Université de Montréal

Effets préventifs et thérapeutiques des polyphénols dans un modèle *in vitro* et *in vivo* de maladie inflammatoire de l'intestin: caractérisation des polyphénols de la pelure de pomme et de la canneberge par spectrométrie de masse

par
Marie-Claude Denis

Département de Nutrition
Faculté de Médecine

Thèse présentée à la Faculté de Médecine
en vue de l'obtention du grade de Docteur en Nutrition

Août 2015

Université de Montréal
Faculté des études supérieures et postdoctorales

Cette thèse intitulée :

Effets préventifs et thérapeutiques des polyphénols dans un modèle *in vitro* et *in vivo* de maladie inflammatoire de l'intestin : caractérisation des polyphénols de la pelure de pomme et de la canneberge par spectrométrie de masse

Présentée par :
Marie-Claude Denis

A été évaluée par un jury composé des personnes suivantes :

Dr Dominique Garrel, président-rapporteur
Dr Emile Levy, directeur de recherche
Dr Edgard Delvin, co-directeur de recherche
Dre Stéphanie Fulton, membre du jury
Dr Gilles Gouspillou, membre externe
Dr Éric Thorin, représentant du doyen de la FESP

Résumé

La muqueuse intestinale est exposée à des agents oxydants provenant de l'ingestion d'aliments modifiés, de cellules immuno-inflammatoires et de la flore intestinale. Une diète élevée en fruits et légumes peut diminuer le stress oxydant (SOx) ainsi que l'inflammation via plusieurs mécanismes. Ces effets bénéfiques peuvent être attribuables à leur contenu élevé en polyphénols. La première étude de mon doctorat consistait à tester l'hypothèse que les polyphénols extraits de pelures de pomme (DAPP) pouvaient diminuer le stress oxydant et l'inflammation impliqués dans les maladies inflammatoires de l'intestin (MII). Nous avons caractérisé les polyphénols des DAPP par spectrométrie de masse (LC-MS) et examiné leur potentiel antioxydant et anti-inflammatoire au niveau des cellules intestinales. L'identification des structures chimiques des polyphénols a été effectuée par LC-MS. Le SOx a été induit par l'ajout du complexe fer/ascorbate (Fe/Asc, 200 µM/2 mM) et l'inflammation par la lipopolysaccharide (LPS, 200µg/mL) à des cellules intestinales Caco-2/15 pré-incubées avec les DAPP (250 µg/mL). L'effet du SOx est déterminé par le dosage du malondialdéhyde (MDA), de la composition des acides gras polyinsaturés et de l'activité des enzymes antioxydantes endogènes (SOD et GPx). L'impact des DAPP sur l'inflammation a été testé par l'analyse de l'expression des marqueurs inflammatoires: cyclooxygénase-2 (COX-2), le facteur de nécrose tumorale alpha (TNF-α), l'interleukine-6 (IL-6) et les facteurs de transcription NF-κB, Nrf-2 et PGC1α par immunobuvardage. Nos données ont montré que les flavonols et les flavan-3-ols constituent les composés polyphénoliques majoritaires des DAPP. L'ajout de Fer^{2+}/Asc a provoqué une augmentation de la peroxidation lipidique comparativement aux cellules contrôles, un appauvrissement des acides gras polyinsaturés n-3 et n-6, et une modulation des enzymes antioxydantes, se traduisant par une augmentation de l'activité de la SOD et une diminution de la GPx. En contrepartie, les DAPP ont exhibé leur potentiel à corriger la plupart des perturbations, y compris l'expression protéique anormalement élevée du COX-2 et la production de la prostaglandine E2 (PGE2), ainsi que l'inflammation telle que réflétée par les facteurs NF-κB, TNF-α et IL-6. Par ailleurs, les mécanismes sous-jacents à ces changements bénéfiques des DAPP ont fait intervenir les facteurs de transcription antioxydants (Nrf-2, PGC1α). Vraisemblablement, cette première étude a permis de démontrer la capacité des DAPP à amoindrir le SOx et à réduire l'inflammation, deux processus étroitement impliqués dans les MII.

Dans la deuxième étape de mon doctorat, nous avons voulu comparer les résultats de DAPP à ceux des polyphenols dérivant de la canneberge qui est considérée par la communauté scientifique comme le fruit ayant le plus fort potentiel antioxydant. À cette fin, nous avons caractérisé l'effet des composés polyphénoliques de la canneberge (CPC) sur le SOx, la défense antioxydante et l'inflammation au niveau intestinal tout en définissant leur métabolisme intraluminal. Les différents CPC ont été séparés selon leur poids moléculaire par chromatographie et leurs structures chimiques ont été identifiées par LC-MS. Suite à une pré-incubation des cellules Caco-2/15 avec les extraits CPC (250 µg/mL), le Fe/Asc et la LPS ont été administrés comme inducteurs du SOx et de l'inflammation, respectivement. La caractérisation globale des CPC a révélé que les acides phénoliques composaient majoritairement l'extrait de canneberge de petit poids moléculaire (LC) alors que les flavonoïdes et les procyanidines dimériques/trimériques représentaient l'extrait de poids moléculaire moyen (MC) tout en laissant les procyanidines oligo et polymériques à l'extrait de

haut poids moléculaire (HC). Les CPC ont permis de restaurer la plupart des perturbations engendrées dans les Caco-2/15 par le Fe/Asc et le LPS. Les CPC exhibaient le potentiel d'abaisser les niveaux de MDA, de corriger la composition des acides gras polyinsaturés n-3 et n-6, d'augmenter l'activité des enzymes antioxydantes (SOD, GPx et CAT) et d'élever l'expression de Nrf2 et PGC1α. En outre, les CPC pouvaient aussi réduire les niveaux élevés des protéines inflammatoires COX-2, TNF-α et IL-6 ainsi que la production des PGE2 par un mécanisme impliquant le NF-κB. Au niveau mitochondrial, les procyanidines oligomériques ont réussi à corriger les dysfonctions reliées à la production d'énergie (ATP), l'apoptose (Bcl-2, Cyt C et AIF) et le statut des facteurs de transcription mitochondriaux (mtTFA, mtTFB1, mtTFB2). Dans le but de bien comprendre les mécanismes d'action des CPC, nous avons défini par LC-MS les composés polyphénoliques qui ont été transportés ou absorbés par l'entérocyte. Nos analyses soulignent le transport (i) des acides cinnamiques et benzoïques (LC); (ii) la quercétine glycosylée et conjuguée et les procyanidines dimériques de type A (MC); et (iii) l'épicatéchine et les procyanidines oligomériques (HC). Les processus de métabolisation (méthylation, glucuronidation et sulfatation) au niveau de l'entérocyte ont probablement permis le transport de ces CPC surtout sous leur forme conjuguée. Les procyanidines oligomériques ayant un degré de polymérisation supérieur à 2 (HC) ont semblé adhérer aux cellules Caco-2/15. L'épicatéchine suivi par les procyanidines dimériques de type A ont été trouvés majoritaires au niveau des mitochondries. Même si nous ignorons encore l'action biologique de chaque composé polyphénolique, nous pouvons suggérer que leurs effets combinatoires exercent des fonctions antioxydantes, anti-inflammatoires et mitochondriales dans le modèle intestinal Caco-2/15.

Dans une troisième étape, nous avons procédé à l'évaluation des aspects préventifs et thérapeutique des DAPP tout en sondant les mécanismes sous-jacents dans une étude préclinique. À cette fin, nous avons exploité le modèle de souris avec colite expérimentale provoquée par le Dextran Sulfate de Sodium (DSS). L'induction de l'inflammation intestinale chez la souris C57BL6 a été effectuée par l'administration orale de DSS à 2.5% pendant 10 jours. Des doses physiologiques et supra-physiologiques de DAPP (200 et 400 mg/kg/j, respectivement) ont été administrées par gavage pendant 10 jours pré- et post-DSS. L'inflammation par le DSS a provoqué une perte de poids, un raccourcissement du côlon, le décollement dystrophique de l'épithélium, l'exulcération et les infiltrations de cellules mono et polynucléaires au niveau du côlon. De plus, le DSS a induit une augmentation de la peroxidation lipidique, une régulation à la baisse des enzymes antioxydantes, une expression protéique à la hausse de la myéloperoxidase (MPO), du COX-2 et de la production des PGE2. Par ailleurs, les DAPP ont permis de corriger ou du moins d'alléger la plupart de ces anomalies en situation préventive ou thérapeutique, en plus d'abaisser l'expression protéique de NF-κB et des cytokines inflammatoires (TNF-α et l'IL-6) tout en stimulant les facteurs de transcription antioxydants (Nrf-2, PGC1α). Conséquemment, les polyphénols des DAPP ont exhibé leur puissant pouvoir antioxydant et anti-inflammatoire au niveau intestinal dans un modèle *in vivo*. Leurs actions sont associées à la régulation des voies de signalisation cellulaire et des changements dans la composition du microbiote. Ces trois projets de recherche permettent d'envisager l'évaluation des effets préventifs et thérapeutiques des DAPP cliniquement chez les patients avec des désordres inflammatoires de l'intestin.

Mots clés : maladie inflammatoire de l'intestin, polyphénol, stress oxydant, inflammation, cyclooxygénase, facteur de transcription, spectrométrie de masse, microbiote.

Abstract

The intestinal mucosa is exposed to oxidizing agents from the ingestion of modified foods, immuno-inflammatory cells and intestinal flora. Diet high in fruits and vegetables may reduce oxidative stress and inflammation via several mechanisms. These beneficial effects may be due to their high polyphenol content. The first aims for my PhD was to define the nature of polyphenols extracted from dried apple peels (DAPP) and to determine their antioxidant and anti-inflammatory potential in the intestine. Caco-2/15 cells were used to study the role of DAPP preventive actions against oxidative stress (OxS) and inflammation induced by iron-ascorbate (Fe/Asc) and lipopolysaccharide (LPS), respectively. The combination of HPLC with fluorescence detection, HPLC-ESI-MS TOF and UPLC-ESI-MS/MS QQQ allowed us to characterize the phenolic compounds present in the DAPP (phenolic acids, flavonols glycosides, flavan-3-ols, procyanidins). The addition of Fe/Asc to Caco-2/15 cells induced OxS as demonstrated by the rise in malondialdehyde, depletion of n-3 polyunsaturated fatty acids, and alterations in the activity of endogenous antioxidants (SOD, GPx, G-Red). However, preincubation with DAPP prevented Fe/Asc-mediated lipid peroxidation and counteracted LPS-mediated inflammation as evidenced by the down-regulation of cytokines (TNF-α and IL-6), and prostaglandin E2. The mechanisms of action triggered by DAPP induced also a down-regulation of cyclooxygenase-2 and nuclear factor-κB, respectively. These actions were accompanied by the induction of Nrf2 (orchestrating cellular antioxidant defenses and maintaining redox homeostasis), and PGC-1α (the "master controller" of mitochondrial biogenesis). Our findings provide evidence of the capacity of DAPP to reduce OxS and inflammation, two pivotal processes involved in inflammatory bowel diseases.

The cranberry fruit has been reported to have high antioxidant effectiveness that is potentially linked to its richness in diversified polyphenolic content. Therefore, the second objective was to compare the results for apple to those for the cranberry. More specifically, the aim of this study was to determine the role of cranberry polyphenolic fractions in oxidative stress, inflammation and mitochondrial functions using intestinal Caco-2/15 cells. The second aim of this work was to determine the polyphenolic species that were responsible for the observed biological activity. The combination of HPLC and UPLC-TDQ techniques allowed us to characterize the profile of low, medium and high molecular weight polyphenolic compounds in cranberry extracts. The medium molecular weight fraction was enriched with flavonoids and procyanidin dimers whereas procyanidin oligomers (degree of polymerization > 4) were the dominant class of polyphenols in the high molecular weight fraction. Pre-incubation of Caco-2/15 cells with these cranberry extracts prevented Fer/Asc-mediated lipid peroxidation and counteracted LPS-mediated inflammation as evidenced by the decrease in pro-inflammatory cytokines (TNF-α and IL-6), cyclooxygenase-2 and prostaglandin E2. Cranberry polyphenols fractions limited both NF-κB activation and Nrf2 down-regulation. Consistently, cranberry procyanidins alleviated oxidative stress-dependent mitochondrial dysfunctions as showed by the rise in ATP production and the up-regulation of Bcl-2, as well as the decline of protein expression of cytochrome C and apoptotic inducing factor. These mitochondrial effects were associated with a significant stimulation of PGC1α, a central inducing factor of mitochondrial biogenesis and transcriptional co-activator of numerous downstream mediators. Finally, cranberry procyanidins forestalled the effect of Fer/Asc on the

protein expression of mitochondrial transcription factors (mtTFA, mtTFB1, mtTFB2). The analysis of different pathways, including absorption and transport of polyphenol species revealed which species in the three cranberry fractions have been responsible for the antioxidant activity observed. Especially, the identification of flavan-3-ols and A-type procyanidins in mitochondria suggested that these polyphenol species were responsible for the antioxidant activity in this organelle. Our findings provide evidence for the capacity of cranberry polyphenols to reduce intestinal oxidative stress and inflammation while improving mitochondrial dysfunction.

Subsequently, we evaluated the preventive and therapeutic aspects of DAPP polyphenols on intestinal inflammation while elucidating the underlying mechanisms and clinical benefits. Induction of intestinal inflammation in the C57BL6 mice was performed by oral administration of the inflammatory agent DSS (Dextran Sodium Sulfate, 2.5% for 10 days). Physiological and supraphysiological doses of DAPP (200 and 400 mg/ kg/day, respectively) were administered by gavage for 10 days pre- and during-DSS. DSS caused weight loss, shortening of the colon, dystrophic detachment of the epithelium, erosion and infiltration of mono- and polymorphonuclear cells in the colon. Additionally, the DSS induced an increase in lipid peroxidation, a down-regulation of antioxidant enzymes, a rise in MPO and COX-2 expression, and PGE2 production. However, the DAPP corrected or at least alleviated most of these abnormalities in preventive and therapeutic situations, in addition to lowering protein expression of NF-κB and inflammatory cytokines (TNF-α and IL-6) while stimulating antioxidant transcription factors (Nrf2, PGC1α). The supraphysiological dose of DAPP in therapeutic situation has corrected mitochondrial dysfunction, as evidenced by the raised ADP/ATP ratio, reduced apoptosis (Cyt C and AIF) and the DNA repair enzyme (OGG1) that eliminated DNA damage, caused by oxidative stress, thereby preventing the initiation of the ROS vicious cycle. The relative abundance of colitogenic bacteria was slightly decreased in DAPP-treated mice compared to DSS-induced colitis group. Conclusions: Polyphenols of DAPP exhibit a powerful anti-oxidant and anti-inflammatory power in the intestine. Their actions are associated with the regulation of cellular signaling pathways and changes in microbiota composition. Therefore, preventive and therapeutic effects of DAPP may be clinically feasible in individuals with intestinal disorders such as colonic cancer.

Keywords: Inflammatory bowel disease, polyphenol, oxidative stress, inflammation, cylooxygenase, transcription factor, mass spectrometry, microbiota

TABLE DES MATIÈRES

Liste des Tableaux

Liste des Figures

Liste des Abréviations

ABC	ATP-binding cassette transporters
ADN	Deoxyribonucleic acid
ADNmt	Mitochondrial deoxyribonucleic acid
AGPI	Polyunsaturated fatty acid
AKT	Protein kinase B
AP-1	Activator protein 1
5-ASA	5-aminosalicyclic acid
ARN	Ribonucleic acid
ATP	Adenosine triphosphate
Balb/c	Albinos mice
Caco-2	Human epithelial colorectal adenocarcinoma cells
CAT	Catalase
C57BL6/J	Inbred strain mice
CD14	Cluster of differentiation 14
COMT	Catechol-O-methyltransferase
COX	Cyclooxygenase
CU	Ulcerative colitis
CumOOH	Cumene hydroperoxide
DAI	Disease Activity Index
DMNT	Deoxyribonucleic acid methyltransferase
DSS	Dextran sulfate sodium
ERK	Extracellular signal-regulated kinases
ERRα	Estrogen-related receptor alpha
FADH2	Flavin adenine dinucleotide H2
FMN	Flavin mononucleotide
GALT	Gut-Associated Lymphoid Tissu
GM-CSF	Granulocyte macrophage colony stimulating factor
GPx	Glutathione peroxydase
GR	Glutathione reductase
GSH	Reduced glutathione
GSSG	Oxidized glutathione
GST	Glutathione S-transferase
GSTT2	Glutathione S-tranferase T2
H_2O_2	Hydrogen peroxide
4-HNE	4-hydroxynonenal
HNF4α	Hepatocyte nuclear factor-4-alpha
HOCl	Hypochlorous acid
HT29	Human colon adenocarcinoma grade II cell line
ICAM-1	Intercellular Adhesion Molecule 1
IFNγ	Interferon γ
IKK	IκB kinase
IL	Interleukin
iNOS	Inducible nitric oxide synthase

INRA	National Institute for Agricultural Research
JAK	Janus kinase protein
JAM	Junctional Adhesion Molecule
JNK	c-Jun N-terminal kinase
$LOO^{\cdot}$	Lipid peroxide radical
LOOH	Lipid hydroperoxide
LOX	Lipoxygenase
LPH	Lactase-phlorizin hydrolase
LPS	Lipopolysaccharide
MAP	Mitogen-activated protein
MAPAQ	Ministère de l'Agriculture, des Pêcheries et de l'Alimentation du Québec
MAGUK	Membrane Associated Guanylate Kinase Homologs
MC	Crohn's disease
MCP	Monocyte chimioattractant protein-1
MDA	Malondialdehyde
MD-2	Myeloid differentiation protein-2
MII	Inflammatory bowel disease
MMP	Metalloproteinase
MPO	Myeloperoxidase
MRP	Multidrug-resistance-associated protein
MUC	Mucin
NF-κB	Nuclear factor-kappa B
$NO^{\cdot}$	Nitric oxide
Nrf2	Nuclear respiratory factor 2
$OH^{\cdot}$	Hydroxyl radical
8-OH-G	8-hydroxy-guanine
$ONOO^{-}$	Peroxynitrite anion
O_2	Molecular dioxygen
$O_2^{-\cdot}$	Superoxide anion
PGC1α	Peroxisome proliferator-activated receptor gamma, coactivator 1 alpha
PGE2	Protaglandin E2
P-gp	Permeability-GlycoProtein
PI 3-kinase	Phosphoinositide 3-kinase
PLA2	Phospholipase A2
PNN	Polynuclear neutrophil
POLRMT	Mitochondrial RNA polymerase gene
PPARy	Peroxisome proliferator-activated receptor gamma
RLO	Reactive oxygen species
$RO^{\cdot}$	Alkoxyl radical
$ROO^{\cdot}$	Peroxide radical
SAH	S-adenosyl-l-homocysteine
SAM	Sorting and assembly machinery
SOD	Superoxide dismutase
SGLT1	Sodium-glucose transport protein 1
SOC3	Suppressor of cytokine signalling 3

STAT	Signal Transducer and Activator of Transcription
TBARS	Thiobarbituric acid reactive substance
TER	Transepithelial Electrical Resistance
TFAM	Mitochondrial transcription factor A
TFB1M	Transcription factor B1 mitochondrial
TFB2M	Transcription factor B2 mitochondrial
Th1	Type 1 T helper
TIM	Transmembrane immunoglobulin and mucin domain
TLR4	Toll-like receptor 4
TOM	Translocase of the outer membrane
TNFα	Tumor necrosis factor alpha
UbH	Ubiquitin hydrolase
UbH2	Ubiquitin hydrolase-2
UDPGT	Uridine diphospho-glucuronosyltransferase
SULT	Sulfotransferase
VCAM-1	Vascular cell adhesion molecule 1
VDAC	Voltage-dependent anion-selective channel
ZO	Zonula occluden

À Samuel, mon grand garçon de 2 ans

Les remerciements

J'ai gardé cette section à la fin pour me gâter! Les premiers mots qui me viennent sont : « Wow, quelle belle aventure! ». J'ai eu la chance de faire un projet de recherche doctoral que j'aimais particulièrement et qui me tenait à cœur. Mes connaissances ultérieures en biochimie, pharmacologie et en spectrométrie de masse m'ont permis de mener à bien mes recherches. Par conséquent, je dois d'abord remercier mes directeurs de recherche, le Dr.Emile Lévy et le Dr.Edgard Delvin, pour m'avoir donné l'opportunité de réaliser ce projet de recherche. Je les remercie également pour leur confiance, leur patience, leur compréhension mais surtout pour leurs nombreux conseils scientifiques qui m'ont été donnés durant ces années.

J'ai eu la chance de côtoyer une superbe équipe composée de jeunes chercheurs, d'étudiants de tous les niveaux et de coordinatrices. La personne qui nous suit dans nos expériences scientifiques outre que nos directeurs de recherche est la coordonnatrice de recherche Carole. Je te remercie Carole pour ton aide, tes conseils et pour tes encouragements. J'ai également eu l'occasion de travailler avec Zola pour l'écriture de mes articles scientifiques. Je te remercie Zola pour ton travail et ta disponibilité. Je remercie également tous les étudiants et jeunes chercheurs de ce labo : Léa, Sabrina, Émilie, Élodie, Marie-Laure, Louis-Philippe, Thierry, Rami, Alain S, Alain M, Sylvain, Sophia, Pantea, Nour, Jade, Maryse et Valérie. Je suis certaine que j'en oublie! Nos échanges scientifiques et l'entraide que nous partageons font la force de cette équipe.

J'ai une pensée particulière pour ma mentor en chimie analytique : Alexandra. Cette chercheure extraordinaire me suit dans tous mes projets scientifiques depuis mes études de premier cycle à l'Université. Chère Alex, je te remercie pour ton aide, pour tes bons conseils et surtout pour ton amitié! Je remercie également son équipe: Karine, Marie-Christine et Louiza. J'ai tellement eu du plaisir à travailler avec vous!

Je remercie le Dr.Jean-Claude Lavoie qui a toujours été disponibile à répondre à mes questions concernant les statistiques et qui m'a bien suivi comme parrain. Je remercie

également ma marraine scientifique : Dre.Christine Desrosiers pour ses bons conseils. Je remercie également nos collaborateurs de l'INAF : Dr.Yves Desjardins, Pascal, Stéphanie et Thibault ainsi que ceux de l'Université de Sherbrooke : Dr.Jean-François Beaulieu et Éric Tremblay.

Je remercie le département de Nutrition, la faculté de Médecine et les Études Supérieures de l'Université de Montréal pour m'avoir donné accès aux études graduées. Je remercie les organismes suivants pour leur soutien financier : la chaire J.A. DeSève de recherche en nutrition du Dr.Levy, la Fondation des Étoiles de l'Hôpital Sainte-Justine et les Fonds de Recherche Québécois en Nature et Technologies (FQRNT).

Pour terminer, je dois également la réussite de ce projet doctoral à mon conjoint Alexandre qui m'a tellement aidé quotidiennement à prendre soin de notre petit garçon Samuel, à faire la vaisselle, le souper, etc. surtout durant mon examen de pré-doc et l'écriture de cette thèse. J'ai la chance d'avoir une belle-famille extraordinaire. Je vous remercie pour vos encouragements et votre aide! Mes derniers mots vont à ma mère, mon père et à ma sœur que j'aime tant. Je vous remercie de m'avoir toujours écouté, encouragé et aidé de toutes les façons inimaginables!

1. INTRODUCTION

En 2008, près de 201 000 Canadiennes et Canadiens sont atteints d'une maladie inflammatoire de l'intestin (MII). On diagnostique chaque année plus de 9 200 nouveaux cas. Le Canada montre une prévalence et une incidence des MII parmi les plus élevées dans le monde entier. Plusieurs voies de recherche et de développement sont en cours pour améliorer les traitements des MII. La nutraceutique et les aliments fonctionnels ont démontré depuis quelques années leur potentiel thérapeutique contre les maladies inflammatoires chroniques.

En collaboration avec l'Institut sur la nutrition et les aliments fonctionnels de l'Université Laval, nous avions l'intérêt de trouver une molécule à la fois anti-inflammatoire et antioxydante agissant au niveau intestinal et, bien entendu, ne causant pas d'effets secondaires supplémentaires à ceux provenant de la médication chez les individus atteints de MII. L'étude de l'influence directe des polyphénols sur l'intestin a fait l'objet de mes recherches doctorales.

Dans ce présent projet, afin de bien comprendre les MII, une courte présentation de l'anatomie du tractus gastro-intestinal et des cellules qui le composent est présentée en premier dans l'introduction. La seconde section contient les caractéristiques physiopathologiques des MII et les traitements associés. Une recension des écrits concernant les deux composantes majeures des MII, le stress oxydant et l'inflammation, est présentée par la suite. Un volet présentant les régimes alimentaires des individus atteints de MII et les bienfaits d'une nutrition par les polyphénols met en contexte le vif du sujet, soit les polyphénols. Une section importante a été dédiée à ces molécules. On retrouve essentiellement de l'information concernant la consommation, les caractéristiques, la biodisponibilité et les mécanismes d'action des polyphénols pour contrer le stress oxydant et l'inflammation. La dernière partie illustre les effets des polyphénols sur le stress oxydant et l'inflammation présents dans l'intestin.

Nous espérons que ce projet de recherche permettra un jour en arriver à recommander aux individus atteints de MII de prendre à la fois leur médicament et un certain nombre d'aliments fonctionnels riches en polyphénols au quotidien. Pour ceux ayant une incapacité à

tolérer les fibres, des suppléments de polyphénols provenant d'extraits de fruits et/ou légumes pourront être préparés par les compagnies nutraceutiques. Ainsi, les équipes médicales pourront suggérer la prise de ces suppléments à leurs patients en mode préventif et thérapeutique et, plus particulièrement en période de phase aiguë de MII.

1.1 Le tube digestif

Le tube digestif est composé d'une suite d'organes creux (œsophage, estomac, duodénum, jéjunum, iléon, côlon et le rectum) et il s'étend de la cavité buccale à l'anus (Figure 1). Le processus de digestion est segmenté entre ces organes : l'estomac assure une digestion primaire en milieu acide, le grêle absorbe majoritairement les nutriments et les acides biliaires, et le côlon digère le reste du bol alimentaire et absorbe l'eau et les minéraux. Ces processus offrent à l'organisme un équilibre des apports énergétique et minéraux essentiels au maintien de la bonne santé.

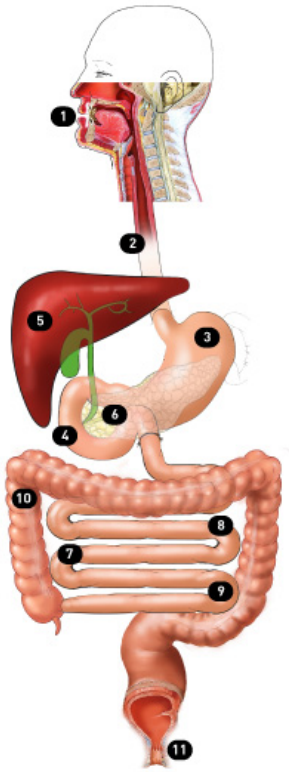

1) Cavité buccale
2) Œsophage (±10 secondes)
3) Estomac (± 1-6 heures)
4) Duodénum
5) Foie
6) Pancréas
7) Intestin grêle (± 7-9 heures)
8) Jéjunum
9) Iléon
10) Côlon (± 25-30 heures)
11) Rectum (± 30-120 heures)

Figure 1: Anatomie et transit des aliments dans le tube digestif
Adaptée de Von Rosenvinge *et al*., 2013(1)

1.1.1 L'anatomie tissulaire et cellulaire

La paroi de l'ensemble du tube digestif possède une anatomie tissulaire et cellulaire adaptée aux fonctions de chacune de ses sections. La Figure 2 illustre les quatres couches de la paroi du tube digestif en allant vers la lumière intestinale: la séreuse, la musculeuse, la sous-muqueuse et la muqueuse (2).

La séreuse est la couche externe de la plupart des organes du tube digestif. Elle est formée d'une couche d'épithélium pavimenteux simple ou mésothélium et d'une couche sous-jacente de tissu conjonctif servant de soutien. La musculeuse est constituée de fibres musculaires lisses disposées en deux couches de cellules permettant de contrôler la motricité du tube digestif. Des plexus ganglionnaires myentériques (plexus d'Auerbach) s'y retrouvent également assurant l'innervation du tube digestif. La sous-muqueuse est composée de tissu conjonctif qui relie la muqueuse à la musculeuse. Elle est richement vascularisée et contient une partie du plexus ganglionnaire submuqueux (plexus de Meissner). Ce plexus est constitué de fibres du système nerveux autonome qui innervent la musculaire-muqueuse. Son rôle est de réguler les sécrétions du tube digestif. La muqueuse est formée de l'épithélium, de la musculaire et de la *lamina propria*. La couche musculaire est caractérisée par une fine couche de tissu musculaire lisse qui plie la muqueuse intestinale. Ces plis permettent d'augmenter la surface de digestion et d'absorption. La *lamina propria* (ou le chorion) est constituée du tissu conjonctif très riche en vaisseaux sanguins et lymphatiques. La *lamina propria* soutient l'épithélium, le rattache à la musculaire et lui fournit le sang et la lymphe. Les vaisseaux sanguins et lymphatiques sont des voies empruntées par les nutriments pour atteindre les autres tissus de l'organisme. Le tissu lymphatique contient plusieurs cellules immunitaires qui protègent le tube digestif des agressions. L'épithélium de la muqueuse constitue une barrière cellulaire composée d'entérocytes entre lesquels s'intercalent des cellules à gobelet, des cellules entéro-endocrines et des cellules immunitaires (Figure 3).

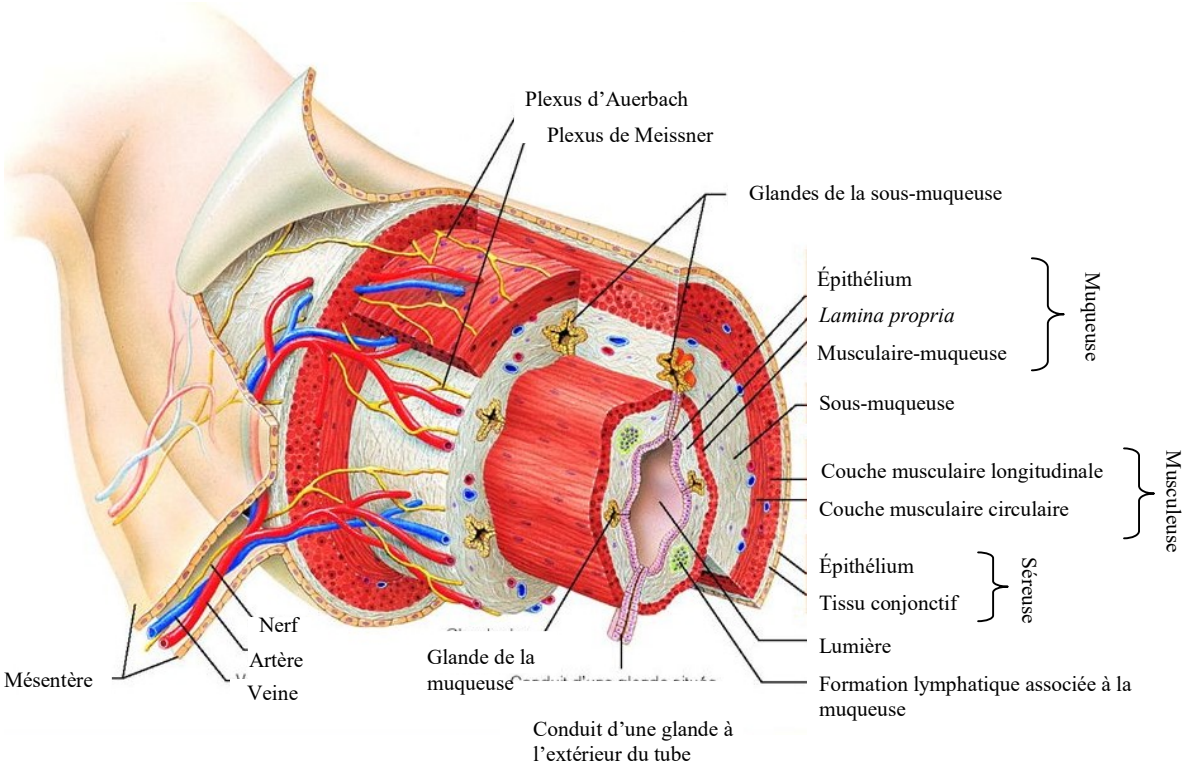

Figure 2: Les couches et les composantes du tube digestif
Adaptée de Tortora et Grabowski, 1999 (3)

1.1.2 L'épithélium de la muqueuse intestinale

1.1.2.1 Les entérocytes

Ces cellules, à renouvellement rapide (tous les 5 jours approximativement), sont reliées par des jonctions serrées formant un tapis cellulaire monocouche pratiquement étanche. Les cellules composant cette barrière intestinale sont polarisées. Elles possèdent un pôle apical en contact avec la lumière intestinale et un pôle basolatéral en contact avec les tuniques successives du côlon (2). Sur la surface du pôle apical des entérocytes se retrouve une membrane hautement spécialisée en forme de bordure en brosse : les microvillosités (2). La surface de contact entre la muqueuse et la lumière intestinale est augmentée par ces microvillosités permettant ainsi une plus grande surface d'absorption d'eau, de minéraux et de nutriments (2). Les entérocytes ont comme fonction, outre l'absorption, de former une barrière physique contre l'invasion de pathogènes.

La barrière physique est composée de jonctions serrées qui maintient une cohésion entre les cellules et offre une étanchéité à la membrane cellulaire (4). Les jonctions serrées sont composées de différentes familles de protéines dont les occludines (5) et les claudines (6). Les occludines sont des protéines transmembranaires qui forment les jonctions serrées des cellules épithéliales (7, 8). Les claudines scellent les jonctions serrées (9). Toutefois, les claudines-2, 10b et 15 permettent le passage sélectif des ions de sodium et de chlore pour le bon fonctionnement de l'organisme (10-12). Lorsque l'intégrité de ces jonctions serrées est altérée, la perméabilité intestinale est augmentée, ce qui accroit la susceptibilité de développer une maladie inflammatoire de l'intestin (MII) (13). De plus, des variations génétiques chez les patients avec MII avaient été trouvées dans les protéines de zonula occludens (ZO). Ces protéines de la famille MAGUK (Membrane Associated Guanylate Kinase Homologs) sont impliquées dans l'assemblage des jonctions serrées ou dans leur régulation par le facteur de transcription HNF4α (hepatocyte nuclear factor-4) (14-16).

1.1.2.2 Les cellules à gobelet

Les cellules à gobelet, appelées également cellules caliciformes ou cellule à mucus, sont juxtaposées aux entérocytes et sécrètent du mucus qui recouvre la surface de l'épithélium intestinal. Le mucus est principalement composé de mucine (glycoprotéines) protégeant la surface de l'épithélium contre les agressions causées par le bol alimentaire, les microbes et les sous-produits bactériens. Le mucus a également comme rôle de lubrifier les parois afin de faciliter l'évacuation des fèces et d'assurer l'adhérence de la flore intestinale par la présence de granules de mucines localisées sous la membrane apical (17, 18). Une modification qualitative des mucines et une diminution du mucus peuvent entraîner un défaut dans la barrière physique de l'épithélium. Une réponse immunitaire est alors déclenchée pouvant générer une inflammation intestinale. Des changements d'expression des mucines (MUC) ont été démontrés par diverses équipes de recherche dans le domaine des MII (19). Neuf gènes de la mucine ont été identifiés chez l'humain et six d'entre eux ont été associés aux MII. Les mucines suivantes : MUC1 (20), MUC2 (21) et MUC3A (22) ont été trouvés reliés à la maladie de Crohn alors que dans la colite ulcéreuse, MUC3A, MUC4 et MUC13 ont été repertoriés (18). Le mucus contient également des peptides régissant la régulation de sa

sécrétion (23). Une perturbation dans la barrière chimique formée par le mucus augmente la perméabilité de l'intestin, amplifiant ainsi la susceptibilité des MII et du cancer colo-rectal.

1.1.2.3 Les cellules entéro-endocrines

L'épithélium gastro-intestinal contient au moins dix types de cellules endocrines différentes qui ont la particularité d'être regroupées ou dispersées parmi les autres cellules digestives. Bien que les cellules entéro-endocrines constituent seulement 1 % des cellules du revêtement du tube digestif, elles font de l'épithélium gastro-intestinal le principal organe endocrinien. Après un repas, chaque type de cellules endocrines sécrète une hormone ou un peptide différent : cholecystokinine (24), ghréline (25-27), sécrétine (28), glucagon-like peptide-1 (29, 30), peptide YY (31, 32), qui passe dans la circulation sanguine et régule la digestion. Ces hormones peuvent par exemple entraîner un effet de satiété, déclencher la vidange de l'estomac ou stimuler la sécrétion d'insuline par le pancréas. Le rôle de ces cellules était jusqu'à présent sous-estimé car les hormones qu'elles sécrètent n'agissent pas seulement au niveau du tube gastro-intestinal mais également au niveau d'autres organes périphériques (cerveau, cœur, pancréas, tissu adipeux, estomac et vésicule biliaire) où elles régulent de nombreux processus métaboliques.

1.1.2.4 Les cellules immunitaires

Malgré le bon fonctionnement de la barrière physique et chimique de la paroi intestinale, certaines bactéries réussissent quand même à pénétrer l'épithélium et à coloniser la *lamina propria*. Le tissu lymphoïde de la muqueuse constitue la dernière barrière intestinale; à lui seul il contient plus de 80% des cellules immunitaires de l'organisme. Cette barrière immunologique, appelée GALT (Gut-Associated Lymphoid Tissu) s'oppose à la propagation des bactéries dans l'organisme (33, 34).

Les cellules de Paneth sécrètent des défensines, des lyxozymes et des cathélicidines. La composition de ces peptides permet de par son organisation d'éliminer les substances nuisibles de l'intestin.

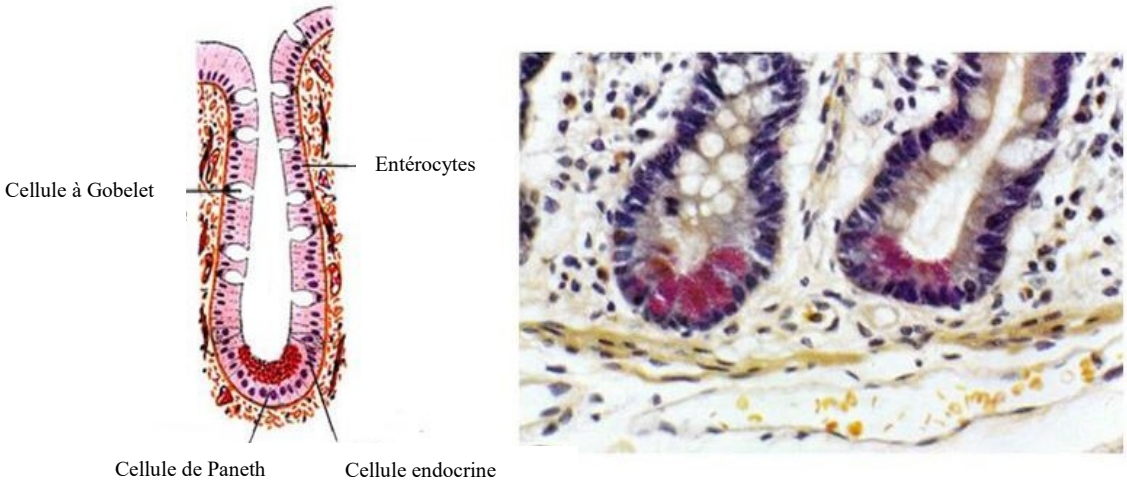

Figure 3: Les différentes cellules de l'épithélium de la muqueuse intestinale
Adaptée de Von Rosenvinge *et al*., 2013 (1)

1.2 Les maladies inflammatoires de l'intestin

Les maladies inflammatoires de l'intestin (MII) regroupent la maladie de Crohn (MC) et la colite ulcéreuse (CU) (35). Elles se caractérisent toutes par une inflammation chronique de la paroi du tube digestif. Ces maladies évoluent par poussées inflammatoires de durée et de fréquence extrêmement variables alternant avec des phases de rémission (36-38).

La qualité de vie des personnes atteintes peut être grandement diminuée durant les poussées inflammatoires nécessitant plusieurs consultations médicales et hospitalisations (39-43), générant des coûts importants pour le système de santé et pour l'individu atteint (44-48). Les MII sont présentes dans tous les coins du monde, mais particulièrement dans les zones industrialisées et les régions nordiques (49-51). En 2000, on dénombrait 206 000 individus atteints au Canada (52, 53) dont 32% provennaient du Québec (54). L'incidence moyenne de développer une MII est de 16.3 individus pour la MC et de 12.9 pour la CU par 100 000 individus au Canada. La prévalence est de 468.1 par 100 000 individus canadiens. À partir de 2000, on a remarqué que le Canada dispose d'une incidence et d'une prévalence des MII parmis les plus élevées au monde (52, 53, 55-58).

L'étiologie et les mécanismes responsables des MII sont encore méconnus, toutefois plusieurs études ont démontré qu'elles sont multifactorielles impliquant des anomalies à la fois du système immunitaire (59, 60) ainsi que des facteurs génétiques (59, 61-65) et environnementaux (59, 66-69).

1.2.1 La maladie de Crohn

Dans la maladie de Crohn (MC), le phénotype inflammatoire peut se retrouver de la bouche à l'anus. Les lésions inflammatoires sont discontinues et peuvent traverser la totalité de la paroi intestinale (61). Lors des poussées inflammatoires, les symptômes sont variés : douleurs abdominales, diarrhées fréquentes souvent sanguinolentes, fatigue, fièvre, malabsorption et perte de poids. Des manifestations extra-intestinales peuvent également être présentes au niveau articulaire, cutané, oculaire et hépatique. L'évolution de la maladie peut entraîner le rétrécissement d'un segment intestinal atteint puis éventuellement une occlusion ou encore un abcès pouvant aboutir à une fistule. Ces complications nécessitent souvent une intervention chirurgicale (70-72).

1.2.2 La colite ulcéreuse

Le désordre inflammatoire chronique de la colite ulcéreuse (CU) n'atteint que le côlon mais se manifeste surtout au niveau du rectum. Les lésions sont continues et touchent uniquement la muqueuse épithéliale. Toutefois, les symptômes sont bien similaires à la MC. Les saignements et l'irritation de la muqueuse épithéliale par les aliments ingérés sont principalement les complications de la CU (73).

1.2.3 Traitements et effets secondaires de la médication

Il n'existe pas de traitement radical de guérison des MII. Les médicaments disponibles permettent toutefois un contrôle durable de la maladie et une qualité de vie acceptable. Comme toutes les maladies inflammatoires chroniques, la prise en charge repose sur un traitement de fond et un traitement de crise. Le premier traitement est consacré à prévenir l'apparition des poussées inflammatoires et à prolonger les phases de rémission. Le second permet de réduire la durée des poussées inflammatoires et de limiter les symptômes (73).

1.2.3.1 Traitements lors des poussées inflammatoires

Lors des poussées inflammatoires, les 5-aminosalicylés (5-ASA) sont les premiers anti-inflammatoires prescrits en raison de leur bonne tolérance (74). En cas d'inefficacité des 5-ASA, les corticoïdes sont utilisés (75). Toutefois, ces derniers présentent des effets secondaires considérables tels que l'ostéopénie, l'ostéoporose (76), l'insuffisance corticotrope (77), l'hypertension artérielle et le diabète (78).

1.2.3.2 Traitements de fond

Lors du traitement de fond, afin de mieux contrôler l'immunité des individus atteints et de réduire l'inflammation à long terme, les immunomodulateurs (azathioprine, mercaptopurine et méthotrexate) et les biothérapies sont utilisés. Depuis 1990, les biothérapies (79) ont grandement amélioré la qualité de vie des individus atteints de formes sévères de la maladie et résistants aux autres traitements. Elles bloquent spécifiquement le facteur d'inflammation TNF-α (80). L'infliximab (81) et l'adalimumab (82) sont les deux molécules indiquées pour la MC alors que pour la CU seulement l'infliximab est souvent recommandé. Ils sont par contre très coûteux et peuvent avoir des effets secondaires graves dans une faible proportion d'individus, tels qu'un choc anaphylactique avec réactions d'hypersensibilité retardée (83), une insuffisance cardiaque congestive (84), des atteintes démyélisantes centrales (sclérose en plaque) ou périphériques (syndrome de Guillain Barré) (85), lupus érythémateux (86), et même le cancer (87).

1.3 La nutrition

1.3.1 Régimes alimentaires

Un régime alimentaire varié est encouragé par les diététiciens lors des périodes de rémission. Toutefois, un régime sans résidus est recommandé pendant les poussées inflammatoires. Ce régime exclut les fruits et légumes crus ou cuits ainsi que les céréales complètes du régime alimentaire. Le régime sans résidus supprime au maximum l'apport en fibre afin d'éviter que des aliments non-digérés augmentent le volume des selles et aggravent

les diarrhées. Suite à une poussée inflammatoire, il est vivement suggéré de suivre un régime pauvre en fibres. Les crudités, les céréales complètes et les fruits et légumes difficiles à digérer pour chaque individu sont proscrits dans le régime pauvre en fibre. La réintroduction du régime alimentaire varié se fait au rythme d'un nouvel aliment par repas selon la tolérance de l'individu. Seuls les individus avec une sténose doivent éviter certains aliments (noyaux fruits, fruits secs et certains fibres tels que le céleri et le poireau) dans leur régime alimentaire afin que ceux-ci ne constituent pas un obstacle physique.

La fréquence des diarrhées et la malabsorption des nutriments peuvent entraîner une carence nutritionnelle. Une supplémentation *per os* ou en intraveineuse de fer, d'acide folique, de zinc, de magnésium et de vitamines peut être nécessaire. Le recours à la nutrition entérale, exclusive ou en complément, peut s'avérer indispensable lorsque l'alimentation orale spontanée ne permet pas de couvrir les besoins nutritionnels de l'individu atteint de MII (88).

1.3.2 Les bienfaits

À part de combler les besoins nutritionnels, la nutrition joue un rôle important dans la prévention des poussées inflammatoires et dans le maintien des périodes de rémission des individus atteints de MII. Dans la dernière décennie, la nutraceutique et les aliments fonctionnels ont démontré leur potentiel thérapeutique contre les maladies inflammatoires. Les prébiotiques (89), les probiotiques (90), les oméga-3 (91), les acides gras surtout essentiels (92), la vitamine D (93, 94) et les antioxydants (95), pour ne nommer que ceux-là, ont réduit ou neutralisé le processus inflammatoire dans diverses maladies. Bien évidemment, l'inflammation est la composante centrale dans les MII, mais elle s'accompagne d'un stress oxydant persistant (96-98). Afin de bien comprendre les effets d'un stress oxydant dans les MII, une recension des écrits concernant cette composante est présentée dans la prochaine section.

1.4 La composante du stress oxydant dans les MII

Les radicaux libres de l'oxygène (RLO) peuvent être exogènes et endogènes. L'exposition à la pollution, au soleil prolongé, l'absorption de médicaments, d'alcool et le tabagisme provoquent une production de RLO qui peut surpasser les défenses antioxydantes endogènes. Malheureusement l'alimentation nord-américaine, et encore moins celle des individus atteints d'une MII, n'est pas suffisante en fruits et légumes (polyphénols, vitamine C, vitamine E et caroténoïdes) afin de combler les défenses antioxydantes endogènes.

Toutes les cellules par leur métabolisme produisent de faibles quantités de dérivés réactifs de l'oxygène. En effet 1 à 2% de l'oxygène présent est dévié vers la formation de radicaux libres. Les RLO sont essentiellement formés au niveau mitochondrial lors du processus de conversion de l'oxygène en eau, produisant le radical superoxyde (O_2^-). Ce radical superoxyde peut également être produit au niveau microsomial et plasmatique par les NADPH oxydases. Le radical superoxyde est transformé en peroxyde d'hydrogène (H_2O_2) (plus stable) par la superoxyde dismutase et ensuite en eau, soit par la catalase ou la glutathion peroxydase. Les RLO peuvent réagir avec différents substrats biologiques tels que les lipides, les protéines et l'ADN. Leurs effets sont décrits dans les paragraphes suivants.

Lorsqu'il y a déséquilibre de la balance des composés pro-oxydants et antioxydants (Figure 4), qui ne peut être compensé, le stress oxydant apparaît. L'exposition chronique à ce débalancement peut entraîner le développement de plusieurs pathologies dont les MII (99-102).

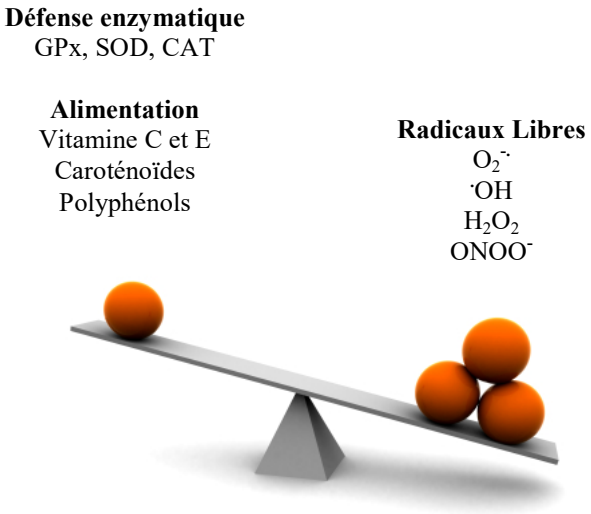

Figure 4 : Balance entre stress oxydant et antioxydants

1.4.1 Les radicaux libres de l'oxygène (RLO)

Les RLO sont impliqués dans l'expression et la régulation des fonctions de prolifération et de mort cellulaire. L'étude de divers pathologies telles que les MII, athérosclérose et le cancer, a démontré que les RLO agissent également comme des médiateurs inflammatoires.

Les RLO sont très instables et leur durée de vie est très courte (10^{-4} secondes). Leur réactivité réside dans leur recherche d'un électron afin d'apparier leur électron célibataire. Les différents RLO selon leur réactivité sont les suivants :

La Figure 5 résume le processus de formation des radicaux libres. L'ion superoxyde $O_2^{\bullet-}$ et le peroxyde d'hydrogène H_2O_2 sont peu actifs. L'$O_2^{\bullet-}$ peut capter un H^+ pour donner $HO_2^{\bullet}$ qui serait la forme réactive de $O_2^{\bullet-}$ capable d'initier la peroxydation lipidique. L'$O_2^{\bullet-}$ peut aussi se dismuter en H_2O_2 et O_2 (réaction spontanée ou catalysée par la superoxyde dismutase), réagir avec $NO^{\bullet}$ pour former l'anion peroxynitrite $ONOO^-$, un oxydant puissant, ou réduire les ions de métaux de transition. L'$O_2^{\bullet-}$ est produit notamment par réduction monoélectronique de l'oxygène moléculaire dans les mitochondries par la NADPH oxydase ou par la xanthine oxydase, une enzyme du métabolisme des purines. Le radical hydroxyle

$HO^{\bullet}$ est l'une des espèces chimiques les plus oxydantes et peut attaquer très rapidement la plupart des molécules biologiques. $HO^{\bullet}$ est produit par réduction monoélectronique de H_2O_2 par les ions métalliques de basse valence comme Fe^{2+} ou Cu^{+}, libres ou complexés (hème) (réaction de Fenton). Le dioxygène singulet $^1O_2$ peut être généré par excitation de $^3O_2$ en présence de photosensibilisateurs mais aussi par des processus chimiques (par exemple, la réaction de H_2O_2 avec ClO^-). $^1O_2$ est très réactif et peut par exemple s'additionner rapidement sur des doubles liaisons carbone-carbone.

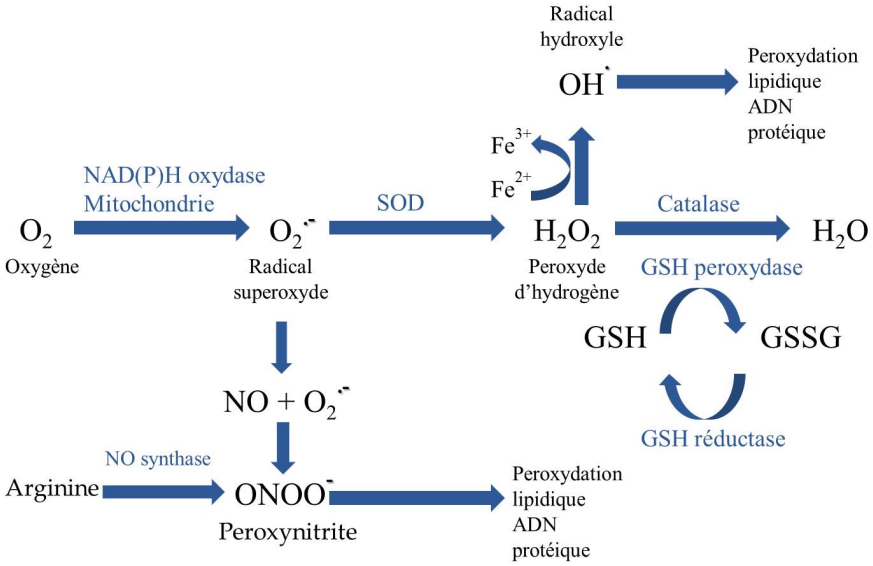

Figure 5: Processus de formation des radicaux libres
Adaptée de Halliwell *et al*., 1994 (103)

1.4.2 Principale source de RLO : la mitochondrie

Les mitochondries sont les organites essentiels à l'origine de la production d'énergie, sous forme d'ATP, nécessaire au fonctionnement cellulaire. Elles sont caractérisées par deux membranes délimitant l'espace inter-membranaire et le compartiment matriciel.

La membrane externe est une bicouche lipidique composée de 50% de protéines et de 50% lipides polaires qui est perméable. Les protéines peuvent traverser la membrane externe via les translocases (TOM) alors que les ions et petites molécules de taille inférieure à 10 kDa entrent par les porines ou les VDAC (voltage-dependent anion channel).

La membrane interne est constituée de 80% de protéines et de 20% de lipides. Elle est imperméable aux ions surtout aux protons. Mais, elle est perméable à l'oxygène, à l'eau, à l'oxyde nitrique, à l'ammoniac et au gaz carbonique. La translocase de nucléotide adénylique assure l'entrée de l'ADP et la sortie de l'ATP. Les autres molécules peuvent franchir la membrane interne par les différents transporteurs suivants: cotransporteur de phosphate ionorganique/proton, le symporteur pyruvate/proton, la navette du glycérol-3-phosphate, la navette malate/aspartate, le transporteur du citrate et la carnitine palmitoyltransferase II. Les translocases TIM permettent aux protéines de traverser également la membrane interne mitochondriale. La membrane interne est composée également de replis formant des crètes. Les complexes de la chaîne respiratoire et l'ATP synthase sont majoritairement retrouvés dans ces crètes. Le compartiment interne de la mitochondrie s'appelle la matrice. Les voies métaboliques suivantes : cycle de krebs et la β-oxydation des acides gras s'y retrouvent. La mitochondrie détient son propre génome (ADN mitochondrial) et synthétise ses protéines grâce aux mitoribosomes.

1.4.2.1 Sites mitochondriaux de production de RLO : complexes I et III

La chaîne respiratoire est une source permanente de RLO (Figure 6). Les complexes I et III sont des sites prédilection de production de RLO. Toutefois, il y a cinq autres sites qui produisent des RLO, à plus petite échelle, au sein des mitochondries : la glycerol-3-phosphate deshydrogénase (GPDH), la flavoprotéine de transfert d'électron ubiquinone oxydoréductase (ETFQOR), la 2-oxoglutarate deshydrogénase (OGDH), la pyruvate deshydrogénase (PDH) et le NADH-coenzyme Q oxydoréductase (104).

Dans les années 80, les équipes de recherche avaient démontré que le complexe III était le plus grand site de production d'$O_2^{\cdot-}$ et que le complexe I venait en seconde place (105-107). L'ajout successif et non combiné de succinate (fournisseur de FADH2) et de roténone (inhibiteur du complexe I) a permis de démontrer l'existence d'un flux inverse d'électrons. Ce flux d'électrons provient de l'oxydation du FADH2 remontant du complexe II au complexe I. Le complexe I est devenu la source majeure de RLO via ce flux inverse d'électrons (108, 109). Même à ce jour, l'endroit exact de la production de RLO du complexe I est encore controversé. Les équipes de recherche ont démontré que la production de RLO de ce complexe

pourrait venir des quinones (110), du groupe des flavines mononucléotides (FMN) (111) ou du groupe fer-soufre (112, 113). Comme ces trois structures interagissent ensemble, il est difficile de dire laquelle intervient majoritairement dans la production de RLO.

La réduction partielle de l'ubiquinone du complexe III génère des RLO. L'électron libre provenant de la chaîne respiratoire s'attache à l'ubiquinone pour former le radical semi-ubiquinone ($UbH^{\cdot}$) qui est instable. Le radical de la semi-ubiquinone est stabilisé par un deuxième électron au niveau du UbH_2 qui permettra le transfert du proton. Toutefois, si le radical semi-quinone rencontre une molécule d'oxygène avant d'être stabilisé, l'oxygène captera l'électron libre générant un anion superoxyde (114).

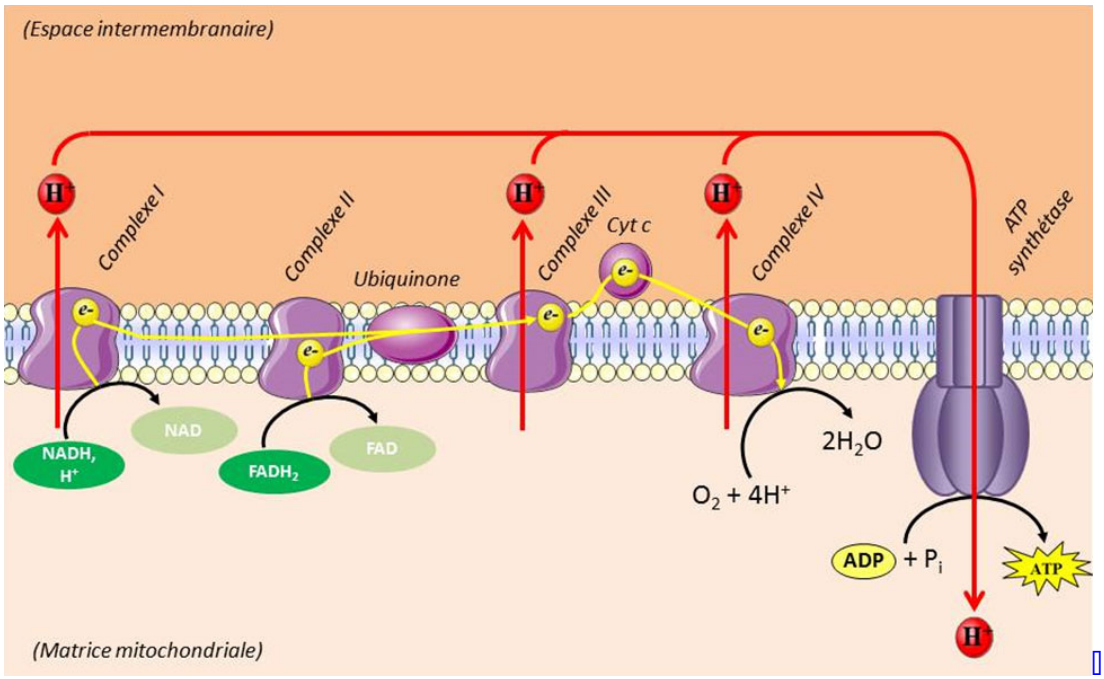

Figure 6 : Chaîne respiratoire et phosphorylation oxydative
Adaptée de Voet et Voet, 1998 (115)

1.4.2.2 Régulation transcriptionnelle mitochondriale

La mitochondrie possède son propre génome. Les protéines de la chaîne respiratoire sont codées par le génome mitochondrial ou le génome nucléaire. Le complexe II, par exemple, est 100% encodé par l'ADN nucléaire. Par conséquent, il y a des facteurs régulateurs

codés par le génome nucléaire qui vont permettre à la fois la transcription du génome mitochondrial et l'expression des gènes nucléaires codant pour les protéines mitochondriales (116).

1.4.2.2.1 ADN mitochondrial

L'ADN mitochondrial (ADNmt) est une molécule bicaténaire circulaire d'environ 16 kilobases dépourvue d'introns et d'histones. Chaque mitochondrie possède un nombre variable de copies d'ADNmt (2 à 10) qui code pour 13 protéines de la chaîne respiratoire mitochondriale, 22 ARN de transfert et 2 ARN ribosomiques.

1.4.2.2.2 Facteurs de transcription mitochondriaux

La mitochondrie possède son propre système de transcription composé de l'ARN polymérase mitochondriale (POLRMT) et des facteurs de transcription mitochondriaux A (TFAM), B1 (TFB1M) et B2 (TFB2M).

1.4.2.2.2.1 POLRMT

L'ARN polymérase mitochondriale a été découvert dans les cellules humaines en 1997 par l'équipe de Tiranti *et al*.(117). La POLRMT a besoin de la présence de TFAM et au moins un des deux facteurs de transcription TFB1M ou TFB2M afin d'interagir avec la région promotrice et initier la transcription de l'ADNmt (118).

1.4.2.2.2.2 TFAM

Le facteur de transcription TFAM se fixe à l'ADN au niveau du site d'initiation de la transcription mitochondriale afin de jouer son rôle essentiel dans la transcription mitochondriale mais aussi dans le maintien et la stabilisation de l'ADNmt ainsi que dans la régulation de la réplication de l'ADNmt (119, 120).

1.4.2.2.2.3 TFB1M et TFB2M

Les facteurs de transcription TFB1M et TFB2M interagissent avec TFAM et la POLRMT pour initier la transcription de l'ADNmt (121, 122). Selon l'équipe de Matsushima

et al.(123) le TFB1M jouerait essentiellement un rôle dans la régulation de la traduction alors que le TFB2M interviendrait dans la transcription (124). En fait, trois modèles ont été suggérés quant au fonctionnement de TFB1M et TFB2M : TFB1M et TFB2M se lient à l'ARN nouvellement synthétisé pour prévenir la formation d'un hybride ARN-ADN au niveau du promoteur; (ii) TFB1M ou TFB2M interagissent avec l'ADNmt mono brin et stabilisent le complexe de transcription; et (iii) TFB1M ou TFB2M interagit avec des molécules régulatrices de l'ARN pour réguler la transcription de l'ADNmt (125).

1.4.2.2.3 Régulateurs transcriptionnels des gènes nucléaires codant pour des protéines mitochondriales

L'expression des gènes nucléaires codant pour les protéines mitochondriales ainsi que les mécanismes de réplication et de transcription de l'ADNmt sont régulés principalement par des facteurs de transcription et par des coactivateurs transcriptionnels.

1.4.2.2.3.1 Nuclear respiratory factor 2 (Nrf2)

Le Nrf2 est un important facteur de transcription qui protège la mitochondrie du stress oxydant en induisant des gènes anti-oxydants et de detoxification par sa liaison à l'élément de réponse antioxydante (ARE). Le Nrf2 a été identifié dans l'étude de Scarpulla en 2002 (126) comme l'activateur transcriptionnel du gène codant pour la sous-unité IV du cytochrome c oxydase. De plus, le Nrf2 active la transcription des gènes codant pour les protéines mitochondriales : TFAM, TFB1M, TFB2M (127, 128).

1.4.2.2.3.2 Proliferator-activated receptor y (PPARγ) coactivator 1a (PGC1α)

Le PGC1α fait partie des coactivateurs transcriptionnels ayant un rôle majeur dans la biogenèse mitochondriale. Cette protéine travaille de concert avec Nrf2 afin d'induire l'expression de gènes codant pour les protéines de la chaîne respiratoire, et les facteurs de réplication et de transcription mitochondriaux (129). De plus, l'interaction de PGC1α avec PPARγ et ERRα permet la régulation de l'expression des gènes codant pour les protéines impliquées dans l'oxydation mitochondriale des acides gras (130).

1.4.2.3 Dysfonction mitochondriale

Les RLO produits par la mitochondrie peuvent modifier l'ADNmt. Comme ce dernier a moins d'histones protectrices et de mécanismes de réparation des bases altérées que l'ADN nucléaire, il se trouve très vulnérable aux RLO (131). En fait, la base guanine est souvent transformée en 8-oxoguanine qui peut produire des mutations géniques. L'enzyme de réparation OGG1 se fixe sur la base endommagée et excise la partie ciblée. La régulation de l'excision de la 8-oxoguanine par OGG1 peut prévenir l'activation de la voie intrinsèque de l'apoptose ainsi que l'activation des voies de signalisation des protéines RAS qui sont impliquées dans l'inflammation de l'intestin (131-133).

Un dommage de l'ANDmt, lorsque non réparé, peut entraîner une production accrue de RLO, une perte du potentiel membranaire mitochondrial, l'inhibition de la chaîne de transport des électrons et la libération de marqueurs pro-apoptotiques tels que le cytochrome C et le facteur inducteur d'apoptose (AIF) (134-136). Les conséquences de la libération du cytochrome C dans le cytosol favorisent par exemple la formation mitochondriale d'O_2^- par deux voies : (i) le cytochrome C est un scavenger de $O_2^{\cdot -}$ et (ii) lorsque le cytochrome C est relaché, le flux d'électron entre le complexe III et IV de la chaîne respiratoire ralentit et peut même s'arrêter dans certains cas (137, 138).

La mitochondrie joue ainsi un rôle clé dans la régulation de l'apoptose (139). En effet, la phase effectrice de l'apoptose comporte l'ouverture des pores de transition de perméabilité (PTP) des mitochondries et la libération de molécules apoptogènes telles que le cytochrome c, les caspases 2, 3 et 9 ainsi que le facteur AIF. Cette phase s'accompagne d'une diminution du potentiel transmembranaire mitochondrial, suivi du gonflement de la matrice mitochondriale, et d'une interruption du métabolisme énergétique aérobique. Cette phase de libération est sous le contrôle des protéines de la famille Bcl-2 (140). En fait, Bcl-2 forment des hétérodimères avec les membres pro-apoptotiques Bax et Bak (141), contrebalancent leur activité et permettent la stabilité de la mitochondrie en se liant à la membrane externe de la mitochondrie et en prévenant l'ouverture des PTP.

1.4.3 Effets dommageables du stress oxydant sur les cibles biologiques

Les principales cibles radicalaires sont les lipides, les macromolécules et l'ADN.

1.4.3.1 Les lipides

Les lipides sont une cible privilégiée des RLO qui provoquent l'oxydation des acides gras polyinsaturés (AGPI) estérifiés aux phospholipides membranaires, créant ainsi la peroxydation lipidique (Figure 7). L'attaque d'un AGPI par un radical $OH^{\bullet}$ par exemple (le radical peut être également un atome ferreux complexé à une molécule organique, une particule hautement énergétique, etc.) va former un radical lipidique qui subira un réarrangement interne de ses doubles liaisons pour devenir un diène conjugué. Ce réarrangement se définit par le déplacement de la double liaison la plus proche de l'électron célibataire et s'appelle la phase d'initiation de la peroxidation lipidique. En présence d'oxygène, le diène conjugué va se transformer en un radical peroxyde ($LOO^{\bullet}$) qui va déstabiliser un autre AGPI pour former un hydroperoxyde lipidique (LOOH) et un autre radical lipidique : c'est la phase de propagation de la peroxydation lipidique. Les réactions de cette phase prolongent les effets des radicaux libres intramembranaires provoquant une augmentation croissante de la perméabilité membranaire pouvant altérer de façon irréversible les fonctions de la cellule. Les réactions de la peroxydation lipidique se termineront par la formation des hydroperoxydes et de ses dérivés.

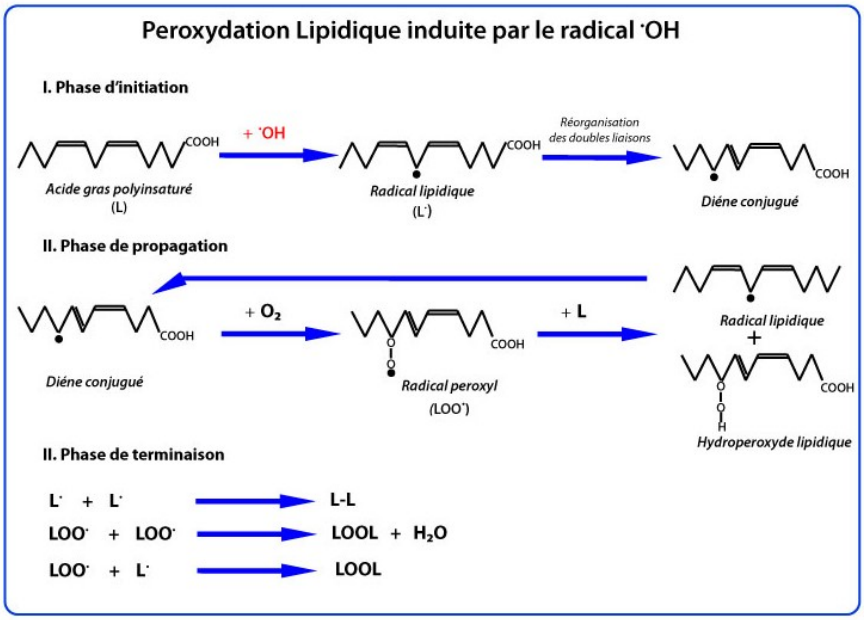

Figure 7 : Peroxydation lipidique
Adaptée de Boots *et al*., 2008 (142)

Toutefois, en présence de fer, ils seront transformés en radicaux alkoxyles. Le malondialdéhyde (MDA) est un des dérivés de la peroxydation lipidique qui a une demi-vie bien plus longue qu'un radical libre. Le MDA réagit avec la désoxyadénosine et la désoxyguanosine pour former des adduits au niveau de l'ADN (Figure 8), notamment le M_1G, qui est mutagène (143).

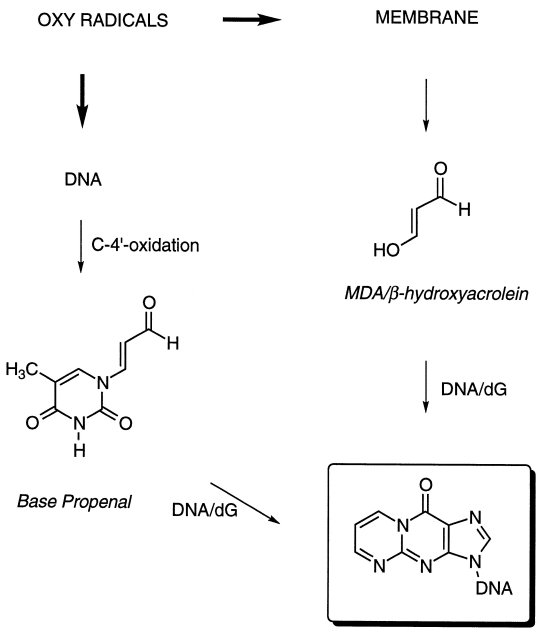

Figure 8 : Réaction du MDA sur l'ADN
Tirée de Marnett *et al*., 1999 (143)

1.4.3.2 Les protéines

Comme pour les lipides, le radical hydroxyle est très réactif et contribue aux altérations des fonctions des protéines telles que l'inactivation enzymatique des sérine-protéases. Les RLO peuvent modifier la conformation tridimensionnelle de la protéine, induire des réticulations inter- et intra-protéines par addition d'un groupement lysine sur le groupement carbonyle d'une protéine oxydée, briser les ponts disulfures de la protéine, et créés de la fragmentation. Le tryptophane, la tyrosine, la phénylalanine, la méthionine et la cystéine sont les acides aminés les plus touchés par les RLO.

1.4.3.3 L'ADN

L'ADN nucléaire et l'ADN mitochondrial sont des cibles des RLO. L'hydroxylation des bases puriques et pyrimidiques et du squelette désoxyribose provoque le clivage des brins et des mutations génétiques (144). Par exemple, l'oxydation de la guanine par le radical hydroxyle forme la 8-hydroxy-guanine (8-OH-G). Ces altérations conduisent à l'arrêt de

l'induction de la transcription ou de la traduction des voies de signalisation, aux erreurs de réplication et à l'instabilité génomique (144).

Les effets délétères des RLO peuvent être contrecarrés par les défenses antioxydantes cellulaires décrites brièvement dans les paragraphes suivants.

1.4.4 Défenses antioxydantes

1.4.4.1 Systèmes de défenses enzymatiques

Les systèmes enzymatiques sont les systèmes de défense cellulaire les plus importants pour contrer les attaques oxydatives. Ils protègent ou détoxifient l'organisme contre les RLO. Les superoxydes dismutases (SOD) et la catalase (CAT) jouent un rôle de protection alors que les glutathion peroxydases (GPx) jouent plutôt un rôle de détoxification des RLO.

La première ligne de défense antioxydante endogène a été découverte en 1969 (145). Il s'agit des enzymes superoxydes dismutases (SOD). Il existe trois SOD : celle localisée dans le cytoplasme fait intervenir le cuivre et le zinc comme co-facteur, nommée Cu^{2+}/Zn^{2+}-SOD (SOD-1), celle localisée dans les mitochondries dont le co-facteur est le manganèse, Mn^{2+}-SOD (SOD-2); et la Cu^{2+}/Zn^{2+}-SOD extracellulaire sécrétée (SOD-3). Les SOD sont des métalloenzymes qui catalysent la dismutation des anions superoxydes en peroxyde d'hydrogène et en oxygène 10 000 fois plus rapidement que la dismutation spontanée de l'anion superoxyde (146). La réduction du H_2O_2 dans le cytosol va dépendre de la Cu^{2+}/Zn^{2+}-SOD et du glutathion peroxydase (GPx) (147). La catalase localisée dans la mitochondrie et les peroxysomes peuvent également réduire le H_2O_2 mais étant donné sa faible affinité pour ce radical, la GPx est plus efficace (148). Par contre, un excès de H_2O_2 et/ou la présence de métaux de transition, Fe^{2+} et le Cu^{2+}, peuvent mener à la formation du radical hydroxyl ($OH^{\cdot}$) et des métabolites réactifs nitrés (149).

Les GPx détoxifient le peroxyde d'hydrogène et les peroxydes lipidiques en couplant leur réduction à l'oxydation d'un substrat réducteur, le glutathion (150). Les GPx sont des enzymes séléno-dépendantes qui contiennent 4 atomes de sélénium dans le centre actif de l'enzyme. Ainsi, un déficit en sélénium entraîne une diminution de l'activité de la GPx alors

qu'une abondance la restaure. Deux formes de GPx se différencient l'une de l'autre de part leur structure et leur activité (151). L'une est intracellulaire et l'autre est extracellulaire ayant des ponts disulfures et de forme glycosylée. La GPx utilise le glutathion réduit (GSH) présent dans le cytosol et les mitochondries comme co-facteur. Le mécanisme de détoxification du peroxyde d'hydrogène par la GPx est représenté dans la figure 9.

Figure 9: Mécanisme de détoxification du peroxyde d'hydrogène par la GPX

La détoxification des hydroperoxydes par la GPx nécessite l'enzyme PLA2. Cette seconde enzyme permet la libération des peroxydes d'acides gras des membranes cellulaires en hydrolysant les liens esters des phospholipides membranaires. Les peroxydes sont transformés par la suite dans le cytosol par la GPx. La figure 10 représente le mécanisme d'action de la GPx dans la detoxification des hydroperoxydes.

Figure 10: Mécanisme de détoxification des hydroperoxydes par la GPx

La CAT se retrouve dans les peroxysomes et les érythrocytes. Son rôle est d'empêcher le peroxyde d'hydrogène de participer à la réaction de Fenton et de le transformer en eau et en oxygène moléculaire (152). L'affinité qu'elle a au peroxyde d'hydrogène reste toutefois bien inférieure à celle du GPx pour prévenir la peroxydation lipidique.

$$2H_2O_2 \Longrightarrow 2H_2O + O_2$$

1.4.4.2 Systèmes antioxydants non-enzymatiques

Les antioxydants non-enzymatiques peuvent être des agents hydrosolubles endogènes (glutathion, acide urique, bilirubine et ubiquinol) ou être fournis par l'alimentation (vitamine C et E, caroténoïdes, polyphénols) (153-155).

Le glutathion est un agent hydrosoluble endogène qui a un pouvoir antioxydant important. Le glutathion prévient l'oxydation des groupements thiols grâce à son pouvoir réducteur. La régénération de la fonction thiol GSH à partir de forme oxydée se fait grâce à l'activité de la glutathion réductase (GR). Il peut chélater les ions cuivreux et limiter ainsi leur participation à la réaction de Fenton. De plus, il est impliqué directement dans la réparation des atteintes oxydatives à l'ADN.

La vitamine C, également appelée acide ascorbique, peut se comporter comme un antioxydant ou un prooxydant dépendamment de la dose employée. Une trop grande dose d'acide ascorbique à l'organisme devient toxique pour celui-ci. L'acide ascorbique peut prendre une forme réduite ou oxydée selon le pH du milieu dans lequel elle est et la présence de métaux de transition. Le passage d'une forme à l'autre est effectué par le glutathion/glutathion réductase et génère un radical ascorbyle. Ainsi, il est considéré comme un couple redox avec un radical ascorbyle capable de capter les RLO et l'oxygène singulet.

1.4.5 Les sources d'agents oxydants dans l'intestin

La muqueuse intestinale est exposée de façon constante à des agents oxydants provenant de l'ingestion d'aliments modifiés (156), de cellules immuno-inflammatoires (157) et de la flore intestinale (158). Ces agents oxydants par la formation de radicaux libres (RL), peuvent présenter un danger ou une première ligne de défense contre les agents pathogènes

(152). En quantité limitée, les RL peuvent entraîner des réponses adaptatives telles que la croissance cellulaire et même l'expression d'enzymes. En situation physiologique normale, un équilibre existe entre la formation de radicaux libres et la neutralisation de ceux-ci par des molécules antioxydantes (159). Cependant, une production excessive de radicaux libres ou une insuffisance de mécanismes antioxydants entraîne un déséquilibre qualifié de stress oxydant tel que vu dans les sections précédentes (160). Un surcroît de stress oxydant peut culminer en une perte d'homéostasie de la barrière intestinale, qui favorise la formation de lésions et l'augmentation de la perméabilité de la paroi intestinale (161, 162).

1.5 La composante majeure de la MII : l'inflammation

Dans les conditions physiologiques, une inflammation basale existe dans l'intestin. Les leucocytes présents dans les tissus intestinaux induisent une inflammation contrôlée faisant face à une variété d'antigènes alimentaires et bactériens permettant de maintenir l'homéostasie intestinale (163).

Toutefois, l'inflammation peut résulter des effets d'agents infectieux tels que les bactéries, les champignons ou même les virus. Elle peut aussi résulter de l'exposition à des produits chimiques, d'une brûlure, d'un traumatisme ou bien d'autres facteurs. La cause de la MII est inconnue, mais les recherches indiquent fortement que des interactions entre les facteurs environnementaux, les bactéries intestinales, un dérèglement immunitaire et une prédisposition génétique en sont responsables. De plus, le risque est accru pour ceux dont un membre de la famille souffre de la maladie.

1.5.1 Origine de l'inflammation intestinale

Avec un système immunitaire inapproprié et bien souvent une prédisposition génétique, trois catégories de facteurs (environnementaux, microbiens et cellulaires) pourraient occasionner de l'inflammation :

Dans la catégorie des facteurs environnementaux, l'hypothèse « hygiéniste » de Bach *et al*. (164) revient très souvent dans la littérature. Cette hypothèse affirme que le changement de modes de vie des populations, dû à l'évolution socio-économique, a réduit l'exposition

microbienne pouvant conduire au développement d'un système immunitaire moins adapté pour contrer certains antigènes et infections intestinales (165, 166). D'autres facteurs tels que le tabagisme (68), le régime alimentaire (167), le statut social (168) et même le stress (169) pourraient en combinaison avec une prédisposition génétique déclencher une MII.

Quand aux facteurs microbiens, les études scientifiques des dernières années ont de plus en plus écarté la théorie microbienne dans l'étiologie du développement de MII. Toutefois, quelques souches bactériennes ont été identifiées dans les MII. C'est le cas de *Listeria monocytogenes*, d'*Escherichia coli* ou encore de *Mycobacterium paratuberculosis* (170). La *Listeria monocytogenes* a été retrouvée dans les tissus intestinaux des individus atteints de MC à 75% (13% pour ceux avec une CU). *Le Mycobacterium paratuberculosis* est impliquée dans l'entérocolite granulomateuse des ruminants (similitudes histologiques et cliniques avec la MC) et a été identifié dans les tissus réséqués des individus atteints de MC (171, 172). Même si l'origine microbienne des MII n'est pas certaine, le lien avec la flore commensale, cible de la réponse immunitaire, est bien établi (173). Toutefois, une stabilité de la diversité des phylas bactériens semble s'installer depuis quelques années chez les individus et les animaux reflétant une homéostasie des rapports entre l'hôte et le microbiome intestinal (174). Les *Bacteroides* et les *Firmicutes* représentent à eux seuls plus de 90% de la totalité du microbiote intestinal chez tous les individus. Le 10% restant du microbiote intestinal est composé de *Proteobacteria*, *Actinobacteria*, *Fusobacteria*, et *Verrucomicrobia* (175). Des altérations de cette diversité d'espèces semblent devenir une valeur prédictive du développement de certaines pathologies telles que les MII.

L'implication des facteurs cellulaires est majeure dans le développement d'une MII. Dès qu'il y a une réponse immunitaire inappropriée et persistante des anomalies anatomiques et fonctionnelles apparaissent dans l'intestin. Des cellules immunitaires telles que les polynucléaires neutrophiles (PNN), les macrophages et les lymphocytes T sont activées et libèrent de nombreux marqueurs inflammatoires; tels que des RLO, des protéines cytotoxiques, des enzymes lytiques et des cytokines conduisant à la destruction des entérocytes et à une inflammation pathologique du tissu intestinal (176). De plus, les cellules dendritiques et les macrophages sécrètent également des cytokines qui déclenchent une réponse immunitaire adaptative via l'activation des lymphocytes T (177, 178).

1.5.2 Modèles inflammatoires de l'intestin

1.5.2.1 Induction de l'inflammation *in vitro* par les lipopolysaccharides (LPS)

La LPS est un complexe macromoléculaire qui compose la membrane externe des bactéries à gram-négatif. Elle est constituée de deux parties : une partie lipidique, lipide A, et une partie polysaccharide. La structure hydrophobique du lipide A permet l'ancrage de la LPS à la membrane cellulaire alors que la partie polysaccharide déborde la membrane externe. La propriété inflammatoire de la LPS est due au lipide A qui est libéré après la lyse de la bactérie. C'est une endotoxine qui induit une réaction inflammatoire pouvant aller jusqu'à la septicémie chez l'homme (179).

La reconnaissance de la LPS par la protéine LBP (LPS binding protein) va permettre le transfert de la LPS vers le récepteur membranaire CD14. Le complexe LPS/CD14 est reconnu par le récepteur TLR4 (toll-like receptor 4) qui est associé à la protéine MD-2 (myeloid differentiation protein-2). Une fois que le complexe TLR4/MD-2 interagit avec celui du LPS/CD14, le facteur de transcription NFκB (Nuclear Facteur kappa-B) est activé entraînant à son tour la sécrétion de cytokines pro-inflammatoires, telles que le TNFα (tumor necrosis factor), l'IL-1 (interleukine-1), le MCP-1 (Monocyte chimioattractant protein-1) et iNOS (inducible nitric oxide synthase) provoquant une réaction inflammatoire.

1.5.2.2 L'inflammation colique induite par l'administration de sulfate de sodium dextran (DSS)

Le DSS est un polysaccharide sulfaté composé de dextran et d'unités d'anhydroglucose (180). Le modèle murin d'inflammation intestinale par le DSS a été découvert en 1990 par l'équipe d'Okayasu *et al*. (181). Le DSS est reconnu comme agent d'inflammation intestinale lorsqu'il est administré dans l'eau de boisson des animaux, il provoque une colite similaire à celle retrouvée chez l'homme.

Comme pour les MII, la pathogénèse exacte de la colite induite par le DSS reste encore inconnue (182, 183). L'importance des groupements sulfatés a déjà été démontrée dans l'initiation des mécanismes d'inflammation (184). L'action toxique du DSS sur les entérocytes induirait une destruction des structures épithéliales de la muqueuse intestinale autant au niveau

in vivo (185) qu'*in vitro* sur les Caco-2 (186). Ainsi, lorsque la muqueuse est altérée les macrophages colonisent le tissu et développent l'inflammation avec les lymphocytes T.

Le degré d'inflammation de la colite induite par le DSS dépend du poids moléculaire de celui-ci, de la dose et de la durée de l'administration (181, 187-190). L'étude de Kitajima *et al*. en 2000 (191) a démontré que l'analyse histologique des côlon de souris Balb/c ayant reçu 5% de DSS à différents poids moléculaire (5, 40 et 500kDa) pendant 7 jours était différente à chacun des poids moléculaire du DSS. Le DSS de 500 kDa n'a pas eu d'effet délétère sur la muqueuse du côlon. Par contre, le DSS à 5 et à 40kDa a créé de l'inflammation intestinale caractérisée par l'érosion et l'ulcération de l'épithélium, la perte de cryptes, l'infiltration de la muqueuse et de la sous-muqueuse par des cellules inflammatoires et de l'oedème de la sous-muqueuse. L'utilisation du DSS à 5kDa a permis d'inflammer la région du caecum et du côlon proximal alors que celle du DSS à 40 kDa a inflammé de manière plus sévère l'intestin particulièrement dans la partie distale du côlon dans le modèle murin. Une seconde étude sur les souris Balb/c ayant reçu des concentrations de DSS de 2.5, 5 ou 7.5% a dévoilé que la sévérité de la colite est corrélée à la concentration du DSS et non de la quantité consommée. L'équipe de Vowinkel *et al*.(192) a confirmé les résultats de l'étude précédente chez des souris C57BL6/J recevant 3 et 5% de DSS. De plus, cette étude a montré que l'accentuation de l'inflammation colique était directement liée à l'exposition de la muqueuse à la concentration de DSS. Les souris ayant reçues 30 mg ou plus de DSS/g de poids de souris avaient une activité bien plus élevée du marqueur inflammatoire « myéloperoxydase » que les souris avec des concentrations inférieures. Par conséquent, la concentration de DSS ajustée au poids des animaux permet d'obtenir une inflammation plus soutenue au niveau de la muqueuse intestinale. La propagation de l'inflammation dépend également de la durée d'exposition de la muqueuse intestinale au DSS. Trois jours après l'apparition des signes cliniques (atteintes macroscopiques décrites au point suivant), l'étude des coupes histologiques du côlon a démontré les premières atteintes morphologiques de l'épithélium. L'infiltration de la muqueuse par les cellules inflammatoires a été aperçue après le quatrième jour du début des signes cliniques (189).

1.5.2.2.1 Les atteintes macroscopiques

Les signes cliniques ou les atteintes macroscopiques ont permis de contrôler et de mesurer le développement et la progression de l'inflammation intestinale. Les atteintes macroscopiques sont caractérisées principalement par l'évaluation des paramètres concernant le poids de l'animal, la consistance des fécès, la présence de sang dans les selles et la longueur du côlon. L'évaluation de ces trois premiers paramètres a permis d'établir un score de maladie « disease activity index (DAI) » que l'expérimentateur pouvait utiliser pour évaluer l'intensité de l'inflammation (189). La présence de sang dans les selles et au pourtour de l'anus ainsi que la diminution de la longueur du côlon sont des atteintes macroscopiques caractéristiques de l'induction de l'inflammation intestinale par le DSS (185, 189, 193).

1.5.2.2.2 Les atteintes microscopiques

L'analyse histologique de l'inflammation intestinale est effectuée au microscope optique après coloration des coupes tissulaires habituellement par un pathologiste. Les atteintes histologiques observées par l'induction de l'inflammation par le DSS affecteront principalement le côlon distal. Ces atteintes ont révélé une érosion et un amincissement de l'épithélium associés à la dilation des cryptes. La muqueuse est infiltrée par les cellules immunitaires telles que les polynucléaires neutrophiles, et peut présenter de l'œdème. L'illustration d'une perte de cellules calciformes, de la présence focale d'abcès ou de congestion vasculaire peut également être observée au microscope (194).

Chacun des paramètres permettant l'évaluation des atteintes macroscopiques et histologiques est mesuré généralement par un système de score allant de 0 à 3 (195).

1.5.2.2.3 Les marqueurs de l'inflammation intestinale

1.5.2.2.3.1 Myéloperoxidase

La myéloperoxidase (MPO) est une peroxydase hémique présente en concentrations importantes (2 à 5 %) dans les granules primaires des cellules polymorphonucléaires neutrophiles (196-198). On la trouve également dans les monocytes en concentration plus

faible, mais la présence de l'enzyme devient indétectable lors de la maturation en macrophages (199). Cet enzyme est un homodimère symétrique, formé de 2 hémi-enzymes, chacune à 2 sous-unités (une chaîne légère de 15 kDA et une chaîne lourde de 59 à 64 kDa) reliées par un pont disulfure (200). Elle est habituellement glycosylée, ce qui explique les variations de son poids moléculaire allant de 120 à 150 kDa.

La MPO possède une activité de peroxydase et de chloration. Elle utilise le peroxyde d'hydrogène (H_2O_2) et catalyse l'oxydation à 2 électrons des ions Cl^- pour former l'acide hypochloreux (HOCl). Son fonctionnement est régulé par différents paramètres : le pH, la production d'$O_2^{\bullet}$ conduisant à la formation d'H_2O_2, la concentration en Cl^- (100 mM dans le plasma), les concentrations en réducteurs (ascorbate, méthionine, etc.), mais aussi le monoxyde d'azote ($NO^{\bullet}$) (201). L'activité de la MPO est proportionnelle aux nombres de neutrophiles présents dans la muqueuse intestinale. Ainsi, une concentration élevée en MPO est signe d'une activation des PNN. Les équipes de recherche l'utilisent régulièrement comme marqueur de l'inflammation intestinale (202).

1.5.2.2.3.2 Les cytokines

Les cytokines pro-inflammatoires, secrétées par les cellules immunitaires, présentent dans le côlon sont principalement de type Th1 (Type 1 T helper). L'élévation de la production de l'IL-1, IL-6 et TNFα est caractéristique de l'inflammation intestinale. Ces mêmes cytokines régulent également la production des RLO, du monoxyde d'azote et des prostaglandines.

Le TNFα est sécrété par les lymphocytes et les cellules présentatrices d'antigène. L'induction de la production de l'IL-1β et IL-6 est effectuée par les TNFα. Une augmentation du TNFα a révélé la présence d'inflammation. La mesure du TNFα est par conséquent utilisée comme marqueur d'inflammation intestinale autant dans les modèles *in vitro* qu'*in vivo*. La production d'anticorps anti-TNF a permis de fabriquer une classe de médicament qui permet de contrôler la MII chez certains individus.

Les macrophages dans la réaction inflammatoire de l'intestin produisent également de l'IL-6. La liaison entre IL-6 et son récepteur permet d'activer le facteur de transcription STAT3 qui est impliqué dans le développement des réactions immunitaires pendant

l'inflammation (176, 203). Un blocage de cette voie de signalisation a permis d'induire l'apoptose des lymphocytes T chez les individus atteints de MC (204).

1.5.2.2.3.3 La cyclooxygénase

La cyclooxygénase (COX) est l'enzyme clé dans la synthèse des prostaglandines, des prostacyclines et des thromboxanes à partir de l'acide arachidonique (205). En fait, la COX convertit l'acide arachidonique hydrolysé par les phospholipases à partir des phospholipides membranaires en prostaglandine H2, le précurseur commun de tous les prostanoïdes (206). En période d'inflammation, la COX-2 va être induite par la présences de cytokines pro-inflammatoires (207). Une augmentation de l'expression de COX-2 induira une augmentation de la production du taux de prostanglandine E2 (PGE2) (208, 209). Les prostanoïdes tels que PGE2 sont impliqués dans de nombreux mécanismes pathophysiologiques comme la réaction inflammatoire, les ulcères de l'estomac, l'angiogenèse et la carcinogenèse (210).

Lors des périodes actives d'inflammation intestinale chez les individus atteints de MII, COX-2 est retrouvée à la surface des cellules épithéliales ainsi que dans les cellules immunitaires de la *lamina propria* (211, 212).

1.5.2.2.3.4 Facteur de transcription NF-κB

Les protéines NF-κB sont exprimées de façon ubiquitaire et se lient particulièrement au promoteur du gène codant pour la chaîne légère kappa dans les cellules B. Les dimères de NF-κB sont séquestrés dans le cytosol de la cellule par des protéines inhibitrices IκB. L'activation de la voie NF-κB par un stress oxydatif et/ou l'inflammation stimule la phosphorylation du complexe IκB kinase-kinases (IKK) qui est un trimère associant la sous-unité régulatrice NEMO et des deux sous-unités catalytiques IKKa et IKKb. IKK activé induit la phosphorylation de IκB puis son ubiquitinylatin et sa dégradation par le protéasome. La dégradation de IκB permet alors la translocation de NF-κB vers le noyau et de réguler l'expression de nombreux gènes codant pour des cytokines et chemokines (IL-1β, TNFα, IL-2, IL-6, IL-8, IL-12), récepteurs à la surface de la cellule (IL2R, CD40), molécules d'adhésion (ICAM-1, VCAM-1, E-sélectine), protéines immuno-régulatrices (molécules MHC I et MHC

II), protéines réponses de phase aiguë (β-defensines, TLR4) et les enzymes inflammatoires (induction du iNOS, COX-2 et PLA_2) (213).

Des études ont démontré que chez des individus atteints de MII, l'expression de NF-κB et des cytokines pro-inflammatoires (IL-1β, TNFα et IL-6) est augmentée dans leurs cellules épithéliales et macrophages (35, 214, 215).

1.6 Les polyphénols

L'intérêt de trouver une molécule à la fois anti-inflammatoire et antioxydante agissant au niveau intestinal, et bien entendu ne causant pas d'effets secondaires supplémentaires à ceux provenant de la médication, est devenu primordial dans le traitement préventif/thérapeutique des MII. Les recherches des dernières années en nutraceutique ont permis d'identifier les polyphénols contenus dans les fruits et les légumes. Ces molécules détiennent un potentiel antioxydant et anti-inflammatoire prometteur de par leur structure chimique. Cette présente section illustre principalement les caractéristiques, la classification, la biosynthèse ainsi que les mécanismes de biodisponibilité des polyphénols dans l'intestin.

1.6.1 Consommation journalière

L'estimation de la consommation journalière moyenne en polyphénols chez un individu est difficile à déterminer étant donné la diversité structurale, la distribution et l'abondance des polyphénols dans un fruit ou un légume. Par exemple, la concentration en polyphénols totaux peut varier de 140 mg/kg de poids frais pour la pomme de terre à 5.5 g/kg de poids frais pour la cerise (216). Des tables de composition affichant la concentration en polyphénols pour un aliment donné peuvent transmettre une estimation de l'apport quotidien en polyphénols. La table Phenol-Explorer (www.phenolexplorer.com), développée par l'INRA avec l'industrie et les partenaires académiques, recense les polyphénols dans l'alimentation de manière beaucoup plus large que ce qui était disponible auparavant par « United States Department of Agriculture » (http://www.ars.usda.gov/Services/docs.htm?docid=6231) et rassemble des caractéristiques portant sur 502 polyphénols dans 452 aliments (217-219). Cette table est en constante mise à jour grâce à l'identification de nouvelles structures de

polyphénols par des scientifiques oeuvrant avec des instruments analytiques performants tels que les spectromètres de masse. Les travaux scientifiques de Kühnau *et al*. (220) ont estimé la consommation en polyphénols aux USA à 1 g/j comprenant 460 mg de proanthocyanidines, 200 mg de catéchines, 180 à 215 mg d'anthocyanes et 115 mg de flavones et de flavonols sans tenir compte des acides phénoliques, des lignanes ou des stilbènes. La comparaison de la consommation de la vitamine C (90 mg/j), des caroténoïdes (5 mg/j) et de la vitamine E (12 mg/j) à celle des polyphénols (1g/j) révèle que cette dernière est bien supérieure aux autres (216).

Si on assume qu'un individu ayant une diète occidentale consomme environ 1g de polyphénols par jour et que le volume de l'intestin est d'environ 6.25 litres, les entérocytes sont alors exposés à une concentration de 235 μg/mL de polyphénols par jour.

1.6.2 Consommation de la pomme et de la canneberge

Au Canada, la culture de la pomme se situe au premier rang des cultures fruitières en 2009 avec un volume de production de 432 306 tonnes métriques. La production des pommes représentait 55% des cultures fruitières totales. Au second rang, on y retrouvait le bleuet avec 13% du total de la production des cultures fruitières. La canneberge se situait au troisième rang (11% du total des fruits cultivés) de la production des cultures fruitières au Canada en 2009 (Statistics Canada. Agriculture and Agri-Food Canada Fall Survey, 2009).

Le Ministère de l'Agriculture, des Pêcheries et de l'Alimentation du Québec (MAPAQ) a déposé, en 2011, une monographie concernant l'industrie de la pomme. Ce rapport démontre que la consommation de fruits frais et transformés au Canada est de 136,29 kg/personne pour l'année 2008. En fait, la consommation de la pomme a été évaluée à 10,58 kg/personne/année, ce qui représente 14.4% des fruits frais consommés par les Canadiens lors de cette même année, lui conférant la seconde place des fruits frais consommés en grande quantité. Au premier rang en 2008, on retrouvait la banane avec 19.5% des fruits frais consommés par Canadien.

Le Canada est le deuxième plus grand producteur de canneberges après les États-Unis. En 2008, la quantité de canneberges dans le régime alimentaire canadien s'élevait à 1,12

kilogramme par personne par année, ce qui équivaut à 35 % de plus qu'en 2007 (Statistics Canada. Agriculture and Agri-Food Canada Fall Survey, 2009).

1.6.3 Caractéristiques, classification et biosynthèse des polyphénols

Les fruits et les légumes consommés fournissent plus de 8000 polyphénols classés en différentes familles selon la nature de leur squelette carboné (220). Tel que le montre le Tableau 1, les polyphénols se déclinent en 4 grandes familles : les acides phénoliques (C_6-C_1 et C_6-C_3), les flavonoïdes (C_6-C_3-C_6), les stilbènes (C_6-C_2-C_6) et les lignanes (C_6-C_3-C_3-C_6).

Tableau 1: Structures du squelette carboné des classes majeures de polyphénols

Squelette	Classes	Structure générale
C_6-C_1	Acides phénoliques	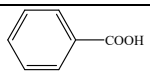
C_6-C_3		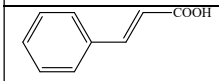
C_6-C_3-C_6	Flavonoïdes	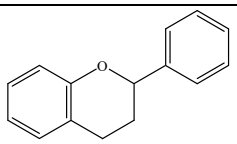
C_6-C_2-C_6	Stilbènes	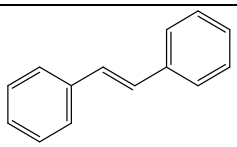
C_6-C_3-C_3-C_6	Lignanes	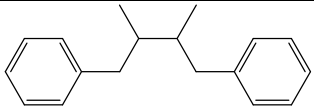

Le nombre de carbone est représenté par la nomenclature « C_n ».

C_6 : cycle aromatique de 6 carbones et C_3 : chaîne carbonée composée de 3 atomes de carbone.

Les flavonoïdes sont les polyphénols les plus abondants dans notre alimentation et plus de 4000 polyphénols ont pu être identifiés (221). Les flavonoïdes présentent une structure

commune en C_6-C_3-C_6 (Figure 11). Deux cycles aromatiques (A et B) sont liés par une chaîne de 3 carbones formant un hétérocycle oxygéné (C) (222).

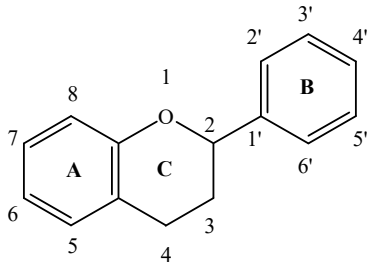

Figure 11 : Structure chimique commune des flavonoïdes
Adaptée de Crozier *et al*., 2009 (223)

La biosynthèse des flavonoïdes se fait à partir du malonyl CoA et des dérivés CoA de l'acide cinnamique, soit le cinnamoyl CoA (224). Deux voies complémentaires, la voie « acétate-malonate » et la voie shikimate (Figure 12), sont essentielles à la formation du squelette carboné des flavonoïdes (225). La voie shikimate engendre la synthèse de l'acide cinnamique et conséquemment celle du cycle aromatique B et de la chaîne de 3 carbones qui formera le cycle oxygéné C de la structure commune des flavonoïdes. Les précurseurs de cette voie sont l'érythrose 4-phosphate de la voie des pentoses et le phosphoénolpyruvate (P-énolpyruvate) résultant de la glycolyse (226). La voie acétate malonate constitue la voie de synthèse du cycle aromatique A. Ce cycle aromatique est formé par condensation répétée d'unités d'acétate (227). Ces deux voies sont par la suite condensées pour former la structure commune du flavonoïde.

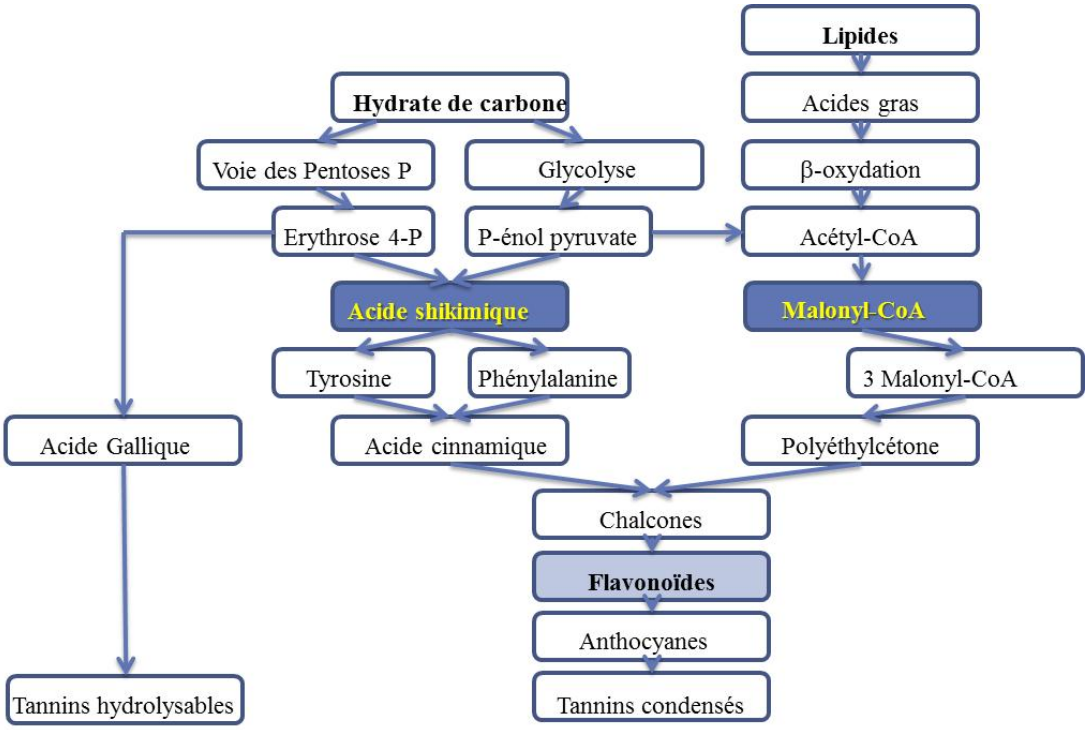

Figure 12 : Voies de biosynthèse des flavonoïdes
Adaptée de Casanal *et al*., 2013 (228)

1.6.3.1 Flavonoïdes

Les flavonoïdes sont subdivisés en sous-classes selon la structure de l'hétérocycle C. On distingue alors les 4-oxoflavonoïdes (flavones, isoflavones, flavonols et flavanones), les flavan-3-ols et les procyanidines, les anthocyanes ainsi que les composés chalcones et dihydrochalcones (223). Il existe dans chaque sous-classe de nombreux composés selon les substitutions des cycles aromatiques par divers groupements fonctionnels (groupements hydroxyles, méthylés ou glycosylés). La plupart des flavonoïdes sont glycosylés mais on retrouve également leur forme native que l'on appelle également « aglycone » (223, 229).

1.6.3.1.1 4-oxoflavonoïdes

Les flavones, les isoflavones, les flavonols et les flavanones constituent les groupes polyphénoliques principaux de la sous-classe des 4-oxo-flavonoïdes (Figure 13).

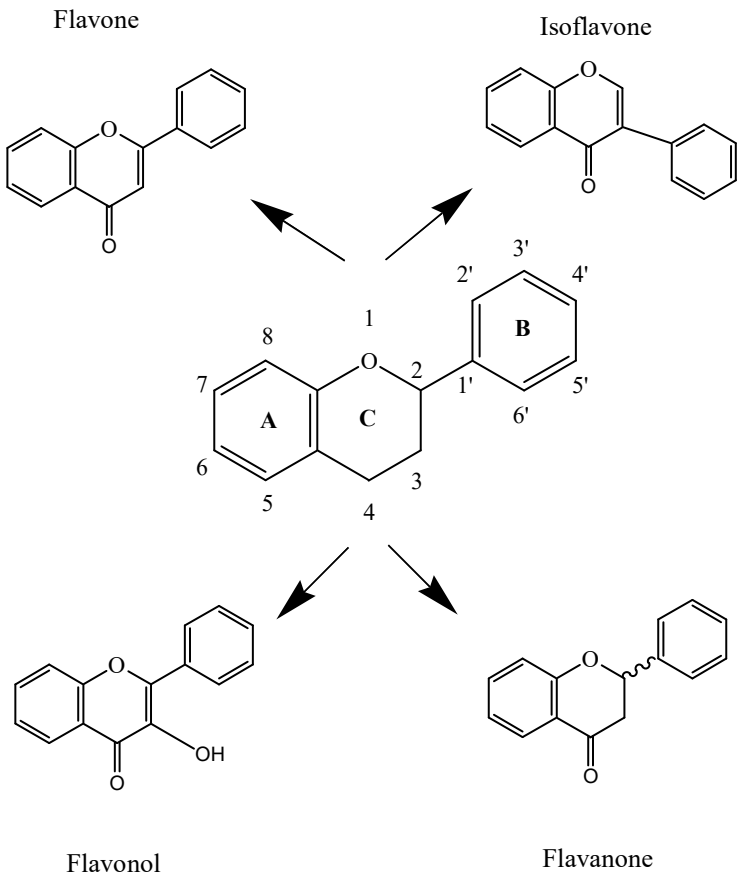

Figure 13: Structures chimiques de la sous-classe des 4-oxoflavonoïdes

1.6.3.1.1.1 Flavones

Les flavones sont principalement présentes dans les céréales, les herbes (par exemple : persil, origan), le céleri, la laitue, les bettraves, les piments et les pommes (230). Les flavones possèdent une double liaison en position 2-3 du cycle hétérogené oxygéné C et le cycle aromatique B est fixé en position 2 (Figure 14). Plusieurs substitutions sont possibles sur les flavones, telles que l'hydroxylation, la méthylation, la O- et C-glycosylation, et l'alkylation. De manière générale, les flavones sont présentes sous la forme de 7-O-glycosides. Moins répandues dans les fruits et légumes que les flavonols, les flavones sont principalement présentes sous forme de glycosides de lutéoline et d'apigénine (231) .

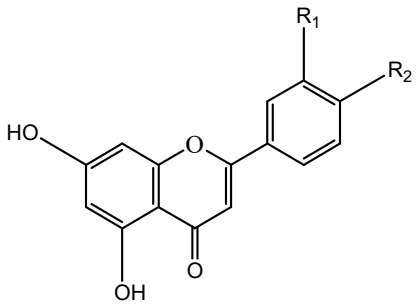

Flavones	R_1	R_2
Apigénine	H	OH
Lutéoline	OH	OH

Figure 14 : Structures chimiques des flavones

1.6.3.1.1.2 Isoflavones

La structure chimique des isoflavones est différente des flavones, le cycle B des isoflavones est lié au carbone 3 au lieu du carbone 2 (Figure 15). Sa structure est donc similaire à celle des phytoestrogènes, classée comme un non-flavonoïde lignane. Les isoflavones se retrouvent particulièrement dans les légumineuses et les grains de céréale. Le soja est riche en daidzéine et génistéine comme 7-O-(6''-O-malonyl) glucosides avec une faible quantité de 7-O-(6''-O-acetyl) glucosides, 7-O-glucosides, et l'aglycone. Le lait de soja et le tofu peuvent se présenter sous la forme d'aglycone (232).

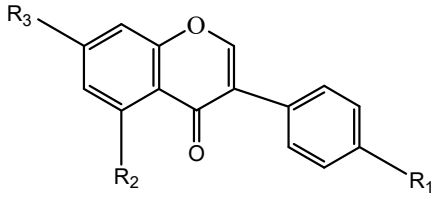

Isoflavones	R_1	R_2	R3
Daidzein	OH	H	OH
Genistein	OH	OH	OH

Figure 15 : Structures chimiques des isoflavones

1.6.3.1.1.3 Flavonols

Les flavonols sont caractérisés par la présence d'une double liaison en position 2-3 et d'un groupement hydroxyle à l'hétérocycle oxygéné (Figure 16). Dans plus de 90% des cas, le

noyau A des flavonols est substitué par deux hydroxyles phénoliques en carbone 5 et en carbone 7. D'autre substitutions peuvent être possibles: les groupements hydroxyles peuvent être libres ou méthylés, ou même impliqués dans une liaison glycosidique. Le noyau B est monosubstitué dans 80% des cas en position 4', ou disubstitué en positions 3' et 4', ou trisubstitué (moins fréquemment) en positions 3', 4' et 5'. Ces substitutions peuvent être des groupes OH ou OMe. Les positions 2' et 6' ne sont qu'exceptionnellement substituées. Le noyau C peut être substitué par un groupement OH, OMe ou O-Gly. Les principaux flavonols identifiés sont le kaempférol, la quercétine, l'isorhamnétine et la myricétine. Ils sont le plus souvent présents sous forme de glycosides, avec une molécule de glucose ou de rhamnose mais le galactose, l'arabinose, le xylose et l'acide glucuronique peuvent être présents. Leur conjugaison se fait le plus fréquemment en position 5, 7, 4', 3' et 5' et il existe plus de 200 conjugués O-glycosylés différents pour le kaempférol (233). La biosynthèse des flavonols étant stimulée par la lumière, on les retrouve principalement dans les parties extérieures et aériennes des végétaux, soit l'épiderme et les feuilles. Donc, au sein d'un même fruit, il existe des différences de concentration de flavonols selon le degré d'exposition à la lumière du soleil (234, 235). Les onions jaune et rouge sont des sources alimentaires à concentration élevée de quercetine-4'-O-glucoside et quercetine-3,4'-O-diglucoside (1.2g/kg de poids frais). Dans la myrtille et le bleuet, le flavonol ayant la plus grande concentration est la quercétine, soient 158 mg/kg et 17-30 mg/kg respectivement. La mûre contient principalement de la myricétine (89-203 mg/kg) suivi par de la quercétine (70-122 mg/kg) et du kaempférol (9-23 mg/kg). Dans les baies, les flavonols glycosides suivants ont été identifiés : la quercétine-3-O-glucoside, la quercétine-3-O-rutinoside, la quercétine-3-O-galactoside et la quercétine-3-O-xylosylglucuronide, myricétine-3-O-glucoside, myricétine-3-O-galactoside et myricétine-3-O-rutinoside.

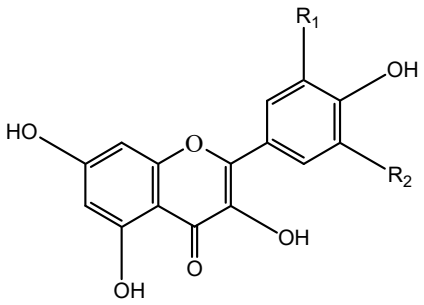

Flavonols	R_1	R_2
Kaempferol	H	H
Quercétine	OH	H
Myricétine	OH	OH
Isorhamétine	OCH3	H

Figure 16 : Structures chimiques des flavonols

1.6.3.1.1.4 Flavanones

Les flavanones se caractérisent par la saturation de l'hétérocycle C, l'absence des doubles liens $\Delta^{2,3}$ et la présence d'un centre chiral en carbone 2 (Figure17). Cette classe de flavonoïdes est caractéristique des agrumes. Le plus souvent glycosylée par un disaccharide en carbone 7, on distingue deux sous-familles: les rutinosides et les néohespéridosides. Ces sous-familles de flavonones ont comme caractéristiques organoleptiques d'être insipides et amers (233). La hespérétine-7-O-rutinoside est considérée comme étant le flavonone rutinoside le plus connu; on la retrouve dans les citrons, les mandarines et les oranges. La présence de la hespéridine-7-O-néohespéridoside dans les oranges et la naringinine-7-O-néohespéridoside dans le citron est celle des flavonones néohespéridosides. Il est toutefois possible de distinguer également des dérivés d'hydroxylation et de O-méthylation dans cette classe de flavonoïde.

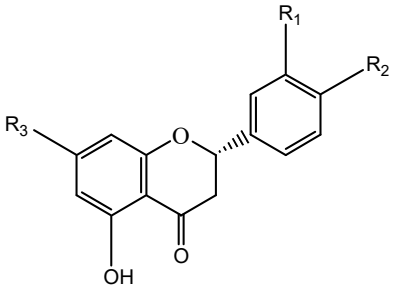

Flavanones	R_1	R_2	R_3
Hesperetin	OH	OCH_3	OH
Naringenin	H	OH	OH
Hesperetin-7-O-rutinoside	OH	OCH_3	$C_{11}H_{18}O_{10}$
Naringinine-7-O-neohesperidoside	H	OH	$C_{11}H_{18}O_{10}$

Figure 17 : Structures chimiques des flavanones

1.6.3.1.1.5 Flavan-3-ols et tanins condensés

Les flavan-3-ols sont les seuls flavonoïdes qui n'existent pas naturellement sous forme de glycosides. Ils existent sous forme de monomères également appelés catéchines ainsi que sous forme d'oligomères et de polymères, les tanins condensés. Les flavan-3-ols présentent un hétérocycle C saturé auquel s'ajoute une fonction hydroxyle en carbone 3 (Figure 18). La présence de deux centres chiraux en carbone 2 et 3 donne 4 isomères potentiels pour chaque niveau d'hydroxylation du cycle B. Dans les baies, les monomères principaux sont la (+)-catéchine et son isomère l'(-)-épicatéchine (236, 237). Ces monomères peuvent être hydroxylés en carbone 4' et former la (+)-gallocatéchine et l'(-)-épigallocatéchine.

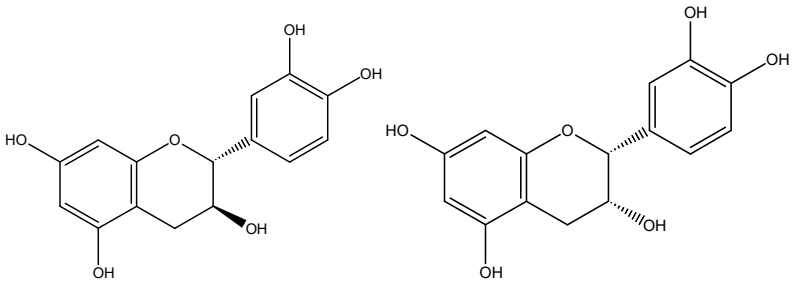

Figure 18 : Structures chimiques de (+)-catéchine et (-)-épicatéchine

Les tanins condensés, communément appelés les proanthocyanidines, sont liés entre eux par des liaisons carbone-carbone difficilement hydrolysables. Les proanthocyanidines sont des oligomères et des polymères de la (+)-catéchine et (-)-épicathéchine qui sont formés par des liaisons entre le carbone 4 et 8 ou le carbone 6, on leur donne le nom de liaisons structures de type B (proanthocyanidine type-B). Les liaisons formées entre le carbone 2 et oxygène 5 ou carbone 2 et l'oxygene 7 sont appelées liaisons structurales de type A (proanthocyanidine type-A) (Figure 19). Les proanthocyanidines comportant uniquement des unités successives d'épicathéchine sont nommées procyanidines. Les polymères de proanthocyanidines peuvent aller jusqu'à 50 unités de flavan-3-ol. Les bleuets (238) ainsi que les canneberges (239, 240) contiennent une quantité élevée de proanthocyanidines.

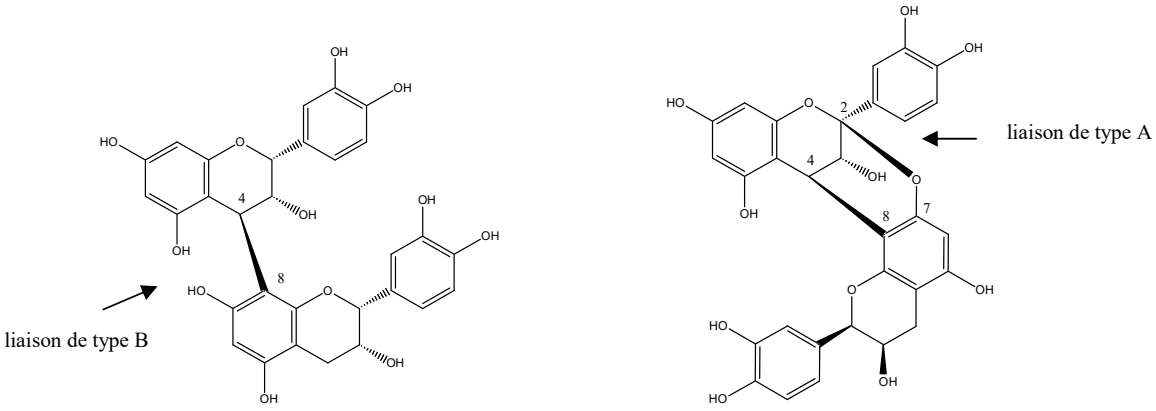

Figure 19: Structures chimiques des proanthocyanidines dimérique type-B2 et type-A2

Les proanthocyanidines (Figure 20) contenant des unités de (epi)afzelechin ou (epi)gallocatechin sont des propelargonidines et prodelphinidines, respectivement.

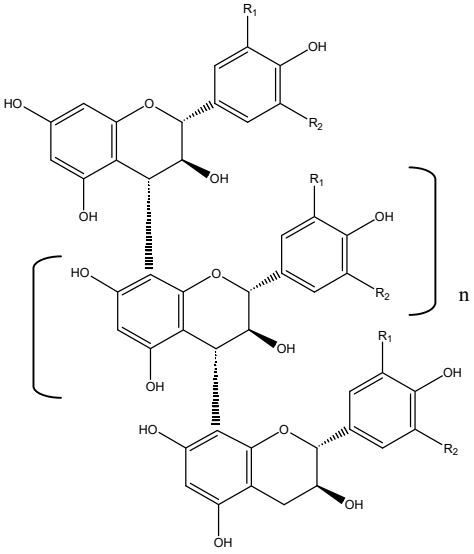

Proanthocyanidine	R_1	R_2
Propelargonidine	H	H
Procyanidine	OH	H
Prodelphinidine	OH	OH

Figure 20 : Structures chimiques des proanthocyanidines

1.6.3.1.1.6 Anthocyanes

Parmi les nombreux composés polyphénoliques présents dans les petits fruits, les anthocyanes sont probablement les plus connus (241). En 2006, 539 anthocyanes étaient recensés. Elles se forment à partir d'anthocyanidines telles que la cyanidine, la delphinidine, la pélargonidine, la péonidine, la pétunidine et la malvidine (Figure 21). Le squelette flavylium est commun à tous ces composés et il est responsable des pigments qui donnent la

couleur rouge, bleue, mauve, violette ou rouge-mauve aux fruits et légumes (242). Les anthocyanes sont très rarement présentes sous la forme aglycone car le squelette flavylium, qui est responsable de la couleur, est aussi un noyau très réactif aux nucléophiles qui confère une instabilité à ces composés. Les anthocyanes existent naturellement sous forme glycosides comme les flavonols. La diversification des anthocyanes est produite par le nombre et la position des différents groupements hydroxyles et méthoxyles, la nature, le nombre et la position des sucres et l'acylation éventuelle de ces sucres (223). Les glycosides les plus connus dans les petits fruits sont formés par l'ajout de glucose, de galactose, de rhamnose, d'arabinose, de xylose et de sophorose. Ils se présentent sous la forme de 3-glycosides ou 3,4-diglycosides. Les agents alkylants pouvant être des acides phénoliques tels que l'acide caféique, p-coumarique, férulique et sinapique. La groseille et la baie de surreau contiennent seulement des anthocyanes provenant de la cyanidine (236, 242-244). Le cassis est caractérisé par la présence de delphinidines et de cyanidines rutinosides et glucosides; les delphinidines et cyanidines rutinoside sont les plus abondantes (242-244). La groseille et les cassis contiennent majoritairement de la cyanidine diglycoside et de la cyanidine monoglycoside en faible quantité (236, 242, 243). La partie osidique des anthocyanes peut être un monosaccharide (glucose, galactose, rhamnose), un diholoside (rutinose constitué d'un glucose lié à un rhamnose, xyloglucose) ou parfois un triholoside. La plupart des anthocyanes sont des 3-monosides et des 3, 5-diosides d'anthocyanidines (245). Il existe aussi des diosides liés en position 3, 7 et des triosides liés en position 3, 5, 3'. De nombreux anthocyanes sont en outre acylés par des acides hydroxycinnamiques : acides 4-coumarique, caféique, férulique, sinapique; des acides benzoïques : acide gallique; des acides aliphatiques carboxyliques : acide acétique, ou des acides dicarboxyliques comme les acides malonique, malique, oxalique et succinique (246, 247). Les fraises (248), les mûres (249) et les framboises (250-252) contiennent divers anthocyanes. La majorité des anthocyanes dans les framboises et les mûres sont des dérivés des cyanidines (253) alors que dans la fraise, la pelargonidine-3-O-glucoside prédomine (254). Dans les bleuets, les anthocyanes principaux sont la malvidine-3-O-arabinoside et les 3-O-galactosides de cyanidine, delphinidine, pétunidine et malvidine (236, 243). Pour ce qui est des canneberges, les anthocyanes majoritaires sont des composés dérivés des cyanidines et péonidines (236, 239, 243).

Les anthocyanes sont présentes dans les fruits mais aussi dans certains légumes feuillus ou racinaires (chou rouge, oignon rouge, radis). La quantité d'anthocyanes est souvent proportionnelle à l'intensité de la pigmentation du fruit et leur concentration peut atteindre 2 à 4 g/kg dans certaines baies comme le cassis ou les mûres.

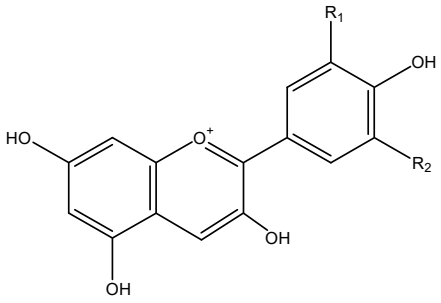

Anthocyanidine	R_1	R_2
Pelargonidine	H	H
Cyanidine	OH	H
Delphinidine	OH	OH
Peonidine	OCH_3	H
Pétunidin	OCH_3	OH
Malvidine	OCH_3	OCH_3

Figure 21 : Structures chimiques des anthocyanidines

1.6.3.1.1.7 Chalcones et dihydrochalcones

Les chalcones sont caractérisées par l'ouverture de l'hétérocycle C avec formation d'une double liaison en position carbone 2 et 3 (Figure 22). La présence de chalcone est faible dans l'alimentation en plus de se transformer en flavanone en milieu acide. La réduction de la double liaison entre carbone 2 et 3 est caractéristique des dihydrochalcones. La plus grande source dihydrochalcone est la pomme et ses produits dérivés. La phloridzine (phlorétine 2'-glucoside), la phlorétine 2'(2''-xylosyl-glucoside) et la 3-hydroxyphloridzine (255) sont les trois principales dihydrochalcones présentes dans la peau et les pépins des pommes (256).

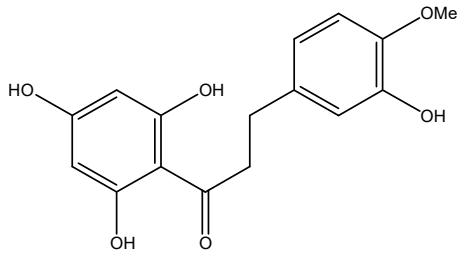

Figure 22 : Structure chimique des dihydrochalcones

1.6.3.2 Les acides phénoliques et les tannins hydrolysables

Les fruits contiennent une grande variété d'acides phénoliques : les acides hydroxybenzoïques et les acides hydroxycinnamiques (Figure 23).

(A)

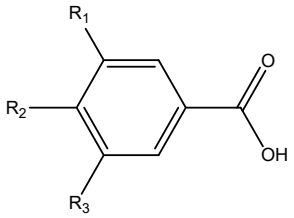

Acides hydroxybenzoïques	R_1	R_2	R_3
Acide protocatéchique	OH	OH	H
Acide gallique	OH	OH	OH

(B)

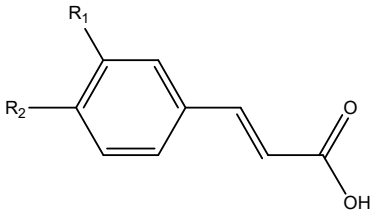

Acides hydroxycinnamiques	R_1	R_2
Acide coumarique	OH	H
Acide caféique	OH	OH
Acide férulique	OCH_3	OH

Figure 23: Structures chimiques des acides hydroxybenzoïques (A) et hydroxycinnamiques (B)

1.6.3.2.1 Les acides hydroxybenzoïques

Les acides hydroxybenzoïques découlent de l'acide benzoïque (C_6-C_1) (Tableau I). Il y a une grande diversité structurale qui a été rapportée dans la littérature pour ces acides. Plusieurs hydroxylations et/ou méthoxylations sont possibles au niveau du cycle aromatique (Figure 23A) créant l'acide protocatéchique, l'acide gallique et plusieurs autres (257). Dans les fruits, les acides hydrobenzoïques sont très présents : les framboises (5.8 mg/kg), les fraises (18 mg/kg) et les mûres (88 mg/kg) (258). Par exemple, l'acide ellagique représente plus de 50% des acides phénoliques totaux dans la fraise (259). Dans l'alimentation, l'acide gallique et l'acide salicylique sous forme conjugués (dérivés d'esters ou glycosylés) sont les deux acides hydrobenzoïques les plus répandus. Toutefois, l'acide gallique a été retrouvé sous forme libre dans certains fruits tels que le kaki.

1.6.3.2.2 Les acides hydroxycinnamiques

Les acides hydroxycinnamiques émanent de l'acide cinnamique. Leur squelette carboné possède une structure de type C_6-C_3 (Tableau I). Leur diversité structurale est davantage influencée par la variabilité des hydroxylations au niveau du cycle aromatique que les acides hydroxybenzoïques (230) (Figure 23B). De plus, la littérature a démontré qu'ils sont présents sous forme de diastéréoisomères (*cis* et *trans*). La forme *trans* est bien plus abondante que la *cis* due à la stabilité de sa thermodynamie. Le composé le plus courant est l'acide caféique qui représente à lui seul 75 à 100% des acides hydroxycinnamiques totaux dans la plupart des fruits (230). Les acides hydroxycinnamiques sont rarement présents sous forme libre et sont retrouvés essentiellement sous forme conjuguée. Il s'agit de dérivés glycosylés ou estérifiés avec des acides quinique, tartrique ou shikimique (241). Le conjugué le plus commun est l'acide 5-cafféoylquinique, également appelé l'acide chlorogénique, qui représente jusqu'à 90% des polyphénols dans la pomme de terre. Les acides hydroxycinnamiques sont présents dans les fruits comme les myrtilles, le kiwi, les prunes, les fraises ou les pommes (de 0,5 à 2 g/kg poids frais). L'acide férulique est le plus abondant dans les céréales mais également dans certains légumes comme l'aubergine (600 à 660 mg/kg PF). L'acide 4-coumarique est présent en quantité importante dans les épinards (300 à 350 mg/kg PF) (241).

1.6.3.2.3 Les tannins hydrolysables

En plus des tannins condensés, il y a également dans les fruits et légumes des tannins hydrolysables. Ces derniers ont une voie de synthèse bien différente à celle des tannins condensés : ils proviennent de l'acide gallique (Figure 12). Ils portent le nom de tannins hydrolysables à cause de leurs liaisons qui sont facilement hydrolysable peu importe qu'ils soient dans un milieu acide ou basique. Ils sont subdivisés en deux classes : les gallotannins et les ellangitannins (Figure 24). Ils possèdent un noyau polyol (souvent le D-glucopyranose) dont les fonctions hydroxyles sont estérifiées par des unités d'acide gallique; ce qui formera des oligomères tels que l'épigallocatéchine 3-gallate (EGCG) et l'épicatéchine 3-gallate particulièrement présent dans le thé vert (260). Les ellagitannins, présents dans les mûres, les

framboises noires, les framboises rouges et les fraises sont plutôt formés par estérification avec de l'acide hexahydroxydiphénique (261).

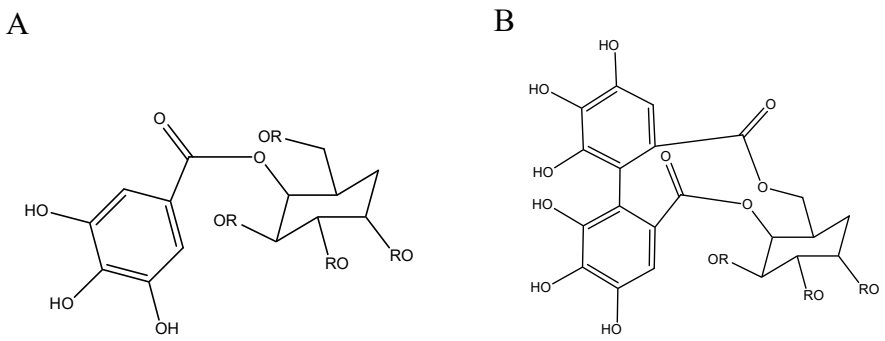

Figure 24 : Structures chimiques des tannins hydrolysables: gallotannin (A) et ellangitannin (B)

1.6.3.3 Les stilbènes

Les stilbènes présentent une structure en C_6-C_2-C_6 (Tableau I), avec un cycle A portant deux fonctions hydroxyles en position méta et un cycle B portant des fonctions hydroxyles ou méthoxyles en méta, ortho et para. Ils sont synthétisés à partir de dérivés d'acides cinnamiques dont la substitution déterminera celle du cycle B. La molécule la plus courante et la plus étudiée est le resvératrol (3,5,4'-trihydroxystilbène) qui existe sous forme *cis* ou *trans* (Figure 25). Cependant, la forme trans est majoritaire et les dérivés conjugués tels que le trans-resvératrol-3-O-glucoside, peuvent être également présents. Les sources principales de stilbènes sont le raisin et son jus, les cacahuètes et le beurre de cacahuètes (262), le chou rouge, les épinards et certaines plantes médicinales (233). La concentration en stilbènes dans le vin est en partie déterminée par les étapes de macération avec la peau et les pépins de raisin. Ainsi, c'est dans le vin rouge que l'on en mesure la plus grande quantité avec une concentration jusqu'à 8 mg/L selon les variétés (263). Le jus de raisin rouge contient 0,7 à 14 mg/L de resvératrol et le jus de raisin blanc environ 1,4 mg/L. Dans les jus, les formes glycosylées représentent plus de 90% du resvératrol (223, 241).

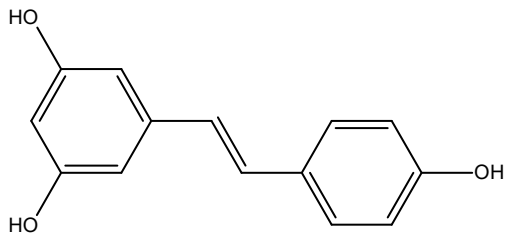

Figure 25 : Structure chimique du resvératrol

1.6.3.4 Les lignanes

Une dimérisation oxydative de deux unités de phénylpropane permet la formation de la lignane (Figure 26). Il y a peu de lignane dans les fruits et les légumes comparativement à ce qui est retrouvé dans la graine de lin. Selon les études, il y en aurait dans le blé, les légumineuses, les poires, les prunes et les petites baies (264) et elle y compterait environ 1000 fois moins que dans la graine de lin où une concentration de 3,7 g/kg de poids sec a été estimée (265, 266). La flore colique métabolise les lignanes en entérodiol et en entérolactone, et leur structure chimique est comparable aux phytoestrogènes.

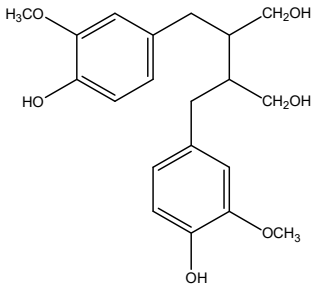

Figure 26 : Structure chimique de la lignane

1.6.4 Biodisponibilité

Les polyphénols sont présents dans notre alimentation sous plusieurs formes (267-271). Cette particularité va leur conférer des types de métabolisme différents. La biodisponibilité des polyphénols dépend de trois facteurs essentiels : la capacité de transport à travers la bordure en brosse des entérocytes, l'intensité de la sécrétion intestinale des

polyphénols conjugués vers le sang et la capacité de la sécrétion biliaire. Les polyphénols présentent une faible biodisponibilité avec une élimination lente qui diffère d'un polyphénol à l'autre. En effet, les polyphénols peuvent être absorbés par l'intestin dans leur forme aglycone ou encore être conjugués par méthylation, sulfatation ou glucuronidation (Figure 27). Une partie de ces polyphénols est déversée dans le sang tandis qu'une autre est destinée à poursuivre le transit vers le grêle et le côlon, ce qui représente l'un des mécanismes de contrôle de l'absorption intestinale des polyphénols. Dans le sang, les polyphénols ne sont pas présents sous leur forme native car ils ont été modifiés à cause de leur transformation au niveau du foie et des cellules intestinales. La fraction des polyphénols conjugués, destinée finalement aux différents tissus, pourrait résulter en un effet biologique potentiel ou être éliminée dans les urines. Cependant, d'autres polyphénols conjugués pourraient être déversés dans l'intestin via la bile et y être hydrolysés par des enzymes de la flore intestinale libérant ainsi de nouveaux aglycones. Ce recyclage entérohépatique des polyphénols permettrait de maintenir une concentration de polyphénols non négligeable dans le sang (223, 272-274).

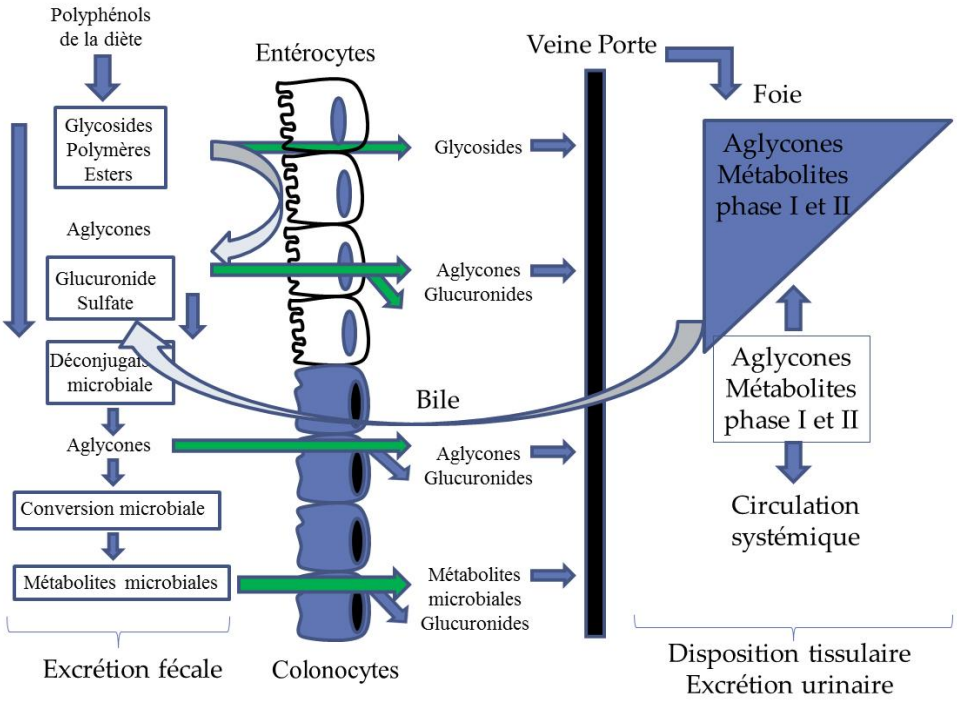

Figure 27 : Métabolisme intestinal des polyphénols chez l'humain
Adaptée de Scalbert *et al*., 2000 (275)

Le tractus gastro-intestinal est responsable de l'absorption, de la transformation des aliments, de leur dégradation en protéines, en glucides, en sels minéraux, en oligo-éléments, en lipides et en d'autres substances utilisables par l'organisme. Il assure également le passage de ces nutriments dans la circulation sanguine de façon à ce qu'ils puissent être employés par l'ensemble des organes. Ces substances constituent les matières premières pour la fabrication, la réparation et le contrôle des différents systèmes de l'organisme. La section suivante a pour objectif d'élucider le devenir des flavonoïdes dans l'intestin par l'étude des différents mécanismes d'absorption, d'excrétion vers la lumière intestinale, de conjugaison, de métabolisation par la microflore et d'élimination. Étant donné que les fruits et légumes contiennent principalement des flavonoïdes, seule cette sous-classe est présentée dans ce présent travail. Un schéma des mécanismes majeurs impliqués dans la métabolisation intestinal des flavonoïdes est illustré à la fin de cette section (Figure 28).

1.6.4.1 Absorption

Les propriétés bioactives des flavonoïdes dépendent principalement de leur absorption au travers de la paroi gastro-intestinale. Les flavonoïdes provenant de l'apport alimentaire, tels que la pomme et la canneberge, se retrouvent en général sous forme de glycoside, d'esters ou de polymères. Les glycosides des flavonoïdes résistent au pH acide et ne sont donc pas absorbés par la paroi stomacale sauf pour les formes aglycones qui sont rapidement absorbées dans l'estomac et l'intestin grêle (272). Les flavonoïdes, excepté les flavan-3-ols, sont glycosylés le plus souvent par une molécule de glucose, de rhamnose, d'arabinose, de xylose, de rutinose, de galatose et même de sophorose. Cette glycosylation des polyphénols ne permet pas à ces derniers de traverser la membrane plasmique des entérocytes par diffusion passive à cause de leur caractère polaire. Une étape de déglycosylation catalysée par une enzyme est essentielle à l'absorption des flavonoïdes par les entérocytes. La première voie de déglycosylation fait intervenir une glucosidase présente au niveau de la bordure en brosse de l'intestin grêle, la lactase phloridzine hydrolase (LPH). Cette enzyme catalyse l'hydrolyse extracellulairement des glucosides, permettant ainsi aux flavonoïdes de traverser passivement, sous forme aglycone, la membrane plasmique des entérocytes grâce à leur caractère lipophile (276). La LPH présente une affinité pour les substrats tels que les flavonoïdes-O-β-glucosides.

La deuxième voie de déglycosylation fait intervenir un transporteur de glucose sodium dépendant (SGLT1 : sodium-glucose transport protein 1) qui permet l'entrée des glucosides polaires des flavonoïdes dans les entérocytes par transport actif (273, 277). Par la suite, une β-glucosidase cytosolique située dans les entérocytes hydrolyse les glycosides des flavonoïdes.

Le site et le taux d'absorption des flavonoïdes glycosylés sont dépendants du type de sucre attaché sur ce dernier. La position du sucre, quant à elle, affectera les mécanismes impliqués dans l'absorption intestinale. La position des glycosides sur le squelette carboné des flavonoïdes à la position 3' et 4' influence leur absorption. L'équipe de Day *et al*. en 2003 a montré que la quercétine-3-O-glucoside n'était pas un substrat de la β-glucosidase cytosolique et que ce composé empruntait préférentiellement la voie de la LPH, alors que la quercétine-4'-O-glucoside empruntait les deux voies métaboliques (278). Le kaempferol ayant un groupe 4'-hydroxyle est plus biodisponible que la quercétine, lequel a un groupement 3',4'-dihydroxyle (279, 280). Par exemple, la 3-hydroxyanthocyane dans les fraises, pélargonidine-3-O-glucoside, est absorbée plus facilement que son analogue en 3',4'-dihydroxy, la cyanidine-3-O-glucoside (248, 281). Il y a des polyphénols glycosylés par d'autres sucres (rhamnose, arabinose, xylose), des proanthocyanidines ou des esters d'acides phénoliques comme l'acide chlorogénique qui ne sont pas ou peu absorbés au niveau de l'intestin (241). Un exemple qui revient fréquemment dans la littérature est celui de l'absorption de la quercétine glycosylée chez l'humain: le pic d'absorption de la quercétine 4'-glucoside se fait entre 0,5 à 0,7 h alors que celui de la quercétine 3-rutinoside se fait de 6 à 9 h après son ingestion (273). De plus, comme le rutoside n'est pas un substrat de l'enzyme LPH dans la bordure en brosse, la quercétine 3-rutinoside se retrouve intacte dans le côlon.

Ainsi, les flavonoïdes qui ne sont pas absorbés dans l'intestin grêle se dirigent vers le côlon où la microflore peut hydrolyser les glycosides en aglycone grâce à l'action d'enzymes telles que les rhamnosidases, les estérases, etc. La microflore peut également O- et C-déglycosyler, hydrolyser les esters et les amines, et déglucuronider les métabolites produits. Les aglycones libérés sont absorbés au niveau du côlon mais de façon moins importante qu'au niveau de l'intestin où la surface d'échange est bien plus grande ainsi que le nombre de transporteurs (241).

Les flavan-3-ols sont la seule sous-classe des flavonoïdes qui ne sont pas présents comme glycosides dans le régime alimentaire. L'absorption de la catéchine par l'intestin grêle est directement proportionnelle à la dose apportée par la diète (282). Les données suggèrent que la catéchine pénètre dans les cellules intestinales par diffusion passive, un mécanisme d'absorption qui est généralement proportionnelle à la dose. L'absorption d'oligomères de flavan-3-ols, les procyanidines, a été principalement étudiée dans le modèle cellulaire Caco-2, c'est un modèle communément utilisé pour évaluer les paramètres d'absorption intestinale. L'équipe de Ou *et al*. ont démontré, en 2012, que les procyanidines dimériques, trimériques et tétramériques de type-A pouvaient être absorbées par la voie paracellulaire via les jonctions serrées des cellules (283). A cause du caractère polaire des procyanidines, le transport passif se fait par voie paracellulaire au lieu transcellulaire. Toutefois, dans cette même année, l'équipe de Zumdick *et al*. a révélé que les procyanidines sont des substrats pour la p-glycoprotéine, ce qui signifie que les procyanidines de type-B peuvent être transportées par la voie para et transcellulaire dans les cellules Caco-2. Les procyanidines internalisées dans les cellules Caco-2, par voie transcellulaire, s'exposent à de l'efflux diminuant ainsi leur taux d'absorption nette (284).

1.6.4.2 Métabolisme

Les flavonoïdes sont métabolisés dans l'intestin grêle par conjugaison ou dans le côlon par la microflore. Au niveau intestinal, les flavonoïdes peuvent subir trois types de conjugaisons (méthylation, glucuronidation et sulfatation) suite à leur absorption. La méthylation des flavonoïdes est effectuée par la catéchol-O-méthyltransférase (COMT). Cet enzyme catalyse le transfert d'un groupe méthyle de la S-adénosyl-L-méthionine au flavonoïde ayant un groupement o-diphénolique (catéchol). Cette réaction de conjugaison est bien connue à la position 3' de la quercétine et de la catéchine, et elle se produit dans plusieurs tissus autres que l'intestin (35). La seconde conjugaison est la glucuronidation produite par l'UDP-glucuronosyltransférase (UDPGT). Cet enzyme lié aux membranes du réticulum endoplasmique catalyse cette fois-ci le transfert d'un acide glucuronique de l'acide UDP-glucuronique vers le flavonoïde. La sulfatation des flavonoïdes est la troisième conjugaison possible dans l'intestin. La sulfatation est réalisée par des sulfotransférases (SULT), présentes

dans le cytosol de la cellule intestinale, qui catalysent le transfert d'un groupement sulfate de la 3'-phosphoadénosine-5'-phosphosulfate sur les groupements hydroxyles des flavonoïdes. La proportion de chacune des trois réactions de conjugaison est dépendante de la structure chimique des flavonoïdes et elle est très variable. Ainsi, il est possible d'observer de la quercétine diglucuronidée, de la phlorétine glucuronidée-sulfatée ou encore de la catéchine méthylée-glucuronidée et sulfatée. Le taux de conjugaison des flavonoïdes étant particulièrement élevé, le niveau d'aglycone mesuré du coté basolatéral des cellules Caco-2 ou dans le plasma est relativement faible (241, 285).

Les aglycones non-absorbés dans l'intestin grêle se retrouvent au niveau du côlon où la microflore pourra leur faire subir une ou plusieurs transformations telles qu'une déhydroxylation, une déméthoxylation et une déméthylation aromatique en plus d'une hydrogénation, α–oxidation et β-oxidation des éléments aliphatiques générés après l'ouverture de l'hétérocycle. Les transformations effectuées par la microflore libéreront divers métabolites dont des acides hydroxyphénylacétiques issus du métabolisme des flavonols, des acides hydroxyphénylpropioniques issus du métabolisme des flavones et des flavanones ainsi que des phénylentérolactones et des acides hydroxyphénylpropioniques issus du métabolisme des flavanols. Ces acides aromatiques sont par la suite eux-mêmes métabolisés en dérivés d'acide benzoïque (241). Il est rare que les études quantifient les produits non-aromatiques (l'oxaloacétate, le CO_2) résultant de ces réactions. Pourtant, ils ne sont pas négligeables car la principale étape du catabolisme des flavonoïdes est la rupture du cycle A et la perte des carbones 5 à 8 comme l'acide oxaloacétique qui est lui-même utilement métabolisé en CO_2. Ces métabolites peuvent être absorbés au niveau du côlon (286). Par conséquent, les acides phénoliques ou aromatiques générés dans le tractus gastro-intestinal sont indépendants des classes de polyphénols provenant des aliments consommés. Les anthocyanes et les proanthocyanidines vont produire les acides benzoïques (C6-C1) dont les acides protocatéchique (3,4-dihydroxybenzoïque) et 4-hydrobenzoïques et aussi les acides phenylpropionates (C6-C3) dont les acides dihydrocaféique et dihydroférulique, avec quelques acides phenylvalérique (C6-C5)-γ-OH lors du début de la dégradation des proanthocyanidines. De plus, il y aurait une augmentation des acides benzoïques vers la fin étant donné que la microflore ou les systèmes enzymatiques vont réduire la chaîne latérale. Les acides

cinnamiques peuvent être absorbés tels quels ou être réduits à des acides dihydro C6-C3; les flavonols peuvent être réduits en acides phenylacétique (C6-C2) et peuvent être formés également suite à une α-oxidation des acides dihydro C6-C3 en les réduisant en acides C6-C1 par le même mécanisme (287). La description de ces groupes de métabolites dans les paragraphes suivants démontre la complexité du métabolisme des flavonoïdes dans un modèle *in vivo* où la microflore intervient. Il est toutefois important pour les équipe de recherche, travaillant sur le métabolisme des polyphénols, d'en tenir compte puisqu'il y a sans doute une partie de l'activité biologique qui est due à ces métabolites (287).

Acides benzoïques (C6-C1)

Les études avec les cellules Caco-2 ont démontré que les acides benzoïques et les 3 isomères des acides mono-hydroxybenzoïques sont les substrats du transporteur monocarboxylate (288). Suite à leur transport, ils sont métabolisés en conjugués sulfatés et glucuronidés par les cellules Caco-2. Les acides 3-methoxy-4-hydroxy-phénylacétique ou homovanillique sont des substrats pour le transporteur organique anionique des rats (289). Suite à l'absorption, la catechol-O-methyl transferase méthyle l'acide protocatéchique donnant de l'acide vanillique (290).

Acides phenylacétique (C6-C2)

Dans les matières fécales, le contenu du côlon est composé d'acide phénylacétique, d'acide 3-phenylpropionique, d'acide 3-hydroxyphénylacétique, d'acide 3,4-dihydroxyphenylacétique, d'acide 3-(4'hydroxyphenyl)-propionique et d'acide 4-hydroxy-3-methoxycinnamique (connu aussi sous le nom d'acide férulique) dont les concentrations moyennes sont 188, 197, 110, 64, 61 et 10 μM, respectivement (291).

Acides phenylpropionate (C6-C3)

L'acide dihydrocaféique est principalement absorbé par diffusion passive transcellulaire ce qui permet son entrée dans la circulation majoritairement sous forme libre. Cependant, une faible proportion d'acide dihydrocaféique est glucuronidé (292). Les acides dihydrocaféiques sont rapidement sulfatés ou méthylés puis sulfatés par le foie alors que les métabolites majoritairement entrant dans la circulation sanguine sont des acides dihydroféruliques libres, acide dihydrocaféique-3-O-sulfate ou acide dihydroférulique-4-O-sulfate. L'acide dihydroférulique est absorbé par l'intestin partiellement par diffusion passive transcellulaire et par transport actif par le transporteur monocarboxylique (292, 293). L'acide

3-hydroxycinnamique et ses dihydroformes, et l'acide 3-(3'-hydroxyphenyl)-propionique sont les deux absorbés partiellement par le transporteur monocarboxylique dans les cellules Caco-2 (294).

Acides phenylvalérique (C6-C5)

Plusieurs catabolites ont été détectés dans le plasma et les urines comme conjugués méthylés et/ou glucuronidés/sulfatés (295).

1.6.4.3 Efflux

L'efflux intestinal est un mécanisme important qui limite l'absorption de certains flavonoïdes. Une proportion importante de flavonoïdes conjugués formés dans l'intestin grêle est activement retournée à la lumière intestinale. L'interaction de ces molécules avec les transporteurs membranaires MRP (multidrug-resistance-associated protein) et la P-gp (P-glycoprotéine) de la famille ABC (ATP-binding cassette transporters) est impliquée dans l'efflux (296, 297). L'efflux de la quercétine et les métabolites est supposé se produire par MRP2, situé sur le côté luminal des cellules épithéliales (298, 299). La quercétine-3'-O-glucuronide a été excrétée dans la lumière de façon sélective, laissant probablement d'autres métabolites tels que le 3- et 7-O-glucuronides disponibles pour la circulation systémique (300). La proportion de l'efflux intestinal de certains flavonoïdes a été étudiée suite à une perfusion intestinale *situ*. Par exemple, pour la quercétine 52% de la dose perfusée a été ré-excrétée de retour dans la lumière alors que seulement 10 à 20% de la dose de kaempférol a été de nouveau éliminée (301). La catéchine ne semble toutefois pas être un substrat de choix pour ces protéines de transport, ce qui pourrait expliquer la différence du taux d'absorption entre la catéchine et l'épicatéchine. Par conséquent, la communauté scientifique s'interroge sur les différences d'absorption des flavonoïdes. Est-ce que le taux d'absorption des flavonoïdes dépend davantage de l'interaction des flavonoïdes avec les protéines responsables de l'efflux ou de la quantité de flavonoïdes pouvant être absorbée au niveau intestinal ?

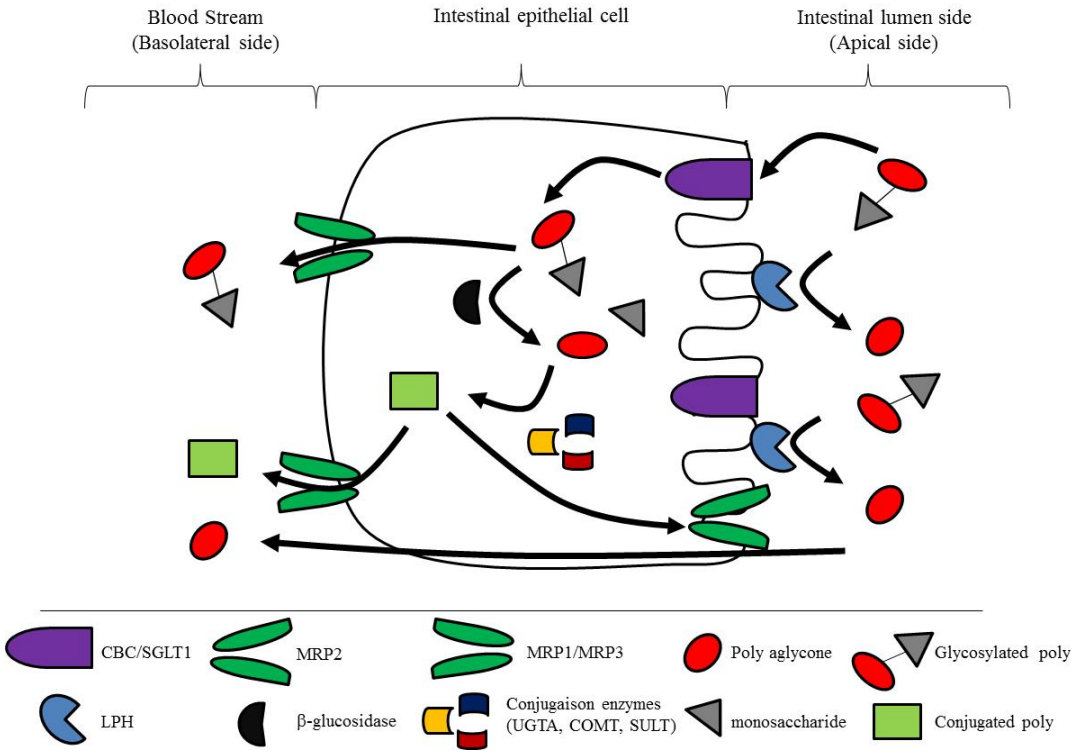

Où LPH, lactase phloridzin hydrolase; SGLT, sodium-dependent glucose transporter; MRP, multi resistance-associated protein; Poly, polyphenol.

Figure 28: Schéma représentant les processus d'absorption et de métabolisation des polyphénols dans les cellules Caco-2/15

1.6.4.4 Distribution et élimination

Les flavonoïdes glycosylés ou estérifiés natifs ne sont généralement pas présents dans la circulation sanguine sauf pour les anthocyanines ayant une forme native glycosylée. Les flavonoïdes conjugués issus du métabolisme intestinal et même hépatique sont identifiés dans le sang. La forme glucuronidée des flavonoïdes est le métabolite conjugué principal au niveau sanguin.

Des études menées avec des flavonoïdes marqués (quercétine, épigallocatéchine, quercétine 4'-glucoside, cyanidine 3-glucoside) ont montré que, 1 à 6 heures après l'ingestion, la radioactivité était détectée majoritairement dans la circulation sanguine et les organes du système digestif. Toutefois, les flavonoïdes ont également été détectés dans d'autres organes tels que le cerveau, le cœur, les reins, le thymus, le pancréas et la prostate. Les concentrations

en polyphénols dans ces tissus étaient de 30 à 3000 ng d'équivalents aglycones/g de tissu selon le polyphénol considéré, la dose administrée et le tissu analysé (241).

Les principales voies d'excrétion des flavonoïdes sont les voies biliaires et urinaires. Le choix de la voie d'excrétion dépend de la structure chimique des molécules. Ainsi, les métabolites hautement conjugués seront principalement éliminés dans la bile tandis que les petits conjugués comme les monosulfatés seront préférentiellement éliminés par voie urinaire (302). Les métabolites excrétés dans la bile pourront être réabsorbés au niveau de la muqueuse colique permettant ainsi la formation d'un cycle entérohépatique (241). L'excrétion urinaire des flavonoïdes varie d'une molécule à l'autre et peut aller de 0,3 à 43 % de la dose ingérée (pour 50 mg d'aglycone). Ce type d'excrétion est faible pour les anthocyanes, les flavan-3-ols et les flavonols. Toutefois, l'excrétion urinaire des acides phénoliques et des isoflavones est très élevée (303).

1.7 Impacts des polyphénols sur le stress oxydant

Le régime alimentaire peut jouer un rôle dans la modulation du statut antioxydant, soit en augmentant les niveaux d'antioxydants alimentaires, par exemple par l'apport des polyphénols, soit via la synthèse des antioxydants endogènes (304). Les polyphénols sont des micro-nutriments dont la capacité antioxydante permet de maintenir l'équilibre de la balance oxydante/antioxydante par cinq mécanismes d'action: 1) en piégeant de manière directe les RL (305-307); 2) en inhibant les enzymes impliquées dans le stress oxydant et la chélation des ions métalliques responsables de la production des RL (308, 309); 3) en modulant la protection des systèmes de défense antioxydant ainsi que celui du processus de détoxification par les enzymes de phase II (159, 310-318); 4) en diminuant la peroxydation lipidique, l'oxydation des protéines et les dommages de l'ADN (319-328); et 5) en préservant la perméabilité des membranes et les fonctions mitochondriales (160, 329-334).

1.7.1 Mécanismes d'action des polyphénols pour contrer le stress oxydant

1.7.1.1 Les polyphénols piègent de manière directe les radicaux libres (RL)

Les polyphénols, plus particulièrement les flavonoïdes, sont thermodynamiquement capables de réduire rapidement les radicaux superoxydes ($O_2^{-\cdot}$), peroxyles ($ROO^{\cdot}$), alkoxyles ($RO^{\cdot}$) et hydroxyles ($OH^{\cdot}$) par transfert d'hydrogènes. Pour les radicaux peroxyles et alkoxyles, R désigne un substrat organique. Le radical aryloxyle peut réduire le dioxygène (O_2) pour donner une quinone ($C_6H_4O_2$) et un anion superoxyde ($O_2^{-\cdot}$). Cette réaction est toutefois responsable d'un effet prooxydant des flavonoïdes. Plusieurs études ont prouvé la relation entre la structure chimique des polyphénols et leur capacité à piéger les radicaux libres. Les flavonoïdes les plus actifs sont ceux qui combinent les 3 critères suivants : 1) la structure ortho-dihydroxy sur le cycle B (groupement catéchol); 2) la double liaison C_2-C_3 en conjugaison avec la fonction 4-oxo; et 3) la présence du groupe C_3-OH en combinaison avec la double liaison C_2-C_3. Les flavonoïdes possédant une structure catéchol sur le cycle B et en particulier la catéchine, sont de bons piégeurs du dioxygène singulet. La quercétine piège efficacement les radicaux hydroxyles et peroxyles (impliqués dans la peroxydation lipidique). Une étude de Carrasco-Pozo *et al*. (335) a démontré que 50 µg/mL d'extrait de pelure pomme, comportant principalement de la quercétine et ses glycosides (60% de l'extrait), piégeait efficacement le dioxygène singulet, les radicaux hydroxyles et peroxyles générés par une exposition des cellules Caco-2 à 50 µM d'indométhacine pendant 60 minutes.

1.7.1.2 Les polyphénols inhibent les enzymes impliquées dans le stress oxydant et la chélation des ions métalliques responsables de la production des RL

L'inhibition de la production des RL par les polyphénols, particulièrement les flavonoïdes, peut procéder directement par la formation de complexe inhibiteur-enzyme et/ou par piégeage directe des RL. Cos *et al*. ont établi les relations entre la structure chimique des flavonoïdes et leur capacité d'inhiber la formation de superoxyde par inhibition de la xanthine oxydase (formation de complexes enzyme-inhibiteur) et/ou par réduction du superoxyde produit (336). Les résultats de cette étude démontrent que les flavanones, les dihydroflavonols et les flavan-3-ols (cycle C non plan) ne sont pas inhibiteurs de la xanthine oxydase; les

flavonols et les flavones (cycle C plan et conjugué avec les cycles A et B) ont la capacité d'inhiber l'enzyme; et l'absence du groupe hydroxyle en C_3 augmente légèrement l'activité inhibitrice. Les flavonoïdes glycosylées ont des activités inférieures à celles des composés non glycosylés. La rutine est presque dix fois moins active que la quercétine et les flavonoïdes (présentant un cycle B de type catéchol) sont de bons piègeurs de superoxyde en raison de la stabilité des radicaux semiquinones formés lors de la capture.

Les ions du fer ou du cuivre sont essentiels pour de nombreuses fonctions physiologiques. Ils entrent dans la composition des cofacteurs d'enzymes du système de défense antioxydant (ions de fer pour la catalase et ions de cuivre pour la superoxyde dismutase). Mais, ils sont aussi responsables de la production du radical hydroxyle par la réduction du peroxyde d'hydrogène selon la réaction de Fenton. L'auto-oxydation des ions Fe^{2+} et Cu^{2+} est une source de superoxyde et de peroxyde d'hydrogène. Donc, le remplacement des ions de fer et de cuivre par une forme qui bloque leur activité rédox est un mécanisme d'action antioxydante. Les études menées par Van Acker *et al*. sur la chélation des ions du fer par certains flavonoïdes ont mis en évidence les sites essentiels de la chélation des ions métalliques (337): (i) les groupes 3'-hydroxy et 4'-hydroxy du cycle B; (ii) les groupes 3-hydroxy et 4-oxo du cycle C; et (iii) les groupes 4-oxo et 5-hydroxy. La quercétine a tous ces substituants, ce qui lui donne la propriété d'être un complexant métallique particulièrement efficace.

1.7.1.3 Les polyphénols modulent la protection des systèmes de défense antioxydant ainsi que celui du processus de détoxification par les enzymes de phase II

Soyalan *et al*. (318) ont montré que les polyphénols de la pomme provoquent une modulation à la hausse de l'expression des gènes antioxydants (SOD, GPx, CAT) chez les rats recevant du jus de pomme *ad libitum* pendant 10 jours. L'analyse de l'expression génique des côlons distaux a montré que le jus de pomme brut offrait le meilleur potentiel polyphénolique antioxydant.

Le glutathion (GSH) est présent dans tous les types cellulaires et il fait partie de la défense antioxydante endogène. Il a pour action de maintenir l'équilibre rédox de la cellule,

chimiquement à cause du groupement thiol de la cystéine qui le compose. Le GSH a plusieurs rôles et les principaux sont de servir de cofacteur à la GPx pour la détoxification du H_2O_2 et des lipides peroxydés, ce qui produit le glutathion disulfide ou oxydé (GSSG) et lui permet d'agir comme piégeur de RL en neutralisant entre autres le peroxynitrite, le radical peroxyl et le radical hydroxyl. Le ratio glutathion réduit/glutathion disulfide (GSH/GSSG) est souvent utilisé comme biomarqueur de l'état rédox de la cellule. Une pré-incubation de 90 minutes avec 100 µg/mL d'extrait de pelure de pomme Granny Smith (composé de 60% de flavonoïdes, 5% de flavan-3-ols et de 24% de procyanidines) sur des cellules Caco-2 exposées à 250 µM d'indométhacine durant 60 minutes rétablit à 100% le ratio GSH/GSSG comparativement aux cellules contrôles (335).

Le processus de détoxification enzymatique impliquent les enzymes de phase II, soient le glutathion S-transferase, la thiorédoxine réductase et l'hème oxygénase 1. Le glutathion S-transférase (GST) catalyse la conjugaison des électrophiles avec la glutathion en dérivés moins réactifs et hydrophiles. Par conséquent, la GST est une des enzymes de phase II la plus efficace pour détoxifier les RLO. L'équipe de Petermann *et al*. (338) a révélé que les polyphénols de la pomme induisent l'expression génique du glutathion S-tranférase T2 (GSTT2) dans les cellules HT29. Une surexpression de GSTT 2 dans les cellules HT29 réduit significativement le dommage d'ADN induit par le cumene hydroperoxide (CumOOH).

1.7.1.4 Les polyphénols diminuent la peroxydation lipidique, l'oxydation des protéines et les dommages de l'ADN

Les premières cibles des RLO sont les lipides des membranes cellulaires et subcellulaires. Les membranes riches en acides gras polyinsaturés (AGPI) sont très sensibles à l'oxydation à cause de leur degré élevé d'insaturation (339). L'oxydation des lipides génère des peroxydes lipidiques qui sont eux-mêmes très réactifs. Parmi les produits formés lors de la peroxydation lipidique, l'isoprostane, le malondialdéhyde (MDA), le acides thiobarbiturique (TBARS) et le 4-hydroxynonenal (4-HNE) sont étudiés comme marqueurs de la peroxydation lipidique. Les flavonoïdes provenant d'extraits de pomme (311), de raisin (339) et de myrtille (340) préviennent efficacement la peroxydation lipidique puisqu'ils peuvent réagir avec la

plupart des RL susceptibles d'arracher un hydrogène sur le groupement CH_2 situé entre les deux doubles liaisons des AGPI.

De façon comparable à l'oxydation des lipides, les protéines sont aussi susceptibles d'être oxydées par les RL. Cette oxydation provoque l'introduction d'un groupe carbonyl dans la protéine (115). Ces réactions d'oxydation, fréquemment influencées par les cations métalliques comme le Cu^{2+} et le Fe^{2+}, peuvent être classées en deux catégories: celles qui brisent les liaisons peptidiques et modifient la chaîne protéique, et celles associées aux modifications des peptides par l'addition de produits issus de la peroxydation lipidique. Ces changements sont susceptibles de conduire à une modification structurale des protéines dont les conséquences sont majeures (perte de fonction catalytique, augmentation de la sensibilité aux protéases) (341).

Le stress oxydant étant principalement d'origine mitochondriale, ces organites sont les premières cibles des RL. En effet, le génome mitochondrial présente une susceptibilité au stress oxydant qui est 10 fois supérieure à celle du génome nucléaire (342). Les mécanismes explicatifs proposés sont : 1° l'absence d'histones protectrices autour de l'ADN mitochondrial; 2° sa localisation proche de la membrane interne; 3° des mécanismes de réparations frustres; et 4° une structure circulaire sans introns augmentant statistiquement le risque de mutations pathogènes (342-345). Comme le génome mitochondrial code pour quelques sous-unités de protéines impliquées dans la phosphorylation oxydative, leur défaut d'expression pourrait exacerber la fuite d'électrons de la chaîne respiratoire au profit de la production de RL. L'indométhacine inhibe l'activité du complexe I mitochondriale (346) générant ainsi une augmentation de la production de superoxide (347, 348) et une diminution de l'ATP (349). Les polyphénols de l'extrait de pomme sont capables de contrecarrer l'inhibition du complexe I mitochondrial dans les cellules Caco-2 (346).

1.7.1.5 Les polyphénols préservent la perméabilité des membranes et possiblement les fonctions mitochondriales

La barrière épithéliale intestinale a comme premier rôle de se défendre contre un environnement hostile provenant de la lumière intestinale tout en assurant le transport actif et passif de manière efficace pour les nutriments et autres molécules essentielles au bon

fonctionnement de l'intestin. Le passage des polyphénols à travers l'épithélium intestinal peut se faire par voie transcellulaire ou paracellulaire en impliquant les jonctions serrées et l'espace intercellulaire. Les jonctions serrées sont composées de protéines transmembranaires [occludine, claudines et JAM-A (Junctional Adhesion Molecule)] auxquelles se fixent des protéines intracellulaires (ZO, Zonula Occludens) dont le rôle est d'assurer les liaisons avec les protéines du cytosquelette. Des études *in vitro* (331, 350) ont permis d'affirmer que les polyphénols de la pomme (les procyanidines, la quercétine et la phlorétine ainsi que leurs glycosides) pouvaient réguler à la hausse la résistance transépithéliale (TER) et l'expression des protéines des jonctions serrées ZO-1, occludine et claudine-4. L'équipe de Carrasco-Pozo *et al*. (331) a démontré que la quercétine (20 µg/mL) avait également la capacité d'inhiber la redistribution des protéines ZO-1 de la membrane cellulaire au cytosol dans les jonctions serrées (351) et de prévenir la diminution de l'expression ZO-1 et de l'occludine dans les cellules Caco-2 lors d'un stress oxydant.

La barrière épithéliale intestinale dépend également de la composition du mucus qui communique avec la lumière intestinale (352). Les cellules de Gobelet de l'intestin sécrètent des glycoprotéines que l'on appelle des mucines. Ces protéines sont essentielles et jouent un rôle critique dans le maintien de l'intérgrité de la muqueuse intestinale. L'invalidation des gènes encodant pour la mucine 2 entraîne une colite spontanée (353).L'étude de Pierre *et al*. (354) a démontré que les proanthocyanidines de canneberge stimulent le niveau de mucines tout en maitenant celui des cytokines des Th2 de la lamina propria chez des souris recevant leur diète par voie entérale.

La détection de la quercétine intra-mitochondriale a permis de réaliser que la mitochondrie serait un site préférentiel d'accumulation de flavonoïdes de par son compartiment hydrophobe et de ses protéines-hémiques (332). La capacité de la quercétine à se lier à une variété de molécules grâce à sa structure chimique permettrait ainsi de multiplier ses sites de liaisons d'hydrogène et d'interactions hydrophobes. Par conséquent, la quercétine pourrait se lier à plusieurs protéines cytosoliques et compartiments lipidiques tels que les membranes. Elle pourrait éventuellement être relâchée de ces compartiments afin de venir en aide à d'autres compartiments cellulaires lorsque la machinerie antioxydante en place n'est pas suffisante pour contrer le stress oxydant.

De plus, la revue de Sandoval-Acuna *et al*.(355) a schématisé les actions majeures des polyphénols sur la mitochondrie (Figure 29). Les polyphénols sont capables d'induire la biogénèse mitochondriale par l'activation du mécanisme SIRT1-PGC1α; de stimuler ou d'inhiber la voie intrinsèque de l'apoptose par la modulation des protéines Bcl-2 (Bak et Bax); de moduler l'ouverture des canaux de perméabilité mitochondriale (MPTP); d'inhiber les complexes I, II et III de la chaîne de transport des électrons ou d'interagir avec eux comme une molécule d'ubiquinone.

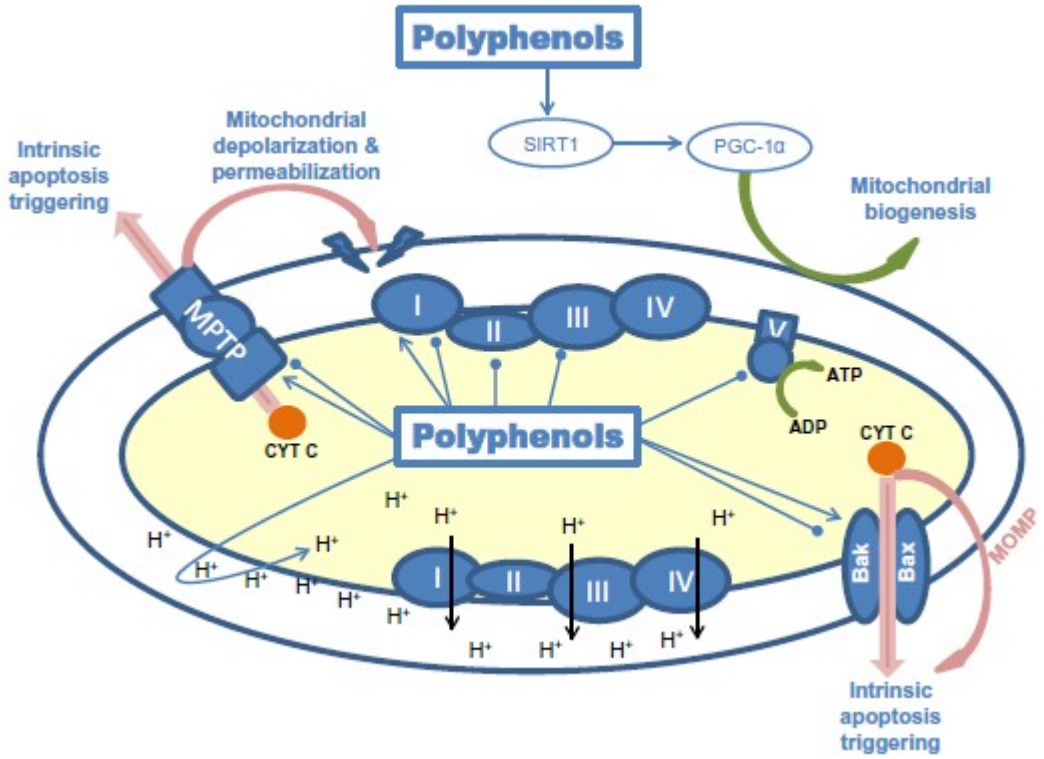

Figure 29 : Représentation schématique des actions majeures des polyphénols sur la mitochondrie
Tirée de Sandoval-Acuna *et al*.(356)

L'inflammation et le stress oxydant sont deux phénomènes reliés. Il est difficile encore aujourd'hui de déterminer si le stress oxydant est un agent causal ou une conséquence de l'inflammation dans les MII.

1.8 Effets des polyphénols sur l'inflammation intestinale

Dans l'intestin, des médiateurs du stress oxydant peuvent aussi être produits par les neutrophiles et les macrophages qui infiltrent la paroi intestinale lors d'une réaction inflammatoire, en réponse à des pathogènes (160).

Plusieurs études démontrent que les polyphénols modulent l'inflammation intestinale par trois différents mécanismes anti-inflammatoires : 1) en inhibant les enzymes pro-inflammatoires telles que la cyclooxygénase (COX-2), la lipoxygénase (LOX) et l'oxyde nitrique synthase inductible (iNOS), et en activant des récepteurs activés par les proliférateurs de peroxysomes (peroxisome proliferators-activated receptor gamma (PPARγ) (311, 357-366); 2) en inhibant les cytokines/chemokines, la phosphoinositide 3-kinase (PI 3-kinase), le NFκB, les MAP kinases (mitogen activated protein kinases) et les JAK/STAT (59, 311, 364, 367-383); et 3) en activant les mécanismes épigénétiques (méthylation de l'ADN/histones et activité des sirtuines) (384-403).

1.8.1 Les mécanismes d'action des polyphénols pour contrer l'inflammation

1.8.1.1 Les polyphénols inhibent les enzymes pro-inflammatoires

Un des importants mécanismes anti-inflammatoires consiste en l'inhibition des enzymes phospholipase A_2 (PLA_2), cyclooxygénase-2 (COX-2) et lipoxygénase (LOX), générant les eicosanoïdes (leucotriènes et prostanoïdes) par des activateurs spécifiques des PPARγ. La PLA_2 va permettre de libérer l'acide arachidonique des phospholipides membranaires, qui peut être métabolisé par la voie des COX-2 en protaglandines et en thromboxanes A_2 ou par la voie de la LOX en acides hydroperoxyeicosatétraénoïques, hydroxyeicosatétranoïques et leucotriènes (366). Les polyphénols ont démontré leur capacité à inhiber ces enzymes inflammatoires. Les flavonoïdes avaient une plus grande capacité à inhiber la LOX que la COX-2 (404). L'inhibition sélective de la 5-LOX requiert un flavonoïde qui peut chélater et réduire les ions de fer. Vasquez-Martines *et al*. (405) concluent que le groupe catéchol est essentiel pour l'inhibition de la 12 et 15-LOX alors qu'il est important mais pas essentiel pour l'inhibition de la 5-LOX (365). La quercétine, le kaempférol et la morine peuvent arrêter l'inflammation en inhibant la PLA_2 selon l'étude de Lattig *et al*. (406).

Par conséquent, les flavonols peuvent être considérés comme les flavonoïdes les plus efficaces pour l'inhibition de la LOX et la PLA_2 (407).

L'étude de Lau et al. a démontré que les polyphénols provenant de 100 µg/mL d'un extrait de bleuet diminuait l'expression de COX-2 et de iNOS en présence d'inflammation induite par 100 ng/mL de LPS dans les cellules microgliales. Dans les modèles *in vivo* d'inflammation intestinale, les polyphénols de la pomme ont confirmé la diminution de l'expression protéique de COX-2 (408) et de iNOS (409) par administration intra-rectale de 7.6% de pomme lyophilisée dans la diète.

1.8.1.2 Les polyphénols inhibent les cytokines/chemokines, la phosphoinositide 3-kinase, les facteurs de transcription nucléaire NF-κB, les MAP kinases et les JAK/STAT

Les cytokines sont des modulateurs majeurs de la réponse immune et inflammatoire. Depuis quelques années, la balance de cytokines pro-inflammatoires (IL-1β, IL-2, TNFα, IL-6, IL-8 et IFNγ)/anti-inflammatoire (IL-10, IL-4, TGFβ) est devenue un indicateur de l'évolution de plusieurs maladies inflammatoires. L'identification des polyphénols capables d'interférer sélectivement avec la production et/ou les fonctions des cytokines pourraient offrir une alternative dans les traitements des maladies inflammatoires. Plusieurs études ont observé l'aptitude des flavonoïdes à diminuer l'expression des différentes cytokines et chemokines, telles que le TNFα, IL-1β, IL-6, IL-8, MCP1, dans l'inflammation intestinale que c'est le cas dans les modèles *in vitro* ou *in vivo* (59, 311, 364, 410-412). Ces études supportent l'idée que les flavonoïdes ont la capacité de moduler la réponse immunitaire et l'activité anti-inflammatoire. Toutefois, la capacité de rétablir le déséquilibre de la balance cytokines pro-inflammatoires/anti-inflammatoires dépend non seulement des structures chimiques des flavonoïdes, mais aussi de leur action spécifique. Par exemple, la quercétine et la catéchine exercent une action inhibitrice de l'expression du TNFα et IL-1β et peuvent promouvoir la libération de l'IL-10 (413, 414).

Les polyphénols modulent les voies de signalisation intracellulaire de PI3 kinase/Akt, de NF-κB, des MAP kinases, de JAK/STATs. La phophatidylinositol-3kinase (PI3K) peut être activée par les récepteurs à activité tyrosine-kinase ou d'autres types de récepteurs comme

ceux couplés aux protéines G. Elle est impliquée principalement dans la croissance et la prolifération cellulaire. L'activation de PI3K génère un signal qui recrute la protéine-kinase B (Akt) à la membrane cellulaire. Celle-ci se lie alors avec la PI(3,4,5)P3 et change de conformation permettant son activation par une protéines-kinase phosphatidylinositol dépendante (PDK1). L'Akt activée est relâchée dans le cytosol où il favorise la survie cellulaire en inhibant les protéines pro-apoptotiques et/ou la transcription des gènes qui les codent. Une étude *in vivo* de Banerjee *et al* (415) a démontré que les polyphénols de la grenade peuvent diminuer l'inflammation intestinale en régulant à la baisse l'activation de NF-κB suite à la suppression de la phosphorylation de PI3K et AKT.

NF-κB joue un rôle pivot dans les réponses immunitaires, inflammatoires, prolifératives, apoptotiques et même dans le stress oxydant dans les cellules. Plusieurs polyphénols (acide éllagique, quercétine (416, 417), 3'-hydroxy-flavone (418), 2',4',6'-tris(methoxy-methoxy)-chalcone (419), et EGCG (383) (pour ne nommer que ces molécules) se comportent comme des anti-inflammatoires par l'inhibition d'une des étapes contrôlant l'activation de NF-κB via l'activité enzymatique IKK qui contrôle la phosphorylation IκB, la dégradation de la phosphorylation IκB associé avec la libération du NF-κB actif et l'activité transcriptionnelle de NF-κB elle-même. Toutefois, seulement la génistéine et le resvératrol ont démontré qu'ils pouvaient augmenter l'activité du NF-κB (420).

La voie des MAP Kinases est la seconde des 2 grandes voies pro-inflammatoires dans l'intestin. Cette voie implique trois sous voies, définies par les dernières kinases de la cascade : les kinases « extracellular signal-regulated kinases » (ERK1 et ERK2), p38 MAP kinases (avec quatre isoformes dénommés α, β, γ et δ) et de « C-Jun N-terminal kinases » (JNK1, JNK2 et JNK3). L'activation de ces sous voies permet l'activation de la phosphorylation de plusieurs facteurs de transcription nucléaires. La sous voie de la kinase ERK ½ cible les facteurs de transcription de l'activation protéine 1 (AP-1) et ElK-1 (421) et les protéines membranaires (PLA_2). Le rôle majeur de l'ERK ½ est de promouvoir la croissance et la différenciation cellulaire. Dans le processus inflammatoire, ERK ½ peut activer la production des lymphocytes T auxilliaires « cytokines T-cell » (422) et leur apoptose (423). L'activation de la sous voie de la kinase JNK par phosphorylation par des MAP kinase-kinase (MAP2K), également stimulées elles-mêmes par des MAP kinase-kinase-kinase

(MAP3K), stimule le facteur de transcription c-Jun qui peut alors former le complexe de facteurs de transcription AP-1 par homo ou hétérodimérisation avec les facteurs de transcription Jun et Fos. AP-1 régule principalement l'expression des métalloprotéases (MMP) et de cytokines inflammatoires. La 3^{e} sous voie de MAP kinase est la p38 MAP Kinase ciblant l'ATF-2, le facteur activateur des myocytes ainsi que la voie de signalisation de NF-κB. La kinase p38 MAPK régule plusieurs aspects de la physiologie cellulaire (prolifération, différenciation et mort cellulaire) en plus d'être un joueur critique dans la réponse inflammatoire normale. Chez des individus avec une maladie inflammatoire de l'intestin, l'expression de la kinase p38α s'est avérée être élevée dans les macrophages et les neutrophiles de la *lamina propria* (424). L'étude de Essafi-Benkhadir *et al*. (425) a démontré que 20 µg/mL d'extrait de poires de Cydonie, contenant principalement de l'acide 5-O-caféylquinique et de la quercétine-3-O-rutinoside, diminuait l'inflammation (1 µg/mL LPS) dans les cellules macrophagiques THP-1 par l'inhibition des trois effecteurs pro-inflammatoires NF-κB, p38α MAPK kinase et AKT. Dans un modèle *in vivo*, 10% d'extrait de bleuet dans la diète journalière des souris ApoE-/- a inhibé l'expression protéique et génique du TNFα et de l'IL-6 en plus d'inhiber la phosphorylation de IκB, NF-κB p65, p38 MAPK et JNK (426). De plus, les polyphénols du thé vert peuvent réduire l'activité des facteurs transcriptionnels STAT-3 et STAT-1 ciblés par les MAPKs, diminuant conséquemment l'inflammation (427). La génistéine réduit l'activité de la voie de MAP Kinase (377) alors que le 3-hydroxy-flavone et 2',4',6'-tris(methoxy-methoxy)-chalcone ont des effets opposés (375, 379).

La voie de « Janus kinase » (JAK) est la voie d'activation de nombreuses cytokines telles que l'interféron, l'IL-6, IL-15, les facteurs de croissance comme l'hormone de croissance et le « granulocyte macrophage colony stimulating factor » (GM-CSF). Les JAK sont des tyrosine-kinases intra-cytoplasmiques qui, une fois activés, stimulent la phosphorylation des protéines STAT qui migrent vers le noyau et induisent la transcription de gènes cibles à l'origine des modifications du comportement cellulaire. De plus, les JAK stimulent aussi les sous voies de MAP kinases Ras/MAPK ERK1/2 et de PI3K/AKT. STAT induit également la production de protéines qui exercent un rétro-contrôle négatif sur la voie de JAK comme les protéines « suppressor of cytokine signalling 3 » (SOC3) et STAT5. JAK

peut être inhibée par une tyrosine-phosphatase, la SHP1.Une étude *in vitro* de Senggunprai *et al*. (428) a démontré que la quercétine et l'épigallocatéchine-3-gallate (EGCG) diminuaient l'expression des cytokines inflammatoires en supprimant la phosphorylation de STAT1 et STAT3.

1.8.1.3 Les polyphénols activent les mécanismes épigénétiques

Depuis les dernières années, la métabolomique a permis de découvrir des molécules bioactives provenant de nutriments mais également de micronutriments tels que les polyphénols ayant un impact sur les mécanismes épigénétiques, incluant la méthylation de l'ADN et des histones, l'acétylation des histones et des protéines non-histones, et l'expression des micro-ARNs. Les polyphénols provenant de la pomme, du thé vert, du café et autres peuvent affecter l'épigénome, l'activité des sirtuines, être des inhibiteurs des histones acétyl-transférases et des modulateurs de la méthylation des résidus de lysines sur les histones. Les polyphénols en ciblant les mécanismes épigénétiques affectent les voies de transduction du signal médié par les récepteurs nucléaires et des facteurs de transcription tels que NF-κB, de progression du cycle cellulaire, de différenciation cellulaire, d'induction de l'apoptose et de la sénescence (429-435).

Les sirtuines sont des protéines enzymatiques qui ont comme mandat de déacétyler les protéines histones ou non-histones telles que le NF-κB, forkhead box class O (FOXO) 3, p53, PPARγ, PGC1α et eNOS (436-438). La protéine SIRT1 est associée directement à la sous-unité RelA/p65 de NF-κB, et elle déacétyle le résidue de la lys310 qui est un site critique dans l'activité transcriptionnelle de NF-κB. De plus, des récentes études ont démontré que la SIRT1 pouvait également déacétyler et supprimer l'activité transcriptionnelle de AP-1 conduisant à une diminution de la régulation de l'expression génique de COX-2. La catéchine et la curcumine ont démontré qu'elles induisaient une hypoacétylation de RelA/p65 en inhibant directement l'activité des enzymes histones acétyltransférase qui conduisent à réguler à la baisse les fonctions de NF-κB et les réponses inflammatoires associées. L'activation de la SIRT1 par le resvératrol régule à la baisse le NF-κB lequel est associé avec l'abrogation de la colite induite par le DSS chez des rats (439). De plus, l'expression de nombreux gènes pro-inflammatoires, tels que COX-2, métalloprotéinases matricielles (MMPs), molécules adhésion

et iNOS a été significativement inhibée par le resvératrol, la quercétine, la curcumine et la catéchine via la régulation à la baisse des facteurs de transcription de NF-κB et AP-1 (440-443).

Les flavonoïdes des pommes, des agrumes, des raisins ont été identifiés dans les études *in vitro* comme des inhibiteurs de l'activité de la ADN méthyltransférase (DNMT). ECGC a été le premier polyphénol décrit capable d'inhiber la méthylation de l'ADN en se liant sur le site catalytique de la DNMT (444). D'autres études ont suggéré que les flavonoïdes dont les catéchines inhibent l'activité de la DNMT en favorisant la méthylation de l'ADN et en catalysant le groupement méthyle provenant de la SAM vers une cytosine. Par ailleurs, ils pourraient actionner un mécanisme indirect via la déplétion de l'adénosylméthionine (SAM), le transfert d'un groupement méthyle de SAM vers une cytosine, due à la méthylation des composés eux-mêmes, et par rétro-inhibition de la DNMT due à l'accumulation de SAH (392, 445, 446).

2. RÉSUMÉ ET PROBLÉMATIQUE

La muqueuse intestinale est exposée de façon constante à des agents oxydants provenant de l'ingestion d'aliments modifiés, de cellules immuno-inflammatoires et de la flore intestinale. Une diète élevée en fruits et légumes peut diminuer le stress oxydant ainsi que l'inflammation via plusieurs mécanismes tout en préservant l'intégrité des lipides, protéines et acides nucléiques intracellulaires. Ces effets bénéfiques peuvent être en partie attribuables à leur contenu élevé en vitamines, micronutriments et polyphénols qui sont considérés comme de puissants antioxydants. La biodisponibilité, la qualité nutritionnelle et le potentiel thérapeutique des classes de polyphénols sont dépendants des différences dans leur structure et de leur absorption par le tractus gastro-intestinal. À ce jour peu d'études ont étudié leurs effets directs sur la muqueuse intestinale et précisé les mécanismes d'action. Des efforts considérables sont donc nécessaires pour établir un tableau exhaustif des événements cellulaires et moléculaires. De plus, le besoin d'évaluer les effets des polyphénols dans les MII est criant étant donné leur caractère antioxydant et possiblement anti-inflammatoire.

3. HYPOTHÈSE GÉNÉRALE

En raison de leur puissante capacité antioxydante, nous avons émis l'hypothèse que les polyphénols de la pomme et/ou de la canneberge aideraient à maintenir l'homéostasie intestinale en situation de stress oxydant et d'inflammation. Nous proposons également que ces polyphénols puissent consolider l'équilibre pro- et antioxydant en plus de contrôler le niveau d'inflammation lors de MII.

4. OBJECTIFS PRINCIPAUX

L'objectif principal de cette thèse est d'analyser le profil et la capacité fonctionnelle des polyphénols contenus dans les pommes et les canneberges, deux fruits connus pour l'apport et la diversité en antioxydants, ainsi que par leur influence bénéfique sur la santé des individus. Plus précisément, nos travaux visent à déterminer les différentes classes polyphénoliques ayant le meilleur potentiel antioxydant et anti-inflammatoire au niveau de l'intestin autant dans un modèle *in vitro* qu'*in vivo*.

Pour cela, quatre buts doivent être atteints pour confronter l'objectif principal de ce programme scientifique :

1-Définir la concentration et la composition des polyphénols de la pomme tout en établissant la comparaison avec ceux de la canneberge, tenue comme référence en vue de sa richesse en plusieurs classes de polyphénols;

2-Déterminer le pouvoir antioxydant et anti-inflammatoire des polyphénols de la pomme et de la canneberge et élucider les mécanismes d'action dans les cellules Caco-2/15, un excellent modèle intestinal;

3- Identifier les voies d'absorption et de métabolisation des polyphénols de la canneberge dans les cellules Caco-2/15;

4- Évaluer la capacité des polyphénols de la pomme à contenir le stress oxydant et l'inflammation dans un modèle murin de MII, et en mesurer l'impact sur les anomalies cliniques.

5. MÉTHODOLOGIE

Trois principaux volets expérimentaux ont été envisagés :

Volet 1 : Définir le profil des polyphénols de la pelure de pomme et leurs actions sur le stress oxydant et l'inflammation au niveau intestinal;

Volet 2 : Caractériser les polyphénols des canneberges, définir leur métabolisme intraluminal, examiner leur caractère antioxydant et anti-inflammatoire, et élucider les mécanismes d'action;

Volet 3 : Évaluer les aspects préventifs et thérapeutiques des polyphénols sur les MII en spécifiant leurs bénéfices cliniques et voies mécanistiques.

Les publications qui découlent de ces volets expérimentaux et qui répondent aux objectifs du projet sont présentées dans la prochaine section.

6. ARTICLES

Article 1: « Apple peel polyphenols and their beneficial actions on oxidative stress and inflammation ».

Denis MC *et al*. Apple peel polyphenols and their beneficial actions on oxidative stress and inflammation. PLoSOne.2013; 8(1): e53725

Author Contributions:

Conceived and designed the experiments: MCD, CG, AF and EL. Performed the experiments: MCD, CG, AM and SD. Analyzed the data: MCD, ED and EL. Contributed reagents/materials/analysis tools: MCD, AF, CG, AM, YD and SD. Wrote the paper: MCD and EL.

Apple peel polyphenols and their beneficial actions on oxidative stress and inflammation

Marie-Claude Denis[1,2], Alexandra Furtos[3], Stéphanie Dudonné[4], Alain Montoudis[1], Carole Garofalo[1], Yves Desjardins[4] , Edgard Delvin[1,3], Emile Levy[1,2,4 *]

[1]Research Centre, CHU Sainte-Justine and [2]Departments of Nutrition, [3]Biochemistry, Université de Montréal, Montreal, Quebec, Canada, H3T 1C5
[4]Institute of Nutraceuticals and Functional foods (INAF), Université Laval, Quebec, Quebec, Canada, G1V 0A6

Running Head*: Antioxidant and anti-inflammatory effects of apple peel*

Key words List: Polyphenol; Peroxidation; Oxidative stress; PUFA; Cyclooxygenase; Inflammation; Transcription factors.

Address correspondence to: **Dr. Emile Levy*
GI-Nutrition Unit
Research Centre
CHU-Sainte-Justine
3175 Ste-Catherine Road
Montreal, Quebec, Canada H3T 1C5

ABSTRACT

Since gastrointestinal mucosa is constantly exposed to reactive oxygen species from various sources, the presence of antioxidants may contribute to the body's natural defenses against inflammatory diseases. **Hypothesis:** To define the polyphenols extracted from dried apple peels (DAPP) and determine their antioxidant and anti-inflammatory potential in the intestine. Caco-2/15 cells were used to study the role of DAPP preventive actions against oxidative stress (OxS) and inflammation induced by iron-ascorbate (Fe/Asc) and lipopolysaccharide (LPS), respectively. **Results:** The combination of HPLC with fluorescence detection, HPLC-ESI-MS TOF and UPLC-ESI-MS/MS QQQ allowed us to characterize the phenolic compounds present in the DAPP (phenolic acids, flavonol glycosides, flavan-3-ols, procyanidins). The addition of Fe/Asc to Caco-2/15 cells induced OxS as demonstrated by the rise in malondialdehyde, depletion of n-3 polyunsaturated fatty acids, and alterations in the activity of endogenous antioxidants (SOD, GPx, G-Red). However, preincubation with DAPP prevented Fe/Asc-mediated lipid peroxidation and counteracted LPS-mediated inflammation as evidenced by the down-regulation of cytokines (TNF-α and IL-6), and prostaglandin E2. The mechanisms of action triggered by DAPP induced also a down-regulation of cyclooxygenase-2 and nuclear factor-κB, respectively. These actions were accompanied by the induction of Nrf2 (orchestrating cellular antioxidant defenses and maintaining redox homeostasis), and PGC-1α (the "master controller" of mitochondrial biogenesis). **Conclusion**: Our findings provide evidence of the capacity of DAPP to reduce OxS and inflammation, two pivotal processes involved in inflammatory bowel diseases.

LIST OF ABBREVIATIONS

ARE;	Antioxidant response element
COX-2;	Cyclooxygenase-2
DAPP;	Dried apple peel
FA;	Fatty acid
Fer/Asc;	Iron-Ascorbate
GPx;	Glutathione peroxidase
G-Red;	Glutathione reductase
IBD;	Inflammatory bowel disease
IL-6;	Interleukin-6
LPS;	Lipopolysaccharide
MDA;	Malondialdehyde
NF-kB;	Nuclear factor-kappa B
Nrf-2;	Nuclear factor erythro-derived 2
OxS	Oxidative stress
PGC-1α;	Peroxisome proliferator-activated receptor gamma coactivator-1-a
PGE2;	Prostaglandin E2
PUFA;	Polyunsaturated fatty acid
ROS;	Reactive oxygen species
SOD;	Superoxide dismutase
TNF-α;	Tumor Necrosis Factor-α

INTRODUCTION

Gastrointestinal mucosa is constantly exposed to luminal oxidants from ingested nutrients, such as alcohol, cholesterol oxides, and key among these is the simultaneous consumption of iron salts and ascorbic acid, which can cause oxidative damage to biomolecules (447, 448). Moreover, local microbes or infections, ischemia/reperfusion, gastric acid production and nonsteroidal anti-inflammatory drugs may promote the formation of reactive radicals (449-451). Additionally, the intestinal mucosa is subject to prolonged oxidative stress (OxS) from reactive oxygen species (ROS) generated during aerobic metabolism (452, 453). The influx of neutrophils and monocytes associated with inflammation can further generate ROS via respiratory burst enzymes as well as those involved in prostaglandin and leukotriene metabolism (454). Even if the etiology of inflammatory bowel diseases (IBD) has yet to be fully elucidated, a close relationship has been noted between ROS and the mucosal inflammatory process (160, 455-458). Although the specific events by which oxidants contribute to inflammation are not entirely elucidated, potential mechanisms include the activation of cyclooxygenage-2 (COX-2) and the transcription factor nuclear factor-kappa B (NF-κB) by pro-oxidants, thereby resulting in the initiation of the expression of genes controlling several aspects of the inflammatory, immune and acute phase responses (459-463). Current epidemiological and experimental studies support a beneficial role of dietary polyphenols in several gastrointestinal diseases, including IBD (59, 329, 464). Polyphenols are the most abundant antioxidants in the diet, (i.e. fruit, vegetables, beverages, herbs and spices) (241, 465-468). However, their poor intestinal absorption is responsible for luminal concentrations of phenolic compounds up to several hundred μmols in the gastrointestinal tract (469). Most of these polyphenols exhibit powerful antioxidant activity by acting as free

radical scavengers, hydrogen donating compounds, singlet oxygen quenchers and metal ion chelators, while they are also able to induce cellular antioxidant defense modulating protein and gene expressions (465, 467, 468, 470). In the present investigation, we hypothesize that apple peel-derived polyphenols act in the gut as powerful antioxidants and anti-inflammatory agents capable of exerting protective effects against harmful intraluminal components in the gut, which may maintain the body's natural defenses against a variety of intestinal diseases, including IBD.

MATERIALS AND METHODS

Chemical and reagents

HPLC-grade acetonitrile, methanol, acetone and Optima grade water were from Fisher Scientific (New Jersey, USA). Formic acid was purchased from Fluka (Steinheim, Germany). MTT was from Sigma (MO, USA). Apple peel crude extract (AB powder) and a purified polyphenolic fraction (JC-047) derived from dried apple peel powder (DAPP) were supplied from Leahy Orchards Inc. and AppleBoost Products Inc.

DAPP extraction

The phenolic compounds of apples (80 % McIntosh and 20% a blend of Northern Spy, Cortland, Empire, Ida Red, Jonagold and Spartan) were extracted by a method similar to that reported previously by Liu's laboratory (465, 471, 472). Briefly, 25 g apple peels were blended with 200 g chilled 80% acetone solution in a Waring blender for 5 min. The sample was then homogenized for 3 min using a Virtis 45 homogenizer. The slurry was filtered through Whatman No. 1 filter paper in a Buchner funnel under vacuum. The solids were scraped into 150 g of 80% acetone and homogenized again for 3 min before refiltering. The filtrate was recovered and evaporated using a rotary evaporator at 45°C. This residue represented the apple peel crude extract (AB powder) while the purified polyphenolic fraction (JC-047) was isolated by preparative HPLC.

LC-MS analysis of DAPP crude extract and purified fraction

A reversed phase LC-MS method has been developed to separate and identify the mass and chemical structure of phenolic compounds derived from crude extract and purified fraction. Separations were performed on HPLC with fluorescence detection and HPLC-ESI-MS TOF (Agilent Technologies, Santa Clara, CA). The chromatographic column was a Halo C18, 3.0 x

100 mm, 2.7 µm particle sizes (Advanced Materials Technology Inc., Wilmington, DE) maintained at 50°C and operated at 0.3 mL/min. A two-step linear acetonitrile gradient was used for elution. The acetonitrile concentration was increased from 2 to 40 % over 20 min then from 40 to 90 % over the next 15 min followed by an equilibration step with the initial mobile phase composition for a total run time of 40 minutes. The mass spectrometer was operated in negative electrospray mode with a dual spray configuration allowing for internal calibration and therefore for a very good mass accuracy. This allowed us to extract narrow mass range peaks for quantitation purposes and increase the selectivity of the method. Mass spectra were acquired from m/z 100 to 2000 with an acquisition cycle of 0.89 s and a resolution greater than 10 000. The electrospray voltage was set at 3.5 kV, the fragmentor at 200 V and the source temperature at 300°C. Major phenolic compounds identified by HPLC-ESI-MS TOF were quantified by ultra-performance liquid chromatography system (UPLC) coupled to a tandem quadrupole mass spectrometer (MS/MS QQQ) equipped with an ESI source (UPLC-ESI-MS/MS QQQ). The UPLC-ESI-MS/MS QQQ system consisting of a Waters-ACQUITY UPLC with an AQUITY TDQ mass spectrometer (Waters, MA, USA). An Agilent Plus C18 column (2.1 x 100 mm, 1.8 µm particle sizes) (CA, USA) was used, and column temperature was maintained at 30°C. The phenolic compounds were separated using a gradient mobile phase consisted of 0.1% formic acid in ultrapure water and acetonitrile (solvent A and B respectively) with the flow rate of 0.4 µL/min. The following gradient was used: 0-8 min, 3-35% B; 8-9 min, 35-60% B; 9-10 min, 60-85% B; 10-11 min, 85% B; 11-11.10 min, 85-3% B; 11.10-14 min, 3% B. Data were acquired by MassLynx V4.1 software and processed for quantification with QuanLynx V4.1 (Waters, MA, USA). The UPLC-ESI-MS/MS QQQ system was operated with an ESI interface in negative ionization mode. Cone and collision gas

flow rates, obtained from a nitrogen generator N2 were 80 L/h and 900 L/h, respectively. The mass spectrometer parameters were defined with Waters IntelliStart software (automatic tuning and calibration of the AQUITY TQD), and manually optimized as follow: capillary voltage of 3 kV, source temperature at 130°C and desolvation temperature at 400°C. Cone voltage was 30 V, and collision energy was 18 eV for all phenolic compounds. Quantification was determined using multiple reactions monitoring mode for all transitions of phenolic acids, flavonols, flavan-3-ols, procyanidins and dihydrochalcones.

Determination of total phenolic content of DAPP crude extract and purified fraction

The total phenolic content of AB powder or JC-047 fraction was determined using the Folin-Ciocalteu method (473), with gallic acid as a main standard. Briefly, 100 µL Folin-Ciocalteu reagent (diluted 10-fold in ultrapure water) and 80 µL sodium carbonate solution (7.5% in ultrapure water) were added to 20 µL MeOH (50% solution of extracts) in a 96-well plate. A blank sample and five calibration solutions of gallic acid (12.5 to 200 µg/mL) were analyzed under the same conditions. After 1h-incubation at room temperature, the absorbance was measured at 765 nm using a Fisher Scientific Multiskan GO microplate reader (MA, USA). All determinations were carried out in triplicate and results were expressed as percentage of extract weight ± SEM.

Heterogeneity of fractionated oligomers and polymers of DAPP on normal-phase HPLC

The procyanidin composition of AB powder and purified JC-047 fraction was analyzed as previously described (474) by normal phase analytical HPLC using an Agilent 1260/1290 Infinity system. Samples (5 µL of 25 mg/mL solutions in acetone/ultrapure water/acetic acid, 70:29.5:0.5) were injected into the HPLC system, and the separation was performed at 35°C with a flow rate of 0.8 mL/min using a Develosil Diol column (250 mm × 4.6 mm, 5 µm

particle size), protected with a Cyano SecurityGuard column (Phenomenex, CA, USA). The elution was performed using a solvent system comprising solvents A (acetonitrile/acetic acid, 98:2) and B (methanol/water/acetic acid, 95:3:2) mixed using a linear gradient from 0% to 40% B in 35 min, 40% to 100% B in 40 min, 100% isocratic B in 45 min and 100% to 0% B in 50 min. The column was re-equilibrated for 5 min between samples. Fluorescence of the procyanidins was monitored at excitation and emission wavelengths of 230 and 321 nm with the fluorescence detector, set to low sensitivity with a gain of 7X for the entire run. Individual procyanidins with DP from DP1 to DP>10 were quantified using an external calibration curve of (-)-epicatechin, taking into account their relative response factors in fluorescence (475). The results were expressed as percentage of extract weight ± SEM.

Intestinal Caco-2/15 cell culture

The human epithelial colorectal adenocarcinoma Caco-2/15 cell line, a stable clone of the parent Caco-2 cells (American Type Culture Collection, Rockville, MD), was obtained from Dr. JF Beaulieu (Department of Cellular Biology, Faculty of Medicine, Université de Sherbrooke, Sherbrooke, Quebec, Canada). Intestinal Caco-2/15 cells were cultured as described previously (476-484). Briefly, they were grown in MEM supplemented with 10% decomplemented fetal bovine serum, 1% Penicillin-Streptomycin and 1% non-essential amino acids (all reagents from GIBCO-BRL, Grand Island, NY) at 37°C, 95% humidity and 5% CO_2 as described previously (476-484). Caco-2/15 cells were maintained in T-75 cm^2 flasks (Corning Glass Works, Corning, NY) and were split (1:5) when they reached 90% confluence using 0.05% trypsin-0.5mM EDTA (GIBCO-BRL). For individual experiments, cells were plated at a density of 1 X 10^6 cells/well on six-well culture plates, and were cultured for 10

days postconfluence, a period at which they are highly differentiated and appropriate for experimental treatments (476-484). The medium was refreshed every second day.

Caco-2/15 cell integrity

After various treatments, cell integrity was estimated by viability, morphology and differentiation assays. Briefly, cell differentiation was assessed by determination of villin protein expression. Monolayer intactness and physical barrier function were tested by evaluating morphology, transepithelial electric resistance and occludin protein expression. Finally, cell viability was appraised with 3-(4,5-dimethyldiazol-2-yl)-2,5 diphenyl Tetrazolium Bromid (MTT).

Induction of oxidative stress and inflammation

Differentiated intestinal Caco-2/15 cells were used to study the effects of the aforementioned polyphenols in OxS (Fe, 200 µM/Asc, 2 mM) and inflammation (LPS, 200 µg/mL) (483). Crude extract (AB powder, 250 µg/mL) and purified (JC-047, 250 µg/mL) fraction were added to the apical compartment of Caco-2/15 cells for 24h before incubation with iron/ascorbate (Fe/Asc) and/or lipopolysaccharide (LPS) for 6h at 37^{o}C. In order to distinguish between acute and chronic inflammation, Caco-2/15 cells were also incubated with LPS for a 24-h period. To highlight the mechanisms behind the beneficial actions of DAPP against OxS and inflammation, some experiments were carried out with 50 µM caffeic acid phenethyl ester (CAPE; Sigma, MO, USA) and 0.4 µM indomethacin heptyl esters (Cayman Chemical, Ann Arbor, MI) to inhibit NF-κB and COX-2, respectively.

Lipid peroxidation

Estimation of lipid peroxidation was assessed by measuring the release of malondialdehyde (MDA) from Caco-2/15 cells exposed to Fe/Asc (200 µM/2 mM) by HPLC. Briefly, proteins

were precipitated with 8% sodium tungstate (Na_2WO_4) (Aldrich, Milwaukee, WI). The protein-free supernatants were then reacted with an equivalent volume of 0.5% (wt/vol) thiobarbituric acid solution (TBA; Sigma, MO, USA) at 95°C for 60 min. After cooling to room temperature, the pink chromogene [MDA-$(TBA)_2$] was extracted with 1-butanol and dried over a stream of nitrogen at 50°C for 3 hours. The dry extract was then resuspended in 100% MeOH before MDA determination by HPLC with a fluorescence detection (Jasco Corporation, Tokyo, Japan) set at 515 nm excitation and 550 nm emission.

Fatty acid analysis

Following differentiation, Caco-2/15 cells were incubated for 6h at 37°C in the absence or presence of Fe/Asc (200 µM/2mM), LPS (200 µg/mL) or both following pre-incubation with 250 µg/mL AB powder or JC-047 fraction, cells were then homogenized in PBS containing 0.005% (w/v) 2,6-Di-tert-butyl-4-methylphenol (Sigma, St-Louis, MO). Samples were subjected to transesterification and injected into a gas chromatograph using a 90 m×0.32 mm WCOT-fused silica capillary column VF-23ms coated with 0.25 µm film thickness (Varian, Canada) according to the method described previously (485).

Endogenous antioxidant enzyme activities

Differentiated Caco-2/15 cells were harvested in hypotonic lysis buffer (10 mM HEPES, 1.5 mM $MgCl_2$, 10 mM KCl, 0.5 mM DTT, 0.2 mM PMSF). Total superoxide dismutase (SOD) activity was determined as described by McCord *et al*. (486). Briefly, superoxide radicals (O_2^-) were generated by the addition of xanthine and xanthine oxidase, and the oxidation of the SOD assay cocktail was followed using a spectrophotometer at 550 nm for 5 min. The same reaction was then repeated with the addition of the sample, and the SOD assay cocktail was less oxidized because of the SOD activity in the sample. The total SOD activity was then

calculated. For glutathione peroxidase (GPx) activity, aliquots of cell homogenates were added to a PBS buffer containing 10 mM GSH, 0.1 U G-Red and 2 mM NADPH with 1.5% H_2O_2 to initiate the reaction. Absorbance was monitored every 30 sec at 340 nm for 5 min (483). For G-Red activity, cell homogenates were added to a PBS buffer containing 2 mM NADPH and 10 mM of GSSG to initiate the reaction. Absorbance was monitored every 30 sec at 340 nm for 5 min (483).

Immunoblot analysis

Following the incubation with the various stimuli, differentiated Caco-2/15 cells were sonificated and the Bradford assay (Bio-Rad, Mississauga, Ontario) was used to determine the protein concentration of each sample. Proteins were denatured in sample buffer containing SDS and ß-mercaptoethanol, separated on a 7.5 % SDS-PAGE and electroblotted onto Hybond nitrocellulose membranes (Amersham, Baie D'Urfé, Quebec, Canada). Signals were detected with an enhanced chemiluminescence system for antigen-antibody complexes. No specific binding sites of the membranes were blocked using defatted milk proteins followed by the addition of one of the following primary antibodies: 1/1000 polyclonal anti-villin (94 kDa; BD Biosciences, Mississauga, Ontario); 1/1000 polyclonal anti-occludin (59 kDa; Abcam, Campbridge, MA); 1:1000 polyclonal anti-COX-2 (70 kDa; Novus, Oakville, ON); 1:10000 polyclonal anti-NF-κB (65 kDa; Santa Cruz Biotechnology, Santa Cruz, CA); 1:5000 polyclonal anti-IκB (39 kDa; Cell Signaling, Beverly MA); 1/5000 polyclonal anti- tumor necrosis factor (TNF)-α (26 kDa; R&D, Canada); 1/5000 monoclonal anti- interleukin (IL)-6 (25 kDa; R&D, Canada), 1/1000 polyclonal anti-Nrf2 (68 kDa; Abcam, MA, USA) and 1/1000 polyclonal anti-PGC-1α (92 kDa; Abcam, MA, USA), and 1:40000 monoclonal anti-β-actin (42 kDa; Sigma, MO, USA).

The relative amount of primary antibody was detected with specie-specific horseradish peroxidase-conjugated secondary antibody (Jackson Laboratory, Bar Harbor, Maine). The β-actin protein expression was determined to confirm equal loading. Molecular size markers (Fermentas, Glen Burie, Maryland) were simultaneously loaded on gels. Blots were developed and the protein mass was quantitated by densitometry using an HP Scanjet scanner equipped with a transparency adapter and the UN-SCAN-IT gel 6.1 software.

Prostaglandin E2 determination

Cellular prostaglandin E2 (PGE2) was measured by enzyme-linked immunosorbent assay (Arbor Assay, Michigan, USA). After a short incubation, the reaction was stopped and the intensity of the generated color was detected in a microtiter plate reader (EnVision Multilabel Plate Readers, PerkinElmer) capable of measuring 450 nm wavelengths.

Nuclear extraction for immunoblot analysis of NF-κB, Nrf2 and PGC-1α

Differentiated Caco-2/15 cells were washed twice with PBS and left on ice for 4 min in a lysis buffer containing 10 mM HEPES, 10 mM KCl, 1.5 mM $MgCl_2$, 2 mM DTT, and 0.4% Nonidet and antiproteases. Cells were then scraped and centrifuged for 5 min at 1,500 *g* at 4°C. Pellets were then washed with the same buffer, but without the Nonidet, and centrifuged again under the same conditions. The resulting pellets were then resuspended in 50 µL of final hypertonic lysis buffer (20 mM HEPES, 400 mM NaCl, 1.5 mM MgCl2, 0.2 mM EDTA, 2 1,4-dithio-DL-treitol, and 20% glycerol and antiproteases) and left on ice for 1h with vortexing. They were then centrifuged for 10 min at 10,000 *g* at 4^{o}C, and the supernatants were collected for protein and Western blotting to analyze NF-κB, nuclear factor erythroid-2-related factor 2 (Nrf2) and peroxisome proliferator-activated receptor gamma coactivator-1 alpha (PGC-1α protein expression.

Statistical analysis

All values are expressed as mean ± SEM. Data were analyzed by using a one-way analysis variance and the two-tailed Student's *t* test using the Prism 5.01 (GraphPad Software) and the differences between the means were assessed post-hoc using Tukey's test. Statistical significance was defined as $P<0.05$.

RESULTS

Profile of phenolic compounds of crude and purified DAPP

A reversed phase LC-MS method has been developed in order to separate and identify masses and chemical structures of polyphenolic compounds contained in the crude extract (AB powder) and purified polyphenol fraction (JC-047) derived from DAPP. Flavonoids figured among the major polyphenol classes: they were identified on the basis of their common structure consisting of two aromatic rings bound together by three carbon atoms that form an oxygenated heterocycle. Representative extracted ion chromatograms of identified polyphenolic compounds (using accurate mass measurement) are shown in Figures 1A and 2A. In the crude extract, flavonols constituted the dominant subclass of flavonoids and were present as a mixture of aglycone and glycosylated quercetin and dihydrochalcone (Figure 1B). Negative electrospray mass spectra of the deprotonated species $[M-H]^-$ were observed [Table 1 and Figure 1C and at m/z 463,090 for quercetin 3-O-glucoside (1A); quercetin 3-O-galactoside (1B); m/z 433,079 for quercetin 3-O-arabinoside (1C); m/z 447,079 for quercetin 3-O-xyloside (1D); m/z 447,095 for quercetin 3-O-rhamnoside (1E) and m/z 435,131 for phloridzin (1F)]. On the other hand, the purified fraction was mainly composed of catechin, epicatechin and their oligomers eluting between 15 to 18 min (Figure 2B). Extracted ion chromatograms at m/z 289.076 are shown (+)-catechin eluting at 15.4 min and (-)-epicatechin eluting at 16.9 min (Figure 2B, left). The trimeric oligomers as proanthocyanidin trimer C1-C4 (Figure 2B, right) share the same m/z of 865.199 (Figure 2C). Colorimetric methods, including the Folin-Ciocalteu, were used for quantifying total phenolics content. The purified fraction contains a higher proportion (26%, $P<0.01$) of total phenolic compounds (1900 ± 160 mg of gallic acid equivalents/100 g of extract weight) compared to the crude extract (1410 ±

120 mg of gallic acid equivalents/100 g of extract weight). Furthermore, the combination of high performance liquid chromatography system (HPLC), coupled to a time-of-flight mass spectrometer (TOF) equipped with an HPLC-ESI-MS TOF; and UPLC-ESI-MS/MS QQQ analysis revealed higher amounts (mg/100 g) of flavonols + procyanidins and phenolic acids in purified JC-047 fraction compared to controls (137 ± 9 vs. 369 ± 10 and 74 ± 1 vs. 43.0 ± 6, respectively). However, the crude extract (AB powder) contained more flavonols and dihydrochalcones than the purified JC-047 fraction (346 ± 14 vs. 207 ± 16 and 261 ± 6 vs. 255 ± 11, respectively).

The distribution of oligomers in the AB powder and JC-047 fraction was from degrees of polymerization (DP1 to DP10) [Table 2 and Figure 3]. However, the determination of total procyanidins content was 3 times higher in the JC-047 compared to the AB powder extract (Table 2)**.** No procyanidin oligomers higher than decamers were detected in the polymeric procyanidin signal.

Cell integrity following various treatments

The effects of Fe/Asc and LPS on Caco-2/15 cells integrity were examined by morphology assessment, protein content quantification and MTT assay after incubation periods of 6 and 24h. The morphology and the protein content remained unchanged with the administration of Fe/Asc, LPS and their combination, as well as following treatment with the AB powder or JC-047 (data not shown). Similarly, Caco-2/15 cell viability was not affected by the addition of the various treatments (Figure 4). Interestingly, an enhancement of villin protein mass was observed when Caco-2/15 cells were cultured in the presence of AB powder. Finally, there was no impact on Caco-2/15 cell monolayer transepithelial resistance (an indicator of cell confluence and monolayer integrity) (Figure 4) and on occludin protein mass (a biomarker for

tight junction and mucosal barrier functions) (Figure 4). Therefore, it could be concluded that our experimental conditions, including the use of DAPP, did not exert any cytotoxic effects on Caco-2/15 cells.

Effects of DAPP on lipid peroxidation

The extent of lipid peroxidation following the treatment of Caco-2/15 cells with Fe/Asc during 6h was assessed by determining cellular levels of MDA. HPLC analyses indicated a four-fold increase in MDA (P<0,001) following the administration of the oxygen free radical-generating system Fe/Asc compared to controls (Figure 5A). The presence of the AB powder or JC-047 fraction counteracted Fe/Asc-mediated lipid peroxidation with a more favorable impact of the former.

Since OxS markedly altered the composition and properties of the bilayer lipid environment, we determined the profile of fatty acids (FA). In fact, the addition of Fe/Asc resulted in substantial differences in FA following the 6h-period of cell incubation (Table 3). In particular, a significant decrease was noted in n-3 and n-6 polyunsaturated fatty acids (PUFA) (EPA, 20:5n-3; DHA, 22:6n-3; AA 20:4n-6) as well as in monounsaturated FAs (18:1n-9) (Table 2). As a consequence, the calculated total n-3, n-6 and n-9 was reduced by 3-fold, 0.5-fold and 2-fold compared to controls (Table 3). As n-3 FAs were more affected by OxS than n-6 FAs, a decline was recorded in the ratio n-6/n-3, which indicates an inflammatory state. Nevertheless, preincubation with the AB powder or JC-047 fraction restored the levels and composition of PUFAs.

Mechanisms for the action of DAPP on oxidative stress

As failure of antioxidant defense may explain the induction of OxS, we examined various endogenous antioxidant enzymes in Caco-2/15 cell line. Treatment with Fe/Asc alone or in

combination with LPS caused a significant augmentation in the SOD activity, but preincubation of Caco-2/15 cells with the AB powder or JC-047 fraction blunted the effects of OxS and inflammation (Figure 5B). Under these conditions, GPx activity was down-regulated by Fe/Asc and LPS, and restored by treatment with the AB powder or JC-047 (Figure 5C). On the other hand, G-Red (Figure 5D) showed a trend of increase with the polyphenol treatments.

Effects of DAPP on inflammatory markers

Cytokines and eicosanoids are pro-inflammatory compounds produced by the cells in response to injury. We therefore assessed the production of TNF-α and IL-6, two powerful inflammatory biomarkers, in Caco-2/15 cells incubated with Fe/Asc, LPS or their combination for 6h. Analysis by Western Blot disclosed an elevation of protein mass of TNF-α (1.5 to 2.0-fold) and IL-6 (1.5 to 1.8-fold) in the presence of Fe/Asc and LPS, respectively, compared to control cells (Figure 6). Pre-treatment with the AB powder or JC-047 fraction abolished the increase in TNF-α and IL-6 protein expression in Caco-2/15 cell line.

We next turned to the formation of inflammatory eicosanoids such as PGE2 that is synthesized from arachidonic acid by COX-2. Our experiments showed that Fe/Asc and LPS elicited exaggerated synthesis of PGE2 whereas preincubation with the AB powder displayed high ability to prevent PGE2 accumulation in response to LPS but not Fe/Asc (Figure 6).

Mechanisms for the action of DAPP on inflammation

Since the COX-2 enzyme may be behind the elevation of Fe/Asc- and LPS-induced PGE2, we determined its protein expression. Both stimuli raised its protein mass as evidenced by Western blot (Figure 7). Pre-incubation of Caco-2/15 cells with the AB powder or JC-047 fraction averted the positive action of the oxidative and inflammatory stimuli on COX-2 protein expression. Importantly, the polyphenol antioxidants were as effective as indomethacin

heptyl ester, a selective COX-2 inhibitor (487) in preventing the elevation of PGE2. In addition, their combination provided a more substantial synergetic effect, which is indicative of different mechanisms of action for LPS-induced inflammation (Figure 8).

Mechanisms for the action of DAPP on transcription factors

NF-κB signaling pathway plays a crucial role in the initiation and amplification of inflammation via the modulation of multiple inflammatory mediators. Figure 9 shows that Caco-2/15 cells exposed to Fe/Asc or LPS displayed a high NF-κB signal in the nucleus along with a low level of IκB protein expression in the cytoplasm, which suggests that the inhibitory protein is degraded by the proteasome, leaving NF-κB free to enter the nucleus and activate the transcription of its target genes. As a consequence, the NF-κB/IκB ratio was increased under the presence of Fe/Asc (Figure 9A) and LPS (Figure 9B and 7C). Importantly, the AB powder or JC-047 fraction displayed their great potential to neutralize IκB degradation and NF-κB mobilization to the nucleus compared to CAPE, the NF-κB inhibitor, with LPS at 6h (Figure 9B) and LPS at 24h (Figure 9C) to mimic an acute and a long inflammation, respectively. The combined administration of CAPE and AB powder or JC-047 fraction did not produce significant changes, thereby indicating the same mechanisms of action.

To decipher the mechanisms of action of the AB powder or JC-047 fraction, we examined the transcription factors that are involved in the regulation of antioxidant genes expression. The protein mass of Nrf2 in homogenates (Figure 10A) and nuclei (Figure 10B) was down-regulated by Fe/Asc- or LPS-induced OxS and inflammation, respectively. However, treatment with the AB powder or JC-047 fraction restored Nrf2 protein expression to the basal level. We also assessed the protein expression of PGC-1α a powerful transcriptional co-activator that up-regulates Nrf2. PGC-1α protein mass was down-regulated in response to OxS

and inflammation in homogenates (Figure 10C) and nuclei (Figure 10D) in Caco-2/15 cells. However, the effect was reestablished when Caco-2/15 cells were pre-incubated with the AB powder or JC-047 fraction.

DISCUSSION

Growing evidence suggests important roles of dietary factors in preserving health and even reversing the progression of chronic diseases, with anti-inflammatory effects as important underlying mechanisms. In the present study, we first characterize the polyphenol compounds of DAPP by HPLC-ESI-MS TOF and then tested their impact on cell integrity and viability. After we excluded any possible toxicity of this natural DAPP (crude extract) and its purified fraction, which has frequently been detected in various chemical drugs, we could subsequently document their remarkable capacity in scavenging ROS and neutralizing inflammation in intestinal absorptive cells. By dissecting the mechanisms of action, our *in vitro* experiments highlighted the ability of apple peel polyphenols to increase the antioxidant/anti-inflammatory defense by (i) preventing LPS-induced inflammation via limitation of the pro-inflammatory expression and activity of COX-2; (ii) ruling out LPS-mediated cytokine production through downregulation of NF-κB, an essential transcription factor for numerous cytokines and (iii) up-regulating the expression of transcription factors (Nrf2 and PGC-1α), key redox-sensitive transcription factors and crucial elements for mitochondrial biogenesis.

The results of our comprehensive study provide fundamental information on the apple peel polyphenols. The high-resolution HPLC-ESI-MS TOF delivers the composition of the different biomolecules in DAPP (AB powder or JC-047 fraction). In the former, flavonols (composed of aglycone and glycosylated quercetin and dihydrochalcone) are the major subclasses of flavonoids present, while in the purified fraction, we mostly found the flavan-3-ols and their oligomers. Noteworthy, quercetin represents the preponderant flavonol in DAPP and, according to previous studies; it has exhibited anti-inflammatory and antioxidant activities, prevented platelet aggregation and promoted relaxation of cardiovascular smooth

muscle (488). As a matter of fact, flavan-3-ols are a family of bioactive compounds and potent antioxidants as has been described in *in vitro* and *in vivo* studies. Importantly, in the current work, we have evaluated the antioxidant and anti-inflammation power of both the crude extract (AB powder) and purified polyphenol fraction (JC-047) derived from DAPP since there was a need to prove that the beneficial effects are derived from the polyphenos contained in apple peels.

In the present work, we used the Caco-2/15 cell line that undergoes a process of spontaneous differentiation leading to the formation of a monolayer of cells expressing several morphological and functional characteristics of the mature enterocyte. This remarkable intestinal model is regarded as the most appropriate for the investigation of gut absorption and interactions, nutrition, toxicology food microbiology, bioavailability tests, and screening of drug permeability in discovery programs. Multiple studies from our laboratory have shown that Caco-2/15 cell monolayers are fully appropriate for the study of OxS and inflammation (480, 481, 483, 489).

To produce OxS, we employed the Fe/Asc complex, a widely used oxygen-radical generating system (476, 478, 481, 483, 484) since our laboratory reported the ability of iron to initiate strong lipid peroxidation, whereas ascorbic acid can amplify iron-oxidative potential by promoting metal ion-induced lipid peroxidation (476). The data of the present study clearly indicate that the Fe/Asc system functioned as a producer of lipid peroxidation given the production of MDA and the degradation of PUFAs and the production of pro-inflammatory eicosanoids. Additionally, with the Fe/Asc complex, the antioxidant/oxidative balance deteriorated the endogenous antioxidant enzymes. In this context, co-supplementation of iron and vitamin C worsens OxS in the gastrointestinal tract, thereby leading to ulceration in

healthy individuals, and exacerbates chronic gastrointestinal inflammatory diseases, which may result in the development of cancers (490). Importantly, supplementation of DAPP by crude extract or its purified fraction significantly prevented lipid peroxidation and restored the depletion of some n-3 PUFA, likely by strengthening the endogenous antioxidant defense as illustrated, in our results, through SOD down-regulation and GPx up-regulation activities.

For the induction of inflammation, we used LPS that has been extensively studied for the past two decades. This is a ubiquitous endotoxin mediator of gram-negative bacteria, which facilitates microbial translocation by a mechanism implicating physical perturbation of the gut mucosal barrier (447, 491). LPS is also a potent inducer of the host's immune response via its capacity to stimulate the pro-inflammatory cytokine cascade. In our studies, LPS led to amplification of the inflammatory response in Caco-2/15 cells given the enhanced production of PGE2 and the raised protein expression of TNF-α and IL-6, probably due to elevated COX-2 and NF-κB, respectively. DAPP was effective in preventing the elevation of PGE2, TNF-α and IL-6 via the down-regulation of COX-2 and NF-κB, as evidenced by the co-administration of their specific inhibitors indomethacin heptyl ester and CAPE, respectively. The combination of CAPE and DAPP (either as crude extract or its purified JC-047 fraction) did not further anti-inflammatory benefits, which suggests a common mechanism of action. On the other hand, compounding indomethacin heptyl ester and DAPP resulted in amplified anti-inflammatory effects, which argues in favor of synergetic mechanisms.

Since the Keap1-Nrf2-antioxidant response element (ARE) is an integrated redox sensitive signaling system that regulates from 1% to 10% of our genes (492, 493), we assessed the protein expression of Nrf2 and could document its significant increase. It is therefore possible that, upon exposure to AB powder or JC-047 fraction, Nrf2 was able to escape Keap1-

mediated ubiquitin-dependent proteasomal degradation, translocate to the nucleus, and activate ARE-dependent gene expression of a series of antioxidative and cytoprotective proteins that include SOD and GPx. Our study went even further since it revealed the positive modulation of PGC-1α by DAPP. PGC-1α controls many aspects of oxidative metabolism, including mitochondrial biogenesis and respiration through the coactivation of many nuclear receptors (494, 495). As an example, Nrf2 is a key target of the PGC-1α in mitochondrial biogenesis and important protective molecules against ROS generation and damage. It is therefore possible that PGC-1α activates NRF2 to induce the SOD and GPx that were altered by Fe/Asc-mediated lipid peroxidation. However, additional efforts are needed to understand the role of DAPP in PGC-1α and Nrf2 cross-talk.

Noteworthy, in some experiments, Caco-2/15 cells were serum-starved for 24h prior to the addition OxS or inflammation. The serum-depleted media were used to minimize the formation of adducts between DAPP and serum proteins, and to exclude the interferences originating from available factors present in fetal bovine serum, as described in previous studies with other types of antioxidants (496). The pre-incubation time of 24h with DAPP was used to maximally strengthen the antioxidant and anti-inflammatory defense before the addition of the iron-ascorbate oxygen radical-generating system or LPS that triggers inflammation. By allocating this period of time, we allow Caco-2/15 cells to deploy various powerful protection mechanisms via transcription factors and signaling pathways. The transport and processing of DAPP have been elaborated in the Discussion section.

Following their consumption, polyphenols are extensively metabolized by hydrolyzing and conjugating enzymes (497, 498). They are first conjugated in the small intestine to form O-glucuronides, sulphate esters and O-methyl ether (499) before reaching the liver for further

metabolism (500). The formation of anionic derivatives by conjugation with glucuronides and sulphate groups facilitates their urinary and biliary excretion and explains their rapid elimination. Non-absorbed polyphenols and the fraction re-excreted by the bile are extensively metabolized and transformed by the microbiota before absorption (501, 502). The transformation by commensal bacteria via esterase, glucosidase, demethylation, dehydroxylation, and decarboxylation is often essential for absorption and modulates the biological activity of these polyphenols (502). In our intestinal model, no flora is present, which suggests an absorption via paracellular route of transport as suggested previously (503). However, additional studies are still needed to highlight the contribution of trans-membrane vs. intercellular absorption as well as the influence of polyphenols of enterocyte metabolism just by adherence to the brush border membrane.

Previous studies investigated the preventive effectiveness of polyphenolic content of flesh apple in cultured gastric mucous cells under conditions independent of acid secretion or systemic factors (504). They identified the composition of phenolic compounds (chlorogenic acid, caffeic acid, catechin, epicatechin, rutin and phloridizin) in apple flesh extracts, which prevented OxS-induced injury to gastric epithelial cells by permeating cell membranes, increasing intracellular antioxidant activity, and inhibiting ROS-dependent lipid peroxidation. In further studies, the same apple flesh extracts demonstrated prevention of aspirin-induced damage to the rat gastric mucosa (505) and an anti-inflammatory effect on colonic injury in rats with trinitrobenzensulphonic acid-induced colitis (506). Even though these reports with apple flesh extracts, and ours with DAPP show anti-inflammatory and antioxidant effects, it is not possible to compare their effectiveness given the differences in the apple species, extraction methodology, experimental models and techniques.

In conclusion, a plethora of studies demonstrates significant health benefits of nutrient rich fruits. If various studies have shown this relationship by indirect evidences, the present work demonstrated the presence of a nonpolar bioactivity in extracts of DAPP and their direct beneficial actions, which negated operational OxS and inflammation, both elicited by state-of-the-art techniques. Our results suggest that DAPP may represent a new strategy for the prevention of OxS and inflammation associated with IBD. Further studies are needed to investigate this hypothesis.

COMPETING INTERESTS

The authors have declared that no competing interests exist.

ACKNOWLEDGMENTS

The authors thank Leahy Orchards Inc. and Appleboost Products Inc. for supplying DAPP and for providing substantial support. Mrs Schohraya Spahis is acknowledged for excellent technical assistance.

REFERENCES

1. Parks DA (1989) Oxygen radicals: mediators of gastrointestinal pathophysiology. Gut 30: 293-298.
2. Young IS, Woodside JV (2001) Antioxidants in health and disease. J Clin Pathol 54: 176-186.
3. Biswas K, Bandyopadhyay U, Chattopadhyay I, Varadaraj A, Ali E et al. (2003) A novel antioxidant and antiapoptotic role of omeprazole to block gastric ulcer through scavenging of hydroxyl radical. J Biol Chem 278: 10993-11001.
4. Parks DA, Williams TK, Beckman JS (1988) Conversion of xanthine dehydrogenase to oxidase in ischemic rat intestine: a reevaluation. Am J Physiol 254: G768-G774.
5. Sanchez S, Martin MJ, Ortiz P, Motilva V, Alarcon dlL (2002) Effects of dipyrone on inflammatory infiltration and oxidative metabolism in gastric mucosa: comparison with acetaminophen and diclofenac. Dig Dis Sci 47: 1389-1398.
6. Brown DI, Griendling KK (2009) Nox proteins in signal transduction. Free Radic Biol Med 47: 1239-1253.
7. Gillespie MN, Pastukh V, Ruchko MV (2009) Oxidative DNA modifications in hypoxic signaling. Ann N Y Acad Sci 1177: 140-150.
8. Babbs CF (1992) Oxygen radicals in ulcerative colitis. Free Radic Biol Med 13: 169-181.
9. Fiocchi C (1998) Inflammatory bowel disease: etiology and pathogenesis. Gastroenterology 115: 182-205.

10. Kruidenier L, Verspaget HW (2002) Review article: oxidative stress as a pathogenic factor in inflammatory bowel disease--radicals or ridiculous? Aliment Pharmacol Ther 16: 1997-2015.

11. Nishikawa M, Oshitani N, Matsumoto T, Nishigami T, Arakawa T et al. (2005) Accumulation of mitochondrial DNA mutation with colorectal carcinogenesis in ulcerative colitis. Br J Cancer 93: 331-337.

12. Pravda J (2005) Radical induction theory of ulcerative colitis. World J Gastroenterol 11: 2371-2384.

13. Rezaie A, Parker RD, Abdollahi M (2007) Oxidative stress and pathogenesis of inflammatory bowel disease: an epiphenomenon or the cause? Dig Dis Sci 52: 2015-2021.

14. Bonizzi G, Piette J, Schoonbroodt S, Greimers R, Havard L et al. (1999) Reactive oxygen intermediate-dependent NF-kappaB activation by interleukin-1beta requires 5-lipoxygenase or NADPH oxidase activity. Mol Cell Biol 19: 1950-1960.

15. Campbell KJ, Perkins ND (2006) Regulation of NF-kappaB function. Biochem Soc Symp 165-180.

16. Natarajan R, Ghosh S, Fisher BJ, Diegelmann RF, Willey A et al. (2001) Redox imbalance in Crohn's disease intestinal smooth muscle cells causes NF-kappaB-mediated spontaneous interleukin-8 secretion. J Interferon Cytokine Res 21: 349-359.

17. Schreck R, Rieber P, Baeuerle PA (1991) Reactive oxygen intermediates as apparently widely used messengers in the activation of the NF-kappa B transcription factor and HIV-1. EMBO J 10: 2247-2258.

18. Sen CK, Packer L (1996) Antioxidant and redox regulation of gene transcription. FASEB J 10: 709-720.

19. Carrasco-Pozo C, Speisky H, Brunser O, Pastene E, Gotteland M (2011) Apple peel polyphenols protect against gastrointestinal mucosa alterations induced by indomethacin in rats. J Agric Food Chem 59: 6459-6466.

20. Romier B, Schneider YJ, Larondelle Y, During A (2009) Dietary polyphenols can modulate the intestinal inflammatory response. Nutr Rev 67: 363-378.

21. Shapiro H, Singer P, Halpern Z, Bruck R (2007) Polyphenols in the treatment of inflammatory bowel disease and acute pancreatitis. Gut 56: 426-435.

22. Eberhardt MV, Lee CY, Liu RH (2000) Antioxidant activity of fresh apples. Nature 405: 903-904.

23. Kang NJ, Shin SH, Lee HJ, Lee KW (2011) Polyphenols as small molecular inhibitors of signaling cascades in carcinogenesis. Pharmacol Ther 130: 310-324.

24. Korycka-Dahl MB, Richardson T (1978) Activated oxygen species and oxidation of food constituents. CRC Crit Rev Food Sci Nutr 10: 209-241.

25. Lavelli V, Hippeli S, Peri C, Elstner EF (1999) Evaluation of radical scavenging activity of fresh and air-dried tomatoes by three model reactions. J Agric Food Chem 47: 3826-3831.

26. Manach C, Scalbert A, Morand C, Remesy C, Jimenez L (2004) Polyphenols: food sources and bioavailability. Am J Clin Nutr 79: 727-747.

27. Scalbert A, Deprez S, Mila I, Albrecht AM, Huneau JF et al. (2000) Proanthocyanidins and human health: systemic effects and local effects in the gut. Biofactors 13: 115-120.

28. Kim DO, Lee KW, Lee HJ, Lee CY (2002) Vitamin C equivalent antioxidant capacity (VCEAC) of phenolic phytochemicals. J Agric Food Chem 50: 3713-3717.

29. Wolfe K, Wu X, Liu RH (2003) Antioxidant activity of apple peels. J Agric Food Chem 51: 609-614.

30. He X, Liu RH (2008) Phytochemicals of apple peels: isolation, structure elucidation, and their antiproliferative and antioxidant activities. J Agric Food Chem 56: 9905-9910.

31. Kevers C, Pincemail J, Tabart J, Defraigne JO, Dommes J (2011) Influence of cultivar, harvest time, storage conditions, and peeling on the antioxidant capacity and phenolic and ascorbic acid contents of apples and pears. J Agric Food Chem 59: 6165-6171.

32. Brownmiller C, Howard LR, Prior RL (2009) Processing and storage effects on procyanidin composition and concentration of processed blueberry products. J Agric Food Chem 57: 1896-1902.

33. Prior RL, Gu L (2005) Occurrence and biological significance of proanthocyanidins in the American diet. Phytochemistry 66: 2264-2280.

34. Bernotti S, Seidman E, Sinnett D, Brunet S, Dionne S et al. (2003) Inflammatory reaction without endogenous antioxidant response in Caco-2 cells exposed to iron/ascorbate-mediated lipid peroxidation. Am J Physiol Gastrointest Liver Physiol 285: G898-G906.

35. Courtois F, Delvin E, Ledoux M, Seidman E, Lavoie JC et al. (2002) The antioxidant BHT normalizes some oxidative effects of iron + ascorbate on lipid metabolism in Caco-2 cells. J Nutr 132: 1289-1292.

36. Courtois F, Seidman EG, Delvin E, Asselin C, Bernotti S et al. (2003) Membrane peroxidation by lipopolysaccharide and iron-ascorbate adversely affects Caco-2 cell function: beneficial role of butyric acid. Am J Clin Nutr 77: 744-750.

37. Levy E, Mehran M, Seidman E (1995) Caco-2 cells as a model for intestinal lipoprotein synthesis and secretion. FASEB J 9: 626-635.

38. Levy E, Trudel K, Bendayan M, Seidman E, Delvin E et al. (2007) Biological role, protein expression, subcellular localization, and oxidative stress response of paraoxonase 2 in the intestine of humans and rats. Am J Physiol Gastrointest Liver Physiol 293: G1252-G1261.

39. Marcil V, Seidman E, Sinnett D, Boudreau F, Gendron FP et al. (2010) Modification in oxidative stress, inflammation, and lipoprotein assembly in response to hepatocyte nuclear factor 4alpha knockdown in intestinal epithelial cells. J Biol Chem 285: 40448-40460.

40. Precourt LP, Seidman E, Delvin E, Amre D, Deslandres C et al. (2009) Comparative expression analysis reveals differences in the regulation of intestinal paraoxonase family members. Int J Biochem Cell Biol 41: 1628-1637.

41. Precourt LP, Marcil V, Ntimbane T, Taha R, Lavoie JC et al. (2012) Antioxidative properties of paraoxonase 2 in intestinal epithelial cells. Am J Physiol Gastrointest Liver Physiol .

42. Taha R, Seidman E, Mailhot G, Boudreau F, Gendron FP et al. (2010) Oxidative stress and mitochondrial functions in the intestinal Caco-2/15 cell line. PLoS One 5: e11817.

43. Spahis S, Vanasse M, Belanger SA, Ghadirian P, Grenier E et al. (2008) Lipid profile, fatty acid composition and pro- and anti-oxidant status in pediatric patients with attention-deficit/hyperactivity disorder. Prostaglandins Leukot Essent Fatty Acids 79: 47-53.

44. McCord JM, Fridovich I (1969) Superoxide dismutase. An enzymic function for erythrocuprein (hemocuprein). J Biol Chem 244: 6049-6055.

45. Kalgutkar AS, Marnett AB, Crews BC, Remmel RP, Marnett LJ (2000) Ester and amide derivatives of the nonsteroidal antiinflammatory drug, indomethacin, as selective cyclooxygenase-2 inhibitors. J Med Chem 43: 2860-2870.

46. Moon SK, Cho GO, Jung SY, Gal SW, Kwon TK et al. (2003) Quercetin exerts multiple inhibitory effects on vascular smooth muscle cells: role of ERK1/2, cell-cycle regulation, and matrix metalloproteinase-9. Biochem Biophys Res Commun 301: 1069-1078.

47. Brunet S, Thibault L, Lepage G, Seidman EG, Dube N et al. (2000) Modulation of endoplasmic reticulum-bound cholesterol regulatory enzymes by iron/ascorbate-mediated lipid peroxidation. Free Radic Biol Med 28: 46-54.

48. Qutub AA, Popel AS (2008) Reactive oxygen species regulate hypoxia-inducible factor 1alpha differentially in cancer and ischemia. Mol Cell Biol 28: 5106-5119.

49. Wells CL, Jechorek RP, Olmsted SB, Erlandsen SL (1993) Effect of LPS on epithelial integrity and bacterial uptake in the polarized human enterocyte-like cell line Caco-2. Circ Shock 40: 276-288.

50. Tkachev VO, Menshchikova EB, Zenkov NK (2011) Mechanism of the Nrf2/Keap1/ARE signaling system. Biochemistry (Mosc) 76: 407-422.

51. Li J, Lee JM, Johnson JA (2002) Microarray analysis reveals an antioxidant responsive element-driven gene set involved in conferring protection from an oxidative stress-induced apoptosis in IMR-32 cells. J Biol Chem 277: 388-394.

52. Martinez-Jimenez CP, Gomez-Lechon MJ, Castell JV, Jover R (2006) Underexpressed coactivators PGC1alpha and SRC1 impair hepatocyte nuclear factor 4 alpha function and promote dedifferentiation in human hepatoma cells. J Biol Chem 281: 29840-29849.

53. Ramachandran B, Yu G, Gulick T (2008) Nuclear respiratory factor 1 controls myocyte enhancer factor 2A transcription to provide a mechanism for coordinate expression of respiratory chain subunits. J Biol Chem 283: 11935-11946.

54. Tang Y, Zheng S, Chen A (2009) Curcumin eliminates leptin's effects on hepatic stellate cell activation via interrupting leptin signaling. Endocrinology 150: 3011-3020.

55. Scalbert A, Morand C, Manach C, Remesy C (2002) Absorption and metabolism of polyphenols in the gut and impact on health. Biomed Pharmacother 56: 276-282.

56. Manach C, Scalbert A, Morand C, Remesy C, Jimenez L (2004) Polyphenols: food sources and bioavailability. Am J Clin Nutr 79: 727-747.

57. Crespy V, Aprikian O, Morand C, Besson C, Manach C et al. (2001) Bioavailability of phloretin and phloridzin in rats. J Nutr 131: 3227-3230.

58. Donovan JL, Crespy V, Manach C, Morand C, Besson C et al. (2001) Catechin is metabolized by both the small intestine and liver of rats. J Nutr 131: 1753-1757.

59. Selma MV, Espin JC, Tomas-Barberan FA (2009) Interaction between phenolics and gut microbiota: role in human health. J Agric Food Chem 57: 6485-6501.

60. Blaut M, Clavel T (2007) Metabolic diversity of the intestinal microbiota: implications for health and disease. J Nutr 137: 751S-755S.

61. Kosinska A, Andlauer W (2012) Cocoa polyphenols are absorbed in Caco-2 cell model of intestinal epithelium. Food Chem 135: 999-1005.

62. Graziani G, D'Argenio G, Tuccillo C, Loguercio C, Ritieni A et al. (2005) Apple polyphenol extracts prevent damage to human gastric epithelial cells in vitro and to rat gastric mucosa in vivo. Gut 54: 193-200.

63. D'Argenio G, Mazzone G, Tuccillo C, Grandone I, Gravina AG et al. (2008) Apple polyphenol extracts prevent aspirin-induced damage to the rat gastric mucosa. Br J Nutr 100: 1228-1236.

64. D'Argenio G, Mazzone G, Tuccillo C, Ribecco MT, Graziani G et al. (2012) Apple polyphenols extract (APE) improves colon damage in a rat model of colitis. Dig Liver Dis 44: 555-562.

Table 1: Identification of procyanidins in DAPP

AB powder		Formula	Ion formula $[M-H]^-$	Experimental mass (m/z)	Theoretical mass (m/z)	Diff. ppm (< 5 ppm)
Flavonols	Quercetin 3-O-glucoside	$C_{21}H_{20}O_{12}$	$C_{21}H_{19}O_{12}$	463,09050	463,08820	4.96
	Quercetin 3-O-galactoside	$C_{21}H_{20}O_{12}$	$C_{21}H_{19}O_{12}$	463,09018	463,08820	4.27
	Quercetin 3-O-arabinoside	$C_{20}H_{18}O_{11}$	$C_{20}H_{17}O_{11}$	433,07914	433,07763	3.47
	Quercetin 3-O-xyloside	$C_{20}H_{18}O_{11}$	$C_{20}H_{17}O_{11}$	433,07977	433,07763	4.92
	Quercetin 3-O-rhamnoside	$C_{21}H_{20}O_{11}$	$C_{21}H_{19}O_{11}$	447,09506	447,09329	3.96
Dihydrochalcone	Phloridzin	$C_{21}H_{24}O_{10}$	$C_{21}H_{23}O_{10}$	435,13171	435,12967	4.68

Experimental mass measurement and empirical formula calculation for quercetin glycosides and dihydrochalcone. A good agreement between the theoretical and the experimental m/z values was obtained for all compounds examined (< 5 ppm). Separations were performed on an 1100 LC system coupled to an ESI-MSD-TOF mass spectrometer (Agilent Technologies, Santa Clara, CA).

Table 2: Heterogeneity of fractionated procyanidin oligomers and polymers of DAPP on normal-Phase HPLC

Procyanidin content	DAPP (mg/100 g extract weight)	
	Crude extract (AB powder)	**Purified fraction (JC-047)**
Monomers	25.0 ± 0.4	42.0 ± 1.0***
Dimers	38.0 ± 3.0	97.0 ± 2.0***
Trimers	19.0 ± 2.0	53.0 ± 2.0***
Tetramers	13.0 ± 1.0	46.0 ± 1.0***
Pentamers	10.0 ± 0.3	34.0 ± 2.0***
Hexamers	9.0 ± 1.0	29.0 ± 2.0***
Heptamers	4.0 ± 0.3	13.0 ± 1.0*
Octamers	2.0 ± 0.1	6.0 ± 1.0
Nonamers	2.0 ± 0.5	7.0 ± 1.0
Decamers	1.0 ± 1.0	2.0 ± 0.5
Polymers DP>10	13.0 ± 5.0	40.0 ± 4.0***
Total	**137.0 ± 9.0**	**369.0 ± 10.0*** **

The procyanidin composition of DAPP from 25 mg/mL crude extract (AB powder) and purified fraction (JC-047) was analyzed by normal phase analytical HPLC using an Agilent 1260/1290 Infinity system coupled to a fluorescence detector. Individual procyanidins with degrees of polymerization (DP) from DP1 to DP>10 were quantified using external calibration curve of (-)-epicatechin, taking into account their relative response factors in fluorescence. The results were expressed as mg/100 g of extract weight ± SEM. *P<0.05, ***P<0.001 vs. AB powder

Table 3: Effects of DAPP on fatty acid composition in Caco-2/15 cells

Fatty acids	Ctl (ug/mg protein)	Fe/Asc (ug/mg protein)	AB powder + Fe/Asc (ug/mg protein)	JC-047 + Fe/Asc (ug/mg protein)
14:0	6,93 ± 0,76	4,36 ± 0,08	5,46 ± 0,66	7,78 ± 0,41
16:0	61,70 ± 5,20	41,85 ± 0,164***	55,27 ± 7,71	70,43 ± 6,04$^{###}$
18:0	56,14 ± 2,04	49,57 ± 0,41	54,7 ± 6,36	62,88 ± 9,35$^{##}$
20:0	1,97 ± 0,27	1,24 ± 0,01	2,08 ± 0,44	2,32 ± 0,54
22:0	1,33 ± 0,14	0,80 ± 0,02	1,37 ± 0,32	1,51 ± 0,39
24:0	2,50 ± 0,30	1,32 ± 0,01	2,55 ± 0,78	3,08 ± 0,79
ALA:18:3n-3	0,12 ± 0,02	0,14 ± 0,01	0,17 ± 0,03	0,15 ± 0,02
20:3n-3	0,07 ± 0,02	0,12 ± 0,03	0,13 ± 0,04	0,16 ± 0,09
EPA:20:5n-3	3,40 ± 0,26	1,10 ± 0,12***	3,06 ± 0,72$^{##}$	3,38 ± 1,04$^{###}$
22:5n-3	1,66 ± 0,23	0,550 ± 0,05	1,55 ± 0,58	1,58 ± 0,75
DHA:22:6n-3	4,62 ± 0,45	1,24 ± 0,18***	4,04 ± 1,09$^{##}$	4,61 ± 1,67$^{###}$
AL:18:2n-6	3,92 ± 0,17	5,72 ± 0,19**	4,20 ± 0,57	4,00 ± 0,46$^{#}$
18:3n-6	0,71 ± 0,13	0,33 ± 0,01	0,72 ± 0,13	0,87 ± 0,22
20:2n-6	0,10 ± 0,03	0,01 ± 0,01	0,23 ± 0,12	0,19 ± 0,09
20:3n-6	2,05 ± 0,20	1,44 ± 0,06	1,81 ± 0,36	2,17 ± 0,62
AA:20:4n-6	9,55 ± 0,81	5,76 ± 0,66***	8,97 ± 2,22$^{###}$	9,42 ± 3,13$^{###}$
22:2n-6	0,35 ± 0,09	0,11 ± 0,04	0,37 ± 0,23	0,51 ± 0,31
22:4n-6	0,20 ± 0,08	0,02 ± 0,00	0,26 ± 0,16	0,30 ± 0,17
16:1n-7	14,17 ± 1,06	4,67 ± 0,26***	12,50 ± 1,86	15,21 ± 0,54
18:1n-7	32,09 ± 3,47	10,83 ± 0,31***	29,07 ± 4,92$^{###}$	37,10 ± 7,47$^{###}$
18:1n-9	64,69 ± 5,67	29,50 ± 0,50***	60,81 ± 10,81$^{###}$	72,99 ± 12,11$^{###}$
20:1n-9	4,27 ± 0,75	1,59 ± 0,01	4,46 ± 1,26	5,15 ± 1,46
20:3n-9	0,63 ± 0,03	0,33 ± 0,05	0,56 ± 0,09	0,58 ± 0,09
22:1n-9	10,69 ± 3,43	3,65 ± 0,10	4,58 ± 0,72	4,97 ± 1,16
24:1n-9	2,59 ± 0,43	1,03 ± 0,04	2,86 ± 1,35	4,16 ± 1,81
Total	300.78 ± 21.86	177.44 ± 2.56***	274.48 ± 43.71$^{###}$	332.52 ± 50.49$^{###}$
Total n-3	9,87 ± 1,32	3,15 ± 0,484**	8,93 ± 2,39$^{#}$	9,88 ± 3,51$^{##}$
Total n-6	16,9 ± 1,97	13,4 ± 1,22	16,6 ± 3,70	17,5 ± 4,80
Total n-7	49,7 ± 6,20	17,1 ± 0,797***	44,5 ± 6,90$^{###}$	56,0 ± 8,11$^{###}$
Total n-9	82,9 ± 13,3	36,1 ± 0,669***	73,3 ± 13,9$^{###}$	87,8 ± 15,9$^{###}$
Saturated FA	137 ± 9,58	105 ± 0,270***	127 ± 16,2$^{###}$	156 ± 18,0$^{###}$
Mono-unsaturated	135 ± 19,5	54,4 ± 1,70***	120 ± 21,3$^{###}$	146 ± 24,3$^{###}$
PUFA	27,4 ± 2,32	16,0 ± 1,26***	26,1 ± 6$^{#}$	27,9 ± 8,39$^{#}$
DHA/AA	0,48 ± 0,02	0,21 ± 0,01**	0,44 ± 0,02$^{#}$	0,47 ± 0,03$^{##}$
ALA/LA	0,031 ± 0,004	0,024 ± 0,002**	0,039 ± 0,003$^{###}$	0,037 ± 0,003$^{###}$
n-6/n-3	1,73 ± 0,04	4,29 ± 0,19***	1,95 ± 0,14$^{###}$	0,17 ± 0,04$^{###}$

After 10 days differentiation, Caco-2/15 cells were incubated for 6h at 37ºC in the absence or presence of Fe/Asc (200 µM/ 2mM) with DAPP from 250 µg/mL AB powder or JC-047 and

collected for fatty acid (FA) composition. Data represent the means ± SEM of two experiments, each done in duplicate (n=4). Student's *t* test (two-tailed) was used to compare differences between means (X±SEM). $^{*}P<0.05$, $^{**}P<0.01$, $^{***}P<0.001$ vs. Ctrl; $^{\#}P<0.05$, $^{\#\#}P<0.01$, $^{\#\#\#}P<0.001$ vs. Fe/Asc.

AA: arachidonic acid, ALA: alpha-linolenic acid, DHA: docosahexaenoic acid, EPA: eicosapentaenoic acid, LA: linoleic acid, PUFA: polyunsaturated fatty acids.

FIGURE LEGENDS

Figure 1 **Separation and identification of polyphenolic compounds in DAPP crude AB powder.** Extracted ion chromatograms of some identified polyphenolic compounds in AB powder using accurate mass measurement; (A). Extracted ion chromatograms of quercetin glycosides and dihydrochalcone (B) and their related mass spectra (C): quercetin 3-O-glucoside, m/z 463.0905 (1A); quercetin 3-O-galactoside, m/z 463.09018 (1B); quercetin 3-O-arabinoside, m/z 433.07914 (1C); quercetin 3-O-xyloside, m/z 447.07977 (1D); quercetin 3-O-rhamnoside, m/z 447.09506 (1E); and phloridzin, m/z 435.13171 (1F) obtained with negative ion electrospray ionisation. These polyphenols are provided from a mixture of 250 μg of crude extract DAPP in 1 mL Optima grade water.

Figure 2 **Separation and identification of polyphenolic compounds in DAPP purified JC-047 fraction.** Extracted ion chromatograms of some identified polyphenolic compounds in JC-047 using accurate mass measurement (A). Extracted ion chromatograms of catechin, epicatechin and trimeric flavan-3-ol oligomers C1 to C4 (B) and their related mass spectra (C): (+)-catechin, m/z 289.07541 (1A) and (-)-epicatechin, m/z 289.07659 (1B) and that trimeric flavan-3-ol oligomers C1 to C4 (2A to 2D) obtained with negative ion electrospray ionisation. These polyphenols provided of a mixture of 250 μg of purified fraction DAPP in 1 mL Optima grade water.

Figure 3 **Identification of procyanidins in DAPP.** Representative chromatograms of DAPP (25 mg/mL) from AB powder (A) or JC-047 (B) were obtained by

normal phase analytical HPLC using an Agilent 1260/1290 Infinity system coupled to a fluorescence detector.

Figure 4 **Effects of DAPP on cell integrity in Caco-2/15 cells.** Integrity of the monolayer was determined by cell viability, morphology (data not shown), differentiation and tight junction assays using fully differentiated Caco-2/15 cells. Crude AB powder (250 µg/mL) and purified JC-047 fraction (250 µg/mL) were added to the apical compartment of Caco-2/15 cells for 24h before incubation with Fe/Asc (200 µM/2 mM) and LPS (200 µg/mL) for 6h at 37^{o}C as described in Materials and Methods. MTT (A), villin protein mass (B), transepithelial resistance (C) and occludin protein expression (D) were assessed. Results represent the means ± SEM of n=3 independent experiments. *P<0.05 vs. Ctrl; $^{\#\#}P$<0.01 vs. Fe/Asc.

Figure 5 **Effects of DAPP on lipid peroxidation and regulatory endogenous antioxidant activities in Caco-2/15 cells.** Crude AB powder (250 µg/mL) and purified JC-047 fraction (250 µg/mL) were added to the apical compartment of differentiated Caco-2/15 cells for 24h before incubation with Fe/Asc (200 µM/2 mM) and LPS (200 µg/mL) for 6h at 37^{o}C as described in Materials and Methods. Estimation of lipid peroxidation was assessed by measuring the MDA by HPLC (A). The activity of SOD (B), GPx (C) and G-Red (D) was then measured. Results represent the means ± SEM of n=3 independent experiments. **P<0.01, ***P<0.001 vs. Ctrl; $^{\#}P$<0.05, $^{\#\#}P$<0.01, $^{\#\#\#}P$<0.001 vs. Fe/Asc; $^{\$\$}P$<0.01, $^{\$\$\$}P$<0.001 vs. Fe/Asc + LPS.

Figure 6 **Effects of DAPP on oxidative stress or LPS-induced inflammation on inflammatory markers in Caco-2/15 cells.** Crude AB powder (250 µg/mL) and purified JC-047 fraction (250 µg/mL) were added to the apical compartment of differentiated Caco-2/15 cells for 24h before incubation with Fe/Asc (200 µM/2 mM) and LPS (200 µg/mL) for 6h at 37°C as described in Materials and Methods. Protein expression of the inflammatory markers TNF-α (A to C) and IL-6 (D to F) was determined by Western blot, respectively. Results represent the means ± SEM of n=3 independent experiments. **P*<0.05, ***P*<0.01, ****P*<0.001 vs. Ctrl; $^{\#\#\#}$*P*<0.001 vs. Fe/Asc; †*P*<0.05, †††*P*<0.001 vs. LPS; $^{\$\$\$}$*P*<0.001 vs. Fe/Asc + LPS.

Figure 7 **Effects of DAPP on oxidative stress and LPS-induced inflammation on prostaglandin E2 in Caco-2/15 cells.** Crude AB powder (250 µg/mL) and purified JC-047 fraction (250 µg/mL) were added to the apical compartment of differentiated Caco-2/15 cells for 24h before incubation with Fe/Asc (200 µM/2 mM) and LPS (200 µg/mL) (A), as well as indomethacin heptyl ester (0.4 µM) (B), as a selective cyclooxygenase (COX)-2 inhibitor, for 6h at 37°C as described in Materials and Methods. PGE2 was determined by enzymatic immunoassay. Results represent the means ± SEM of N=3 independent experiments. ****P*<0.001 vs. Ctrl; †††*P*<0.001 vs. LPS; $^{\$\$\$}$*P*<0.001 vs Fe/Asc+LPS.

Figure 8 **Effects of DAPP on oxidative stress or LPS-induced inflammation on cyclooxygenase 2 modulation in Caco-2/15 cells**. Crude AB powder (250 µg/mL) and purified JC-047 fraction (250 µg/mL) were added to the apical

compartment of differentiated Caco-2/15 cells for 24h before incubation with Fe/Asc (200 µM/2 mM) and LPS (200 µg/mL) (A to C), as well as indomethacin heptyl ester (0.4 µM) (D), as a selective cyclooxygenase (COX)-2 inhibitor, for 6h at 37°C as described in Materials and Methods. Protein expression of COX-2 was determined by Western blotting. Results represent the means ± SEM of n=3 independent experiments. $^{**}P<0.01$, $^{***}P<0.001$ vs. Ctrl; $^{\#\#\#}P<0.001$ vs. Fe/Asc; $^{\dagger\dagger}P<0.01$, $^{\dagger\dagger\dagger}P<0.001$ vs. LPS; $^{\$\$\$}P<0.001$ vs Fe/Asc+LPS.

Figure 9 **Effects of DAPP on oxidative stress or LPS-induced inflammation on NF-κB in Caco-2/15 cells.** Crude AB powder (250 µg/mL) and purified JC-047 fraction (250 µg/mL) in the presence or absence of 50 µM caffeic acid (CAPE, a specific NF-κB inhibitor) were added to the apical compartment of differentiated Caco-2/15 cells for 24h before incubation with Fe/Asc (200 µM/2 mM) (A) and LPS (200 µg/mL) (B) for 6h at 37°C, and LPS (200 µg/mL) (C) for 24h at 37°C to mimic a chronic inflammation as described in Materials and Methods. Results represent the means ± SEM of n=3 independent experiments. $^{**}P<0.01$, $^{***}P<0.001$ vs. Ctrl; $^{\#}P<0.05$, $^{\#\#}P<0.01$, $^{\#\#\#}P<0.001$ vs. Fe/Asc; $^{\dagger\dagger\dagger}P<0.001$ vs. LPS.

Figure 10 **Effects of DAPP oxidative stress or LPS-induced inflammation on transcription factors in Caco-2/15 cells.** AB powder (250 µg/mL) and purified JC-047 fraction (250 µg/mL) were added to the apical compartment of differentiated Caco-2/15 cells for 24h before incubation with Fe/Asc (200 µM/2 mM) and LPS (200 µg/mL) for 6h at 37°C as described in Materials and

Methods. Protein expression of the transcription factors Nrf2 in homogenates (A) and in nucleus (B), as well as PGC-1α in homogenates (C) and in nucleus (D) was determined by Western blot. Results represent the means ± SEM of n=3 independent experiments. **P*<0.05, ***P*<0.01, ****P*<0.001 vs. Ctrl; $^{\#}$*P*<0.05, $^{\#\#}$*P*<0.01, $^{\#\#\#}$*P*<0.001 vs. Fe/Asc; $^{\$}$*P*<0.05, $^{\$\$}$*P*<0.01, $^{\$\$\$}$*P*<0.001 vs. Fe/Asc + LPS.

Figure 1

A

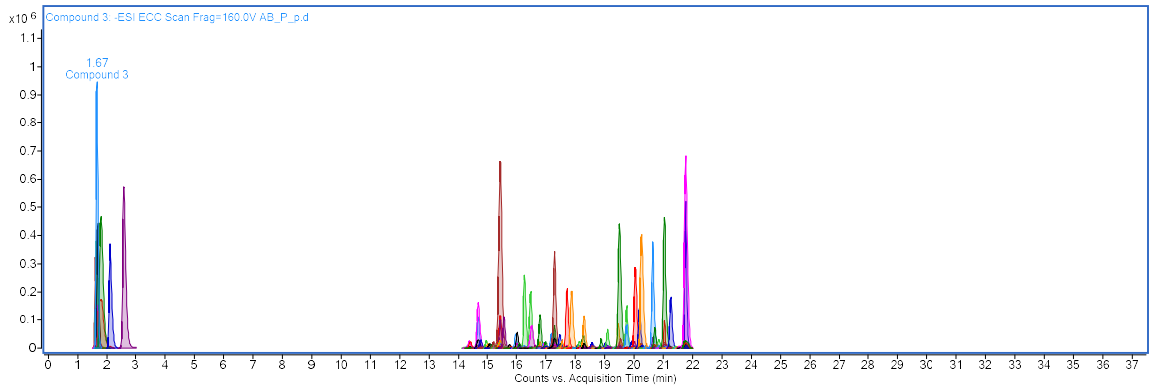
Compound 3 : -ESI ECC Scan Frag=160.0V AB_P_p.d
1.67
Compound 3
Counts vs. Acquisition Time (min)

B

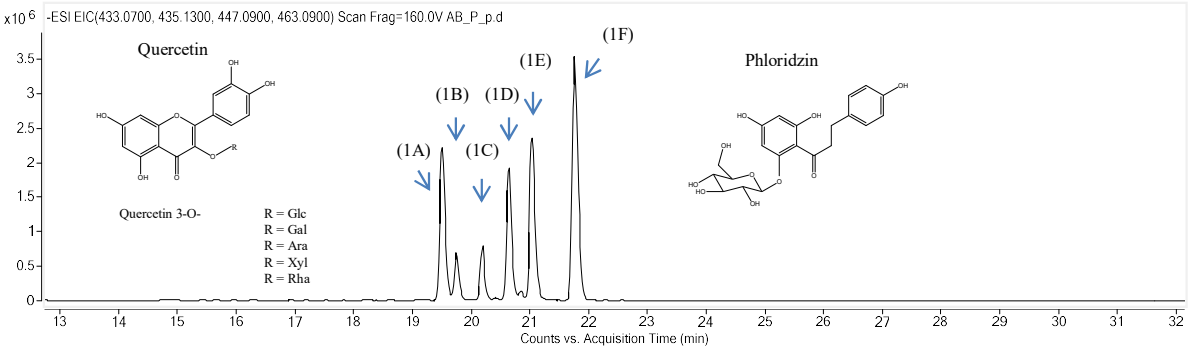
-ESI EIC(433.0700, 435.1300, 447.0900, 463.0900) Scan Frag=160.0V AB_P_p.d
Quercetin
Quercetin 3-O-
R = Glc
R = Gal
R = Ara
R = Xyl
R = Rha
(1A)
(1B)
(1C)
(1D)
(1E)
(1F)
Phloridzin
Counts vs. Acquisition Time (min)

C

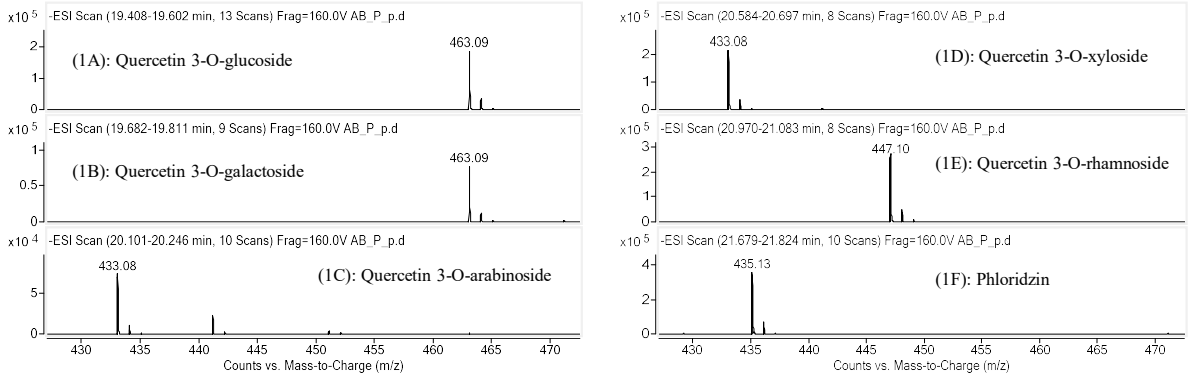
-ESI Scan (19.408-19.602 min, 13 Scans) Frag=160.0V AB_P_p.d
(1A): Quercetin 3-O-glucoside
463.09
-ESI Scan (19.682-19.811 min, 9 Scans) Frag=160.0V AB_P_p.d
(1B): Quercetin 3-O-galactoside
463.09
-ESI Scan (20.101-20.246 min, 10 Scans) Frag=160.0V AB_P_p.d
433.08
(1C): Quercetin 3-O-arabinoside
-ESI Scan (20.584-20.697 min, 8 Scans) Frag=160.0V AB_P_p.d
433.08
(1D): Quercetin 3-O-xyloside
-ESI Scan (20.970-21.083 min, 8 Scans) Frag=160.0V AB_P_p.d
447.10
(1E): Quercetin 3-O-rhamnoside
-ESI Scan (21.679-21.824 min, 10 Scans) Frag=160.0V AB_P_p.d
435.13
(1F): Phloridzin
Counts vs. Mass-to-Charge (m/z)

Figure 2

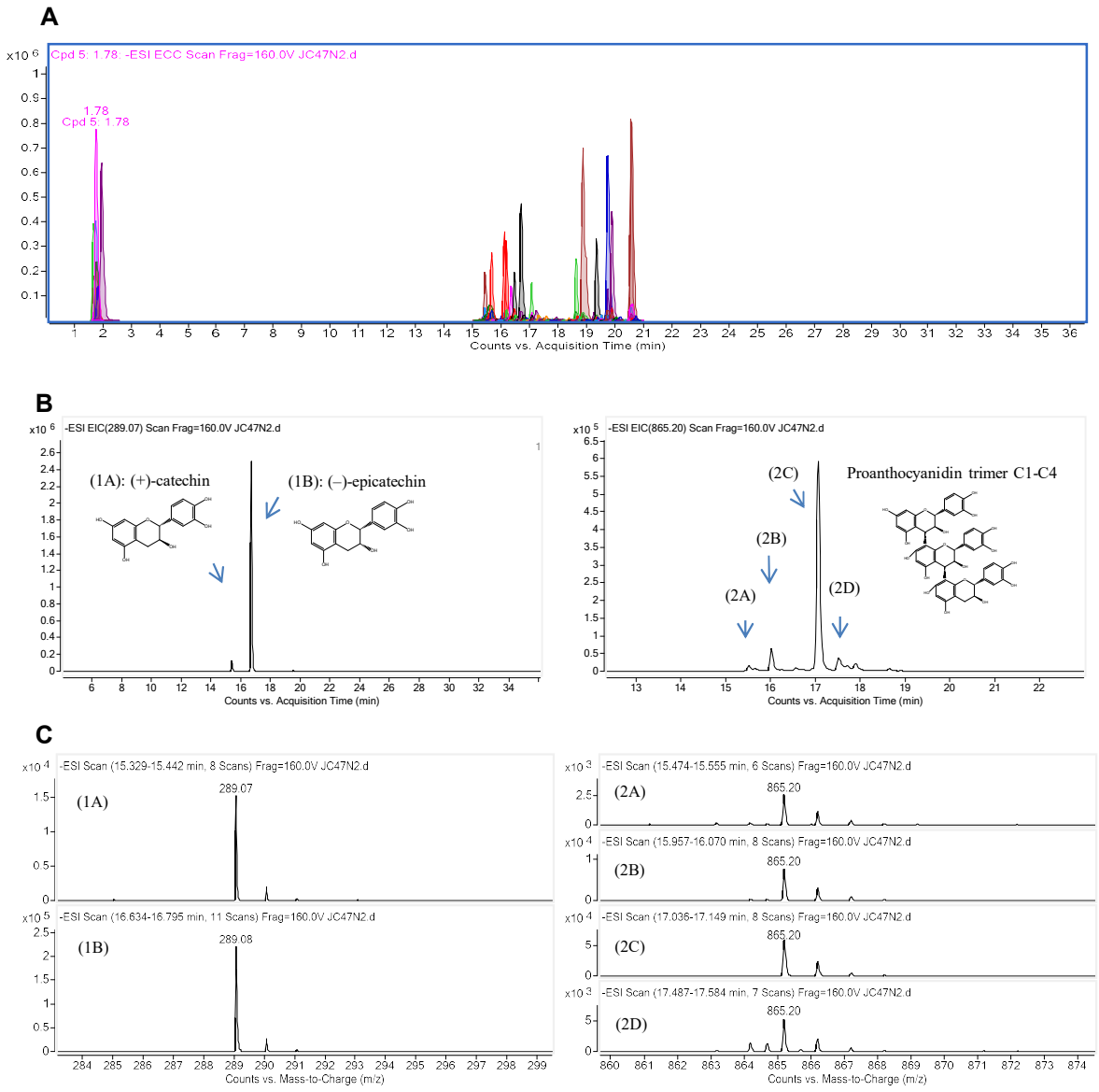
A
Cpd 5: 1.78: -ESI ECC Scan Frag=160.0V JC47N2.d
1.78
Cpd 5: 1.78
Counts vs. Acquisition Time (min)
B
-ESI EIC(289.07) Scan Frag=160.0V JC47N2.d
(1A): (+)-catechin
(1B): (−)-epicatechin
Counts vs. Acquisition Time (min)
-ESI EIC(865.20) Scan Frag=160.0V JC47N2.d
(2A)
(2B)
(2C)
(2D)
Proanthocyanidin trimer C1-C4
Counts vs. Acquisition Time (min)
C
-ESI Scan (15.329-15.442 min, 8 Scans) Frag=160.0V JC47N2.d
(1A)
289.07
-ESI Scan (16.634-16.795 min, 11 Scans) Frag=160.0V JC47N2.d
(1B)
289.08
Counts vs. Mass-to-Charge (m/z)
-ESI Scan (15.474-15.555 min, 6 Scans) Frag=160.0V JC47N2.d
(2A)
865.20
-ESI Scan (15.957-16.070 min, 8 Scans) Frag=160.0V JC47N2.d
(2B)
865.20
-ESI Scan (17.036-17.149 min, 8 Scans) Frag=160.0V JC47N2.d
(2C)
865.20
-ESI Scan (17.487-17.584 min, 7 Scans) Frag=160.0V JC47N2.d
(2D)
865.20
Counts vs. Mass-to-Charge (m/z)

Figure 3

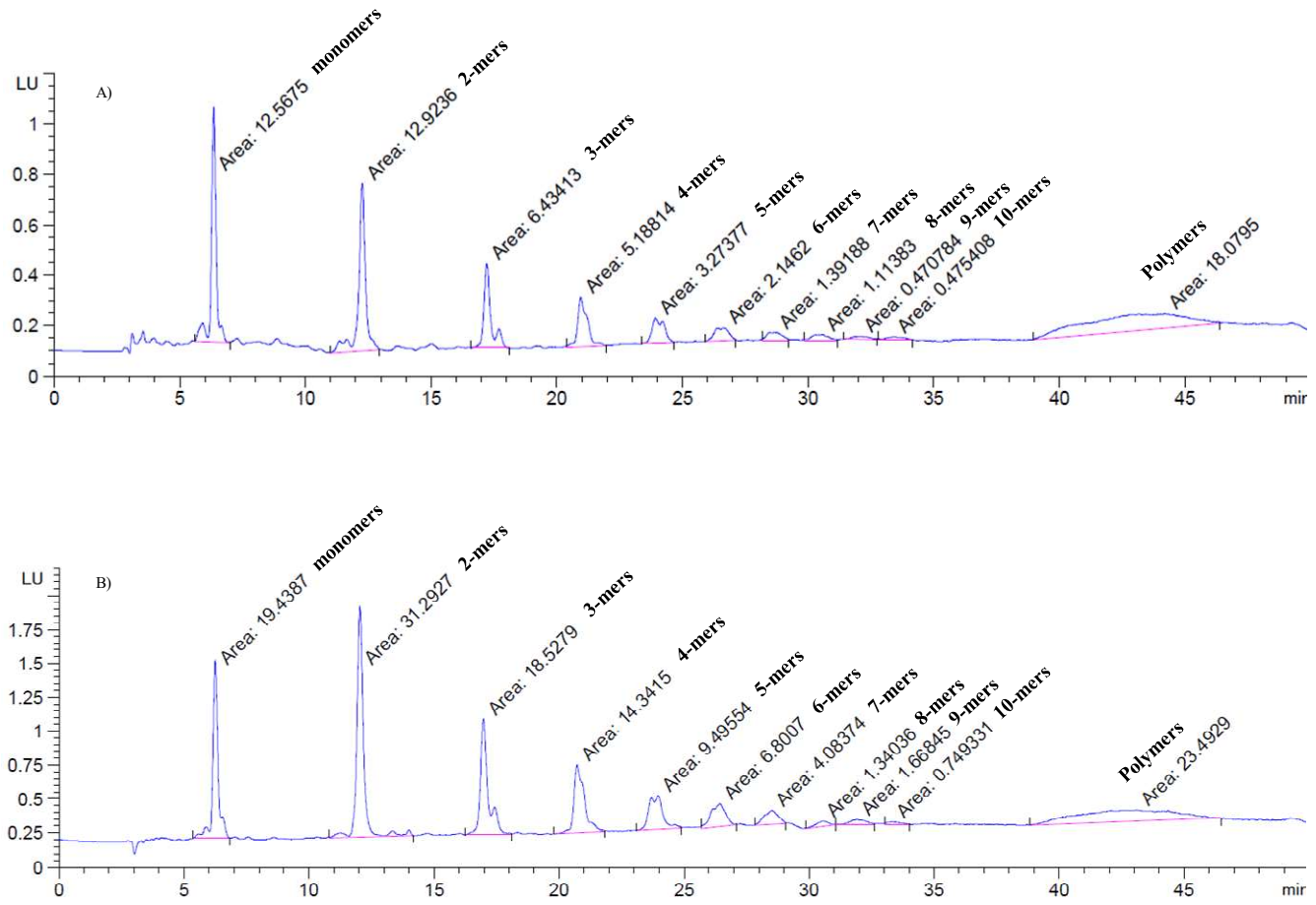
A)
LU
Area: 12.5675 monomers
Area: 12.9236 2-mers
Area: 6.43413 3-mers
Area: 5.18814 4-mers
Area: 3.27377 5-mers
Area: 2.1462 6-mers
Area: 1.39188 7-mers
Area: 1.11383 8-mers
Area: 0.470784 9-mers
Area: 0.475408 10-mers
Polymers
Area: 18.0795
mir
B)
LU
Area: 19.4387 monomers
Area: 31.2927 2-mers
Area: 18.5279 3-mers
Area: 14.3415 4-mers
Area: 9.49554 5-mers
Area: 6.8007 6-mers
Area: 4.08374 7-mers
Area: 1.34036 8-mers
Area: 1.66845 9-mers
Area: 0.749331 10-mers
Polymers
Area: 23.4929
mir

Figure 4

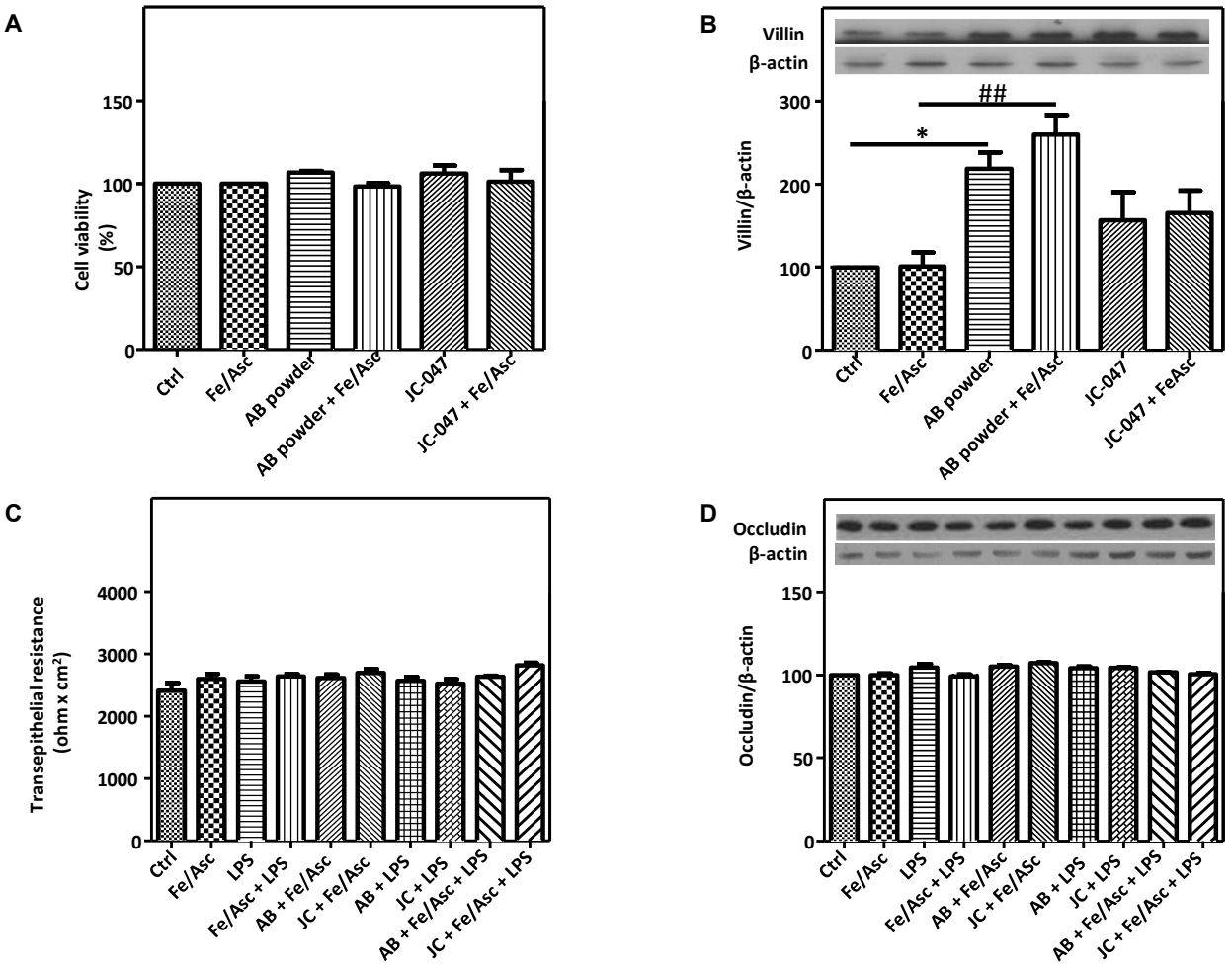
A
Cell viability (%)
150
100
50
0
Ctrl
Fe/Asc
AB powder
AB powder + Fe/Asc
JC-047
JC-047 + Fe/Asc
B
Villin
β-actin
Villin/β-actin
300
200
100
0
##
*
Ctrl
Fe/Asc
AB powder
AB powder + Fe/Asc
JC-047
JC-047 + FeAsc
C
Transepithelial resistance (ohm x cm²)
4000
3000
2000
1000
0
Ctrl
Fe/Asc
LPS
Fe/Asc + LPS
AB + Fe/Asc
JC + Fe/Asc
AB + LPS
JC + LPS
AB + Fe/Asc + LPS
JC + Fe/Asc + LPS
D
Occludin
β-actin
Occludin/β-actin
150
100
50
0
Ctrl
Fe/Asc
LPS
Fe/Asc + LPS
AB + Fe/Asc
JC + Fe/ASc
AB + LPS
JC + LPS
AB + Fe/Asc + LPS
JC + Fe/Asc + LPS

Figure 5

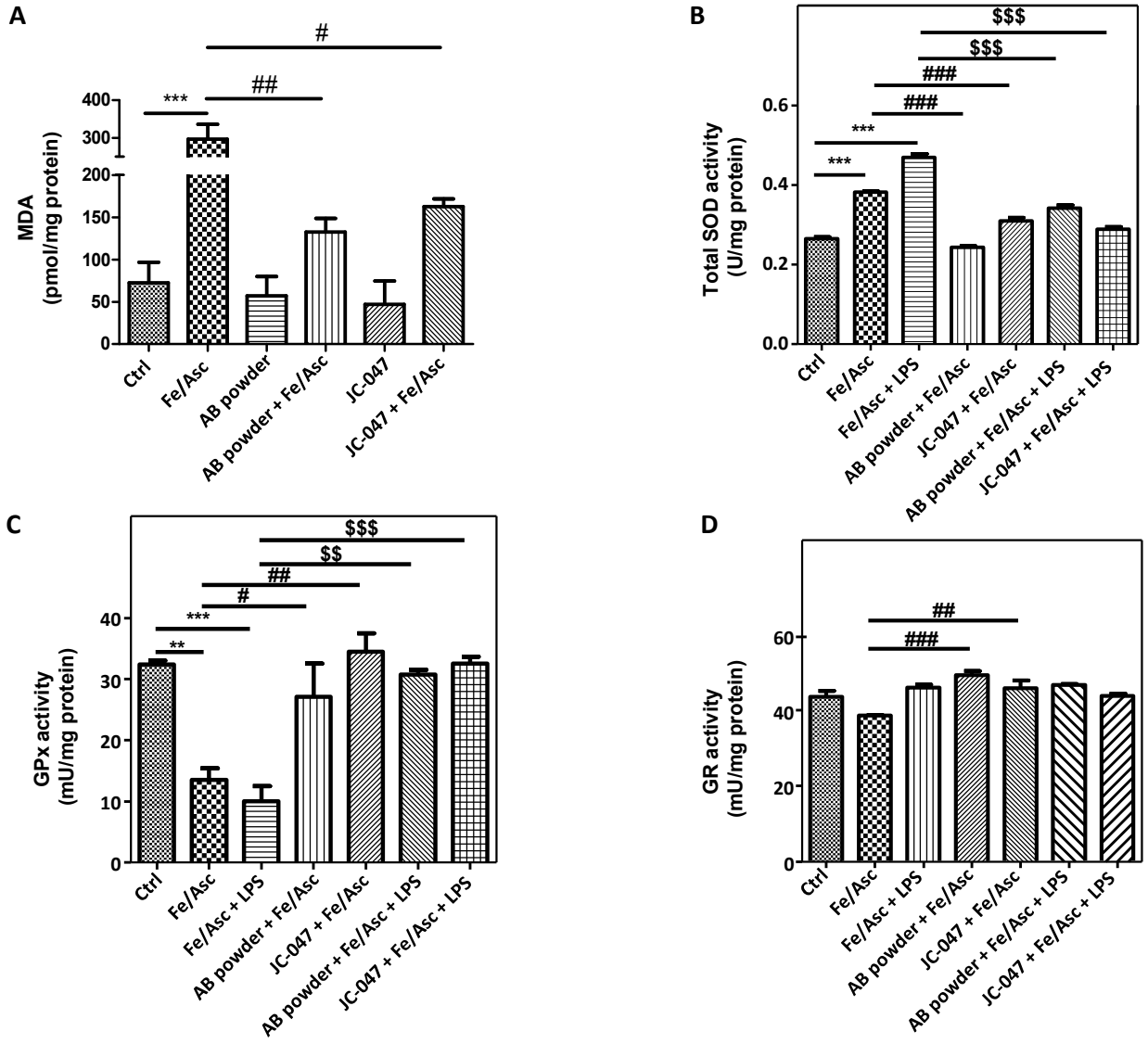
A
MDA (pmol/mg protein)
400
300
200
150
100
50
0
***
##
#
Ctrl
Fe/Asc
AB powder
AB powder + Fe/Asc
JC-047
JC-047 + Fe/Asc
B
Total SOD activity (U/mg protein)
0.6
0.4
0.2
0.0
***
***
###
###
$$$
$$$
Ctrl
Fe/Asc
Fe/Asc + LPS
AB powder + Fe/Asc
JC-047 + Fe/Asc
AB powder + Fe/Asc + LPS
JC-047 + Fe/Asc + LPS
C
GPx activity (mU/mg protein)
40
30
20
10
0
**
***
#
##
$$
$$$
Ctrl
Fe/Asc
Fe/Asc + LPS
AB powder + Fe/Asc
JC-047 + Fe/Asc
AB powder + Fe/Asc + LPS
JC-047 + Fe/Asc + LPS
D
GR activity (mU/mg protein)
60
40
20
0
##
###
Ctrl
Fe/Asc
Fe/Asc + LPS
AB powder + Fe/Asc
JC-047 + Fe/Asc
AB powder + Fe/Asc + LPS
JC-047 + Fe/Asc + LPS

Figure 6

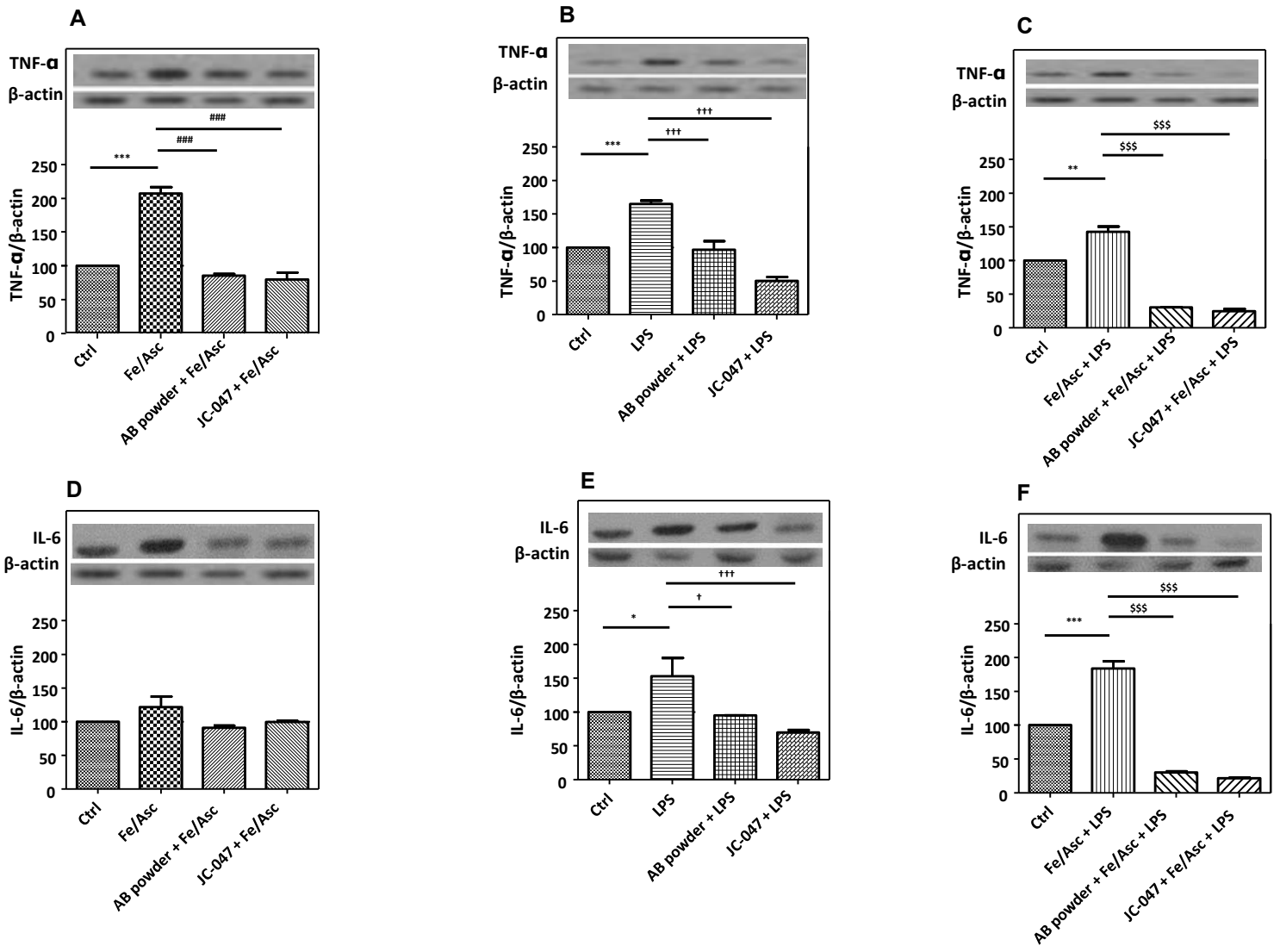
A
TNF-α
β-actin
TNF-α/β-actin
***
###
###
Ctrl
Fe/Asc
AB powder + Fe/Asc
JC-047 + Fe/Asc
B
TNF-α
β-actin
TNF-α/β-actin
***
†††
†††
Ctrl
LPS
AB powder + LPS
JC-047 + LPS
C
TNF-α
β-actin
TNF-α/β-actin
**
$$$
$$$
Ctrl
Fe/Asc + LPS
AB powder + Fe/Asc + LPS
JC-047 + Fe/Asc + LPS
D
IL-6
β-actin
IL-6/β-actin
Ctrl
Fe/Asc
AB powder + Fe/Asc
JC-047 + Fe/Asc
E
IL-6
β-actin
IL-6/β-actin
*
†
†††
Ctrl
LPS
AB powder + LPS
JC-047 + LPS
F
IL-6
β-actin
IL-6/β-actin
***
$$$
$$$
Ctrl
Fe/Asc + LPS
AB powder + Fe/Asc + LPS
JC-047 + Fe/Asc + LPS

Figure 7

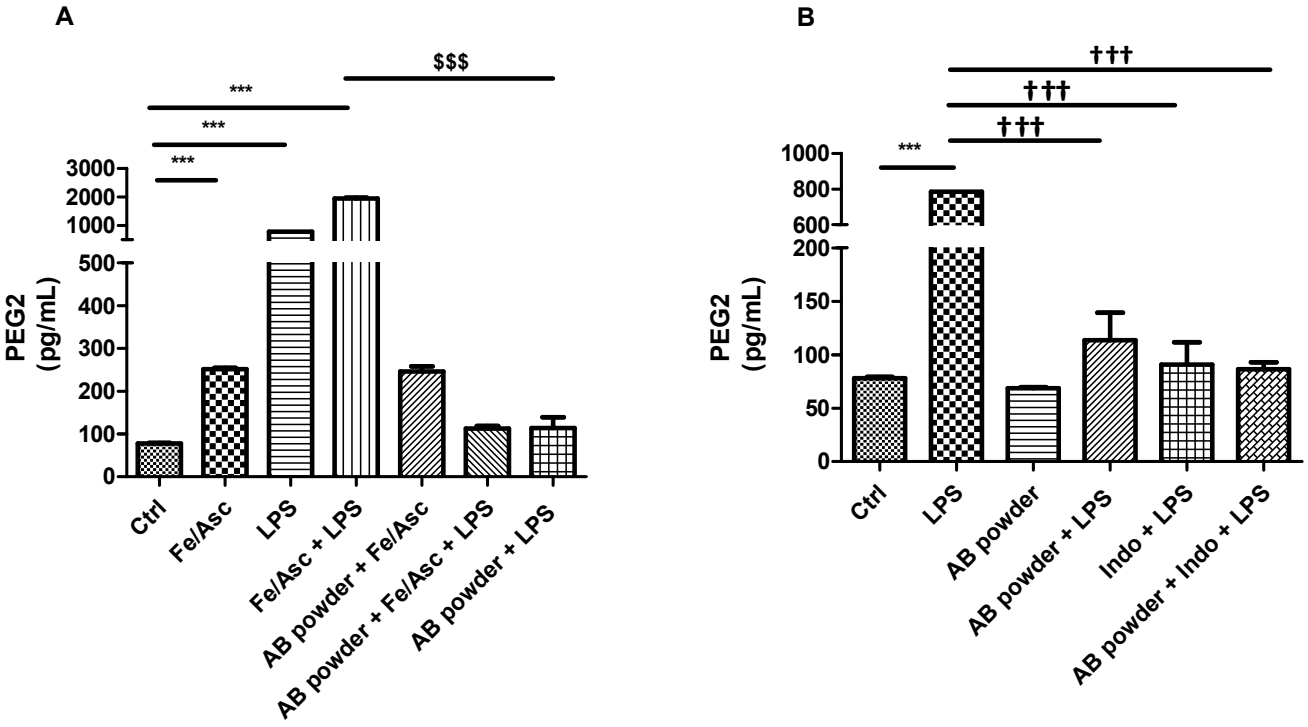
A
B
PEG2 (pg/mL)
***
$$$
†††
Ctrl
Fe/Asc
LPS
Fe/Asc + LPS
AB powder + Fe/Asc
AB powder + Fe/Asc + LPS
AB powder + LPS
AB powder
AB powder + LPS
Indo + LPS
AB powder + Indo + LPS

Figure 8

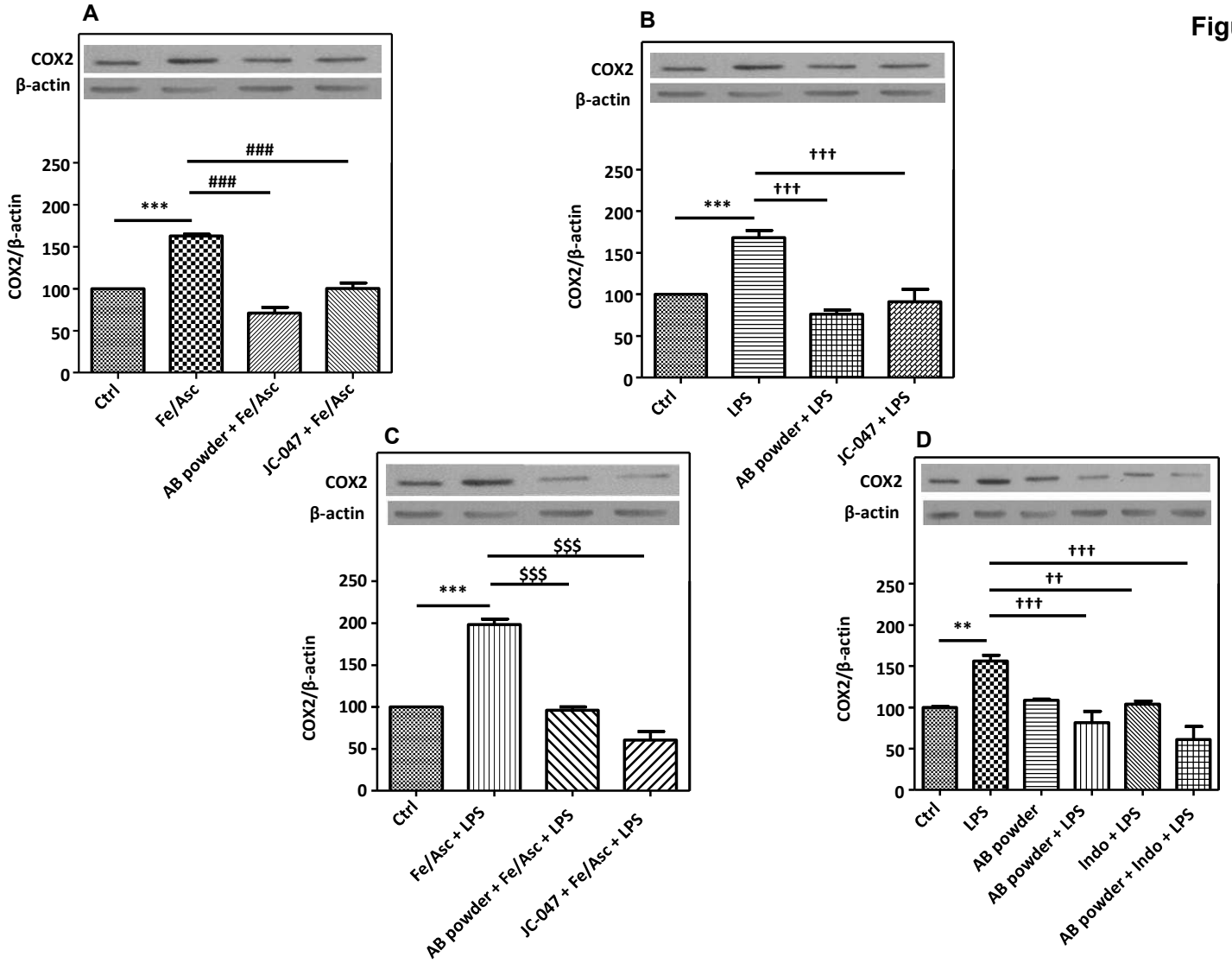
A
COX2
β-actin
COX2/β-actin
***
###
###
Ctrl
Fe/Asc
AB powder + Fe/Asc
JC-047 + Fe/Asc
B
COX2
β-actin
COX2/β-actin
***
†††
†††
Ctrl
LPS
AB powder + LPS
JC-047 + LPS
C
COX2
β-actin
COX2/β-actin
***
$$$
$$$
Ctrl
Fe/Asc + LPS
AB powder + Fe/Asc + LPS
JC-047 + Fe/Asc + LPS
D
COX2
β-actin
COX2/β-actin
**
†††
††
†††
Ctrl
LPS
AB powder
AB powder + LPS
Indo + LPS
AB powder + Indo + LPS

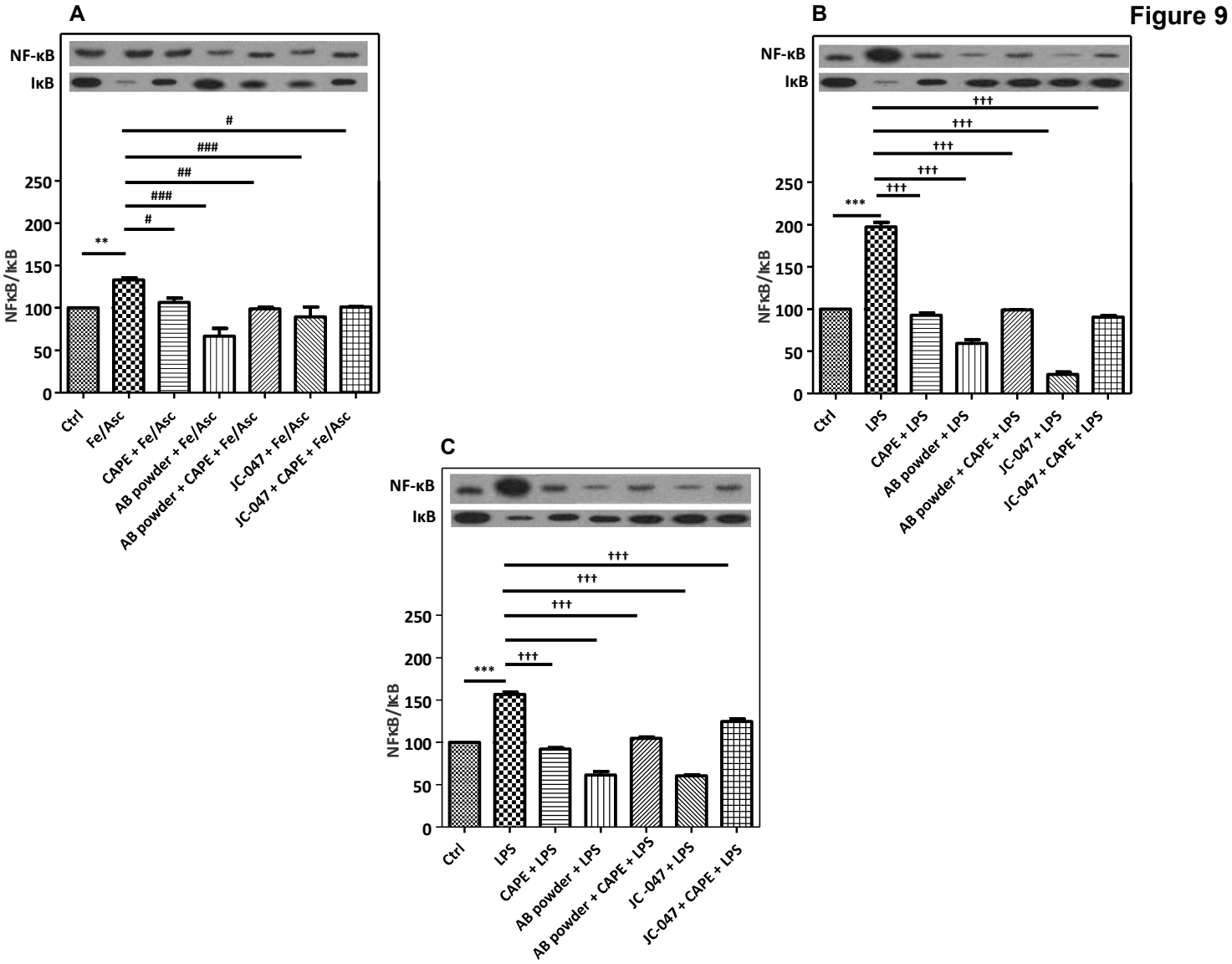
A
NF-κB
IκB
NFκB/IκB
0
50
100
150
200
250
**
#
###
##
###
#
Ctrl
Fe/Asc
CAPE + Fe/Asc
AB powder + Fe/Asc
AB powder + CAPE + Fe/Asc
JC-047 + Fe/Asc
JC-047 + CAPE + Fe/Asc
B
NF-κB
IκB
NFκB/IκB
0
50
100
150
200
250
***
†††
†††
†††
†††
†††
Ctrl
LPS
CAPE + LPS
AB powder + LPS
AB powder + CAPE + LPS
JC-047 + LPS
JC-047 + CAPE + LPS
C
NF-κB
IκB
NFκB/IκB
0
50
100
150
200
250
***
†††
†††
†††
†††
†††
Ctrl
LPS
CAPE + LPS
AB powder + LPS
AB powder + CAPE + LPS
JC-047 + LPS
JC-047 + CAPE + LPS

Figure 9

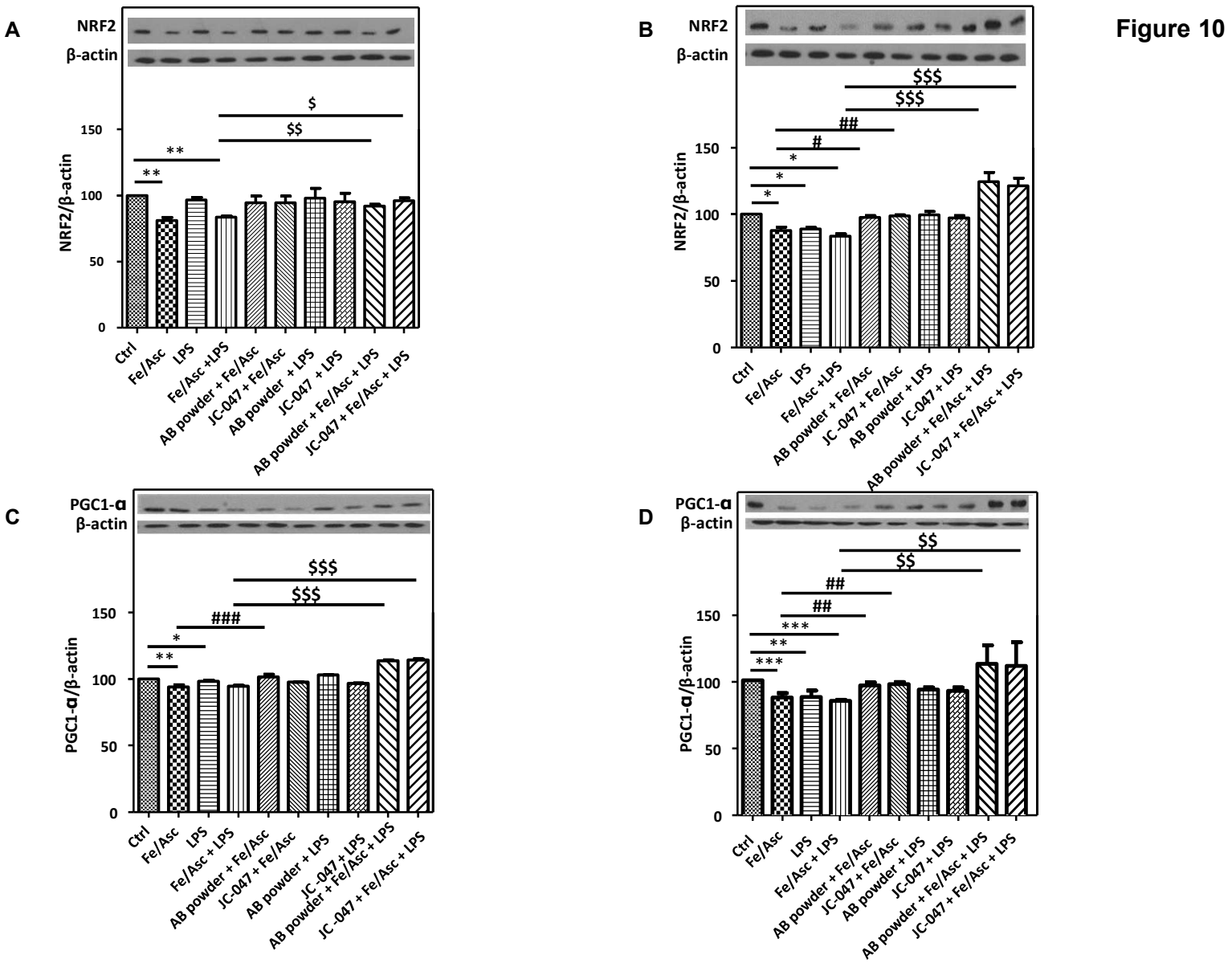
A
NRF2
β-actin
NRF2/β-actin
0
50
100
150
**
**
$
$$
Ctrl
Fe/Asc
LPS
Fe/Asc+LPS
AB powder + Fe/Asc
JC-047 + Fe/Asc
AB powder + LPS
JC-047 + LPS
AB powder + Fe/Asc + LPS
JC-047 + Fe/Asc + LPS
B
NRF2
β-actin
NRF2/β-actin
0
50
100
150
*
*
*
#
##
$$$
$$$
Ctrl
Fe/Asc
LPS
Fe/Asc+LPS
AB powder + Fe/Asc
JC-047 + Fe/Asc
AB powder + LPS
JC-047 + LPS
AB powder + Fe/Asc + LPS
JC-047 + Fe/Asc + LPS
C
PGC1-α
β-actin
PGC1-α/β-actin
0
50
100
150
**
*
###
$$$
$$$
Ctrl
Fe/Asc
LPS
Fe/Asc + LPS
AB powder + Fe/Asc
JC-047 + Fe/Asc
AB powder + LPS
JC-047 + LPS
AB powder + Fe/Asc + LPS
JC-047 + Fe/Asc + LPS
D
PGC1-α
β-actin
PGC1-α/β-actin
0
50
100
150
***
**
***
##
##
$$
$$
Ctrl
Fe/Asc
LPS
Fe/Asc + LPS
AB powder + Fe/Asc
JC-047 + Fe/Asc
AB powder + LPS
JC-047 + LPS
AB powder + Fe/Asc + LPS
JC-047 + Fe/Asc + LPS

Figure 10

Article 2: « Prevention of oxidative stress, inflammation and mitochondrial dysfonction in the intestine by different cranberry phenolic fractions ».

Denis *et al*. Prevention of oxidative stress, inflammation and mitochondrial dysfunction in the intestine by different cranberry phenolic fractions. Clin Sci. (Lond.).2015 Feb; 128 (3): 197-212.

Author contributions:

Marie-Claude Denis, Alexandra Furtos and Emile Levy participated in the design of the study. Marie-Claude Denis, Stéphanie Dudonné, Carole Garofalo and Alain Montoudis conducted the experiments. Marie-Claude Denis, Yves Desjardins, Edgar Delvin and Emile Levy analyzed and interpreted the data. Marie-Claude Denis, Valérie Marcil, Yves Desjardins, André Marette and Emile Levy contributed to the writing of the paper.

Prevention of oxidative stress, inflammation and mitochondrial dysfunction in the intestine by different cranberry phenolic fractions

Marie-Claude Denis[*†], Yves Desjardins[‡], Alexandra Furtos[§], Valérie Marcil[*], Stéphanie Dudonné[‡], Alain Montoudis[*], Carole Garofalo[*], Edgard Delvin[*§], André Marette[‡‖], Emile Levy[*†‡]

[*]Research Centre, CHU Sainte-Justine and [†]Departments of Nutrition, [§]Biochemistry, Université de Montréal, Montreal, Quebec, Canada, H3T 1C5

[‡]Institute of Nutrition and Functional foods (INAF), and [‖]Heart and Lung Institute, Université Laval, Quebec, Quebec, Canada, G1V 0A6

Key words: Polyphenol; Peroxidation; mitochondria; Cyclooxygenase; Inflammation; Transcription factors.

Running Head: Antioxidant and anti-inflammatory effects of cranberry

Abbreviations: AIF, apoptosis-inducing factor; ATP, adenosine triphosphate; Bcl-2, b-cell lymphoma 2; COX-2, cyclooxygenase-2; CP, cranberry polyphenols; DP, degree of polymerization; FA, fatty acid; Fer/Asc, iron-ascorbate; GPx, glutathione peroxidase; GSH-Red, glutathione reductase; IBD, inflammatory bowel diseases; HC, high molecular weight CP; IL-6, interleukin-6; LC**,** low molecular weight CP**;** LPS, lipopolysaccharide**;** MC**,** medium molecular weight CP**;** MDA, malondialdehyde; mt TFA, mitochondrial transcription factor A; mtTFB, mitochondrial transcription factor B; NF-κB, nuclear factor-kappa B; Nrf-2, nuclear factor erythroid 2-related factor 2; OGG1, 8-oxoG-DNA glycosylase; OxS, oxidative stress; Polrmt, mitochondrial RNA polymerase; PGC-1α, peroxisome proliferator-activated receptor gamma coactivator-1-α; PGE2, prostaglandin E2; PUFA, polyunsaturated fatty acid; ROS, reactive oxygen species; SOD, superoxide dismutase; TNF-α, tumor necrosis factor-α

Correspondence: Dr Emile Levy, GI-Nutrition Unit, Research Centre, CHU-Sainte-Justine, 3175 Sainte-Catherine Road, Montreal, Quebec, Canada H3T 1C5

Summary Statement: Our findings demonstrate the capacity of cranberry procyanidins to reduce intestinal oxidative stress and inflammation while improving mitochondrial dysfunction.

ABSTRACT

Cranberry fruit has been reported to have high antioxidant effectiveness that is potentially linked to its richness in diversified polyphenolic content. The aim of the present study is to determine the role of cranberry polyphenolic fractions in oxidative stress, inflammation and mitochondrial functions using intestinal Caco-2/15 cells. The combination of HPLC and UPLC-TDQ techniques allowed us to characterize the profile of low, medium and high molecular weight polyphenolic compounds in cranberry extracts. The medium molecular weight fraction was enriched with flavonoids and procyanidin dimers whereas procyanidin oligomers (degree of polymerization > 4) were the dominant class of polyphenols in the high molecular weight fraction. Pre-incubation of Caco-2/15 cells with these cranberry extracts prevented iron/ascorbate-mediated lipid peroxidation and counteracted lipopolysaccharide-mediated inflammation as evidenced by the decrease in pro-inflammatory cytokines (TNF-α and IL-6), cyclooxygenase-2 and prostaglandin E2. Cranberry polyphenols fractions limited both NF-κB activation and Nrf2 down-regulation. Consistently, cranberry procyanidins alleviated oxidative stress-dependent mitochondrial dysfunctions as showed by the rise in ATP production and the up-regulation of Bcl-2, as well as the decline of protein expression of cytochrome C and apoptotic inducing factor. These mitochondrial effects were associated with a significant stimulation of PGC-1α, a central inducing factor of mitochondrial biogenesis and transcriptional co-activator of numerous downstream mediators. Finally, cranberry procyanidins forestalled the effect of iron/ascorbate on the protein expression of mitochondrial transcription factors (mtTFA, mtTFB1, mtTFB2). Our findings provide evidence for the capacity of cranberry polyphenols to reduce intestinal oxidative stress and inflammation while improving mitochondrial dysfunction.

INTRODUCTION

Polyphenols, a large class of plant-based organic compounds, are found in many fruits and vegetables, and thus serve as important dietary micronutrients. They are involved in plant defence against pathogens and ultraviolet damage (241) and are currently receiving much attention given their multiple related physiological and health effects, including anti-oxidative, anti-inflammatory and immune-regulatory actions (507, 508). Their potent free-radical scavenging activity and capacity to reduce inflammation (509) make them ideal candidate molecules not only for prevention, but also for complementary treatment strategies to improve health outcomes.

The dynamic crosstalk between intestinal epithelial cells and microflora represents one of the fundamental features of intestinal homeostasis (510, 511). Given the unique environmental challenges, the gastrointestinal tract has become exquisitely sensitive to perturbations that affect its capacity to resolve oxidative stress (OxS). Accumulation of oxidative damage occurs when pro-oxidants overwhelm the endogenous antioxidant capacity, thereby leading to excessive production of reactive oxygen species (ROS). Free radical generation, which is intensively catalyzed by redox-active metals such as iron owing to its catalyzing role in Fenton chemistry, may be linked to gut-related diseases (512-514). Undoubtedly, the intestine is highly vulnerable to oxidative damage due to its constant exposure to aerobic metabolism or luminal oxidants from ingested nutrients, local microbes or infections, ischemia/reperfusion, gastric acid production and non-steroidal anti-inflammatory drugs (449-451). Currently, OxS appears as an essential component of the signaling cascade of inflammation. It plays a significant role in inflammatory bowel diseases (IBD), chronic pathologies that are

characterized by uncontrolled inflammation ultimately leading to mucosal disruption and ulceration (515).

Although polyphenols exhibit powerful antioxidant activity by acting as free radical scavengers, namely hydrogen donating compounds, singlet oxygen quenchers and metal ion chelators (465, 467, 468, 470), very few studies have evaluated their protective effects and mechanisms of actions in the intestinal mucosa. Moreover, only limited work has been carried out to explore their impact on the induction of cellular antioxidant defense via the modulation of gene and protein expressions. Such antioxidant defense may maintain intestinal epithelial cells in a reduced environment, thereby protecting them from OxS while preserving their innate function. Additionally, the influence of polyphenols on the interplay between mitochondria and OxS has not been thoroughly examined in the gut epithelium. Thus, in the present study, we have tested the hypothesis that polyphenols can attenuate OxS and inflammation in enterocytes. We investigated their inherent potential using Caco-2/15 cells, a recognized human intestinal model for the investigation of gut absorption and interactions, nutrition, toxicology, food microbiology, bioavailability tests, and screening of drug permeability in discovery programs (516-518). To this end, we employed extracts containing polyphenolic compounds derived from cranberries whose polyphenols (CP) have a wide range of biological effects, including the ability to fight several bacterial strains through antimicrobial activity, to serve as antioxidants in conditions of OxS, to modulate activities of various enzymes and to regulate the expression of numerous genes (519, 520). Finally, we took advantage of this study to analyze the impact of the degree of CP polymerization , which modulates CP uptake by the intestinal mucosa, bioavailability at both local and systemic levels, and action on peripheral tissues.

MATERIALS AND METHODS

General chemicals and reagents

HPLC-grade acetonitrile, methanol, acetone and Optima grade water were from Fisher Scientific (New Jersey, USA). Formic acid was purchased from Fluka (Steinheim, Germany). 3-(4,5-dimethyldiazol-2-yl)-2,5 diphenyl Tetrazolium Bromid (MTT) was from Sigma (MO, USA). Chemicals and reagents for specific assays will be described in the respective sections. Fresh cranberries (*Vaccinium macrocarpon* Ait.) underwent chemical treatments for the extraction of fractions with different molecular weights, which were then lyophilized, milled and kept frozen at -20°C.

Extraction of polyphenolic fractions of different molecular weights

Freeze-dried cranberries (150 g) were extracted twice with 500 mL of an extraction solvent mixture containing acetone/water/acetic acid (70:29.5:0.5, v/v). The extracts were combined and the acetone was evaporated at 50°C using a rotary evaporator under partial vacuum. The resultant slurry (approximately 300 mL) was extracted three times with 250 mL hexane to remove lipid substances. The water slurry was evaporated again on a rotary evaporator to eliminate the residual hexane. The remaining aqueous fraction was diluted with an equal volume of 20% methanol in water (v/v) and applied to a Sephadex LH-20 column (30 X 600 mm) that had previously been hydrated for more than 2 h in 20% aqueous methanol. The samples were collected in three different fractions consisting of low, medium and high molecular weight CP compounds. Elution was performed with 500 mL of 60% methanol/water (v/v) for the low molecular weight CP (LC fraction) followed by 1 L of 100% methanol (v/v) to obtain the medium molecular weight CP (MC fraction) and finally by 2 L of 70% acetone/water (v/v) for elution of the high molecular weight CP compounds (HC

fraction). A rotary evaporator operated at 50°C under partial vacuum was used to remove the organic solvent from each fraction. The residual concentrated water solutions were freeze-dried and generated three solid (powder) fractions.

Determination and characterization of cranberry polyphenol fractions

The total phenolic content of LC, MC and HC fractions was determined using the Folin-Ciocalteu method (473) with gallic acid as a standard. Briefly, 100 µL Folin-Ciocalteu reagent (diluted 10-fold in ultrapure water) and 80 µL sodium carbonate solution (7.5% in ultrapure water) were added to 20 µL MeOH in a 96-well plate. A blank sample and five calibration solutions of gallic acid (12.5 to 200 µg/mL) were analyzed under the same conditions. After a 1h-incubation at room temperature, the absorbance was measured at 765 nm using the Fisher Scientific Multiskan GO microplate reader (MA, USA). All determinations were carried out in triplicate, and results were expressed as g/100 g of extract weight ± SEM.

Flavonoids were identified and quantified using an ultra-performance ACQUITY UPLC liquid chromatography system coupled to a TDQ tandem quadrupole mass spectrometer equipped with an ESI source, all from Waters (MA, USA). An Agilent Plus C18 column (2.1 × 100 mm, 1.8 µm particle sizes) (CA, USA), operated at 30°C, was employed. The flavonoids were separated using 0.2% acetic acid in ultrapure water and acetonitrile (solvent A and B, respectively) with a flow rate of 0.4 µL/min under the following gradient: 0-8 min, 5-50% B; 8-9.10 min, 50-90% B; 9.10-10 min, 90% B; 10-10.10 min, 90-5% B; 10.10-13 min, 5% B. Data were acquired with MassLynx V4.1 software and processed for quantification with QuanLynx V4.1 (Waters, MA, USA). The UPLC-TQD system was operated in negative electrospray ionization mode for flavonoids. Cone and collision gas (nitrogen) flow rates were 80 L/h and 800 L/h, respectively. The mass spectrometer parameters were first generated with

Waters' IntelliStart software (automatic tuning and calibration of the AQUITY- TQD), which were then manually optimized as following: capillary voltage 2.75 kV, source temperature 150^{o}C and desolvation temperature 400^{o}C. Quantification was performed in multiple reaction monitoring modes, tracking the transition of parent and product ions specific for each compound with the inclusion of an external calibration.

The procyanidin composition of cranberry fractions was analyzed as previously described (474) by normal phase analytical HPLC using an Agilent 1260/1290 Infinity System. Samples (5 µL of 25 mg/mL solutions in acetone/ultrapure water/acetic acid, 70:29.5:0.5) were injected into the HPLC system and the separation was performed at 35°C with a flow rate of 0.8 mL/min using a Develosil Diol column (250 mm × 4.6 mm, 5 µm particle size) protected with a Cyano Security Guard column (Phenomenex, CA, USA). The elution was performed using a solvent system comprising solvents A (acetonitrile/acetic acid, 98:2) and B (methanol/water/acetic acid, 95:3:2) in a linear gradient from 0% to 40% B in 35 min, 40% to 100% B in 40 min, 100% isocratic B up to 45 min and 100% to 0% B in 50 min. The column was re-equilibrated for 5 min between injections. Fluorescence of the procyanidins was monitored at excitation and emission wavelengths of 230 and 321 nm respectively with the fluorescence detector set to low sensitivity with a gain of 7X for the entire run. Individual procyanidins with degrees of polymerization (DP) ranging from DP1 to DP>10 were quantified using an external calibration curve of (-)-epicatechin, taking into account their relative response factors in fluorescence (475). The results were expressed as g/100 g of extract weight ± SEM.

Intestinal Caco-2/15 cell culture

The human epithelial colorectal adenocarcinoma Caco-2/15 cell line, a stable clone of the parent Caco-2 cells (American Type Culture Collection, Rockville, MD), was employed. Intestinal Caco-2/15 cells were cultured as described previously (476-484). Briefly, they were grown in MEM supplemented with 10% decomplemented fetal bovine serum, 1% Penicillin-Streptomycin and 1% non-essential amino acids (all reagents from GIBCO-BRL, Grand Island, NY) at 37°C, 95% humidity and 5% CO_2 as described previously (476-484). Caco-2/15 cells were maintained in T-75 cm^2 flasks (Corning Glass Works, Corning, NY) and were split (1:5) when they reached 90% confluence using 0.05% trypsin-0.5mM EDTA (GIBCO-BRL). For individual experiments, cells were plated at a density of 1×10^6 cells/well on six-well culture plates and were cultured for 10 days post-confluence, a period at which they are highly differentiated and appropriate for experimental treatments (476-484). The medium was refreshed every second day.

Caco-2/15 cell integrity

After various treatments, cell integrity was estimated by viability, morphology and differentiation assays. Briefly, cell differentiation was assessed by determination of villin protein expression. Monolayer intactness and physical barrier function were tested by evaluating morphology, transepithelial electric resistance and occludin protein expression. Finally, cell viability was appraised using the MTT test.

Induction of oxidative stress and inflammation

Differentiated intestinal Caco-2/15 cells were used to explore the effects of the polyphenol fractions on OxS (induced by the mixture of 200 μM iron and 2 mM Ascorbate, Fe/Asc) and inflammation [prompted by 200 μg/mL lipopolysaccharide (LPS)] as previously reported

(483). CP fractions of different molecular weights (LC, MC and HC) at the concentration of 250 µg/mL were added to the apical compartment of Caco-2/15 cells for 24h before incubation with Fe/Asc or LPS for 6h at 37°C.

Measurement of lipid peroxidation

Estimation of lipid peroxidation was assessed by quantifying malondialdehyde (MDA) by HPLC following exposure of Caco-2/15 cells to Fe/Asc. Briefly, proteins were precipitated with 8% sodium tungstate (Na_2WO_4) (Aldrich, Milwaukee, WI). The protein-free supernatants were then reacted with an equivalent volume of 0.5% (wt/vol) thiobarbituric acid solution (TBA; Sigma, MO, USA) at 95°C for 60 min. After cooling to room temperature, the pink chromophore [MDA-$(TBA)_2$] was extracted with 1-butanol and dried over a stream of nitrogen at 50°C for 3 hours. The dry extract was then resuspended in 100% MeOH before MDA determination by HPLC with a fluorescence detection (Jasco Corporation, Tokyo, Japan) set at 515 nm excitation and 550 nm emission.

Fatty acid analysis

Following differentiation, Caco-2/15 cells were incubated for 6h at 37°C in the absence or presence of Fe/Asc (200 µM/2 mM) following pre-incubation with 250 µg/mL CP fractions. Cells were then homogenized in PBS containing 0.005% (w/v) 2,6-Di-tert-butyl-4-methylphenol (Sigma, St-Louis, MO). Samples were subjected to trans-esterification and injected into a gas chromatograph using a 90 m × 0.32 mm WCOT-fused silica capillary column VF-23ms coated with 0.25 µm film thickness (Varian, Canada) according to the method described previously (485).

Endogenous antioxidant enzyme activities

Differentiated Caco-2/15 cells were harvested in hypotonic lysis buffer (10 mM HEPES, 1.5 mM $MgCl_2$, 10 mM KCl, 0.5 mM DTT, 0.2 mM PMSF). Total superoxide dismutase (SOD) activity was determined as described by McCord *et al*. (486). Briefly, superoxide radicals (O_2^-) were generated by the addition of xanthine and xanthine oxidase, and the oxidation of the SOD assay cocktail was followed using a spectrophotometer at 550 nm for 5 min. The same reaction was then repeated with the addition of the sample. The total SOD activity was then calculated. For glutathione peroxidase (GPx) activity, aliquots of cell homogenates were added to a PBS buffer containing 10 mM GSH, 0.1 U glutathione reductase (GSH-Red) and 2 mM NADPH with 1.5% H_2O_2 to initiate the reaction. Absorbance was monitored every 30 sec at 340 nm for 5 min (483). For GSH-Red activity, cell homogenates were added to a PBS buffer containing 2 mM NADPH and 10 mM of GSSG to initiate the reaction. Absorbance was monitored every 30 sec at 340 nm for 5 min (483).The assay for catalase (CAT) activity was adapted from the protocol reported by Jiang *et al.*(521) with measurement of xylenol orange oxidation at 560 nm in the presence of ferrous ions. Briefly, 100 μM of H_2O_2 were added and the absorbance was monitored at 560 nm. Samples were then incubated on ice with the same H_2O_2 concentrations and allowed to react for 5 min. CAT activity can then be calculated using a standard curve.

Immunoblot analysis

Following the incubation with the various stimuli, differentiated Caco-2/15 cells were sonicated and the Bradford assay (Bio-Rad, Mississauga, Ontario) was used to determine the protein concentration of each sample. Proteins were denatured in sample buffer containing

SDS and ß-mercaptoethanol, separated on a 7.5 % SDS-PAGE and electroblotted onto Hybond nitrocellulose membranes (Amersham, Baie D'Urfé, Qc, Canada). Signals were detected with an enhanced chemiluminescence system for antigen-antibody complexes. No specific binding sites of the membranes were blocked using defatted milk proteins followed by the addition of one of the following primary antibodies: 1/1000 polyclonal anti-villin (94 kDa; BD Biosciences, Mississauga, On, Canada); 1:1,000 polyclonal anti-occludin (59 kDa; Abcam, Campbridge, MA); 1:1,000 polyclonal anti-cyclooxygenase-2 (COX-2) (70 kDa; Novus, Oakville, ON); 1:10,000 polyclonal anti-NF-κB (65 kDa; Santa Cruz Biotechnology, Santa Cruz, CA); 1:5,000 polyclonal anti-IκB (39 kDa; Cell Signaling, Beverly MA); 1:5,000 polyclonal anti-tumor necrosis factor (TNF)-α (26 kDa; R&D, Canada); 1:5,000 monoclonal anti-interleukin (IL)-6 (25 kDa; R&D), 1:1,000 polyclonal anti-Nrf2 (68 kDa; Abcam); 1:1,000 polyclonal anti-PGC-1α (92 kDa; Abcam); 1:40,000 monoclonal anti-β-actin (42 kDa; Sigma, MO, USA); 1:1,000 anti-mtTFA (25 kDa; Santa Cruz Biotechnology); 1:1,000 polyclonal anti-mitochondrial transcription factor (mtTF) B1M (39 kDa; Novus Biologicals, CO, USA); 1:1,000 polyclonal anti-mtTFB2M (40 kDa; Novus Biologicals); 1:1,000 polyclonal anti-mtRNA polymerase (135 kDa; Abcam); 1:1,000 polyclonal anti-OGG1 (39 kDa; Novus Biologicals), 1:1,000 monoclonal anti-cytochrome C (15 kDa; Novus Biologicals), 1:1,000 anti-inducing factor (AIF) (67 kDa; Abcam) and 1:1,000 anti-Blc2 (26 kDa; Abcam).

The relative amount of primary antibody was detected with species-specific horseradish peroxidase-conjugated secondary antibody (Jackson Laboratory, Bar Harbor, Maine). The β-actin protein expression was determined to confirm equal loading. Molecular size markers (Fermentas, Glen Burie, Maryland) were simultaneously loaded on gels. Blots were developed

and the protein mass was quantitated by densitometry using an HP Scanjet scanner equipped with a transparency adapter and the UN-SCAN-IT gel 6.1 software.

Prostaglandin E2 determination

Cellular prostaglandin E2 (PGE2) was measured by enzyme-linked immunosorbent assay (Arbor Assay, MI, USA). After a short incubation, the reaction was stopped and the intensity of the generated color was detected in a microtiter plate reader (EnVision Multilabel Plate Readers, PerkinElmer) capable of measuring 450 nm wavelengths.

Mitochondrial and nucleus separation

Differentiated Caco-2/15 cells were washed twice with PBS and left on ice for 5 min in a buffer containing 250 mM sucrose, 3 mM EDTA, 1 mM DTT at pH 7.4. Cells were then scraped and homogenized with a glass pestle Dounce homogenizer. The homogenate was centrifuged at 1,000 *g* for 10 min at 4^{o}C to obtain the pellets containing nuclei. The supernatant was then collected and centrifuged at 10,000 *g* for 10 min to obtain the pellets containing mitochondria. The pellet was resuspended in the above mentioned buffer, then was quick-frozen and stored at -80^{o}C. The nuclear samples were collected for protein expression analysis using Western blotting to evaluate NF-κB, nuclear factor erythroid-2-related factor 2 (Nrf2), peroxisome proliferator-activated receptor gamma coactivator-1 alpha (PGC-1α), while mitochondrial organelles were employed to assess their specific transcription factors (mtTF: mtTFA, mtTFB1, mtTFB2 and POLRMT), as well as 8-oxoguanine-DNA glycosylase (OGG1), apoptosis-inducing factor (AIF), and cytochrome C and B-cell lymphoma 2 (Bcl-2).

Assessment of Intracellular Adenosine triphosphate (ATP)

Intracellular ATP was measured using luciferase driven bioluminescence using EnzyLight^{TM} ADP/ATP Ratio Assay Kit (Bioassay systems, CA, USA) as reported previously (139). Values for mitochondria were then normalized further with regard to the protein content.

Statistical analyses

All values are expressed as mean ± SEM. Data were analyzed by using a one-way analysis variance and the two-tailed Student's *t* test using the Prism 5.01 (GraphPad Software) and the differences between the means were assessed post-hoc using Tukey's test. Statistical significance was defined as $P<0.05$.

RESULTS

Profile of phenolic compounds of cranberry fractions

Total contents of phenolic compounds in the different cranberry fractions were determined by the colorimetric Folin-Ciocalteu method (Table 1). A large variation was found in the composition of the different CP fractions ranging from 5.0 ± 0.1 to 54.5 ± 0.9 g of gallic acid equivalents/100 g of extract weight. The combination of UPLC coupled to a TDQ tandem quadrupole mass spectrometer revealed that the LC was essentially constituted of small absorbable phenolic acids and some anthocyanins. The MC fraction was constituted of anthocyanin, flavonols and proanthocyanidin monomers and dimers. The HC fraction was devoid of phenolic acids and of anthocyanin but contained flavonols (35% of total) and procyanidins (65% of total). The latter were essentially composed of dimers (47 %), oligomers (3 to 5 DP) (38%) and polymers (DP 5 to 10) (15%).

Cell integrity following various treatments

The effects of Fe/Asc and LPS on Caco-2/15 cells integrity were examined by morphological assessment, protein content quantification and MTT assay after a 6h-incubation period. The morphology and the protein content remained unchanged with the administration of Fe/Asc and LPS, as well as following treatment with the CP fractions (data not shown). Similarly, Caco-2/15 cell viability and monolayer membrane permeability were not affected by the addition of the different treatments (Supplementary Figure S1). On the other hand, an enhancement of cell viability and protein expression of occludin (a biomarker for tight junction and mucosal barrier function) was noticed when Caco-2/15 cells were cultured in the presence of the MC fraction (Supplementary Figure S1). Thus, it can be concluded that cell integrity was not compromised by the experimental conditions.

Effects of CP fractions on lipid peroxidation

The extent of lipid peroxidation following the treatment of Caco-2/15 cells with Fe/Asc during 6h was assessed by determining MDA levels. HPLC analyses indicated a four-fold increase in MDA (P<0.001) following the administration of the oxygen free radical-generating system Fe/Asc as compared to controls (Figure 1A). The presence either of the LC, MC or HC cranberry fraction was found to counteract Fe/Asc-mediated lipid peroxidation, with a more favorable impact for HC (Figure 1A).

Since OxS may alter the composition and properties of the bilayer lipid environment, we next determined whether Fe/Asc was able to affect cellular fatty acid (FA) profile. A significant decrease was noted in n-3 and n-6 polyunsaturated fatty acids (PUFA) (EPA, 20:5n-3; DHA, 22:6n-3; AL, 18:2n-6) as well as in monounsaturated FAs (18:1n-9), which led to a reduction in the calculated total n-3, n-7 and n-9 PUFA contents compared to controls (Table 2). As n-3 PUFAs were more affected by OxS than n-6 PUFAs, an increase was observed in the n-6/n-3 ratio, which might promote an inflammatory state. On the other hand, pre-incubation with CP fractions restored the levels and composition of PUFAs. Once again, HC fraction polymers had a more favorable impact on bilayer lipid environment after the induction of OxS (Table 2).

Mechanisms for the action of CP fractions on oxidative stress

As failure of antioxidant defense may favor the induction of OxS, we examined various endogenous antioxidant enzymes and we found that treatment of Caco-2/15 cells with Fe/Asc caused a significant augmentation in total SOD activity. In accordance with our previous results, pre-incubation with the CP fractions blunted the effects of OxS (Figure 1B). Under these same conditions, GPx activity was down-regulated by Fe/Asc and restored by treatment with the MC and HC fractions (Figure 1C). CAT activity was also affected by Fe/Asc and

normalized by treatment with the CP fractions (Figure 1E). On the other hand, GSH-Red activity was not significantly affected by either the Fe/Asc or polyphenol treatments (Figure 1D).

Effects of cranberry polyphenolic fractions on inflammatory markers

Eicosanoids and cytokines are pro-inflammatory compounds produced by cells in response to injury. The formation of inflammatory eicosanoids such as PGE2 is synthesized from arachidonic acid by specific enzymes, especially COX-2. Our experiments showed that Fe/Asc and LPS elicited exaggerated synthesis of PGE2 and that pre-incubation with CP fractions completely blocked COX-2 induction by these pro-inflammatory treatments (Figures 2C and 2D). Noteworthy, we found distinct effects of the CP fractions on PGE2 production: while the HC fraction was the more efficient in lessening Fe/Asc-mediated PGE2 accumulation (Figure 2A), the LC fraction was more potent in lowering LPS-induced PGE2 accretion (Figure 2B). We then assessed the production of TNF-α and IL-6, two powerful inflammatory mediators, following the incubation of Caco-2/15 cells with Fe/Asc and LPS. Western blot analyses indicated that the CP fractions were able to significantly decrease and, in most cases, to completely abolish TNF-α and IL-6 production (Figures 3A-D).

Effects of CP fractions on key transcription factors

The NF-κB signaling pathway plays a crucial role in the initiation and amplification of inflammation via the modulation of multiple inflammatory mediators. Figure 4 shows that Caco-2/15 cells exposed to Fe/Asc or LPS displayed a high NF-κB/IκB protein ratio, which is indicative of elevated transcriptional activation of its target inflammatory genes (Figures 4A and 4D). Importantly, the CP fractions were found to blunt the activation of the NF-κB pathway in these cells. To further decipher the mechanisms of action of the CP fractions, we

examined the transcription factors that are involved in the regulation of antioxidant genes expression and mitochondrial biogenesis. The protein mass of Nrf2 was down-regulated by Fe/Asc- or LPS-induced OxS and inflammation (Figures 4B and 4E). However, treatment with the CP fractions prevented the downregulation of Nrf2 protein expression when the cells were pre-incubated with CP fractions before their exposure to Fe/Asc or LPS. We also assessed PGC-1α, a transcriptional co-activator known for up-regulating Nrf2. PGC-1α protein mass was reduced in response to both Fe/Asc and LPS treatments in Caco-2/15 cells (Figures 4C and 4F). However, pre-incubation with the CP fractions was able to prevent PGC-1α downregulation by the inflammatory agents.

Effect of cranberry procyanidin rich fraction (HC) on mitochondrial functions

The main function of the mitochondrion is the production of energy in the form of ATP via oxidative phosphorylation and oxygen consumption. We therefore assessed the amount of ATP levels in mitochondria extract from Caco-2/15 cells exposed to the Fe/Asc oxygen radical generating system. As noted in Figure 5A, the administration of Fe/Asc led to a 6-fold reduction of ATP level compared with untreated cells. However, pre-incubation with the HC fraction almost fully prevented the reduction of ATP levels.

Protective effect of procyanidin rich fraction against oxidative stress-induced apoptosis

In the process of programmed cell death, mediators of apoptosis are released from mitochondria through disruptions in the outer mitochondrial membrane and then participate in caspase activation and DNA degradation. In our study, we focused on one specific mediator of the outer mitochondrial membrane, the anti-apoptotic protein Bcl-2. Treatment of Caco-2/15 cells with Fe/Asc lowered Bcl-2 protein expression and pre-incubation with the HC fraction blunted this effect (Figure 5C). AIF is normally located in the inter-membrane space of

mitochondria and is involved in initiating a caspase-independent pathway of apoptosis by causing DNA fragmentation and chromatin condensation. Furthermore, when cell death is triggered by an apoptotic stimulus, cytochrome C is released into the cytosol and contributes to the caspase-dependent pathway of apoptosis. Western blot analysis revealed an increase in the level of AIF (1.5-fold) and cytochrome C (2.5-fold) protein masses in the mitochondrial extract following the addition of Fe/Asc to Caco-2/15 cells (Figures 5B and 5D, respectively). Pre-incubation with the HC fraction prior to Fe/Asc administration prevented the rise in both AIF and cytochrome C protein mass.

Effect of procyanidin rich fraction on OGG1 repair enzyme level

The base excision repair pathway is primarily responsible for removing 8-OHdG from mitochondrial DNA (522). In humans, 8-OHdG is repaired by 8-oxoguanine DNA glycosylase (OGG1), an enzyme that recognizes and hydrolyzes the aberrant base from the DNA backbone. As illustrated in Figure 6A, treatment with Fe/Asc resulted in a significant ($P < 0.01$) reduction of OGG1 protein mass as compared to control cells. However, pre-incubation of Caco-2/15 cells with the HC fraction prevented the decline in OGG1 expression.

Effects of procyanidin rich fraction on mitochondrial transcription factors

Human mitochondrial transcription requires bacteriophage-related RNA polymerase, POLRMT, mtDNA-binding protein, h-mtTFA/TFAM, and two transcription factors/rRNA methyltransferases, h-mtTFB1 and h-mtTFB2. These crucial proteins define mitochondrial biogenesis and gene expression that together are believed to fine-tune mitochondrial functions (126, 139, 523). Given the deleterious effects of Fe/Asc, it was mandatory to explore how OxS modulates the core protein components required for mitochondrial transcription. Western blot analyses showed a significant increase in POLRMT, mtTFA, mtTFB1 and mtTFB2 protein

expression (Figures 6B-6E) in Caco-2/15 cells treated with Fe/Asc compared with control untreated cells. However, pre-incubation with the HC fraction was found to fully block the changes in these transcription factors.

DISCUSSION

Emerging data provides substantial evidence to classify numerous fruits as functional nutrients with several preventive and therapeutic health benefits (388, 524-526). Among them, cranberries have recently received attention as a result of their association with protection against urinary tract infections (527), glycemic response improvement (528) and cardiovascular risk prevention (529, 530), but only few reports have focused on gastrointestinal health. This study was therefore conducted in order to test the potential effects of CP fractions on cell viability, membrane permeability, OxS, inflammation and mitochondrial functions in intestinal epithelial cells. We were particularly interested in determining which polyphenolic species was responsible for the presumed biological activity. We thus separated three fractions differing in their molecular size and intestinal absorption capacity. The LC fraction was composed of anthocyanins (1/3) and phenolic acids (2/3). The former of these molecules are relatively poorly absorbed and the latter have been shown to be readily absorbable by the enterocyte (223, 285). The MC fraction was composed of some poorly bioavailable anthocyanins, flavonols and small molecular weight procyanidins in approximately equal quantity. Importantly, the bioavailability of both the flavonols and the procyanidin monomers and dimers was previously evidenced (531). On the other hand, the HC fraction contained flavonols and procyanidin dimers but was particularly enriched in procyanidins, molecules with higher molecular weight and of which the oligomeric and polymeric forms are poorly absorbed (283). Hence, the distinctive difference between the MC and the HC fractions was the higher proportion of procyanidins that are not as well absorbed by the enterocyte.

The effects of polyphenols were tackled with Caco-2/15 cells that undergo a process of spontaneous differentiation leading to the formation of a monolayer of cells expressing several morphological and functional characteristics of mature human enterocytes. This remarkable intestinal model is regarded as the most appropriate for the investigation of gut absorption and interactions, nutrition, toxicology food microbiology, bioavailability tests, and screening of drug permeability in discovery programs. Multiple studies from our laboratory (532-539) have shown that Caco-2/15 monolayers are fully appropriate for the study of fat absorption, lipid/lipoprotein homeostasis, oxidative stress and inflammation. Importantly, when seeded on porous filters (Transwell), Caco-2/15 cells permit access to both sides of the bipolar intestinal epithelium: apical and basolateral compartments corresponding to intestinal lumen or serosal circulation, respectively. Therefore, the Caco-2/15 cell model has been proved to be a good alternative for human and animal studies and has emerged as one of the standard *in vitro* tools to predict *in vivo* intestinal absorption of various substances, such as polyphenols (540). For example, Caco-2 cells have been shown to produce sulfate and glucuronide conjugates of resveratrol (541) and to achieve sulfation that constitutes the primary route of intestinal metabolism of epicatechin, an antioxidant flavonoid in tea (299).

If one assumes a Western person consumes 1 g of polyphenols per day (275) and the volume of the intestine is about 6.25 L, one would expect that the enterocytes are exposed to a concentration of about 235 μg / ml, which is very close to what we used in our experiments. Taking into account the volume of the colon (approximately 4.25 L), we may obtain even higher values, which justifies the concentration (250 μg/mL) that was administered to Caco-

2/15 cells. Therefore, the dose employed in our experiments is physiologically representative (542).

Our results showed that treatment of Caco-2/15 cells with CP fractions evoked no cell damage, but significantly increased occludin, a tight junction protein, suggesting an improved intestinal mucosal barrier that efficiently restricts paracellular permeability. The MC fraction caused the highest stimulation of occludin production, while HC improved the production of the protein under exposure to Fe/Asc stress. The high flavonol content of both the MC and HC fractions may explain this response since it was reported that quercetin enhances intestinal barrier by increasing the assembly of the tight junction protein occludin (543). This class of molecules, along with procyanidins, has shown to improve the mucosal intestinal integrity (544) and kidney epithelial layer tightness (545).

Additionally, our experiments revealed the remarkable capacity of CP fractions to stimulate endogenous antioxidant mechanisms as they protected Caco-2/15 cells from Fe/Asc-induced OxS. CP prevented the increase of LPS-mediated pro-inflammatory cytokines, lowered PGE2 production via COX-2 inhibition and suppressed inflammation and NF-κB activation. Finally, procyanidin oligomers and polymers (HC fraction) restored mitochondrial functioning as suggested by the normalization of mitochondrial ATP production and apoptosis through modulation of local transcription factors and of PGC-1α, a key protein that controls mitochondrial biogenesis and respiration.

PGE2 production/biosynthesis during inflammatory processes is primarily modulated by the concerted activities of three enzymes: prostaglandin E synthase-1 (mPGES-1), cyclooxygenase-2 (COX-2) and 15-hydroxyprostaglandin dehydrogenase (15-PGDH). The

former two enzymes are involved in the synthesis of PGE2 and are inducible by a huge range of stimuli, which include pro-inflammatory IL-1β, TNF-α and IL-6 (546, 547), whereas 15-PGDH is an enzyme degrading PGE2. The role of polyphenols in PGE2 pathway remains quite unclear. It is possible that different types of polyphenols may have distinct actions on the three enzymes, which may explain the discrepancy between COX-2 abundance and PGE2 concentrations.

ROS are highly reactive transient chemical molecules. In limited concentrations, they are indispensable in many normal cellular processes, but their generation under physiological condition is tightly controlled by a large number of antioxidant systems. Among the efficient antioxidant enzymes, the SOD catalyzed the conversion of O_2^- to H_2O_2 and molecular oxygen, whereas the decomposition of H_2O_2 to nontoxic compounds is the main function of CAT and GPx (548). An imbalance between ROS and antioxidant defence causes OxS (549) that can elicit general damage to cells by promoting the oxidation of proteins, DNA and lipids (550) with a direct implication in the pathogenesis of inflammatory bowel diseases (96, 98). Limited efforts have been devoted to understand the influence of CP fractions on the gastrointestinal tract, despite being recognized for developing OxS in response to constant noxious luminal oxidant exposure. Our data clearly disclosed that the CP fractions acted as potent antioxidants that markedly reduced the extent of OxS. Apparently, one of the critical mechanisms for inactivating OxS by CP fractions was via the induction of endogenous antioxidant proteins (SOD, GPx, catalase). Also, our studies clearly pointed out that CP fractions positively modulated the antioxidant defence by up-regulating Nrf2, a central transcription factor that

initiates the transcription of cytoprotective genes following binding to specific DNA sites termed anti-oxidant response elements (ARE) (551).

Caco-2/15 cells have the ability to activate the transcription factor Nrf2, a master regulator of cellular defenses against oxidative stress. Under basal conditions, Nrf2 is bound to its cytosolic inhibitor Keap1, which functions as an adaptor protein in the cullin 3 (Cul3)-based E3 ligase complex that ubiquitinates Nrf2 resulting in proteasomal degradation (552). In the presence of oxidative or electrophilic stress, ubiquitination of Nrf2 is disturbed allowing the accumulation of Nrf2 in the nucleus where Nrf2 binds to the antioxidant response element (ARE) (553) in the regulatory regions of the target genes and drives their expression. In our studies, Nrf2 was assessed in the nucleus, which reflects its full potential to play its cytoprotective regulatory role.

In the present work, CP fractions not only targeted antioxidant components, but also reinforced anti-inflammatory mechanisms. Indeed, the incubation of Caco-2/15 cells with LPS in presence of CP fractions led to the prevention of NF-κB activation and to the reduced generation of the pro-inflammatory mediators TNF-α and IL-6. The CP fractions also targeted the COX-2 pathway further amplifying the protection against inflammation. The inactivation of NF-κB likely led to the downregulation of COX-2, a pro-inflammatory enzyme responsible for the elevated levels of PGE2 prostanoids (554). Overall, our data demonstrated that the different CP fractions are able to suppress LPS-induced pro-inflammatory cytokines and COX-2 expression via the control of NF-κB signal transduction pathway. We therefore propose that maintaining anti-oxidant and anti-inflammatory homeostasis of intestinal tissue by CP may help prevent and/or provide added benefit to treatments of intestinal diseases leading to obvious health benefits.

Mitochondrial processes are of great importance to cells of multiple organs and include energy metabolism, generation of free radicals, calcium homeostasis, and initiation of apoptosis via release of the respiratory protein cytochrome C. Their membranes are potential targets of OxS, but mitochondria are also a source of pro-oxidants and critical regulators of survival and death, thereby contributing to complex diseases (555-557). Based on the facts that grape seed procyanidins (containing a mixture of monomers, dimers, oligomers and polymers) modulate energy metabolism in skeletal muscle mitochondria (558) and that quercetin flavonols preferentially accumulate in mitochondria and prevent damage by ROS (332), we specifically studied the impact of the HC fraction on mitochondrial activity and integrity, assuming that this fraction contained a high quantity of both flavonols and procyanidins. Our data point out that OxS activated apoptotic signaling pathway as indicated by a significant increase of the pro-apoptic protein cytochrome C and a downregulation of the anti-apoptotic protein Bcl-2. It is believed that the accumulation of OxS by-products in mitochondria probably constitutes the upstream cascade trigger that leads to apoptosis (559). Accordingly, we showed the anti-apoptotic effects of cranberry flavonols and procyanidins given the increment of mitochondrial Bcl-2 and the reduced expression of cytochrome C and AIF in their presence. Since Bcl-2 is a key anti-apoptotic regulator of mitochondrial outer membrane permeabilization and a prerequisite for cytochrome C release from mitochondria to cytosol, the positive modulation of this pathway by cranberry flavonols and procyanidins definitely suggests an inhibition of apoptosis. According to available studies, the flavonol quercetin altered the intramitochondrial Ca^{2+} mobilization, cytotoxicity and apoptosis induced by indomethacin and thus appears to prevent mitochondrial dysfunction by regulating

intracellular Ca^{2+} homeostasis and preventing apoptosis (330).

Mitochondrial biogenesis is dependent on the crosstalk between the nuclear and mitochondrial genomes orchestrated by PGC-1α (560). PGC-1α also mediates mitochondrial DNA transcription and replication through two nuclear-encoded genes, including mTFA and mTFB (561). Our studies support the notion of a protective effect of cranberry flavonols and procyanidins on mitochondrial functioning perturbations by restoring ATP synthesis via the rise of PGC-1α protein expression. Additional studies are necessary to delineate whether the stimulation of ATP production by CP is accomplished via mitochondrial biogenesis and/or bio-energetically mitochondrion efficiency. The former action is favoured since it is already known that quercetin induces muscle mitochondrial biogenesis and contributes to improving exercise recuperation by increasing PGC-1α and SIRT1 expression (562). Finally, as suggested by our findings, cranberry flavonols and procyanidins were able to raise OGG1, the DNA repair enzyme, which eliminated DNA damage caused by OxS, thereby preventing the initiation of the vicious cycle of ROS.

The polymers of the HC fraction are not absorbed by intestinal epithelial cells, but could provide a physical barrier for free radicals and antioxidant protection (563). In addition, they may interact with the lipid bilayer and proteins of the membrane, which may alter its chemico-physical properties, thereby generating signals that constitute input for the enterocytes to adjust their metabolism and to influence a number of physiological processes, including glucose uptake via alterations of glucose transporter genes (564, 565) and insulin sensitivity (566) through enhancing insulin signaling inflammatory, cholesterol, and lipogenic pathways in intestinal enterocytes (567). Additional studies are evidently necessary to uncover the mechanisms of action of HC polyphenols to modulate mitochondrial adaptations.

In conclusion, our data support the importance of examining the roles of cranberry polyphenols in regulating cellular processes related to OxS and inflammation, as well as the cross-talk between cellular compartments, which increases our understanding of the mode of actions of this unique blend of polyphenols. Such advances may help determine whether cranberry polyphenols constitute novel therapeutic approaches to better treat inflammatory bowel diseases.

CLINICAL PERSPECTIVES

i) L'inflammation est la composante centrale dans les MII, mais elle s'accompagne d'un stress oxydant persistant. Ainsi, l'intérêt de trouver une molécule à la fois anti-inflammatoire et antioxydante agissant au niveau intestinal, et bien entendu ne causant pas d'effets secondaires supplémentaires à ceux provenant de la médication, est devenu primordial dans le traitement des MII; ii) Our findings provide evidence for the capacity of cranberry polyphenols to reduce intestinal oxidative stress and inflammation while improving mitochondrial dysfunction and iii) The potent free-radical scavenging activity and capacity to reduce inflammation make cranberry polyphenol ideal candidate molecules not only for prevention, but also for complementary treatment strategies to improve health outcomes. Cranberry polyphenols may represent efficient functional foods capable of exerting beneficial actions on intestinal disorders such as inflammatory bowel diseases.

AUTHOR CONTRIBUTION

Marie-Claude Denis, Alexandra Furtos and Emile Levy participated in the design of the study. Marie-Claude Denis, Stéphanie Dudonné, Carole Garofalo and Alain Montoudis conducted the experiments. Marie-Claude Denis, Yves Desjardins, Edgar Delvin and Emile Levy analyzed and interpreted the data. Marie-Claude Denis, Valérie Marcil, Yves Desjardins, André Marette and Emile Levy contributed to the writing of the paper.

FUNDING

This study was supported by the J. A. DeSève Research Chair in Nutrition, the Canadian Foundation of Innovation (EL), Leahy Orchards Inc. & Appleboost Products Inc. and scholarship award from Fonds de recherche du Québec-Nature et technologies (MCD). The funders had no role in study design, data collection and analysis, decision to publish, or

preparation of the manuscript. Therefore, the authors have declared that no competing interests exist.

ACKNOWLEDGEMENTS

Mrs Schohraya Spahis is acknowledged for her excellent technical assistance.

REFERENCES

1. Manach C, Scalbert A, Morand C, Remesy C, Jimenez L. Polyphenols: food sources and bioavailability. Am J Clin Nutr 2004;79:727-47.

2. Galleano M, Calabro V, Prince PD, Litterio MC, Piotrkowski B, Vazquez-Prieto MA et al. Flavonoids and metabolic syndrome. Ann N Y Acad Sci 2012;1259:87-94.

3. Landete JM. Updated knowledge about polyphenols: functions, bioavailability, metabolism, and health. Crit Rev Food Sci Nutr 2012;52:936-48.

4. Salah N, Miller NJ, Paganga G, Tijburg L, Bolwell GP, Rice-Evans C. Polyphenolic flavanols as scavengers of aqueous phase radicals and as chain-breaking antioxidants. Arch Biochem Biophys 1995;322:339-46.

5. Artis D. Epithelial-cell recognition of commensal bacteria and maintenance of immune homeostasis in the gut. Nat Rev Immunol 2008;8:411-20.

6. Hooper LV, Macpherson AJ. Immune adaptations that maintain homeostasis with the intestinal microbiota. Nat Rev Immunol 2010;10:159-69.

7. Srigiridhar K, Nair KM. Iron-deficient intestine is more susceptible to peroxidative damage during iron supplementation in rats. Free Radic Biol Med 1998;25:660-5.

8. Gonzalez PK, Doctrow SR, Malfroy B, Fink MP. Role of oxidant stress and iron delocalization in acidosis-induced intestinal epithelial hyperpermeability. Shock 1997;8:108-14.

9. Reifen R, Matas Z, Zeidel L, Berkovitch Z, Bujanover Y. Iron supplementation may aggravate inflammatory status of colitis in a rat model. Dig Dis Sci 2000;45:394-7.

10. Biswas K, Bandyopadhyay U, Chattopadhyay I, Varadaraj A, Ali E, Banerjee RK. A novel antioxidant and antiapoptotic role of omeprazole to block gastric ulcer through scavenging of hydroxyl radical. J Biol Chem 2003;278:10993-1001.

11. Parks DA, Williams TK, Beckman JS. Conversion of xanthine dehydrogenase to oxidase in ischemic rat intestine: a reevaluation. Am J Physiol 1988;254:G768-G774.

12. Sanchez S, Martin MJ, Ortiz P, Motilva V, Alarcon dlL. Effects of dipyrone on inflammatory infiltration and oxidative metabolism in gastric mucosa: comparison with acetaminophen and diclofenac. Dig Dis Sci 2002;47:1389-98.

13. Sartor RB, Muehlbauer M. Microbial host interactions in IBD: implications for pathogenesis and therapy. Curr Gastroenterol Rep 2007;9:497-507.

14. Eberhardt MV, Lee CY, Liu RH. Antioxidant activity of fresh apples. Nature 2000;405:903-4.

15. Kim DO, Lee KW, Lee HJ, Lee CY. Vitamin C equivalent antioxidant capacity (VCEAC) of phenolic phytochemicals. J Agric Food Chem 2002;50:3713-7.

16. Korycka-Dahl MB, Richardson T. Activated oxygen species and oxidation of food constituents. CRC Crit Rev Food Sci Nutr 1978;10:209-41.

17. Lavelli V, Hippeli S, Peri C, Elstner EF. Evaluation of radical scavenging activity of fresh and air-dried tomatoes by three model reactions. J Agric Food Chem 1999;47:3826-31.

18. Rubas W, Cromwell ME, Shahrokh Z, Villagran J, Nguyen TN, Wellton M et al. Flux measurements across Caco-2 monolayers may predict transport in human large intestinal tissue. J Pharm Sci 1996;85:165-9.

19. Yang F, Wang J, Li X, Ying T, Qiao S, Li D, Wu G. 2-DE and MS analysis of interactions between Lactobacillus fermentum I5007 and intestinal epithelial cells. Electrophoresis 2007;28:4330-9.

20. Sun H, Chow EC, Liu S, Du Y, Pang KS. The Caco-2 cell monolayer: usefulness and limitations. Expert Opin Drug Metab Toxicol 2008;4:395-411.

21. McKay DL, Blumberg JB. Cranberries (Vaccinium macrocarpon) and cardiovascular disease risk factors. Nutr Rev 2007;65:490-502.

22. Puupponen-Pimia R, Nohynek L, Alakomi HL, Oksman-Caldentey KM. Bioactive berry compounds-novel tools against human pathogens. Appl Microbiol Biotechnol 2005;67:8-18.

23. Kevers C, Pincemail J, Tabart J, Defraigne JO, Dommes J. Influence of cultivar, harvest time, storage conditions, and peeling on the antioxidant capacity and phenolic and ascorbic acid contents of apples and pears. J Agric Food Chem 2011;59:6165-71.

24. Brownmiller C, Howard LR, Prior RL. Processing and storage effects on procyanidin composition and concentration of processed blueberry products. J Agric Food Chem 2009;57:1896-902.

25. Prior RL, Gu L. Occurrence and biological significance of proanthocyanidins in the American diet. Phytochemistry 2005;66:2264-80.

26. Bernotti S, Seidman E, Sinnett D, Brunet S, Dionne S, Delvin E, Levy E. Inflammatory reaction without endogenous antioxidant response in Caco-2 cells exposed to iron/ascorbate-mediated lipid peroxidation. Am J Physiol Gastrointest Liver Physiol 2003;285:G898-G906.

27. Courtois F, Delvin E, Ledoux M, Seidman E, Lavoie JC, Levy E. The antioxidant BHT normalizes some oxidative effects of iron + ascorbate on lipid metabolism in Caco-2 cells. J Nutr 2002;132:1289-92.

28. Courtois F, Seidman EG, Delvin E, Asselin C, Bernotti S, Ledoux M, Levy E. Membrane peroxidation by lipopolysaccharide and iron-ascorbate adversely affects Caco-2 cell function: beneficial role of butyric acid. Am J Clin Nutr 2003;77:744-50.

29. Levy E, Mehran M, Seidman E. Caco-2 cells as a model for intestinal lipoprotein synthesis and secretion. FASEB J 1995;9:626-35.

30. Levy E, Trudel K, Bendayan M, Seidman E, Delvin E, Elchebly M et al. Biological role, protein expression, subcellular localization, and oxidative stress response of paraoxonase 2 in the intestine of humans and rats. Am J Physiol Gastrointest Liver Physiol 2007;293:G1252-G1261.

31. Marcil V, Seidman E, Sinnett D, Boudreau F, Gendron FP, Beaulieu JF et al. Modification in oxidative stress, inflammation, and lipoprotein assembly in response to hepatocyte nuclear factor 4alpha knockdown in intestinal epithelial cells. J Biol Chem 2010;285:40448-60.

32. Precourt LP, Seidman E, Delvin E, Amre D, Deslandres C, Dominguez M et al. Comparative expression analysis reveals differences in the regulation of intestinal paraoxonase family members. Int J Biochem Cell Biol 2009;41:1628-37.

33. Precourt LP, Marcil V, Ntimbane T, Taha R, Lavoie JC, Delvin E et al. Antioxidative properties of paraoxonase 2 in intestinal epithelial cells. Am J Physiol Gastrointest Liver Physiol 2012.

34. Taha R, Seidman E, Mailhot G, Boudreau F, Gendron FP, Beaulieu JF et al. Oxidative stress and mitochondrial functions in the intestinal Caco-2/15 cell line. PLoS One 2010;5:e11817.

35. Spahis S, Vanasse M, Belanger SA, Ghadirian P, Grenier E, Levy E. Lipid profile, fatty acid composition and pro- and anti-oxidant status in pediatric patients with attention-deficit/hyperactivity disorder. Prostaglandins Leukot Essent Fatty Acids 2008;79:47-53.

36. McCord JM, Fridovich I. Superoxide dismutase. An enzymic function for erythrocuprein (hemocuprein). J Biol Chem 1969;244:6049-55.

37. Jiang ZY, Woollard AC, Wolff SP. Lipid hydroperoxide measurement by oxidation of Fe2+ in the presence of xylenol orange. Comparison with the TBA assay and an iodometric method. Lipids 1991;26:853-6.

38. Taha R, Seidman E, Mailhot G, Boudreau F, Gendron FP, Beaulieu JF et al. Oxidative stress and mitochondrial functions in the intestinal Caco-2/15 cell line. PLoS One 2010;5:e11817.

39. Bohr VA, Stevnsner T, de Souza-Pinto NC. Mitochondrial DNA repair of oxidative damage in mammalian cells. Gene 2002;286:127-34.

40. Esposito LA, Melov S, Panov A, Cottrell BA, Wallace DC. Mitochondrial disease in mouse results in increased oxidative stress. Proc Natl Acad Sci U S A 1999;96:4820-5.

41. Scarpulla RC. Transcriptional activators and coactivators in the nuclear control of mitochondrial function in mammalian cells. Gene 2002;286:81-9.

42. Wang SY, Lin HS. Antioxidant activity in fruits and leaves of blackberry, raspberry, and strawberry varies with cultivar and developmental stage. J Agric Food Chem 2000;48:140-6.

43. Sun J, Chu YF, Wu X, Liu RH. Antioxidant and antiproliferative activities of common fruits. J Agric Food Chem 2002;50:7449-54.

44. Fang MZ, Wang Y, Ai N, Hou Z, Sun Y, Lu H et al. Tea polyphenol (-)-epigallocatechin-3-gallate inhibits DNA methyltransferase and reactivates methylation-silenced genes in cancer cell lines. Cancer Res 2003;63:7563-70.

45. Wu X, Beecher GR, Holden JM, Haytowitz DB, Gebhardt SE, Prior RL. Lipophilic and hydrophilic antioxidant capacities of common foods in the United States. J Agric Food Chem 2004;52:4026-37.

46. Burleigh AE, Benck SM, McAchran SE, Reed JD, Krueger CG, Hopkins WJ. Consumption of sweetened, dried cranberries may reduce urinary tract infection incidence in susceptible women -- a modified observational study. Nutr J 2013;12:139.

47. Wilson T, Meyers SL, Singh AP, Limburg PJ, Vorsa N. Favorable glycemic response of type 2 diabetics to low-calorie cranberry juice. J Food Sci 2008;73:H241-H245.

48. McKay DL, Blumberg JB. Cranberries (Vaccinium macrocarpon) and cardiovascular disease risk factors. Nutr Rev 2007;65:490-502.

49. Ruel G, Couillard C. Evidences of the cardioprotective potential of fruits: the case of cranberries. Mol Nutr Food Res 2007;51:692-701.

50. Crozier A, Jaganath IB, Clifford MN. Dietary phenolics: chemistry, bioavailability and effects on health. Nat Prod Rep 2009;26:1001-43.

51. Manach C, Williamson G, Morand C, Scalbert A, Remesy C. Bioavailability and bioefficacy of polyphenols in humans. I. Review of 97 bioavailability studies. Am J Clin Nutr 2005;81:230S-42S.

52. Deprez S, Mila I, Huneau JF, Tome D, Scalbert A. Transport of proanthocyanidin dimer, trimer, and polymer across monolayers of human intestinal epithelial Caco-2 cells. Antioxid Redox Signal 2001;3:957-67.

53. Ou K, Percival SS, Zou T, Khoo C, Gu L. Transport of cranberry A-type procyanidin dimers, trimers, and tetramers across monolayers of human intestinal epithelial Caco-2 cells. J Agric Food Chem 2012;60:1390-6.

54. Courtois F, Suc I, Garofalo C, Ledoux M, Seidman E, Levy E. Iron-ascorbate alters the efficiency of Caco-2 cells to assemble and secrete lipoproteins. Am J Physiol Gastrointest Liver Physiol 2000;279:G12-G19.

55. Grenier E, Maupas FS, Beaulieu JF, Seidman E, Delvin E, Sane A et al. Effect of retinoic acid on cell proliferation and differentiation as well as on lipid synthesis, lipoprotein secretion, and apolipoprotein biogenesis. Am J Physiol Gastrointest Liver Physiol 2007;293:G1178-G1189.

56. Levy E, Menard D, Suc I, Delvin E, Marcil V, Brissette L et al. Ontogeny, immunolocalisation, distribution and function of SR-BI in the human intestine. J Cell Sci 2004;117:327-37.

57. Levy E, Harmel E, Laville M, Sanchez R, Emonnot L, Sinnett D et al. Expression of Sar1b enhances chylomicron assembly and key components of the coat protein complex II system driving vesicle budding. Arterioscler Thromb Vasc Biol 2011;31:2692-9.

58. Mailhot G, Ravid Z, Barchi S, Moreau A, Rabasa-Lhoret R, Levy E. CFTR knockdown stimulates lipid synthesis and transport in intestinal Caco-2/15 cells. Am J Physiol Gastrointest Liver Physiol 2009;297:G1239-G1249.

59. Marcil V, Delvin E, Seidman E, Poitras L, Zoltowska M, Garofalo C, Levy E. Modulation of lipid synthesis, apolipoprotein biogenesis, and lipoprotein assembly by butyrate. Am J Physiol Gastrointest Liver Physiol 2002;283:G340-G346.

60. Ravid Z, Bendayan M, Delvin E, Sane AT, Elchebly M, Lafond J et al. Modulation of intestinal cholesterol absorption by high glucose levels: impact on cholesterol transporters, regulatory enzymes, and transcription factors. Am J Physiol Gastrointest Liver Physiol 2008;295:G873-G885.

61. Sane AT, Sinnett D, Delvin E, Bendayan M, Marcil V, Menard D et al. Localization and role of NPC1L1 in cholesterol absorption in human intestine. J Lipid Res 2006;47:2112-20.

62. Cencic A, Langerholc T. Functional cell models of the gut and their applications in food microbiology--a review. Int J Food Microbiol 2010;141 Suppl 1:S4-14.

63. Li Y, Shin YG, Yu C, Kosmeder JW, Hirschelman WH, Pezzuto JM, van Breemen RB. Increasing the throughput and productivity of Caco-2 cell permeability assays using liquid chromatography-mass spectrometry: application to resveratrol absorption and metabolism. Comb Chem High Throughput Screen 2003;6:757-67.

64. Vaidyanathan JB, Walle T. Transport and metabolism of the tea flavonoid (-)-epicatechin by the human intestinal cell line Caco-2. Pharm Res 2001;18:1420-5.

65. Scalbert A, Williamson G. Dietary intake and bioavailability of polyphenols. J Nutr 2000;130:2073S-85S.

66. Farrell TL, Poquet L, Dew TP, Barber S, Williamson G. Predicting phenolic acid absorption in Caco-2 cells: a theoretical permeability model and mechanistic study. Drug Metab Dispos 2012;40:397-406.

67. Suzuki T, Hara H. Quercetin enhances intestinal barrier function through the assembly of zonula [corrected] occludens-2, occludin, and claudin-1 and the expression of claudin-4 in Caco-2 cells. J Nutr 2009;139:965-74.

68. Pierre JF, Heneghan AF, Feliciano RP, Shanmuganayagam D, Roenneburg DA, Krueger CG et al. Cranberry proanthocyanidins improve the gut mucous layer morphology and function in mice receiving elemental enteral nutrition. JPEN J Parenter Enteral Nutr 2013;37:401-9.

69. Lipson SM. Cranberry and Grape Juices Affect Tight Junction Function and Structural Integrity of Rotavirus-Infected Monkey Kidney Epithelial Cell Monolayers. Food Environ Virol 2011;3:46-54.

70. Stichtenoth DO, Thoren S, Bian H, Peters-Golden M, Jakobsson PJ, Crofford LJ. Microsomal prostaglandin E synthase is regulated by proinflammatory cytokines and glucocorticoids in primary rheumatoid synovial cells. J Immunol 2001;167:469-74.

71. Thoren S, Jakobsson PJ. Coordinate up- and down-regulation of glutathione-dependent prostaglandin E synthase and cyclooxygenase-2 in A549 cells. Inhibition by NS-398 and leukotriene C4. Eur J Biochem 2000;267:6428-34.

72. MacMillan-Crow LA, Crow JP. Does more MnSOD mean more hydrogen peroxide? Anticancer Agents Med Chem 2011;11:178-80.

73. Sies H. Role of reactive oxygen species in biological processes. Klin Wochenschr 1991;69:965-8.

74. Cadenas E, Davies KJ. Mitochondrial free radical generation, oxidative stress, and aging. Free Radic Biol Med 2000;29:222-30.

75. Pavlick KP, Laroux FS, Fuseler J, Wolf RE, Gray L, Hoffman J, Grisham MB. Role of reactive metabolites of oxygen and nitrogen in inflammatory bowel disease. Free Radic Biol Med 2002;33:311-22.

76. Karp SM, Koch TR. Oxidative stress and antioxidants in inflammatory bowel disease. Dis Mon 2006;52:199-207.

77. Moi P, Chan K, Asunis I, Cao A, Kan YW. Isolation of NF-E2-related factor 2 (Nrf2), a NF-E2-like basic leucine zipper transcriptional activator that binds to the tandem NF-E2/AP1 repeat of the beta-globin locus control region. Proc Natl Acad Sci U S A 1994;91:9926-30.

78. Kobayashi A, Kang MI, Okawa H, Ohtsuji M, Zenke Y, Chiba T et al. Oxidative stress sensor Keap1 functions as an adaptor for Cul3-based E3 ligase to regulate proteasomal degradation of Nrf2. Mol Cell Biol 2004;24:7130-9.

79. Rushmore TH, Morton MR, Pickett CB. The antioxidant responsive element. Activation by oxidative stress and identification of the DNA consensus sequence required for functional activity. J Biol Chem 1991;266:11632-9.

80. Li Q, Verma IM. NF-kappaB regulation in the immune system. Nat Rev Immunol 2002;2:725-34.

81. Yan MH, Wang X, Zhu X. Mitochondrial defects and oxidative stress in Alzheimer disease and Parkinson disease. Free Radic Biol Med 2013;62:90-101.

82. Schapira AH. Mitochondrial diseases. Lancet 2012;379:1825-34.

83. Newsholme P, Gaudel C, Krause M. Mitochondria and diabetes. An intriguing pathogenetic role. Adv Exp Med Biol 2012;942:235-47.

84. Pajuelo D, Diaz S, Quesada H, Fernandez-Iglesias A, Mulero M, Arola-Arnal A et al. Acute administration of grape seed proanthocyanidin extract modulates energetic metabolism in skeletal muscle and BAT mitochondria. J Agric Food Chem 2011;59:4279-87.

85. Fiorani M, Guidarelli A, Blasa M, Azzolini C, Candiracci M, Piatti E, Cantoni O. Mitochondria accumulate large amounts of quercetin: prevention of mitochondrial damage and release upon oxidation of the extramitochondrial fraction of the flavonoid. J Nutr Biochem 2010;21:397-404.

86. Wang GW, Klein JB, Kang YJ. Metallothionein inhibits doxorubicin-induced mitochondrial cytochrome c release and caspase-3 activation in cardiomyocytes. J Pharmacol Exp Ther 2001;298:461-8.

87. Carrasco-Pozo C, Pastene E, Vergara C, Zapata M, Sandoval C, Gotteland M. Stimulation of cytosolic and mitochondrial calcium mobilization by indomethacin in Caco-2 cells: modulation by the polyphenols quercetin, resveratrol and rutin. Biochim Biophys Acta 2012;1820:2052-61.

88. Ruchko M, Gorodnya O, LeDoux SP, Alexeyev MF, Al-Mehdi AB, Gillespie MN. Mitochondrial DNA damage triggers mitochondrial dysfunction and apoptosis in oxidant-challenged lung endothelial cells. Am J Physiol Lung Cell Mol Physiol 2005;288:L530-L535.

89. Poulsen HE, Prieme H, Loft S. Role of oxidative DNA damage in cancer initiation and promotion. Eur J Cancer Prev 1998;7:9-16.

90. Davis CS, Mock KE, Bentz BJ, Bromilow SM, Bartell NV, Murray BW et al. Isolation and characterization of 16 microsatellite loci in the mountain pine beetle, Dendroctonus ponderosae Hopkins (Coleoptera: Curculionidae: Scolytinae). Mol Ecol Resour 2009;9:1071-3.

91. Fraga CG, Galleano M, Verstraeten SV, Oteiza PI. Basic biochemical mechanisms behind the health benefits of polyphenols. Mol Aspects Med 2010;31:435-45.

92. Johnston K, Sharp P, Clifford M, Morgan L. Dietary polyphenols decrease glucose uptake by human intestinal Caco-2 cells. FEBS Lett 2005;579:1653-7.

93. Alzaid F, Cheung HM, Preedy VR, Sharp PA. Regulation of glucose transporter expression in human intestinal Caco-2 cells following exposure to an anthocyanin-rich berry extract. PLoS One 2013;8:e78932.

94. Solomon TP, Blannin AK. Changes in glucose tolerance and insulin sensitivity following 2 weeks of daily cinnamon ingestion in healthy humans. Eur J Appl Physiol 2009;105:969-76.

95. Qin B, Dawson HD, Schoene NW, Polansky MM, Anderson RA. Cinnamon polyphenols regulate multiple metabolic pathways involved in insulin signaling and intestinal lipoprotein metabolism of small intestinal enterocytes. Nutrition 2012;28:1172-9.

Table 1: Profile of cranberry fractions

	Cranberry fractions		
	LC	MC	HC
Polyphenol compounds	Polyphenol content (g/100 g extract dry weight)		
Total polyphenols	5.0 ± 0.1	54.5 ± 0.9	52.0 ± 1.0
Anthocyanins	1.1 ± 0.1	5.2 ± 0.1	0.1 ± 0.002
Flavonols	-	13.7 ± 0.3	16.0 ± 0.2
Phenolic acids	2.5 ± 0.1	-	-
Procyanidins	-	11.5 ± 0.1	29.0 ± 0.2
Monomers		1.1 ± 0.1	-
Dimers		10.2 ± 0.1	13.8 ± 0.1
Oligomers (DP 3 and 4)		-	10.9 ± 0.1
Polymers (DP 5 to > 10)		-	4.3 ± 0.1

Phenolic content of low-molecular weight (LC), medium-molecular weight (MC) and hight-molecular-weight (HC) in terms of phenolic acid, flavonoid, procyanidins and total phenolics. The total phenolic content was determined using the Folin-Ciocalteu method (473), with gallic acid as a main standard. The flavonoids were analyzed by UPLC-TDQ and the quantification was performed in multiple reactions monitoring mode, tracking the transition of parent and product ions specific for each compound with external calibration. The procyanidin content (DP 2 to > 10) was analyzed by normal phase analytical HPLC using an Agilent 1260/1290 Infinity system coupled to a fluorescence detector, using external calibration curve of (-)-epicatechin. The results were expressed as g/100 g of extract weight ± SEM.

Table 2: Effects of cranberry on fatty acid composition in Caco-2/15 cells

Fatty acids	Ctrl (%)	Fe/Asc (%)	LC + Fe/Asc (%)	MC + Fe/Asc (%)	HC + Fe/Asc (%)
14:0	1.64 ± 0.08	2.25 ± 0.02 *	1.71 ± 0.01	1.68 ± 0.01	1.72 ± 0.02
16:0	16.74 ± 0.61	24.04 ± 0.21***	17.81 ± 0.21###	17.25 ± 0.16###	17.02 ± 0.21###
18:0	11.78 ± 0.16	20.75 ± 0.47***	12.51 ± 0.41###	14.01 ± 0.12###	13.20 ± 0.13###
20:0	0.660 ± 0.026	0.674 ± 0.003	0.551 ± 0.019	0.633 ± 0.005	0.740 ± 0.023
22:0	0.730 ± 0.012	0.530 ± 0.009	0.481 ± 0.013	0.611 ± 0.005	0.685 ± 0.017
24:0	1.02 ± 0.029	0.909 ± 0.016	0.896 ± 0.010	1.060 ± 0.001	1.12 ± 0.05
ALA:18:3n-3	0.048 ± 0.004	0.080 ± 0.004	0.027 ± 0.003	0.117 ± 0.001	0.080 ± 0.002
20:3n-3	0.040 ± 0.003	0.060 ± 0.003	0.065 ± 0.005	0.069 ± 0.001	0.085 ± 0.002
EPA:20:5n-3	1.830 ± 0.030	0.576 ± 0.084***	1.47 ± 0.04###	1.47 ± 0.01###	1.59 ± 0.02###
22:5n-3	0.694 ± 0.013	0.506 ± 0.018	0.531 ± 0.015	0.552 ± 0.005	0.528 ± 0.001
DHA:22:6n-3	2.12 ± 0.04	1.15 ± 0.081***	1.69 ± 0.02	1.64 ± 0.01	2.12 ± 0.08###
AL:18:2n-6	1.68 ± 0.03	2.78 ± 0.024***	1.83 ± 0.03###	1.87 ± 0.01###	1.93 ± 0.02###
18:3n-6	0.355 ± 0.001	0.225 ± 0.021	0.376 ± 0.023	0.480 ± 0.006	0.477 ± 0.009
20:2n-6	0.015 ± 0.001	0.010 ± 0.001	0.012 ± 0.001	0.007 ± 0.001	0.039 ± 0.007
20:3n-6	1.04 ± 0.02	0.577 ± 0.027	0.891 ± 0.023	0.889 ± 0.008	1.03 ± 0.02
AA:20:4n-6	4.33 ± 0.02	4.24 ± 0.14	3.84 ± 0.16	4.18 ± 0.02	4.66 ± 0.12
22:2n-6	0.306 ± 0.008	0.116 ± 0.013	0.297 ± 0.054	0.184 ± 0.061	0.095 ± 0.014
22:4n-6	0.015 ± 0.001	0.012 ± 0.001	0.012 ± 0.001	0.021 ± 0.002	0.074 ± 0.014
16:1n-7	5.65 ± 0.24	5.70 ± 0.30	5.87 ± 0.04	4.890 ± 0.005###	5.10 ± 0.07#
18:1n-7	12.40 ± 0.23	9.21 ± 0.14***	12.70 ± 0.48###	12.78 ± 0.09###	12.38 ± 0.19###
18:1n-9	30.07 ± 0.60	19.92 ± 0.21***	30.44 ± 0.96###	29.37 ± 0.20###	29.11 ± 0.37###
20:1n-9	2.28 ± 0.11	1.76 ± 0.07	1.75 ± 0.04	1.75 ± 0.02	1.78 ± 0.02
20:3n-9	0.268 ± 0.004	0.195 ± 0.008	0.190 ± 0.001	0.242 ± 0.005	0.258 ± 0.002
22:1n-9	3.00 ± 0.04	2.92 ± 0.01	3.21 ± 0.04	3.08 ± 0.008	3.22 ± 0.11
24:1n-9	1.30 ± 0.05	0.817 ± 0.021	0.854 ± 0.001	1.16 ± 0.03	0.970 ± 0.022
Total n-3	4.73 ± 0.05	2.37 ± 0.04***	3.78 ± 0.08###	3.85 ± 0.03###	4.57 ± 0.10###
Total n-6	7.74 ± 0.08	7.95 ± 0.17	7.25 ± 0.18##	7.63 ± 0.10	8.31 ± 0.14
Total n-7	19.61 ± 0.51	14.92 ± 0.37***	20.08 ± 0.56###	19.01 ± 0.11###	18.25 ± 0.32###
Total n-9	59.92 ± 1.08	25.61 ± 1.09***	36.44 ± 1.05###	35.61 ± 0.20###	35.33 ± 0.41###
Saturated FA	36.04 ± 0.43	35.86 ± 0.30	38.67 ± 0.65###	39.39 ± 0.43###	38.02 ± 0.42###
Mono-unsaturated	80.49 ± 1.05	66.03 ± 0.84***	58.90 ± 0.84###	56.46 ± 0.36###	54.78 ± 0.80###
PUFA	12.73 ± 0.13	10.52 ± 0.08***	11.22 ± 0.26##	11.72 ± 0.14###	13.14 ± 0.24###
ALA/LA	0.012 ± 0.002	0.015 ± 0.005	0.005 ± 0.001	0.026 ± 0.001	0.011 ± 0.001
DHA/AA	0.204 ± 0.001	0.145 ± 0.001	0.005 ± 0.001	0.026 ± 0.001	0.011 ± 0.001
n-6/n-3	0.684 ± 0.001	1.800 ± 0.003***	0.688 ± 0.002###	0.835 ± 0.005###	0.476 ± 0.003###
Δ6 20:3n6/18:2n6	0.259 ± 0.018	0.111 ± 0.015	0.175 ± 0.012	0.201 ± 0.011	0.139 ± 0.010
Δ9 18:1n9/18:0	1.07 ± 0.14	0.515 ±0.100*	0.875 ± 0.110	0.883 ± 0.110	0.574 ± 0.160
Δ7 16:1n7/16:0	0.141 ± 0.002	0.127 ± 0.003	0.118 ± 0.002	0.119 ± 0.005	0.078 ± 0.002

Following differentiation, Caco-2/15 cells were incubated for 6h at 37ºC in the absence or presence of Fe/Asc (200 µM/ 2mM) with low (LC), medium (MC) or high (HC) molecular weight phenolic compounds (250 µg/mL) and analyzed for fatty acid (FA) composition. Results are expressed as % of total fatty acid content. Data represent the means ± SEM of three experiments, each done in duplicate (n=6). Student's *t* test (two-tailed) was used to compare differences between means (X±SEM). **P*<0.05, ****P*<0.001 vs. Ctrl; $^{\#\#}P$<0.01, $^{\#\#\#}P$<0.001 vs. Fe/Asc.

AA: arachidonic acid; ALA: alpha-linolenic acid; DHA: docosahexaenoic acid; EPA: eicosapentaenoic acid; LA: linoleic acid; PUFA: polyunsaturated fatty acids.

FIGURE LEGENDS

Figure 1 **Effects of cranberry on lipid peroxidation and on regulatory endogenous antioxidant activities in Caco-2/15 cells.** Low (LC), medium (MC) or high (HC) molecular weight phenolic compounds (250 µg/mL) isolated from cranberry were added to the apical compartment of differentiated Caco-2/15 cells for 24h before incubation with Fe/Asc (200 µM/2 mM) and LPS (200 µg/mL) for 6h at 37°C as described in Materials and Methods. Estimation of lipid peroxidation was assessed by measuring MDA by HPLC (A). The activity of superoxide dismutase (SOD, B), glutathione peroxidase (GPx), glutathione reductase (GSH-Red, D) and catalase (CAT, E) was then measured. Results represent the means ± SEM of n=3 independent experiments. $^{**}P<0.01$, $^{***}P<0.001$ vs. Ctrl; $^{\#}P<0.05$, $^{\#\#}P<0.01$, $^{\#\#\#}P<0.001$ vs. Fe/Asc.

Figure 2 **Regulatory effects of cranberry polyphenols on oxidative stress and LPS-induced inflammation on prostaglandin E2 and cyclooxygenase 2 in Caco-2/15 cells.** Low (LC), medium (MC) or high (HC) molecular weight phenolic compounds (250 µg/mL) were added to the apical compartment of differentiated Caco-2/15 cells for 24h before incubation with Fe/Asc (200 µM/2 mM) and LPS (200 µg/mL), for 6h at 37°C as described in Materials and Methods. PGE2 (A and B) was determined by enzymatic immunoassay while protein expression of COX-2 (C and D) was determined by Western blotting. Results represent the means ± SEM of N=3 independent experiments. $^{**}P<0.01$, $^{***}P<0.001$ vs. Ctrl; $^{\#\#\#}P<0.001$ vs. Fe/Asc; $^{\$\$}P<0.01$, $^{\$\$\$}P<0.001$ vs. LPS

Figure 3 **Effects of cranberry polyphenols on oxidative stress or LPS-induced inflammation on proinflammatory cytokines in Caco-2/15 cells.** Low (LC), medium (MC) or high (HC) molecular weight phenolic compounds (250 µg/mL) were added to the apical compartment of differentiated Caco-2/15 cells for 24h before incubation with Fe/Asc (200 µM/2 mM) or LPS (200 µg/mL) for 6h at 37°C as described in Materials and Methods. Protein expression of the inflammatory markers TNF-α (A and C) and IL-6 (B and D) was determined by Western blot. Results represent the means ± SEM of n=3 independent experiments. $^{**}P<0.01$, $^{***}P<0.001$ vs. Ctrl; $^{\#\#\#}P<0.001$ vs. Fe/Asc; $^{\$\$\$}P<0.001$ vs. LPS.

Figure 4 **Effects of cranberry polyphenols on oxidative stress or LPS-induced inflammation on key transcription factors in Caco-2/15 cells.** Low (LC), medium (MC) or high (HC) molecular weight phenolic compounds (250 µg/mL) were added to the apical compartment of differentiated Caco-2/15 cells for 24h before incubation with Fe/Asc (200 µM/2 mM) and LPS (200 µg/mL) for 6h at 37°C as described in Materials and Methods. Protein expression of the transcription factors NF-κB (A and D), Nrf2 (B and E) and PGC-1α (C and F) in nucleus and IκB in cytosol was determined by Western blot. Results represent the means ± SEM of n=3 independent experiments. $^{*}P<0.05$, $^{**}P<0.01$, $^{***}P<0.001$ vs.Ctrl; $^{\#}P<0.05$, $^{\#\#\#}P<0.001$ vs. Fe/Asc; $^{\$}P<0.05$, $^{\$\$}P<0.01$, $^{\$\$\$}P<0.001$ vs. LPS.

Figure 5 **Effects of high molecular weight phenolic cranberry compounds on mitochondrial fonctions induced by oxidative stress in Caco-2/15 cells.** High

(HC) molecular weight phenolic compounds (250 µg/mL) were added to the apical compartment of differentiated Caco-2/15 cells for 24h before incubation with Fe/Asc (200 µM/2 mM) for 6h at 37°C as described in Materials and Methods. Mitochondrial ATP content was measured by luciferase driven bioluminescence while the protein expression of AIF (B), Bcl-2 (C) and CytC (D) in mitochondria was determined by Western blot. Results represent the means ± SEM of n=3 independent experiments. **P*<0.05, ****P*<0.001 vs.Ctrl; ###*P*<0.001 vs. Fe/Asc.

Figure 6 **Effects of high molecular weight phenolic cranberry compounds on the mitochondrial protein expression of OGG1 and transcription factors by oxidative stress in Caco-2/15 cells.** High (HC) molecular-weight phenolic compounds (250 µg/mL) isolated from cranberry were added to the apical compartment of differentiated Caco-2/15 cells for 24h before incubation with Fe/Asc (200 µM/2 mM) for 6h at 37°C as described in Materials and Methods. Protein expression of the OGG1 (A), TFA (B), TFB_1 (C) and TFB_2 (D) in mitochondria was determined by Western blot. Results represent the means ± SEM of n=3 independent experiments. **P*<0.05, ** *P*<0.01, ****P*<0.001 vs. Ctrl; #*P*<0.05, ###*P*<0.001 vs. Fe/Asc.

Figure 1

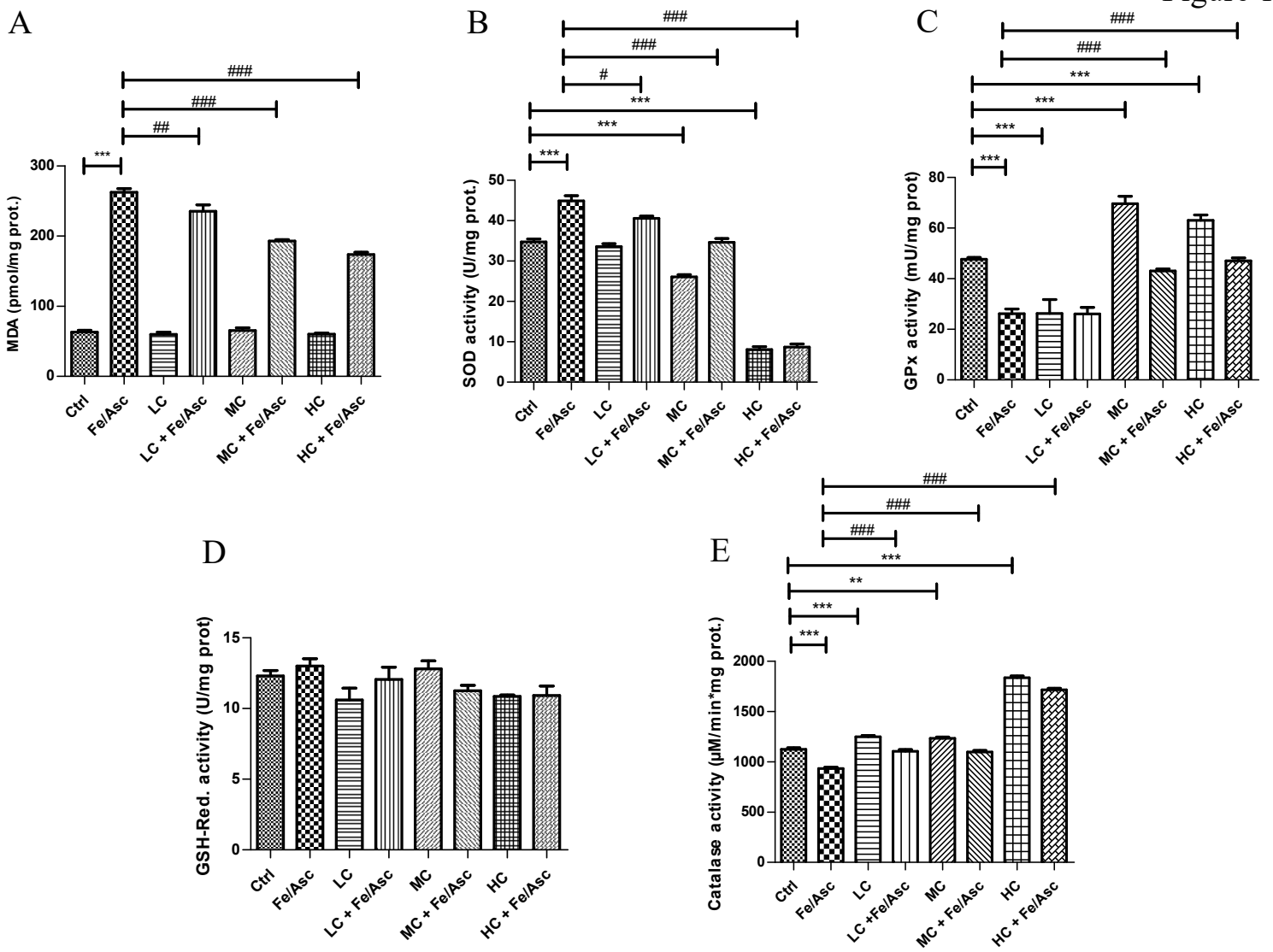
A
MDA (pmol/mg prot.)
300
200
100
0
***
##
###
###
Ctrl
Fe/Asc
LC
LC + Fe/Asc
MC
MC + Fe/Asc
HC
HC + Fe/Asc
B
SOD activity (U/mg prot.)
50
40
30
20
10
0
***
***
***
#
###
###
C
GPx activity (mU/mg prot)
80
60
40
20
0
***
***
***
***
###
###
D
GSH-Red. activity (U/mg prot)
15
10
5
0
E
Catalase activity (µM/min*mg prot.)
2000
1500
1000
500
0
***
***
**
###
###
###

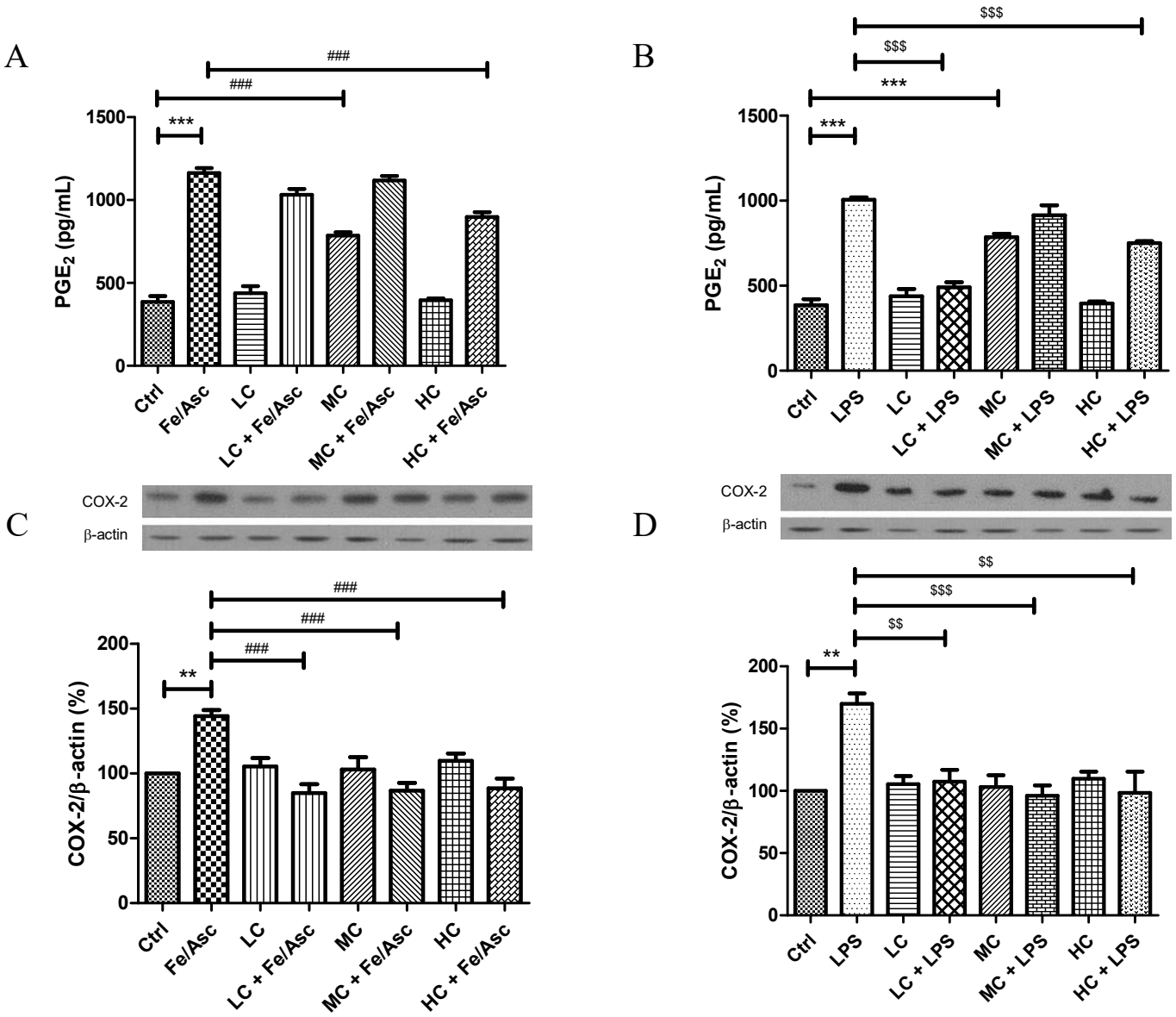
A
B
C
D
PGE2 (pg/mL)
COX-2/β-actin (%)
COX-2
β-actin
Ctrl
Fe/Asc
LPS
LC
LC + Fe/Asc
LC + LPS
MC
MC + Fe/Asc
MC + LPS
HC
HC + Fe/Asc
HC + LPS
***
**
###
$$
$$$

Figure 2

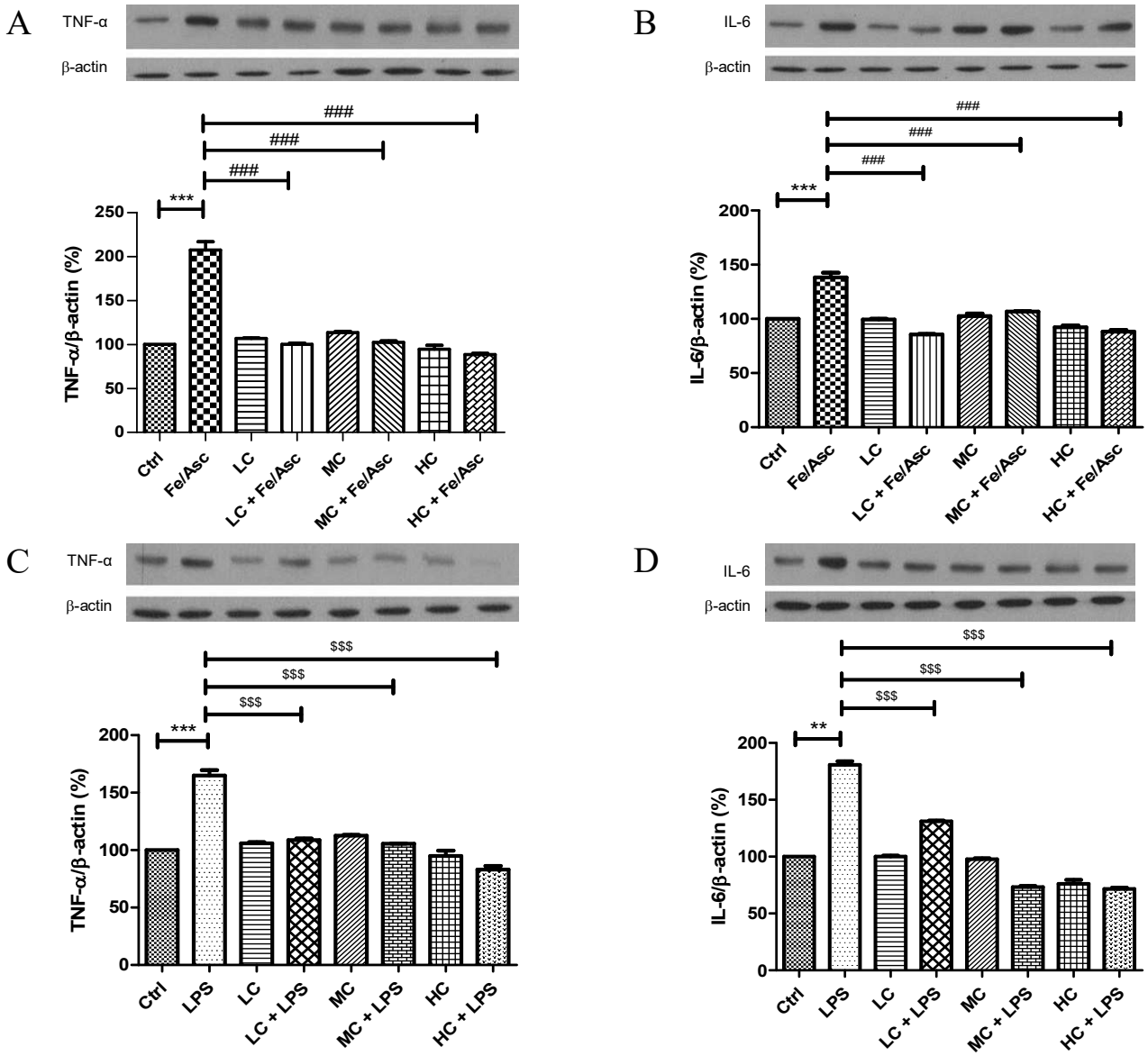
A
TNF-α
β-actin
###
###
###
***
250
200
150
100
50
0
TNF-α/β-actin (%)
Ctrl
Fe/Asc
LC
LC + Fe/Asc
MC
MC + Fe/Asc
HC
HC + Fe/Asc
B
IL-6
β-actin
###
###
###
***
200
150
100
50
0
IL-6/β-actin (%)
Ctrl
Fe/Asc
LC
LC + Fe/Asc
MC
MC + Fe/Asc
HC
HC + Fe/Asc
C
TNF-α
β-actin
$$$
$$$
$$$
***
200
150
100
50
0
TNF-α/β-actin (%)
Ctrl
LPS
LC
LC + LPS
MC
MC + LPS
HC
HC + LPS
D
IL-6
β-actin
$$$
$$$
$$$
**
200
150
100
50
0
IL-6/β-actin (%)
Ctrl
LPS
LC
LC + LPS
MC
MC + LPS
HC
HC + LPS

Figure 3

Figure 4

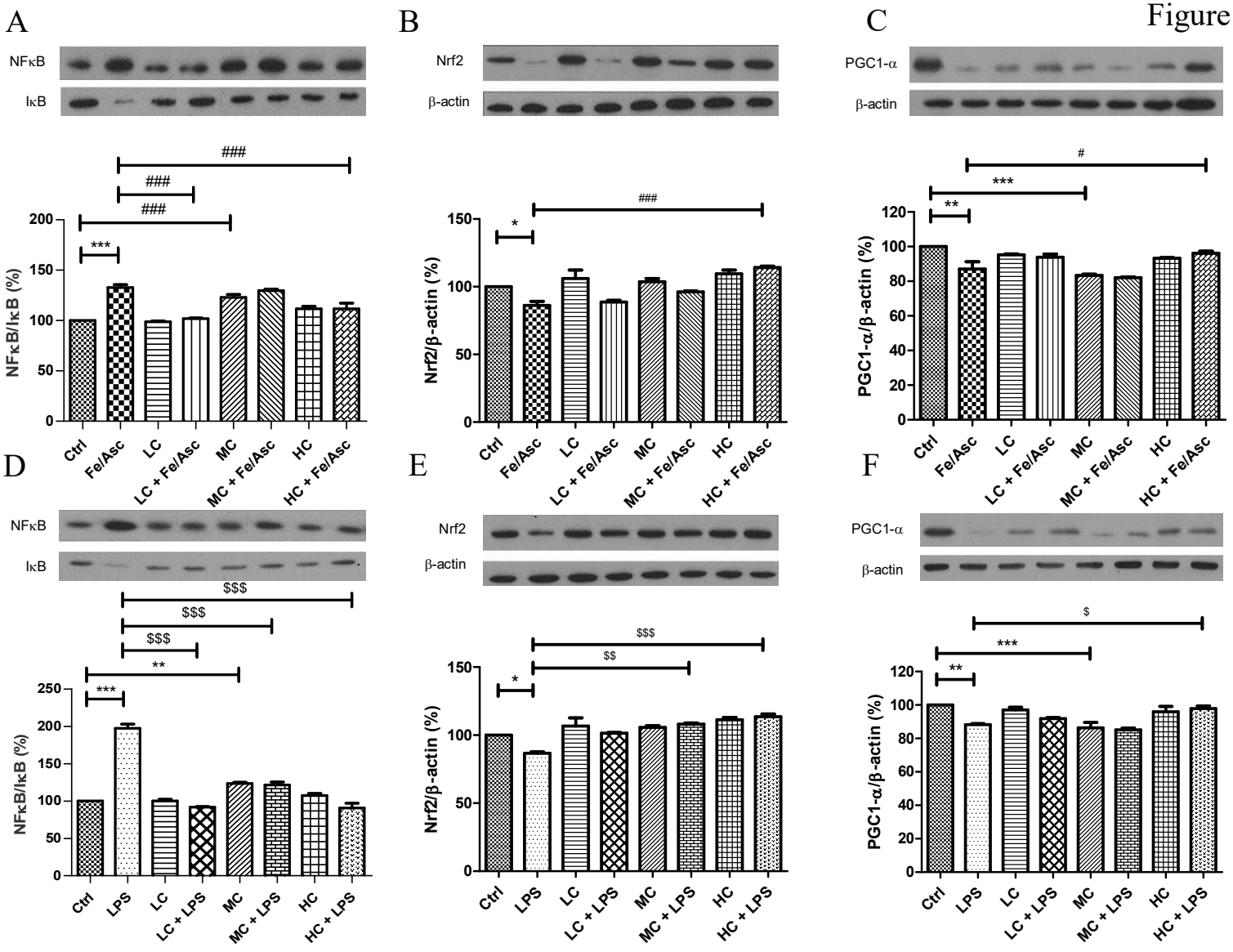
A
NFκB
IκB
NFκB/IκB (%)
###
###
###
***
Ctrl
Fe/Asc
LC
LC + Fe/Asc
MC
MC + Fe/Asc
HC
HC + Fe/Asc
B
Nrf2
β-actin
Nrf2/β-actin (%)
*
###
C
PGC1-α
β-actin
PGC1-α/β-actin (%)
#
***
**
D
NFκB
IκB
NFκB/IκB (%)
$$$
$$$
$$$
**
***
Ctrl
LPS
LC
LC + LPS
MC
MC + LPS
HC
HC + LPS
E
Nrf2
β-actin
Nrf2/β-actin (%)
$$$
$$
*
F
PGC1-α
β-actin
PGC1-α/β-actin (%)
$
***
**

Figure 5

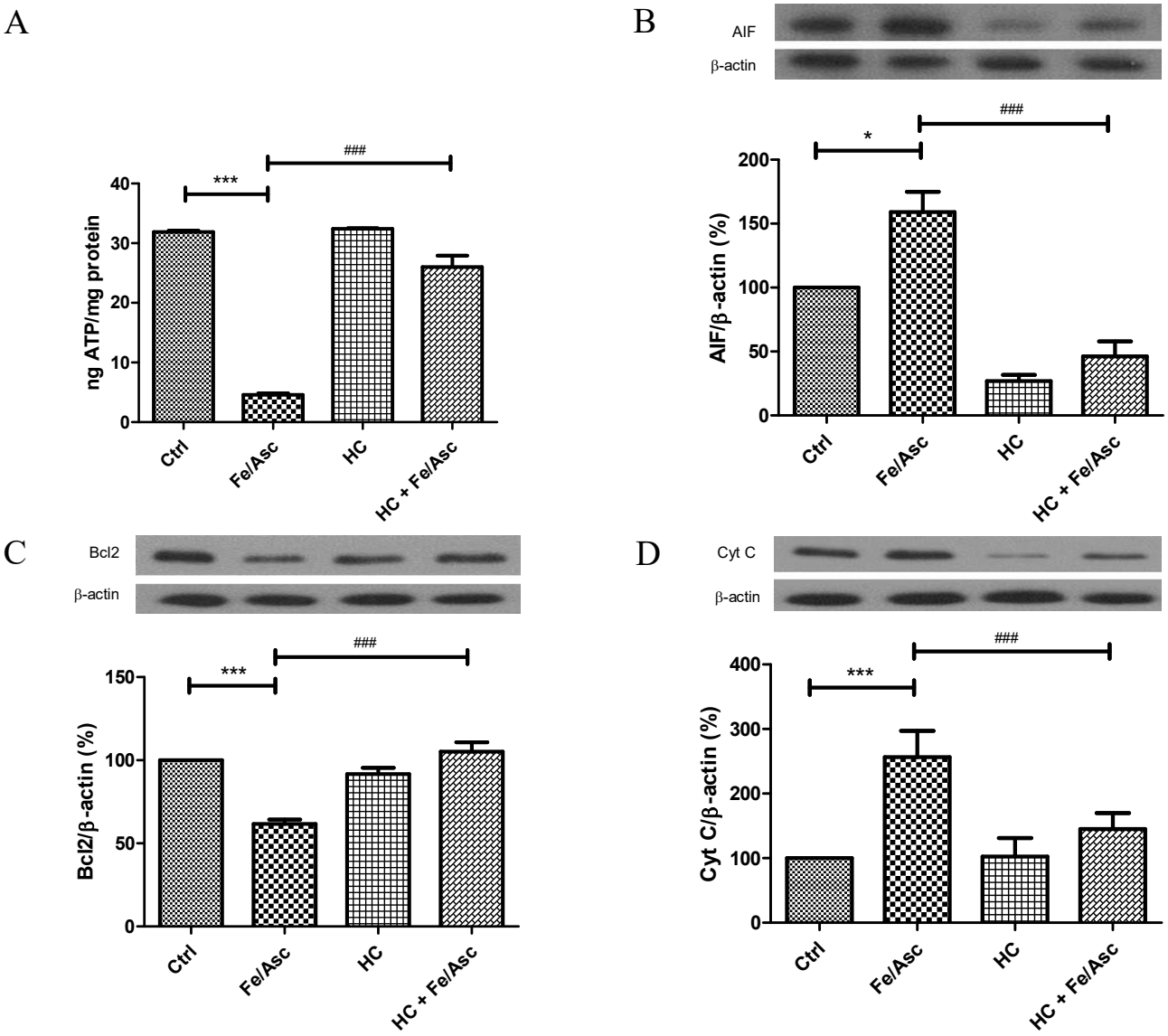
A
ng ATP/mg protein
***
###
Ctrl
Fe/Asc
HC
HC + Fe/Asc
B
AIF
β-actin
AIF/β-actin (%)
*
###
C
Bcl2
β-actin
Bcl2/β-actin (%)
D
Cyt C
β-actin
Cyt C/β-actin (%)

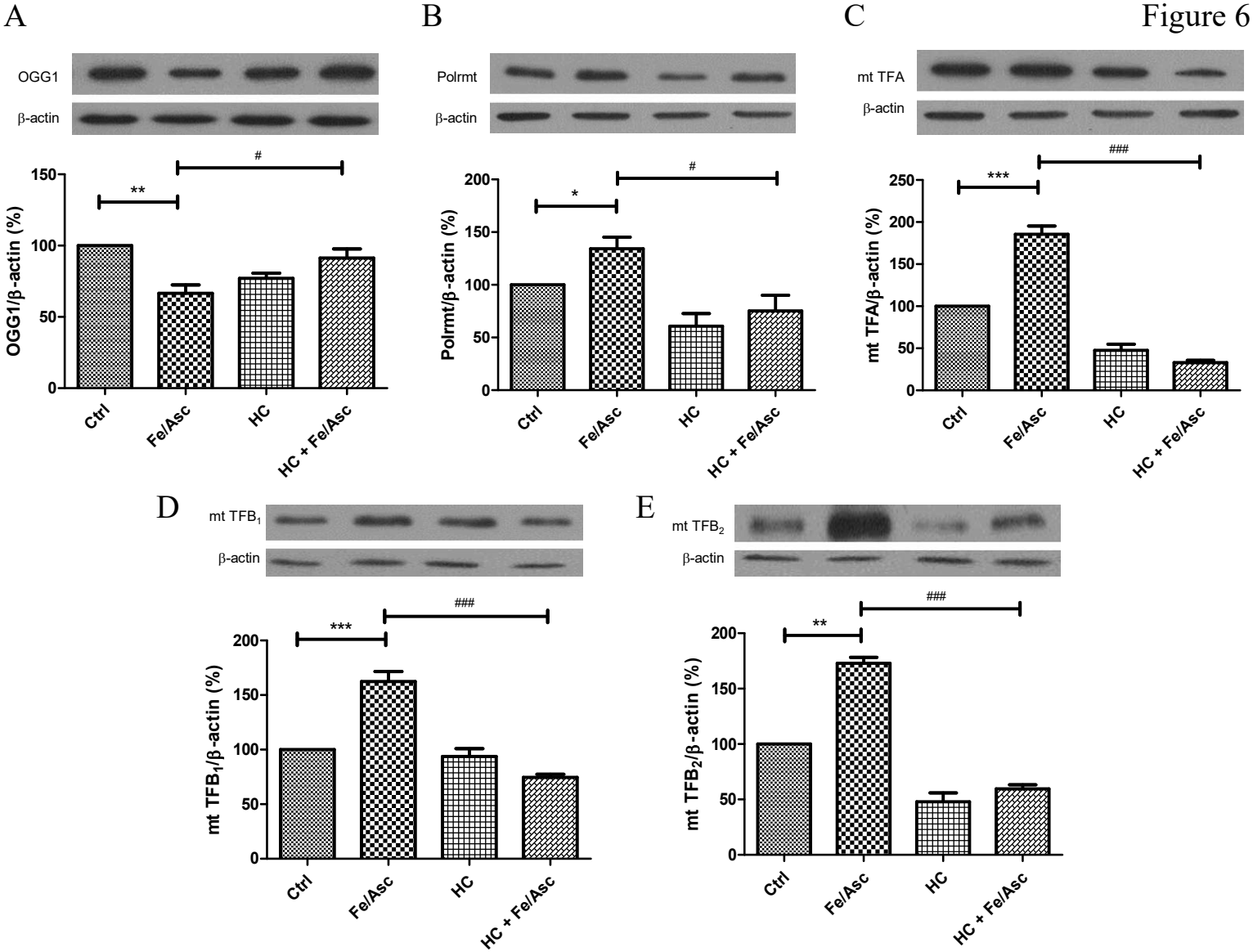
A
OGG1
β-actin
OGG1/β-actin (%)
150
100
50
0
**
#
Ctrl
Fe/Asc
HC
HC + Fe/Asc
B
Polrmt
β-actin
Polrmt/β-actin (%)
200
150
100
50
0
*
#
Ctrl
Fe/Asc
HC
HC + Fe/Asc
C
mt TFA
β-actin
mt TFA/β-actin (%)
250
200
150
100
50
0
***
###
Ctrl
Fe/Asc
HC
HC + Fe/Asc
D
mt TFB1
β-actin
mt TFB1/β-actin (%)
200
150
100
50
0
***
###
Ctrl
Fe/Asc
HC
HC + Fe/Asc
E
mt TFB2
β-actin
mt TFB2/β-actin (%)
200
150
100
50
0
**
###
Ctrl
Fe/Asc
HC
HC + Fe/Asc

Figure 6

Article 3: « Characterization of bioactive cranberry fractions by mass spectrometry »

Denis *et al*. Characterization of bioactive cranberry fractions by mass spectrometry. Nutr.Metab. (Lond.) 2015; sera soumis en septembre. Attente de corrections des co-auteurs.

Author contributions:

Marie-Claude Denis, Alexandra Furtos and Emile Levy participated in the design of the study. Marie-Claude Denis, Alexandra Furtos, Pascal Dubé and Stéphanie Dudonné conducted the experiments. Marie-Claude Denis, Alexandra Furtos, Yves Desjardins and Emile Levy analyzed and interpreted the data. Marie-Claude Denis, Alexandra Furtos, and Emile Levy contributed to the writing of the paper.

Characterization of bioactive cranberry fractions by mass spectrometry

Marie-Claude Denis[1,2], Yves Desjardins[3], Pascal Dubé[3], Stéphanie Dudonné[3], Edgard Delvin[1,4], Emile Levy[1,2,4], Alexandra Furtos[5]

[1]Research Centre, CHU Sainte-Justine, Departments of [2]Nutrition, [4]Biochemistry, [5]Chemistry, Université de Montréal, Montreal, Quebec, Canada, H3T 1C5
[3]Institute of Nutrition and Functional foods (INAF), Université Laval, Quebec, Quebec, Canada, G1V 0A6

Key words: Polyphenol; Mass spectrometry, Oxidative stress

Running Head: Characterization of bioactive cranberry

Abbreviations: CP, cranberry polyphenols; DP, degree of polymerization; Fer/Asc, iron-ascorbate; IBD, inflammatory bowel diseases; CH, high molecular weight CP; CL**,** low molecular weight CP**;** CM**,** medium molecular weight CP**;** OxS, oxidative stress; ROS, reactive oxygen species;

Correspondence: Dr Alexandra Furtos, Chemistry department, University of Montreal, 2900 Edouard-Montpetit Blvd, Montreal, Quebec, Canada H3T 1J4

ABSTRACT

Increasing evidence indicates that fruits contain functional nutrients with several preventive and therapeutic health benefits. Among them, cranberries have recently received particular attention as a result of their association with protection against urinary tract infections, glycemic response enhancement, cardiovascular risk prevention and gastrointestinal health improvement. Our group has recently conducted a study in order to assess the potential effects of cranberry polyphenolic fractions on intestinal Caco-2/15 epithelial cells. An obvious reduction in oxidative stress and inflammation was observed and several of the mechanisms were highlighted. The aim of the present work is to determine the polyphenolic species that were responsible for the observed biological activity. Low (CL), medium (CM) and high (CH) cranberry fractions were generated with a SephadexLH-20 column by elution with 60% MeOH, 100% MeOH and 70% acetone respectively. Total phenol quantity in the three fractions was determined by the Folin-Ciocalteu method. A combination of LC-MS/MS and MALDI-TOF methods were used to characterize the nature of polyphenolic compounds in the cranberry extracts. Reversed phase and hilic chromatography coupled to high resolution mass spectrometry were first used to generate empirical formulae for the species identified in the three fractions. Additionally, MALDI-TOF/TOF was performed on the CH sample in order to obtain complementary information on larger size oligomers. The LC-MS analysis revealed that the CL was essentially constituted of small absorbable phenolic acids: hydroxycinnamic and hydroxybenzoic acids. The CM fraction was mostly composed of anthocyanin, flavonols (quercetin, myricetin, isorhamnetin, kaempferol) and procyanidins monomers (epicatechin, catechin), dimers and small oligomers. A particular attention was paid to

characterization of the CH fraction in view of its dominant antioxidant and anti-inflammatory actions noted on intestinal epithelial cells exposed to various stressors. The CH fraction was devoid of phenolic acids and anthocyanins, but it contained for the most part procyanidins, the latter essentially composed of oligomers and polymers. By both HILIC-LC-MS, and MALDI-TOF-MS, procyanidin oligomers up to degrees of polymerization (DP) 16 were detected. These species could be responsible for the perceived antioxidant and anti-inflammatory activity of CH. A major abundance of ellagic acid, caffeoylquinic acid and hydroxybenzoic acids into the Caco-2 cells after incubation with the CL fraction showed that these phenolic acids were transported across the membrane and could have been responsible for the antioxidant activity observed. After treatment with the CM fraction, the following flavonoids, in descending order of abundance, were detected into the Caco-2 cells: quercetin glucoside, myricetin glucoside, A-type procyanidin dimer, kaempferol glucoside, cyanidin 3- arabinoside, cyanidin 3-glucoside and phloretin. These species could therefore be responsible for the biological activity of CM fraction. For the CH fraction, oligomers of procyanidins up to DP8 were identified in the Caco-2 cell lysate. The same oligomer species were detected in mitochondria enriched fraction of the Caco-2 cells. These species could be responsible for the antioxidant protection revealed by the CH fraction.

INTRODUCTION

Gastrointestinal mucosa is constantly exposed to luminal oxidants from ingested foods. Key among these is the simultaneous consumption of iron salts and ascorbic acid, which can cause oxidative damage to biomolecules. Additionally, the intestinal mucosa is subject to prolonged oxidative stress from reactive oxygen species generated during aerobic metabolism. Finally, the influx of neutrophils and monocytes associated with inflammation can generate further reactive oxygen species via respiratory burst enzymes as well as those involved in prostaglandin and leukotriene metabolism (447, 449, 451).

In vitro experimental systems showed that cranberry polyphenols possess antioxidant and free radical-scavenging activities, but also metal chelation, antiproliferative, anticarcinogenic, antibacterial, antiallergenic, and antiviral properties (568-570). These benefits have been linked to its various polyphenolic compounds such as anthocyanins, phenolic acids, flavonols, flavan-3-ols and proanthocyanidins (571). The presence of these phytochemicals in cranberry appears to be responsible for reducing oxidative stress and inflammation in many diseases and infections, including cardiovascular diseases (529, 572), cancers (573), and infections involving the urinary tract (574), dental health and Helicobacter pylori-induced stomach ulcers (575, 576).

Over the last years, considerable efforts have been devoted to understand the influence of polyphenols on the gastrointestinal tract (577, 578). Several studies using *in vitro* and *in vivo* models demonstrated that the biological activities of polyphenols are dependent on their intestinal absorption (579, 580). Furthermore, numerous studies *in vivo* have shown that dietary polyphenols are subjected to metabolic conversion not only in the liver, but

also during their absorption in the intestinal epithelial cells before reaching the systemic circulation (579).On the other hand, previous research indicated that > 95% of proanthocyanidins (PACs) remained in the intestinal lumen during transit, suggesting that beneficial dietary effects of PACs may occur through interactions at the mucosal surface of the gastrointestinal tract (275) such as the secretion of mucins in the small intestine (581). This suggests that PACs may influence health without being actually absorbed in the gastrointestinal tract (354).

In our previous studies, the data clearly disclosed that cranberries reduced the extent of OxS in Caco-2/15 cells. Apparently, one of their critical mechanisms for inactivating OxS was via the induction of endogenous antioxidant proteins (SOD, GPx and CAT). Our studies also clearly pointed out that cranberries positively modulated the antioxidant defense by up-regulating Nrf2, a central transcription factor that initiates the transcription of cytoprotective genes following binding to specific DNA sites termed antioxidant response elements (AREs). The cranberry fraction containing proanthocyanidins has been the most efficient to reduce OxS in Caco-2/15 cells (582).

Research on the role of PACs in health and nutrition is impaired by the lack of analytical methods that are able to deal with their structural complexity in food. Because of the difficulty of isolating this class of compounds, PACs are often characterized as being homopolymers with identical B-type interflavan bonds which is oversimplifying and not always true. Number methods for the separation of oligomeric and polymeric proanthocyanidins with various molecular weights have been described in the past (474, 583-588). Understanding structural differences among PACs is very important for their

biological activity. For example, procyanidin oligomers containing A-type bonds, isolated from cranberry, were able to inhibit the adherence or uropathogenic *Escherichia coli* to uroepithalial cells and prevent the urinary tract infections, whereas the procyanidins containing B-type only, were not (589). However, characterizing the complex cranberry procyanidins (linkage types for example) requires very performant analytical techniques. Mass spectrometry that uses soft ionization sources such as matrix assisted laser desorption ionization (MALDI) or electrospray ionization (ESI) is capable of elucidating the different degrees of polymerization, presence of A- or B-type linkages and hydroxylation patterns on the flavan-3-ols (589-596). Therefore, MALDI and ESI mass spectrometry based techniques have been used in the present work for (i) characterization of polyphenols in cranberry fractions; (ii) detection of their metabolites; (iii) study their absorption and transport in a Caco-2 cell model.

MATERIALS AND METHODS

General chemicals and reagents

HPLC-grade acetonitrile, methanol, acetone and Optima grade water were from Fisher Scientific (New Jersey, USA). Formic acid was purchased from Fluka (Steinheim, Germany). Chemicals and reagents for specific assays will be described in the respective sections. Fresh cranberries (*Vaccinium macrocarpon* Ait.) underwent physical treatments for the extraction of fractions with different molecular weights, which were then lyophilized, milled and kept frozen at -20°C.

Extraction of polyphenolic fractions of different molecular weights

Freeze-dried cranberries (150 g) were extracted twice with 500 mL of an extraction solvent mixture containing acetone/water/acetic acid (70:29.5:0.5, v/v). The extracts were combined and the acetone was evaporated at 50°C using a rotary evaporator under partial vacuum. The resultant slurry (approximately 300 mL) was extracted three times with 250 mL hexane to remove lipid species. The water slurry was evaporated again on a rotary evaporator to eliminate the residual hexane. The remaining aqueous fraction was diluted with an equal volume of 20% methanol in water (v/v) and applied to a Sephadex LH-20 column (30 X 600 mm) that had previously been hydrated for more than 2 h in 20% aqueous methanol. The samples were collected in three different fractions consisting of low (CL), medium (CM) and high (CH) molecular weight cranberry polyphenol compounds. Elution was performed with 500 mL of 60% methanol/water (v/v) for the CL fraction followed by 1 L of 100% methanol (v/v) to obtain the CM fraction and finally by 2 L of 70% acetone/water (v/v) for elution of the CH fraction. A rotary evaporator operated at 50°C under partial vacuum was used to remove the organic solvent from each fraction. The residual concentrated water solutions were freeze-dried and generated three solid (powder) fractions.

Determination and characterization of cranberry polyphenol fractions

Total phenolic content of cranberry fractions

The total phenolic content of CL, CM and CH fractions was determined using the Folin-Ciocalteu method (597), with gallic acid as a standard. Briefly, 100 µL Folin-Ciocalteu

reagent (diluted 10-fold in ultrapure water) and 80 µL sodium carbonate solution (7.5% in ultrapure water) were added to 20 µL MeOH in a 96-well plate. A blank sample and five calibration solutions of gallic acid (12.5 to 200 µg/mL) were analyzed under the same conditions. After 1h incubation at room temperature, the absorbance was measured at 765 nm using the Fisher Scientific Multiskan GO microplate reader (MA, USA). All determinations were carried out in triplicate, and results were expressed as g/100 g of extract weight ± SEM.

LC-MS analysis of cranberry fractions

A reversed phase LC-MS method has been developed to separate and identify phenolic compounds comprised in CL and CM fractions. Separations were performed on an UPLC-ESI-Synapt G2S system equipped with an ion mobility separation (IMS) module (Waters, Beverly, MA). The chromatographic column was an Acquity CSH C18, 2.1 x75 mm, 1.7 µm particle size (Waters, Milford, MA) maintained at 40^{o}C. The compounds were separated using 2% acetic acid in ultrapure water and acetonitrile (solvent A and B, respectively) with a flow rate of 0.55 mL/min under the following gradient: 0-0.5 min, 3% B; 0.5-8 min, 3-30% B; 8-9 min, 30-60% B; 9-10 min, 60-85% B; 10-11 min, 85% B; 11-11.2 min, 85-3% and 11.2-15 min, 3%B. Mass spectra were acquired in resolution negative MS^{e} mode from m/z 100 to 5000 with a 0.3 s scan time. No collision energy was applied in function 1 and a transfer collision energy ramp from 20-55 V was applied in function 2. LeuEnk at 1 ng/mL, infused at 20 µL/min, was used as lock-spray solution for accurate mass determination.

A HILIC-MS method has been developed to separate and identify phenolic compounds comprised in the CH fraction. Separations were performed on an UPLC-ESI-Synapt G2S

system. The chromatographic column was a Luna HILIC, 2.0 X 100 mm, 3.0 μm particle size (Phenomenex,Torrance, CA) maintained at 40°C. The compounds were separated using 10 mM Ammonium Acetate in ultrapure water and 2% acetic acid in acetonitrile (solvent A and B, respectively) with a flow rate of 0.6 mL/min under the following gradient: 0-0.5 min, 95% B; 0.5-8 min, 95-65% B; 8-9 min, 65% B; 9-9.2 min, 65-95% B; 9.2-12 min, 95% B. Mass spectra were acquired in positive and negative HDMS^e mode from m/z 100 to 5000 with a 0.3 s scan time. A transfer collision energy ramp of 20-45 eV was applied in function 2. IMS wave velocity was linearly changed from 1000-500 m/s at 40V. Other parameters were as following: capillary voltage 1.2 kV, cone voltage 30V, source temperature 120°C and desolvation temperature 400°C. Cone and collision gas flow rates were 100 L/h and 700 L/h, respectively. LeuEnk (1 ng/mL) was infused at 20 μL/min as lock spray solution. The instrument control and data processing were performed with MassLynx 4.1 from Waters.

MALDI-TOF/TOF analysis of CH fraction

A mixture of H_2O/ACN/TFA (50:50:0.1) was used as solvent for the cranberry fractions, for the MALDI matrix (DHB) and for the cationization agent, Cesium Trifluoroacetate (CsTFA). The CH fraction solution was prepared at 1mg/mL and the CsTFA at 10 mM. Following, 1 μL of the CsTFA solution was mixed with 10 μL DHB matrix and 1 μL CH solution. Aliquots of 1 μL of the resulting mix were spotted onto the MALDI plate and air dried. MALDI-TOF measurements were performed using a UltrafleXtreme MALDI-TOF/TOF mass spectrometer (Bruker Daltonics) equipped with SmartBeam-II Nd:YAG/ 355 nm laser operated at a repetition rate of 1 kHz. Ions generated by laser desorption were introduced into the flight tube with an acceleration voltage of 25 kV. All

mass spectra were collected by averaging 5000 laser shots per spectrum in the MS and MS/MS modes between m/z 500-5000. Angiotensin I and bovine insulin were used for external mass calibration. The instrument was controlled by FlexControl 3.4 software and data was processed with FlexAnalysis 3.4, both from Bruker Daltonics.

Determination of phenolic compounds profile in medium, cells and mitochondrial extracts by UPLC-MS/MS

CL, CM or CH molecular weight fractions (250 µg/mL) were added to the apical compartment of differentiated Caco-2/15 cells for 24h. Following, the cells were incubated with Fe/Asc (200 µM/2 mM) for 6h at 37°C. After that, the medium from the apical and basolateral side of membrane, Caco-2/15 cells and mitochondria (CH fraction only) were analyzed by UPLC-MS/MS.

Prior to the UPLC-MS/MS analysis, the medium, the cells and mitochondrial lysates samples were pre-treated by off-line µSPE. The extraction of phenolic compounds was realized as previously described (598). Briefly, waters OASIS HLB µelution plates (Milford, MA) were preconditioned sequentially with 250 µL of methanol and 250 µL of 0.2% acetic acid. Medium samples, cell and mitochondrial lysates were centrifuged for 5 min (4°C, 5000 rpm) and the supernatants were mixed with phosphoric acid 4% (v/v) to disrupt phenol-protein bonds prior to loading into the plates. The loaded plates were washed with 200 µL of ultrapure water and 200 µL 0.2% acetic acid. The retained phenolic compounds were then eluted with 2 x 50 µL of acetone/ultrapure water/acetic acid solution (70/29.5/0.5, v/v/v) in presence of rosmarinic acid as internal standard (1 µg/mL final concentration). The eluted solutions were directly injected in the UPLC-

MS/MS for the analysis of phenolic acids and flavonoids (negative mode), followed by the analysis of anthocyanins (positive mode).

An ultra-performance ACQUITY UPLC liquid chromatography system coupled to a TDQ tandem quadrupole mass spectrometer equipped with an ESI source, all from Waters (Milford, MA) was used. The chromatography was performed on an Agilent Plus C18 column (2.1 x 100 mm, 1.8 µm particle size) (Santa Clara, CA) operated at 30°C. The phenolic acids and flavonoids were separated using 0.2% acetic acid in ultrapure water and acetonitrile (solvent A and B respectively) with a flow rate of 0.4 mL/min under the following gradient: 0-8 min, 5-50% B; 8-9.10 min, 50-90% B; 9.10-10 min, 90% B; 10-10.10 min, 90-5% B; 10.10-13 min, 5% B. For anthocyanins, a gradient consisting of A (water/acetic acid, 90:10, v/v) and B (acetonitrile) at a flow rate of 0.45 mL/min was applied as follows: 0-3.50 min, 2-50% B; 3.50-4 min, 50-90% B; 4-4.50 min, 90% B; 4.50-4.55 min, 90-2% B; 4.55-6 min, 2% B. Data were acquired with MassLynx V4.1 software and processed for quantification with QuanLynx V4.1 from Waters. The UPLC-TQD system was operated in negative electrospray ionization mode for phenolic acids and flavonoids. Cone and collision gas flow rates (both nitrogen) were 80 L/h and 800 L/h, respectively. The mass spectrometer parameters were first generated with Waters' IntelliStart software (automatic tuning and calibration of the AQUITY-TQD) then manually optimized as following: capillary voltage 2.75 kV, source temperature 150^{o}C and desolvation temperature 400^{o}C. For anthocyanins, the UPLC-TQD system was operated with an ESI interface in positive mode. Cone and collision gas flow rates were 80 L/h and 1100 L/h, respectively. The mass spectrometer parameters were first generated with Waters' IntelliStart software then manually optimized as

following: capillary voltage 1.3 kV, source temperature 130°C and desolvation temperature 350°C. Quantification was performed in multiple reactions monitoring (MRM) mode, tracking the transition of parent and product ions specific for each compound, with external calibration. Supplementary data show the MS/MS transitions for quantification and confirmation as well as the cone voltage and collision energy values optimized for each of the standard compounds. In order to identify additional potential metabolites in the CH treated cells, an untargeted experiment on the Synapt G2S instrument was performed as well. The chromatographic column was a Kinetex EVO C18, 5um, 150x2.1mm maintained at 40°C and operated at 0.5 mL/min. Water and acetonitrile both containing 0.1 % formic acid (solvents A and B respectively) were used for elution under the following gradient: 0-0.5 min, 1% B; 0.5-6.0 min, 1-35% B; 6.0-9.5 min, 35-95% B; 9.5-10.0 min, 95% B; 10.0-10.2 min, 95-1% B; 10.2-12.0 min, 1%B. Mass spectra were acquired from 100-3000 m/z with a scan time of 0.3 s in negative MS^e mode. No collision energy was applied in function 1. A 20-55 V collision energy gradient was applied in the transfer cell in function 2.

Determination of transport ratio and recovery rate of polyphenols

The transport ratio and recovery rate were calculated using the following equations:

$$Transport\ ratio = (polyphenol\ transported | total\ polyphenols) \times 100\%$$

$$Recovery\ rate = [polyphenol(transported + remaining) \div total\ polyphenols] \times 100\ \%$$

Polyphenol transported represents the amount of polyphenols on the basolateral side of the transwell after transport. Total polyphenols was the total amount of polyphenols added on the apical side of the transwell at the beginning of the experiment. Polyphenols

(transported + remaining) were the sum of polyphenols that passed across Caco-2 membranes and those that remained in the apical side after transport.

RESULTS

Total contents of phenolic compounds in the different cranberry fractions were determined by the colorimetric Folin-Ciocalteu method. A large variation was found in the composition of the different cranberry fractions, ranging from 5.0 ± 0.1 in the CL fraction to 54.5 ± 0.9 in the CM fraction and 51.98 ± 1.11 in the CH fraction, all expressed as g of gallic acid equivalents/100 g of dry extract weight.

LC-MS analysis of cranberry fractions

High-resolution mass spectrometry was employed for identification of polyphenolic species in the cranberry fractions. For the monoisotopic m/z values experimentally obtained, molecular formulae were generated under certain elemental composition restrictions (Table 1). For this purpose, we considered potential phenolic species containing C (3 to 50), H (10 to 150), O (0 to 30) and Na (up to 1) and a mass accuracy of 5 ppm. We created a homemade database specific for cranberry polyphenols derived from the phenol-explorer database (218) and the USDA database for flavonoid content of foods (599). Those databases still have certain limitations due to variations in the polyphenol content generated by seasonal effects, local climate, varietal differences and storage conditions (600).

A reversed phase LC-MS method has been used in order to separate and identify polyphenols contained in the CL and CM fractions derived from cranberries. The

polyphenols expected in these two fractions are identified by accurate mass and by comparing the theoretical and experimental isotopic pattern. Representative extracted ion chromatograms (EIC) of these species identified in CL and CM fractions are shown in Figures 1 and 2 respectively. In the CL fraction, phenolic acids constituted the dominant class of polyphenols amongst which the caffeoylquinic acid, the benzoic acid and the coumaric acid were the most abundant (Figure 1). The observed deprotonated species $[M-H]^-$ generated in negative electrospray are presented in Table 1 and comprised mainly hydroxybenzoic and hydroxycinnamic acids. The CM fraction was mainly composed of four subclasses of flavonoids: flavonols, flavan-3-ols, dihydrochalcones and anthocyanines that were all identified with a mass error lower than 5 ppm. Figure 2 (A, B and C) shows the EIC of the $[M-H]^-$ ion signals for flavonols, flavan-3-ols and dihydrochalcones respectively. The main flavonols were present as a mixture of aglycone and glycosylated quercetin, kaempferol, isorhamnetin and myricetin. The (+)-catechin, (-)-epicatechin and procyanidine dimers and trimers characterize the subclass of flavan-3-ols. For dihydrochalcones, we recognized the phloretin and phloretin glucoside (phloridzin) at m/z 273.0763 and 435.1281 respectively. For anthocyanins, the EIC of the protonated $[M+H]^+$ species are presented in Figure 2D. The aglycone and glycosylated cyanidin and peonidin are found in the CM fraction. All compounds identified by reversed phase LC-MS in the CM fraction are presented in Table 1.

HILIC-MS analysis of CH fraction

A HILIC-MS method has been developed to separate and identify procyanidins comprised in the CH fraction. In negative electrospray mode we observed single charged

species $[M-H]^{1-}$ of procyanidins with degrees of polymerization (DP) from DP2 to DP5, double charged species $[M-2H]^{2-}$ of oligomer procyanidins with DP4 to DP9 and triple charged species $[M-3H]^{3-}$ from DP9 to DP16 (Figure 3). These different charge states, due to the differences in their size and shape are neatly separated by ion mobility as shown in the inset in Figure 3. Beside the degree of polymerization, cranberry procyanidins present an additional degree of heterogeneity due to two possible types of linkages: type A and type B, as shown by the structure in Figure 4. For example, we identified procyanidin tetramers with four different linkage types: the AAA-type bond at m/z 1149.25 (panel A); BAA-type bond at m/z 1151.27 (panel B); BBA-type bond at m/z 1153.28 (panel C) and BBB-type bond at m/z 1155.30 (panel D).

MALDI-TOF analysis of CH fraction

MALDI TOF analysis of CH fraction revealed the presence of procyanidins $[M+Cs]^{+}$ up to n=16 (m/z 4739) in positive-ion reflector mode (Figure 5). The most intense series of peaks correspond to procyanidin containing pure (epi)catechin units. Smaller oligomers contained at least one A-type linkage and an increasing number of B-type linkages, as proven by the repetition unit of 288. The probability of additional A-type bonds being present increases with the chain length. For example, starting with the heptamer, the most abundant signal in the isotopical pattern belongs to the structure containing two A-type linkages (m/z 2147.7). Additional smaller peaks at 2 mass units from each other confirm the heterogeneity of the bonds in larger chain oligomers. By MALDI-TOF, as previously shown by LC-ESI-MS, we identified procyanidin tetramers with four different linkage types: the AAA-type bond at m/z 1281.4; AAB-type bond at m/z 1283.4; ABB-type bond

at m/z 1285.4 and BBB-type bond at m/z 1287.4 (Figure 6). Once again, the most abundant tetramer was the ABB-type bond isomer. As an additional source of structural information, MS/MS was performed on m/z 3876.8 as shown in the inset in Figure 5. This confirms that most of the bonds were B-type (a 288 mass unit difference between the fragments) and few of them were A-type (between m/z 2436 and m/z 2150 for example).

Polyphenolic compounds in cells, medium, and mitochondrial extracts by UPLC-MS/MS

Identification and quantification of major polyphenols and metabolites from pre-incubation with CL, CM or CH fraction in Caco-2/15 cells and mitochondria were performed by a targeted UPLC-MRM method.

Bioavailability of polyphenols from cranberry fractions

The evaluation of absorption and transport of 19 different phenolic acids, targeted for their potential protection effect against OxS, was performed by UPLC-TDQ. Among these compounds only 12 phenolic acids were detected in the Caco-2 cells after preincubation with CL fraction and induction of OxS (Figure 7). The hydroxycinnamic acids (16.4 mg/100 g of extract weight; 78.3% of total phenolic acids) were found in higher concentration than hydroxybenzoic acids (4.56 mg/100 g of extract weight; 21.7 % of total phenolic acids) in the Caco-2/15 cells. Ellagic acid (11.3 ± 3.24 mg/100g extract weight) was the most abundant hydroxycinnamic acid followed by caffeoylquinic acid (4.95 ± 1.36 mg/100g of extract weight) and by p-coumaric (0.074 ± 0.007 mg/100g of extract weight), m-coumaric (0.057 ± 0.028 mg/100g of extract weight), caffeic (0.042 ±

0.023 mg/100g of extract weight) and ferulic acid (0.019 ± 0.001 mg/100g of extract weight). Among hydroxybenzoic acids, benzoic acid (2.87 ± 0.074 mg/100g of extract weight) was the most abundant compound followed by protocatechuic acid (0.723 ± 0.022 mg/100g of extract weight), hydroxybenzoic acid (0.521 ± 0.104 mg/100g of extract weight) and vanillic acid (0.259 ± 0.182 mg/100g of extract weight). The transport ratios (Table 2) of hydroxybenzoic acids (from 4.15 to 58.3 %) were much higher than the values of hydroxycinnamic acids (from 1.92 to 38.6%). These results showed that ellagic and caffeoylquinic acids (transport ratios 1.92 and 1.99%) were better absorbed by Caco-2/15 cells than benzoic and hydroxybenzoic acids (transport ratios 53.8 and 49.1%).

So, a major abundance of ellagic acid, caffeoylquinic acid and hydroxybenzoic acids into the Caco-2 cells after incubation with the CL fraction showed that these phenolic acids were transported across the membrane and could have been responsible for the antioxidant activity observed.

A total of 44 different flavonoids identified in the CM fraction, including four major subclasses: flavonols, flavan-3-ols, dihydrochalcones, anthocyanidines and their metabolites were also targeted for evaluating their protection against oxidative stress by UPLC-TDQ. After preincubation with CM fraction, most flavonoids are present in the cells as glycosides and other conjugates. The subclass with the higher amount of flavonoids was the flavonols (118.3 ± 2.95 mg/100g of extract weight), followed by flavan-3-ols (5.87 ± 1.84 mg/100g of extract weight), anthocyanidins (3.64 ± 0.574 mg/100g of extract weight) and dihydrochalcone (1.19 ± 0.073 mg/100g of extract

weight). The major flavonoids included in these subclasses are quercetin, myricetin, kaempferol and isorhamnetin for flavonols, epicatechin and catechin for flavan-3-ols, cyanidin and peonidin for anthocyanins, and phloretin for dihydrochalcones.

Among the flavonols identified, we found quercetin, myricetin, kaempferol and isorhamnetin as glycosides, aglycones or conjugates. The most abundant flavonol glycoside in Caco-2/15 cells (Figure 8A) was quercetin-glucoside (93.8 ± 1.14 mg/100g of extract weight) followed by myricetin-glucoside (17.1 ± 0.283 mg/100g of extract weight). All these flavonol-glucosides were transported across the Caco-2/15 cells monolayer and appear in the basolateral side (Table 2). A low amount of flavonols as aglycones (0.138 ± 0.049 to 0.640 ± 0.280 mg/100g extract weight) was absorbed and remained in Caco-2/15 cells. Flavonols conjugated by glucuronidation and sulfation or a combination of the two characterizes the flavonol metabolites after absorption and transport of flavonols from CM fraction. Quercetin, myricetin, isorhamnetin and kaempferol have been glucuronided and were found in apical side after transport across Caco-2/15 monolayer. Furthermore, the kaempferol sulfate metabolite was found in greater quantity than native molecule on apical side after transporting (Table 2). Only a low amount of these flavonols conjugated by glucuronidation was found in basolateral side. The transport ratios of isorhamnetin and kaempferol aglycone (respectively 44.3 and 21.4%) were much higher that the values of their glycosylated counterparts (3.6 % and 2.03% respectively). These results showed that glycosylated forms of quercetin and myricetin were better absorbed by Caco-2/15 cells than their aglycone forms.

With regard to the individual anthocyanins in Caco-2/15 cells after preincubation with CM fraction, the cyanidin and peonidin are all glycosylated (Table 2). The linked sugar is often glucose but can also be galactose and arabinose (601). The cyanidin-3-arabinoside (1.12 ± 0.113 mg/100g of extract weight) was the most abundant anthocyanin, followed by cyanidin-3-glucoside (0.960 ± 0.073 mg/100g of extract weight), peonidin-3-glucoside (0.750 ± 0.282 mg/100g of extract weight), cyanidin-3-galactoside (0.470 ± 0.018 mg/100g of extract weight), and peonidin-3-galactoside (0.341 ± 0.088 mg/100g of extract weight). In the basolateral side (Table 2), cyanidin-3-arabinoside (9.62 ± 0.810 mg/100g extract weight) was the most abundant anthocyanin, followed by peonidin 3-galactoside (3.07 ± 0.259 mg/100g extract weight), cyanidin 3-galactoside (2.26 ± 0.001 mg/100g extract weight) and peonidin-3-arabinoside (1.93 ± 0.348 mg/100g extract weight). The transport ratios of cyanidin (7.06%) and peonidin (0.884%) bound to galactose are higher than those bound with a glucose or arabinose. However, the anthocyanins bound to glucose were more absorbed by Caco-2/15 cells (Figure 8C).

Glucuronidation and/or sulfation metabolites of hydrochalcones were detected after preincubation with CM fraction (Figure 8D and Table 2). The phloretin sulfate metabolite was found in greater quantity in basolateral side (0.595 ± 0.029 mg/100g of extract weight) than apical side (0.231 ± 0.020mg/100g of extract weight) after transport across Caco-2/15 cells. The sum of phloretin and metabolites (in the basolateral side + remaining in the apical side) was 22.4 ± 2.60 mg/100 g extract weight (95.0% total dihydrochalcone). On the basolateral side of differentiated Caco-2/15 cell monolayer, the transport ratio of total phloretin and metabolites was 18.2%.

Flavan-3-ols in cranberries occur as monomers ((-)-epicatechin and (+)-catechin), and oligomeric and polymeric forms, when they are called procyanidins (Table 2). Procyanidins in cranberry vary according to the nature of the interflavan linkage, constitutive units, and degree of polymerization. According to the nature of the interflavan linkage, both A- and B-type procyanidins are found in cranberry. The total content of flavan-3-ols in Caco-2/15 cells was 5.87 ± 1.84mg/100g extract weight for CM fraction (Figure 8B) and 0.392 ± 0.073mg/100g extract weight for CH fraction (Figure 9). A-type procyanidin dimers were found in both CM and CH cranberry fractions.

Methylation, glucuronidation and/or sulfation metabolites of flavan-3-ols were detected after preincubation with CM or CH fraction. Methyl catechin sulfate (0.744 ± 0.402mg/100g extract weight) and methyl catechin glucuronide sulfate (0.059 ± 0.001mg/100g extract weight) were found in Caco-2/15 cells after preincubation with CM fraction (Figure 8B). We have not identified metabolite in Caco-2/15 cells from the CH fraction. However, two flavan-3-ol metabolites are found in medium (apical and basolateral sides) after preincubation with CH fraction: catechin diglucuronide (2.42 ± 1.32 mg/100g of extract weight) and methyl catechin sulfate (0.954 ± 0.365mg/100g of extract weight). The transport ratios of flavan-3-ols and procyanidin dimers ranged from 0.742 to 5.65% after preincubation with CM fraction (table 4) and ranged from 19.7 to 23.3% for CH fraction (Table 2).

An untargeted LC-MS experiment in scan mode offered a global view of the apical side, basolateral side, Caco-2/15 cell and mitochondria content after CH incubation. This approach allowed the detection of small molecules as well as larger oligomeric procyanidin species (Figure 10). In the apical side, procyanidin polymers up to n=11

were detected either as doubly charged $[M-2H]^{2-}$ or triply charged $[M-3H]^{3-}$ species. In Caco-2 cells, procyanidin oligomers and polymers with DP2 to DP8 were identified while in the mitochondrial lysate procyanidins from DP2 to DP11 were detected (Figure 10). No procyanidins were observed in the basolateral side.

So, after treatment with the CM fraction, the following flavonoids, in descending order of abundance, were detected into the Caco-2 cells: quercetin glucoside, myricetin glucoside, A-type procyanidin dimer, kaempferol glucoside, cyanidin 3- arabinoside, cyanidin 3-glucoside and phloretin. These species could therefore be responsible for the biological activity of CM fraction. For the CH fraction, oligomers of procyanidins up to DP8 were identified in the Caco-2 cell lysate. The oligomer species up to DP11 were detected in mitochondria enriched fraction of the Caco-2 cells. These species could be responsible for the antioxidant protection revealed by the CH fraction.

DISCUSSION

Analysis of phenolic compounds in food has been mainly carried out by reverse-phase liquid chromatography. Normal-phase chromatography has also been applied to certain phenolic classes such as the procyanidin oligomers (587, 588). Apart from UV-VIS and fluorescence detection (588, 602), mass spectrometry coupled to LC through atmospheric pressure chemical ionization (APCI) and electrospray ionization (ESI) interfaces have been successfully applied to the analysis of phenolic compounds (236). Matrix-assisted laser desorption ionization (MALDI) interfaces combined with time-of-flight (TOF)

analyzers have been seen as a promising and powerful technique for characterizing proanthocyanidins and other complex phenolic mixtures (593).

In this paper, the determination of total phenolic content in cranberry fractions was firstly done by the Folin-Ciocalteu method. This assay provides very useful qualitative and quantitative information. Its main disadvantage is that it only determines the total phenolic content without providing information on the individual polyphenol components (603).

In this study a combination of LC-MS and MALDI-TOF methods was used to characterize the nature of polyphenolic compounds in the cranberry fractions. Reversed and hilic phase chromatography coupled to high resolution mass spectrometry were first used to generate empirical formulae for the species identified in the three fractions. The LC-MS analysis revealed that the CL was essentially constituted of phenolic acids (hydroxycinnamic acid, hydroxybenzoic acid). The CM fraction was mostly composed of anthocyanin, flavonols (quercetin, myricetin, isorhamnetin, kaempferol) and procyanidins monomers (epicatechin, catechin), dimers and small oligomers. It is noteworthy that other lower abundance species were detected as well in this extremely complex fraction.

A particular attention was paid to characterizing the CH fraction in view of its dominant antioxidant and anti-inflammatory actions noted on intestinal epithelial cells exposed to Fe/Asc (604). The MALDI-TOF MS equipped with delayed extraction provided the mass resolution necessary for the visualization of isotopic distributions, allowing for characterization of mass differences due to variation of A-type vs. B-type linkage (589). This technique is very well suited for characterizing polydispersed oligomers because it produces only singly charged molecular ions and allows detection, in reflector mode, of

high molecular weight species with good mass accuracy (605, 606). The presence of a single charge state simplifies the mass spectra interpretation and, in our particular application, allows distinguishing between oligomers with different linkage types. This could be an interesting, less expensive alternative for laboratories not equipped with high resolution LC-MS instruments. Feliciano et al. mentioned that the linear mode MALDI-TOF MS will be capable of detecting oligomers with a DP of up to 26 flavan units in cranberry PAC, but does not have sufficient baseline resolution to adequately deconvolution isotope patterns. The use of reflectron mode MALDI-TOF MS as described in this paper gave baseline resolution of 1 amu for oligomers up to the undecamers and therefore was able to determine ratios of type linkage for oligomers with DP from 2 to 11 (607). However, MALDI-TOF is not applicable for detecting smaller molecules. At m/z below 600, signals coming from the matrix are very intense and interfere with the detection. It is therefore very difficult to determine the structure of individual proanthocyanidin oligomers below DP3 (589).

In our ESI-MS experiments, procyanidins were detected in both positive and negative ionization modes as mixtures of different charge states. Single and doubly charged species were detected in positive mode while single, doubly and triply charged species were detected in negative mode. The ion mobility feature of the Synapt G2S instrument allowed to separate procyanidins of different charges and offered an additional dimension of separation. However, ion mobility cannot prevent ion suppression in the source, when highly complex mixtures, such as natural product extracts, are analyzed. A good chromatography prior to MS detection is still highly suitable. In this study, by both HILIC-LC-MS, and MALDI-TOF-MS, procyanidin oligomers up to DP16 were detected.

The high resolution of the TOF detector allowed characterizing quite easily linkage types in the cranberry oligomers. The cranberry has previously been shown to contain PAC that predominately includes one or more A-type linkages (593, 595). The apple conversely has been shown to contain PAC that predominately contain all B-type linkage (608). In our determination, dimers seemed to be formed exclusively by A-type bonds. Trimers were identified with 2A, 2B and AB linkages, the AB-type being the most abundant. Among the tetramers, with both MALDI-TOF and ESI-TOF techniques, the ABB type was detected with the highest intensity. The incidence of A-type bonds increased with the chain length and for polymers larger than DP7, the most abundant isomer started to be the one containing two A-type linkages. No particular rule could be found in the chain growing process. However, if we assume that cranberry procyanidins are formed by successive additions of epicathechin units, they all should start from the dimer we observed, which has an A-bond linkage. This head-chain, different from the one in apple for example, could be responsible for the particular biological activity of cranberry procyanidins. For the first time, we demonstrated that cranberries contain procyanidins up to 16-mers. Neto et al. identified oligomers as large as 12 DP; however, the primary constituents appear to be around four units size (591). Moreover, we are able to identify type linkage (A and B-type) in the detected polymers and these by two different analytic approaches: LC-MS and MALDI-TOF.

Mechanisms regulating the bioavailability of flavonoids

The notion of bioavailability integrates several variables, such as intestinal absorption, excretion of glucuronides toward the intestinal lumen, metabolism by the microflora,

intestinal and hepatic metabolism, plasma kinetics, the nature of circulating metabolites, binding to albumin, cellular uptake, intracellular metabolism, accumulation in tissues, and biliary and urinary excretion. The difficulty lies in integrating all the information and relating the variables to health effects at the organ level. These tasks are made all the more difficult because the relative weight of each variable may depend on the polyphenol considered. Some polyphenols may be less efficiently absorbed than are others but nevertheless reach equivalent plasma concentrations because of lower secretion toward the intestinal lumen and lower metabolism and elimination. Better knowledge of bioavailability is essential for investigating the health effects of polyphenols. Our study evaluated the following parameters: intestinal absorption, excretion of polyphenols toward the intestinal lumen and intestinal metabolism of cranberry polyphenols on a Caco-2 *in vitro* model (Figure 11).

Intestinal absorption

The majority of flavonoids, with the exception of flavan-3-ols, are present as various glycosides in cranberries. The hydrolysis of the moiety is a required step for absorption. The type of sugar attached to the flavonoid is the determinant factor of the site and extend of absorption, but the position of the sugar affects the mechanisms involved in intestinal uptake. Lactase phloridzin hydrolase (LPH) is present on the brush-border of small intestine epithelial cells (609). This enzyme has a broad specificity for β-glucosides conjugated to flavonoids and will hydrolyze the glucoside to the aglycone prior to absorption. The resulting aglycone may then enter epithelial cells by passive diffusion due to its increased hydrophobicity, and this process is possibly enhanced by proximity to the cellular membrane. Alternatively, a broad specificity cytosolic β-glucosidase (CBG)

has been identified in epithelial cells (610). For hydrolysis by CBG, the polar glucosides would need to be transported into epithelial cells, possibly by the active sodium-dependent glucose transporter SGLT1 (272). The relative contribution of LPH/diffusion and transport/CBG depend on the position of glycosylation. Quercetin-3-glucoside is not a substrate for CBG (611) and larger molecules such as quercetin-3,4'-O-diglucoside interact poorly with the sugar transporter whereas quercetin-4'-O-glucoside is a good substrate for CBG (272). Quercetin rhamnoglucosides (rutin) are substrates for neither CBG nor LPH (273) although anthocyanins were not substrates for CBG (610). The flavan-3-ols are the only subclass of flavonoids that are not present as glycoside in the diet. The absorption of (+)-catechin by the small intestine is directly proportional to the dose over concentrations expected to occur in the small intestine after customary dietary intakes. The data suggested that (+)-catechin enters intestinal epithelial cells by passive diffusion, a mechanism that is generally proportional to the dose. The absorption of proanthocyanidins with different degrees of polymerization was investigated with colonic carcinoma (caco-2) cells, a commonly used model of intestinal absorption. Monomeric (+)-catechin and low molecular weight proanthocyanidins could be absorbed by the small intestine but larger molecular weight proanthocyanidins were not absorbed (531).

Intestinal efflux of absorbed flavonoids

Intestinal excretion is an important mechanism that limits the absorption of certain flavonoids (612). Conjugated metabolites formed in the small intestine are actively effluxed back into the intestinal lumen by interaction with membrane-bound transporters in the ABC family including multidrug resistance protein (MRP) and P-glycoprotein (P-gp). The efflux of quercetin and epicatechin metabolites is thought to occur by MRP2,

located on the luminal side of epithelial cells (613, 614). The quercetin-3'-O-glucuronide was selectively excreted into the lumen, presumably leaving other metabolites such as the 3- and 7-O-glucuronides available for systemic circulation (615). The amount of active intestinal efflux of flavonoids representing the major subclasses of flavonoids was studied after in situ intestinal perfusion. For quercetin, 52% of the perfused dose was re-excreted back into the lumen, whereas only 10-20% of the dose was re-excreted for kaempferol (616). The (+)-catechin, alternatively, did not appear to be a substrate for these efflux transport proteins. Some studied suggest that significant differences exist in the extent of absorption between (+)-catechin and (-)-epicatechin. The reasons for the apparent differences in the net absorption of some of these flavonoids may be more dependent upon interaction with efflux transporters than on the amount of intestinal absorption.

Intestinal metabolism

Our results on the identification of metabolic profile confirm that intestinal metabolism pathway of phenolic compounds is common to drug metabolism. Except for catechin, the major phenolic compounds were first deglycosylated to the free aglycone before being absorbed by the intestinal barrier and then converted to glucuronides or sulfates or a combination of the two, with or without methylation. Lactase phlorizin hydrolase (LPH) and β-glucosidase cytosolic (CBG) (610, 617) have been suggested to play an important role in the metabolism of phenolic compound glucosides, because they catalyze the hydrolysis of a wide range of phenolic compound glucosides. After absorption by Caco-2/15 cells, phenolic compounds are methylated by catechol-O-methyltransferase (COMT), a reaction which also occurs in a wide range of tissues. The COMT catalyzes

the transfer of a methyl group from S-adenosyl-L-methionine to polyphenols having an o-diphenolic (catechol) moiety. This reaction is well known for quercetin and catechin (618). The methylation generally occurs predominantly in the 3' position of the polyphenol, but a minor proportion of 4'-O-methylated product is also formed. The UDP glucuronosyl transferase (UDPGT) catalyzes the conjugation of phenolic compounds to glucuronic acid. It is situated in the endoplasmic reticulum and exists as a large family of related enzymes. Glucuronidation of phenolic compounds is predominantly performed by the UGT1A family, which occurs in intestine, liver and kidney (619). For most flavonoids, a significant proportion of the glucuronides that are formed in the intestinal mucosa are secreted back to the gut lumen, which reduces net absorption (612). The transporter multiresistant protein 2 (MRP2) or the P-glycoprotein may be involved in the efflux (620, 621). A third conjugation may take place in the enterocyte; sulfation is realized by phenol sulfotransferases (SULT) which are a small group of cytosolic enzymes that are widely distributed (622). The SULT catalyze the transfer of a sulfate moiety from 3'-phosphoadenoside-5'-phosphosulfate to a hydroxyl group on polyphenol (623). A significant amount of free aglycones was identified in the basolateral side. However, the proportion of conjugated compounds in the basolateral side was much higher that their free aglycones counterparts.

Antioxidant mechanisms of cranberry polyphenols in Caco-2/15 cells

Phenolic acids contained in CL fraction are known to act as antioxidants not only because of their ability to donate hydrogen or electrons but also because of their stable radical intermediates, which prevent the oxidation of various food ingredients. Preliminary structure-activity relationship studies of cinnamic acids and derivatives have pointed out

the importance of the catechol group in the antiradical efficacy (624). The p-coumaric acid is the most prevalent hydroxycinnamic acid (625). The gene expression of antioxidant enzymes is up-regulated by gallic, p-coumaric and ferulic acids. Ferulic and caffeic acids are better inhibitors of peroxynitrite-mediated tyrosine nitration than coumaric acid (626). Furthermore, the ferulic acid has high antioxidant properties due to its resonance-stabilized phenoxy radical structure, and has been approved in certain countries as a food additive to prevent lipid peroxidation (627). Zeng and Wang also found that p-coumaric and caffeic acids were in very similar proportion in cranberry extracts (235). Ellagic acid (628) is a potent inhibitor of NF-kB which regulates the expression of cytokines, inducible nitric oxide synthase (iNOS), cyclo-oxygenase 2 (COX-2), growth factors and inhibitors of apoptosis. Caffeoylquinic acid suppressed the ROS-mediated NF-kB and AP-1 signaling pathways (629). Phenylpropionic acid, hydroxyphenylacetic acid and hydroxyphenylpropionic acid decreased the expression of cyclo-oxygenase-2 in HT20 cells (630). These results are in concordance with previous studies which also found that benzoic acid was the most concentrated hydroxybenzoic acid in cranberry juice (31-32). Benzoic acid forms 80% of the total organic acids contained in cranberry juice. Also in line with our results, Prior et al (33) found that protocatechuic acid was among the most abundant hydroxybenzoic acids in a commercial cranberry powder.

Flavonols, anthocyanins, dihydrochalcones and procyanidins monomers and dimers were presented in CM fraction. In aglycone form, flavonols are powerful antioxidants in vitro (631), and have a relatively longer circulation time in vivo. On the other hand, quercetin conjugates have a reduced tendency to undergo redox cycling, although their ability to

function as antioxidants is not completely abolished. The total amount of flavonols in cranberry ranges from 200 to 400 mg/kg (235, 573, 632). Cranberry is the best source of flavonols among 30 flavonol-containing plant foods studied (633), and the flavonol content of cranberry is almost twice as high as 12 other commonly consumed fruit juices, including pomegranate and grape (634). Quercetin is the most abundant flavonol in cranberry, and it varies from 11 to 25 mg/100g, primarily as the 3-*O*-galactoside (632, 635). Cranberry is also the best source of quercetin (241). Myricetin is the second most abundant flavonol, followed by kaempferol (636). Cranberry, compared to many other berries, has a very small number of anthocyanin isomers, the major ones being galactosides and arabinosides of cyanidin and peonidin (637, 638). Whole cranberries contain a very broad concentration range of anthocyanins, 180-596 mg/kg fresh weight (639), which also varies according to maturity from 0.8 to 111.0 mg/kg fresh weight from the green to dark red stage. Anthocyanins were shown to induce phase II antioxidant and detoxifying enzymes in cultured cells (640). In our study, the low absorption of anthocyanins resulted from their poor lipophilic properties. The profile where higher contents of cyanidin-3-arabinoside than cyanidin- and peonidin-3-galactoside were found, has been reported to occur in cranberry pomace (641). Anthocyanins enhanced antioxidant capacity through the activation of both NADPH: quinone reductase and three glutathione-related enzymes, glutathione reductase, glutathione peroxidase, and glutathione S-transferase (642, 643). Phloridzin is the most prevalent member of the class of dihydrochalcones present in cranberries at 120 mg/kg (644). Dihydrochalcones showed significant radical scavenging and suppressing lipid peroxidation activities (645).

Cranberries have the highest levels of monomers (catechin + epicatechin) among berries, and monomer levels in cranberries are twice as high as those in blueberries (240). Total catechins in cranberry average around 17 mg/100g, with epicatechin being the most abundant (646). The proanthocyanidins, commonly called condensed tannins, are responsible for the bitter astringent taste of cranberries due to their binding to saliva proteins. Their average concentration is 419 mg/100g by weight (240). Cranberries have the most dimers, trimers and 4-10mers compared with other fruit studied (240, 269). The most unique aspect of cranberry polyphenols is the occurrence of A-type linkages (C2→O→C7) between epicatechin units. It has been estimated that A-type procyanidins account for 65% of their total procyanidins (595, 647). A-type procyanidin oligomers isolated from cranberries were able to inhibit adherence of uropathogenic *Escherichia coli*, whereas the B-type procyanidins were not (590). Previous studies and the profile of A-type procyanidins dimers actually suggest that A-type procyanidins are the major bioactive components in cranberries. These observations are consistent with the results of Appledoorn et al. (648), who found that A-type procyanidin dimers were absorbable from the small intestine of rats during an in situ perfusion. Procyanidins oligomers and polymers characterize the CH fraction. Ou et al. showed in 2012 that cranberry A-type procyanidin dimers, trimers, and tetramers passed across Caco-2 cell monolayers (649) and revealed that A-type procyanidin dimers from peanut skin were absorbed and their transport ratios were higher than that of B-type procyanidin dimers, suggesting that they could be absorbed by humans after cranberry consumption. However, Gu et al. revealed in 2002 that these same absorbable oligomers only account for 15% of total procyanidins, while the rest are polymers. This composition of the cranberry could limited its

bioavailability and bioactivities of procyanidins (650). A team of researchers interested in understanding the mechanism of action of antioxidant procyanidins, showed that B-type procyanidin induced Nrf2 translocation and glutathione S-transferase P1 expression via ERKs and p38-MAPK pathways that will protect human colonic cells against oxidative stress (651).

In addition to the total amount of epicatechin/catechin present in procyanidin molecules, their tridimensional structure and disposition on the membrane surface contribute to flavonoid-membrane interactions. A relationship between membrane integrity and polymer length has also been observed in other models of interfacial adsorption. The flavan-3-ols and procyanidins can interact with membrane phospholipids through hydrogen bonding to the polar head groups of phospholipids. As a consequence, these compounds can accumulate at the membranes' surface, both outside and inside the cells. A set of structural characteristics determine the adsorption or penetration of the polyphenol into the lipid bilayer (216, 652). Taking in consideration the antioxidant effects, when adsorbed on the membrane surface, polyphenols could provide a physical barrier for hydrosoluble radicals (653). Inserted into the lipid bilayer, polyphenols would be in close proximity to scavenge $L^{\cdot}$, $LOO^{\cdot}$, and other lipid soluble radicals (654, 655). Thus, polyphenols can protect membranes and membrane components from oxidation by providing an antioxidant protection through mechanisms not completely related to free radical scavenging or metal chelating actions.

Mitochondria represent a critical source of ROS and their ability to accumulate polyphenols and their metabolites may be important for protection of mitochondrial

function and integrity. This hydrophobic compartment may represent a site of preferential accumulation of the polyphenols. The flavan-3-ols and A-type procyanidin dimers are efficient cranberry polyphenols exerting a protective effect against mitochondrial dysfunction probably due to their ability to enter cells and potentially to accumulate in mitochondria. The results reported in this study lead to the identification of mitochondria as an important site of action in which flavan-3-ols and procyanidin oligomers can to prevent the damage initiated by reactive species.

CONCLUSIONS

The study demonstrated that cranberries contain procyanidins up to 16-mers. Moreover, we are able to identify type linkage (A and B-type) in the detected polymers and these by two different analytic approaches: LC-MS and MALDI-TOF. The identification of metabolites has elucidated the mechanisms of absorption and transport of cranberry polyphenols in the Caco-2/15 model. We demonstrated the presence of procyanidin oligomers in the Caco-2/15 cells and in the enriched extract of mitochondria. The identification of bioavailability mechanisms of procyanidin oligomers in Caco-2/15 cells and mitochondria remains to be clarified. These results could support the main metabolizing pathway of procyanidin oligomers and polymers would not happen in enterocytes.

AUTHOR CONTRIBUTION

Marie-Claude Denis, Stéphanie Dudonné, Alexandra Furtos and Emile Levy participated in the design of the study. Marie-Claude Denis, Alexandra Furtos, Pascal Dubé and Stéphanie Dudonné conducted the experiments. Marie-Claude Denis, Alexandra Furtos,

Yves Desjardins and Emile Levy analyzed and interpreted the data. Marie-Claude Denis, Alexandra Furtos, Yves Desjardins, Edgard Delvin and Emile Levy contributed to the writing of the paper.

REFERENCES

1. Biswas K, Bandyopadhyay U, Chattopadhyay I, Varadaraj A, Ali E, Banerjee RK. A novel antioxidant and antiapoptotic role of omeprazole to block gastric ulcer through scavenging of hydroxyl radical. J Biol Chem 2003;278:10993-1001.

2. Parks DA. Oxygen radicals: mediators of gastrointestinal pathophysiology. Gut 1989;30:293-8.

3. Sanchez S, Martin MJ, Ortiz P, Motilva V, Alarcon dlL. Effects of dipyrone on inflammatory infiltration and oxidative metabolism in gastric mucosa: comparison with acetaminophen and diclofenac. Dig Dis Sci 2002;47:1389-98.

4. Merken HM, Beecher GR. Measurement of food flavonoids by high-performance liquid chromatography: A review. J Agric Food Chem 2000;48:577-99.

5. Merken HM, Beecher GR. Liquid chromatographic method for the separation and quantification of prominent flavonoid aglycones. J Chromatogr A 2000;897:177-84.

6. Nijveldt RJ, van NE, van Hoorn DE, Boelens PG, van NK, van Leeuwen PA. Flavonoids: a review of probable mechanisms of action and potential applications. Am J Clin Nutr 2001;74:418-25.

7. Pappas E, Schaich KM. Phytochemicals of cranberries and cranberry products: characterization, potential health effects, and processing stability. Crit Rev Food Sci Nutr 2009;49:741-81.

8. McKay DL, Blumberg JB. Cranberries (Vaccinium macrocarpon) and cardiovascular disease risk factors. Nutr Rev 2007;65:490-502.

9. Ruel G, Couillard C. Evidences of the cardioprotective potential of fruits: the case of cranberries. Mol Nutr Food Res 2007;51:692-701.

10. Neto CC. Cranberry and its phytochemicals: a review of in vitro anticancer studies. J Nutr 2007;137:186S-93S.

11. Burleigh AE, Benck SM, McAchran SE, Reed JD, Krueger CG, Hopkins WJ. Consumption of sweetened, dried cranberries may reduce urinary tract infection incidence in susceptible women -- a modified observational study. Nutr J 2013;12:139.

12. Burger O, Weiss E, Sharon N, Tabak M, Neeman I, Ofek I. Inhibition of Helicobacter pylori adhesion to human gastric mucus by a high-molecular-weight constituent of cranberry juice. Crit Rev Food Sci Nutr 2002;42:279-84.

13. Burger O, Ofek I, Tabak M, Weiss EI, Sharon N, Neeman I. A high molecular mass constituent of cranberry juice inhibits helicobacter pylori adhesion to human gastric mucus. FEMS Immunol Med Microbiol 2000;29:295-301.

14. Gonthier MP, Donovan JL, Texier O, Felgines C, Remesy C, Scalbert A. Metabolism of dietary procyanidins in rats. Free Radic Biol Med 2003;35:837-44.

15. Reed JD. Nutritional toxicology of tannins and related polyphenols in forage legumes. J Anim Sci 1995;73:1516-28.

16. Del RD, Rodriguez-Mateos A, Spencer JP, Tognolini M, Borges G, Crozier A. Dietary (poly)phenolics in human health: structures, bioavailability, and evidence of protective effects against chronic diseases. Antioxid Redox Signal 2013;18:1818-92.

17. Rodriguez-Mateos A, Vauzour D, Krueger CG, Shanmuganayagam D, Reed J, Calani L et al. Bioavailability, bioactivity and impact on health of dietary flavonoids and related compounds: an update. Arch Toxicol 2014;88:1803-53.

18. Scalbert A, Williamson G. Dietary intake and bioavailability of polyphenols. J Nutr 2000;130:2073S-85S.

19. Pierre JF, Heneghan AF, Feliciano RP, Shanmuganayagam D, Roenneburg DA, Krueger CG et al. Cranberry Proanthocyanidins improve the gut mucous layer morphology and function in mice receiving elemental enteral nutrition. Journal of Parenteral and Enteral Nutrition 2013;37:401-9.

20. Pierre JF, Heneghan AF, Feliciano RP, Shanmuganayagam D, Roenneburg DA, Krueger CG et al. Cranberry proanthocyanidins improve the gut mucous layer morphology and function in mice receiving elemental enteral nutrition. JPEN J Parenter Enteral Nutr 2013;37:401-9.

21. Moi P, Chan K, Asunis I, Cao A, Kan YW. Isolation of NF-E2-related factor 2 (Nrf2), a NF-E2-like basic leucine zipper transcriptional activator that binds to the tandem NF-E2/AP1 repeat of the beta-globin locus control region. Proc Natl Acad Sci U S A 1994;91:9926-30.

22. Cote J, Caillet S, Doyon G, Sylvain JF, Lacroix M. Analyzing cranberry bioactive compounds. Crit Rev Food Sci Nutr 2010;50:872-88.

23. Prior RL, Fan E, Ji H, Howell A, Nio C, Payne MJ, Reed J. Multi-laboratory validation of a standard method for quantifying proanthocyanidins in cranberry powders. J Sci Food Agric 2010;90:1473-8.

24. Feliciano RP, Shea MP, Shanmuganayagam D, Krueger CG, Howell AB, Reed JD. Comparaison of isolated Cranberry (Vaccinium macrocarpon Ait.) proanthocyanidins to catechin and procyanidins A2 and B2 for use as standards in the 4-(dimethylamino)cinnamaldehyde assay. Journal of Agricultural and Food Chemistry 2012;60:4578-85.

25. Brownmiller C, Howard LR, Prior RL. Processing and storage effects on procyanidin composition and concentration of processed blueberry products. J Agric Food Chem 2009;57:1896-902.

26. Kelm MA, Johnson JC, Robbins RJ, Hammerstone JF, Schmitz HH. High-performance liquid chromatography separation and purification of cacao (Theobroma cacao L.) procyanidins according to degree of polymerization using a diol stationary phase. J Agric Food Chem 2006;54:1571-6.

27. Robbins RJ, Leonczak J, Johnson JC, Li J, Kwik-Uribe C, Prior RL, Gu L. Method performance and multi-laboratory assessment of a normal phase high pressure liquid chromatography-fluorescence detection method for the quantitation of flavanols and procyanidins in cocoa and chocolate containing samples. J Chromatogr A 2009;1216:4831-40.

28. Wallace DC, Giusti M. Extraction and normal-phase HPLC-fluorescence-electrospray MS characterization and quantification of procyanidins in cranberry extracts. Journal of Food Science 2010;75:C690-C696.

29. Howell AB, Reed JD, Krueger CG, Winterbottom R, Cunningham DG, Leahy M. A-type cranberry proanthocyanidins and uropathogenic bacterial anti-adhesion activity. Phytochemistry 2005;66:2281-91.

30. Foo LY, Lu Y, Howell AB, Vorsa N. A-Type proanthocyanidin trimers from cranberry that inhibit adherence of uropathogenic P-fimbriated Escherichia coli. J Nat Prod 2000;63:1225-8.

31. Neto CC, Krueger CG, Lamoureux TL, Kondo M, Vaisberg AJ, Hurta RAR. MALDI-TOF MS characterization of proanthocyanidins from cranberry fruit Vaccinium macrocarpon that inhibit tumor cell growth and matrix metalloproteinase expression in vitro. Journal of the Science of Food and Agriculture 2006;81:18-25.

32. Porter ML, Krueger CG, Wiebe DA, Cunningham DG, Reed JD. Cranberry proanthocyanidins associate with low-density lipoprotein and inhibit in vitro Cu2+-induced oxidation. Journal of the Science of Food and Agriculture 2001;81:1306-13.

33. Reed JD, Krueger CG, Vestling MM. MALDI-TOF mass spectrometry of oligomeric food polyphenols. Phytochemistry 2005;66:2248-63.

34. Carpenter JL, Caruso FL, Tata A, Vorsa N, Neto CC. Variation in proanthocyanidin content and composition among commonly grown North American cranberry cultivars (Vaccinium macrocarpon). J Sci Food Agric 2014;94:2738-45.

35. Foo LY, Lu Y, Howell AB, Vorsa N. The structure of cranberry proanthocyanidins which inhibit adherence of uropathogenic P-fimbriated Escherichia coli in vitro. Phytochemistry 2000;54:173-81.

36. Feliciano RP, Meudt JJ, Shanmuganayagam D, Krueger CG, Reed JD. Ratio of "A-type" to "B-type" proanthocyanidin interflavan bonds affects extra-intestinal pathogenic Escherichia coli invasion of gut epithelial cells. J Agric Food Chem 2014;62:3919-25.

37. Kevers C, Pincemail J, Tabart J, Defraigne JO, Dommes J. Influence of cultivar, harvest time, storage conditions, and peeling on the antioxidant capacity and phenolic and ascorbic acid contents of apples and pears. J Agric Food Chem 2011;59:6165-71.

38. Marti MP, Pantaleon A, Rozek A, Soler A, Valls J, Macia A et al. Rapid analysis of procyanidins and anthocyanins in plasma by microelution SPE and ultra-HPLC. J Sep Sci 2010;33:2841-53.

39. Neveu V, Perez-Jimenez J, Vos F, Crespy V, du CL, Mennen L et al. Phenol-Explorer: an online comprehensive database on polyphenol contents in foods. Database (Oxford) 2010;2010:bap024.

40. USDA. USDA database for the flavonoid content of selected foods release. 21 st edn. 2007. USDA, Belstville.

41. Rodriguez-Mateos A, Vauzour D, Krueger CG, Shanmuganayagam D, Reed J, Calani L et al. Bioavailability, bioactivity and impact on health of dietary flavonoids and related compounds: an update. Arch Toxicol 2014;88:1803-53.

42. Harborne JB. The Flavonoids: Advances in Research since 1986. In: Chapman and Hall, ed. London, U.K.: 1994.

43. Häkkinen S, Heinonen M, Karenlampi S, Mykkanen H, Ruuskanen J, Torronen R. Screening of selected flavonoids and phenolic acids in 19 berries. Food Res Int 1999;32:345-53.

44. Prior RL, Lazarus SA, Cao G, Muccitelli H, Hammerstone JF. Identification of procyanidins and anthocyanins in blueberries and cranberries (Vaccinium spp.) using high-performance liquid chromatography/mass spectrometry. J Agric Food Chem 2001;49:1270-6.

45. Singleton VL, Orthofer R, and Lamuela-Raventos RM. Analysis of total phenols and other oxidation substrates and antioxidants by means of Folin-Ciocalteu Reagent. Methods in Enzymology 1999;299:152-78.

46. Denis MC, Desjardins Y, Furtos A, Marcil V, Dudonne S, Montoudis A et al. Prevention of oxidative stress, inflammation and mitochondrial dysfunction in the intestine by different cranberry phenolic fractions. Clin Sci (Lond) 2015;128:197-212.

47. Hanton SD. Mass spectrometry of polymers and polymer surfaces. Chem Rev 2001;101:527-69.

48. Alicata R, Montaudo G, Puglisi C, Samperi F. Influence of chain end groups on the matrix-assisted laser desorption/ionization spectra of polymer blends. Rapid Commun Mass Spectrom 2002;16:248-60.

49. Feliciano RP, Krueger CG, Shanmuganayagam D, Vestling MM, Reed JD. Deconvolution of matrix-assisted laser desorption/ionization time-of-flight mass spectrometry isotope patterns to determine ratios of A-type to B-type interflavan bonds in cranberry proanthocyanidins. Food Chem 2012;135:1485-93.

50. Ohnishi-Kameyama M, Yanagida A, Kanda T, Nagata T. Identification of catechin oligomers from apple (Malus pumila cv. Fuji) in matrix-assisted laser desorption/ionization time-of-flight mass spectrometry and fast-atom bombardment mass spectrometry. Rapid Commun Mass Spectrom 1997;11:31-6.

51. Day AJ, Canada FJ, Diaz JC, Kroon PA, Mclauchlan R, Faulds CB et al. Dietary flavonoid and isoflavone glycosides are hydrolysed by the lactase site of lactase phlorizin hydrolase. FEBS Lett 2000;468:166-70.

52. Day AJ, DuPont MS, Ridley S, Rhodes M, Rhodes MJ, Morgan MR, Williamson G. Deglycosylation of flavonoid and isoflavonoid glycosides by human small intestine and liver beta-glucosidase activity. FEBS Lett 1998;436:71-5.

53. Gee JM, DuPont MS, Rhodes MJ, Johnson IT. Quercetin glucosides interact with the intestinal glucose transport pathway. Free Radic Biol Med 1998;25:19-25.

54. Day AJ, Gee JM, DuPont MS, Johnson IT, Williamson G. Absorption of quercetin-3-glucoside and quercetin-4'-glucoside in the rat small intestine: the role of lactase phlorizin hydrolase and the sodium-dependent glucose transporter. Biochem Pharmacol 2003;65:1199-206.

55. Hollman PC, Katan MB. Dietary flavonoids: intake, health effects and bioavailability. Food Chem Toxicol 1999;37:937-42.

56. Deprez S, Mila I, Huneau JF, Tome D, Scalbert A. Transport of proanthocyanidin dimer, trimer, and polymer across monolayers of human intestinal epithelial Caco-2 cells. Antioxid Redox Signal 2001;3:957-67.

57. Crespy V, Morand C, Manach C, Besson C, Demigne C, Remesy C. Part of quercetin absorbed in the small intestine is conjugated and further secreted in the intestinal lumen. Am J Physiol 1999;277:G120-G126.

58. Walgren RA, Karnaky KJ, Jr., Lindenmayer GE, Walle T. Efflux of dietary flavonoid quercetin 4'-beta-glucoside across human intestinal Caco-2 cell monolayers by apical multidrug resistance-associated protein-2. J Pharmacol Exp Ther 2000;294:830-6.

59. Vaidyanathan JB, Walle T. Transport and metabolism of the tea flavonoid (-)-epicatechin by the human intestinal cell line Caco-2. Pharm Res 2001;18:1420-5.

60. Petri N, Tannergren C, Holst B, Mellon FA, Bao Y, Plumb GW et al. Absorption/metabolism of sulforaphane and quercetin, and regulation of phase II enzymes, in human jejunum in vivo. Drug Metab Dispos 2003;31:805-13.

61. Crespy V, Morand C, Besson C, Cotelle N, Vezin H, Demigne C, Remesy C. The splanchnic metabolism of flavonoids highly differed according to the nature of the compound. Am J Physiol Gastrointest Liver Physiol 2003;284:G980-G988.

62. Lambert N, Kroon PA, Faulds CB, Plumb GW, McLauchlan WR, Day AJ, Williamson G. Purification of cytosolic beta-glucosidase from pig liver and its reactivity towards flavonoid glycosides. Biochim Biophys Acta 1999;1435:110-6.

63. Wu X, Cao G, Prior RL. Absorption and metabolism of anthocyanins in elderly women after consumption of elderberry or blueberry. J Nutr 2002;132:1865-71.

64. Mojarrabi B, Mackenzie PI. Characterization of two UDP glucuronosyltransferases that are predominantly expressed in human colon. Biochem Biophys Res Commun 1998;247:704-9.

65. Walle UK, Galijatovic A, Walle T. Transport of the flavonoid chrysin and its conjugated metabolites by the human intestinal cell line Caco-2. Biochem Pharmacol 1999;58:431-8.

66. Ayrton A, Morgan P. Role of transport proteins in drug absorption, distribution and excretion. Xenobiotica 2001;31:469-97.

67. Coughtrie MW, Sharp S, Maxwell K, Innes NP. Biology and function of the reversible sulfation pathway catalysed by human sulfotransferases and sulfatases. Chem Biol Interact 1998;109:3-27.

68. Falany CN. Enzymology of human cytosolic sulfotransferases. FASEB J 1997;11:206-16.

69. Silva FA, Borges F, Guimaraes C, Lima JL, Matos C, Reis S. Phenolic acids and derivatives: studies on the relationship among structure, radical scavenging activity, and physicochemical parameters. J Agric Food Chem 2000;48:2122-6.

70. Zuo Y, Wang C, Zhan J. Separation, characterization, and quantitation of benzoic and phenolic antioxidants in American cranberry fruit by GC-MS. J Agric Food Chem 2002;50:3789-94.

71. Yeh CT, Ching LC, Yen GC. Inducing gene expression of cardiac antioxidant enzymes by dietary phenolic acids in rats. J Nutr Biochem 2009;20:163-71.

72. Graf E. Antioxidant potential of ferulic acid. Free Radic Biol Med 1992;13:435-48.

73. Zheng W, Wang SY. Oxygen radical absorbing capacity of phenolics in blueberries, cranberries, chokeberries, and lingonberries. J Agric Food Chem 2003;51:502-9.

74. Yang F, Oz HS, Barve S, de Villiers WJ, McClain CJ, Varilek GW. The green tea polyphenol (-)-epigallocatechin-3-gallate blocks nuclear factor-kappa B activation by inhibiting I kappa B kinase activity in the intestinal epithelial cell line IEC-6. Mol Pharmacol 2001;60:528-33.

75. Feng R, Lu Y, Bowman LL, Qian Y, Castranova V, Ding M. Inhibition of activator protein-1, NF-kappaB, and MAPKs and induction of phase 2 detoxifying enzyme activity by chlorogenic acid. J Biol Chem 2005;280:27888-95.

76. Karlsson PC, Huss U, Jenner A, Halliwell B, Bohlin L, Rafter JJ. Human fecal water inhibits COX-2 in colonic HT-29 cells: role of phenolic compounds. J Nutr 2005;135:2343-9.

77. Rice-Evans C, Miller N. Measurement of the antioxidant status of dietary constituents, low density lipoproteins and plasma. Prostaglandins Leukot Essent Fatty Acids 1997;57:499-505.

78. Vvedenskaya IO, Rosen RT, Guido JE, Russell DJ, Mills KA, Vorsa N. Characterization of flavonols in cranberry (Vaccinium macrocarpon) powder. J Agric Food Chem 2004;52:188-95.

79. Aherne SA, O'Brien NM. Dietary flavonols: chemistry, food content, and metabolism. Nutrition 2002;18:75-81.

80. Mullen W, Marks SC, Crozier A. Evaluation of phenolic compounds in commercial fruit juices and fruit drinks. J Agric Food Chem 2007;55:3148-57.

81. Yan X, Murphy BT, Hammond GB, Vinson JA, Neto CC. Antioxidant activities and antitumor screening of extracts from cranberry fruit (Vaccinium macrocarpon). J Agric Food Chem 2002;50:5844-9.

82. Manach C, Scalbert A, Morand C, Remesy C, Jimenez L. Polyphenols: food sources and bioavailability. Am J Clin Nutr 2004;79:727-47.

83. Vvedenskaya IO, Rosen RT, Guido JE, Russell DJ, Mills KA, Vorsa N. Characterization of flavonols in cranberry (Vaccinium macrocarpon) powder. J Agric Food Chem 2004;52:188-95.

84. Ohnishi R, Ito H, Kasajima N, Kaneda M, Kariyama R, Kumon H et al. Urinary excretion of anthocyanins in humans after cranberry juice ingestion. Biosci Biotechnol Biochem 2006;70:1681-7.

85. Prior RL, Lazarus SA, Cao G, Muccitelli H, Hammerstone JF. Identification of procyanidins and anthocyanins in blueberries and cranberries (Vaccinium spp.) using high-performance liquid chromatography/mass spectrometry. J Agric Food Chem 2001;49:1270-6.

86. Bilyk A, Sapers GM. Varietal differences in the quercetin, kaempferol, and myricetin contents of highbush blueberry, cranberry, and thornless blackberry fruits. J Agric Food Chem 1986;34:585-8.

87. Shih PH, Yeh CT, Yen GC. Effects of anthocyanidin on the inhibition of proliferation and induction of apoptosis in human gastric adenocarcinoma cells. Food Chem Toxicol 2005;43:1557-66.

88. White BL, Howard LR, Prior RL. Proximate and polyphenolic characterization of cranberry pomace. J Agric Food Chem 2010;58:4030-6.

89. Shih PH, Yeh CT, Yen GC. Anthocyanins induce the activation of phase II enzymes through the antioxidant response element pathway against oxidative stress-induced apoptosis. J Agric Food Chem 2007;55:9427-35.

90. Singletary KW, Jung KJ, Giusti M. Anthocyanin-rich grape extract blocks breast cell DNA damage. J Med Food 2007;10:244-51.

91. Turner A, Chen SN, Nikolic D, van BR, Farnsworth NR, Pauli GF. Coumaroyl iridoids and a depside from cranberry (Vaccinium macrocarpon). J Nat Prod 2007;70:253-8.

92. Nakamura Y, Watanabe S, Miyake N, Kohno H, Osawa T. Dihydrochalcones: evaluation as novel radical scavenging antioxidants. J Agric Food Chem 2003;51:3309-12.

93. Gu L, Kelm MA, Hammerstone JF, Beecher G, Holden J, Haytowitz D et al. Concentrations of proanthocyanidins in common foods and estimations of normal consumption. J Nutr 2004;134:613-7.

94. Harnly JM, Doherty RF, Beecher GR, Holden JM, Haytowitz DB, Bhagwat S, Gebhardt S. Flavonoid content of U.S. fruits, vegetables, and nuts. J Agric Food Chem 2006;54:9966-77.

95. Gu L, Kelm MA, Hammerstone JF, Beecher G, Holden J, Haytowitz D, Prior RL. Screening of foods containing proanthocyanidins and their structural characterization using LC-MS/MS and thiolytic degradation. J Agric Food Chem 2003;51:7513-21.

96. Gu L, Kelm MA, Hammerstone JF, Beecher G, Holden J, Haytowitz D, Prior RL. Screening of foods containing proanthocyanidins and their structural characterization using LC-MS/MS and thiolytic degradation. J Agric Food Chem 2003;51:7513-21.

97. Appeldoorn MM, Vincken JP, Gruppen H, Hollman PC. Procyanidin dimers A1, A2, and B2 are absorbed without conjugation or methylation from the small intestine of rats. J Nutr 2009;139:1469-73.

98. Ou K, Percival SS, Zou T, Khoo C, Gu L. Transport of cranberry A-type procyanidin dimers, trimers, and tetramers across monolayers of human intestinal epithelial Caco-2 cells. J Agric Food Chem 2012;60:1390-6.

99. Gu L, Kelm M, Hammerstone JF, Beecher G, Cunningham D, Vannozzi S, Prior RL. Fractionation of polymeric procyanidins from lowbush blueberry and quantification of procyanidins in selected foods with an optimized normal-phase HPLC-MS fluorescent detection method. J Agric Food Chem 2002;50:4852-60.

100. Rodriguez-Ramiro I, Ramos S, Bravo L, Goya L, Martin MA. Procyanidin B2 induces Nrf2 translocation and glutathione S-transferase P1 expression via ERKs and p38-MAPK pathways and protect human colonic cells against oxidative stress. Eur J Nutr 2012;51:881-92.

101. Fiorani M, Guidarelli A, Blasa M, Azzolini C, Candiracci M, Piatti E, Cantoni O. Mitochondria accumulate large amounts of quercetin: prevention of mitochondrial damage and release upon oxidation of the extramitochondrial fraction of the flavonoid. J Nutr Biochem 2010;21:397-404.

102. Scalbert A, Williamson G. Dietary intake and bioavailability of polyphenols. J Nutr 2000;130:2073S-85S.

103. Verstraeten SV, Keen CL, Schmitz HH, Fraga CG, Oteiza PI. Flavan-3-ols and procyanidins protect liposomes against lipid oxidation and disruption of the bilayer structure. Free Radic Biol Med 2003;34:84-92.

104. Verstraeten SV, Hammerstone JF, Keen CL, Fraga CG, Oteiza PI. Antioxidant and membrane effects of procyanidin dimers and trimers isolated from peanut and cocoa. J Agric Food Chem 2005;53:5041-8.

105. Verstraeten SV, Lanoue L, Keen CL, Oteiza PI. Relevance of lipid polar headgroups on boron-mediated changes in membrane physical properties. Arch Biochem Biophys 2005;438:103-10.

Table 1: Identification of polyphenols in cranberry fractions

Cranberry fraction	Polyphenol subclass	Polyphenol name	Formula	Ion formula	Experimental mass (m/z)	Theoretical mass (m/z)	Diff.ppm (<5ppm)
CL fraction	Hydroxybenzoic acids	Benzoic acid	$C_7H_6O_2$	$[C_7H_6O_2\text{-}H]^-$	121.0294	121.0290	3.3
		Hydroxybenzoic acids	$C_7H_6O_3$	$[C_7H_6O_3\text{-}H]^-$	137.0234	137.0239	-3.6
		Dihydroxybenzoic acids	$C_6H_6O_4$	$[C_6H_6O_4\text{-}H]^-$	153.0191	153.0188	2.0
		Protocatechuic acid					
		Vanillic acid	$C_8H_8O_4$	$[C_8H_8O_4\text{-}H]^-$	167.0340	167.0344	-2.4
		Ellagic acid	$C_{14}H_6O_8$	$[C_{14}H_6O_8\text{-}H]^-$	300.9980	300.9984	-1.3
	Hydroxycinnamic acid	Coumaric acid	$C_9H_8O_3$	$[C_9H_8O_3\text{-}H]^-$	163.0398	163.0395	1.8
		p-coumaroyl glycolic acid	$C_8H_8O_4$	$[C_8H_8O_4\text{-}H]^-$	167.0337	167.0344	-4.2
		Caffeic acid	$C_9H_8O_4$	$[C_9H_8O_4\text{-}H]^-$	179.0351	179.0344	3.9
		Ferulic acid	$C_{10}H_{10}O_4$	$[C_{10}H_{10}O_4\text{-}H]^-$	193.0498	193.0501	-1.6
		Sinapic acid	$C_{11}H_{12}O_5$	$[C_{11}H_{12}O_5\text{-}H]^-$	223.0600	223.0606	-2.7
		Caffeolquinic acid	$C_{16}H_{18}O_9$	$[C_{16}H_{18}O_9\text{-}H]^-$	377.0868	377.0848	5.0
	Hydroxyphenylacetic acid	4-Hydroxyphenylacetic acid	$C_8H_8O_3$	$[C_8H_8O_3\text{-}H]^-$	151.0400	151.0395	3.3
	Hydroxyphenyl-propanoic acid	Dihydrocaffeic acid	$C_9H_{10}O_4$	$[C_9H_{10}O_4\text{-}H]^-$	181.0502	181.0501	1.1
CM fraction	Flavonols	Kaempferol	$C_{15}H_{10}O_6$	$[C_{15}H_{10}O_6\text{-}H]^-$	285.0390	285.0399	3.2
		6,8-Dihydroxykaempferol	$C_{15}H_{12}O_8$	$[C_{15}H_{12}O_8\text{-}H]^-$	319.0461	319.0454	2.2
		Quercetin	$C_{15}H_{10}O_7$	$[C_{15}H_{10}O_7\text{-}H]^-$	301.0336	301.0348	4.0
		Isorhamnetin	$C_{16}H_{12}O_7$	$[C_{16}H_{12}O_7\text{-}H]^-$	315.0498	315.0505	2.2
		Myricetin	$C_{15}H_{10}O_8$	$[C_{15}H_{10}O_8\text{-}H]^-$	317.0292	317.0298	1.6
		Kaempferol 3-O-galactoside	$C_{21}H_{20}O_{11}$	$[C_{21}H_{20}O_{11}\text{-}H]^-$	447.0930	447.0927	0.7
		Kaempferol 3-O-glucoside	$C_{21}H_{20}O_{11}$	$[C_{21}H_{20}O_{11}\text{-}H]^-$			
		Kaempferol 7-O-glucoside	$C_{21}H_{20}O_{11}$	$[C_{21}H_{20}O_{11}\text{-}H]^-$			
		Quercetin 3-O-rhamnoside	$C_{21}H_{20}O_{11}$	$[C_{21}H_{20}O_{11}\text{-}H]^-$			
		Myricetin 3-O-arabinoside	$C_{20}H_{18}O_2$	$[C_{20}H_{18}O_2\text{-}H]^-$	449.0740	449.0720	4.5
		Isorhamnetin 7-O-rhamnoside	$C_{22}H_{22}O_{11}$	$[C_{22}H_{22}O_{11}\text{-}H]^-$	461.1089	461.1084	1.1
		Kaempferol 3-O-glucuronide	$C_{21}H_{18}O_{12}$	$[C_{21}H_{18}O_{12}\text{-}H]^-$	461.0714	461.0720	1.3
		Myricetin 3-O-rhamnoside	$C_{21}H_{20}O_{12}$	$[C_{21}H_{20}O_{12}\text{-}H]^-$	463.0894	463.0876	3.7
		Quercetin 3-O-galactoside	$C_{21}H_{20}O_{12}$	$[C_{21}H_{20}O_{12}\text{-}H]^-$			
		Quercetin 3-O-glucoside	$C_{21}H_{20}O_{12}$	$[C_{21}H_{20}O_{12}\text{-}H]^-$			
		Isorhamnetin 3-O-galactoside	$C_{21}H_{22}O_{12}$	$[C_{21}H_{20}O_{12}\text{-}H]^-$	477.1009	477.1033	5.0
		Isorhamnetin 3-O-glucoside	$C_{21}H_{22}O_{12}$	$[C_{21}H_{20}O_{12}\text{-}H]^-$			
		Isorhamnetin 4'-O-glucoside	$C_{21}H_{22}O_{12}$	$[C_{21}H_{22}O_{12}\text{-}H]^-$			
		Myricetin 3-O-galactoside	$C_{21}H_{20}O_{13}$	$[C_{21}H_{20}O_{13}\text{-}H]^-$	479.0838	479.0826	2.5
		Myricetin 3-O-glucoside	$C_{21}H_{20}O_{13}$	$[C_{21}H_{20}O_{13}\text{-}H]^-$			

Flavan-3-ols	(+)-Catechin	$C_{15}H_{14}O_6$	$[C_{15}H_{14}O_6\text{-}H]^-$	289.0709	289.0712	1.0
	(-)-Epicatechin	$C_{15}H_{14}O_6$	$[C_{15}H_{14}O_6\text{-}H]^-$			
	Prodelphinidin dimer B3	$C_{30}H_{26}O_{13}$	$[C_{30}H_{26}O_{13}\text{-}H]^-$	593.1312	593.1295	2.9
	Procyanidin trimer C1	$C_{45}H_{38}O_{18}$	$[C_{45}H_{38}O_{18}\text{-}H]^-$	865.1987	865.1980	0.8
	Procyanidin trimer C2	$C_{45}H_{38}O_{18}$	$[C_{45}H_{38}O_{18}\text{-}H]^-$			
Dihydrochalcones	Phloretin	$[C_{15}H_{14}O_5\text{-}H]^-$	$[C_{15}H_{14}O_5\text{-}H]^-$	273.0769	273.0763	2.2
	Phloridzin	$[C_{21}H_{24}O_{10}\text{-}H]^-$	$[C_{21}H_{24}O_{10}\text{-}H]^-$	435.1281	435.1291	2.1
Anthocyanines	Cyanidin	$[C_{15}H_{11}O_6]^+$	$[C_{15}H_{11}O_6]^+$	288.0639	288.0634	1.7
	Peonidin	$[C_{16}H_{13}O_6]^+$	$[C_{16}H_{13}O_6]^+$	301.0721	301.0712	3.0
	Cyanidin 3-O-arabinoside	$[C_{20}H_{19}O_{10}]^+$	$[C_{20}H_{19}O_{10}]^+$	420.0971	420.1057	-1.7
	Cyanidin 3-O-xyloside	$[C_{20}H_{19}O_{10}]^+$	$[C_{20}H_{19}O_{10}]^+$			
	Cyanidin 3-O-galactoside	$[C_{21}H_{21}O_{11}]^+$	$[C_{21}H_{21}O_{11}]^+$	450.1165	450.1162	0.7
	Cyanidin 3-O-glucoside	$[C_{21}H_{21}O_{11}]^+$	$[C_{21}H_{21}O_{11}]^+$			
	Peonidin 3-O-galactoside	$[C_{22}H_{23}O_{11}]^+$	$[C_{22}H_{23}O_{11}]^+$	464.1324	464.1319	1.1
	Peonidin 3-O-glucoside	$[C_{22}H_{23}O_{11}]^+$	$[C_{22}H_{23}O_{11}]^+$			
	Cynidin 3,5-O-diglucoside	$[C_{27}H_{31}O_{16}]^+$	$[C_{27}H_{31}O_{16}]^+$	611.1621	611.1612	1.5
	Cyanidin 3,5-O-diglucoside	$[C_{27}H_{31}O_{16}]^+$	$[C_{27}H_{31}O_{16}]^+$			

Experimental mass measurement and empirical formula calculation for polyphenols. A good agreement between the theoretical and the experimental m/z values was obtained for all compounds examined (< 5 ppm). Separations were performed on a UPLC-ESI-Synapt G2S system (Waters, Beverly, MA).

Table 2: Characterization of polyphenols of cranberry in medium

Cranberry fraction	Polyphenol subclass	Polyphenol name	Polyphenols (mg/100g extract weight)			Transport ratio (%)	Recovery rate (%)
			Apical side before transport	Basolateral side after transport	Apical side after transport		
CL fraction	*Phenolic acids*	Caffeoylquinic acid	392.5	7.82 ± 4.87	379.7 ± 21.4	1.99	98.7
		p-coumaric acid	82.2	20.6 ± 2.38	61.5 ± 18.3	25.1	99.9
		m-coumaric acid	16.9	4.05 ± 0.752	12.8 ± 0.493	24.0	99.7
		Caffeic acid	19.4	0.421 ± 0.003	18.9 ± 0.739	2.17	99.6
		Ferulic acid	13.6	5.21 ± 0.056	8.32 ± 1.09	38.6	99.5
		Benzoic acid	162.7	87.6 ± 0.081	72.2 ± 8.64	53.8	98.2
		Protocatechuic acid	106.7	4.43 ± 0.252	101.8 ± 1.77	4.15	99.6
		Hydroxybenzoic acid	22.0	10.8 ± 0.287	10.7 ± 1.74	49.1	97.7
		Vanillic acid	53.4	16.2 ± 1.17	36.9 ± 0.08	30.3	99.4
		Ellagic acid	66.9	1.29 ± 0.001	54.3 ± 9.00	1.92	83.1
		Sinapic acid	12.8	1.15 ± 0.480	11.6 ± 1.56	9.02	100
		Dihydroxyphenylpropionic acid	11.4	2.30 ± 0.124	9.00 ± 2.36	20.2	99.1
		Hydroxyphenylacetic acid	22.2	5.78 ± 0.831	16.4 ± 1.96	26.0	99.9
		Dihydroxyphenylacetic acid	-	-	5.82 ± 0.993	-	-
CM fraction	*Flavonols*	Quercetin glucoside	1260.9	219.2 ± 7.15	947.9 ± 86.9	17.4	92.6
		Quercetin	54.3	1.31 ± 0.260	52.3 ± 10.1	2.41	99.3
		Quercetin glucuronide	-	1.10 ± 0.849	56.6 ± 8.54	-	-
		Quercetin diglucuronide	-	-	14.1 ± 1.44	-	-
		Quercetin glucuronide sulfate	-	-	0.080 ± 0.024	-	-
		Myricetin glucoside	180.4	29.1 ± 1.13	134.2 ± 10.6	16.1	90.5
		Myricetin	-	-	6.20 ± 1.05	-	-
		Myricetin glucuronide	-	0.841 ± 0.613	1.78 ± 0.671	-	-
		Myricetin diglucuronide	-	-	12.7 ± 1.23	-	-
		Isorhamnetin glucoside	15.6	0.567 ± 0.310	13.6 ± 1.17	3.6	90.8
		Isorhamnetin	48.8	21.6 ± 2.49	26.7 ± 5.94	44.3	99.0
		Isorhamnetin glucuronide	-	1.04 ± 0.001	1.76 ± 0.695	-	-
		Kaempferol glucoside	150.5	3.06 ± 2.49	145.0 ± 20.4	2.03	98.4
		Kaempferol	2.63	0.564 ± 0.026	1.93 ± 0.309	21.4	94.8
		Kaempferol glucuronide	-	-	0.883 ± 0.048	-	-
		Kaempferol sulfate	-	1.33 ± 0.152	403.4 ± 89.5	-	-
	Flavan-3-ols	Epicatechin	104.1	5.88 ± 0.001	97.6 ± 0.443	5.65	99.4
		Catechin	59.7	2.44 ± 2.16	57.1 ± 7.82	4.09	99.7
		Methyl catechin	-	-	-	-	-
		Catechin diglucuronide	-	1.49 ± 0.599	1.18 ± 0.280	-	-
		Catechin sulfate	-	6.27 ± 2.15	17.3 ± 2.04	-	-
		Methyl catechin sulfate	-	9.64 ± 2.17	15.8 ± 0.160	-	-
		Methyl catechin glucuronide sulfate	-	-	3.42 ± 0.730	-	-
		A-type procyanidin dimer	148.2	1.10 ± 0.089	142.8 ± 11.4	0.742	97.1
	Anthocyanins	Cyanidin 3-glucoside	-	-	-	-	-
		Cyanidin 3-galactoside	32.0	2.26 ± 0.001	29.3 ± 0.740	7.06	98.6
		Cyanidin 3-arabinoside	575.2	9.62 ± 0.810	564.5 ± 123.5	1.67	99.8
		Peonidin 3-glucoside	-	-	14.7 ± 0.841	-	-
		Peonidin 3-galactoside	347.3	3.07 ± 0.259	343.9 ± 17.1	0.884	99.9
		Peonidin 3-arabinoside	355.8	1.93 ± 0.348	353.9 ± 7.45	0.542	100
		Peonidin glucuronide	-	-	0.291 ± 0.051	-	-
	Dihydrochalcones	Phloridzin	10.2	0.336 ± 0.115	9.86 ± 1.17	3.29	99.9
		Phloretin	10.2	2.07 ± 0.411	7.14 ± 0.745	20.3	90.3
		Phloretin glucuronide	-	0.828 ± 0.054	1.30 ± 0.048	-	-
		Phloretin diglucuronide	-	-	0.089 ± 0.004	-	-
		Phloretin sulfate	-	0.595 ± 0.029	0.231 ± 0.020	-	-
		Phloretin glucuronide sulfate	-	-	-	-	-
CH fraction	*Flavan-3-ols*	Epicatechin	4.16	0.942 ± 0.001	3.07 ± 0.815	22.6	96.4
		Catechin	7.26	1.69 ± 0.898	5.52 ± 1.16	23.3	99.3
		Methyl catechin	-	-	-	-	-

Catechin diglucuronide	-	1.60 ± 0.982	0.823 ± 0.339	-	-
Catechin sulfate	-	-	-	-	-
Methyl catechin sulfate	-	0.412 ± 0.145	0.542 ± 0.220	-	-
Methyl catechin glucuronide sulfate	-	-	-	-	-
A-type procyanidin dimer	29.9	5.91 ± 0.045	23.7 ± 5.26	19.7	99.0
B-type procyanidin dimer	-	-	-	-	-

Major polyphenols were identified and quantified by UPLC-TDQ equipped with an ESI source as described in Materials and Methods. For quantification, data were collected in the multiple reaction monitoring (MRM) mode, tracking the transition of parent and product ions specific for each compound (supplementary data), and using external calibration curves. Transport of polyphenols on Caco-2/15 cells was evaluated in both of monolayer side (apical and basolateral). The results were expressed as mg/100 g of extract weight of cranberry fraction ± SD. The transport ratio and recovery rate were calculated using the following equations: Transport ratio = [(polyphenol transported) / (total polyphenols)] x 100 % and Recovery rate = {[(polyphenol (transported + remaining)] / [total polyphenols]} x 100%

FIGURES AND LEGENDS

Figure 1 **Separation and identification of phenolic acids in the CL fraction.** Extracted ion chromatograms of some identified phenolic acids in CL fraction using accurate mass measurement are presented. These phenolic acids are provided from a mixture of 250 mg of CL fraction in 1 mL Optima grade water.

Figure 2 **Separation and identification of flavonoids in the CM fraction.** Extracted ion chromatograms of flavonols (A), flavan-3-ols (B), dihydrochalcones (C) and anthocyanidins (D) are presented. These flavonoids are provided from a mixture of 250 mg of CM fraction in 1 mL Optima grade water.

Figure 3 **Separation and identification of procyanidins oligomers in CH fraction.** Extracted ion chromatograms of procyanidins oligomers of different charge stated are presented. Ion mobility separations are perceived in the inset.

Figure 4 **Separation and identification of procyanidin tetramers in the CH fraction with different linkage types.** Extracted ion chromatograms of m/z 1149.9 of AAA-type linkage (A), m/z 1151 of AAB-type linkage (B), m/z 1153 of ABB-type linkage (C), m/z 1155 of BBB-type linkage (D) of procyanidin tetramer are presented.

Figure 5 **Separation and identification of [M+Cs]+ ion species of procyanidin oligomers in the CH fraction by MALDI-TOF.** The MS/MS on m/z 3876 is presented in the inset.

Figure 6 **Structural characterization of procyanidin tetramer in the CH fraction by MALDI-TOF.** Mass spectra of procyanidin tetramers with four different linkage types: the AAA-type bond at m/z 1281.4; AAB-type bond at m/z 1283.4; ABB-type bond at m/z 1285.4 and BBB-type bond at m/z 1287.4 is presented.

Figure 7 **Identification of phenolic acids of CL fraction from CP in Caco-2 cells.** Representative of some identified phenolic acids in Caco-2 cells incubated with CL fraction (250 µg/mL) from cranberry extract for 24h before incubation with Fe/Asc (200 µM/2 mM) for 6h at 37^{o}C as described in Materials and Methods is presented.

Figure 8 **Identification of polyphenols of CM fraction from CP in Caco-2 cells.** Representative of flavonols (A), flavan-3-ols (B), dihydrochalcones (C) and anthocyanidins (D) in Caco-2 cells incubated with CM fraction (250 µg/mL) from cranberry extract for 24h before incubation with Fe/Asc (200 µM/2 mM) for 6h at 37^{o}C as described in Materials and Methods are presented.

Figure 9 **Identification of polyphenols of CH fraction from CP in Caco-2 cells.** Representative of some identified polyphenols in Caco-2 cells incubated with CH fraction (250 µg/mL) from cranberry extract for 24h before incubation with Fe/Asc (200 µM/2 mM) for 6h at 37°C as described in Materials and Methods is presented.

Figure 10 **Identification of procyanidins from cranberry in medium, Caco-2 cells and mitochondria by UPLC-MS.** Mass spectra of procyanidin oligomers in apical side (A), in Caco-2 cells (B), in mitochondria (C) and in basolateral side (D) are presented. The doubly charged $[M-2H]^{2-}$ for DP4 to DP8 or triply charged $[M-3H]^{3-}$ for DP8 to DP11 were observed. No procyanidins was detected in the basolateral side. The Caco-2 cells incubated with CH fraction from cranberry extract for 24h before incubation with Fe/Asc (200 µM/2 mM) for 6h at 37°C as described in Materials and Methods.

Figure 11 **Overall diagram showing the mechanisms of intestinal release and absorption of cranberry polyphenols in Caco-2/15 cells.** LPH, lactase phloridzin hydrolase; SGLT, sodium-dependent glucose transporter; MRP, multi resistance-associated protein; Poly, polyphenol.

Figure 1

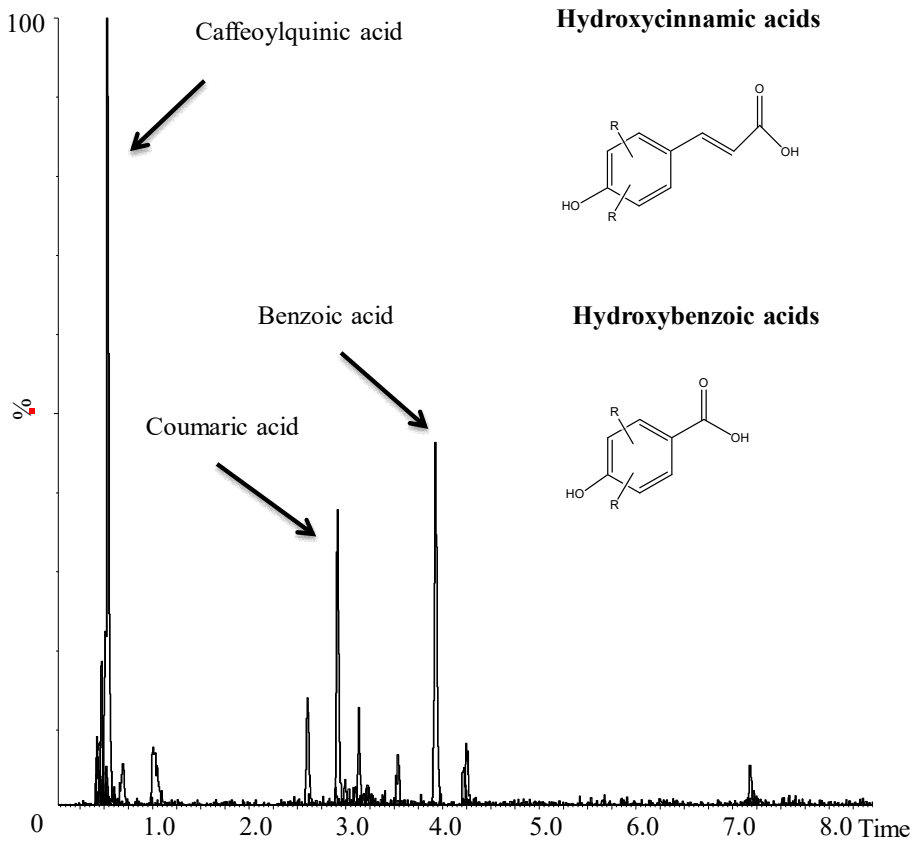
100
Caffeoylquinic acid
Hydroxycinnamic acids
R
O
OH
HO
R
Benzoic acid
Hydroxybenzoic acids
Coumaric acid
%
O
R
OH
HO
R
0
1.0
2.0
3.0
4.0
5.0
6.0
7.0
8.0 Time

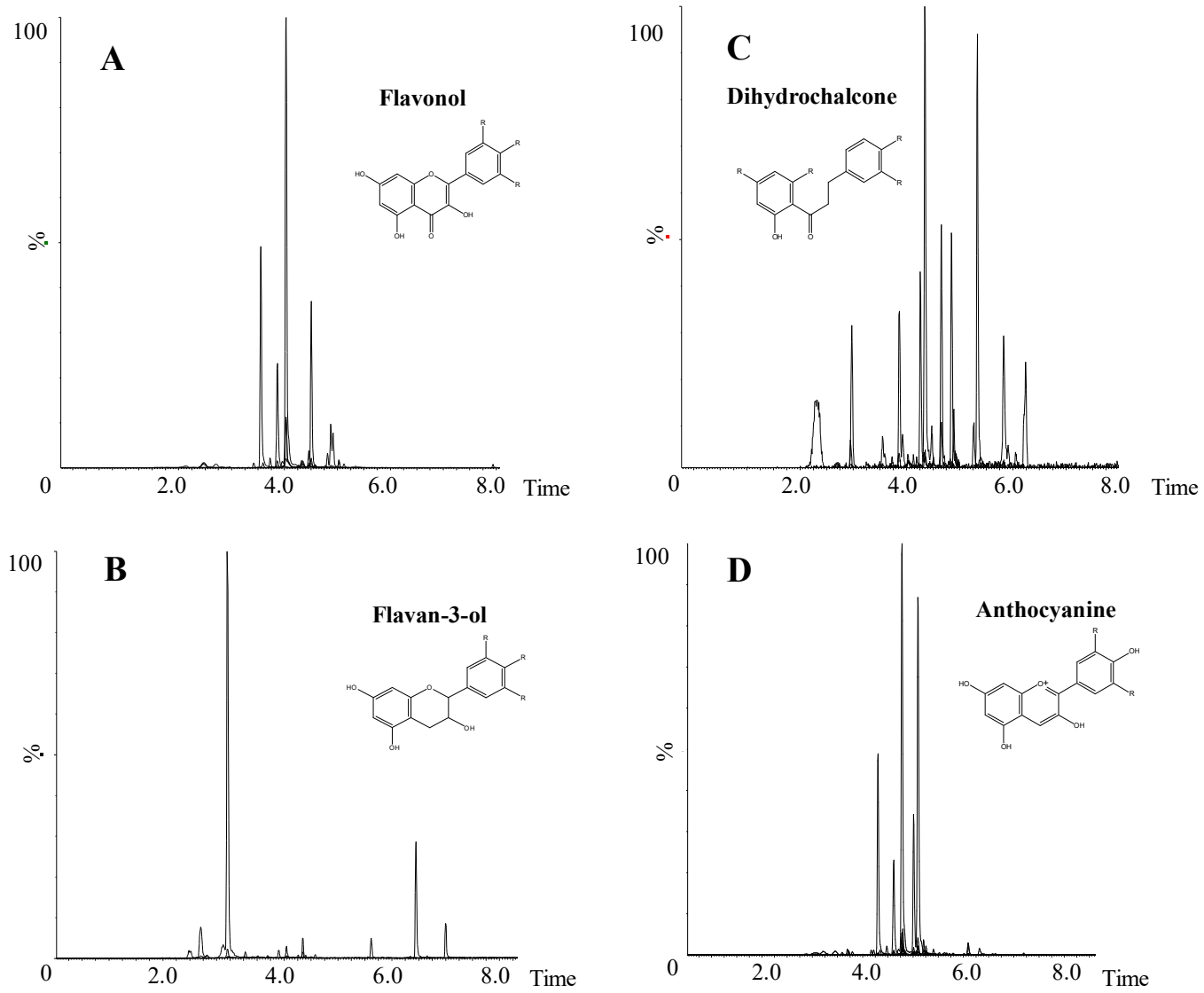
A
Flavonol
100
%
0
2.0
4.0
6.0
8.0
Time
C
Dihydrochalcone
100
%
0
2.0
4.0
6.0
8.0
Time
B
Flavan-3-ol
100
%
0
2.0
4.0
6.0
8.0
Time
D
Anthocyanine
100
%
0
2.0
4.0
6.0
8.0
Time

Figure 2

Figure 3

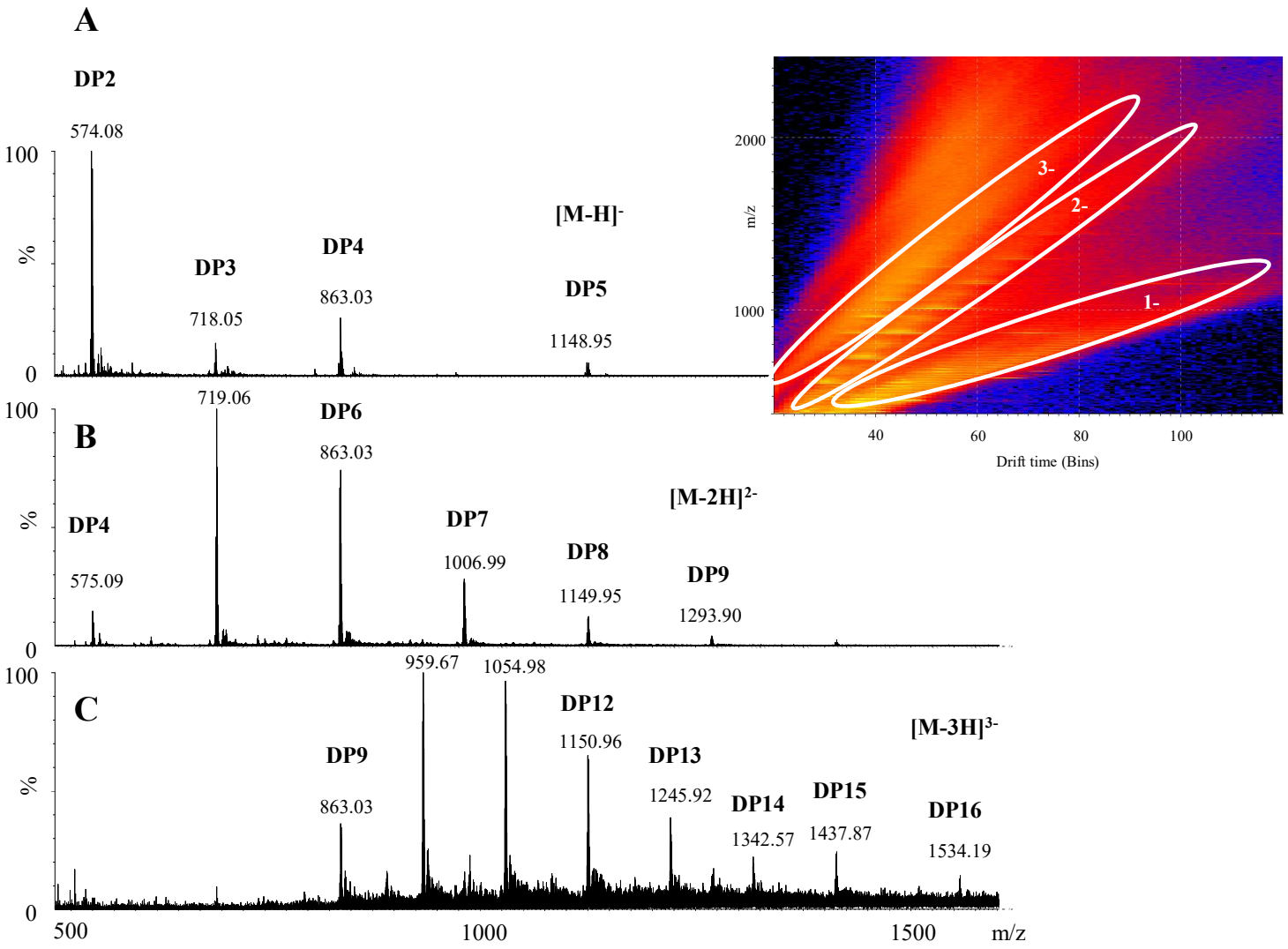
A
DP2
574.08
100
%
0
DP3
718.05
DP4
863.03
[M-H]-
DP5
1148.95
719.06
B
DP6
863.03
DP4
575.09
DP7
1006.99
DP8
1149.95
[M-2H]2-
DP9
1293.90
959.67
1054.98
C
DP12
1150.96
DP9
863.03
DP13
1245.92
DP14
1342.57
DP15
1437.87
[M-3H]3-
DP16
1534.19
500
1000
1500
m/z
2000
m/z
1000
3-
2-
1-
40
60
80
100
Drift time (Bins)

Figure 4

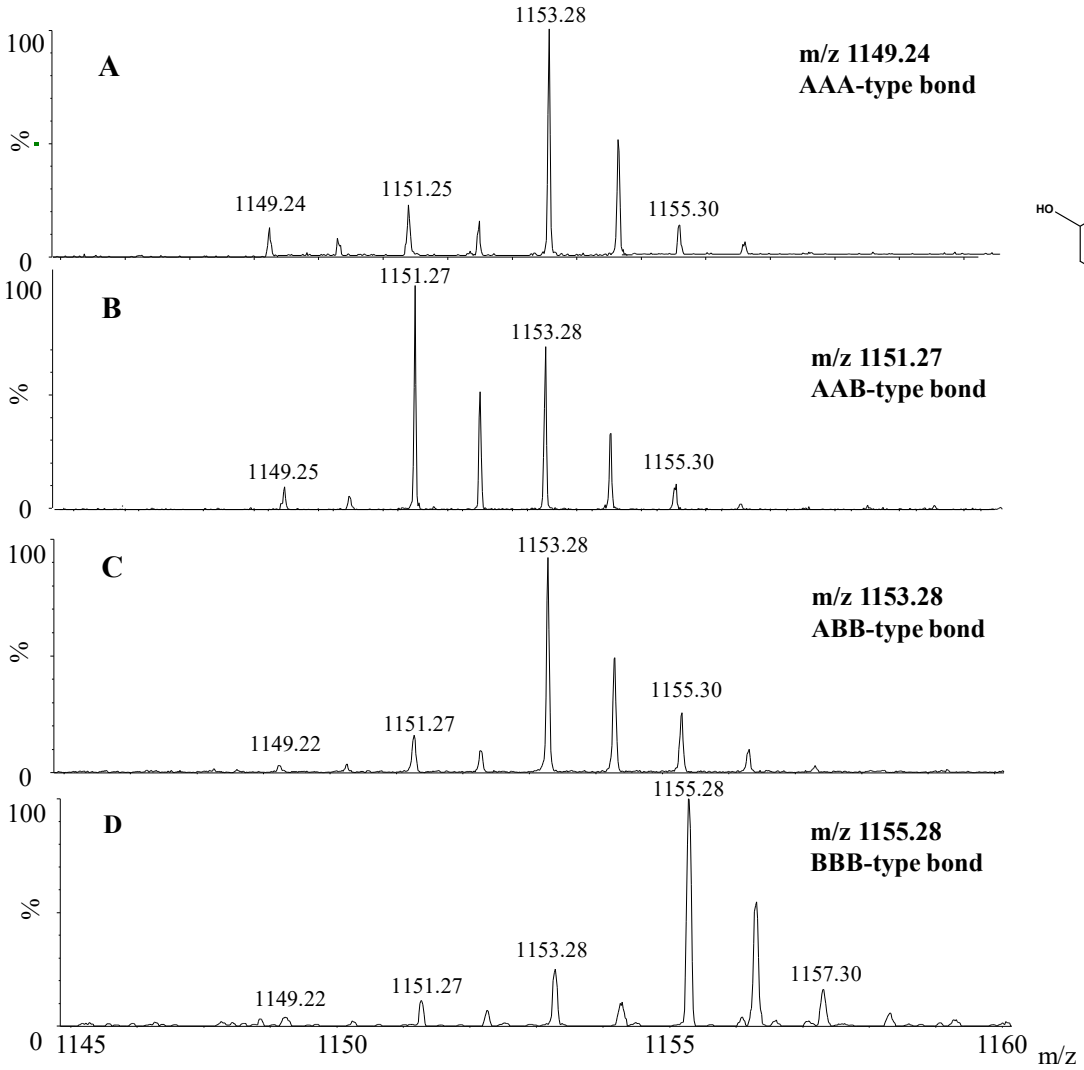
A
m/z 1149.24
AAA-type bond
1153.28
1151.25
1149.24
1155.30
B
m/z 1151.27
AAB-type bond
1151.27
1153.28
1149.25
1155.30
C
m/z 1153.28
ABB-type bond
1153.28
1155.30
1151.27
1149.22
D
m/z 1155.28
BBB-type bond
1155.28
1153.28
1157.30
1151.27
1149.22
100
%
0
1145
1150
1155
1160
m/z

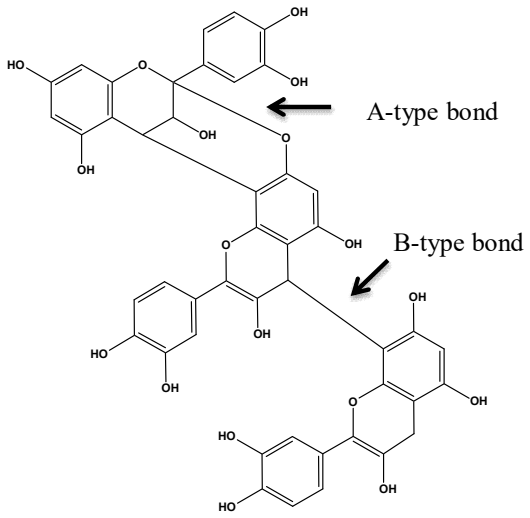
A-type bond
B-type bond
HO
OH
O

Figure 5

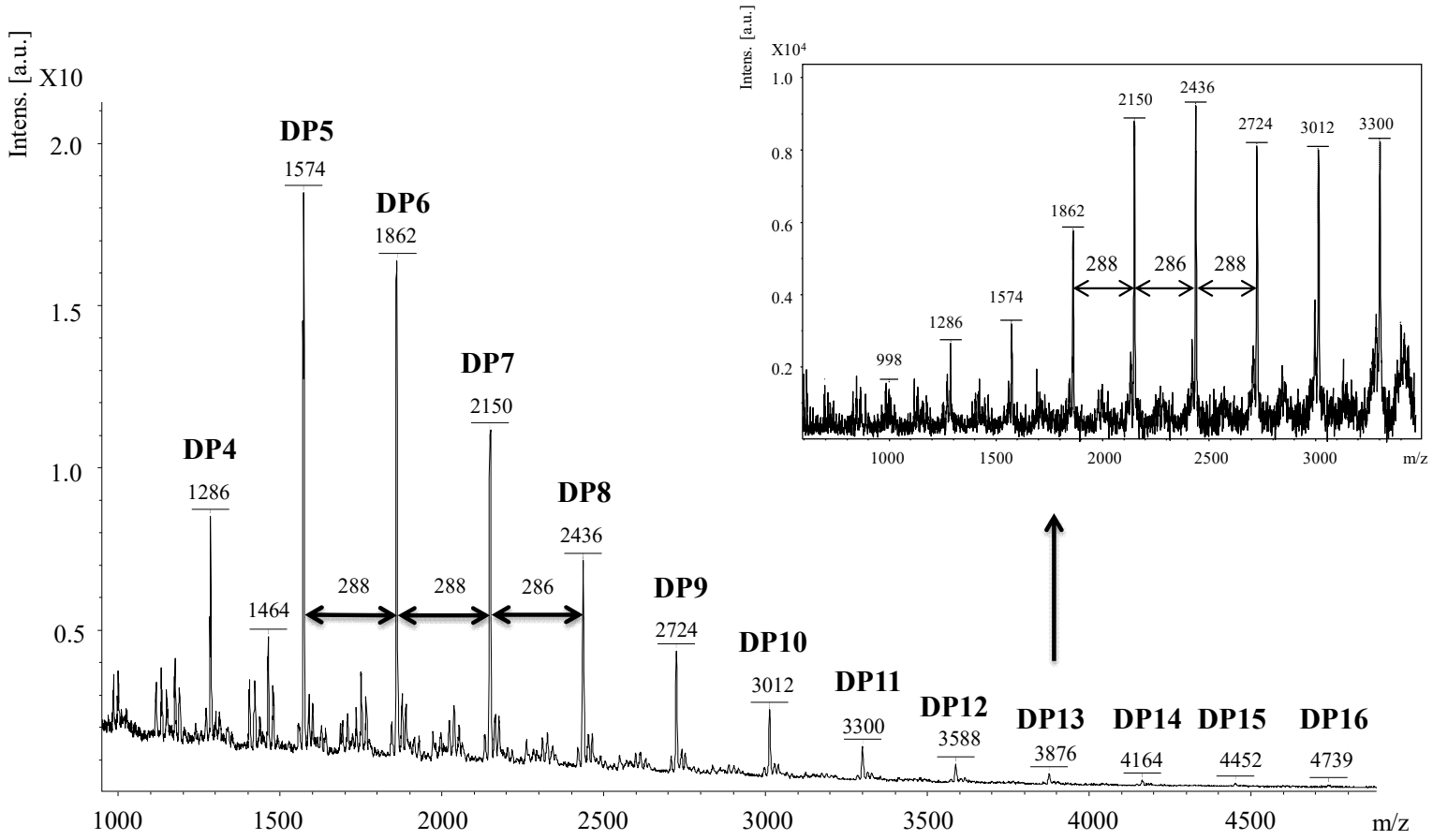
Intens. [a.u.]
X10
2.0
1.5
1.0
0.5
DP4
1286
1464
DP5
1574
DP6
1862
DP7
2150
DP8
2436
DP9
2724
DP10
3012
DP11
3300
DP12
3588
DP13
3876
DP14
4164
DP15
4452
DP16
4739
288
288
286
1000
1500
2000
2500
3000
3500
4000
4500
m/z
Intens. [a.u.]
X10⁴
1.0
0.8
0.6
0.4
0.2
998
1286
1574
1862
2150
2436
2724
3012
3300
288
286
288
1000
1500
2000
2500
3000
m/z

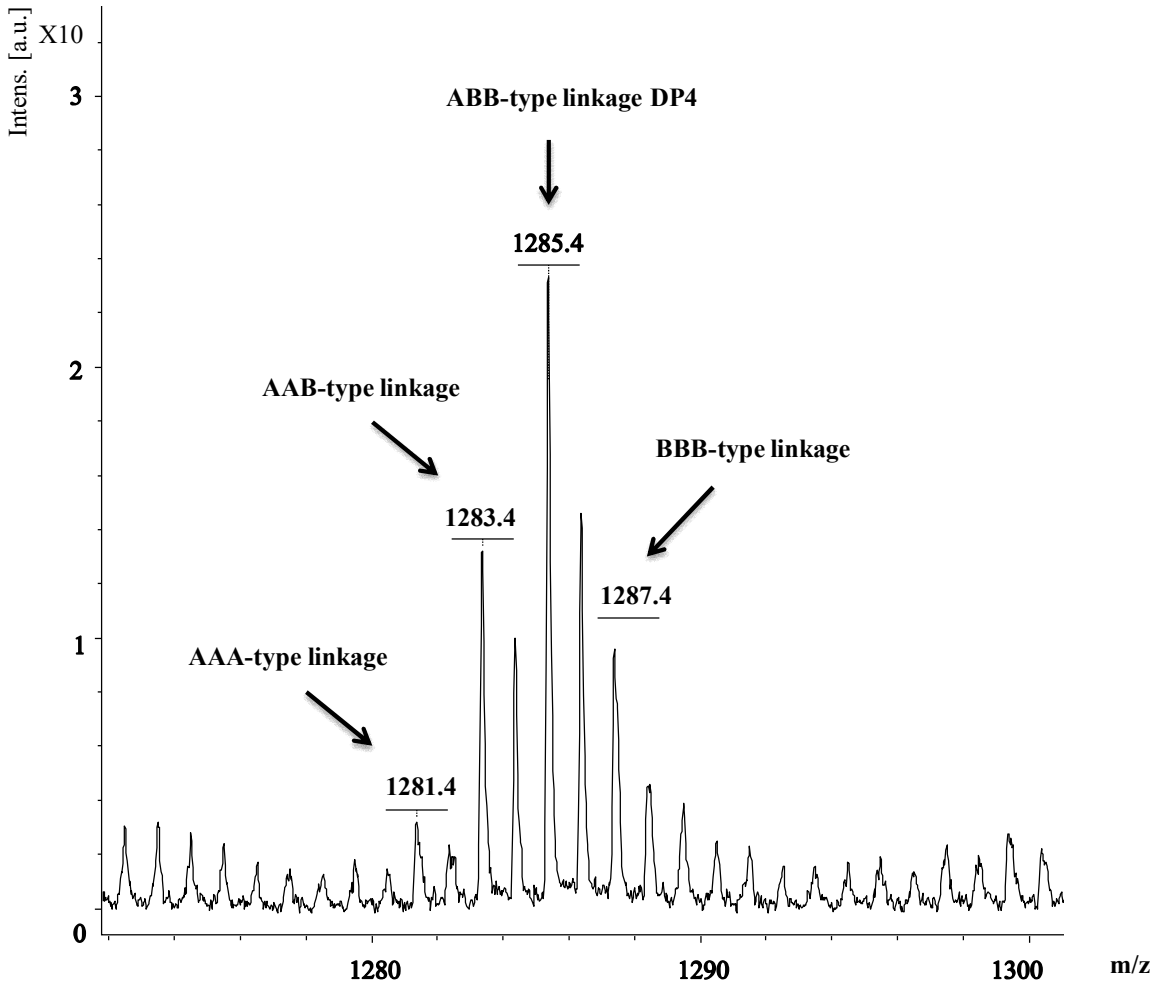
Intens. [a.u.]
X10
3
2
1
0
ABB-type linkage DP4
1285.4
AAB-type linkage
1283.4
BBB-type linkage
1287.4
AAA-type linkage
1281.4
1280
1290
1300
m/z

Figure 6

Figure 7

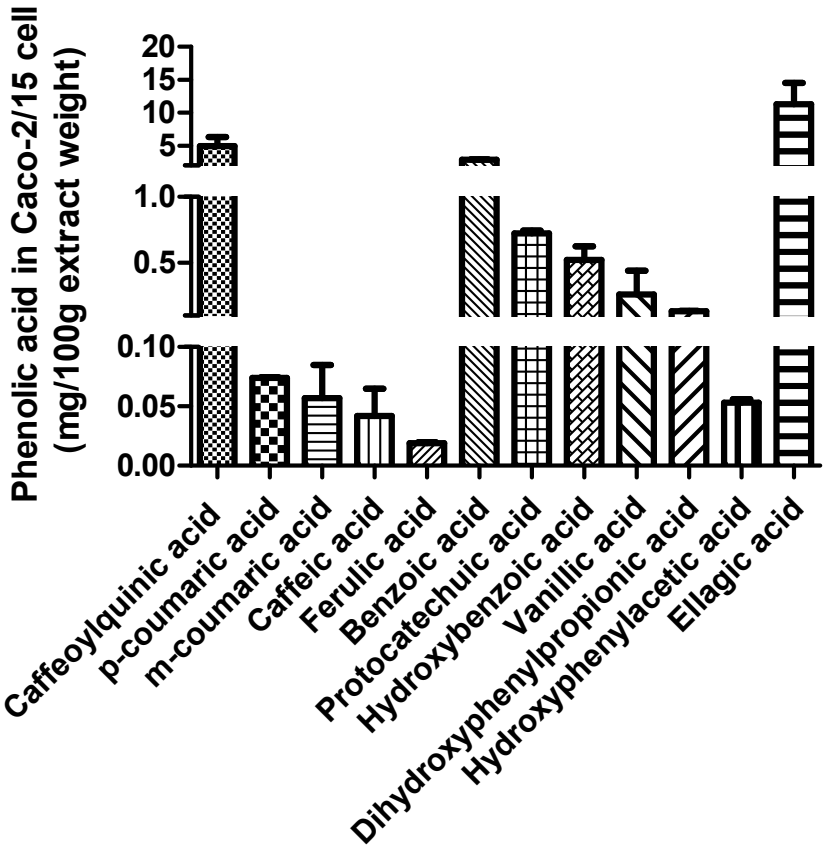
Phenolic acid in Caco-2/15 cell
(mg/100g extract weight)
20
15
10
5
1.0
0.5
0.10
0.05
0.00
Caffeoylquinic acid
p-coumaric acid
m-coumaric acid
Caffeic acid
Ferulic acid
Benzoic acid
Protocatechuic acid
Hydroxybenzoic acid
Vanillic acid
Dihydroxyphenylpropionic acid
Hydroxyphenylacetic acid
Ellagic acid

Figure 8

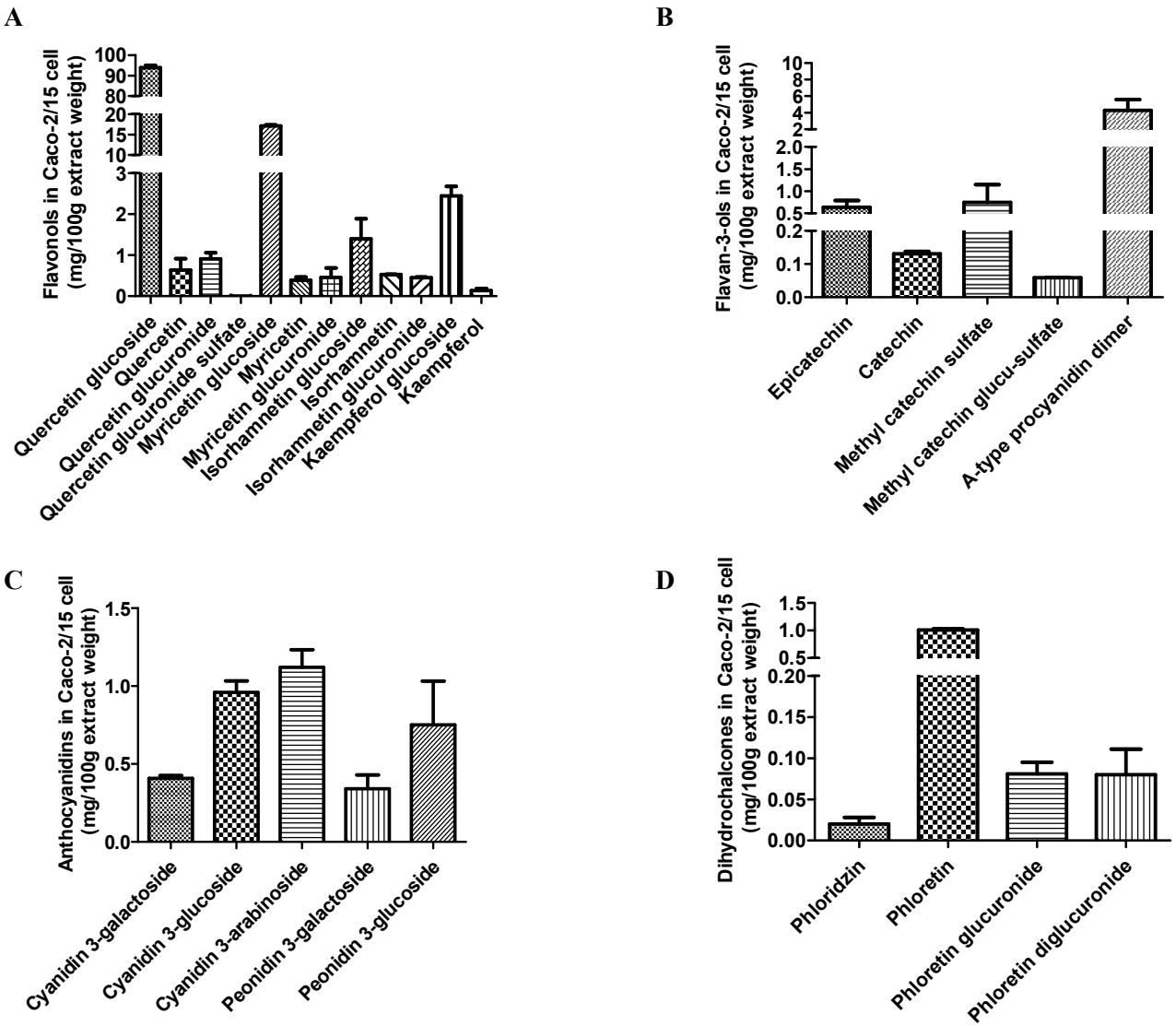
A
Flavonols in Caco-2/15 cell (mg/100g extract weight)
Quercetin glucoside
Quercetin
Quercetin glucuronide
Quercetin glucuronide sulfate
Myricetin glucoside
Myricetin
Myricetin glucuronide
Isorhamnetin glucoside
Isorhamnetin
Isorhamnetin glucuronide
Kaempferol glucoside
Kaempferol
B
Flavan-3-ols in Caco-2/15 cell (mg/100g extract weight)
Epicatechin
Catechin
Methyl catechin sulfate
Methyl catechin glucu-sulfate
A-type procyanidin dimer
C
Anthocyanidins in Caco-2/15 cell (mg/100g extract weight)
Cyanidin 3-galactoside
Cyanidin 3-glucoside
Cyanidin 3-arabinoside
Peonidin 3-galactoside
Peonidin 3-glucoside
D
Dihydrochalcones in Caco-2/15 cell (mg/100g extract weight)
Phloridzin
Phloretin
Phloretin glucuronide
Phloretin diglucuronide

Figure 9

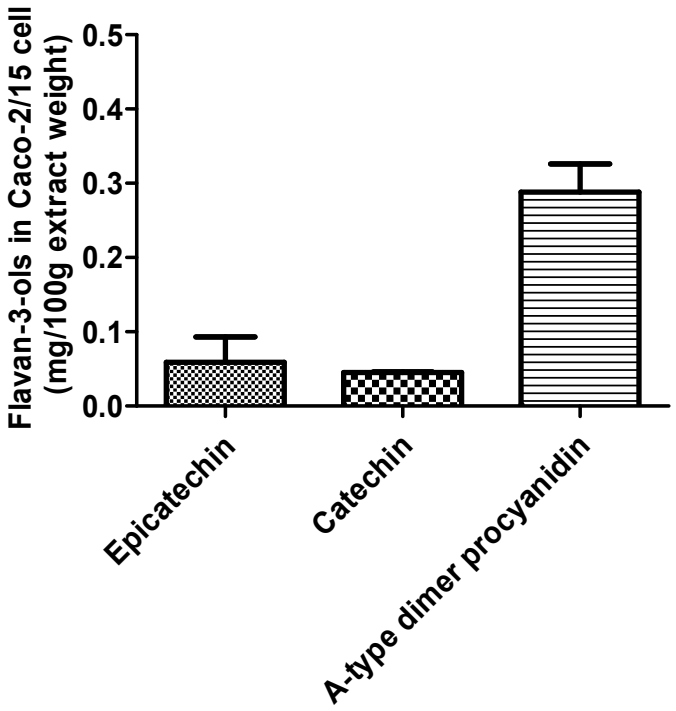
Flavan-3-ols in Caco-2/15 cell
(mg/100g extract weight)
0.5
0.4
0.3
0.2
0.1
0.0
Epicatechin
Catechin
A-type dimer procyanidin

Figure 10

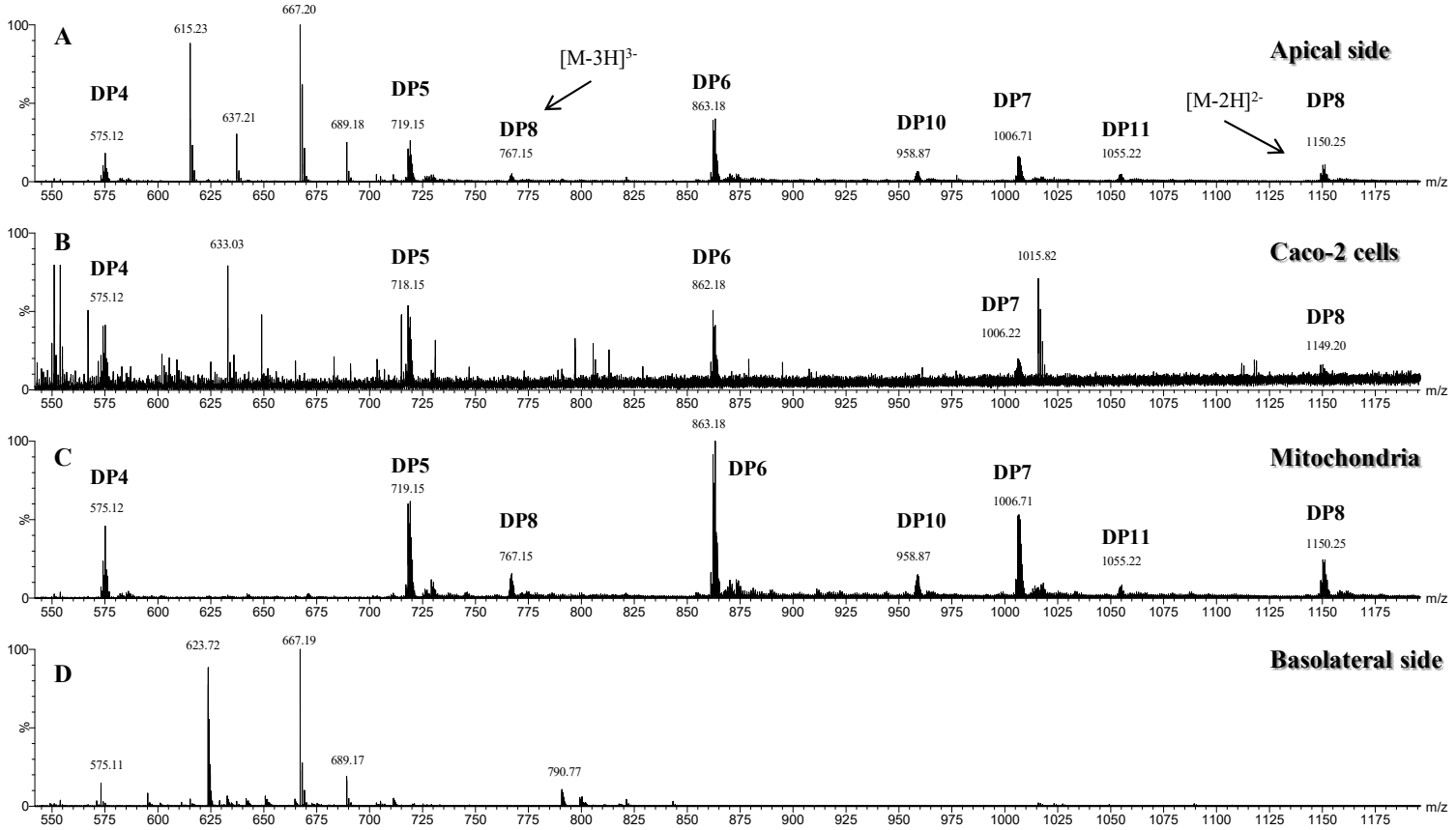
A
Apical side
DP4
575.12
615.23
637.21
667.20
689.18
DP5
719.15
[M-3H]3-
DP8
767.15
DP6
863.18
DP10
958.87
DP7
1006.71
DP11
1055.22
[M-2H]2-
DP8
1150.25
B
Caco-2 cells
DP4
575.12
633.03
DP5
718.15
DP6
862.18
1015.82
DP7
1006.22
DP8
1149.20
C
Mitochondria
DP4
575.12
DP5
719.15
DP8
767.15
863.18
DP6
DP10
958.87
DP7
1006.71
DP11
1055.22
DP8
1150.25
D
Basolateral side
575.11
623.72
667.19
689.17
790.77
%
m/z

Figure 11

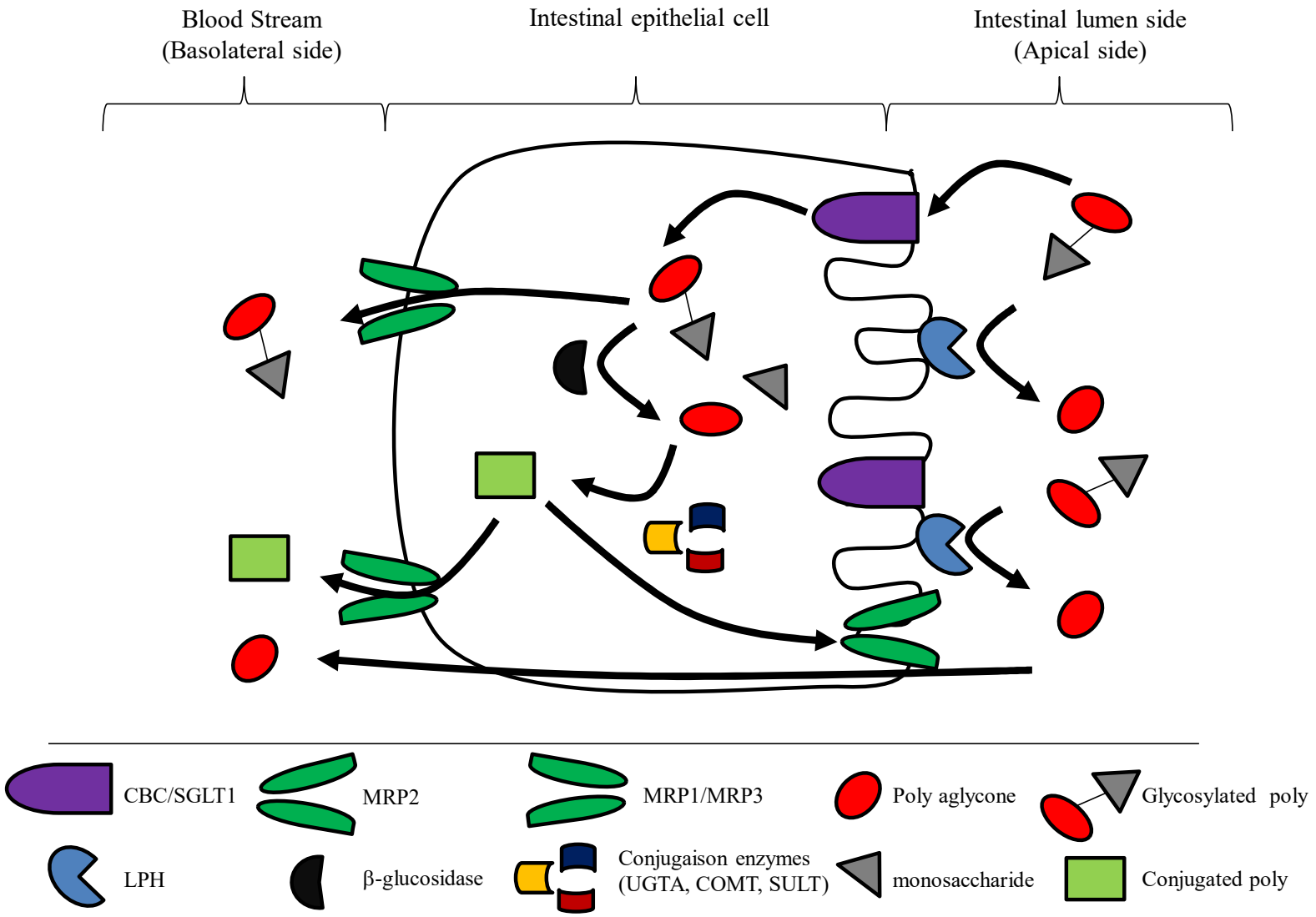
Blood Stream
(Basolateral side)
Intestinal epithelial cell
Intestinal lumen side
(Apical side)
CBC/SGLT1
MRP2
MRP1/MRP3
Poly aglycone
Glycosylated poly
LPH
β-glucosidase
Conjugaison enzymes
(UGTA, COMT, SULT)
monosaccharide
Conjugated poly

Supplementary data: Fragmentation parameters of polyphenols

Phenolic compounds	Fragmentation parameters			
	MS (-)	MS/MS	Cone (V)	E coll (eV)
Caffeoylquinic acid	353.1	191.0	24	15
p-coumaric acid	163.2	119.0	26	12
m-coumaric acid	163.2	119.0	26	12
Caffeic acid	179.2	135.0	28	15
Ferulic acid	193.2	134.0	28	16
Benzoic acid	121.0	77.0	22	12
Protocatechuic acid	153.1	109.0	28	13
Hydroxybenzoic acid	137.2	93.0	25	14
Vanillic acid	167.2	152.2	31	15
Ellagic acid	301.2	145.0	55	37
Sinapic acid	223.2	164.0	27	15
Dihydroxyphenylpropionic acid	181.1	137.0	22	8
Hydroxyphenylacetic acid	151.2	107.2	21	8
Dihydroxyphenylacetic acid	167.2	123.0	26	12
Quercetin glucoside	463.2	301.0	42	29
Quercetin	301.2	151.2	42	22
Quercetin glucuronide	477.2	301.0	42	29
Quercetin diglucuronide	653.0	301.0	40	22
Quercetin glucuronide sulfate	557.2	301.0	45	30
Myricetin glucoside	479.2	317.0	42	25
Myricetin	317.2	151.2	42	25
Myricetin glucuronide	493.2	317.0	42	22
Myricetin diglucuronide	669.2	317.0	40	22
Isorhamnetin glucoside	477.2	315.0	45	32
Isorhamnetin	315.2	151.2	45	30
Isorhamnetin glucuronide	491.2	315.2	45	32
Kaempferol glucoside	447.2	285.2	45	25
Kaempferol	285.2	93.2	53	32
Kaempferol glucuronide	461.2	285.0	43	22
Kaempferol sulfate	365.2	285.0	45	20
Epicatechin	289.2	245.1	37	14
Catechin	289.2	245.1	37	14
Methyl catechin	303.2	289.2	40	20
Catechin diglucuronide	641.2	289.0	45	22
Catechin sulfate	369.2	289.2	40	20
Methyl catechin sulfate	383.2	303.2	40	20
Methyl catechin glucuronide sulfate	559.2	289.0	45	25
A-type procyanidin dimer	575.2	289.0	35	24
B-type procyanidin dimer	575.2	289.0	35	24
Cyanidin 3-glucoside	449.2	287.0	35	20
Cyanidin 3-galactoside	449.2	287.0	35	20
Cyanidin 3-arabinoside	419.2	287.0	35	20
Peonidin 3-glucoside	463.2	301.0	35	20
Peonidin 3-galactoside	463.2	301.0	35	20
Peonidin 3-arabinoside	433.2	301.0	35	20
Peonidin glucuronide	447.2	301.0	35	20
Phloridzin	435.2	273.2	31	15
Phloretin	273.2	167.0	32	18
Phloretin glucuronide	449.2	273.0	40	20
Phloretin diglucuronide	625.2	273.0	40	25
Phloretin sulfate	353.2	273.2	36	15
Phloretin glucuronide sulfate	529.2	273.0	42	25

Phenolic compounds were identified by UPLC-TDQ equipped with an ESI source as described in Materials and Methods. The data were collected in the multiple reaction monitoring (MRM) mode, tracking the transition of parent and product ions specific for each compounds, and using external calibration curves.

Article 4: « Apple peel polyphenolic content as a key player for the prevention and treatment of experimental inflammatory bowel disease ».

Denis M.C.*et al*. Apple peel polyphenolic content as a key player for the prevention and treatment of experimental inflammatory bowel disease. Journal of Crohn's and Colitis, 2016; manuscript ID: ECCO-JCC-2016-0010.

Author contributions:

MCD, CG and EL participated in the design of the study. MCD, PYR, NH, CG, ATS, NP, TV, and ET conducted the experiments. MCD, PYR, ATS, TV, NP, ET and EL analyzed and interpreted the data. MCD, DR, YD, AF, ED, AM, JFB, DA and EL contributed to the writing of the paper.

Apple peel polyphenolic content as a key player for the prevention and treatment of experimental inflammatory bowel disease

Marie-Claude Denis[1,2], Denis Roy[3], Pantea RahmaniYeganeh [1,2], Yves Desjardins[3], Thibault Varin[3], Nour Haddad[1], Devendra Amre[1,4], Alain Théophile Sané[1], Carole Garofalo[1], Alexandra Furtos[5], Natalie Patey[1,6], Edgard Delvin[1,7], Eric Tremblay[8], André Marette[3], Jean-François Beaulieu[8], Emile Levy[1,2,3,8]

[1]Research Centre, CHU Sainte-Justine and [2]Departments of Nutrition, [4]Pediatrics, [5]Chemistry, [6]Pathology and [7]Biochemistry, Université de Montréal, Montreal, Quebec, Canada, H3T 1C5

[3]Institute of Nutrition and Functional foods (INAF), Université Laval, Quebec, Quebec, Canada, G1V 0A6

[8]Laboratory of intestinal physiopathology, Department of Anatomy and Cellular Biology, Faculty of Medicine and Health Sciences
Université de Sherbrooke, Sherbrooke, Quebec, Canada, J1H 5N4

Key words: Polyphenol; Peroxidation; Mitochondria; Cyclooxygenase; Inflammation; Transcription factors.

Running Head: Antioxidant and anti-inflammatory effects of apple

Abbreviations: DAPP, apple peel extract polyphenols; AIF, apoptosis-inducing factor; ATP, adenosine triphosphate; COX-2, cyclooxygenase-2; DP, degree of polymerization; FA, fatty acid; GPx, glutathione peroxidase; IBD, inflammatory bowel diseases; IL-6, interleukin-6; MDA, malondialdehyde; NF-κB, nuclear factor-kappa B; Nrf-2, nuclear factor erythroid 2-related factor 2; OGG1, 8-oxoG-DNA glycosylase; OxS, oxidative stress; PGC-1α, peroxisome proliferator-activated receptor gamma coactivator-1-α; PGE2, prostaglandin E2; PUFA, polyunsaturated fatty acid; ROS, reactive oxygen species; SOD, superoxide dismutase; TNF-α, tumor necrosis factor-α

Correspondence: Dr Emile Levy, GI-Nutrition Unit, Research Centre, CHU Sainte-Justine, 3175 Sainte-Catherine Road, Montreal, Quebec, Canada H3T 1C5

ABSTRACT

The intestinal mucosa is exposed to oxidizing agents from the ingestion of modified foods, immuno-inflammatory cells and the intestinal flora. Diet high in fruits and vegetables may reduce oxidative stress and inflammation via several mechanisms. These beneficial effects may be due to their high polyphenol content. **Objective:** To evaluate the preventive and therapeutic aspects of polyphenols in apple peel extract (DAPP) on intestinal inflammation while elucidating the underlying mechanisms and clinical benefits. **Methods**: Induction of intestinal inflammation in the C57BL6 mice is performed by oral administration of the inflammatory agent DSS (Dextran Sodium Sulfate) at 2.5% for 10 days. Physiological and supraphysiological doses of DAPP (200 and 400 mg/kg/day, respectively) were administered by gavage for 10 days pre- and post-DSS treatment. **Results:** The inflammation caused by DSS: weight loss, shortening of the colon, dystrophic detachment of the epithelium, erosion and infiltration of mono- and polymorphonuclear cells in the colon. Additionally, the DSS induced an increase in lipid peroxidation, a down-regulation of antioxidant enzymes, an augmented expression of myeloperoxidase (MPO) and COX-2, an elevated production of prostaglandin PGE2 and a shift in mucosa-associated microbial composition. However, DAPP normalized or at least alleviated most of these abnormalities in preventive or therapeutic situation in addition to lowering protein expression of NF-kB and inflammatory cytokines (TNF-α and IL-6) while stimulating antioxidant transcription factors (Nrf-2, PGC1-α) and modulating other potential healing pathways. The supraphysiological dose of DAPP in therapeutic situation also corrected mitochondrial dysfunctions as evidenced by ADP/ATP ratio, apoptosis (Cytochrome C and AIF) reduction and raise of DNA repair

enzyme (OGG1) capable of eliminating DNA damage caused by oxidative stress, thereby preventing the initiation of ROS vicious cycle. Relative abundance of colitogenic bacteria was slightly decreased in DAPP-treated mice compared to DSS-induced colitis group. **Conclusions**: DAPP Polyphenols exhibit a powerful anti-oxidant and anti-inflammatory power in the intestine where they mitigate murine colitis severity. Their actions are associated with the regulation of cellular signaling pathways and changes in microbiota composition. Therefore, evaluation of preventive and therapeutic effects of DAPP may be clinically feasible in individuals with intestinal inflammatory bowel diseases.

INTRODUCTION

Inflammatory bowel diseases (IBD), clinically manifested as Crohn's disease (CD) and ulcerative colitis, represents a widespread, chronic and debilitating set of disorders characterized by aberrant inflammation and immune-mediated injury to the gastrointestinal tract.[1] Despite the recent advances in the fields of IBD genetics and mucosal immunology, our understanding of the pathogenesis of IBD remains incomplete. The most widely accepted general hypothesis encompasses three main factors: genetic predisposition, environmental influences and the loss of homeostasis between the intestinal microbiome and host immunity.[2, 3] A disruption of immune tolerance to commensal bacteria and dysregulation of the intestinal microbiota balance ('dysbiosis') may result in gut inflammation, epithelial dysfunction and enhanced mucosal permeability.[4] Although genome-wide association studies and meta-analyses have resulted in the discovery of an ever-increasing number of genetic susceptibility loci,[5-7] the findings can only explain ~25% of the predictable heritability risk of CD. In addition, the complex, as yet poorly understood, the interaction of the aforementioned factors is ultimately believed to induce chronic relapsing intestinal inflammation leading to the various clinical phenotypes of disease expression. Noteworthy, among environmental risk factors, diet is the most commonly implicated, as epidemiological studies have shown that different dietary macro- and micronutrients may play a role in CD.[8]

IBD significantly impacts on quality of life and accounts for a substantial financial burden to our health care system and to society.[9, 10] Patients often require lifelong medication and the conventional treatment for IBD involves the use of corticosteroids, immunosuppressive agents, anti-tumour necrosis factor (TNF) antibodies and

antibiotics.[8-10] Some of these agents have been associated with the risks of infection and malignancy,[11, 12] as well as numerous side effects.[13-15] Moreover, not all patients are responsive to drug therapy. On the other hand, due to its perceived natural and healthy properties, complementary and alternative medicine is increasingly being used by pediatric and adult patients with IBD.[16-19] It may reach 60% in adult IBD populations from North America and Europe.[20] However, scientific evidence regarding their efficacy or safety remains inadequate, and the majority of studies have produced inconsistent results.[21] If in the late 90's, the nutritional spotlight focused on the antioxidant capabilities of carotenoids, vitamins, and minerals, growing strong support has more recently been devoted to dietary polyphenols, secondary plant metabolites, ubiquitously present in fruits and vegetables, which represents a significant class within the family of phytonutrients. This rising scientific interest could probably account for by their antioxidant capacity and their role in the prevention of certain cancers, diabetes and cardiovascular diseases.[22-25] The resurgence of interest in the last decade is also aroused by the revelations about their anti-inflammatory effects.[26, 27] Although protective or preventive anti-inflammatory properties of a number of polyphenol species have been noted in IBD, the mechanisms of action underlying their health-promoting effects remain largely unknown. In addition, the quite unrealistic doses that cannot be reached in a common diet and the mode of administration (i.e., intraperitoneal) have prevented their incorporation into the mainstream of medical care.[28]

The major aim of the present study was to investigate the preventive (200 mg) and therapeutic (400 mg/kg/day) capacity of polyphenols isolated from apple peel extract (DAPP) in IBD-related disorders. We chose this fruit since the apple ranks second for the

total polyphenol concentrations and had the highest portion of free polyphenols when compared to other fruits.[16] Furthermore, 20% of polyphenols consumed from fruits are from apples in Canada and the United States (Statistics Canada, and Economic Research Service, United States Department of Agriculture, Food Availability, compilation MAPAQ). To examine the preventive and therapeutic effects of DAPP, we employed the valuable dextran sulfate sodium (DSS)-induced colitis animal model in view of its simplicity and wide applicability and since it is the most frequently used in studies of IBD. It exhibits many symptoms similar to those seen in human ulcerative colitis and has various advantages when compared to other animal models of colitis.[29] Experimental intestinal inflammation induced by DSS is associated with changes in overall bacterial composition, suggesting that host-mediated inflammation and the altered mucosal inflammatory milieu selectively affect the composition of the intestinal microbiota by eliminating a subset of bacteria while supporting the relative abundances of others.[30] In particular, we dissected the DAPP effects by focusing on the antioxidant status, neutrophil infiltration, eicosanoid-generating enzymes, cytokine-induced inflammatory response and gastrointestinal integrity protection. Insights into the mechanisms were gained by analyzing mitochondrial functions, transcription factors activation, transcriptomic signature and microbiota profiling in connection with the pathophysiological conditions.

MATERIALS AND METHODS

DAPP extraction

The phenolic compounds of apples (80 % McIntosh and 20% Northern Spy blend, Cortland, Empire, Ida Red, Jonagold and Spartan) were extracted by a method similar to that reported previously by Liu's laboratory.[31-33] Briefly, 25 g apple peels were blended with 200 g chilled 80% acetone solution in a Waring blender for 5 min. The sample was then homogenized for 3 min using a Virtis 45 homogenizer. The slurry was filtered through Whatman No. 1 filter paper in a Buchner funnel under vacuum. The solids were scraped into 150 g of 80% acetone and homogenized again for 3 min before refiltering. The filtrate was recovered and evaporated using a rotary evaporator at 45°C. This residue represented the DAPP extract.

LC-MS analysis of DAPP extract

A reversed phase LC-MS method has been developed to separate and identify the mass and chemical structure of phenolic compounds derived from DAPP extract by ultra-performance liquid chromatography system (UPLC) coupled to a QuanTOF mass spectrometer (MS/MS QTOF) equipped with an ESI source (UPLC-ESI-MS/MS QTOF) as well described previously.[34]

Animals

Male C57BL6 mice (7-8 week of age) were purchased from Charles River (Senneville, Montreal) and housed in individual cages at 24 ± 1^{o}C under a 12-h light/dark cycle with free access to a standard laboratory chow diet (2018 Teklad Global, containing 18.6% protein, 3.5% carbohydrates and 6.2 % fat for 3.1 kcal/g, Harlan Laboratories,

Indianapolis, IN). Experiments were performed during the light phase of cycle. Animal experiments were conducted according to the Canadian Council on Animal Care guidelines for the care and use of experimental animals and were approved by the Institutional Animal Care Committee of the Sainte-Justine UHC Research Center.

Induction of DSS-induced colitis and collection of biological specimens

After a one-week adaptation under standard conditions, the mice were randomly divided into six groups. All mice were received water and were fed *ad libitum* throughout the whole experimental period (20 days) with the chow diet (Controls). Colitis was induced by adding 2.5% (w/v) DSS (average molecular weight 36 000-50 000, MP Biomedicals) in the drinking water for 10 days (**Supplementary Figure 1**). In addition to the noncolitis control group (CTL), the five DSS colitis groups were distributed as follows: DSS colitis group received only the vehicle (water used to administer DAPP) by oral gavage; the preventive groups were orally treated by gavage with 200 mg/kg/day DAPP (DAPP-200/DSS) or 400 mg/kg/day DAPP (DAPP-400/DSS) starting 10 days before colitis induction; and the therapeutic groups were orally treated by gavage with 200 mg/kg/day DAPP (DSS/DAPP-200) or 400 mg/kg/day DAPP (DSS/DAPP-400) starting with colitis induction for 10 days. Fresh DAPP solution was provided daily and the DSS solution was replaced every day. Similarly, body weight and food/water intake were measured on a daily basis. Thereafter, mice were fasted overnight, weighed and anesthetized. Blood samples were collected on EDTA by cardiac puncture and plasma was separated by centrifugation at 3000 g for 20 min at 4 °C. The peritoneal cavity was then opened and the colon from the ileocecal junction to the rectum was rapidly excised, measured (length

and weight), cut open lengthwise and the content removed with saline for the analysis of mucosa-associated microbiota, flash-frozen, and stored at −80°C for experiments. In several experiments, prior to freezing, cross-sections of distal colon were fixed in 10% neutral buffered formalin for histological examination.

Disease activity index

The severity of DSS-induced colitis was evaluated using the disease activity index (DAI), which combines scores for the mean values of body weight loss as well as stool consistency and occult blood. The body weight loss was determined by calculating the percentage of weight change from the start of DSS administration until sacrifice (0 = none; 1 = 1-5%; 2 = 5-10%; 3 = 10-20% and 4 = >20%). The stool consistency and occult blood scores were determined using the scoring systems (0 = normal; 1 = moist/sticky stool; 2 = soft stool; 3 = soft stool with mild diarrhea; 4 = diarrhea only) and (0 = no blood; 1 = minimal blood in stool; 2 = mild blood in stool; 3 = evidence blood in stool and 4 = only blood), respectively.

Histological analyses

As mentioned, at the end of the experimental period, a specimen of the colon was fixed in 10% neutral buffered formalin, dehydrated in gradient ethanol series and embedded in paraffin. For histological evaluation, 5µm-thick tissue sections were stained with hematoxylin phloxine saffron and examined under an optic microscope (ZEISS IMAGER A1 microscope) by a pathologist who was unaware of the experimental protocol. The pictures were taken using a digital camera at 10X and 20X resolution. To quantitatively

compare the severity of lesions between mouse treatments, tissues were assessed for injury and inflammation using a semi-quantitative scoring system.[35] Sections were scored as focal (<10% of specimen), multifocal (10–50% of specimen), or diffuse (>50% of specimen) for mucosa, submucosa and muscularis. The muscularis damage was evaluated in a blind manner by estimating the amount of myocytes, vacuoles, necrosis and infiltration of cells (maximum score = 9). The submucosa damage was evaluated by estimating the infiltration of mononuclear, polymorphonuclear and eosinophilic cells (maximum score = 3). The characterization of the damage of the surface mucosal epithelium was evaluated by erosion, necrosis, exulceration, loss of the mucus layer (maximum score = 12). All scores on the individual parameters together could results in a total score ranging from 0 to 24.

Myeloperoxidase activity assay

Tissue samples from distal colon were used to determine myeloperoxidase (MPO) activity. Tissue homogenates were centrifuged at 5000 x g at 4°C for 15 min and MPO activity in the supernatant was analyzed by ELISA (Hycult biotech, Uden, the Netherlands). All the samples of the six mouse groups were analyzed on the same plate at 450 nm.

Lipid peroxidation

Estimation of lipid peroxidation was assessed by measuring the content of malondialdehyde (MDA) in tissue samples of the distal colon by HPLC as described previously.[34]

Endogenous antioxidant enzyme activities

Total superoxide dismutase (SOD) activity was determined as described previously. For glutathione peroxidase (GPx) activity, aliquots of distal colon were added to a PBS buffer containing 10 mM GSH, 0.1 U G-Red and 2 mM NADPH with 1.5% H_2O_2 to initiate the reaction as described previously. [38]

Prostaglandin E2 determination

Tissue samples from the distal colon were homogenized in 1 mL of 0.1M phosphate pH 7.4 containing 1 mM EDTA and centrifuged at 5 000 x g at 4^{o}C for 15 min. A dilution of sample supernatant 1:3000 was assayed. Prostaglandin E2 (PGE2) levels were measured by ELISA (Arbor Assay, Michigan, USA). The intensity of the generated color was detected at the 450 nm wavelength using a microtiter plate reader (EnVision Multilabel Plate Readers, PerkinElmer).

RNA isolation and reverse transcription

Total RNA was isolated from distal colonic tissues from the 6 mouse groups using QIAzol Lysis Reagent (QIAGEN, Maryland, USA) according to the manufacturer's instructions. Precipitated total RNA was then resuspended in RNAse-free sterile water and further purified through sequential precipitation with lithium chloride and sodium acetate to prevent the inhibitory effect of DSS on polymerase enzymatic activity.[39] The RNA quality was assessed by agarose gel electrophoresis, and cDNAs were synthesized from 400 ng of RNA using the Reverse Transcriptase Kit (Invitrogen, Carlsbad, CA).

Gene expression was quantified by RT-PCR and the GAPDH was used as an internal control.[40, 41]

Immunoblot analysis

Tissue samples from the distal colon were homogenized in cold PBS buffer with 4 mM EDTA and 10 μL protease inhibitor cocktail (leupeptin, pepstatin, PMSF, ALV and BHT). The Bradford assay (Bio-Rad, Mississauga, Ontario) was used to determine the protein concentration. Proteins were denatured in sample buffer containing SDS and ß-mercaptoethanol, separated on a 7.5 % SDS-PAGE and electroblotted onto Hybond nitrocellulose membranes (Amersham, Baie D'Urfé, Quebec, Canada).[40] Specific binding sites of the membranes were blocked using defatted milk proteins followed by the addition of one of the following primary antibodies: 1/1000 polyclonal anti-COX-2 (70 kDa, Novus, Oakville, ON); 1/10000 polyclonal anti-NF-κB (65 kDa, Santa Cruz Biotechnology, Santa Cruz, CA); 1/5000 polyclonal anti-IκB (39 kDa, Cell Signaling, Beverly MA); 1/5000 polyclonal anti- tumor necrosis factor (TNF)-α (26 kDa, R&D, Canada); 1/5000 monoclonal anti-interleukin (IL)-6 (25 kDa, R&D, Canada), 1/1000 polyclonal anti-Nrf2 (68 kDa, Abcam, MA, USA); 1/1000 polyclonal anti-PGC-1α (92 kDa, Abcam, MA, USA); 1/1000 polyclonal anti-OGG1 (39 kDa, Novus Biologicals); 1/1000 monoclonal anti-cytochrome C (15 kDa, Novus Biologicals); 1/1000 anti-inducing factor (AIF) (67 kDa, Abcam); 1/1000 peroxisome proliferator-activated receptor (PPAR)γ (55kDA, Santa Cruz); 1/40000 monoclonal anti-β-actin (42 kDa, Sigma, MO, USA).

The relative amount of primary antibody was detected with species-specific horseradish peroxidase-conjugated secondary antibody (Jackson Laboratory, Bar Harbor, Maine). The β-actin protein expression was determined to confirm equal loading. Molecular size markers (Fermentas, Glen Burie, Maryland) were simultaneously loaded on gels. Blots were developed and the protein mass was quantitated by densitometry using an HP Scanjet scanner equipped with a transparency adapter and the UN-SCAN-IT gel 6.1 software.

Measurement of ADP and ATP levels

ADP and ATP contents were measured using an ADP/ATP bioluminescent assay kit from BioAssay Systems (Hayward, CA, USA) as described previously.[42, 43] Values for mitochondria were then normalized with regard to the protein content.

Microarray screening and data analysis

Probes for microarray analysis were generated from RNA isolated from 4 mouse groups (CTL, DSS, DAPP-200/DSS, and DSS/DAPP-400, n=3 for each group). The 12 samples were processed at the microarray platform of the Princess Margaret Genomics Centre (Toronto, ON). Illumina mouse whole genome WG-6 expression beadchips were screened, analyzed and quantile normalized via the Princess Margaret Genomics Centre (data are accessible through GEO **** and are all MIAME compliant). For each gene, samples bearing a coefficient of variation larger than 10% (representing less than 1% of all samples) were not considered in the statistical analysis and a Kruskal-Wallis analysis (P<0.05) was used to identify genes expressed differentially (using TMEV 4.9 software).

Ingenuity Pathway Analysis (IPA) analysis

Functional analyses were performed using IPA (Ingenuity Systems Inc., Redwood City, CA, USA) to identify functional pathway enrichment involved in the preventive and therapeutic effects of polyphenols in apple peel on intestinal inflammation. Each gene identifier was mapped to its corresponding gene object in the Ingenuity Knowledge Base. IPA used Fisher's exact test to calculate a *p*-value, which gave the likelihood that the set of genes in this pathway could be explained by chance alone.

16S rRNA gene amplicon sequencing using the Illumina MiSeq platform

A total of 40 gut mucosal samples consisting of pooled material of two or three mice from the same group were kept at -80°C until being processed. Bacterial DNA of these samples was extracted using a mechanical lysis of bacterial cells (Bead-beater) combined with silica-based column purification kit as directed by the manufacturer (ZR Fecal DNA Minprep; Zymo Research, USA). Total extracted DNA was quantified with a Qubit (Life Technologies, USA) and DNA purity was assessed using a ND-1000 Nanodrop (Nanodrop Technologies, USA).

The V3-V4 region of the 16S rDNA gene was amplified by PCR using primers Bakt_341F (5'-CCTACGGGNGGCWGCAG-3') and Bakt_805R (5'-GACTACHVGGGTATCTAATCC-3') adapted to incorporate the transposon-based Illumina Nextera adapters (Illumina, USA) and a sample barcode sequence allowing multiplexed paired-end sequencing. PCR mixtures contained 1X Q5 buffer (NEB), 1X Q5 Enhancer (NEB), 200 µM dNTP (VWR International, Canada), 0.2 µM of forward

and reverse primer (Integrated DNA Technologies, USA), 1 U of Q5 (NEB) and 1 µL of template DNA in a 50 µL reaction. The PCR cycling conditions consisted of an initial denaturation of 30 s at 98°C, followed by a first set of 15 cycles (98°C for 10 s, 55°C for 30 s and 72°C for 30 s), then by a second step of 15 cycles (98°C for 10 s, 65°C for 30 s and 72°C for 30 s) and final elongation of 2 min at 72°C before cooling to 4°C forever. PCR products were purified using 35 µL of magnetic beads (AxyPrep Mag PCR Clean up kit; Axygen Biosciences, USA) per 50 µL PCR reaction. Amplifications were controlled on a Bioanalyzer 2100 using DNA 7500 chips (Agilent Technologies, USA). Samples were pooled at an equimolar ratio, the pool was repurified as described before and checked for quality on a Bioanalyzer 2100 using a DNA high sensitivity chip. The pool was quantified using picogreen (Life Technologies, USA) and loaded on a MiSeq system (Illumina, USA). High-throughput sequencing was performed at the IBIS (Institut de Biologie Intégrative et des Systèmes - Université Laval). The raw sequencing data have been deposited in the NCBI Sequence Read Archive (SRA) (http://www.ncbi.nlm.nih.gov/sra/) under the study accession number XXX.

Bioinformatics of 16S rRNA gene amplicons

After demultiplexing by the MiSeq platform, raw sequence data obtained from the 40 sequenced samples were processed using the QIIME software package (version 1.9.0).[44] Firstly, paired-end reads obtained for each sample were joined on the overlapping ends, then resulting sequences were filtered to remove low read quality score (phred <25). Forward and reverse primers were trimmed from the filtered sequences; reads with at least one reverse primer mismatch or where the reverse primer was not found were

discarded. USEARCH 61 (version 6.1.544)[45] was used to check and filter chimeras from the dataset. Out of a total of 40 original samples, two samples were removed from the dataset because of too low read count. After those filtering steps, we characterized a total of 602 836 sequences for the 38 remaining samples with an average of 15 864 ± 4459 reads per sample. Final amplicon mean length varied between 441-465 bp for all samples. 16S rRNA sequences that successfully passed the pre-processing steps and presenting ≥97% nucleotide sequence identity were binned into OTUs (Operational Taxonomic Units) using USEARCH 61 (version 6.1.544)[45] with an open-reference methodology. Reads that did not hit the Greengenes reference database (August 2013 release)[46] during the closed-reference step were subsequently clustered *de novo* at 97% identity threshold. Taxonomic assignment of representative OTU sequence form each cluster was then performed against the Greengenes reference database using the naive Bayesian RDP classifier at default parameters.[47] Singleton OTUs (cluster with a unique sequence occurring only once among all reads) and OTUs with a number of sequences <0.005% of total number of sequences[48] were discarded at this step. A subsampling depth of 6412 reads (smallest amount of sequences originally found among our 38 metagenomic samples) was chosen to rarefy the OTU tables used in the downstream analyses. OTUs that were unclassified at the genus level with the Greengenes database were further investigated with the RDP classifier against the RDP database (version September 17, 2014)[49] using a minimum bootstrap cutoff of 50%.[50]

Statistical analysis

All values are expressed as mean ± SEM. Data were analyzed by using a one-way analysis variance and the two-tailed Student's *t* test using the Prism 5.01 (GraphPad Software) and the differences between the means were assessed post-hoc using Tukey's test. Statistical significance was defined as $P<0.05$.

The software PC-ORD (version 6; MjM Software, USA) was used to perform a principal coordinates analysis (PCoA) in order to illustrate differences between taxonomic profiles of metagenomic samples at the genus level. This ordination method combined with Bray-Curtis distance measure is well suited for species abundance data avoiding the assumption of linear relationship between variables. STAMP (Statistical Analysis of Metagenomic Profiles, version 2.0.9; Parks & Beiko, 2014) was employed to perform two-way comparisons of taxonomic distributions (at the genus level) between metagenomic samples (e.g. CTL vs DSS-treated), using the White's non-parametric t-test associated with the bootstrap method for calculating confidence intervals (nominal coverage of 95%). A Storey FDR approach was used to indicate the percentages of false positives (reported by q-values) that should be expected among all significant taxonomic units illustrated on bar plots. In order to visualize the relationships between OTUs and samples, a heatmap was constructed with STAMP using the Kruskal-Wallis H-test combined with the Tukey-Kramer test as post-hoc analysis. Multiple test correction for the heatmap analysis was performed with the Storey FDR approach. For all analyses performed within STAMP, only specific families or genera of interest were considered and features (taxa) with a q-value >0.05 were discarded.

RESULTS

Profile of phenolic compounds of DAPP

A reversed phase LC-MS method has been developed in order to separate and identify masses and chemical structures of polyphenolic compounds contained in the DAPP extract. Flavonoids figured among the major polyphenol classes: they were identified on the basis of their common structure consisting of two aromatic rings bound together by three carbon atoms that form an oxygenated heterocycle. Representative extracted ion chromatograms of identified DAPP polyphenolic compounds, using accurate mass measurement, are shown in **Supplementary Figure 2**. The DAPP was essentially constituted of hydroxycinnamic acids (**Supplementary Figure 2**A), dihydrochalcones (**Supplementary Figure 2**B), flavan-3-ols (**Supplementary Figure 2**C), and flavonols (**Supplementary Figure 2**D). The hydroxycinnamic acids were composed of isomers of coumaric acids, p-coumaroylquinic acids and caffeoquinic acids while we found phloretin and phloridzin as dihydrochalcones. The accurate mass measurement revealed that the flavan-3-ol subclass was constituted of (+)-catechin, (-)-epicathechin, (+)-catechin 3-O-gallate, (-)-epicathechin 3-O-gallate and (+)-catechin 3-O-glucose (**Table 1**). Noteworthy, in the DAPP extract, flavonols constituted the dominant subclass of flavonoids and were present as a mixture of aglycone and glycosylated quercetin (**Supplementary Figure 2D** and **Table 1**).

Effects of DAPP on the severity of DSS-induced colitis in mice

Mice exposed to oral administration of 2.5% DSS over 10 days was characterized by sustained weight loss (**Figure 1A**), abnormal stool consistency (**Figure 1B**) and bloody

diarrhea (**Figure 1C**), which presented a significant increase in DAI (**Figure 1D**). To assess the preventive and therapeutic effects of polyphenols, the mice were treated with DAPP before or during induction and development of colitis at two different doses (200 and 400 mg/kg/day). All DAPP animal groups exhibited significantly reduced DAI scores compared with the DSS colitis group without the DAPP treatment (**Figure 1D**). As the colon length is inversely correlated with the severity of colitis and is considered to be an indirect marker of inflammation, we examined colon shrinking. While the DSS group had significantly shorter colons relatively to the control group (**Figures 1E and 1F**), the preventive (200 mg) and the therapeutic 400 mg/kg/day doses of DAPP displayed the most significantly beneficial effect on colon shortening compared with the group on DSS alone (**Figures 1E and 1F**).

In colons from the control group, no histopathological changes were observed (**Figure 2A**). In contrast, the histopathological examination of the distal colon of mice treated with DSS showed mucosal ulceration, which was marked by an increased thickness of the muscle layer, loss of crypt structure, multifocal inflammatory cell infiltration into submucosal, severe denudation of the surface epithelium (erosion) and mucodepletion of glands (**Figure 2B**). Except for the group with the DAPP-400/DSS, DAPP significantly decreased the microscopic inflammation score for DSS-induced colitis in the other groups (**Figure 2G**). For example, mice pretreated with 200 mg/kg/day of DAPP showed less structural damage and inflammatory cell infiltration without a significant effect on muscle layer thickness compared to the DSS group without DAPP treatment (**Figure 2D**). Moreover, the epithelium in various areas remained intact and the mucin layer was clearly visible with stain cells, suggesting the beginning of a reepithelization and healing

process. Noteworthy, the high 400 mg/kg/day therapeutic DAPP dose resulted in near-normal colonic histology (**Figure 2E**) whereas the mice treated with the high 400 mg/kg/day preventive DAPP dose still showed several severe ulcers (**Figure 2F**). The colonic lesions were evaluated by a semi-quantitative scoring system that assesses the muscularis, submucosa and surface mucosal epithelium damages. Representation of total microscopic damage score demonstrated that preventive and therapeutic dose of 200 mg/kg/day of DAPP decreased colonic lesions (Figure 2G). However, therapeutic dose of 400 mg/kg/day of DAPP had the lowest total microscopic damage score (**Figure 2G**).

Effects of DAPP on colonic leukocyte involvement in DSS-induced colitis in mice

The colonic MPO activity, as a marker of inflammatory cell infiltration, was significantly increased in the colitis group (25-fold) compared to control mice (**Figure 2H**). All DAPP groups showed a reduction in the degree of polymorphonuclear neutrophil infiltration. The mice treated with the preventive 200 mg/kg/day dose of DAPP showed only a trend of decrease in MPO activity in distal colonic tissue

Effects of DAPP on Lipid Peroxidation in the distal colon of DSS-induced colitis mice

Compared to the control group, DSS significantly increased lipid peroxidation in the distal colon (**Figure 3A**). When mice were pretreated with 200 or 400 mg/kg/day DAPP, DSS-induced lipid peroxidation was prevented. On the other hand, only the highest therapeutic dose of DAPP (400 mg/kg/day) was able to totally counteract lipid peroxidation occurrence.

Mechanisms for the action of DAPP on oxidative stress

As failure of antioxidant defense may favor the induction of OxS, we examined endogenous antioxidant enzymes and found that the treatment with DSS alone caused a significant augmentation in the SOD activity compared to the CTL group (**Figure 3B**). However, the preventive (200 mg/kg/day) or therapeutic dose of 400 mg/kg/day of DAPP was the most efficient conditions for maintaining SOD activity quite comparable to that of the CTL group (**Figure 3B**). Only a slight decrease was noted in the other DAPP-400/DSS group. Under these conditions, GPx activity was down regulated by DSS (**Figure 3C**), and restored by the same preventive and therapeutic doses.

We examined the transcription factor Nrf2 that regulates antioxidant genes expression. While DSS-induced colitis down regulated the gene (50%) and protein (30%) expression of Nrf2 (**Figures 3D and 3E**), and the preventive DAPP dose of 200 mg/kg/day was capable of inhibiting the decrease of Nrf2 gene expression in DSS-treated mice (**Figure 3D**). Apart from the therapeutic dose of 200 mg/kg/day, the other groups (DAPP-400/DSS and DSS/DAPP-400) showed a particularly favorable influence on protein expression of Nrf2 (**Figure 3E**).

Effects of DAPP on inflammatory markers in the distal colon of DSS-induced colitis mice

As Cyclooxygenase-2 (COX-2) produce excessive inflammatory mediators, which are detrimental to the integrity of the colon and contribute to the development of intestinal damage, we evaluated its protein expressions. As shown in **Figure 4A**, the COX-2 protein expression in the DSS group was higher than in CTL mice. Preventive and therapeutic DAPP treatments were able to lessen the exaggerated induction of COX-2

protein expression noted in DSS mice. To confirm these findings, we assessed the prostaglandin E2 (PGE2) that is a major downstream mediator of COX-2. PGE2 concentrations were significantly decreased by preventive and therapeutic DAPP treatments in DSS mice (**Figure 4B**). Therefore, DAPP is able to down regulate the COX-2-PGE2 pathway that is of high pharmacological interest for IBD.

To further evidence the anti-inflammatory capacity of DAPP, we assessed its influence on cytokines expressions (**Figure 5**). While the DSS resulted in severe inflammatory response as indicated by remarkable increases in colonic levels of the proinflammatory TNF-α and IL6 as compared to the CTL group, DAPP strongly antagonized this inflammation magnitude given the marked drop of the colonic mRNA content and protein expression of these cytokines. Of note, the TNF-α gene expression was decreased only in the group of mice that received 400 mg/kg/day of DAPP (**Figure 5A**).

Mechanisms for the action of DAPP on transcription factors

As the ubiquitous eukaryotic transcription factor NF-κB is mainly responsible for regulating the induction of pro-inflammatory cytokines, we examined the potential of DAPP to inhibit its activation in mouse colonic samples inflamed with DSS (**Figures 5C**). In fact, treatment with DAPP caused a significant inhibition of NF-κB/IκB ratio (**Figure 5F**). Noteworthy, the effect was more pronounced with the 200 mg/kg/day and therapeutic 400 mg/kg/day doses (**Figure 5F**).

We also evaluated the modulation of two crucial transcription factors: peroxisome proliferator-activated receptor γ Coactivator-1α (PGC-1α) and peroxisome proliferator-activated receptor (PPAR)γ. The levels of PGC-1α (Figures 6A and 6B) and PPARγ

(Figures 6C and 6D) were down regulated in the DSS group comparatively to the CTL group. Whereas the therapeutic 200 mg/kg/day dose of DAPP was inefficient in enhancing PGC-1α mRNA and protein levels in DSS-treated mice, a significant trend of increase was noted in the other groups. With regard to PPARγ, an increase was noted in all the groups except for the preventive DAPP-400/DSS group.

Effect of DAPP on mitochondrial functions in mice with DSS-induced colitis

As the ADP/ATP ratio is generally considered a key parameter in mitochondrial energy metabolism and respiration, we established its status (**Figure 7A**) in purified mitochondria from the distal colons. The ADP/ATP ratio for the DSS group increased 4-fold compared to the control group, but the used therapeutic dose of 400 mg/kg/day reduced significantly this ADP/ATP ratio induction.

AIF is located in the inter-membrane space of mitochondria and is involved in initiating a caspase-independent pathway of apoptosis by causing DNA fragmentation and chromatin condensation. Furthermore, when colonic cell death is triggered by an apoptotic stimulus like DSS, cytochrome (Cyt) C is released into the cytosol and contributes to caspase-dependent pathway of apoptosis. Western blot analysis revealed an increase in the AIF and Cyt C protein masse in the mitochondrial preparation following DSS-induced colitis (**Figures 7B and 7C**). However, the therapeutic and preventive dose of 400 mg/kg/day was able to restore their normal levels.

The base excision repair pathway is primarily responsible for removing 8-OHdG from mitochondrial DNA. In human and murine model, 8-OHdG is repaired by 8-oxoguanine DNA glycosylase (OGG1), an enzyme that recognizes and hydrolyses the aberrant base

from the DNA backbone. As illustrated in **Figure 7D**, the DSS treatment resulted in a significant reduction in OGG1 protein mass as compared with CTL group. However, the therapeutic and preventive dose of 400 mg/kg/day prevented the decline in OGG1 expression.

Group comparisons using a score summation index

To compare the outcomes under the different conditions, we employed a score summation index (**Supplementary Table 1**). The total score was calculated by summing the various effects of DAPP in the different animal groups. As higher scores indicate greater improvements of the DSS group in response to polyphenol administration, we could identify two distinctive groups that exhibit the best outcomes, i.e. the preventive group with 200 mg/kg/day and the therapeutic group with 400 mg/kg/day. Therefore, we selected these two groups to conduct a microarray analysis of colonic gene expression and to examine gut microbiota.

Functional pathways involved in the effect of DAPP in mice with DSS-induced colitis.

To further determine the effect of DAPP in mice with DSS-induced colitis, we established colonic gene expression profiles for each group (CTL, DSS, DAPP-200/DSS, and DSS/DAPP-400, n=3 for each group) using Illumina mouse whole genome WG-6 expression beadchips. Statistical analyses revealed that 2152 genes were differentially expressed between each group (**Supplementary Table 2**). Significantly differentially expressed genes were subjected to IPA software. Comparative analysis of the cellular, molecular, physiological and metabolic functions was performed and classified according

to statistical significance in the variation of the expression of genes in DSS/DAPP-400 and DAPP-200/DSS. **Supplementary Tables 3 and 4** list 86 and 89 categories for DSS/DAPP-400 and DAPP-200/DSS, respectively, which were sorted according to their statistical significance as the negative logarithm of *P*-values calculated by IPA. Plotting the negative logarithm of p-values calculated by IPA for each of the functional categories found in the DSS/DAPP-400 group against the negative logarithm of *P*-values of the corresponding categories found in the DAPP-200/DSS group allows visualization of functions that are most relevant to each treatment. In **Figure 8,** we plotted the most significant 25 functional categories in each group, and found that 14 of them were altered in both groups. Among the shared canonical pathways we identified "IL6 signalling", "Atherosclerosis signalling", "LXR/RXR activation", "Acute phase response signalling" and "IL10 signalling", demonstrating that the DAPP treatment could modulate several inflammatory pathways. Interestingly, our results also evidenced that some biological functions were exclusively regulated by the preventive rather than the therapeutic treatment. For instance, preventive effects modulated "PPAR signalling", "Fc epsilon RI signalling" and "Dendritic maturation" while "Gap junction signalling", "FcγRIIB signalling in B lymphocytes" and "Epithelial adherents junctions signalling" were modulated by therapeutic treatment, suggesting differential beneficial effects depending on the treatment period.

Impact of DSS-induced colitis and DAPP treatment on the gut microbiota

In order to assess the effect of DAPP on gut dysbiosis induced by DSS, we performed a 16s rRNA metagenomic analysis of 38 gut mucosal collections from the CTL, DSS-

induced colitis (DSS), preventive (DAPP+DSS) and therapeutic (DSS+DAPP) groups comprising 10, 9, 10, and 9 samples respectively. As no significant difference in gut bacterial composition was found between metagenomic samples from mice treated with different doses (200 and 400 mg/kg/day) of DAPP, only therapeutic DAPP administration at the 400 mg/kg/day dose was considered for further metagenomic analyses.

The PCoA plot (**Figure 9A**) indicates the correlation between bacterial communities and the different treatments administered in mice. A clear shift from the CTL to all the treated animals groups (DSS, DSS+DAPP, DAPP+DSS) occurred along the first (and the most influential) component. The genera *Parabacteroides*, *Ruminococcus*, and more specifically *Barnesiella* and *Anaerostipes*, were strongly associated with the healthy state, while *Akkermansia* and *Mucispirillum* genera were more abundant in the metagenomes of treated mice; in particular, the families *Peptostreptococcaceae* and *Enterobacteriaceae* were significantly correlated with treated animal samples. In addition, the **Figure 9B** illustrates that those two bacterial families were absent from the control metagenomic sample, and consequently, only represented in the groups where DSS was administered; conversely, the genus *Anaerostipes* was only found in the CTL group. The relative abundance of *Akkermansia* and *Mucispirillum* was significantly more important in the metagenomes of treated animals than in the CTL group. The proximity between the CTL and the DSS+DAPP treated mice in the PCoA plot is slightly greater than the one observed between the DSS and CTL groups, likely indicating a more pronounced bacterial profile similarity between the therapeutic and healthy metagenomes.

Associations between gut bacterial composition and treated mice groups were further investigated by pairwise comparisons of gut bacterial profiles with respect to treatment

(**Figure 9B**). *Peptostreptococcaceae* and *Enterobacteriaceae* families were clearly overrepresented in the DSS metagenome, whereas the mean proportion of *Barnesiella* was significantly higher in the CTR group, along with *Parabacteroides* and *Ruminococcus*. Sequences assigned to *Peptostreptococcaceae* and *Enterobacteriaceae* were more abundant in the metagenomes of DSS+DAPP and DAPP+DSS groups in comparison with the CTLs, but to a less extent than in the DSS-treated mice (**Figure 10**). Interestingly, reads classified as *Peptostreptococcaceae* was less numerous in the metagenome of therapeutics DAPP-treated mice than in the DAPP+DSS mice when compared to the CTR group. The genus *Mucispirillum* was overrepresented in both DSS+DAPP and DAPP+DSS metagenomes compared to the CTLs, while the mean proportion of sequences attributed to *Akkermansia* was higher in the metagenome of the preventive DAPP-treated animals only.

DISCUSSION

IBD constitute a major health problem in the Western world. As no cure exists and no definitive therapies are available for this chronic inflammatory disorder, it becomes urgent and crucial to develop novel strategies with high efficacy. Multiple scientific groups studying functional nutrients have identified polyphenolic compounds among complementary and alternative medicines. However, the full spectrum of biological activities and the mechanisms of actions have rarely been reported. Therefore, in this study, we address the following issues: Does oral administration of DAPP protect against sustained oxidative stress and inflammation, characteristic of IBD? Is DAPP efficient in preserving mitochondrial bioenergetics and functions known to be affected in IBD? May DAPP trigger central transcription factors that are master regulators of antioxidant, anti-inflammatory and mitochondrial cytoprotective mechanisms? What is the transcriptomic signature that can be disclosed by microarray analysis of colonic specimens in response to DAPP treatment on a mouse model of induced colitis? What are the microbiota changes elicited by DSS-induced intestinal injury and are they restored by DAPP administration? Is DAPP for prevention and management? At what concentration?

We found that DAPP treatment showed obviously an improvement of weight loss, diarrhea and bloody stools at a macroscopic level, but it also reduced the histological score at a microscopic level given lessening of inflammatory cell invasion into colonic tissue. Our findings also support this inflammation alleviation in response to DAPP supplementation as noted by the reduced expression of pro-inflammatory cytokines (TNF-α) and eicosanoids (PGE2). Consistently, DSS-mediated oxidative stress and mitochondrial dysfunctions were ameliorated given the substantial fall in MDA and the ADP/ATP ratio along with antioxidant defense. The limited oxidative and inflammatory

magnitude displayed following DAPP administration may be due to the regulation of transcription factors and nuclear receptors as well as to the modifications of the microbiota composition and transcript profiling. We also observed a slight decrease of relative abundance of *Peptostreptococcaceae* and colitogenic *Enterobacteriaceae* in DAPP groups compared to DSS-induced colitis group, suggesting that polyphenolic compounds exert an antioxidant effect on the mucosal inflammatory milieu. Our results highlight the potential of using DAPP to prevent and treat IBD via numerous mechanisms.

We employed polyphenols from apples given their abundance of biologically active compounds as well as their significant protecting role in reducing the risk of chronic diseases such as cancer, type II diabetes, cardiovascular disease, pulmonary disease and asthma.[51] We especially selected apple peel polyphenols since they are more diversified and concentrated than those of the flesh.[33] Indeed, in addition to the rich phenolic content (phloretin glycosides, phloridzin, and chlorogenic acid) in apple flesh and peel, the latter contains additional flavonoids that are not found within the flesh.[33] In our study, special attention was given to the analysis of the composition of polyphenols as their concentration and antioxidant activity may vary depending on food processing and seasonal differences. Using the high-resolution of UPLC-ESI-MS/MS QTOF, we evidenced the presence of flavonols (aglycone and glycosylated quercetin), flavan-3-ols [(+)-catechin and (-)-epicatechin], dihydrochalcones (phloretin and phloridzin) and hydroxycinnamic acids, which represent the major flavonoid subclasses that exhibited anti-inflammatory and antioxidant activities in our previous studies.[34]

Noteworthy, not only we have used in the present study apple peels that constitute a good source of phenolic compounds,[31, 33] but the concentrations of phenolic extract administered to our mouse model approximates the total extractable phenolic content of 100 g of fresh apple widely consumable by humans (~ 357 [31, 33]mg/100 g fresh apple).[52, 53] In addition, the phenolic doses used in this study in mice are easily attainable in humans. By applying the US Food and Drug Administration's guidelines to establish the human equivalent dose based on body surface area,[54] we found that a 16 mg/kg dose would be the human equivalent of a 200 mg/kg dose in mice. This is perfectly achievable by supplementation or by incorporating DAPP in other food products. We also doubled the DAPP dose to 400 mg to examine whether large quantities of polyphenols can have more desirable outcomes especially in the therapeutic mode.

It is also important to note that the DSS colitis mouse is highly valuable and the most frequently used model to investigate IBD pathogenesis.[55, 56] It exhibits numerous characteristics that are similar to human colitis, including inflammatory response progression, clinical signs (diarrhea, occult blood, gross rectal bleeding, shortening of the colon), histopathological changes of the intestine, and modifications of intestinal microbiota.[57] Very often, the results obtained using this animal model can be relevant to human.[29] Finally, the conditions of DSS administration (2.5% for 10 days) were chosen to induce a mild-to-moderate colitis that could be more amenable to nutritional prevention or therapy.[58, 59]

Evaluation of the preventive and therapeutic effects of DAPP in the experimental mouse colitis model showed a significant improvement of the DSS-induced clinical

manifestations, as evidenced by the alleviation of body weight loss, diarrhea and fecal bleeding. In addition, supplementation of DAPP ameliorated colon shortening and colonic histological damages in the DSS-induced colitis mouse model. It also lessened neutrophils influx into the colonic tissue since the MPO activity was decreased, which evidenced the role of DAPP in restraining the induction of neutrophils recruitment. Moreover, DAI scores were markedly lower in the DAPP groups than in the DSS group. Taken together, these data demonstrate the preventive and therapeutic efficacy of DAPP against colitis development. Interestingly, the maximal preventive effect of DAPP was mostly achieved at the dose of 200 mg/kg/day and not sustained trend was noted with the curative doses of 200 and 400mg/kg/day.

A large number of experimental and clinical data suggests that chronic intestinal inflammation may be the result of a sustained overproduction of pro-inflammatory cytokines.[60, 61] As inflammatory mediators like TNF-α and IL-6 play critical roles in the pathogenesis of murine colitis, we analyzed their expression by qRT-PCR and Western blot. Consistent with these previous reports, the levels of these pro-inflammatory cytokines in DSS-induced mice were found positively correlated to the severity of colitis in the current study. Furthermore, DAPP significantly provided suppressive effects on intrinsic TNF-α and IL-6 elevations under experimental colitis condition, which probably halts the pathological progression of pro-inflammatory cascade. To delineate the mechanism of DAPP anti-inflammatory action, we assessed the expression of nuclear NF-κB that functions in the transcription regulation of numerous genes[62] and appeared remarkably elevated in colonic tissues of animal with colitis.[63, 64] Estimation of NF-κB and its inhibitory molecule IκB (capable of preventing the translocation of NF-κB to the

nucleus for the transcription activation of pro-inflammatory target genes) showed the capacity of DAPP to reverse NF-κB increase and cytoplasmic IκB degradation in mice with DSS-induced colitis. Indeed, DAPP weakened NF-κB p65 signals while enhancing the expression of the inhibitory subunit IκB-α, which led to the decline of the NF-κB/ IκB ratio. Our results are in accordance with the anti-inflammatory effects in intestinal epithelial Caco-2/15 cells[34] and are also consistent with previous reports that illustrate the efficiency of apple polyphenols to inhibit NF-κB activation in lipopolysaccharide/IFNγ-induced inflammation in human cell lines[65] and HLA-B27 transgenic rats.[66]

Up-regulation of certain proteins such as COX-2 is also implicated in immune dysregulation characterizing IBD.[67] Its induction results in an excessive inflammatory response, which may affect colon mucosa integrity and contributes to the development of intestinal damage.[68] The anti-inflammatory activity of DAPP was further confirmed by measuring colonic COX-2 levels. In fact, DAPP supplementation was able to mediate COX-2 down-regulation and to limit the formation of its PGE_2 product in parallel with the noted TNF-α and IL-6 blocking as well as MPO reduction (as an index of the neutrophils' presence and activation), thereby proving the high efficacy in ameliorating the acute colitis stage. The preventive and therapeutic benefits of DAPP supplementation are likely to stem from a global anti-inflammatory effect probably via the control of NF-κB signal transduction pathway.[69]

As largely reported, IBD is initiated and perpetuated by a combination of deregulated immune response and imbalance between the production of free radical and antioxidant defense.[70, 71] Given the close correlation between the activity of free radicals in the gut and DAI severity, indicating the significance of oxidative stress in the inflammatory

process, we have assessed the impact of DAPP on lipid peroxidation that is responsible for many of the damaging reactions in the cell by causing membrane leakiness and breakdown.[72] Our findings clearly support the protective role of DAPP in the regulation of oxidative stress since it significantly averted the elevation of MDA. Notably, our data also emphasize the indirect antioxidant effect of DAPP through the induction of endogenous protective antioxidative SOD and GPx enzymes through activation of Nrf2, which orchestrates the transcription of antioxidant genes and up-regulation of cytoprotective proteins.[73]

Structurally abnormal mitochondria have been observed in tissue from patients with gut inflammation[74] and in epithelial monolayers treated with prooxidants.[43] Although there are limited data on the role of mitochondria in colitis, there is a growing interest in targeting mitochondria-derived oxidative stress to reduce epithelial barrier dysfunction and colitis.[75] Our findings show the effectiveness of DAPP to enhance mitochondrial ATP generation while lowering apoptosis as evidenced by the fall in AIF and Cyt C protein expression in DSS-treated mice. Furthermore, DAPP was able to counteract the DSS-induced drop of OGG1, an enzyme that recognizes and hydrolyzes the aberrant nucleic bases from the DNA backbone. Our data are consistent with previous investigations showing that polyphenols able to protect against the loss of mitochondrial membrane potential, the increment in lipid peroxidation and the fall in cellular ATP induced by indomethacin in Caco-2 cells.[76] Mechanistically, this mitochondrial regulation by DAPP may be mediated via the increase of PGC-1α that is a master modulator of mitochondrial biogenesis and a transcriptional regulator of cellular energy processes, including OXPHOS and fatty acid oxidation.[77-79] It is tempting to speculate

that DAPP may have salutary effects via the induction of PGC-1α on mitochondrial dysfunctions since quercetin was recently reported to enhance the expression of PGC-1α in conjunction with mitochondrial biogenesis and functions.[80]

The intestinal microbiota of the control group of mice was characterized by a positive correlation with three bacterial phylotypes: *Anaerostipes, Parabacteroide*s and *Barnesiella*. These two latter phylotypes belong to the family of *Porphyromonadaceae*, order Bacteroidales, consisting of anaerobic, bile-resistant, non-spore-forming, gram-negative rods. In the human intestine, member of the order Bacteroidales play a role in the symbiotic relationships with the host, taking part in carbohydrate degradation, influencing the local immunity and preventing gut colonization by pathogenic bacteria.[81, 82] *Parabacteroides* sp. was found to be at higher levels in healthy controls than in Ulcerative Colitis or Irritable Bowel Syndrome patients.[83] In the murine gut, *Barnesiella* is one of the most abundant genera.[84, 85] Higher levels of a *Barnesiella* phylotype correlated with lower activity levels of colitis in IL-deficient mice.[86] In addition, arthritis-resistant mice were characterized by microbiota enriched with *Barnesiella, Bifidobacterium* and *Parabacteroides* spp., with *Barnesiella* being the most abundant genus.[87] However, the representation of *Barnesiella* bacteria in human microbiota might be minor[88] although these bacteria are able to restraint growth of antibiotic-resistant pathogenic bacteria and contribute to survival of hospitalized patients.[82]

DSS treatment induced a reduction in the proportion of Bacteroidales bacteria as compared to the CTL group. In mice with DSS-induced colitis, an increase of the relative abundance of *Enterobacteriaceae* and *Peptostreptococceae* as well as mucin-degrading bacteria *Akkermansia* and *Mucispirillum* was also observed. The cytotoxic effects of DSS

on gut epithelium have been associated with an increase of mucus release, intestinal permeability, and acute barrier damage. The loss of barrier function allows the translocation of pro-inflammatory microbial products.[89, 90] Then, the induced intestinal inflammation could be responsible for the shift in microbial composition observed in mice with DSS treatments, including those with DAPP. The host-mediated inflammation and oxidant-mediated injury also change the environmental conditions in the gut, which may affect proliferation of some phylotypes capable of adapting to these conditions.

According to Bailey *et al*.[84] although the mechanisms are not clear, it is possible that intestinal inflammations, such as that induced by DSS, could reduce the relative abundance of *Porphyromonadaceae* (*Barnesiella* and *Parabacteroides*), resulting in a proliferation of the *Enterobacteriaceae* and *Peptostreptococceae*. Facultative anaerobes such as *Enterobacteriaceae* and *Peptostreptococceae* may be favored over obligate anaerobes such as *Porphyromonadaceae* (*Barnesiella* and *Parabacteroides*) and *Anaerostipes* from increased oxygen availability or resistance to reactive oxygen species produced during inflammation.[91] Lupp *et al*.[30] found that host-mediated inflammation alone is sufficient to perturb the composition of the intestinal microbiota in DSS-induced colitis. They observed a reduction in the proportion of Bacteroidales from 74% to 60% of total microbiota and an overgrowth of *Enterobacteriaceae* and of *Enterococcus faecalis*, suggesting that increased oxygen availability in the inflammed intestine supports colonization by facultative anaerobic bacteria. Schwab *et al*.[92] noted that shifts in relative abundance of 16S rRNA of Clostridiales and Bacteroidales and the increase of *Deferribacteraceae* (*Mucispirillum*) and *Enterobacteriaceae* 16S rRNA were most pronounced in mice that suffered from greatest weight loss and the most severe

inflammation. *Enterobacteriaceae* also contribute in a high proportion of total sequences in the IL-10$^{-/-}$ but not in the wild-type mice.[93] *Peptostreptococcaceae* are commensal organisms in humans that can infect multiple sites of the body including intestinal mucosa under immunosuppressed or traumatic conditions.[94]

Schwab et al.[92] also observed increased *Verrucomicrobiaceae* (mainly *Akkermansia* spp.) and *Deferribacteracae* (mainly *Mucispirillum* spp.) during acute inflammation in agreement with our results for DSS-induced colitis.[91] Intestinal mucus provides a reservoir of glycans that serve as a source of nutrition for *Akkermansia muciniphila*.[95] *Mucispirillum schaedleri* is a spiral-shaped bacterium colonizing the mucus layer of the gastrointestinal tract of laboratory rodents.[96] In DSS-induced colitis, *Mucispirillum* and *Akkermansia* could benefit from the degradation of host-derived mucus secretions. Mucus composition and secretion are altered whereas there is some evidence that mucolytic bacteria and mucolytic activity are increased in inflammation.[91]

In DAPP-treated mice, a reduction in the degree of polymorphonuclear neutrophil infiltration was observed. The mice treated with the preventive 200 mg/kg/day dose of DAPP showed only a trend of decrease in MPO activity in distal colonic tissue. Osman et al.[97] also observed that blueberry reduced leucocytes infiltration in the tissues as indicated by the reduction of MPO compared to colitis control. *Enterobacteriaceae* count decreased significantly in blueberry group compared to the colitis control.

In conclusion, the present investigation provides *in vivo* evidence that administration of DAPP lessens the intestinal oxidative stress magnitude via the modulation of the NRF2/ARE signaling pathway in which NRF2 functions as a master switch for a cascade of antioxidant gene regulation. The findings also show the modulation of intestinal

inflammatory response by DAPP through the inhibition of neutrophil infiltration and deactivation of the NF-κB signaling pathway. These advantageous effects could be attributed, at least partially, to the regulatory role of DAPP in mitochondrial functions, messenger RNA phenotype and microbiota that is essential for optimal health. Overall, these positive modifications were associated with significant benefits such as reduction of bleeding, improvement in stool consistency, improved histological appearance, decreased weight loss, and protection from colon shortening, which indicate that polyphenols may represent potent tools for preventing and treating IBD. Noteworthy, this preclinical study will help define whether improvement of gut dysbiosis by DAPP, in association with the severity of mucosal injury or inflammation may constitute a promising treatment option in IBD. Finally, our study is an appropriate answer to the critically important scientific question seeking whether polyphenols are as effective as people believe.

AUTHORS CONTRIBUTION

MCD, CG and EL participated in the design of the study. MCD, PYR, NH, CG, ATS, NP, TV, and ET conducted the experiments. MCD, PYR, ATS, TV, NP, ET and EL analyzed and interpreted the data. MCD, DR, YD, AF, ED, AM, JFB, DA and EL contributed to the writing of the paper.

COMPETING INTERESTS\ACKNOWLEDGEMENT

This study was supported by the J. A. DeSève Research Chair in Nutrition, the Canadian Foundation of Innovation (EL), Leahy Orchards Inc. & Appleboost Products Inc. (EL), and scholarship award from Fonds de recherche du Québec-Nature et technologies (MCD). The authors thank Mrs Schohraya Spahis for her excellent technical assistance. The funders had no role in study design, data collection and analysis, decision to publish, or preparation of the manuscript. Therefore, the authors have declared that no competing interests exist.

Table 1: Polyphenols identification from DAPP extract

Polyphenol class	Polyphenol subclass	Polyphenol name	Formula	Ion Formula [M-H]-	Experimental mass (m/z)	Theoretical mass (m/z)	Diff.ppm (<5ppm)
Phenolic acids	Hydroxycinnamic acid	Coumaric acids	$C_9H_8O_3$	$C_9H_7O_3$	163.0390	163.0395	-3.1
		Coumaroylquinic acids	$C_{16}H_{18}O_8$	$C_{16}H_{17}O_8$	337.0928	337.0923	1.5
		Caffeoylquinic acids	$C_{16}H_{18}O_9$	$C_{16}H_{17}O_9$	353.0878	353.0872	1.7
Flavonoids	Dihydrochalcone	Phloretin	$C_{15}H_{14}O_5$	$C_{15}H_{13}O_5$	273.0769	273.0763	2.2
		Phloridzin	$C_{21}H_{24}O_{10}$	$C_{21}H_{23}O_{10}$	435.1282	435.1291	-2.1
	Dihydroflavonol	Dihydroquercetin	$C_{15}H_{12}O_7$	$C_{15}H_{11}O_7$	303.0520	303.0505	4.9
		Dihydroquercetin 3-O-rhamnoside	$C_{21}H_{22}O_{11}$	$C_{21}H_{21}O_{11}$	449.1100	449.1084	3.6
	Flavanol	(+)-Catechin (-)-Epicatechin	$C_{15}H1_4O_6$	$C_{15}H_{13}O_6$	289.0709	289.0712	-1.0
		(+)-Catechin 3-O-gallate	$C_{22}H_{18}O_{10}$	$C_{22}H_{18}O_{10}Na$	465.0798*	441.0822	-4.9
		(+)-Catechin 3-O-glucose	$C_{21}H_{24}O_{11}$	$C_{21}H_{23}O_{11}$	451.1223	451.1240	-3.8
	Flavonol	Quercetin	$C_{15}H_{10}O_7$	$C_{15}H_9O_7$	301.0336	301.0348	-4.0
		Quercetin 3-O-arabinoside Quercetin 3-O-xyloside	$C_{20}H_{18}O_{11}$	$C_{20}H_{17}O_{11}$	433.0721	433.0771	-1.2
		Quercetin 3-O-rhamnoside	$C_{21}H_{20}O_{11}$	$C_{21}H_{19}O_{11}$	447.0941	447.0927	3.1
		Quercetin 3-O-galactoside Quercetin 3-O-glucoside	$C_{21}H_{20}O_{12}$	$C_{21}H_{19}O_{12}$	463.0894	463.0876	3.9
		Quercetin 3-O-galactoside-7-O-rhamnoside Quercetin 3-O-rhamnosyl-galactoside Quercetin 3-O-rutinoside	$C_{27}H_{30}O_{16}$	$C_{27}H_{29}O_{16}$	609.1471	609.1456	2.5

Experimental mass measurement and empirical formula calculation for phenolic acids and flavonoids. A good agreement between the theoretical and the experimental m/z values was obtained for all compounds examined (< 5ppm). Separations were performed on an ultra-performance liquid chromatography system (UPLC) coupled to a QuanTOF mass spectrometer (MS/MS QTOF) equipped with an ESI source (UPLC-ESI-MS/MS QTOF). The UPLC-ESI-MS/MS QTOF system consisting of a Waters-ACQUITY UPLC with an Synapt G2-Si High Definition mass spectrometer (Waters, MA, USA).* adduct sodium of $C_{22}H_{18}O_{10}$.

FIGURE LEGENDS

Figure 1 **Effects of DAPP on macroscopic damage in mice with DSS-induced colitis.** The severity of the colitis was determined by the disease activity index score (D), which combines scores for the body weight change (A) and feces condition (stool consistency (B) and fecal bleeding (C). The body weight change was determined by calculating the percentage of weight change relative to the starting weight before DSS treatment (0 = none; 1 = 1-5%; 2 = 5-10%; 3 = 10-20% and 4 = >20%). The fecal condition score was determined using two parameters: stool consistency (0 = normal; 1 = moist/sticky stool; 2 = soft stool; 3 = soft stool with mild diarrhea; 4 = diarrhea only) and fecal bleeding (0 = no blood; 1 = minimal blood in stool; 2 = mild blood in stool; 3 = evidence blood in stool and 4 = only blood). After sacrificing the mice, the colon length was measured between the colocecal junction and the rectum (E and F). In addition to the noncolitis control group (CTL), the five DSS colitis groups were distributed as follows: DSS colitis group received only the vehicle (water used to administer DAPP) by oral gavage; the preventive groups were orally treated by gavage with 200 mg/kg/day DAPP (DAPP-200/DSS) or 400 mg/kg/day DAPP (DAPP-400/DSS) starting 10 days before colitis induction; and the therapeutic groups were orally treated by gavage with 200 mg/kg/day DAPP (DSS/DAPP-200) or 400 mg/kg/day DAPP (DSS/DAPP-400) starting with colitis induction for 10 days. The results shown are representative of three independent experiments with 5 to 6 mice per group. ***P<0.001 vs. CTL group; $^{\#}P$<0.05, $^{\#\#}P$<0.01, $^{\#\#\#}P$<0.001 vs. DSS group.

Figure 2 **Effects of DAPP on microscopic damage and myeloperoxidase in mice with DSS-induced colitis.** Histological characterization was assessed by histological sections of distal colonic mucosa and tissue samples from distal colon were used to determine myeloperoxidase (MPO) concentration (H) from the six groups of mice (as described in Supplementary Figure 1) stained with hematoxylin phloxine saffron: (A) control group (CTL); (B) colitis group (DSS), (C) DSS/DAPP-200, (D) DAPP-200/DSS, (E), DSS/DAPP-400 and (F) DAPP-400/DSS. The pictures were taken using a digital camera at 10X (pictures B, C and F) or 20X (pictures A, D and E) resolution. Colon sections were scored for DSS-induced colonic inflammation and tissue injury (G) as described in Materials and Methods. The results shown are representative of three independent experiments with 5 to 6 mice per group. ***P<0.001 vs. CTL group; $^{\#\#}P$<0.01 vs. DSS group.

Figure 3 **Effects of DAPP on oxidative stress markers in mice with DSS-induced colitis.** Estimation of lipid peroxidation was assessed by measuring malondialdehyde (MDA) by HPLC (A). The activity of superoxide dismutase (SOD, B), glutathione peroxidase (GPx, C) was then measured. Gene and protein expression of the transcription factor Nrf2 (D and E) were determined by qRT-PCR and Western blot respectively. The results from the six groups of mice (as described in Supplementary Figure 1) shown are representative of three independent experiments with 5 to 6 per group. *P<0.05 vs. CTL group; $^{\#}P$<0.05 $^{\#\#}P$<0.01 $^{\#\#\#}P$<0.001 vs. DSS group.

Figure 4 **Regulatory effects of DAPP on cyclooxygenase 2 and prostaglandin E2 in mice with DSS-induced colitis.** Protein expression of COX-2 (A) was determined by Western blotting while PGE_2 (B) was determined by enzymatic immunoassay. The results from the six groups of mice (as described in Supplementary Figure 1) shown are representative of three independent experiments with 5 to 6 per group. **P*<0.05, ****P*<0.001 vs. CTL group; $^{\#}P$<0.05, $^{\#\#}P$<0.01, $^{\#\#\#}P$<0.001 vs. DSS group.

Figure 5 **Effects of DAPP on proinflammatory cytokines in mice with DSS-induced colitis.** Gene and protein expression of the inflammatory markers TNF-α (A and D), IL-6 (B and E) and the transcription factors NF-kB (C and F) were determined by qRT-PCR and Western blot respectively. The ratio NF-κB/IκB was then calculated. The results from the six groups of mice (as described in Supplementary Figure 1) shown are representative of three independent experiments with 5 to 6 per group. **P*<0.05, ***P*<0.01, ****P*<0.001 vs. CTL group; $^{\#}P$<0.05, $^{\#\#}P$<0.01, $^{\#\#\#}P$<0.001 vs. DSS group.

Figure 6 **Regulator effects of DAPP on peroxisome proliferator-coactivator-1 (PGC1-α) and -activated receptor (PPAR) γ in mice with DSS-induced colitis.** The mitochondrial transcription and translation were evaluated by gene and protein expression of PCG1-α (A and B), PPAR-γ (C and D), determined by qRT-PCR and Western blot respectively. The results from the six groups of mice (as described in Supplementary Figure 1) shown are representative of three independent experiments with 5 to 6 per group. **P*<0.05, ***P*<0.01, ****P*<0.001 vs. CTL group; $^{\#}P$<0.05, $^{\#\#}P$<0.01, $^{\#\#\#}P$<0.001 vs. DSS group.

Figure 7 **Effects of DAPP on mitochondrial functions in mice with DSS-induced colitis.** Mitochondrial ADP/ATP ratio (A) was measured by luciferase driven bioluminescence while the protein expression of AIF (B), Cyt C (C) and OGG1 (D) in mitochondria was determined by Western blot. The results from four groups of mice (as described in Supplementary Figure 1) shown are representative of three independent experiments with 5 to 6 per group. $^{**}P<0.01$, $^{***}P<0.001$ vs. CTL group; $^{\#}P<0.05$, $^{\#\#}P<0.01$ vs. DSS group.

Figure 8 **Comparative analysis of functional enriched pathways between preventive and therapeutic DAPP treatments**. The negative logarithm of p-values (Fisher's test), calculated by IPA, for each of the most significant 25 functional categories overrepresented in DSS/DAPP-400 was plotted against those modulated in DAPP-200/DSS. ***Insert***: Venn diagram showing the 155 canonical pathways between DSS/DAPP-400 and DAPP-200/DSS. Thresholds (dotted lines) denote the p=0.05 [-Log (0.05) =1.3]. **B)** List of the most significant twenty-five functional categories for DSS/DAPP-400 and DAPP-200/DSS represented in A with their corresponding genes.

Figure 9A **Principal Coordinates Analysis (PCoA) plot illustrating the clustering of sampled gut mucosal communities at the genus level with respect to treatment (CTL, DSS, DSS+DAPP, DAPP+DSS).** Samples are plotted as colored points and bacterial families or genera of interest as black vectors. This analysis was based on Bray-Curtis similarities of the log-transformed OTU abundances. Randomization test (999 permutations) indicates that the first two PCO axes are significant. The per cent of variation explained for each axis is

given in brackets. OTU, operational taxonomic unit. * Family group with unclassified genus.

Figure 9B **Heatmap of the relative abundance (%) of selected bacterial taxa that were found in the control (CTL) and treated animal metagenomic samples (DSS, DSS+DAPP, DAPP+DSS).** Each row corresponds to a family or genus of interest and each column to a mucosal metagenomics sample. The color scale represents the sample affiliation to its respective treatment, while the gray scale represents the abundance level (%). * Family group with unclassified genus.

Figure 10 **Pairwise mean proportional differences (%) calculated at the genus level between the control (CTL) and the treated animal metagenomic samples (DSS, DSS+DAPP, DAPP+DSS).** The bar graphs on the left side display the mean proportion of sequences assigned to each selected family or genus. The dot plots on the right side show the bacterial genera that were overrepresented in one sample or another. Whiskers denote calculated 95% CIs. Only features of interest with a q-value of >0.05 are represented. * Family group with unclassified genus.

REFERENCES

1. Rubin DC, Shaker A, Levin MS. Chronic intestinal inflammation: inflammatory bowel disease and colitis-associated colon cancer. Front Immunol. 2012;3:107.
2. Baumgart DC, Carding SR. Inflammatory bowel disease: cause and immunobiology. Lancet 2007;369:1627-1640.
3. Podolsky DK. Inflammatory bowel disease. N.Engl.J.Med. 2002;347:417-429.
4. Danese S, Fiocchi C. Etiopathogenesis of inflammatory bowel diseases. World J.Gastroenterol. 2006;12:4807-4812.
5. Genome-wide association study of 14,000 cases of seven common diseases and 3,000 shared controls. Nature 2007;447:661-678.
6. Duerr RH, Taylor KD, Brant SR, et al. A genome-wide association study identifies IL23R as an inflammatory bowel disease gene. Science 2006;314:1461-1463.
7. Jostins L, Ripke S, Weersma RK, et al. Host-microbe interactions have shaped the genetic architecture of inflammatory bowel disease. Nature 2012;491:119-124.
8. Hou JK, Abraham B, El-Serag H. Dietary intake and risk of developing inflammatory bowel disease: a systematic review of the literature. Am.J.Gastroenterol. 2011;106:563-573.
9. Bernstein CN, Loftus EV, Jr., Ng SC, et al. Hospitalisations and surgery in Crohn's disease. Gut 2012;61:622-629.
10. Rocchi A, Benchimol EI, Bernstein CN, et al. Inflammatory bowel disease: a Canadian burden of illness review. Can.J.Gastroenterol. 2012;26:811-817.
11. Lichtenstein GR, Rutgeerts P, Sandborn WJ, et al. A pooled analysis of infections, malignancy, and mortality in infliximab- and immunomodulator-treated adult patients with inflammatory bowel disease. Am.J.Gastroenterol. 2012;107:1051-1063.
12. Toruner M, Loftus EV, Jr., Harmsen WS, et al. Risk factors for opportunistic infections in patients with inflammatory bowel disease. Gastroenterology 2008;134:929-936.
13. Dear KL, Compston JE, Hunter JO. Treatments for Crohn's disease that minimise steroid doses are associated with a reduced risk of osteoporosis. Clin.Nutr. 2001;20:541-546.
14. Sarzi-Puttini P, Ardizzone S, Manzionna G, et al. Infliximab-induced lupus in Crohn's disease: a case report. Dig.Liver Dis. 2003;35:814-817.
15. Steenholdt C, Svenson M, Bendtzen K, et al. Acute and delayed hypersensitivity reactions to infliximab and adalimumab in a patient with Crohn's disease. J.Crohns.Colitis. 2012;6:108-111.
16. Fernandez A, Barreiro-de AM, Vallejo N, et al. Complementary and alternative medicine in inflammatory bowel disease patients: frequency and risk factors. Dig.Liver Dis. 2012;44:904-908.
17. Lakatos PL, Czegledi Z, David G, et al. Association of adherence to therapy and complementary and alternative medicine use with demographic factors and disease phenotype in patients with inflammatory bowel disease. J.Crohns.Colitis. 2010;4:283-290.
18. Rawsthorne P, Clara I, Graff LA, et al. The Manitoba Inflammatory Bowel Disease Cohort Study: a prospective longitudinal evaluation of the use of complementary and alternative medicine services and products. Gut 2012;61:521-527.
19. Weizman AV, Ahn E, Thanabalan R, et al. Characterisation of complementary and alternative medicine use and its impact on medication adherence in inflammatory bowel disease. Aliment.Pharmacol.Ther. 2012;35:342-349.
20. Hilsden RJ. Seeking the ultimate bowel preparation for colonoscopy: is the end in sight? Can.J.Gastroenterol. 2011;25:655-656.

21. Ng SC, Lam YT, Tsoi KK, et al. Systematic review: the efficacy of herbal therapy in inflammatory bowel disease. Aliment.Pharmacol.Ther. 2013;38:854-863.
22. Gonzalez-Vallinas M, Gonzalez-Castejon M, Rodriguez-Casado A, et al. Dietary phytochemicals in cancer prevention and therapy: a complementary approach with promising perspectives. Nutr Rev 2013;71:585-599.
23. Khurana S, Venkataraman K, Hollingsworth A, et al. Polyphenols: benefits to the cardiovascular system in health and in aging. Nutrients. 2013;5:3779-3827.
24. Munir KM, Chandrasekaran S, Gao F, et al. Mechanisms for food polyphenols to ameliorate insulin resistance and endothelial dysfunction: therapeutic implications for diabetes and its cardiovascular complications. Am.J.Physiol Endocrinol.Metab 2013;305:E679-E686.
25. Tangney CC, Rasmussen HE. Polyphenols, inflammation, and cardiovascular disease. Curr.Atheroscler.Rep. 2013;15:324.
26. Chu AJ. Antagonism by bioactive polyphenols against inflammation: a systematic view. Inflamm.Allergy Drug Targets. 2014;13:34-64.
27. Gupta SC, Tyagi AK, Deshmukh-Taskar P, et al. Downregulation of tumor necrosis factor and other proinflammatory biomarkers by polyphenols. Arch.Biochem.Biophys. 2014;559:91-99.
28. Romier B, Schneider YJ, Larondelle Y, et al. Dietary polyphenols can modulate the intestinal inflammatory response. Nutr.Rev. 2009;67:363-378.
29. Perse M, Cerar A. Dextran sodium sulphate colitis mouse model: traps and tricks. J.Biomed.Biotechnol. 2012;2012:718617.
30. Lupp C, Robertson ML, Wickham ME, et al. Host-mediated inflammation disrupts the intestinal microbiota and promotes the overgrowth of Enterobacteriaceae. Cell Host.Microbe 2007;2:119-129.
31. Eberhardt MV, Lee CY, Liu RH. Antioxidant activity of fresh apples. Nature 2000;405:903-904.
32. He X, Liu RH. Phytochemicals of apple peels: isolation, structure elucidation, and their antiproliferative and antioxidant activities. J.Agric.Food Chem. 2008;56:9905-9910.
33. Wolfe K, Wu X, Liu RH. Antioxidant activity of apple peels. J.Agric.Food Chem. 2003;51:609-614.
34. Denis MC, Furtos A, Dudonne S, et al. Apple peel polyphenols and their beneficial actions on oxidative stress and inflammation. PLoS.One. 2013;8:e53725.
35. Cooney RM, Warren BF, Altman DG, et al. Outcome measurement in clinical trials for Ulcerative Colitis: towards standardisation. Trials 2007;8:17.
36. !!! INVALID CITATION !!! {Denis, 2013 #164;McCord, 1969 #453;Denis, 2013 #164;McCord, 1969 #453;Denis, 2013 #164;McCord, 1969 #453}.
37. McCord JM, Fridovich I. Superoxide dismutase. An enzymic function for erythrocuprein (hemocuprein). J.Biol.Chem. 1969;244:6049-6055.
38. Precourt LP, Marcil V, Ntimbane T, et al. Antioxidative properties of paraoxonase 2 in intestinal epithelial cells. Am.J.Physiol Gastrointest.Liver Physiol 2012;303:G623-G634.
39. Viennois E, Chen F, Laroui H, et al. Dextran sodium sulfate inhibits the activities of both polymerase and reverse transcriptase: lithium chloride purification, a rapid and efficient technique to purify RNA. BMC.Res.Notes 2013;6:360.
40. Levy E, Spahis S, Garofalo C, et al. Sar1b transgenic male mice are more susceptible to high-fat diet-induced obesity, insulin insensitivity and intestinal chylomicron overproduction. J Nutr Biochem 2014;25:540-8.
41. Levy E, Ben Djoudi Ouadda A, Spahis S, et al. PCSK9 plays a significant role in cholesterol homeostasis and lipid transport in intestinal epithelial cells. Atherosclerosis 2013;227:297-306.

42. Denis MC, Desjardins Y, Furtos A, et al. Prevention of oxidative stress, inflammation and mitochondrial dysfunction in the intestine by different cranberry phenolic fractions. Clin.Sci (Lond) 2015;128:197-212.
43. Taha R, Seidman E, Mailhot G, et al. Oxidative stress and mitochondrial functions in the intestinal Caco-2/15 cell line. PLoS.One. 2010;5:e11817.
44. Caporaso JG, Kuczynski J, Stombaugh J, et al. QIIME allows analysis of high-throughput community sequencing data. Nat.Methods 2010;7:335-336.
45. Edgar RC. Search and clustering orders of magnitude faster than BLAST. Bioinformatics. 2010;26:2460-2461.
46. DeSantis TZ, Hugenholtz P, Larsen N, et al. Greengenes, a chimera-checked 16S rRNA gene database and workbench compatible with ARB. Appl.Environ Microbiol. 2006;72:5069-5072.
47. Wang Q, Garrity GM, Tiedje JM, et al. Naive Bayesian classifier for rapid assignment of rRNA sequences into the new bacterial taxonomy. Appl.Environ Microbiol. 2007;73:5261-5267.
48. Bokulich NA, Subramanian S, Faith JJ, et al. Quality-filtering vastly improves diversity estimates from Illumina amplicon sequencing Nat.Methods 2013;10:57-59.
49. Cole JR, Wang Q, Fish JA, et al. Ribosomal Database Project: data and tools for high throughput rRNA analysis. Nucleic Acids Res. 2014;42:D633-D642.
50. Claesson MJ, O'Sullivan O, Wang Q, et al. Comparative analysis of pyrosequencing and a phylogenetic microarray for exploring microbial community structures in the human distal intestine. PLoS.One. 2009;4:e6669.
51. Boyer J, Liu RH. Apple phytochemicals and their health benefits. Nutr J. 2004;3:5.
52. Liu RH, Eberhardt MV, Lee CY. Antioxidant and antiproliferative activites of selected New York apple cultivars . . N.Y.Fruit Q. 2001;9:15-17.
53. Podsedek A, Wilska-Jeszka J, Anders B, et al. Compositional characterisation of some apple varieties. European Food Research and Technology 2000;210:268-272.
54. Reagan-Shaw S, Nihal M, Ahmad N. Dose translation from animal to human studies revisited. FASEB J. 2008;22:659-661.
55. Murthy SN, Cooper HS, Shim H, et al. Treatment of dextran sulfate sodium-induced murine colitis by intracolonic cyclosporin. Dig.Dis.Sci 1993;38:1722-1734.
56. Wirtz S, Neurath MF. Mouse models of inflammatory bowel disease. Adv.Drug Deliv.Rev 2007;59:1073-1083.
57. Chassaing B, Aitken JD, Malleshappa M, et al. Dextran sulfate sodium (DSS)-induced colitis in mice. Curr.Protoc.Immunol. 2014;104:Unit.
58. Dieleman LA, Ridwan BU, Tennyson GS, et al. Dextran sulfate sodium-induced colitis occurs in severe combined immunodeficient mice. Gastroenterology 1994;107:1643-1652.
59. Elson CO, Sartor RB, Tennyson GS, et al. Experimental models of inflammatory bowel disease. Gastroenterology 1995;109:1344-1367.
60. Pahl HL. Activators and target genes of Rel/NF-kappaB transcription factors. Oncogene 1999;18:6853-6866.
61. Papadakis KA, Targan SR. Current theories on the causes of inflammatory bowel disease. Gastroenterol.Clin.North Am. 1999;28:283-296.
62. Visekruna A, Joeris T, Seidel D, et al. Proteasome-mediated degradation of IkappaBalpha and processing of p105 in Crohn disease and ulcerative colitis. J.Clin.Invest 2006;116:3195-3203.
63. Andresen L, Jorgensen VL, Perner A, et al. Activation of nuclear factor kappaB in colonic mucosa from patients with collagenous and ulcerative colitis. Gut 2005;54:503-509.
64. Dong WG, Liu SP, Yu BP, et al. Ameliorative effects of sodium ferulate on experimental colitis and their mechanisms in rats. World J.Gastroenterol. 2003;9:2533-2538.

65. Jung M, Triebel S, Anke T, et al. Influence of apple polyphenols on inflammatory gene expression. Mol.Nutr Food Res. 2009;53:1263-1280.
66. Castagnini C, Luceri C, Toti S, et al. Reduction of colonic inflammation in HLA-B27 transgenic rats by feeding Marie Menard apples, rich in polyphenols. Br.J.Nutr 2009;102:1620-1628.
67. Singer II, Kawka DW, Schloemann S, et al. Cyclooxygenase 2 is induced in colonic epithelial cells in inflammatory bowel disease. Gastroenterology 1998;115:297-306.
68. Sanchez-Fidalgo S, Cardeno A, Villegas I, et al. Dietary supplementation of resveratrol attenuates chronic colonic inflammation in mice. Eur.J.Pharmacol. 2010;633:78-84.
69. Li Q, Verma IM. NF-kappaB regulation in the immune system. Nat.Rev.Immunol. 2002;2:725-734.
70. Levy E, Rizwan Y, Thibault L, et al. Altered lipid profile, lipoprotein composition, and oxidant and antioxidant status in pediatric Crohn disease. Am.J.Clin.Nutr. 2000;71:807-815.
71. Lih-Brody L, Powell SR, Collier KP, et al. Increased oxidative stress and decreased antioxidant defenses in mucosa of inflammatory bowel disease. Dig.Dis.Sci 1996;41:2078-2086.
72. Alzoghaibi MA. Concepts of oxidative stress and antioxidant defense in Crohn's disease. World J.Gastroenterol. 2013;19:6540-6547.
73. Huang HC, Nguyen T, Pickett CB. Phosphorylation of Nrf2 at Ser-40 by protein kinase C regulates antioxidant response element-mediated transcription. J.Biol.Chem 2002;277:42769-42774.
74. Nazli A, Yang PC, Jury J, et al. Epithelia under metabolic stress perceive commensal bacteria as a threat. Am.J.Pathol. 2004;164:947-957.
75. Wang A, Keita AV, Phan V, et al. Targeting mitochondria-derived reactive oxygen species to reduce epithelial barrier dysfunction and colitis. Am.J.Pathol. 2014;184:2516-2527.
76. Carrasco-Pozo C, Gotteland M, Speisky H. Apple peel polyphenol extract protects against indomethacin-induced damage in Caco-2 cells by preventing mitochondrial complex I inhibition. J.Agric.Food Chem. 2011;59:11501-11508.
77. Scarpulla RC. Transcriptional activators and coactivators in the nuclear control of mitochondrial function in mammalian cells. Gene 2002;286:81-89.
78. Scarpulla RC. Nuclear control of respiratory chain expression by nuclear respiratory factors and PGC-1-related coactivator. Ann N.Y.Acad.Sci 2008;1147:321-334.
79. Scarpulla RC. Transcriptional paradigms in mammalian mitochondrial biogenesis and function. Physiol Rev 2008;88:611-638.
80. Rayamajhi N, Kim SK, Go H, et al. Quercetin induces mitochondrial biogenesis through activation of HO-1 in HepG2 cells. Oxid.Med.Cell Longev. 2013;2013:154279.
81. Kulagina EV, Efimov BA, Maximov PY, et al. Species composition of Bacteroidales order bacteria in the feces of healthy people of various ages. Biosci.Biotechnol.Biochem. 2012;76:169-171.
82. Ubeda C, Bucci V, Caballero S, et al. Intestinal microbiota containing Barnesiella species cures vancomycin-resistant Enterococcus faecium colonization. Infect.Immun. 2013;81:965-973.
83. Noor SO, Ridgway K, Scovell L, et al. Ulcerative colitis and irritable bowel patients exhibit distinct abnormalities of the gut microbiota. BMC.Gastroenterol. 2010;10:134.
84. Bailey MT, Dowd SE, Parry NM, et al. Stressor exposure disrupts commensal microbial populations in the intestines and leads to increased colonization by Citrobacter rodentium. Infect.Immun. 2010;78:1509-1519.
85. Weiss GA, Chassard C, Hennet T. Selective proliferation of intestinal Barnesiella under fucosyllactose supplementation in mice. Br.J.Nutr 2014;111:1602-1610.

86. Yeh CT, Ching LC, Yen GC. Inducing gene expression of cardiac antioxidant enzymes by dietary phenolic acids in rats. J.Nutr.Biochem. 2009;20:163-171.
87. Gomez A, Luckey D, Yeoman CJ, et al. Loss of sex and age driven differences in the gut microbiome characterize arthritis-susceptible 0401 mice but not arthritis-resistant 0402 mice. PLoS.One. 2012;7:e36095.
88. Wiese DM, Lashner BA, Lerner E, et al. The effects of an oral supplement enriched with fish oil, prebiotics, and antioxidants on nutrition status in Crohn's disease patients. Nutr Clin.Pract. 2011;26:463-473.
89. Kitajima S, Takuma S, Morimoto M. Changes in colonic mucosal permeability in mouse colitis induced with dextran sulfate sodium. Exp.Anim 1999;48:137-143.
90. Mueller C, Macpherson AJ. Layers of mutualism with commensal bacteria protect us from intestinal inflammation. Gut 2006;55:276-284.
91. Berry D, Schwab C, Milinovich G, et al. Phylotype-level 16S rRNA analysis reveals new bacterial indicators of health state in acute murine colitis. ISME.J. 2012;6:2091-2106.
92. Schwab C, Berry D, Rauch I, et al. Longitudinal study of murine microbiota activity and interactions with the host during acute inflammation and recovery. ISME.J. 2014;8:1101-1114.
93. Wohlgemuth S, Keller S, Kertscher R, et al. Intestinal steroid profiles and microbiota composition in colitic mice. Gut Microbes. 2011;2:159-166.
94. Chen W, Liu F, Ling Z, et al. Human intestinal lumen and mucosa-associated microbiota in patients with colorectal cancer. PLoS.One. 2012;7:e39743.
95. Derrien M, Vaughan EE, Plugge CM, et al. Akkermansia muciniphila gen. nov., sp. nov., a human intestinal mucin-degrading bacterium. Int.J.Syst.Evol.Microbiol. 2004;54:1469-1476.
96. Robertson DA, Ray J, Diamond I, et al. Personality profile and affective state of patients with inflammatory bowel disease. Gut 1989;30:623-626.
97. Osman N, Adawi D, Ahrne S, et al. Probiotics and blueberry attenuate the severity of dextran sulfate sodium (DSS)-induced colitis. Dig.Dis.Sci 2008;53:2464-2473.

Figure 1

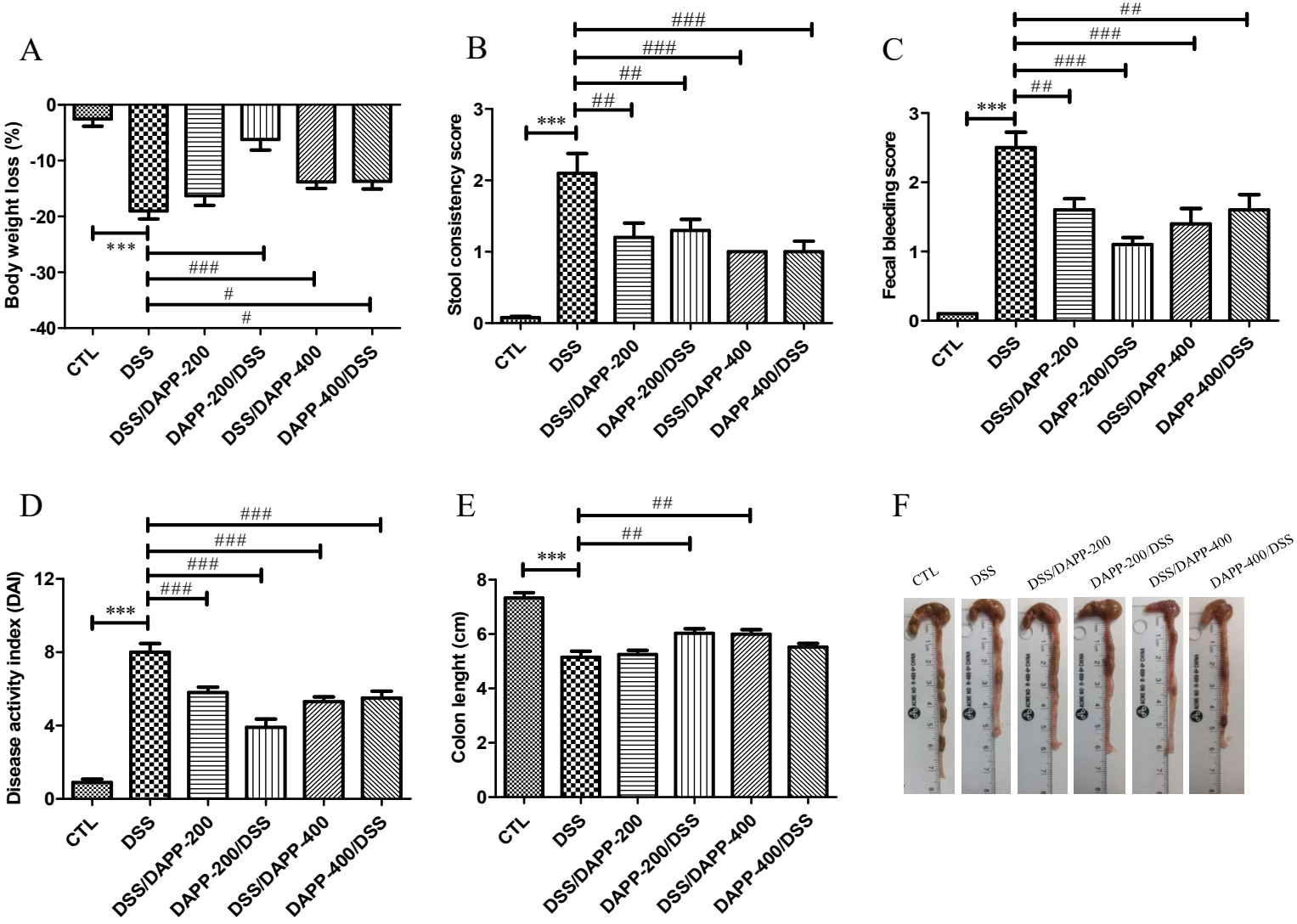
A
Body weight loss (%)
0
-10
-20
-30
-40
***
###
#
#
CTL
DSS
DSS/DAPP-200
DAPP-200/DSS
DSS/DAPP-400
DAPP-400/DSS
B
Stool consistency score
3
2
1
0
***
###
###
##
##
C
Fecal bleeding score
3
2
1
0
***
##
###
###
##
D
Disease activity index (DAI)
12
8
4
0
***
###
###
###
###
E
Colon lenght (cm)
8
6
4
2
0
***
##
##
F
CTL
DSS
DSS/DAPP-200
DAPP-200/DSS
DSS/DAPP-400
DAPP-400/DSS

Figure 2

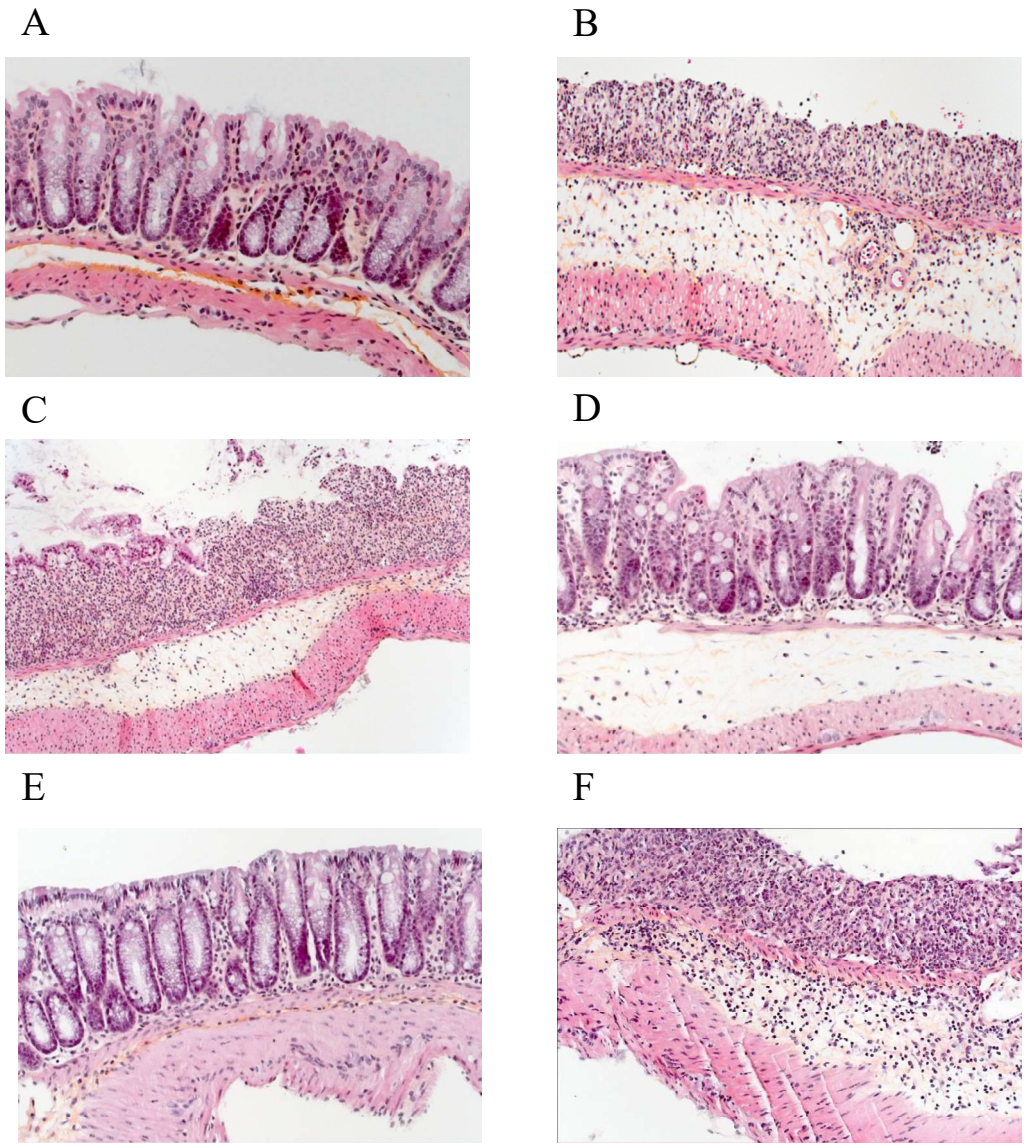
A
B
C
D
E
F

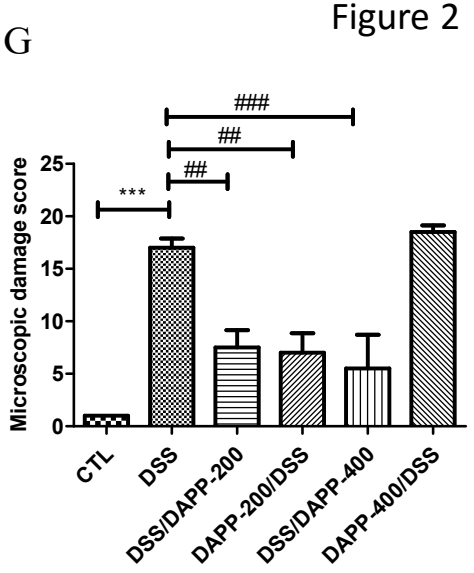
G
Microscopic damage score
0
5
10
15
20
25
***
##
##
###
CTL
DSS
DSS/DAPP-200
DAPP-200/DSS
DSS/DAPP-400
DAPP-400/DSS

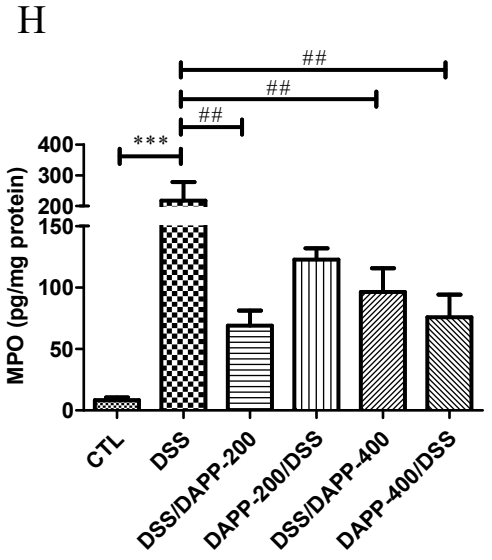
H
MPO (pg/mg protein)
0
50
100
150
200
300
400
***
##
##
##
CTL
DSS
DSS/DAPP-200
DAPP-200/DSS
DSS/DAPP-400
DAPP-400/DSS

Figure 3

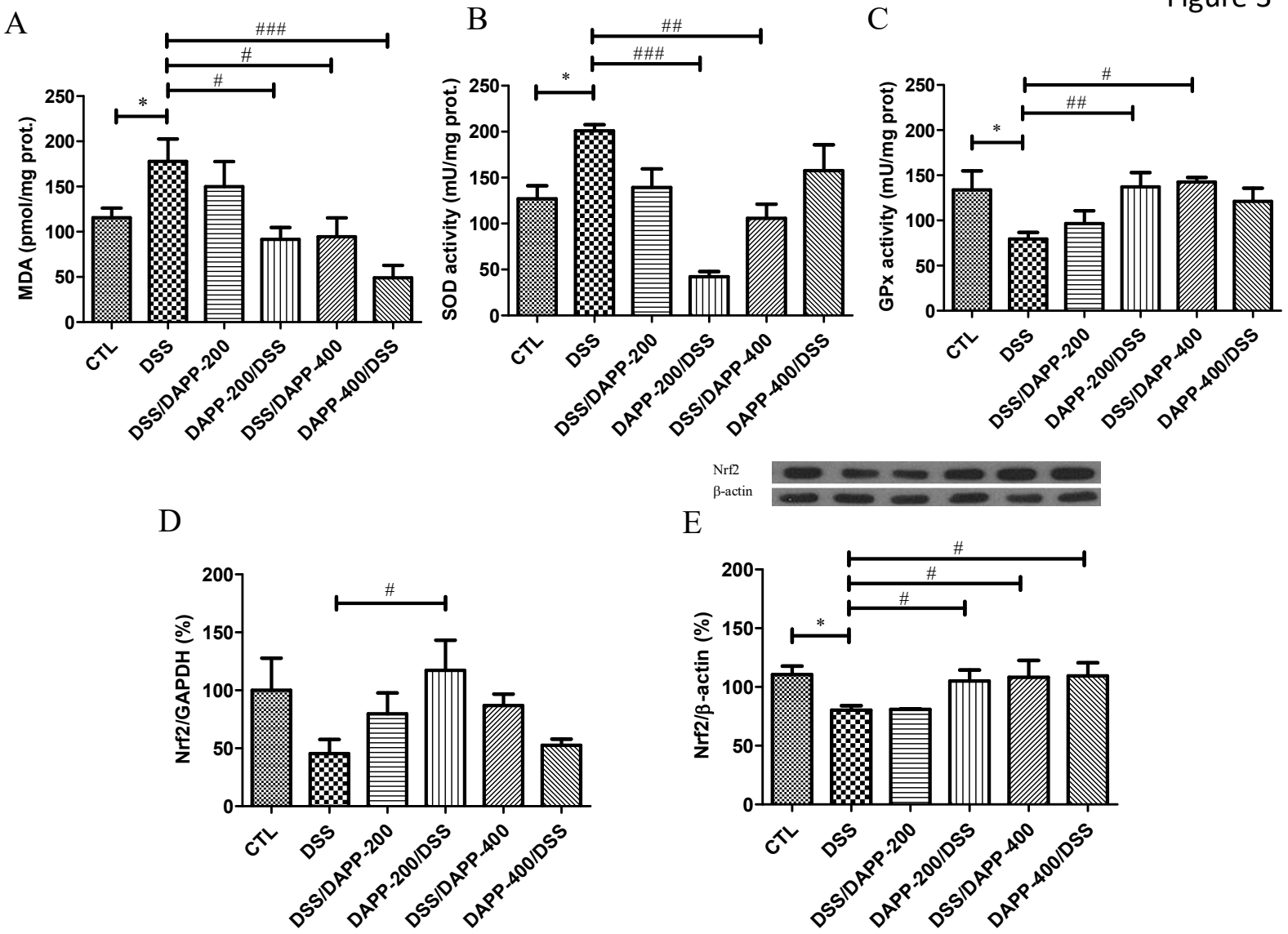
A
MDA (pmol/mg prot.)
B
SOD activity (mU/mg prot.)
C
GPx activity (mU/mg prot)
CTL
DSS
DSS/DAPP-200
DAPP-200/DSS
DSS/DAPP-400
DAPP-400/DSS
Nrf2
β-actin
D
Nrf2/GAPDH (%)
E
Nrf2/β-actin (%)

Figure 4

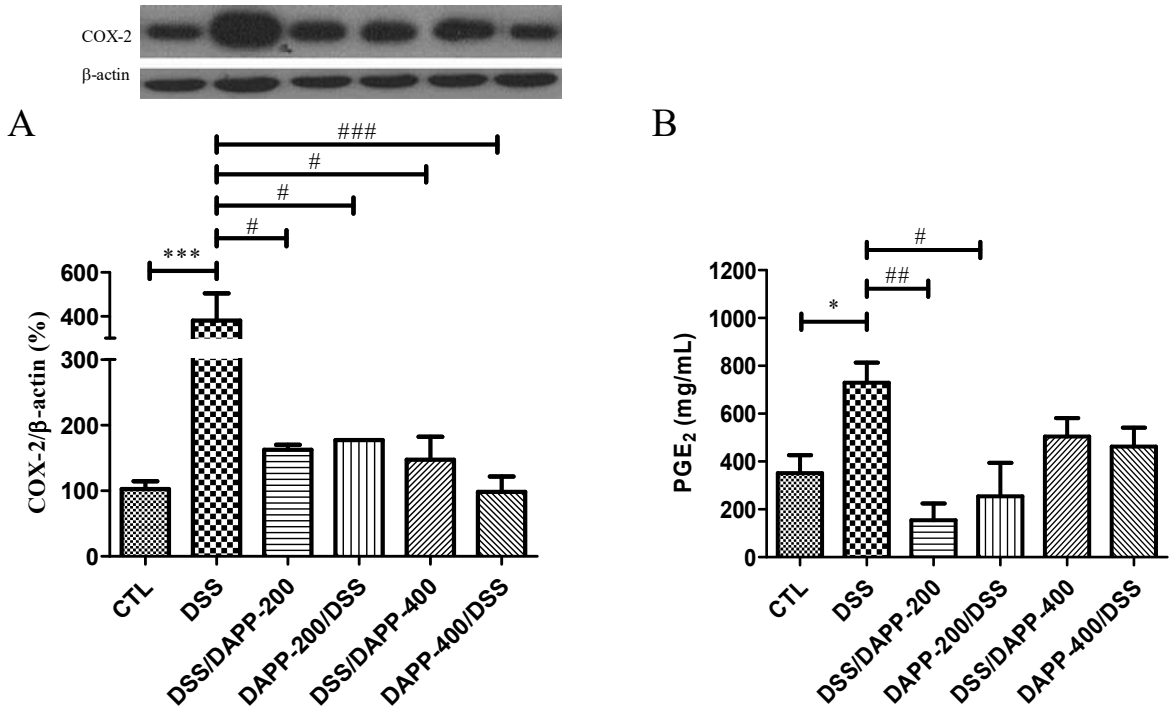
COX-2
β-actin
A
B
###
#
#
#
***
*
#
##
COX-2/β-actin (%)
PGE2 (mg/mL)
600
400
300
200
100
0
1200
1000
800
600
400
200
0
CTL
DSS
DSS/DAPP-200
DAPP-200/DSS
DSS/DAPP-400
DAPP-400/DSS

Figure 5

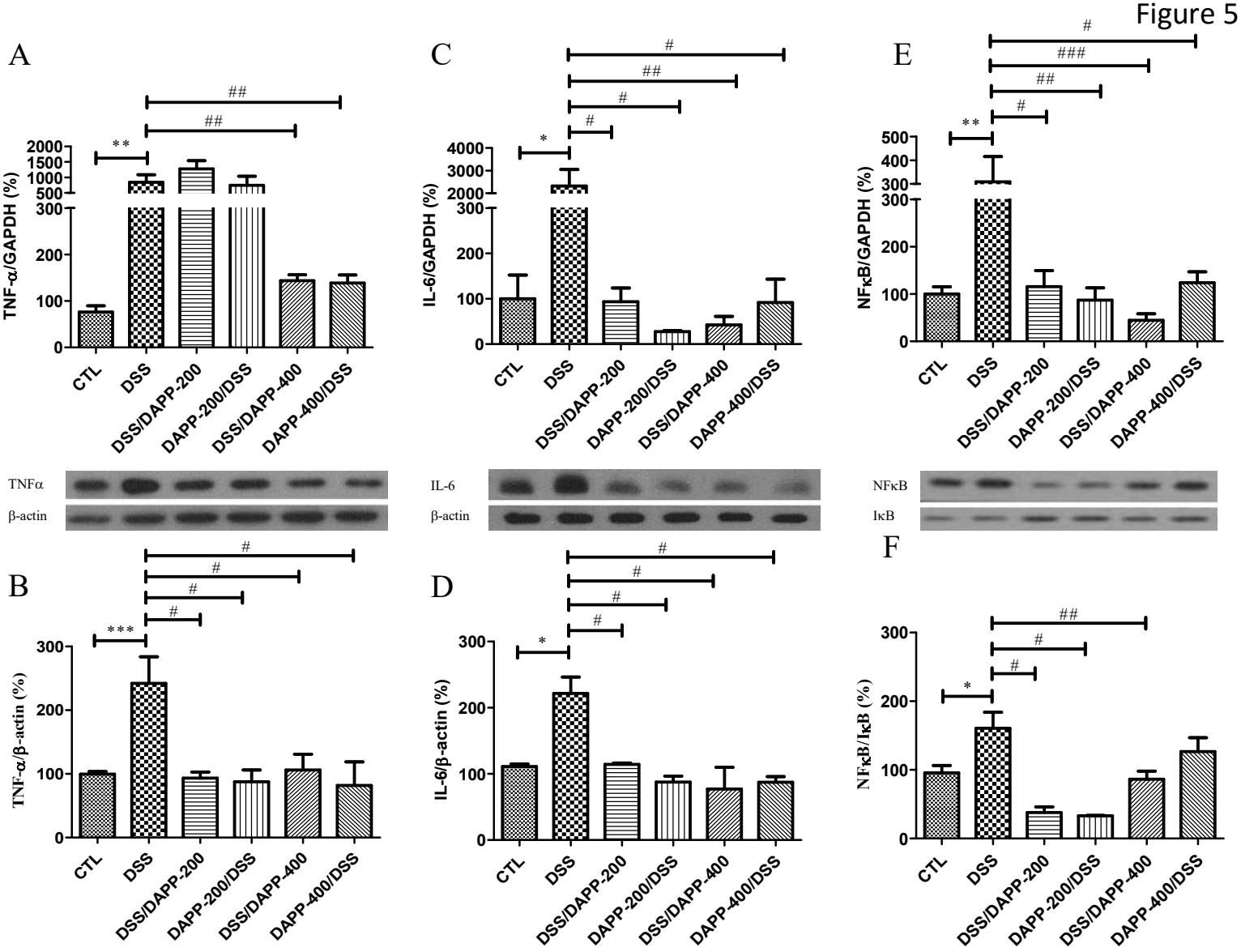
A
TNF-α/GAPDH (%)
2000
1500
1000
500
300
200
100
0
**
##
##
CTL
DSS
DSS/DAPP-200
DAPP-200/DSS
DSS/DAPP-400
DAPP-400/DSS
C
IL-6/GAPDH (%)
4000
3000
2000
300
200
100
0
*
#
#
#
##
E
NFκB/GAPDH (%)
500
400
300
300
200
100
0
**
#
#
##
###
#
TNFα
β-actin
IL-6
β-actin
NFκB
IκB
B
TNF-α/β-actin (%)
300
200
100
0
***
#
#
#
#
D
IL-6/β-actin (%)
300
200
100
0
*
#
#
#
#
F
NFκB/IκB (%)
300
200
100
0
*
#
#
##

Figure 6

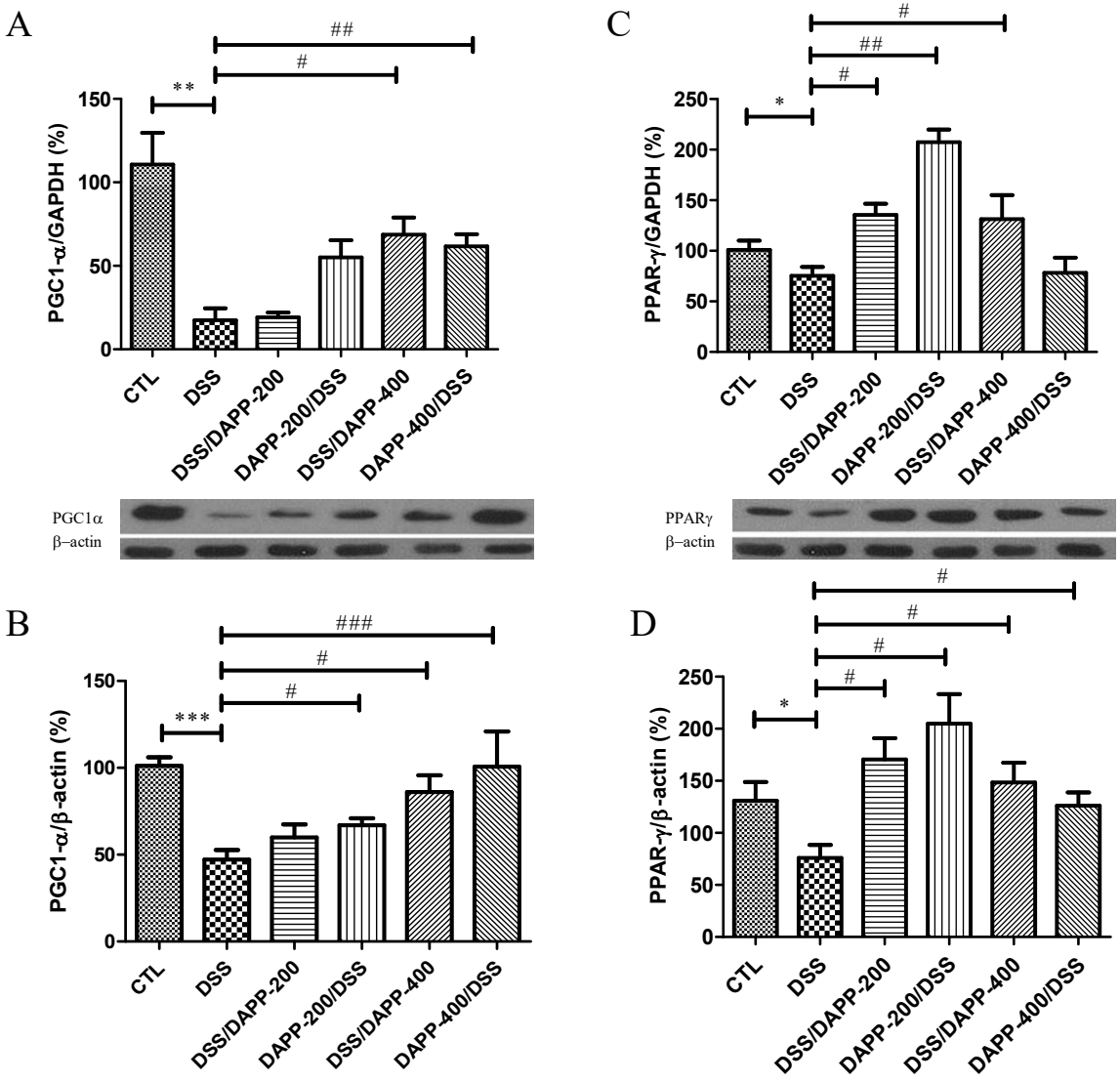
A
PGC1-α/GAPDH (%)
150
100
50
0
**
#
##
CTL
DSS
DSS/DAPP-200
DAPP-200/DSS
DSS/DAPP-400
DAPP-400/DSS
PGC1α
β–actin
C
PPAR-γ/GAPDH (%)
250
200
150
100
50
0
*
#
##
#
CTL
DSS
DSS/DAPP-200
DAPP-200/DSS
DSS/DAPP-400
DAPP-400/DSS
PPARγ
β–actin
B
PGC1-α/β-actin (%)
150
100
50
0
***
#
#
###
CTL
DSS
DSS/DAPP-200
DAPP-200/DSS
DSS/DAPP-400
DAPP-400/DSS
D
PPAR-γ/β-actin (%)
250
200
150
100
50
0
*
#
#
#
#
CTL
DSS
DSS/DAPP-200
DAPP-200/DSS
DSS/DAPP-400
DAPP-400/DSS

Figure 7

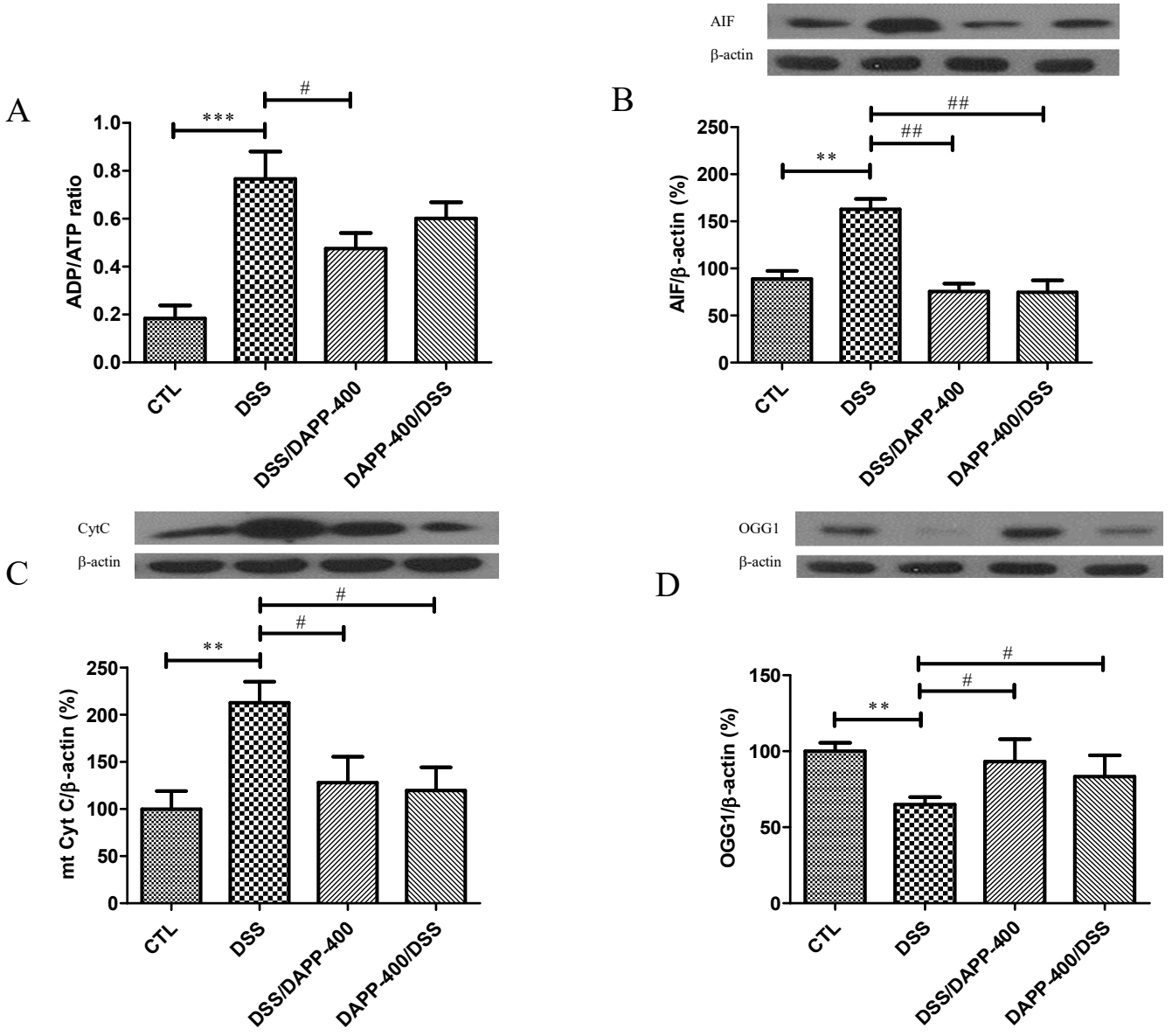
A
ADP/ATP ratio
1.0
0.8
0.6
0.4
0.2
0.0
***
#
CTL
DSS
DSS/DAPP-400
DAPP-400/DSS
B
AIF
β-actin
AIF/β-actin (%)
250
200
150
100
50
0
**
##
##
CTL
DSS
DSS/DAPP-400
DAPP-400/DSS
C
CytC
β-actin
mt Cyt C/β-actin (%)
250
200
150
100
50
0
**
#
#
CTL
DSS
DSS/DAPP-400
DAPP-400/DSS
D
OGG1
β-actin
OGG1/β-actin (%)
150
100
50
0
**
#
#
CTL
DSS
DSS/DAPP-400
DAPP-400/DSS

Figure 8

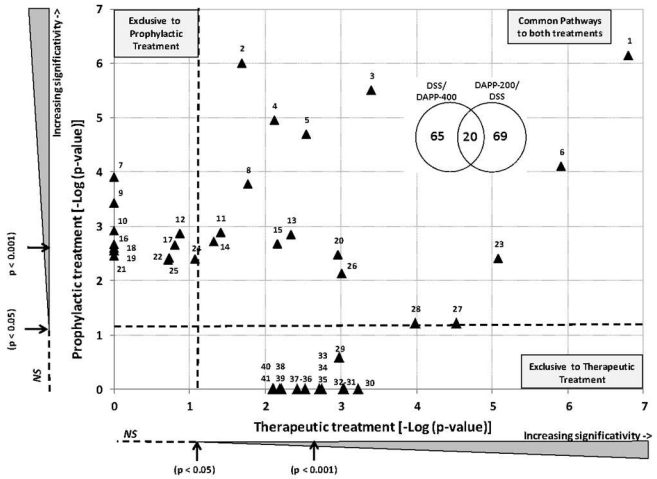

List of the main IPA cannonical pathways modulated by DAPP

#	Ingenuity Canonical Pathways	Gene list
1	Hepatic Fibrosis / Hepatic Stellate Cell Activation	IL1RL1,COL12A1,FN1,MMP9,COL3A1,COL4A2,IL1R2,ACTA2,LBP,CXCL3,IL6
2	IL-6 Signaling	IL1RL1,IL6,KRAS,PIK3R3,IL1R2,LBP,IL6ST
3	Atherosclerosis Signaling	LYZ,COL3A1,PLA2G1B,COL1A2,IL6, MMP9
4	Glucocorticoid Receptor Signaling	DUSP1,TSC22D3,HSPA8,IL1R2,CXCL3,IL6,KRT36,KRAS,PIK3R3
5	Intrinsic Prothrombin Activation Pathway	KNG1,COL3A1,COL1A2
6	LXR/RXR Activation	LYZ,IL1RL1,MMP9,KNG1,IL1R2,LBP,IL6
7	Virus Entry via Endocytic Pathways	KRAS,PIK3R3,ACTA2,TFRC
8	Role of Macrophages, Fibroblasts and Endothelial	IL6,IL1RL1,KRAS,PIK3R3,FN1,IL1R2,IL6ST
9	CNTF Signaling	KRAS,PIK3R3,IL6ST
10	LPS-stimulated MAPK Signaling	KRAS,PIK3R3,LBP
11	PPAR/RXR Activation	IL1R2,IL6,IL1RL1,KRAS,ADIPOQ
12	VEGF Family Ligand-Receptor Interactions	KRAS,PIK3R3,PLA2G1B
13	p38 MAPK Signaling	IL1RL1,PLA2G1B,IL1R2
14	Clathrin-mediated Endocytosis Signaling	LYZ,HSPA8,,PIK3R3,ACTA2,TFRC
15	eNOS Signaling	PIK3R3,KNG1,AQP8,HSPA8
16	VEGF Signaling	KRAS,PIK3R3,ACTA2
17	PPAR Signaling	IL1RL1,KRAS,IL1R2
18	Mouse Embryonic Stem Cell Pluripotency	KRAS,PIK3R3,IL6ST
19	Paxillin Signaling	KRAS,PIK3R3,ACTA2
20	Hepatic Cholestasis	IL1RL1,IL1R2,LBP,HNF4A,IL6
21	Pancreatic Adenocarcinoma Signaling	KRAS,PIK3R3,MMP9
22	Fc Epsilon RI Signaling	KRAS,PLA2G1B
23	Acute Phase Response Signaling	KRAS,CFB,PIK3R3,FN1,LBP,IL6ST,C1S,IL6
24	Dendritic Cell Maturation	PIK3R3,COL3A1,COL1A2,IL6
25	CCR3 Signaling in Eosinophils	KRAS,PIK3R3,PLA2G1B
26	IL-10 Signaling	IL1RL1,IL1R2,LBP,IL6
27	MIF-mediated Glucocorticoid Regulation	KRAS,PIK3R3,FN1,KNG1,ACTA2,LBP,PLA2G1B
28	Actin Cytoskeleton Signaling	MMP9,HSPG2,THBS1,N1,KNG1
29	Germ Cell-Sertoli Cell Junction Signaling	KRAS,TUBA1A,PIK3R3,ACTA2
30	Glioma Invasiveness Signaling	KRAS,PIK3R3,MMP9
31	Gap Junction Signaling	KRAS,TUBA1A,PIK3R3,ACTA2
32	Agrin Interactions at Neuromuscular Junction	KRAS,LAMC1,ACTA2
33	ILK Signaling	PIK3R3,FN1,MMP9,ACTA2
34	Bladder Cancer Signaling	KRAS,MMP9,THBS1
35	FAK Signaling	KRAS,PIK3R3,ACTA2
36	HIF1 Signaling	KRAS,PIK3R3,MMP9
37	Role of NANOG in Mammalian Embryonic Stem Cell Pluri	KRAS,PIK3R3,IL6ST
38	FcRIIB Signaling in B Lymphocytes	KRAS,PIK3R3
39	Melanoma Signaling	KRAS,PIK3R3
40	MSP-RON Signaling Pathway	PIK3R3,ACTA2
41	Epithelial Adherens Junction Signaling	KRAS,TUBA1A,ACTA2

Figure 9

A

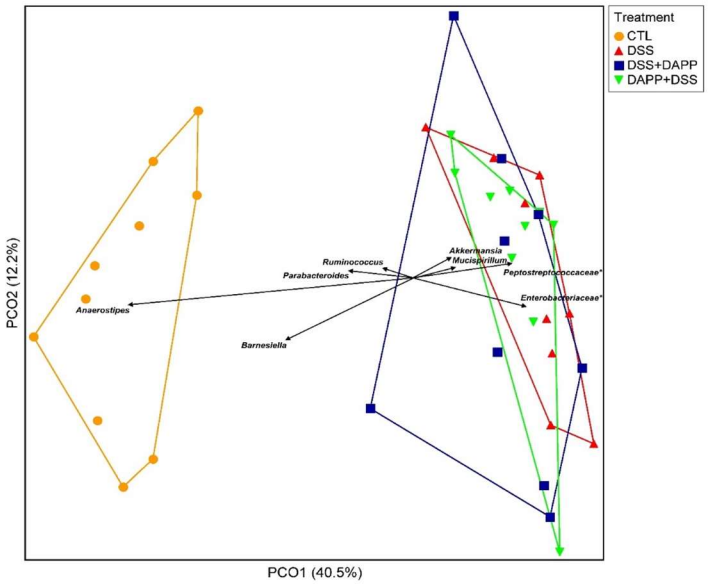
Treatment
CTL
DSS
DSS+DAPP
DAPP+DSS
PCO2 (12.2%)
PCO1 (40.5%)
Ruminococcus
Parabacteroides
Anaerostipes
Barnesiella
Akkermansia
Mucispirillum
Peptostreptococcaceae*
Enterobacteriaceae*

B

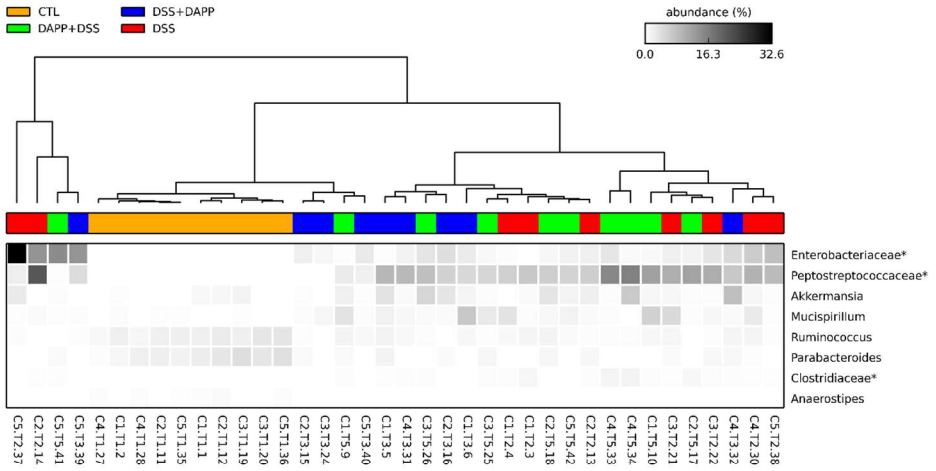
CTL
DSS+DAPP
DAPP+DSS
DSS
abundance (%)
0.0
16.3
32.6
Enterobacteriaceae*
Peptostreptococcaceae*
Akkermansia
Mucispirillum
Ruminococcus
Parabacteroides
Clostridiaceae*
Anaerostipes

Figure 10

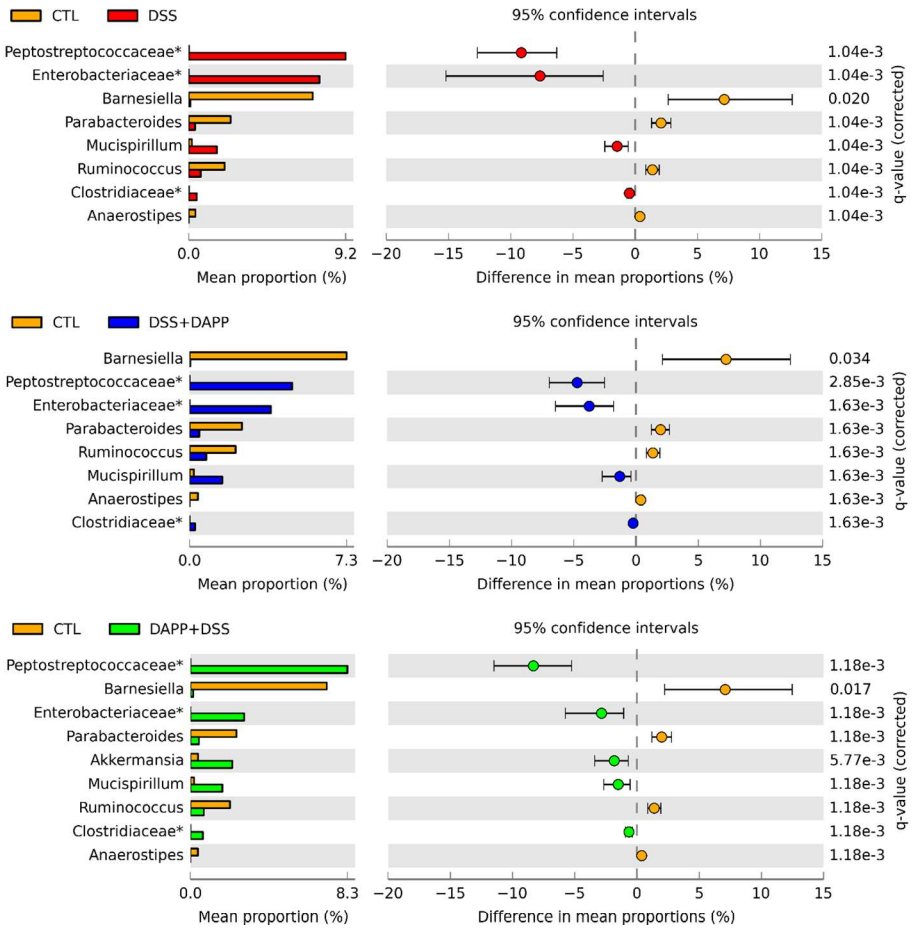
CTL
DSS
95% confidence intervals
Peptostreptococcaceae*
Enterobacteriaceae*
Barnesiella
Parabacteroides
Mucispirillum
Ruminococcus
Clostridiaceae*
Anaerostipes
1.04e-3
1.04e-3
0.020
1.04e-3
1.04e-3
1.04e-3
1.04e-3
1.04e-3
q-value (corrected)
0.0
9.2
Mean proportion (%)
−20 −15 −10 −5 0 5 10 15
Difference in mean proportions (%)
CTL
DSS+DAPP
95% confidence intervals
Barnesiella
Peptostreptococcaceae*
Enterobacteriaceae*
Parabacteroides
Ruminococcus
Mucispirillum
Anaerostipes
Clostridiaceae*
0.034
2.85e-3
1.63e-3
1.63e-3
1.63e-3
1.63e-3
1.63e-3
1.63e-3
q-value (corrected)
0.0
7.3
Mean proportion (%)
−20 −15 −10 −5 0 5 10 15
Difference in mean proportions (%)
CTL
DAPP+DSS
95% confidence intervals
Peptostreptococcaceae*
Barnesiella
Enterobacteriaceae*
Parabacteroides
Akkermansia
Mucispirillum
Ruminococcus
Clostridiaceae*
Anaerostipes
1.18e-3
0.017
1.18e-3
1.18e-3
5.77e-3
1.18e-3
1.18e-3
1.18e-3
1.18e-3
q-value (corrected)
0.0
8.3
Mean proportion (%)
−20 −15 −10 −5 0 5 10 15
Difference in mean proportions (%)

Suppl. Figure 1

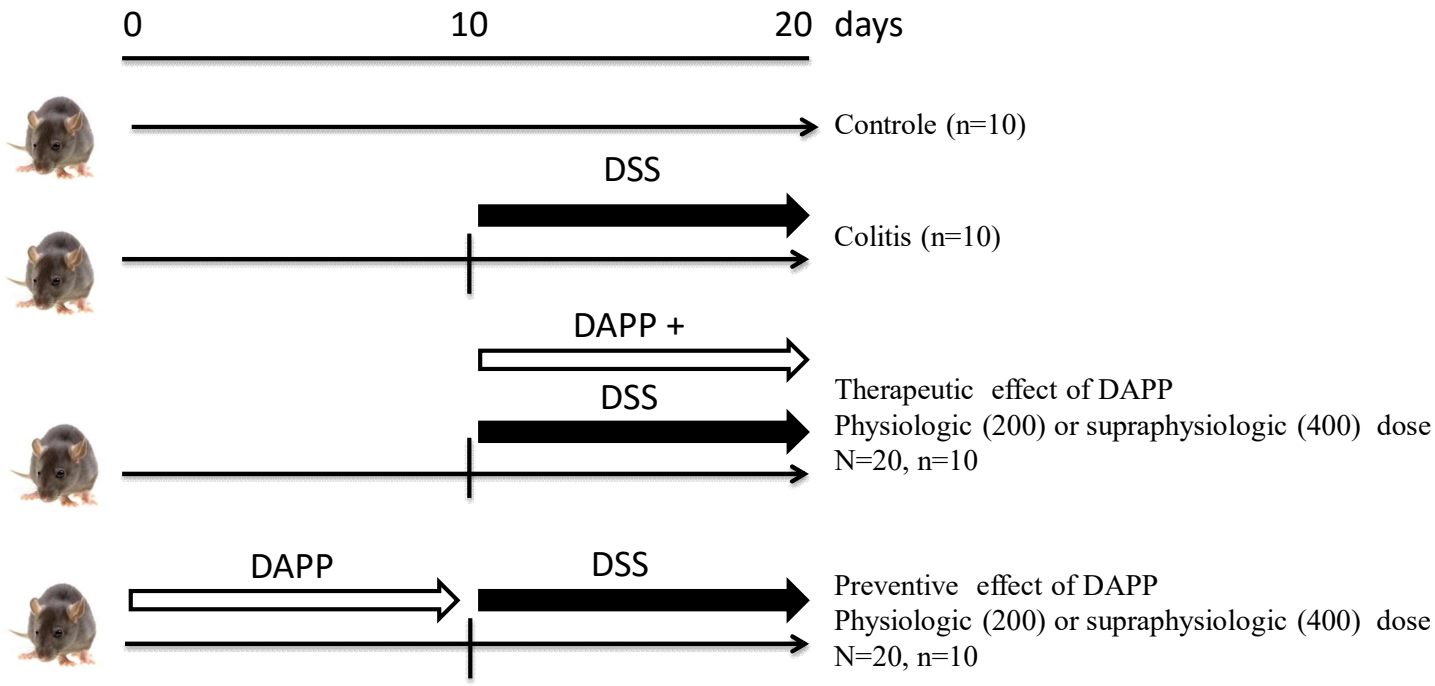

Suppl. Figure 2

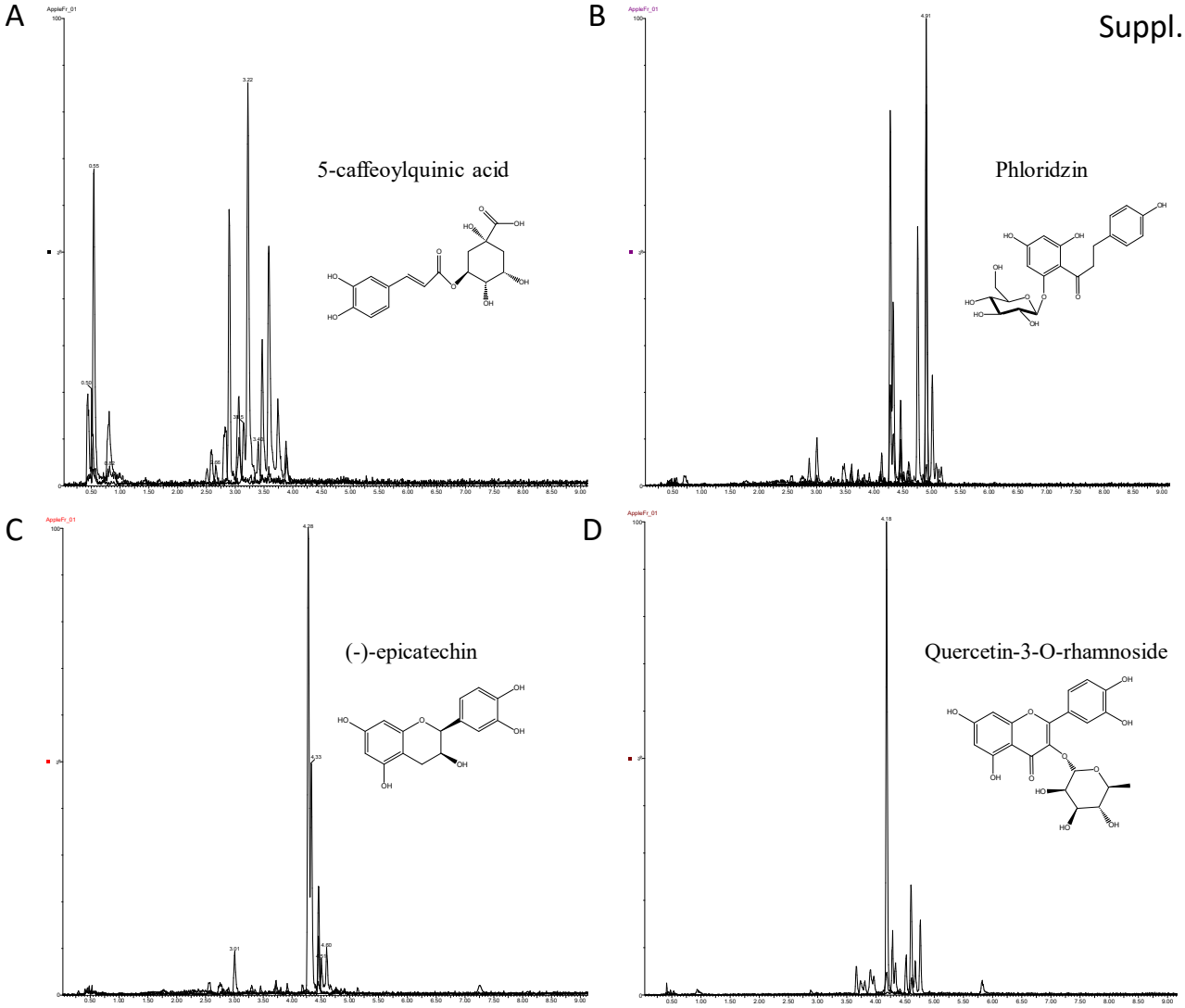

Supplementary Table 1: Positive effects of DAPP on oxidative stress and inflammation markers in distal colon of DSS-induced colitis mice

Markers	DSS/DAPP-200	DAPP-200/DSS	DSS/DAPP-400	DAPP-400/DSS
Body weight loss	+	++++	+++	++
Stool consistency score	++	+	++++	+++
Fecal bleeding score	++	++++	+++	+
DAI	+	++++	+++	++
Colon lenght	+	++++	+++	++
Microscopic damage score	++	+++	++++	+
MPO	++++	+	++	+++
MDA	+	+++	++	++++
SOD activity	++	++++	+++	+
GPx activity	+	+++	++++	++
Nrf2 gene	++	++++	+++	+
Nrf2 protein	+	++	++++	+++
Total OxS	20	37	38	25
COX-2	++	+	+++	++++
PGE_2	++++	+++	+	++
TNF-α gene	+	++	+++	++++
TNF-α protein	++	+++	+	++++
IL-6 gene	+	++++	+++	++
IL-6 protein	+	++	++++	+++
NFκB gene	++	+++	++++	+
NFκB/IκB protein	+++	++++	++	+
PGC1-α gene	+	++	++++	+++
PGC1-α protein	+	++	+++	++++
PPAR-γ gene	++	++++	+++	+
PPAR-γ protein	+++	++++	++	+
Total inflammation	23	34	33	30
Total OxS + Inflammation	43	71	71	55

Expression levels of positive effects of DAPP on different oxidative stress and inflammation markers in mice with DSS-induced colitis and DAPP (as described in Supplementay Figure 1) are represented by (+). When there are four + in a group of mice, the positive effect is the highest. The greater the number of + decreases, the positive effect is reduced. Subsequently, adding the number of + was performed in each of the groups of mice.

Supplementary Table 2. List of differentially expressed genes

ILMN Gene	Symbol	Description	Gene ID	Control	DSS	DSS/DAPP-400	DAPP-200/DSS
ABAT	Abat	Mus musculus 4-aminobutyrate aminotransferase (Abat), nuclear	268860	188	139	134	138
ABAT	Abat	Mus musculus 4-aminobutyrate aminotransferase (Abat), nuclear	268860	5353	1866	2328	2688
ABCA8A	Abca8a	Mus musculus ATP-binding cassette, sub-family A (ABC1), member 8a	217258	301	153	269	172
ABCD4	Abcd4	Mus musculus ATP-binding cassette, sub-family D (ALD), member 4	19300	151	191	171	169
ACAD8	Acad8	Mus musculus acyl-Coenzyme A dehydrogenase family, member 8	66948	134	136	122	118
ACAP2	Acap2	Mus musculus ArfGAP with coiled-coil, ankyrin repeat and PH domains	78618	130	136	133	142
ACBD6	Acbd6	Mus musculus acyl-Coenzyme A binding domain containing 6 (Acbd6),	72482	643	513	529	457
ACOT8	Acot8	Mus musculus acyl-CoA thioesterase 8 (Acot8), mRNA.	170789	2248	2276	1932	2063
ACP2	Acp2	Mus musculus acid phosphatase 2, lysosomal (Acp2), mRNA.	11432	596	697	789	708
ACP2	Acp2	Mus musculus acid phosphatase 2, lysosomal (Acp2), mRNA.	11432	350	432	488	508
ACSBG1	Acsbg1	Mus musculus acyl-CoA synthetase bubblegum family member 1	94180	127	141	157	148
ACSM3	Acsm3	Mus musculus acyl-CoA synthetase medium-chain family member 3	20216	4061	1831	1813	2250
ACSM3	Acsm3	Mus musculus acyl-CoA synthetase medium-chain family member 3	20216	4842	2487	1447	2235
ACSS1	Acss1	Mus musculus acyl-CoA synthetase short-chain family member 1	68738	4153	2585	2452	2298
ACTA2	Acta2	Mus musculus actin, alpha 2, smooth muscle, aorta (Acta2), mRNA.	11475	7751	3572	6065	5035
ACTA2	Acta2			6057	3142	5289	4425
ACTR3	Actr3	Mus musculus ARP3 actin-related protein 3 homolog (yeast) (Actr3),	74117	5304	6595	6700	7095
ACVR1B	Acvr1b			123	123	137	133
ADAM28	Adam28	Mus musculus a disintegrin and metallopeptidase domain 28	13522	121	130	126	145
ADAM4	Adam4	Mus musculus a disintegrin and metallopeptidase domain 4 (Adam4),	11498	140	154	139	148
ADAM9	Adam9	Mus musculus a disintegrin and metallopeptidase domain 9 (meltrin	11502	762	932	1221	1200
ADAMTS16	Adamts16			132	145	138	130
ADAMTS2	Adamts2	Mus musculus a disintegrin-like and metallopeptidase (reprolysin	216725	494	756	999	891
ADAMTS2	Adamts2	Mus musculus a disintegrin-like and metallopeptidase (reprolysin	216725	225	362	595	460
ADAMTS2	Adamts2	Mus musculus a disintegrin-like and metallopeptidase (reprolysin	216725	946	1283	2047	1693
ADAMTS6	Adamts6	Mus musculus a disintegrin-like and metallopeptidase (reprolysin	108154	125	130	162	145
ADAMTS7	Adamts7	Mus musculus a disintegrin-like and metallopeptidase (reprolysin	108153	141	158	194	185
ADAMTS9	Adamts9			129	136	160	144
ADAP1	Adap1	Mus musculus ArfGAP with dual PH domains 1 (Adap1), mRNA.	231821	210	546	906	564
ADH4	Adh4	Mus musculus alcohol dehydrogenase 4 (class II), pi polypeptide	26876	132	136	161	124
ADIPOQ	Adipoq	Mus musculus adiponectin, C1Q and collagen domain containing	11450	790	231	744	272

ADM	Adm	Mus musculus adrenomedullin (Adm), mRNA.	11535	185	298	370	308
ADNP	Adnp	Mus musculus activity-dependent neuroprotective protein (Adnp),	11538	2358	1720	1824	2021
ADNP	Adnp	Mus musculus activity-dependent neuroprotective protein (Adnp),	11538	2999	2634	2341	2614
ADSSL1	Adssl1	Mus musculus adenylosuccinate synthetase like 1 (Adssl1), mRNA.	11565	153	277	331	250
AEBP1	Aebp1	Mus musculus AE binding protein 1 (Aebp1), mRNA.	11568	406	776	1088	908
AGTPBP1	Agtpbp1			132	136	148	160
AHCY	Ahcy	Mus musculus S-adenosylhomocysteine hydrolase (Ahcy), mRNA.	269378	311	230	252	216
AHNAK2	Ahnak2	Mus musculus AHNAK nucleoprotein 2 (Ahnak2), mRNA.	382643	517	273	368	335
AI481316	AI481316			2473	3128	2888	2502
AI607873	AI607873	PREDICTED: Mus musculus expressed sequence AI607873	226691	185	409	379	326
AI661311	AI661311			148	158	148	137
AI747448	AI747448	Mus musculus expressed sequence AI747448 (AI747448), mRNA.	99709	459	2236	1530	2302
AI854703	AI854703	PREDICTED: Mus musculus expressed sequence AI854703	243373	1868	465	420	631
AI931714	AI931714			154	136	140	144
AI987692	AI987692	Mus musculus expressed sequence AI987692 (AI987692), mRNA.	331063	5892	2855	2354	3206
AK2	Ak2	Mus musculus adenylate kinase 2 (Ak2), transcript variant 2, mRNA.	11637	411	634	636	504
AK5	Ak5	Mus musculus adenylate kinase 5 (Ak5), mRNA.	229949	128	123	128	135
AKR1B7	Akr1b7	Mus musculus aldo-keto reductase family 1, member B7 (Akr1b7),	11997	275	261	243	199
AKR1C14	Akr1c14	Mus musculus aldo-keto reductase family 1, member C14 (Akr1c14),	105387	417	240	220	258
AKR1C21	Akr1c21	Mus musculus aldo-keto reductase family 1, member C21 (Akr1c21),	77337	122	121	124	118
ALDH1A3	Aldh1a3			121	114	126	121
ALDH1L2	Aldh1l2	Mus musculus aldehyde dehydrogenase 1 family, member L2	216188	192	286	320	364
ALDH3B1	Aldh3b1	Mus musculus aldehyde dehydrogenase 3 family, member B1	67689	321	519	556	446
ALG6	Alg6	Mus musculus asparagine-linked glycosylation 6 homolog (yeast,	320438	1264	970	895	1287
ALKBH8	Alkbh8	Mus musculus alkB, alkylation repair homolog 8 (E. coli) (Alkbh8),	67667	224	211	151	175
ALOX15	Alox15	Mus musculus arachidonate 15-lipoxygenase (Alox15), mRNA.	11687	125	128	138	142
ALS2	Als2	Mus musculus amyotrophic lateral sclerosis 2 (juvenile) homolog	74018	502	319	301	354
ALX1	Alx1	Mus musculus ALX homeobox 1 (Alx1), mRNA.	216285	143	135	127	126
AMBRA1	Ambra1	Mus musculus autophagy/beclin 1 regulator 1 (Ambra1), transcript	228361	138	127	130	124
AMY2-2	Amy2-2	Mus musculusamylase 2-2, pancreatic (Amy2-2), mRNA.	109959	117	7144	3857	169
AMZ2	Amz2	Mus musculus archaelysin family metallopeptidase 2 (Amz2),	13929	889	727	724	703
ANAPC7	Anapc7	Mus musculus anaphase promoting complex subunit 7 (Anapc7),	56317	896	791	866	661
ANGPTL1	Angptl1	Mus musculus angiopoietin-like 1 (Angptl1), mRNA.	72713	236	179	210	191
ANGPTL2	Angptl2			149	137	126	132

ANK1	Ank1	Mus musculus ankyrin 1, erythroid (Ank1), mRNA.	11733	341	193	213	197
ANK3	Ank3	Mus musculus ankyrin 3, epithelial (Ank3), transcript variant 6, mRNA.	11735	130	128	130	125
ANKFY1	Ankfy1			121	123	130	132
ANKRD33	Ankrd33	Mus musculus ankyrin repeat domain 33 (Ankrd33), mRNA.	208258	147	145	122	124
ANKRD49	Ankrd49	Mus musculus ankyrin repeat domain 49 (Ankrd49), mRNA.	56503	974	914	662	790
ANO4	Ano4	Mus musculus anoctamin 4 (Ano4), mRNA.	320091	153	127	130	126
ANTXR1	Antxr1	Mus musculus anthrax toxin receptor 1 (Antxr1), mRNA.	69538	527	697	914	902
ANTXR1	Antxr1	Mus musculus anthrax toxin receptor 1 (Antxr1), mRNA.	69538	421	627	728	667
ANXA3	Anxa3	Mus musculus annexin A3 (Anxa3), mRNA.	11745	9104	7645	6433	7120
ANXA3	Anxa3	Mus musculus annexin A3 (Anxa3), mRNA.	11745	10544	8919	8394	9191
AOF2	Aof2	Mus musculus amine oxidase (flavin containing) domain 2 (Aof2),	99982	1472	1206	1178	1063
APC	Apc	Mus musculus adenomatosis polyposis coli (Apc), mRNA.	11789	137	127	121	118
APIP	Apip	Mus musculus APAF1 interacting protein (Apip), mRNA.	56369	139	142	172	171
AQP8	Aqp8	Mus musculus aquaporin 8 (Aqp8), mRNA.	11833	6642	960	2491	1481
ARG1	Arg1	Mus musculus arginase 1, liver (Arg1), mRNA.	11846	164	758	1986	578
ARG2	Arg2	Mus musculus arginase type II (Arg2), mRNA.	11847	159	497	482	339
ARHGAP12	Arhgap12	Mus musculus Rho GTPase activating protein 12 (Arhgap12), transcript	75415	1121	599	443	635
ARHGAP8	Arhgap8	Mus musculus Rho GTPase activating protein 8 (Arhgap8), mRNA.	73167	281	287	220	240
ARHGEF1	Arhgef1	Mus musculus Rho guanine nucleotide exchange factor (GEF) 1	16801	327	381	457	446
ARHGEF9	Arhgef9	Mus musculus CDC42 guanine nucleotide exchange factor (GEF) 9	236915	125	129	130	120
ARID4A	Arid4a			135	134	144	153
ARID4A	Arid4a			146	139	137	154
ARID5A	Arid5a	Mus musculus AT rich interactive domain 5A (MRF1-like) (Arid5a),	214855	150	170	176	158
ARL4C	Arl4c	Mus musculus ADP-ribosylation factor-like 4C (Arl4c), mRNA.	320982	146	192	218	220
ARL4C	Arl4c	Mus musculus ADP-ribosylation factor-like 4C (Arl4c), mRNA.	320982	154	177	188	197
ARL6IP5	Arl6ip5	Mus musculus ADP-ribosylation factor-like 6 interacting protein 5	65106	962	1064	1244	1277
ARMC9	Armc9	Mus musculus armadillo repeat containing 9 (Armc9), transcript	78795	183	157	130	152
ARNT	Arnt	Mus musculus aryl hydrocarbon receptor nuclear translocator (Arnt),	11863	131	146	144	158
ARPC1B	Arpc1b	Mus musculus actin related protein 2/3 complex, subunit 1B (Arpc1b),	11867	2790	4504	5120	5019
ARPC1B	Arpc1b	Mus musculus actin related protein 2/3 complex, subunit 1B (Arpc1b),	11867	4400	5539	7543	7417
ARPC2	Arpc2	Mus musculus actin related protein 2/3 complex, subunit 2 (Arpc2),	76709	5315	5752	6300	7705
ARTN	Artn	Mus musculus artemin (Artn), mRNA.	11876	165	217	258	245
ASB1	Asb1	Mus musculus ankyrin repeat and SOCS box-containing 1 (Asb1),	65247	247	246	289	289
ASB12	Asb12	Mus musculus ankyrin repeat and SOCS box-containing protein 12	70392	139	150	162	139

ASB2	Asb2	Mus musculus ankyrin repeat and SOCS box-containing 2 (Asb2),	65256	1326	565	574	642
ASF1A	Asf1a	Mus musculus ASF1 anti-silencing function 1 homolog A (S. cerevisiae)	66403	123	130	128	126
ATG3	Atg3	Mus musculus autophagy-related 3 (yeast) (Atg3), mRNA.	67841	837	910	1193	1295
ATL2	Atl2	Mus musculus atlastin GTPase 2 (Atl2), transcript variant 2, mRNA.	56298	829	833	660	654
ATM	Atm	Mus musculus ataxia telangiectasia mutated homolog (human) (Atm),	11920	352	271	227	299
ATP2B4	Atp2b4	Mus musculus ATPase, Ca++ transporting, plasma membrane 4	381290	145	134	148	143
ATP5C1	Atp5c1	Mus musculus ATP synthase, H+ transporting, mitochondrial F1	11949	15507	12305	10700	11114
ATP5G3	Atp5g3	Mus musculus ATP synthase, H+ transporting, mitochondrial F0	228033	25737	28655	21329	23341
ATP5J	Atp5j	Mus musculus ATP synthase, H+ transporting, mitochondrial F0	11957	592	777	658	665
ATP5J2	Atp5j2	Mus musculus ATP synthase, H+ transporting, mitochondrial F0	57423	22372	22435	16492	17707
ATP5S	Atp5s	Mus musculus ATP synthase, H+ transporting, mitochondrial F0	68055	548	389	381	412
ATP6V0D1	Atp6v0d1	Mus musculus ATPase, H+ transporting, lysosomal V0 subunit D1	11972	2726	2659	2589	2486
ATPIF1	Atpif1	Mus musculus ATPase inhibitory factor 1 (Atpif1), nuclear gene	11983	17707	15261	14113	12908
ATXN10	Atxn10	Mus musculus ataxin 10 (Atxn10), mRNA.	54138	423	425	625	518
AU022508	AU022508			1327	956	1021	1112
AU044581	AU044581			123	125	135	129
AVPI1	Avpi1	Mus musculus arginine vasopressin-induced 1 (Avpi1), mRNA.	69534	319	483	426	416
AVPI1	Avpi1	Mus musculus arginine vasopressin-induced 1 (Avpi1), mRNA.	69534	180	256	237	220
AW538212	AW538212			137	143	131	145
AXL	Axl	Mus musculus AXL receptor tyrosine kinase(Axl), mRNA.	26362	1992	2974	3726	2625
AXL	Axl			124	125	134	137
B130064M22	B130064M22Ri			145	140	133	125
B230208L21R	B230208L21Ri			129	132	136	126
B230217C12	B230217C12Ri			123	126	128	112
B230220B15	B230220B15Ri			122	118	126	123
B230327L12R	B230327L12Ri			130	160	138	141
B230333P14	B230333P14Ri			131	130	144	125
B230339M05	B230339M05R	Mus musculus RIKEN cDNA B230339M05 gene (B230339M05Rik),	228850	1380	977	1139	1189
B230387C07	B230387C07Ri			640	367	283	327
B2M	B2m	Mus musculus beta-2 microglobulin (B2m), mRNA.	12010	12857	21447	18367	21273
B3GALNT1	B3galnt1	Mus musculus UDP-GalNAc:betaGlcNAc beta 1,3-	26879	266	293	390	319
B3GALNT2	B3galnt2	Mus musculus UDP-GalNAc:betaGlcNAc beta 1,3-	97884	549	423	436	510
B3GNT9	B3gnt9	Mus musculus UDP-GlcNAc:betaGal beta-1,3-N-	97440	362	410	518	535
B430202L17R	B430202L17Ri			182	152	137	148

B430216N15	B430216N15			235	202	214	186
B430306N03	B430306N03	Mus musculus RIKEN cDNA B430306N03 gene (B430306N03Rik),	320148	129	141	145	145
B430320O11	B430320O11			117	132	125	140
B4GALNT3	B4galnt3	Mus musculus beta-1,4-N-acetyl-galactosaminyl transferase 3	330406	185	168	160	155
B4GALNT4	B4galnt4	Mus musculus beta-1,4-N-acetyl-galactosaminyl transferase 4	330671	137	162	140	145
B4GALT5	B4galt5	Mus musculus UDP-Gal:betaGlcNAc beta 1,4-galactosyltransferase,	56336	175	163	159	164
B930007L02	B930007L02R			610	518	509	547
B930095G15	B930095G15R			250	171	176	185
BAG5	Bag5	Mus musculus BCL2-associated athanogene 5 (Bag5), mRNA.	70369	499	563	642	594
BAI3	Bai3	Mus musculus brain-specific angiogenesis inhibitor 3 (Bai3), mRNA.	210933	170	153	183	143
BANK1	Bank1	Mus musculus B-cell scaffold protein with ankyrin repeats 1	242248	131	124	143	152
BAT2D	Bat2d	Mus musculus BAT2 domain containing 1 (Bat2d), mRNA.	226562	147	135	142	159
BAZ1A	Baz1a	PREDICTED: Mus musculus bromodomain adjacent to zinc finger	217578	159	206	188	239
BAZ2A	Baz2a	Mus musculus bromodomain adjacent to zinc finger domain, 2A	116848	151	141	125	126
BC003324	BC003324			210	351	430	377
BC004044	BC004044	Mus musculus cDNA sequence BC004044 (BC004044), mRNA.	80752	145	166	163	183
BC005682	BC005682			369	434	526	530
BC021614	BC021614	Mus musculus cDNA sequence BC021614 (BC021614), mRNA.	225884	217	494	382	387
BC030499	BC030499	Mus musculus cDNA sequence BC030499 (BC030499), mRNA.	216976	485	456	350	348
BC034090	BC034090	PREDICTED: Mus musculus cDNA sequence BC034090, transcript	207792	224	208	244	231
BC037112	BC037112	Mus musculus cDNA sequence BC037112 (BC037112), mRNA.	231128	144	144	128	124
BC039210	BC039210	PREDICTED: Mus musculus cDNA sequence BC039210 (BC039210),	234839	225	349	362	433
BC039632	BC039632	Mus musculus cDNA sequence BC039632 (BC039632), mRNA.	330657	154	134	133	146
BC042720	BC042720	PREDICTED: Mus musculus cDNA sequence BC042720 (BC042720),	329178	133	128	128	138
BC094274	BC094274	Mus musculus cDNA sequence BC094274 (BC094274), mRNA.	227717	139	130	134	134
BCAM	Bcam	Mus musculus basal cell adhesion molecule (Bcam), mRNA.	57278	144	136	131	148
BCCIP	Bccip	Mus musculus BRCA2 and CDKN1A interacting protein (Bccip),	66165	2189	2039	1587	1799
BCCIP	Bccip			134	126	119	124
BCL11A	Bcl11a	Mus musculus B-cell CLL/lymphoma 11A (zinc finger protein)	14025	225	169	191	191
BCL6B	Bcl6b	Mus musculus B-cell CLL/lymphoma 6, member B (Bcl6b), mRNA.	12029	133	139	154	149
BCR	Bcr	Mus musculus breakpoint cluster region homolog (Bcr), mRNA.	110279	303	343	421	328
BDNF	Bdnf	Mus musculus brain derived neurotrophic factor (Bdnf), transcript	12064	122	128	129	136
BEST1	Best1	Mus musculus bestrophin 1 (Best1), mRNA.	24115	162	188	227	180
BEX4	Bex4	Mus musculus brain expressed gene 4 (Bex4), mRNA.	406217	632	185	180	167

BEX4	Bex4	Mus musculusbrain expressed gene 4 (Bex4), mRNA.	406217	263	159	149	152
BGN	Bgn	Mus musculus biglycan (Bgn), mRNA.	12111	5024	6667	8843	9221
BICC1	Bicc1	Mus musculus bicaudal C homolog 1 (Drosophila) (Bicc1), mRNA.	83675	639	1217	1787	1262
BIN1	Bin1	Mus musculus bridging integrator 1 (Bin1), transcript variant 2,	30948	139	134	149	145
BMP1	Bmp1	Mus musculus bone morphogenetic protein 1 (Bmp1), mRNA.	12153	208	277	332	296
BMP1	Bmp1	Mus musculus bone morphogenetic protein 1 (Bmp1), mRNA.	12153	211	331	373	372
BNIP1	Bnip1	Mus musculus BCL2/adenovirus E1B interacting protein 1 (Bnip1),	224630	415	435	324	368
BPHL	Bphl	Mus musculus biphenyl hydrolase-like (serine hydrolase, breast	68021	131	128	120	121
BPTF	Bptf	Mus musculus bromodomain PHD finger transcription factor (Bptf),	207165	400	343	488	455
BRAF	Braf	Mus musculus Braf transforming gene (Braf), mRNA.	109880	120	126	128	119
BRCA2	Brca2	Mus musculus breast cancer 2 (Brca2), transcript variant 1, mRNA.	12190	129	149	136	141
BRPF1	Brpf1	Mus musculus bromodomain and PHD finger containing, 1 (Brpf1),	78783	476	571	678	612
BRUNOL4	Brunol4	Mus musculus bruno-like 4, RNA binding protein (Drosophila)	108013	135	145	138	149
C030003M13	C030003M13R			132	134	156	139
C030014K22	C030014K22Ri	Mus musculus RIKEN cDNA C030014K22 gene (C030014K22Rik),	226610	130	129	143	140
C030034I22RI	C030034I22Ri	PREDICTED: Mus musculus RIKEN cDNA C030034I22 gene	77533	309	303	229	239
C130020N16	C130020N16Ri			148	143	159	152
C130022E19R	C130022E19Ri			655	471	328	626
C130032N06	C130032N06Ri			132	139	140	143
C130038G02	C130038G02Ri	Mus musculus RIKEN cDNA C130038G02 gene (C130038G02Rik),	77521	147	133	141	142
C130042F01R	C130042F01Ri			124	125	141	140
C130067A03	C130067A03Ri			220	219	167	191
C130099A20	C130099A20Ri			191	148	151	172
C1QTNF7	C1qtnf7	Mus musculus C1q and tumor necrosis factor related protein 7	109323	140	148	162	162
C1S	C1s	Mus musculus complement component 1, s subcomponent (C1s),	50908	190	332	492	508
C230012O17	C230012O17Ri			137	130	130	121
C230040G06	C230040G06	PREDICTED: Mus musculus hypothetical protein C230040G06	327749	135	132	130	121
C230077C18	C230077C18Ri			133	129	135	120
C230078M08	C230078M08R	Mus musculus RIKEN cDNA C230078M08 gene (C230078M08Rik),	319749	446	247	215	311
C3	C3			1948	7773	10860	11389
C330002I19RI	C330002I19Ri	PREDICTED: Mus musculus RIKEN cDNA C330002I19 gene, transcript	77480	120	130	132	140
C330005L02R	C330005L02Ri			209	165	155	171
C330016O10	C330016O10Ri			133	140	146	171
C330019G07	C330019G07Ri	Mus musculus RIKEN cDNA C330019G07 gene (C330019G07Rik),	215476	162	174	142	154

C330023M	C330023M0	Mus musculus RIKEN cDNA C330023M02 gene	231713	362	602	592	494
C430049B	C430049B0			131	125	123	118
C4A	C4a	Mus musculus complement component 4A (Rodgers blood	625018	502	1879	2622	2730
C4A	C4a	Mus musculus complement component 4A (Rodgers blood	625018	591	1912	2593	2517
C530008M	C530008M1	PREDICTED: Mus musculus RIKEN cDNA C530008M17	320827	579	400	373	517
C530030I18	C530030I18			133	123	135	128
C6	C6	Mus musculus complement component 6 (C6), mRNA.	12274	132	193	167	173
C630001G	C630001G2			161	150	138	136
C630011I2	C630011I23			132	155	139	146
C730004I03	C730004I03			126	132	132	142
C730026J1	C730026J16			1072	756	696	975
C730048C	C730048C1	Mus musculus RIKEN cDNA C730048C13 gene	319800	122	128	141	131
C76746	C76746			120	128	135	146
CACNA1C	Cacna1c			136	146	141	141
CALB2	Calb2	Mus musculus calbindin 2 (Calb2), mRNA.	12308	237	149	186	165
CAMK2D	Camk2d			122	124	127	133
CAMK2N2	Camk2n2	PREDICTED: Mus musculus calcium/calmodulin-dependent	73047	467	612	715	726
CAMK4	Camk4			267	170	163	180
CAMSAP1	Camsap1	PREDICTED: Mus musculus calmodulin regulated spectrin-	227634	122	120	130	140
CAND1	Cand1	PREDICTED: Mus musculus cullin associated and	71902	243	186	182	212
CAPG	Capg	Mus musculus capping protein (actin filament), gelsolin-	12332	162	300	378	336
CAPN1	Capn1	Mus musculus calpain 1 (Capn1), mRNA.	12333	147	148	160	158
CAPSL	Capsl	Mus musculus calcyphosine-like (Capsl), mRNA.	75568	435	159	136	150
CAPZA2	Capza2	Mus musculus capping protein (actin filament) muscle Z-	12343	132	131	138	144
CAR1	Car1	Mus musculus carbonic anhydrase 1 (Car1), transcript	12346	23809	16771	11740	14068
CAR14	Car14	Mus musculus carbonic anhydrase 14 (Car14), mRNA.	23831	191	175	191	152
CAR3	Car3	Mus musculus carbonic anhydrase 3 (Car3), mRNA.	12350	440	202	130	243
CASP1	Casp1	Mus musculus caspase 1 (Casp1), mRNA.	12362	11434	9485	7238	8995
CASP6	Casp6	Mus musculus caspase 6 (Casp6), mRNA.	12368	627	696	705	734
CASP9	Casp9			209	182	168	179
CBFA2T2	Cbfa2t2	Mus musculus core-binding factor, runt domain, alpha	12396	136	157	147	153
CBLN3	Cbln3	Mus musculus cerebellin 3 precursor protein (Cbln3),	56410	118	120	132	124
CBLN3	Cbln3	Mus musculus cerebellin 3 precursor protein (Cbln3),	56410	129	122	127	120
CCBL2	Ccbl2	Mus musculus cysteine conjugate-beta lyase 2 (Ccbl2),	229905	160	136	159	144
CCDC155	Ccdc155	Mus musculus coiled-coil domain containing 155	384619	148	130	122	129
CCDC32	Ccdc32	Mus musculus coiled-coil domain containing 32	269336	1834	1628	1302	1619
CCDC47	Ccdc47	Mus musculus coiled-coil domain containing 47	67163	1126	1056	759	1002
CCDC62	Ccdc62	PREDICTED: Mus musculus coiled-coil domain	208908	152	141	134	145
CCDC93	Ccdc93	Mus musculus coiled-coil domain containing 93	70829	141	182	192	160
CCNB3	Ccnb3			138	134	123	122
CCNO	Ccno	Mus musculus cyclin O (Ccno), mRNA.	218630	128	210	256	170

CCNT2	Ccnt2			202	184	209	237
CCRN4L	Ccrn4l	Mus musculus CCR4 carbon catabolite repression 4-like	12457	555	284	345	341
CD14	Cd14	Mus musculus CD14 antigen (Cd14), mRNA.	12475	781	2997	2975	2289
CD200	Cd200			206	280	297	239
CD226	Cd226	Mus musculus CD226 antigen (Cd226), transcript variant	225825	116	126	147	147
CD247	Cd247	Mus musculus CD247 antigen (Cd247), mRNA.	12503	130	145	141	148
CD38	Cd38	Mus musculus CD38 antigen (Cd38), mRNA.	12494	168	265	210	201
CD44	Cd44	Mus musculus CD44 antigen (Cd44), transcript variant 2,	12505	128	137	158	169
CD44	Cd44			174	141	148	136
CD52	Cd52			364	717	1475	1763
CD84	Cd84			146	195	159	202
CD93	Cd93	Mus musculus CD93 antigen (Cd93), mRNA.	17064	343	587	811	826
CDC14A	Cdc14a	Mus musculus CDC14 cell division cycle 14 homolog A	229776	389	276	261	289
CDC25C	Cdc25c	Mus musculus cell division cycle 25 homolog C (S.	12532	121	118	117	126
CDC42EP1	Cdc42ep	Mus musculus CDC42 effector protein (Rho GTPase	104445	291	263	327	283
CDC42EP3	Cdc42ep	Mus musculus CDC42 effector protein (Rho GTPase	260409	1322	856	889	956
CDCA7	Cdca7	Mus musculus cell division cycle associated 7 (Cdca7),	66953	2178	1035	604	1513
CDH12	Cdh12	Mus musculus cadherin 12 (Cdh12), mRNA.	215654	138	140	126	119
CDK6	Cdk6	Mus musculus cyclin-dependent kinase 6 (Cdk6), mRNA.	12571	138	138	126	126
CDKL1	Cdkl1	Mus musculus cyclin-dependent kinase-like 1 (CDC2-	71091	135	127	132	147
CDKN1A	Cdkn1a	Mus musculus cyclin-dependent kinase inhibitor 1A	12575	838	570	462	434
CDR2L	Cdr2l	Mus musculus cerebellar degeneration-related protein	237988	186	236	258	280
CEACAM3	Ceacam3	PREDICTED: Mus musculus carcinoembryonic antigen-	384557	127	134	121	128
CEBPD	Cebpd	Mus musculus CCAAT/enhancer binding protein	12609	122	123	157	143
CEP250	Cep250	Mus musculus centrosomal protein 250 (Cep250),	16328	133	142	126	133
CEP350	Cep350	PREDICTED: Mus musculus centrosomal protein 350,	74081	152	156	140	143
CFB	Cfb	Mus musculus complement factor B (Cfb), mRNA.	14962	618	821	1382	1231
CFD	Cfd	Mus musculus complement factor D (adipsin) (Cfd),	11537	4824	1767	5434	1847
CHAC1	Chac1	Mus musculus ChaC, cation transport regulator-like 1	69065	181	389	336	316
CHD1	Chd1	Mus musculus chromodomain helicase DNA binding	12648	206	236	192	219
CHORDC1	Chordc1	Mus musculus cysteine and histidine-rich domain	66917	1301	1046	745	1334
CHRNA7	Chrna7	Mus musculus cholinergic receptor, nicotinic, alpha	11441	131	146	141	134
CHST11	Chst11	Mus musculus carbohydrate sulfotransferase 11	58250	124	146	160	157
CHST9	Chst9	Mus musculus carbohydrate (N-acetylgalactosamine 4-	71367	144	126	123	119
CHURC1	Churc1	Mus musculus churchill domain containing 1 (Churc1),	211151	1400	1941	1810	1674

CIB2	Cib2	Mus musculus calcium and integrin binding family	56506	387	320	348	266
CIDEA	Cidea	Mus musculus cell death-inducing DNA fragmentation	12683	147	154	145	140
CISH	Cish	Mus musculus cytokine inducible SH2-containing	12700	927	597	702	561
CKM	Ckm	Mus musculus creatine kinase, muscle (Ckm), mRNA.	12715	210	136	158	148
CKMT1	Ckmt1			2531	1180	1019	1639
CLA3	Cla3			155	168	154	164
CLDN10	Cldn10	Mus musculus claudin 10 (Cldn10), transcript variant 1,	58187	141	239	247	201
CLEC14A	Clec14a	Mus musculus C-type lectin domain family 14, member	66864	169	136	128	137
CLECSF12	Clecsf12			156	242	261	290
CLECSF9	Clecsf9			160	337	290	265
CLIP1	Clip1	Mus musculus CAP-GLY domain containing linker	56430	269	285	326	304
CLOCK	Clock	Mus musculus circadian locomoter output cycles kaput	12753	2511	1710	1244	1756
CLPS	Clps	Mus musculus colipase, pancreatic (Clps), mRNA.	109791	916	10152	5829	332
CLPX	Clpx	Mus musculus caseinolytic peptidase X (E.coli) (Clpx),	270166	409	362	323	346
CMA2	Cma2	Mus musculus chymase 2, mast cell (Cma2), mRNA.	545055	125	143	147	182
CMKBR2	Cmkbr2			140	175	172	190
CML5	Cml5	Mus musculus camello-like 5 (Cml5), mRNA.	69049	130	143	132	125
CNFN	Cnfn	Mus musculus cornifelin (Cnfn), transcript variant 2,	72383	138	158	142	138
CNKSR3	Cnksr3	Mus musculus Cnksr family member 3 (Cnksr3), mRNA.	215748	258	201	248	178
CNN1	Cnn1	Mus musculus calponin 1 (Cnn1), mRNA.	12797	202	157	157	142
CNOT8	Cnot8	Mus musculus CCR4-NOT transcription complex,	69125	145	137	133	118
CNPY1	Cnpy1	Mus musculus canopy 1 homolog (zebrafish) (Cnpy1),	269637	120	123	130	126
CNPY2	Cnpy2	Mus musculus canopy 2 homolog (zebrafish) (Cnpy2),	56530	2876	2245	2499	2518
CNTN3	Cntn3			134	138	143	150
COG8	Cog8			1414	1284	1201	1039
COL12A1	Col12a1	Mus musculus collagen, type XII, alpha 1 (Col12a1),	12816	196	340	535	502

COL12A1	Col12a1	Mus musculus collagen, type XII, alpha 1 (Col12a1), mRNA.	12816	393	624	717	730
COL1A1	Col1a1			400	1089	1268	1458
COL1A2	Col1a2	Mus musculus collagen, type I, alpha 2 (Col1a2), mRNA.	12843	363	751	1104	1154
COL3A1	Col3a1	Mus musculus collagen, type III, alpha 1 (Col3a1), mRNA.	12825	1000	2100	3857	3933
COL4A1	Col4a1	Mus musculus procollagen, type IV, alpha 1 (Col4a1), mRNA.	12826	1982	4890	7046	6713
COL4A2	Col4a2	Mus musculus collagen, type IV, alpha 2 (Col4a2), mRNA.	12827	799	2256	3428	3508
COL4A6	Col4a6	Mus musculus procollagen, type IV, alpha 6 (Col4a6), mRNA.	94216	135	132	115	131
COL5A2	Col5a2			174	221	287	300
COL6A2	Col6a2			192	222	251	236
COL6A3	Col6a3	Mus musculus procollagen, type VI, alpha 3 (Col6a3), mRNA.	12835	2181	2926	3470	4065
COL9A1	Col9a1			124	130	133	122
COPE	Cope	Mus musculus coatomer protein complex, subunit epsilon (Cope),	59042	1276	1623	1405	1441
COPS5	Cops5	Mus musculus COP9 (constitutive photomorphogenic) homolog,	26754	1974	2385	2024	2153
COQ10B	Coq10b	Mus musculus coenzyme Q10 homolog B (S. cerevisiae) (Coq10b),	67876	1062	866	766	855
COQ2	Coq2	Mus musculus coenzyme Q2 homolog, prenyltransferase (yeast)	71883	2676	2023	2392	2333
COQ9	Coq9	Mus musculus coenzyme Q9 homolog (yeast) (Coq9), mRNA.	67914	1234	1046	853	829
CORO1A	Coro1a	Mus musculus coronin, actin binding protein 1A (Coro1a), mRNA.	12721	211	436	562	466
COX17	Cox17	Mus musculus cytochrome c oxidase, subunit XVII assembly protein	12856	5609	5174	4351	4477
COX6B1	Cox6b1	Mus musculus cytochrome c oxidase, subunit VIb polypeptide 1	110323	16412	16412	12352	12083
CPHX	Cphx	Mus musculus cytoplasmic polyadenylated homeobox (Cphx), mRNA.	105594	150	136	123	133
CPNE2	Cpne2	Mus musculus copine II (Cpne2), mRNA.	234577	395	557	705	612
CRAT	Crat	Mus musculus carnitine acetyltransferase (Crat), nuclear gene	12908	138	162	162	146
CRBN	Crbn			150	144	155	140
CREG2	Creg2	Mus musculus cellular repressor of E1A-stimulated genes 2 (Creg2),	263764	137	126	149	124
CRK	Crk	Mus musculus v-crk sarcoma virus CT10 oncogene homolog (avian)	12928	4432	3735	2654	3811
CRMP1	Crmp1	Mus musculus collapsin response mediator protein 1 (Crmp1),	12933	164	132	138	145
CRSP3	Crsp3			127	130	143	128
CRYZ	Cryz	Mus musculus crystallin, zeta (Cryz), mRNA.	12972	359	289	246	230
CSF2RB2	Csf2rb2	Mus musculus colony stimulating factor 2 receptor, beta 2, low-	12984	145	208	239	244

CSF3R	Csf3r	Mus musculus colony stimulating factor 3 receptor (granulocyte)	12986	132	275	338	385
CSF3R	Csf3r	Mus musculus colony stimulating factor 3 receptor (granulocyte)	12986	140	206	191	244
CSF3R	Csf3r	Mus musculus colony stimulating factor 3 receptor (granulocyte)	12986	118	140	136	162
CSNK1D	Csnk1d	Mus musculus casein kinase 1, delta (Csnk1d), transcript variant 2,	104318	835	1205	1293	1053
CSNK1D	Csnk1d	Mus musculus casein kinase 1, delta (Csnk1d), transcript variant 2,	104318	910	1216	1417	1046
CSNK1G2	Csnk1g2	Mus musculus casein kinase 1, gamma 2 (Csnk1g2), mRNA.	103236	6916	5776	5679	5262
CTHRC1	Cthrc1	Mus musculus collagen triple helix repeat containing 1 (Cthrc1),	68588	133	129	117	129
CTNNA3	Ctnna3	Mus musculus catenin (cadherin associated protein), alpha 3	216033	135	123	134	122
CTPS	Ctps	Mus musculus cytidine 5'-triphosphate synthase (Ctps), mRNA.	51797	597	1673	1981	1577
CTSB	Ctsb	Mus musculus cathepsin B (Ctsb), mRNA.	13030	11260	13960	15731	18454
CTSC	Ctsc	Mus musculus cathepsin C (Ctsc), mRNA.	13032	2784	4315	3806	4996
CTSC	Ctsc	Mus musculus cathepsin C (Ctsc), mRNA.	13032	1032	1713	1753	2096
CTSK	Ctsk	Mus musculus cathepsin K (Ctsk), mRNA.	13038	478	998	1192	1032
CUL7	Cul7	Mus musculus cullin 7 (Cul7), mRNA.	66515	476	518	698	568
CXADR	Cxadr	Mus musculus coxsackie virus and adenovirus receptor (Cxadr),	13052	3408	1668	1560	2403
CXADR	Cxadr			2299	1169	980	1443
CXCL17	Cxcl17	Mus musculus chemokine (C-X-C motif) ligand 17 (Cxcl17), mRNA.	232983	135	142	151	134
CXCL2	Cxcl2	Mus musculus chemokine (C-X-C motif) ligand 2 (Cxcl2), mRNA.	20310	124	917	656	296
CXCL2	Cxcl2			135	2858	2357	887
CXCR4	Cxcr4			160	270	364	269
CXCR6	Cxcr6	Mus musculus chemokine (C-X-C motif) receptor 6 (Cxcr6), mRNA.	80901	125	157	143	167
CYB5	Cyb5	Mus musculus cytochrome b-5 (Cyb5), mRNA.	109672	1305	1291	1589	1623
CYB5B	Cyb5b	Mus musculus cytochrome b5 type B (Cyb5b), mRNA.	66427	6673	4806	4203	4881
CYBB	Cybb			125	128	146	143
CYHR1	Cyhr1			257	263	224	206
CYP2B19	Cyp2b19			134	131	129	144
CYP2D34	Cyp2d34	Mus musculus cytochrome P450, family 2, subfamily d, polypeptide	223706	1584	931	1006	1082
CYP2J5	Cyp2j5	Mus musculus cytochrome P450, family 2, subfamily j, polypeptide 5	13109	122	127	122	117
CYP2J9	Cyp2j9	Mus musculus cytochrome P450, family 2, subfamily j, polypeptide 9	74519	313	246	260	215
CYP4B1	Cyp4b1	Mus musculus cytochrome P450, family 4, subfamily b, polypeptide 1	13120	172	153	139	143

CYTIP	Cytip	Mus musculus cytohesin 1 interacting protein (Cytip), mRNA.	227929	929	2110	1807	1329
D030022P06	D030022P06R			197	192	203	231
D030028O16	D030028O16R			472	341	381	422
D030049F17	D030049F17			127	134	123	123
D030065J16R	D030065J16Ri			140	135	121	127
D10BWG137	D10Bwg1379e			270	224	192	196
D10ERTD516	D10Ertd516e			291	203	197	224
D130011K02	D130011K02R			137	121	126	131
D130035C10	D130035C10Ri			120	120	125	128
D130059C03	D130059C03R			119	137	130	139
D130065A14	D130065A14Ri			125	129	132	118
D130084E01	D130084E01R			139	152	163	169
D15MGI27	D15Mgi27	Mus musculus DNA Segment, Chr 15, Mouse Genome Informatics 27	106073	749	906	1164	1007
D15MIT260	D15Mit260			763	725	934	928
D230028J12R	D230028J12Ri			127	139	127	136
D2BWG1423	D2Bwg1423e	PREDICTED: Mus musculus DNA segment, Chr 2, Brigham & Women's	329372	174	165	174	179
D330001K12	D330001K12R			151	129	145	141
D330005C11	D330005C11R			133	128	141	143
D330008E13	D330008E13R			138	141	146	152
D330014H01	D330014H01R			142	151	170	157
D330017J20R	D330017J20Ri	Mus musculus RIKEN cDNA D330017J20 gene (D330017J20Rik),	320609	238	199	168	179
D330030P06	D330030P06R			135	129	147	148
D330036A12	D330036A12Ri			133	131	147	148
D330038K10	D330038K10R			238	188	160	194
D330038O06	D330038O06	Mus musculus RIKEN cDNA D330038O06 gene (D330038O06Rik),	330788	175	162	150	185
D330045A20	D330045A20Ri	Mus musculus RIKEN cDNA D330045A20 gene (D330045A20Rik),	102871	396	220	160	205
D330045A20	D330045A20Ri	Mus musculus RIKEN cDNA D330045A20 gene (D330045A20Rik),	102871	323	198	148	178
D430006B11	D430006B11Ri			125	114	119	118
D430006M22	D430006M22			135	141	144	154
D430036O16	D430036O16R			157	155	138	138

D630003M21	D630003M21	Mus musculus RIKEN cDNA D630003M21 gene (D630003M21Rik),	228846	158	133	137	153
D630013G24	D630013G24R			768	465	319	432
D6ERTD160E	D6Ertd160e			122	126	123	130
D730020K15	D730020K15R			125	143	133	141
D830007F02	D830007F02R	Mus musculus RIKEN cDNA D830007F02 gene (D830007F02Rik),	213435	135	131	141	121
D930026K06	D930026K06R			130	134	138	126
D930044C15	D930044C15R			151	132	141	130
DACH1	Dach1			120	116	137	129
DACH2	Dach2			157	146	129	132
DAPK1	Dapk1	Mus musculus death associated protein kinase 1 (Dapk1), transcript	69635	159	182	212	168
DCT	Dct	Mus musculus dopachrome tautomerase (Dct), mRNA.	13190	139	125	128	137
DCT	Dct	Mus musculus dopachrome tautomerase (Dct), mRNA.	13190	142	127	134	125
DCTN3	Dctn3	Mus musculus dynactin 3 (Dctn3), mRNA.	53598	1661	1881	1445	1637
DDC	Ddc	Mus musculus dopa decarboxylase (Ddc), mRNA.	13195	2473	1138	902	1443
DDC	Ddc			1841	819	652	713
DDIT4	Ddit4	Mus musculus DNA-damage-inducible transcript 4 (Ddit4), mRNA.	74747	842	2328	3005	1658
DDO	Ddo	Mus musculus D-aspartate oxidase (Ddo), mRNA.	70503	214	150	168	165
DDX1	Ddx1	Mus musculus DEAD (Asp-Glu-Ala-Asp) box polypeptide 1 (Ddx1),	104721	1621	2028	1766	2147
DDX1	Ddx1	Mus musculus DEAD (Asp-Glu-Ala-Asp) box polypeptide 1 (Ddx1),	104721	1213	1413	1465	1533
DDX10	Ddx10	PREDICTED: Mus musculus DEAD (Asp-Glu-Ala-Asp) box	77591	258	269	214	225
DECR1	Decr1	Mus musculus 2,4-dienoyl CoA reductase 1, mitochondrial	67460	335	232	190	213
DECR2	Decr2			290	277	214	231
DEF6	Def6	Mus musculus differentially expressed in FDCP 6 (Def6), mRNA.	23853	157	200	228	195
DEFB6	Defb6	Mus musculus defensin beta 6 (Defb6), mRNA.	116746	139	150	138	126
DEFCR3	Defcr3	Mus musculusdefensin related cryptdin 3 (Defcr3), mRNA.	13237	129	137	147	133
DENND4C	Dennd4c	Mus musculus DENN/MADD domain containing 4C (Dennd4c),	329877	130	121	129	143
DERL2	Derl2	Mus musculus Der1-like domain family, member 2 (Derl2), mRNA.	116891	414	575	754	705
DES	Des	Mus musculus desmin (Des), mRNA.	13346	10809	4014	5155	4566
DGKH	Dgkh	Mus musculus diacylglycerol kinase, eta (Dgkh), mRNA.	380921	315	182	196	226
DICER1	Dicer1	Mus musculus Dicer1, Dcr-1 homolog (Drosophila) (Dicer1),	192119	428	340	388	495

DIO1	Dio1	Mus musculus deiodinase, iodothyronine, type I (Dio1), mRNA.	13370	640	262	196	203
DKK4	Dkk4	Mus musculus dickkopf homolog 4 (Xenopus laevis) (Dkk4),	234130	133	134	125	120
DLAT	Dlat	Mus musculus dihydrolipoamide S-acetyltransferase (E2	235339	458	282	284	297
DLX5	Dlx5	Mus musculus distal-less homeobox 5 (Dlx5), transcript variant 1,	13395	135	136	128	129
DMP1	Dmp1	Mus musculus dentin matrix protein 1 (Dmp1), mRNA.	13406	135	122	126	121
DMRT3	Dmrt3	Mus musculus doublesex and mab-3 related transcription factor	240590	131	122	139	123
DNAJB12	Dnajb12	Mus musculus DnaJ (Hsp40) homolog, subfamily B, member 12	56709	314	354	380	298
DNAJB14	Dnajb14	PREDICTED: Mus musculus DnaJ (Hsp40) homolog, subfamily B,	70604	126	115	116	120
DNM1L	Dnm1l			402	411	371	535
DOCK2	Dock2			126	123	136	153
DOCK8	Dock8	Mus musculus dedicator of cytokinesis 8 (Dock8), mRNA.	76088	142	169	191	184
DOK5	Dok5	Mus musculus docking protein 5 (Dok5), mRNA.	76829	138	135	141	148
DPH1	Dph1	Mus musculus DPH1 homolog (S. cerevisiae) (Dph1), mRNA.	116905	649	951	870	851
DPH2L1	Dph2l1			562	835	714	713
DPYD	Dpyd	Mus musculus dihydropyrimidine dehydrogenase (Dpyd), mRNA.	99586	193	135	151	132
DTWD1	Dtwd1	Mus musculus DTW domain containing 1 (Dtwd1), mRNA.	69185	353	295	308	268
DTX2	Dtx2	Mus musculus deltex 2 homolog (Drosophila) (Dtx2), mRNA.	74198	581	675	863	645
DUB1A	Dub1a	Mus musculus deubiquitinating enzyme 1a (Dub1a), mRNA.	381944	129	132	138	127
DUOX2	Duox2	Mus musculus dual oxidase 2 (Duox2), mRNA.	214593	164	360	525	445
DUSP1	Dusp1	Mus musculus dual specificity phosphatase 1 (Dusp1), mRNA.	19252	2083	7060	6579	3744
DUSP10	Dusp10	Mus musculus dual specificity phosphatase 10 (Dusp10), mRNA.	63953	153	153	163	169
DUSP16	Dusp16	Mus musculus dual specificity phosphatase 16 (Dusp16), transcript	70686	1417	1117	1048	998
DUSP28	Dusp28	Mus musculus dual specificity phosphatase 28 (Dusp28), mRNA.	67446	339	256	222	250
DXBWG1396	DXBwg1396e			137	137	165	145
DYSF	Dysf	Mus musculusdysferlin (Dysf), transcript variant 1, mRNA.	26903	317	388	519	431
E030024M20	E030024M20Ri			132	137	142	139
E030028L09R	E030028L09Ri			168	146	153	167
E030030I06RI	E030030I06Rik	PREDICTED: Mus musculus RIKEN cDNA E030030I06 gene, transcript	319887	191	164	206	211
E030034P13R	E030034P13Ri			188	225	254	292

E030040P03R	E030040P03Ri			253	187	213	260
E130014H08	E130014H08Ri			141	148	130	125
E130119H03	E130119H03Ri			128	126	133	141
E230027K01R	E230027K01Ri			337	288	268	299
E2F3	E2f3	Mus musculus E2F transcription factor 3 (E2f3), mRNA.	13557	272	242	235	196
E2F3	E2f3			209	167	190	196
E330022G21	E330022G21Ri			157	134	162	152
E330034G19	E330034G19Ri	Mus musculus RIKEN cDNA E330034G19 gene (E330034G19Rik),	105418	142	119	136	124
E330035H20	E330035H20Ri			148	228	221	185
E330037N20	E330037N20Ri			133	135	142	150
E430002G05	E430002G05Ri			606	318	434	407
E430002G05	E430002G05Ri	Mus musculus RIKEN cDNA E430002G05 gene (E430002G05Rik),	210622	586	326	379	332
E430013K19R	E430013K19Ri			118	126	130	131
E530011J04RI	E530011J04Ri			127	131	128	123
E530018N03	E530018N03Ri			129	123	122	129
EBPL	Ebpl	Mus musculus emopamil binding protein-like (Ebpl), mRNA.	68177	422	318	280	272
ECEL1	Ecel1	Mus musculus endothelin converting enzyme-like 1 (Ecel1), mRNA.	13599	138	124	123	128
ECHDC1	Echdc1			198	185	161	176
EDN1	Edn1	Mus musculus endothelin 1 (Edn1), mRNA.	13614	2206	916	936	670
EDNRA	Ednra	Mus musculus endothelin receptor type A (Ednra), mRNA.	13617	698	1195	1426	1354
EFCAB2	Efcab2	Mus musculus EF-hand calcium binding domain 2 (Efcab2), mRNA.	68226	138	131	134	146
EFCAB2	Efcab2	Mus musculus EF-hand calcium binding domain 2 (Efcab2), mRNA.	68226	132	123	119	120
EG224572	EG224572	PREDICTED: Mus musculus predicted gene, EG224572 (EG224572),	224572	128	120	130	127
EG236892	EG236892	PREDICTED: Mus musculus predicted gene, EG236892 (EG236892),	236892	140	128	144	130
EG237361	EG237361	PREDICTED: Mus musculus predicted gene, EG237361 (EG237361),	237361	2793	3210	3749	3361
EG240038	EG240038	PREDICTED: Mus musculus predicted gene, EG240038, transcript	240038	248	222	169	198
EG245190	EG245190	PREDICTED: Mus musculus predicted gene, EG245190 (EG245190),	245190	251	269	292	313
EG269105	EG269105	PREDICTED: Mus musculus predicted gene, EG269105 (EG269105),	269105	19339	19339	15507	16594
EG317677	EG317677	Mus musculus predicted gene, EG317677(EG317677), mRNA.	317677	188	289	349	349
EG317677	EG317677	Mus musculus predicted gene, EG317677(EG317677), mRNA.	317677	121	125	118	123
EG328314	EG328314	PREDICTED: Mus musculus predicted gene, EG328314 (EG328314),	328314	130	130	145	145

EG384770	EG384770	PREDICTED: Mus musculus predicted gene, EG384770 (EG384770),	384770	135	137	145	131
EG384813	EG384813	Mus musculus predicted gene, EG384813(EG384813), mRNA.	384813	146	142	137	131
EG434280	EG434280	Mus musculus predicted gene, EG434280(EG434280), mRNA.	434280	134	121	127	139
EG434510	EG434510	Mus musculus predicted gene, EG434510(EG434510), mRNA.	434510	133	125	127	129
EG574082	EG574082	Mus musculus predicted gene, EG574082 (EG574082), non-coding	654454	132	130	118	120
EG622976	EG622976	Mus musculus predicted gene, EG622976(EG622976), mRNA.	622976	127	143	131	143
EG623172	EG623172	PREDICTED: Mus musculus predicted gene, EG623172 (EG623172),	623172	124	133	143	128
EG625054	EG625054	Mus musculus predicted gene, EG625054 (EG625054), non-coding	625054	22584	19136	23402	25128
EG626058	EG626058	PREDICTED: Mus musculus predicted gene, EG626058 (EG626058),	626058	127	131	115	121
EG629595	EG629595	PREDICTED: Mus musculus predicted gene, EG629595 (EG629595),	629595	22847	25043	25933	23809
EG665509	EG665509	PREDICTED: Mus musculus predicted gene, EG665509 (EG665509),	665509	690	1361	1615	1619
EG666648	EG666648	PREDICTED: Mus musculus predicted gene, EG666648 (EG666648),	666648	136	138	152	149
EG668668	EG668668	Mus musculus predicted gene, EG668668(EG668668), mRNA.	668668	28655	30092	24106	24106
EGFR	Egfr	Mus musculus epidermal growth factor receptor (Egfr), transcript	13649	676	905	1077	951
EGLN1	Egln1	Mus musculus EGL nine homolog 1 (C. elegans) (Egln1), mRNA.	112405	142	161	141	163
EI24	Ei24			2081	1844	1725	1662
EID3	Eid3	Mus musculus EP300 interacting inhibitor of differentiation 3	66341	131	149	137	126
EIF1AD	Eif1ad	Mus musculus eukaryotic translation initiation factor 1A domain	69860	316	446	364	367
EIF2B2	Eif2b2	Mus musculus eukaryotic translation initiation factor 2B, subunit 2	217715	514	804	786	601
EIF3I	Eif3i	Mus musculus eukaryotic translation initiation factor 3, subunit I	54709	3897	3964	3193	3208
EIF4EBP1	Eif4ebp1	Mus musculus eukaryotic translation initiation factor 4E binding	13685	1640	2682	3445	2820
EIF4EL3	Eif4el3			2136	2676	2501	2249
EIF4ENIF1	Eif4enif1	Mus musculus eukaryotic translation initiation factor 4E nuclear	74203	1113	932	981	944
ELA1	Ela1			132	145	147	138
ELL3	Ell3	Mus musculus elongation factor RNA polymerase II-like 3 (Ell3),	269344	524	220	216	213
ELMO1	Elmo1	Mus musculus engulfment and cell motility 1, ced-12 homolog (C.	140580	145	158	163	152
EMP2	Emp2	Mus musculus epithelial membrane protein 2(Emp2), mRNA.	13731	1238	792	772	660
END3	End3			117	118	123	133

ENO3	Eno3	Mus musculus enolase 3, beta muscle (Eno3), mRNA.	13808	3372	974	277	468
ENPP5	Enpp5	Mus musculus ectonucleotide pyrophosphatase/phosphodiesterase 5	83965	1608	982	1052	913
ENSA	Ensa	Mus musculus endosulfine alpha (Ensa), transcript variant 1, mRNA.	56205	513	436	382	398
ENSMUSG000	ENSMUSG000	Mus musculus predicted gene, ENSMUSG00000053178	208595	728	573	421	465
ENSMUSG000	ENSMUSG000	Mus musculus predicted gene, ENSMUSG00000053178	208595	285	240	214	264
ENSMUSG000	ENSMUSG000	Mus musculus predicted gene, ENSMUSG00000053338	245126	126	159	168	153
ENSMUSG000	ENSMUSG000	Mus musculus predicted gene, ENSMUSG00000068790	545007	113	123	122	119
EPB4.1L1	Epb4.1l1	Mus musculus erythrocyte protein band 4.1-like 1(Epb4.1l1), transcript	13821	351	253	221	264
EPHA7	Epha7	Mus musculus Eph receptor A7 (Epha7), mRNA.	13841	137	134	129	151
EPHX1	Ephx1	Mus musculus epoxide hydrolase 1, microsomal (Ephx1), mRNA.	13849	881	377	418	409
EPN2	Epn2			460	642	924	724
EPN2	Epn2	Mus musculus epsin 2 (Epn2), mRNA.	13855	661	851	1076	920
EPN2	Epn2	Mus musculus epsin 2 (Epn2), mRNA.	13855	180	238	267	293
EPO	Epo	Mus musculus erythropoietin (Epo), mRNA.	13856	119	124	134	131
EPS8	Eps8	Mus musculus epidermal growth factor receptor pathway substrate 8	13860	873	894	652	763
EREG	Ereg	Mus musculus epiregulin (Ereg), mRNA.	13874	132	126	122	123
ESD	Esd	Mus musculus esterase D/formylglutathione hydrolase (Esd), mRNA.	13885	225	195	169	206
ESPNL	Espnl	Mus musculus espin-like (Espnl), mRNA.	227357	143	147	126	122
ESRRG	Esrrg	Mus musculus estrogen-related receptor gamma (Esrrg), mRNA.	26381	319	150	151	144
ETFA	Etfa	Mus musculus electron transferring flavoprotein, alpha polypeptide	110842	8274	7367	5483	6700
ETFB	Etfb	Mus musculus electron transferring flavoprotein, beta polypeptide	110826	4651	4329	3508	3438
EXDL2	Exdl2	Mus musculus exonuclease 3''-5'' domain-like 2 (Exdl2), mRNA.	97827	809	649	697	707
EXDL2	Exdl2	Mus musculus exonuclease 3''-5'' domain-like 2 (Exdl2), mRNA.	97827	833	577	634	679
EXOD1	Exod1	Mus musculus exonuclease domain containing 1 (Exod1), mRNA.	71151	178	163	142	180
EXT1	Ext1	Mus musculus exostoses (multiple) 1 (Ext1), mRNA.	14042	823	1366	1817	1513
F630001K14R	F630001K14Ri			150	218	209	194
F730038L14RI	F730038L14Ri			132	135	122	125
F730046H10R	F730046H10Ri			149	129	136	132
FADS3	Fads3	Mus musculus fatty acid desaturase 3 (Fads3), mRNA.	60527	253	314	355	329
FAM132A	Fam132a	Mus musculus family with sequence similarity 132, member A	67389	324	358	346	307

FAM13B	Fam13b	Mus musculus family with sequence similarity 13, member B (Fam13b),	225358	585	386	387	543
FAM13B	Fam13b	Mus musculus family with sequence similarity 13, member B (Fam13b),	225358	692	396	477	537
FAM169B	Fam169b	Mus musculus family with sequence similarity 169, member B	434197	155	188	190	174
FAM176B	Fam176b	Mus musculus family with sequence similarity 176, member B	230752	152	170	190	195
FARS2	Fars2	Mus musculus phenylalanine-tRNA synthetase 2 (mitochondrial)	69955	1638	1162	1287	947
FBN1	Fbn1			732	930	1383	1367
FBXL5	Fbxl5	Mus musculus F-box and leucine-rich repeat protein 5 (Fbxl5), mRNA.	242960	152	131	127	128
FBXO3	Fbxo3	Mus musculus F-box protein 3 (Fbxo3), transcript variant 1, mRNA.	57443	683	542	497	603
FBXO30	Fbxo30			392	278	215	352
FBXO34	Fbxo34	Mus musculus F-box protein 34 (Fbxo34), mRNA.	78938	853	1181	1219	1022
FBXO36	Fbxo36	Mus musculus F-box protein 36 (Fbxo36), mRNA.	66153	263	215	205	193
FBXO4	Fbxo4			154	172	174	183
FCGR3	Fcgr3	Mus musculus Fc receptor, IgG, low affinity III (Fcgr3), mRNA.	14131	310	1189	1453	1070
FCHSD2	Fchsd2	Mus musculus FCH and double SH3 domains 2 (Fchsd2), mRNA.	207278	2085	1270	1440	1269
FCMD	Fcmd			459	362	333	417
FER1L4	Fer1l4	PREDICTED: Mus musculus fer-1-like 4 (C. elegans) (Fer1l4), mRNA.	74562	131	167	173	195
FGD5	Fgd5	Mus musculus FYVE, RhoGEF and PH domain containing 5 (Fgd5),	232237	153	158	143	154
FJX1	Fjx1	Mus musculus four jointed box 1 (Drosophila) (Fjx1), mRNA.	14221	186	215	257	230
FLOT1	Flot1	Mus musculus flotillin 1 (Flot1), mRNA.	14251	1037	1549	1859	1883
FMNL3	Fmnl3	Mus musculusformin-like 3 (Fmnl3), mRNA.	22379	385	426	547	451
FMO4	Fmo4	Mus musculus flavin containing monooxygenase 4 (Fmo4), mRNA.	226564	177	137	163	150
FN1	Fn1	Mus musculus fibronectin 1 (Fn1), mRNA.	14268	730	1186	2013	1837
FNTA	Fnta	Mus musculus farnesyltransferase, CAAX box, alpha (Fnta), mRNA.	14272	4762	4022	3649	3510
FOXJ2	Foxj2	Mus musculus forkhead box J2 (Foxj2), mRNA.	60611	595	447	552	499
FOXO3	Foxo3			254	169	199	183
FOXP3	Foxp3	Mus musculus forkhead box P3 (Foxp3), mRNA.	20371	154	181	190	174
FRY	Fry	PREDICTED: Mus musculus furry homolog (Drosophila) (Fry), mRNA.	320365	167	177	192	211
FSIP1	Fsip1	Mus musculus fibrous sheath-interacting protein 1 (Fsip1), mRNA.	71313	131	139	131	122
FTL1	Ftl1			10341	8897	12681	12305
FUSIP1	Fusip1	Mus musculus FUS interacting protein (serine-arginine rich) 1 (Fusip1),	14105	192	201	165	180

FUSIP1	Fusip1	Mus musculus FUS interacting protein (serine-arginine rich) 1 (Fusip1),	14105	370	364	302	426
FXR2	Fxr2	Mus musculus fragile X mental retardation, autosomal homolog 2	23879	542	526	781	723
FXYD4	Fxyd4	Mus musculus FXYD domain-containing ion transport regulator 4	108017	1358	547	269	347
FYB	Fyb			133	162	163	192
FZD10	Fzd10	Mus musculus frizzled homolog 10 (Drosophila) (Fzd10), mRNA.	93897	137	116	127	131
FZD5	Fzd5			150	136	134	125
FZD7	Fzd7	Mus musculus frizzled homolog 7 (Drosophila) (Fzd7), mRNA.	14369	441	234	256	299
G0B-ALPHA	G0B-alpha			141	133	128	123
G3BP2	G3bp2	Mus musculus GTPase activating protein (SH3 domain) binding protein	23881	3612	3072	2447	3163
G430079N04	G430079N04Ri			128	143	147	150
G630013P12	G630013P12Ri			125	120	128	132
GABPB2	Gabpb2	Mus musculus GA repeat binding protein, beta 2 (Gabpb2), transcript	213054	142	126	130	146
GABRD	Gabrd	Mus musculus gamma-aminobutyric acid (GABA-A) receptor, subunit	14403	139	146	128	126
GABRG1	Gabrg1			125	134	131	124
GABRG2	Gabrg2			116	123	131	131
GALNT10	Galnt10	Mus musculus UDP-N-acetyl-alpha-D-galactosamine:polypeptide N-	171212	1515	2531	2344	1890
GCA	Gca	Mus musculus grancalcin (Gca), mRNA.	227960	567	396	263	323
GCC2	Gcc2	Mus musculus GRIP and coiled-coil domain containing 2 (Gcc2), mRNA.	70297	497	407	273	313
GCH1	Gch1	Mus musculus GTP cyclohydrolase 1 (Gch1), mRNA.	14528	1680	3481	2984	2877
GDA	Gda	Mus musculus guanine deaminase (Gda), mRNA.	14544	139	276	198	256
GDAP10	Gdap10			125	132	147	155
GDF6	Gdf6	Mus musculus growth differentiation factor 6 (Gdf6), mRNA.	242316	114	143	120	119
GDNF	Gdnf	Mus musculus glial cell line derived neurotrophic factor (Gdnf), mRNA.	14573	303	189	227	216
GFPT2	Gfpt2	Mus musculus glutamine fructose-6-phosphate transaminase 2 (Gfpt2),	14584	211	331	343	304
GGTA1	Ggta1	Mus musculus glycoprotein galactosyltransferase alpha 1, 3 (Ggta1),	14594	211	358	467	486
GHITM	Ghitm	Mus musculus growth hormone inducible transmembrane protein	66092	2080	1397	1604	1858
GIT1	Git1	Mus musculus G protein-coupled receptor kinase-interactor 1 (Git1),	216963	191	172	165	180
GJA8	Gja8	Mus musculus gap junction protein, alpha 8 (Gja8), mRNA.	14616	140	135	124	133
GLB1	Glb1	Mus musculus galactosidase, beta 1 (Glb1), mRNA.	12091	1625	1317	1386	1093

GLCCI1	Glcci1	Mus musculus glucocorticoid induced transcript 1 (Glcci1), transcript	170772	131	124	128	120
GLDC	Gldc	Mus musculus glycine decarboxylase (Gldc), mRNA.	104174	153	196	229	163
GLIPR2	Glipr2	Mus musculus GLI pathogenesis-related 2 (Glipr2), mRNA.	384009	133	162	167	175
GLIS1	Glis1	Mus musculus GLIS family zinc finger 1 (Glis1), mRNA.	230587	162	135	138	148
GLIS3	Glis3	Mus musculus GLIS family zinc finger 3 (Glis3), mRNA.	226075	127	135	140	128
GLIS3	Glis3	Mus musculus GLIS family zinc finger 3 (Glis3), mRNA.	226075	136	148	146	129
GLT25D2	Glt25d2	Mus musculus glycosyltransferase 25 domain containing 2 (Glt25d2),	269132	135	130	125	143
GLYCTK	Glyctk	Mus musculus glycerate kinase (Glyctk), transcript variant 1, mRNA.	235582	148	155	128	138
GM1060	Gm1060	Mus musculus gene model 1060, (NCBI) (Gm1060), mRNA.	381738	151	139	145	170
GM1141	Gm1141	Mus musculus gene model 1141, (NCBI) (Gm1141), mRNA.	382221	151	179	174	163
GM136	Gm136	Mus musculus gene model 136, (NCBI) (Gm136), mRNA.	214568	121	125	119	116
GM1527	Gm1527	Mus musculus gene model 1527, (NCBI) (Gm1527), mRNA.	385263	130	143	136	123
GM1673	Gm1673	Mus musculus gene model 1673, (NCBI) (Gm1673), mRNA. XM_922421	381633	160	197	244	194
GM22	Gm22	PREDICTED: Mus musculus gene model 22, (NCBI) (Gm22), mRNA.	195209	161	226	242	251
GM546	Gm546	PREDICTED: Mus musculus gene model 546, (NCBI) (Gm546), mRNA.	224908	145	138	127	129
GM608	Gm608	Mus musculus gene model 608, (NCBI) (Gm608), mRNA.	207806	128	137	127	138
GM609	Gm609	Mus musculus gene model 609, (NCBI) (Gm609), mRNA.	208166	189	160	154	155
GM70	Gm70	PREDICTED: Mus musculus gene model 70, (NCBI), transcript variant 4	210762	147	136	126	125
GM757	Gm757	Mus musculus gene model 757, (NCBI) (Gm757), mRNA.	329360	155	145	133	143
GM806	Gm806	Mus musculus gene model 806, (NCBI) (Gm806), mRNA.	328250	181	164	157	156
GM846	Gm846	Mus musculus gene model 846, (NCBI) (Gm846), mRNA.	330921	140	126	134	126
GM949	Gm949	Mus musculus gene model 949, (NCBI) (Gm949), mRNA.	381142	154	162	192	165
GM960	Gm960	Mus musculus gene model 960, (NCBI) (Gm960), mRNA.	381196	218	203	218	186
GM97	Gm97	Mus musculus gene model 97, (NCBI) (Gm97), mRNA.	225923	138	130	145	135
GNAI2	Gnai2	Mus musculus guanine nucleotide binding protein (G protein), alpha	14678	3216	3726	4278	4497
GNL2	Gnl2	Mus musculus guanine nucleotide binding protein-like 2 (nucleolar)	230737	332	438	413	405
GNL3L	Gnl3l	Mus musculus guanine nucleotide binding protein-like 3 (nucleolar)-	237107	542	489	507	447
GNPDA1	Gnpda1	Mus musculus glucosamine-6-phosphate deaminase 1 (Gnpda1),	26384	603	866	815	862
GOLGB1	Golgb1	PREDICTED: Mus musculus golgi autoantigen, golgin subfamily b,	224139	126	131	133	141
GOLPH3L	Golph3l	Mus musculus golgi phosphoprotein 3-like (Golph3l), mRNA.	229593	5103	2942	3262	3860

GOSR2	Gosr2	Mus musculus golgi SNAP receptor complex member 2 (Gosr2), mRNA.	56494	544	736	686	716
GOSR2	Gosr2	Mus musculus golgi SNAP receptor complex member 2 (Gosr2), mRNA.	56494	791	1028	1287	1242
GOSR2	Gosr2	Mus musculus golgi SNAP receptor complex member 2 (Gosr2), mRNA.	56494	294	419	355	427
GPATCH3	Gpatch3	Mus musculus G patch domain containing 3 (Gpatch3), mRNA.	242691	146	162	142	161
GPC2	Gpc2	Mus musculus glypican 2 (cerebroglycan) (Gpc2), mRNA.	71951	158	132	126	136
GPC3	Gpc3	Mus musculus glypican 3 (Gpc3), mRNA.	14734	503	292	364	312
GPNMB	Gpnmb	Mus musculus glycoprotein (transmembrane) nmb (Gpnmb), mRNA.	93695	348	1135	1639	1171
GPR126	Gpr126	Mus musculus G protein-coupled receptor 126 (Gpr126), mRNA.	215798	131	129	124	122
GPR133	Gpr133	Mus musculus G protein-coupled receptor 133 (Gpr133), mRNA.	243277	144	151	136	147
GPR176	Gpr176	Mus musculus G protein-coupled receptor 176 (Gpr176), mRNA.	381413	163	266	358	312
GPR182	Gpr182	Mus musculus G protein-coupled receptor 182 (Gpr182), mRNA.	11536	153	184	213	197
GPR182	Gpr182	Mus musculus G protein-coupled receptor 182 (Gpr182), mRNA.	11536	139	153	179	167
GPR49, FEX,	Gpr49, FEX, GPCR			140	122	141	129
GPX7	Gpx7	Mus musculus glutathione peroxidase 7 (Gpx7), mRNA.	67305	230	405	446	382
GRB10	Grb10			161	172	185	192
GRHPR	Grhpr	Mus musculus glyoxylate reductase/hydroxypyruvate reductase	76238	824	1165	1049	951
GRIA1	Gria1	Mus musculus glutamate receptor, ionotropic, AMPA1 (alpha 1)	14799	148	131	118	138
GRIT	Grit	Mus musculus Rho GTPase-activating protein (Grit), mRNA.	330914	1037	891	731	705
GRLF1	Grlf1	Mus musculus glucocorticoid receptor DNA binding factor 1 (Grlf1),	232906	238	234	209	213
GRM4	Grm4	Mus musculus glutamate receptor, metabotropic 4 (Grm4), mRNA.	268934	134	147	138	145
GSDMDC1	Gsdmdc1	Mus musculus gasdermin domain containing 1 (Gsdmdc1), mRNA.	69146	2871	3786	4382	4629
GSS	Gss	Mus musculus glutathione synthetase (Gss), mRNA.	14854	657	577	549	475
GSTZ1	Gstz1	Mus musculus glutathione transferase zeta 1 (maleylacetoacetate	14874	1274	1045	1013	875
GUCA2B	Guca2b	Mus musculus guanylate cyclase activator 2b (retina) (Guca2b), mRNA.	14916	725	1413	1170	1086
GYK	Gyk			872	791	527	633
GYK	Gyk			131	128	120	135
GYPC	Gypc	Mus musculus glycophorin C (Gypc), mRNA.	71683	253	267	357	300
GZF1	Gzf1	Mus musculus GDNF-inducible zinc finger protein 1 (Gzf1), mRNA.	74533	734	621	568	475
H19	H19	Mus musculus H19 fetal liver mRNA (H19), non-coding RNA.	14955	134	216	303	263
H2-M10.6	H2-M10.6	Mus musculus histocompatibility 2, M region locus 10.6 (H2-M10.6),	399549	143	132	143	126

H6PD	H6pd	Mus musculus hexose-6-phosphate dehydrogenase (glucose 1-	100198	648	1228	1491	1080
HAAO	Haao	Mus musculus 3-hydroxyanthranilate 3,4-dioxygenase(Haao), mRNA.	107766	129	143	138	135
HAGHL	Haghl			169	139	162	150
HAND2	Hand2	Mus musculus heart and neural crest derivatives expressed transcript 2	15111	137	150	170	168
HAO1	Hao1	Mus musculus hydroxyacid oxidase 1, liver (Hao1), mRNA.	15112	127	154	152	138
HCFC1R1	Hcfc1r1	Mus musculus host cell factor C1 regulator 1 (XPO1-dependent)	353502	162	186	154	179
HDAC11	Hdac11	Mus musculus histone deacetylase 11 (Hdac11), mRNA.	232232	375	253	260	202
HDAC2	Hdac2			2748	1630	1314	2164
HDAC2	Hdac2			206	177	145	172
HDAC5	Hdac5	Mus musculus histone deacetylase 5 (Hdac5), transcript variant 1,	15184	1016	649	725	706
HDAC7	Hdac7	Mus musculus histone deacetylase 7 (Hdac7), mRNA. XM_001003311	56233	208	246	264	262
HELB	Helb	Mus musculus helicase (DNA) B (Helb), mRNA.	117599	639	589	595	562
HEPACAM2	Hepacam2	Mus musculus HEPACAM family member 2 (Hepacam2), mRNA.	101202	125	124	135	118
HERC1	Herc1	PREDICTED: Mus musculus hect (homologous to the E6-AP (UBE3A)	235439	128	121	127	132
HERC1	Herc1	PREDICTED: Mus musculus hect (homologous to the E6-AP (UBE3A)	235439	309	169	212	191
HES1	Hes1	Mus musculus hairy and enhancer of split 1 (Drosophila) (Hes1),	15205	1305	678	813	964
HGF	Hgf			229	417	352	492
HGF	Hgf			131	171	153	171
HHAT	Hhat	Mus musculus hedgehog acyltransferase(Hhat), mRNA.	226861	198	179	166	173
HIPK2	Hipk2			140	133	149	156
HIST1H2BG	Hist1h2bg	Mus musculus histone cluster 1, H2bg (Hist1h2bg), mRNA.	319181	159	139	148	153
HIST1H2BJ	Hist1h2bj	Mus musculus histone cluster 1, H2bj (Hist1h2bj), mRNA.	319183	4676	3065	2682	3103
HIST1H2BK	Hist1h2bk	Mus musculus histone cluster 1, H2bk (Hist1h2bk), mRNA.	319184	1593	1200	1128	1365
HIST1H2BN	Hist1h2bn	Mus musculus histone cluster 1, H2bn (Hist1h2bn), mRNA.	319187	2394	1764	1614	1903
HIST1H3H	Hist1h3h	Mus musculus histone cluster 1, H3h (Hist1h3h), mRNA.	319152	148	155	127	147
HIST1H4H	Hist1h4h	Mus musculus histone cluster 1, H4h (Hist1h4h), mRNA.	69386	932	498	404	410
HIST2H2AA2	Hist2h2aa2	Mus musculus histone cluster 2, H2aa2 (Hist2h2aa2), mRNA.	319192	3313	2586	2073	2011
HIST2H3C1	Hist2h3c1	Mus musculus histone cluster 2, H3c1 (Hist2h3c1), transcript variant 2,	15077	209	172	167	190
HNF4A	Hnf4a	Mus musculus hepatic nuclear factor 4, alpha (Hnf4a), mRNA.	15378	6072	2802	4235	4746
HNRPK	Hnrpk	Mus musculus heterogeneous nuclear ribonucleoprotein K (Hnrpk),	15387	297	264	302	275

HOOK1	Hook1	Mus musculus hook homolog 1 (Drosophila) (Hook1), mRNA.	77963	223	191	157	184
HOXA11	Hoxa11	Mus musculus homeo box A11 (Hoxa11), mRNA.	15396	136	140	184	170
HP	Hp	Mus musculus haptoglobin (Hp), mRNA.	15439	207	4343	4407	3015
HP	Hp	Mus musculus haptoglobin (Hp), mRNA.	15439	145	2521	2659	1775
HPN	Hpn	Mus musculus hepsin (Hpn), mRNA.	15451	175	133	133	123
HR	Hr	Mus musculus hairless (Hr), mRNA.	15460	969	613	372	630
HRH2	Hrh2	Mus musculus histamine receptor H2 (Hrh2), transcript variant 2,	15466	158	145	152	148
HRSP12	Hrsp12	Mus musculus heat-responsive protein 12 (Hrsp12), mRNA.	15473	531	353	282	329
HSD17B12	Hsd17b12			273	310	246	348
HSN2	Hsn2	Mus musculus hereditary sensory neuropathy, type II (Hsn2), mRNA.	406236	180	157	147	143
HSPA12A	Hspa12a	Mus musculus heat shock protein 12A (Hspa12a), mRNA.	73442	140	139	164	151
HSPA8	Hspa8	Mus musculus heat shock protein 8 (Hspa8), mRNA.	15481	6759	8230	12180	12413
HSPG2	Hspg2	PREDICTED: Mus musculus perlecan (heparan sulfate proteoglycan 2)	15530	1196	1372	2550	2137
HSPG2	Hspg2			934	1103	2287	2043
HUS1B	Hus1b	Mus musculus Hus1 homolog b (S. pombe) (Hus1b), mRNA.	210554	135	127	128	123
HVCN1	Hvcn1	Mus musculus hydrogen voltage-gated channel 1 (Hvcn1), transcript	74096	290	351	433	354
IBRDC3	Ibrdc3			154	208	195	173
IBRDC3	Ibrdc3	PREDICTED: Mus musculus IBR domain containing 3 (Ibrdc3), mRNA.	75234	368	615	648	568
ID4	Id4	Mus musculus inhibitor of DNA binding 4 (Id4), mRNA.	15904	579	219	239	298
IDH3G	Idh3g	Mus musculus isocitrate dehydrogenase 3 (NAD+), gamma (Idh3g),	15929	7303	6129	5800	5470
IER5L	Ier5l	Mus musculus immediate early response 5-like (Ier5l), mRNA.	72500	277	341	387	412
IFNAR2	Ifnar2	Mus musculus interferon (alpha and beta) receptor 2 (Ifnar2), mRNA.	15976	165	255	332	331
IFNAR2	Ifnar2	Mus musculus interferon (alpha and beta) receptor 2 (Ifnar2), mRNA.	15976	124	136	147	148
IFNAR2	Ifnar2	Mus musculus interferon (alpha and beta) receptor 2 (Ifnar2), mRNA.	15976	182	232	272	261
IGFBP4	Igfbp4			972	4051	4815	5909
IGFBP5	Igfbp5			5029	17707	22759	23723
IGFBP7	Igfbp7	Mus musculus insulin-like growth factor binding protein 7 (Igfbp7),	29817	10687	14267	18564	18564
IGHV1S120_A	IGHV1S120_AF025443_Ig_heavy_variable_1S120_8			1077	585	209	409
IGHV1S121_A	IGHV1S121_AF025445_Ig_heavy_variable_1S121_173			165	125	125	140
IGHV1S14_K0	IGHV1S14_K00707$X00161_Ig_heavy_variable_1S14_164			193	161	154	151

IGHV1S35_M	IGHV1S35_M12376_Ig_heavy_variable_1S35_13			1453	645	241	437
IGHV1S59_L1	IGHV1S59_L17134_Ig_heavy_variable_1S59_150			237	143	246	523
IGSF10	Igsf10	PREDICTED: Mus musculus immunoglobulin superfamily, member 10,	242050	251	215	229	245
IGSF6	Igsf6	Mus musculus immunoglobulin superfamily, member 6 (Igsf6), mRNA.	80719	141	150	176	162
IL15	Il15			137	126	125	138
IL17RA	Il17ra	Mus musculus interleukin 17 receptor A (Il17ra), mRNA.	16172	126	144	135	146
IL1R2	Il1r2	Mus musculus interleukin 1 receptor, type II (Il1r2), mRNA.	16178	124	1411	913	626
IL1RAP	Il1rap	Mus musculus interleukin 1 receptor accessory protein (Il1rap),	16180	145	160	154	168
IL1RL1	Il1rl1	Mus musculus interleukin 1 receptor-like 1 (Il1rl1), transcript variant 2,	17082	169	3533	6878	4746
IL20RB	Il20rb	Mus musculus interleukin 20 receptor beta (Il20rb), transcript variant	213208	143	130	146	140
IL2RG	Il2rg			134	160	170	158
IL3RA	Il3ra	Mus musculus interleukin 3 receptor, alpha chain (Il3ra), mRNA.	16188	148	212	189	216
IL4	Il4	Mus musculus interleukin 4 (Il4), mRNA.	16189	123	153	147	165
IL4RA	Il4ra	Mus musculus interleukin 4 receptor, alpha (Il4ra), mRNA.	16190	131	149	200	168
IL6	Il6	Mus musculus interleukin 6 (Il6), mRNA.	16193	128	591	401	298
IL6ST	Il6st	Mus musculus interleukin 6 signal transducer (Il6st), mRNA.	16195	518	673	1106	960
ING5	Ing5	Mus musculus inhibitor of growth family, member 5 (Ing5), mRNA.	66262	142	150	160	148
INO80C	Ino80c	Mus musculus INO80 complex subunit C (Ino80c), mRNA.	225280	232	372	305	302
INO80C	Ino80c	Mus musculus INO80 complex subunit C (Ino80c), mRNA.	225280	216	359	283	245
INPP4A	Inpp4a	Mus musculus inositol polyphosphate-4-phosphatase, type I (Inpp4a),	269180	141	124	124	117
INPP4A	Inpp4a	Mus musculus inositol polyphosphate-4-phosphatase, type I (Inpp4a),	269180	126	121	134	132
INPP4B	Inpp4b			222	171	151	158
INTS12	Ints12	Mus musculus integrator complex subunit 12 (Ints12), mRNA.	71793	474	396	373	448
IPMK	Ipmk	Mus musculus inositol polyphosphate multikinase (Ipmk), mRNA.	69718	1342	925	920	861
IPMK	Ipmk	Mus musculus inositol polyphosphate multikinase (Ipmk), mRNA.	69718	2375	1569	1459	1357
IPPK	Ippk	Mus musculus inositol 1,3,4,5,6-pentakisphosphate 2-kinase (Ippk),	75678	1007	747	698	650
IRAK1BP1	Irak1bp1	Mus musculus interleukin-1 receptor-associated kinase 1 binding	65099	133	139	125	122
IRAK2	Irak2	Mus musculus interleukin-1 receptor-associated kinase 2 (Irak2),	108960	764	544	523	484
IRAK3	Irak3	Mus musculus interleukin-1 receptor-associated kinase 3 (Irak3),	73914	337	643	748	549
IRF8	Irf8	Mus musculus interferon regulatory factor 8 (Irf8), mRNA.	15900	574	875	1173	979

ISL2	Isl2	Mus musculus insulin related protein 2 (islet 2) (Isl2), mRNA.	104360	135	148	160	159
ITGA4	Itga4			158	177	162	180
ITGAD	Itgad	Mus musculus integrin, alpha D (Itgad), mRNA.	381924	132	124	127	123
ITGAE	Itgae	Mus musculus integrin alpha E, epithelial-associated (Itgae), transcript	16407	234	350	392	316
ITGAE	Itgae	Mus musculus integrin alpha E, epithelial-associated (Itgae), transcript	16407	250	369	373	324
ITGAV	Itgav			143	195	170	163
ITGAX	Itgax			128	134	131	141
ITGB3BP	Itgb3bp	Mus musculus integrin beta 3 binding protein (beta3-endonexin)	67733	415	373	268	314
ITGB8	Itgb8			137	140	152	158
ITGB8	Itgb8	Mus musculus integrin beta 8 (Itgb8), mRNA. XM_919665 XM_986358	320910	128	141	137	131
ITIH5	Itih5	Mus musculus inter-alpha (globulin) inhibitor H5 (Itih5), mRNA.	209378	303	217	164	205
ITM2B	Itm2b	Mus musculus integral membrane protein 2B (Itm2b), mRNA.	16432	23555	24828	19193	20839
ITSN1	Itsn1			139	122	126	138
IVD	Ivd	Mus musculus isovaleryl coenzyme A dehydrogenase (Ivd), nuclear	56357	857	816	728	603
IVNS1ABP	Ivns1abp	Mus musculus influenza virus NS1A binding protein (Ivns1abp),	117198	6667	3697	3095	4038
JAK1	Jak1	Mus musculus Janus kinase 1 (Jak1), mRNA.	16451	276	314	355	403
JAK3	Jak3	Mus musculus Janus kinase 3 (Jak3), mRNA.	16453	137	170	180	188
JMJD6	Jmjd6	Mus musculus jumonji domain containing 6 (Jmjd6), mRNA.	107817	1793	2422	2235	1967
JUN	Jun	Mus musculus Jun oncogene (Jun), mRNA.	16476	617	493	529	456
KAZALD1	Kazald1	Mus musculus Kazal-type serine peptidase inhibitor domain 1	107250	285	153	142	145
KCNA5	Kcna5	Mus musculus potassium voltage-gated channel, shaker-related	16493	124	129	125	136
KCNB2	Kcnb2	PREDICTED: Mus musculus potassium voltage gated channel, Shab-	98741	131	121	140	140
KCNE4	Kcne4	Mus musculus potassium voltage-gated channel, Isk-related subfamily,	57814	239	845	942	566
KCNH2	Kcnh2	Mus musculus potassium voltage-gated channel, subfamily H (eag-	16511	294	220	197	191
KCNJ1	Kcnj1	Mus musculus potassium inwardly-rectifying channel, subfamily J,	56379	136	123	151	129
KCNK13	Kcnk13	Mus musculus potassium channel, subfamily K, member 13 (Kcnk13),	217826	157	261	236	223
KCNV1	Kcnv1	Mus musculus potassium channel, subfamily V, member 1 (Kcnv1),	67498	144	135	116	131
KCTD17	Kctd17	Mus musculus potassium channel tetramerisation domain containing	72844	1508	1337	1588	1674
KHDC1C	Khdc1c	Mus musculus KH domain containing 1C (Khdc1c), mRNA.	433278	136	200	152	192
KIFC1	Kifc1	Mus musculus kinesin family member C1 (Kifc1), mRNA.	16580	142	129	136	152

KIFC2	Kifc2	Mus musculus kinesin family member C2 (Kifc2), mRNA.	16581	212	175	169	192
KLB	Klb	Mus musculus klotho beta (Klb), mRNA.	83379	281	166	148	173
KLHL12	Klhl12	Mus musculus kelch-like 12 (Drosophila) (Klhl12), mRNA.	240756	175	205	189	210
KLHL20	Klhl20	Mus musculus kelch-like 20 (Drosophila) (Klhl20), mRNA.	226541	127	121	135	125
KLK6	Klk6	Mus musculus kallikrein related-peptidase 6 (Klk6), mRNA.	19144	139	141	126	125
KLRB1B	Klrb1b	Mus musculus killer cell lectin-like receptor subfamily B member 1B	80782	126	140	151	157
KLRI2	Klri2	Mus musculus killer cell lectin-like receptor family I member 2 (Klri2),	320407	123	135	134	123
KNG1	Kng1	Mus musculus kininogen 1 (Kng1), mRNA.	16644	139	528	311	325
KNG2	Kng2	Mus musculus kininogen 2 (Kng2), mRNA.	385643	149	270	228	208
KPNA1	Kpna1	Mus musculus karyopherin (importin) alpha 1 (Kpna1), mRNA.	16646	607	537	460	519
KRAS	Kras	Mus musculus v-Ki-ras2 Kirsten rat sarcoma viral oncogene homolog	16653	1646	1462	961	1271
KRCC1	Krcc1	Mus musculus lysine-rich coiled-coil 1 (Krcc1), mRNA.	57896	1303	1039	960	1151
KRIT1	Krit1	Mus musculus KRIT1, ankyrin repeat containing (Krit1), mRNA.	79264	182	206	175	205
KRR1	Krr1	Mus musculus KRR1, small subunit (SSU) processome component,	52705	189	162	160	179
KRR1	Krr1	Mus musculus KRR1, small subunit (SSU) processome component,	52705	170	157	156	151
KRT10	Krt10	Mus musculus keratin 10 (Krt10), mRNA.	16661	798	607	461	580
KRT2-19	Krt2-19			140	122	136	125
KRT33A	Krt33a	Mus musculus keratin 33A (Krt33a), mRNA.	71888	199	157	158	142
KRT36	Krt36	Mus musculus keratin 36 (Krt36), mRNA.	16673	154	558	220	476
KRTAP16-9	Krtap16-9	Mus musculus keratin associated protein 16-9 (Krtap16-9), mRNA.	170657	124	121	126	130
KRTCAP3	Krtcap3	Mus musculus keratinocyte associated protein 3 (Krtcap3), mRNA.	69815	6721	5139	4676	4606
LAMA5	Lama5	Mus musculus laminin, alpha 5 (Lama5), mRNA.	16776	208	248	310	295
LAMB1-1	Lamb1-1	Mus musculus laminin B1 subunit 1 (Lamb1-1), mRNA.	16777	150	183	228	240
LAMC1	Lamc1	Mus musculus laminin, gamma 1 (Lamc1), mRNA.	226519	698	1061	1792	1485
LANCL1	Lancl1	Mus musculus LanC (bacterial lantibiotic synthetase component C)-like	14768	211	186	173	172
LARP4	Larp4	Mus musculus La ribonucleoprotein domain family, member 4 (Larp4),	207214	278	212	182	219
LARP6	Larp6	Mus musculus La ribonucleoprotein domain family, member 6 (Larp6),	67557	218	297	357	299
LASS2	Lass2	Mus musculus LAG1 homolog, ceramide synthase 2 (Lass2), mRNA.	76893	1023	1279	1504	1556
LASS2	Lass2	Mus musculus LAG1 homolog, ceramide synthase 2 (Lass2), mRNA.	76893	3714	4852	5705	5762

LAT	Lat			123	137	135	127
LATS2	Lats2	Mus musculus large tumor suppressor 2 (Lats2), mRNA.	50523	120	121	136	132
LAYN	Layn	PREDICTED: Mus musculus layilin (Layn), mRNA.	244864	131	138	152	146
LBH	Lbh	Mus musculus limb-bud and heart (Lbh), mRNA.	77889	2131	2912	3334	3163
LBP	Lbp	Mus musculus lipopolysaccharide binding protein (Lbp), mRNA.	16803	169	488	749	524
LCP2	Lcp2	Mus musculus lymphocyte cytosolic protein 2 (Lcp2), mRNA.	16822	125	129	142	134
LDHC	Ldhc	Mus musculus lactate dehydrogenase C (Ldhc), mRNA.	16833	140	148	127	135
LEAP2	Leap2	Mus musculus liver-expressed antimicrobial peptide 2 (Leap2), mRNA.	259301	126	141	134	127
LGALS4	Lgals4	Mus musculus lectin, galactose binding, soluble 4 (Lgals4), mRNA.	16855	24969	20587	26402	29898
LGALS8	Lgals8	Mus musculus lectin, galactose binding, soluble 8 (Lgals8), mRNA.	56048	661	673	920	931
LHCGR	Lhcgr	Mus musculus luteinizing hormone/choriogonadotropin receptor	16867	156	133	134	128
LHFP	Lhfp	Mus musculus lipoma HMGIC fusion partner (Lhfp), mRNA.	108927	543	1021	1418	1179
LHFP	Lhfp	Mus musculus lipoma HMGIC fusion partner (Lhfp), mRNA.	108927	708	1572	2084	1854
LHFPL3	Lhfpl3	Mus musculus lipoma HMGIC fusion partner-like 3 (Lhfpl3), mRNA.	269629	129	120	135	128
LIAS	Lias	Mus musculus lipoic acid synthetase (Lias), nuclear gene encoding	79464	141	124	140	125
LIMK1	Limk1	Mus musculus LIM-domain containing, protein kinase (Limk1), mRNA.	16885	195	269	251	274
LIMS2	Lims2	Mus musculus LIM and senescent cell antigen like domains 2 (Lims2),	225341	670	377	529	424
LIN7B	Lin7b	Mus musculus lin-7 homolog B (C. elegans) (Lin7b), mRNA.	22342	126	138	125	133
LIP1	Lip1			486	641	662	772
LIP1	Lip1			299	387	412	461
LIPE	Lipe			137	144	139	149
LMCD1	Lmcd1	Mus musculus LIM and cysteine-rich domains 1 (Lmcd1), mRNA.	30937	189	703	822	500
LMNA	Lmna	Mus musculus lamin A (Lmna), transcript variant 1, mRNA.	16905	602	419	561	548
LMOD1	Lmod1	Mus musculus leiomodin 1 (smooth muscle) (Lmod1), mRNA.	93689	541	290	347	310
LOC10003652	LOC10003652	PREDICTED: Mus musculus hypothetical gene LOC100036521	100036521	1076	818	702	948
LOC10003889	LOC10003889	PREDICTED: Mus musculus hypothetical protein LOC100038897	100038897	139	136	124	127
LOC10003934	LOC10003934	PREDICTED: Mus musculus hypothetical protein LOC100039346	100039346	9434	9398	12908	12857
LOC10003962	LOC10003962	PREDICTED: Mus musculus similar to Aph1a protein (LOC100039623),	100039623	223	255	339	291
LOC10003975	LOC10003975	PREDICTED: Mus musculus similar to 40S ribosomal protein S12	100039751	10411	11166	14315	15111
LOC10003982	LOC10003982	PREDICTED: Mus musculus similar to putative, transcript variant 1	100039829	127	156	133	128

LOC10004059	LOC10004059	PREDICTED: Mus musculus similar to Hmgcs1 protein, transcript	100040592	17760	10285	7926	9601
LOC10004060	LOC10004060	PREDICTED: Mus musculus similar to ribosomal protein L13	100040605	21986	20587	19136	18739
LOC10004076	LOC10004076	PREDICTED: Mus musculus similar to hCG2012694 (LOC100040766),	100040766	131	122	123	130
LOC10004141	LOC10004141	PREDICTED: Mus musculus hypothetical protein LOC100041416	100041416	129	135	148	147
LOC10004217	LOC10004217	PREDICTED: Mus musculus similar to mitochondria-associated	100042179	804	785	701	665
LOC10004339	LOC10004339	PREDICTED: Mus musculus similar to QM protein (LOC100043391),	100043391	23193	20682	24505	24581
LOC10004352	LOC10004352	PREDICTED: Mus musculus similar to ribosomal protein S28	100043527	19035	16938	22435	21447
LOC10004401	LOC10004401	PREDICTED: Mus musculus hypothetical protein LOC100044012	100044012	142	148	124	126
LOC10004452	LOC10004452	PREDICTED: Mus musculus similar to Desmoglein 2 (LOC100044529),	100044529	202	177	141	159
LOC100044692	LOC10004469	PREDICTED: Mus musculus similar to aldehyde reductase	100044692	7024	7104	7658	8217
LOC100044756	LOC10004475	PREDICTED: Mus musculus similar to PX domain-containing protein	100044756	543	401	392	356
LOC100044873	LOC10004487	PREDICTED: Mus musculus similar to substance K receptor	100044873	468	357	419	301
LOC100045117	LOC10004511	PREDICTED: Mus musculus similar to Chain A, Crystal Structure Of The	100045117	138	138	146	154
LOC100045250	LOC10004525	PREDICTED: Mus musculus hypothetical protein LOC100045250	100045250	4686	2293	1915	2873
LOC100045280	LOC10004528	PREDICTED: Mus musculus similar to mKIAA1021 protein	100045280	567	572	719	769
LOC100045776	LOC10004577	PREDICTED: Mus musculus similar to DAZ interacting protein 1	100045776	151	154	163	168
LOC100045780	LOC10004578	PREDICTED: Mus musculus similar to metalloprotease-disintegrin	100045780	415	448	583	518
LOC100045869	LOC10004586	PREDICTED: Mus musculus similar to Limb expression 1 homolog	100045869	176	144	135	157
LOC100045958	LOC10004595	PREDICTED: Mus musculus similar to hCG45299, transcript variant 1	100045958	269	188	183	212
LOC100046232	LOC10004623	PREDICTED: Mus musculus similar to NFIL3/E4BP4 transcription factor	100046232	213	2056	2148	1187
LOC100046343	LOC10004634	PREDICTED: Mus musculus similar to CCR4-NOT transcription complex,	100046343	1155	1567	1113	1503
LOC100046546	LOC10004654	PREDICTED: Mus musculus similar to IgM (kappa)light-chain	100046546	133	126	162	136
LOC100046650	LOC10004665	PREDICTED: Mus musculus similar to PRELI domain containing 1	100046650	6064	7268	5960	7315
LOC100046690	LOC10004669	PREDICTED: Mus musculus hypothetical protein LOC100046690	100046690	335	177	216	172
LOC100046775	LOC10004677	PREDICTED: Mus musculus similar to CMP-sialic acid transporter	100046775	6136	3889	3928	4526
LOC100046796	LOC10004679	PREDICTED: Mus musculus similar to polymerase (RNA) II (DNA	100046796	289	317	274	340
LOC100046802	LOC10004680	PREDICTED: Mus musculus similar to Inhbb protein (LOC100046802),	100046802	143	210	251	222
LOC100046883	LOC10004688	PREDICTED: Mus musculus similar to CKLF-like MARVEL	100046883	765	879	1453	1162
LOC100046918	LOC10004691	PREDICTED: Mus musculus similar to Electron transferring	100046918	2399	2032	1620	2022
LOC100046953	LOC10004695	PREDICTED: Mus musculus similar to Rab6 interacting protein 1	100046953	596	719	997	695
LOC100047024	LOC10004702	PREDICTED: Mus musculus similar to [Human Ig rearranged gamma	100047024	119	114	123	125

LOC100047268	LOC10004726	PREDICTED: Mus musculus similar to Immediate early response 5-like	100047268	148	184	188	271
LOC100047273	LOC10004727	PREDICTED: Mus musculus hypothetical protein LOC100047273	100047273	308	214	211	229
LOC100047615	LOC10004761	PREDICTED: Mus musculus similar to 40S ribosomal protein S17	100047615	24626	26119	22193	22435
LOC100047856	LOC10004785	PREDICTED: Mus musculus similar to calponin 3, acidic	100047856	949	1083	1158	1184
LOC100047935	LOC10004793	PREDICTED: Mus musculus similar to ribosomal protein L5	100047935	19822	18693	21447	22030
LOC100048020	LOC10004802	PREDICTED: Mus musculus similar to RIKEN cDNA 0610009K11 gene	100048020	1396	1214	1373	1165
LOC100048280	LOC10004828	PREDICTED: Mus musculus similar to crooked legs CG14938-PB,	100048280	692	430	411	533
LOC100048436	LOC10004843	PREDICTED: Mus musculus similar to CDNA sequence BC049816	100048436	132	141	152	150
LOC100048461	LOC10004846	PREDICTED: Mus musculus similar to dendritic cell-associated C-type	100048461	171	267	255	282
LOC100048508	LOC10004850	PREDICTED: Mus musculus similar to Rpl36 protein, transcript variant	100048508	4765	5277	8002	6474
LOC100048534	LOC10004853	PREDICTED: Mus musculus similar to D19Ertd652e protein	100048534	122	119	126	134
LOC100048583	LOC10004858	PREDICTED: Mus musculus similar to interferon-inducible protein 203,	100048583	129	142	144	156
LOC10004863	LOC10004863	PREDICTED: Mus musculus similar to lens fiber cell beaded-filament	100048638	237	195	165	171
LOC207350	LOC207350			120	120	126	127
LOC208347	LOC208347			124	125	140	134
LOC210583	LOC210583			135	131	127	125
LOC213320	LOC213320	PREDICTED: Mus musculus similar to Crn, crooked neck-like 1	213320	153	133	138	131
LOC214973	LOC214973			137	140	130	134
LOC215633	LOC215633			137	128	146	134
LOC216963	LOC216963			140	136	145	160
LOC218877	LOC218877			141	155	143	162
LOC224582	LOC224582	PREDICTED: Mus musculus similar to putative pheromone receptor	224582	124	132	137	123
LOC225134	LOC225134	PREDICTED: Mus musculus similar to ribosomal protein S4, X-linked	225134	13426	12083	14893	14693
LOC225897	LOC225897			810	845	841	752
LOC226416	LOC226416			22720	19980	27301	27623
LOC230143	LOC230143			134	130	140	144
LOC234911	LOC234911			125	138	141	142
LOC235921	LOC235921			119	121	123	124
LOC236579	LOC236579			132	130	120	123
LOC237684	LOC237684			126	121	132	133

LOC239090	LOC239090			124	134	128	123
LOC239683	LOC239683			127	122	125	138
LOC240672	LOC240672			204	276	278	273
LOC242681	LOC242681			140	137	147	125
LOC243439	LOC243439	PREDICTED: Mus musculus similar to Ig kappa chain V-V region L6	243439	475	149	246	164
LOC244335	LOC244335			126	116	122	131
LOC244495	LOC244495			127	123	134	137
LOC245263	LOC245263	Mus musculus similar to double homeobox, 4 (LOC245263), mRNA.	245263	146	127	132	122
LOC245436	LOC245436			139	125	136	130
LOC245510	LOC245510			127	139	139	131
LOC245892	LOC245892			226	346	529	465
LOC268602	LOC268602			123	132	140	145
LOC268700	LOC268700			11260	10700	12965	14192
LOC268730	LOC268730			130	146	155	176
LOC269251	LOC269251			1792	2178	3226	2840
LOC276837	LOC276837			134	153	167	156
LOC277231	LOC277231			158	138	176	159
LOC277343	LOC277343			135	138	138	132
LOC277385	LOC277385			154	168	173	191
LOC279872	LOC279872			127	133	142	123
LOC280205	LOC280205			2460	1963	2974	3032
LOC328425	LOC328425			134	128	138	127
LOC330693	LOC330693			122	118	130	114
LOC331083	LOC331083			139	142	134	132
LOC331626	LOC331626			138	139	148	158
LOC333818	LOC333818			182	199	204	247
LOC380613	LOC380613			129	133	151	148
LOC380617	LOC380617			208	258	327	261
LOC380651	LOC380651			139	129	130	124
LOC380707	LOC380707			1495	1432	2109	1902

LOC380839	LOC380839			126	140	135	137
LOC380854	LOC380854			195	198	178	211
LOC380870	LOC380870			124	134	127	134
LOC380896	LOC380896			116	132	128	124
LOC380924	LOC380924			117	121	140	126
LOC380973	LOC380973			139	128	132	134
LOC381046	LOC381046			10752	11338	11087	10531
LOC381087	LOC381087			128	130	137	125
LOC381132	LOC381132			650	541	648	506
LOC381133	LOC381133			128	133	138	122
LOC381210	LOC381210			124	122	130	131
LOC381217	LOC381217			185	139	136	150
LOC381222	LOC381222			352	156	135	178
LOC381255	LOC381255			174	179	162	164
LOC381260	LOC381260			143	125	136	127
LOC381273	LOC381273			118	124	138	131
LOC381355	LOC381355	PREDICTED: Mus musculus similar to centrosome-associated protein	381355	122	132	120	118
LOC381365	LOC381365			3696	3867	4780	5727
LOC381448	LOC381448			9141	7559	9601	9485
LOC381514	LOC381514			128	117	121	130
LOC381754	LOC381754			133	126	144	134
LOC381860	LOC381860			3259	997	2176	2415
LOC381931	LOC381931			140	131	132	124
LOC382012	LOC382012			131	131	136	138
LOC382031	LOC382031			129	143	132	138
LOC382145	LOC382145			153	159	166	182
LOC382159	LOC382159			141	150	140	149
LOC382161	LOC382161			120	121	113	119
LOC382262	LOC382262			144	138	137	153
LOC382392	LOC382392			114	115	119	123

LOC382791	LOC382791	149	132	141	126
LOC383021	LOC383021	130	139	149	135
LOC383306	LOC383306	126	120	122	140
LOC383308	LOC383308	9799	10221	12943	13062
LOC383584	LOC383584	138	136	144	149
LOC383749	LOC383749	140	138	146	135
LOC383785	LOC383785	139	138	149	153
LOC383816	LOC383816	120	126	133	123
LOC383836	LOC383836	142	153	150	148
LOC383865	LOC383865	120	120	130	132
LOC383941	LOC383941	140	125	135	130
LOC384061	LOC384061	134	140	128	138
LOC384196	LOC384196	138	128	133	138
LOC384273	LOC384273	132	154	150	141
LOC384313	LOC384313	116	118	120	124
LOC384332	LOC384332	135	130	147	137
LOC384490	LOC384490	127	123	130	138
LOC384521	LOC384521	131	142	145	125
LOC384675	LOC384675	130	130	146	152
LOC384687	LOC384687	138	133	150	129
LOC384721	LOC384721	130	154	136	142
LOC384901	LOC384901	139	141	136	130
LOC385094	LOC385094	138	162	139	145
LOC385242	LOC385242	127	123	133	136
LOC385251	LOC385251	127	123	131	142
LOC385252	LOC385252	146	148	154	158
LOC385453	LOC385453	131	123	142	150
LOC385532	LOC385532	136	137	150	141
LOC385985	LOC385985	157	159	131	149

LOC385989	LOC385989			139	152	156	144
LOC386081	LOC386081			244	178	171	191
LOC386218	LOC386218			2826	3684	3402	5081
LOC386234	LOC386234			151	136	131	127
LOC386246	LOC386246			508	751	703	1004
LOC386552	LOC386552			133	124	129	122
LOC545472	LOC545472	PREDICTED: Mus musculus similar to BTB (POZ) domain containing 1	545472	472	535	644	677
LOC545487	LOC545487	PREDICTED: Mus musculus similar to ribosomal protein L27a-like	545487	297	341	408	476
LOC627424	LOC627424	PREDICTED: Mus musculus similar to nuclear receptor binding factor 2	627424	124	117	114	124
LOC630242	LOC630242	PREDICTED: Mus musculus similar to Ig heavy chain V region MC101	630242	265	152	216	164
LOC632022	LOC632022	PREDICTED: Mus musculus similar to 40S ribosomal protein S18	632022	20515	18821	24262	25043
LOC632684	LOC632684	PREDICTED: Mus musculus hypothetical LOC632684 (LOC632684), misc	632684	718	746	469	581
LOC632784	LOC632784	PREDICTED: Mus musculus similar to Stretchin-Mlck CG18255-PA,	632784	140	124	130	130
LOC633238	LOC633238	PREDICTED: Mus musculus similar to cyclin-dependent kinase 8	633238	166	154	161	165
LOC635470	LOC635470	PREDICTED: Mus musculus similar to ribosomal protein L27a-like	635470	9179	10910	15358	13316
LOC637785	LOC637785	PREDICTED: Mus musculus similar to Ig heavy chain V region 3	637785	1256	583	233	432
LOC665235	LOC665235	PREDICTED: Mus musculus similar to hCG1642689 (LOC665235), misc	665235	6029	5604	8677	8770
LOC665281	LOC665281	PREDICTED: Mus musculus similar to 40S ribosomal protein S12	665281	6852	8002	10094	10448
LOC665408	LOC665408	PREDICTED: Mus musculus similar to SP140 nuclear body protein	665408	117	114	124	120
LOC665425	LOC665425	PREDICTED: Mus musculus similar to T-cell receptor beta chain V region	665425	116	125	131	135
LOC668038	LOC668038	PREDICTED: Mus musculus similar to ribosomal protein (LOC668038),	668038	2066	2344	3666	3730
LOC668387	LOC668387	PREDICTED: Mus musculus similar to ribosomal protein S6	668387	3478	4294	4621	5277
LOC669365	LOC669365	PREDICTED: Mus musculus similar to K+ channel tetramerization	669365	125	119	126	121
LOC671641	LOC671641	PREDICTED: Mus musculus similar to ribosomal protein S12	671641	10566	10976	14441	14243
LOC672274	LOC672274	PREDICTED: Mus musculus similar to Transcription factor SOX-4	672274	149	175	201	197
LOC672445	LOC672445	PREDICTED: Mus musculus similar to engrailed homeobox 1	672445	127	117	132	122
LOC673028	LOC673028	PREDICTED: Mus musculus similar to 60S ribosomal protein L23a	673028	141	139	128	130
LOC673245	LOC673245	PREDICTED: Mus musculus similar to F-box and WD-40 domain protein	673245	141	127	138	133
LOC674050	LOC674050	PREDICTED: Mus musculus similar to adaptor protein Gads	674050	146	153	156	140

LOC674115	LOC674115	PREDICTED: Mus musculus similar to TDPOZ1 (LOC674115), mRNA.	674115	131	131	136	127
LOC674195	LOC674195	PREDICTED: Mus musculus similar to ubiquitin specific protease 48	674195	356	350	426	401
LOC674960	LOC674960	PREDICTED: Mus musculus similar to high-mobility group box 1	674960	131	138	129	139
LOC675567	LOC675567	PREDICTED: Mus musculus similar to RCC1 domain containing 1	675567	149	139	150	139
LOC676420	LOC676420	PREDICTED: Mus musculus similar to ceramide kinases (LOC676420),	676420	1252	1571	1835	1487
LOC676709	LOC676709	PREDICTED: Mus musculus hypothetical protein LOC676709	676709	178	168	154	159
LOC98434	LOC98434			1421	1379	1594	1722
LONP2	Lonp2	Mus musculus lon peptidase 2, peroxisomal (Lonp2), mRNA.	66887	1677	1194	1217	1369
LOXL1	Loxl1			123	134	129	134
LRIT1	Lrit1	Mus musculus leucine-rich repeat, immunoglobulin-like and	239037	132	136	125	135
LRP1	Lrp1	Mus musculus low density lipoprotein receptor-related protein 1	16971	265	289	425	374
LRP5	Lrp5	Mus musculus low density lipoprotein receptor-related protein 5	16973	131	145	130	136
LRRC10	Lrrc10	Mus musculus leucine rich repeat containing 10 (Lrrc10), mRNA.	237560	152	137	133	134
LRRC3	Lrrc3	Mus musculus leucine rich repeat containing 3 (Lrrc3), mRNA.	237387	164	152	139	156
LRRC36	Lrrc36	Mus musculus leucine rich repeat containing 36 (Lrrc36), mRNA.	270091	133	118	138	125
LRRC4C	Lrrc4c	Mus musculus leucine rich repeat containing 4C (Lrrc4c), mRNA.	241568	129	124	118	128
LRRC6	Lrrc6	Mus musculus leucine rich repeat containing 6 (testis) (Lrrc6), mRNA.	54562	147	165	155	143
LRRC8	Lrrc8			148	208	244	217
LRRFIP2	Lrrfip2	Mus musculus leucine rich repeat (in FLII) interacting protein 2	71268	437	327	323	346
LRRK1	Lrrk1	Mus musculus leucine-rich repeat kinase 1 (Lrrk1), mRNA.	233328	850	1046	1161	941
LRRTM4	Lrrtm4	Mus musculus leucine rich repeat transmembrane neuronal 4	243499	125	122	117	131
LSP1	Lsp1			125	139	130	132
LTBP3	Ltbp3	Mus musculus latent transforming growth factor beta binding protein	16998	536	587	861	674
LTBP4	Ltbp4	Mus musculus latent transforming growth factor beta binding protein	108075	1099	477	683	744
LTF	Ltf	Mus musculus lactotransferrin (Ltf), mRNA.	17002	145	659	728	354
LY6A	Ly6a	Mus musculus lymphocyte antigen 6 complex, locus A (Ly6a), mRNA.	110454	8879	24969	21690	22103
LY9	Ly9			124	139	136	149
LYPLAL1	Lyplal1	Mus musculuslysophospholipase-like 1 (Lyplal1), mRNA.	226791	368	236	225	218
LYZS	Lyzs	Mus musculus lysozyme (Lyzs), mRNA.	17105	1860	3132	5064	6271
MAB21L1	Mab21l1	Mus musculus mab-21-like 1 (C. elegans) (Mab21l1), mRNA.	17116	136	129	120	126
MACF1	Macf1	PREDICTED: Mus musculus microtubule-actin crosslinking factor 1,	11426	142	130	146	135

MAGEE2	Magee2	Mus musculus melanoma antigen, family E, 2 (Magee2), mRNA.	272790	125	132	144	129
MAP3K14	Map3k14	Mus musculus mitogen-activated protein kinase kinase kinase 14	53859	195	286	320	275
MAP3K6	Map3k6	Mus musculus mitogen-activated protein kinase kinase kinase 6	53608	235	437	567	353
MAP3K6	Map3k6			284	534	872	500
MAP3K7IP1	Map3k7ip1	Mus musculus mitogen-activated protein kinase kinase kinase 7	66513	1983	1548	1419	1224
MAP4K4	Map4k4	Mus musculus mitogen-activated protein kinase kinase kinase kinase	26921	152	216	241	203
MAP4K5	Map4k5	Mus musculus mitogen-activated protein kinase kinase kinase kinase	399510	149	166	149	160
MAPBPIP-	Mapbpip-		2369	2122	1851	2003	
MAPK1	Mapk1	Mus musculus mitogen-activated protein kinase 1 (Mapk1), transcript	26413	2663	2297	2214	2131
MAPK1	Mapk1	Mus musculus mitogen-activated protein kinase 1 (Mapk1), transcript	26413	785	603	568	628
MAPK12	Mapk12	Mus musculus mitogen-activated protein kinase 12 (Mapk12), mRNA.	29857	161	156	182	170
MAPK15	Mapk15	Mus musculus mitogen-activated protein kinase 15 (Mapk15), mRNA.	332110	149	141	136	134
MAPK9	Mapk9	Mus musculus mitogen-activated protein kinase 9 (Mapk9), transcript	26420	2298	1560	1598	1526
MAPRE2	Mapre2	Mus musculus microtubule-associated protein, RP/EB family, member	212307	2166	1249	1245	1382
MARVELD3	Marveld3	Mus musculus MARVEL (membrane-associating) domain containing 3	73608	1315	1146	880	1077
MBD1	Mbd1			136	160	183	153
MBOAT1	Mboat1	Mus musculus membrane bound O-acyltransferase domain containing	218121	8079	6064	5511	6749
MBTD1	Mbtd1			151	136	131	129
MCART6	Mcart6	Mus musculus mitochondrial carrier triple repeat 6 (Mcart6), mRNA.	67062	136	135	131	124
MCCC1	Mccc1	Mus musculus methylcrotonoyl-Coenzyme A carboxylase 1 (alpha)	72039	285	180	199	214
MCPT1	Mcpt1	Mus musculus mast cell protease 1 (Mcpt1), mRNA.	17224	131	225	180	275
MCPT4	Mcpt4	Mus musculus mast cell protease 4 (Mcpt4), mRNA.	17227	127	143	147	164
MCPT6	Mcpt6	Mus musculus mast cell protease 6 (Mcpt6), mRNA.	17229	123	136	146	125
ME2	Me2	Mus musculus malic enzyme 2, NAD(+)-dependent, mitochondrial	107029	742	563	516	555
MECR	Mecr	Mus musculus mitochondrial trans-2-enoyl-CoA reductase (Mecr),	26922	925	566	503	561
MEGF9	Megf9	Mus musculus multiple EGF-like-domains 9 (Megf9), mRNA.	230316	175	172	159	158
MELA	Mela			172	188	257	238
METTL7A2	Mettl7a2	Mus musculus methyltransferase like 7A2 (Mettl7a2), mRNA.	393082	860	148	131	153
MGL2	Mgl2	Mus musculus macrophage galactose N-acetyl-galactosamine specific	216864	244	425	698	336
MGL2	Mgl2			225	339	516	294

MIA3	Mia3			129	126	125	122
MIC2L1	Mic2l1			1392	749	1076	823
MICAL3	Mical3	Mus musculus microtubule associated monoxygenase, calponin and	194401	133	150	150	140
MKIAA0756	mKIAA0756			129	130	126	138
MKRN1	Mkrn1	Mus musculus makorin, ringfinger protein, 1 (Mkrn1), mRNA.	54484	941	644	799	648
MLL2	Mll2	PREDICTED: Mus musculus myeloid/lymphoid or mixed-lineage	381022	131	136	135	146
MLXIP	Mlxip	Mus musculus MLX interacting protein (Mlxip), transcript variant 2,	208104	138	121	127	125
MMP17	Mmp17	Mus musculus matrix metallopeptidase 17 (Mmp17), mRNA.	23948	461	244	320	275
MMP20	Mmp20	Mus musculus matrix metallopeptidase 20 (enamelysin) (Mmp20),	30800	121	121	126	139
MMP3	Mmp3	Mus musculus matrix metallopeptidase 3 (Mmp3), mRNA.	17392	193	6996	7417	5155
MMP9	Mmp9	Mus musculus matrix metallopeptidase 9 (Mmp9), mRNA.	17395	189	476	742	574
MOSPD4	Mospd4	PREDICTED: Mus musculus motile sperm domain containing 4	72076	128	119	127	132
MPP4	Mpp4	Mus musculus membrane protein, palmitoylated 4 (MAGUK p55	227157	127	117	122	133
MPZL3	Mpzl3	Mus musculus myelin protein zero-like 3 (Mpzl3), transcript variant 1,	319742	259	198	223	159
MRGPRB5	Mrgprb5	Mus musculus MAS-related GPR, member B5 (Mrgprb5), mRNA.	404239	139	140	117	121
MRPL47	Mrpl47	Mus musculus mitochondrial ribosomal protein L47 (Mrpl47), nuclear	74600	265	213	201	224
MRPL9	Mrpl9	Mus musculus mitochondrial ribosomal protein L9 (Mrpl9), nuclear	78523	2091	1879	1484	1460
MRPS31	Mrps31	Mus musculus mitochondrial ribosomal protein S31 (Mrps31), nuclear	57312	2709	2129	1815	1931
MRPS34	Mrps34	Mus musculus mitochondrial ribosomal protein S34 (Mrps34), nuclear	79044	2855	3264	2734	2702
MRPS9	Mrps9	Mus musculus mitochondrial ribosomal protein S9 (Mrps9), mRNA.	69527	2155	1466	1636	1331
MS4A6B	Ms4a6b	Mus musculus membrane-spanning 4-domains, subfamily A, member	69774	132	146	196	169
MSC	Msc	Mus musculus musculin (Msc), mRNA.	17681	197	261	667	264
MSCP	Mscp			282	357	384	360
MSL2L1	Msl2l1	PREDICTED: Mus musculus male-specific lethal 2-like 1 (Drosophila)	77853	259	196	180	235
MSL2L1	Msl2l1	PREDICTED: Mus musculus male-specific lethal 2-like 1 (Drosophila)	77853	247	211	205	202
MSRB2	Msrb2	Mus musculus methionine sulfoxide reductase B2 (Msrb2), mRNA.	76467	391	286	240	242
MT1	Mt1	Mus musculus metallothionein 1 (Mt1), mRNA.	17748	11853	31357	30928	21744
MT2	Mt2	Mus musculus metallothionein 2 (Mt2), mRNA.	17750	197	889	1230	583
MTA2	Mta2	Mus musculus metastasis-associated gene family, member 2 (Mta2),	23942	626	875	806	1035
MTAP7D1	Mtap7d1	Mus musculus microtubule-associated protein 7 domain containing 1	245877	394	431	550	608

MT-CO2	mt-Co2			14732	13162	18196	19822
MTDNA_AT	mtDNA_ATP8			22915	17661	26281	27753
MTDNA_CO	mtDNA_COXII			18511	13316	19623	23121
MTDNA_CY	mtDNA_CytB			28846	30407	24159	27191
MTERF	Mterf	Mus musculus mitochondrial transcription termination factor (Mterf),	545725	750	606	399	502
MTL5	Mtl5	Mus musculus metallothionein-like 5, testis-specific (tesmin) (Mtl5),	17771	142	129	137	129
MT-ND1	mt-Nd1			20839	16840	22969	23490
MT-ND4	mt-Nd4			25351	22435	29898	29074
MTNR1A	Mtnr1a	Mus musculus melatonin receptor 1A (Mtnr1a), mRNA.	17773	140	159	159	149
MTRF1L	Mtrf1l	Mus musculus mitochondrial translational release factor 1-like (Mtrf1l),	108853	429	333	369	439
MTUS1	Mtus1			132	139	121	136
MXRA8	Mxra8	Mus musculus matrix-remodelling associated 8 (Mxra8), mRNA.	74761	273	353	555	424
MYCBPAP	Mycbpap	Mus musculus Mycbp associated protein (Mycbpap), mRNA.	104601	257	156	137	170
MYD88	Myd88			396	558	876	696
MYO1H	Myo1h	PREDICTED: Mus musculus myosin 1H (Myo1h), mRNA.	231646	132	122	121	138
MYO6	Myo6	Mus musculus myosin VI (Myo6), mRNA.	17920	4596	3882	3325	4022
NAALADL1	Naaladl1	Mus musculus N-acetylated alpha-linked acidic dipeptidase-like 1	381204	166	124	137	137
NAALADL1	Naaladl1	Mus musculus N-acetylated alpha-linked acidic dipeptidase-like 1	381204	184	133	131	133
NACA	Naca	Mus musculus nascent polypeptide-associated complex alpha	17938	1400	1632	1208	1300
NAGK	Nagk	Mus musculus N-acetylglucosamine kinase (Nagk), mRNA.	56174	503	461	400	442
NANOS3	Nanos3	Mus musculus nanos homolog 3 (Drosophila) (Nanos3), mRNA.	244551	139	116	125	119
NAPSA	Napsa	Mus musculus napsin A aspartic peptidase (Napsa), mRNA.	16541	250	429	544	391
NARG2	Narg2	Mus musculus NMDA receptor-regulated gene 2 (Narg2), mRNA.	93697	358	283	268	344
NBL1	Nbl1	Mus musculus neuroblastoma, suppression of tumorigenicity 1 (Nbl1),	17965	303	308	411	370
NCAML-	Ncaml-			144	161	147	166
NCK1	Nck1	Mus musculus non-catalytic region of tyrosine kinase adaptor protein 1	17973	1440	822	712	1094
NCKAP1	Nckap1	Mus musculus NCK-associated protein 1 (Nckap1), mRNA.	50884	1250	1311	1251	1489
NDC80	Ndc80	Mus musculus NDC80 homolog, kinetochore complex component (S.	67052	129	150	130	143
NDUFA8	Ndufa8	Mus musculus NADH dehydrogenase (ubiquinone) 1 alpha subcomplex,	68375	2514	2743	2337	2336
NDUFB7	Ndufb7	Mus musculus NADH dehydrogenase (ubiquinone) 1 beta subcomplex, 7	66916	683	723	688	623

NDUFB8	Ndufb8	Mus musculus NADH dehydrogenase (ubiquinone) 1 beta subcomplex 8	67264	13357	12083	11114	11166
NDUFC1	Ndufc1	Mus musculus NADH dehydrogenase (ubiquinone) 1, subcomplex	66377	8274	8601	6022	7029
NDUFC2	Ndufc2	Mus musculus NADH dehydrogenase (ubiquinone) 1, subcomplex	68197	6015	6139	5623	5220
NEDD1	Nedd1			713	543	518	571
NEDD4	Nedd4	Mus musculus neural precursor cell expressed, developmentally down-	17999	119	122	122	115
NEFM	Nefm	Mus musculus neurofilament, medium polypeptide (Nefm), mRNA.	18040	152	151	176	167
NEK1	Nek1	Mus musculus NIMA (never in mitosis gene a)-related expressed kinase	18004	126	128	134	142
NEK10	Nek10	Mus musculus NIMA (never in mitosis gene a)- related kinase 10	238944	135	126	122	118
NEO1	Neo1			339	220	210	245
NEO1	Neo1			229	181	166	197
NETO2	Neto2	PREDICTED: Mus musculus neuropilin (NRP) and tolloid (TLL)-like 2,	74513	122	123	121	134
NEU1	Neu1	Mus musculus neuraminidase 1 (Neu1), mRNA.	18010	6326	3496	3717	2617
NEU2	Neu2	Mus musculus neuraminidase 2 (Neu2), mRNA.	23956	383	262	233	223
NEUROG1	Neurog1	Mus musculus neurogenin 1 (Neurog1), mRNA.	18014	124	133	145	134
NFASC	Nfasc	Mus musculus neurofascin (Nfasc), mRNA.	269116	141	125	117	121
NFKB1	Nfkb1			374	409	450	454
NFKBIA	Nfkbia	Mus musculus nuclear factor of kappa light polypeptide gene	18035	887	1839	2174	1253
NFKBID	Nfkbid	Mus musculus nuclear factor of kappa light polypeptide gene	243910	240	281	315	337
NGP	Ngp	Mus musculus neutrophilic granule protein (Ngp), mRNA.	18054	126	281	261	152
NICN1	Nicn1	Mus musculus nicolin 1 (Nicn1), mRNA.	66257	1043	619	742	715
NID1	Nid1	Mus musculus nidogen 1 (Nid1), mRNA.	18073	345	490	656	768
NINJ2	Ninj2	Mus musculus ninjurin 2 (Ninj2), mRNA.	29862	132	148	142	144
NIPBL	Nipbl	Mus musculus Nipped-B homolog (Drosophila) (Nipbl), transcript	71175	846	553	477	608
NIT2	Nit2	Mus musculus nitrilase family, member 2 (Nit2), mRNA.	52633	360	313	308	279
NLRP4F	Nlrp4f	Mus musculus NLR family, pyrin domain containing 4F (Nlrp4f),	97895	135	120	134	121
NLRP5	Nlrp5	Mus musculus NLR family, pyrin domain containing 5 (Nlrp5),	23968	137	134	121	124
NLRP9B	Nlrp9b	Mus musculus NLR family, pyrin domain containing 9B (Nlrp9b),	243874	138	128	127	140
NMB	Nmb	Mus musculus neuromedin B (Nmb), mRNA.	68039	141	170	158	159
NNAT	Nnat	Mus musculus neuronatin (Nnat), transcript variant 2, mRNA.	18111	149	125	125	130
NOL10	Nol10	Mus musculus nucleolar protein 10 (Nol10), mRNA.	217431	121	119	132	130

NOL3	Nol3	Mus musculus nucleolar protein 3 (apoptosis repressor with CARD	78688	144	150	169	167
NOL7	Nol7	Mus musculus nucleolar protein 7 (Nol7), mRNA.	70078	223	190	152	166
NPSR1	Npsr1	Mus musculus neuropeptide S receptor 1 (Npsr1), mRNA.	319239	140	152	139	144
NPTX1	Nptx1	Mus musculus neuronal pentraxin 1 (Nptx1), mRNA.	18164	135	121	118	127
NPY2R	Npy2r	Mus musculus neuropeptide Y receptor Y2 (Npy2r), mRNA.	18167	142	127	132	131
NQO1	Nqo1	Mus musculus NAD(P)H dehydrogenase, quinone 1 (Nqo1), mRNA.	18104	408	321	296	279
NR1H5	Nr1h5	Mus musculus nuclear receptor subfamily 1, group H, member 5	381463	137	156	149	140
NRP2	Nrp2	Mus musculus neuropilin 2 (Nrp2), transcript variant 2, mRNA.	18187	186	163	184	196
NRXN1	Nrxn1	Mus musculus neurexin I (Nrxn1), mRNA.	18189	120	118	128	137
NSCCN1	Nsccn1			137	145	129	143
NSEP1	Nsep1			19035	22193	16728	17173
NT5C3L	Nt5c3l	Mus musculus 5'-nucleotidase, cytosolic III-like (Nt5c3l), mRNA.	68106	443	376	367	296
NT5C3L	Nt5c3l	Mus musculus 5'-nucleotidase, cytosolic III-like (Nt5c3l), mRNA.	68106	316	267	245	241
NTN2L	Ntn2l	Mus musculus netrin 2-like (chicken) (Ntn2l), mRNA.	18209	250	207	237	210
NTNG1	Ntng1	Mus musculus netrin G1 (Ntng1), mRNA.	80883	120	131	127	123
NTNG2	Ntng2	Mus musculus netrin G2 (Ntng2), transcript variant b, mRNA.	171171	130	134	125	133
NTRK2	Ntrk2	Mus musculus neurotrophic tyrosine kinase, receptor, type 2	18212	129	135	126	134
NUDT12	Nudt12			139	133	141	147
NUDT7	Nudt7	Mus musculus nudix (nucleoside diphosphate linked moiety X)-type	67528	1615	1410	1019	1230
NUFIP2	Nufip2	Mus musculus nuclear fragile X mental retardation protein	68564	158	134	138	163
NUMA1	Numa1	Mus musculus nuclear mitotic apparatus protein 1 (Numa1), mRNA.	101706	296	255	261	269
NUP155	Nup155	Mus musculus nucleoporin 155 (Nup155), mRNA.	170762	135	148	151	157
NUP88	Nup88	Mus musculus nucleoporin 88 (Nup88), transcript variant 1, mRNA.	19069	169	186	201	170
OAS1G	Oas1g	Mus musculus 2'-5' oligoadenylate synthetase 1G (Oas1g), mRNA.	23960	141	130	145	130
ODZ4	Odz4	Mus musculus odd Oz/ten-m homolog 4 (Drosophila) (Odz4), mRNA.	23966	331	185	205	182
ODZ4	Odz4	Mus musculus odd Oz/ten-m homolog 4 (Drosophila) (Odz4), mRNA.	23966	325	188	199	184
OLFM1	Olfm1			185	147	142	131
OLFML2B	Olfml2b	Mus musculus olfactomedin-like 2B (Olfml2b), mRNA.	320078	849	1123	1716	1669
OLFR1032	Olfr1032	Mus musculus olfactory receptor 1032 (Olfr1032), mRNA.	258572	133	129	109	122
OLFR1052	Olfr1052	Mus musculus olfactory receptor 1052 (Olfr1052), mRNA.	259012	128	129	130	117

OLFR1097	Olfr1097	Mus musculus olfactory receptor 1097 (Olfr1097), mRNA.	258840	119	134	119	136
OLFR1135	Olfr1135	Mus musculus olfactory receptor 1135 (Olfr1135), mRNA.	258654	129	136	122	135
OLFR1164	Olfr1164	Mus musculus olfactory receptor 1164 (Olfr1164), mRNA.	258634	136	128	117	120
OLFR1184	Olfr1184	Mus musculus olfactory receptor 1184 (Olfr1184), mRNA.	258820	140	120	132	124
OLFR120	Olfr120	Mus musculus olfactory receptor 120 (Olfr120), mRNA.	258624	132	127	142	122
OLFR1220	Olfr1220	Mus musculus olfactory receptor 1220 (Olfr1220), mRNA.	258902	144	133	123	133
OLFR1223	Olfr1223			136	142	151	134
OLFR1251	Olfr1251	Mus musculus olfactory receptor 1251 (Olfr1251), mRNA.	259145	123	129	126	116
OLFR127	Olfr127	Mus musculus olfactory receptor 127 (Olfr127), mRNA.	258374	129	131	126	122
OLFR1298	Olfr1298	Mus musculus olfactory receptor 1298 (Olfr1298), mRNA.	258888	170	135	130	126
OLFR1311	Olfr1311			112	110	117	113
OLFR1320	Olfr1320	Mus musculus olfactory receptor 1320 (Olfr1320), mRNA.	236784	121	139	130	123
OLFR1352	Olfr1352	Mus musculus olfactory receptor 1352 (Olfr1352), mRNA.	259074	125	132	127	122
OLFR1425	Olfr1425	Mus musculus olfactory receptor 1425 (Olfr1425), mRNA.	258155	138	125	136	128
OLFR1446	Olfr1446	Mus musculus olfactory receptor 1446 (Olfr1446), mRNA.	258699	133	130	130	120
OLFR1475	Olfr1475	Mus musculus olfactory receptor 1475 (Olfr1475), mRNA.	258298	134	128	133	124
OLFR1477	Olfr1477	Mus musculus olfactory receptor 1477 (Olfr1477), mRNA.	258691	160	134	151	139
OLFR153	Olfr153	Mus musculus olfactory receptor 153 (Olfr153), mRNA.	110511	145	129	119	128
OLFR155	Olfr155	Mus musculus olfactory receptor 155 (Olfr155), mRNA.	29845	117	128	117	124
OLFR165	Olfr165	Mus musculus olfactory receptor 165 (Olfr165), mRNA.	258458	329	196	177	200
OLFR166	Olfr166	Mus musculus olfactory receptor 166 (Olfr166), mRNA.	259071	136	133	129	116
OLFR209	Olfr209	Mus musculus olfactory receptor 209 (Olfr209), mRNA.	404311	144	137	123	128
OLFR281	Olfr281	Mus musculus olfactory receptor 281 (Olfr281), mRNA.	258277	154	134	127	123
OLFR301	Olfr301	Mus musculus olfactory receptor 301 (Olfr301), mRNA.	257958	134	128	142	121
OLFR320	Olfr320	Mus musculus olfactory receptor 320 (Olfr320), mRNA.	216783	143	120	135	128
OLFR421	Olfr421			149	140	129	124
OLFR430	Olfr430			134	116	126	124
OLFR450	Olfr450	Mus musculus olfactory receptor 450 (Olfr450), mRNA.	258437	135	134	144	119
OLFR457	Olfr457	Mus musculus olfactory receptor 457 (Olfr457), mRNA.	258989	141	128	134	129
OLFR570	Olfr570	Mus musculus olfactory receptor 570 (Olfr570), mRNA.	259114	134	116	135	126

OLFR576	Olfr576	Mus musculus olfactory receptor 576 (Olfr576), mRNA.	258248	137	118	123	131
OLFR591	Olfr591	Mus musculus olfactory receptor 591 (Olfr591), mRNA.	258139	141	124	137	131
OLFR64	Olfr64	Mus musculus olfactory receptor 64 (Olfr64), mRNA.	18366	149	139	149	139
OLFR646	Olfr646	Mus musculus olfactory receptor 646 (Olfr646), mRNA.	259058	127	145	155	136
OLFR686	Olfr686	Mus musculus olfactory receptor 686 (Olfr686), mRNA.	259072	123	132	132	128
OLFR700	Olfr700	Mus musculus olfactory receptor 700 (Olfr700), mRNA.	258593	131	143	118	131
OLFR707	Olfr707	Mus musculus olfactory receptor 707 (Olfr707), mRNA.	194433	126	141	126	124
OLFR75-PS1	Olfr75-ps1	Mus musculus olfactory receptor 75, pseudogene 1 (Olfr75-ps1), non-	258186	135	134	143	128
OLFR836	Olfr836	Mus musculus olfactory receptor 836 (Olfr836), mRNA.	258557	142	135	146	133
OLFR891	Olfr891			154	145	128	127
OLFR968	Olfr968	Mus musculus olfactory receptor 968 (Olfr968), mRNA.	258605	129	135	124	118
OLIG1	Olig1	Mus musculus oligodendrocyte transcription factor 1 (Olig1), mRNA.	50914	127	126	135	134
OPLAH	Oplah	Mus musculus 5-oxoprolinase (ATP-hydrolysing) (Oplah), mRNA.	75475	313	255	303	229
ORC1L	Orc1l	Mus musculus origin recognition complex, subunit 1-like (S.cereviaiae)	18392	156	168	184	207
ORF19	ORF19	Mus musculus open reading frame 19 (ORF19), transcript variant 1,	68767	317	333	419	377
ORF9	ORF9	Mus musculus open reading frame 9 (ORF9), mRNA.	52793	1823	3413	3113	3251
ORM2	Orm2			138	320	251	247
OSBPL6	Osbpl6	Mus musculus oxysterol binding protein-like 6 (Osbpl6), mRNA.	99031	488	289	255	302
OSTB	Ostb	Mus musculus organic solute transporterbeta (Ostb), mRNA.	330962	731	1592	2164	1148
OTTMUSG0	OTTMUSG000	Mus musculus predicted gene, OTTMUSG00000000231	381531	148	130	137	124
OTUD3	Otud3	PREDICTED: Mus musculus OTU domain containing 3 (Otud3), mRNA.	73162	261	348	322	289
OTUD5	Otud5	Mus musculus OTU domain containing 5 (Otud5), mRNA.	54644	803	849	1085	905
OVOL1	Ovol1	Mus musculus OVO homolog-like 1 (Drosophila) (Ovol1), mRNA.	18426	317	200	180	211
OXCT1	Oxct1	Mus musculus 3-oxoacid CoA transferase 1 (Oxct1), mRNA.	67041	5909	3799	3326	4167
P4HA2	P4ha2			132	128	133	122
PAFAH1B2	Pafah1b2	Mus musculus platelet-activating factor acetylhydrolase, isoform 1b,	18475	127	132	146	135
PALLD	Palld	PREDICTED: Mus musculus palladin, cytoskeletal associated protein,	72333	656	482	580	650
PALMD	Palmd	Mus musculus palmdelphin (Palmd), mRNA.	114301	120	116	136	130
PAPPA2	Pappa2	PREDICTED: Mus musculus pappalysin 2 (Pappa2), mRNA.	23850	122	119	132	126
PATZ1	Patz1	Mus musculus POZ (BTB) and AT hook containing zinc finger 1	56218	138	129	127	130

PAX8	Pax8	Mus musculus paired box gene 8 (Pax8), mRNA.	18510	132	131	120	124
PCDH19	Pcdh19	PREDICTED: Mus musculus protocadherin 19 (Pcdh19), mRNA.	279653	128	124	127	135
PCDHB14	Pcdhb14	Mus musculus protocadherin beta 14 (Pcdhb14), mRNA.	93885	127	138	137	154
PCMT1	Pcmt1	Mus musculus protein-L-isoaspartate (D-aspartate) O-	18537	1504	955	900	938
PCMTD1	Pcmtd1	Mus musculus protein-L-isoaspartate (D-aspartate) O-	319263	298	288	192	285
PCTK3	Pctk3	Mus musculus PCTAIRE-motif protein kinase 3 (Pctk3), mRNA.	18557	144	142	137	131
PDCD10	Pdcd10	Mus musculus programmed cell death 10 (Pdcd10), mRNA.	56426	1288	1052	717	830
PDCD2	Pdcd2	Mus musculus programmed cell death 2 (Pdcd2), mRNA.	18567	1738	1350	1501	1297
PDE7B	Pde7b	Mus musculus phosphodiesterase 7B (Pde7b), mRNA.	29863	185	162	135	150
PDS5A	Pds5a	Mus musculus PDS5, regulator of cohesion maintenance, homolog A	71521	167	174	164	194
PDZD7	Pdzd7	Mus musculus PDZ domain containing 7 (Pdzd7), mRNA.	212684	334	152	143	140
PDZGEF1	Pdzgef1			140	135	144	154
PDZK1	Pdzk1			138	143	124	133
PEAR1	Pear1	Mus musculus platelet endothelial aggregation receptor 1 (Pear1),	73182	129	134	139	145
PECAM1	Pecam1	Mus musculus platelet/endothelial cell adhesion molecule 1	18613	293	319	453	396
PELO	Pelo	Mus musculus pelota homolog (Drosophila) (Pelo), mRNA.	105083	1200	1486	1552	1351
PFKFB4	Pfkfb4	Mus musculus 6-phosphofructo-2-kinase/fructose-2,6-	270198	1657	1234	1109	1045
PFKL	Pfkl	Mus musculus phosphofructokinase, liver, B-type (Pfkl), mRNA.	18641	165	184	160	176
PGK1	Pgk1			118	125	132	126
PGLYRP1	Pglyrp1			4378	10860	8569	10910
PGM2L1	Pgm2l1			171	146	157	159
PGM3	Pgm3	Mus musculus phosphoglucomutase 3 (Pgm3), mRNA.	109785	114	118	125	125
PHF10	Phf10	Mus musculus PHD finger protein 10 (Phf10), mRNA.	72057	605	673	775	881
PHF20L1	Phf20l1	PREDICTED: Mus musculus PHD finger protein 20-like 1, transcript	239510	137	126	123	124
PHLDB2	Phldb2	Mus musculus pleckstrin homology-like domain, family B, member 2	208177	143	129	118	123
PIGF	Pigf	Mus musculus phosphatidylinositol glycan anchor biosynthesis, class	18701	1233	1097	913	991
PIK3CA	Pik3ca	Mus musculus phosphatidylinositol 3-kinase, catalytic, alpha	18706	342	267	275	327
PIK3R3	Pik3r3	Mus musculus phosphatidylinositol 3 kinase, regulatory subunit,	18710	1096	748	494	623
PIK3R3	Pik3r3	Mus musculus phosphatidylinositol 3 kinase, regulatory subunit,	18710	625	325	357	455
PILRA	Pilra	Mus musculus paired immunoglobin-like type 2 receptor alpha	231805	136	186	204	225

PIM3	Pim3			1919	2344	3686	1801
PIPOX	Pipox	Mus musculus pipecolic acid oxidase (Pipox), mRNA.	19193	147	141	151	160
PIRA1	Pira1	Mus musculus paired-Ig-like receptor A1 (Pira1), mRNA.	18722	123	157	186	171
PIT1	Pit1			131	143	151	133
PIWIL2	Piwil2	Mus musculus piwi-like homolog 2 (Drosophila) (Piwil2), mRNA.	57746	130	163	161	156
PKDREJ	Pkdrej	Mus musculus polycystic kidney disease (polycystin) and REJ (sperm	18766	128	132	126	141
PKHD1L1	Pkhd1l1	Mus musculus polycystic kidney and hepatic disease 1-like 1 (Pkhd1l1),	192190	159	149	137	139
PKN2	Pkn2			136	155	126	133
PKP4	Pkp4	Mus musculus plakophilin 4 (Pkp4), transcript variant 2, mRNA.	227937	771	948	1123	879
PLA1A	Pla1a			154	241	283	234
PLA2G1B	Pla2g1b	Mus musculus phospholipase A2, group IB, pancreas (Pla2g1b), mRNA.	18778	121	1493	899	141
PLA2G2E	Pla2g2e	Mus musculus phospholipase A2, group IIE (Pla2g2e), mRNA.	26970	151	152	130	131
PLA2G7	Pla2g7	Mus musculus phospholipase A2, group VII (platelet-activating factor	27226	183	400	556	518
PLAUR	Plaur	Mus musculus plasminogen activator, urokinase receptor (Plaur),	18793	188	526	459	413
PLCH1	Plch1	Mus musculus phospholipase C, eta 1 (Plch1), mRNA.	269437	146	126	139	132
PLCZ1	Plcz1	Mus musculus phospholipase C, zeta 1 (Plcz1), mRNA.	114875	187	183	166	163
PLEKHA4	Plekha4	Mus musculus pleckstrin homology domain containing, family A	69217	136	124	128	133
PLEKHF1	Plekhf1	Mus musculus pleckstrin homology domain containing, family F (with	72287	200	279	274	250
PLG	Plg			143	143	120	133
PLK2	Plk2	Mus musculus polo-like kinase 2 (Drosophila) (Plk2), mRNA.	20620	351	465	554	476
PLN	Pln	Mus musculus phospholamban (Pln), mRNA.	18821	257	143	179	147
PLOD1	Plod1	Mus musculus procollagen-lysine, 2-oxoglutarate 5-dioxygenase 1	18822	213	301	392	373
PLSCR1	Plscr1	Mus musculus phospholipid scramblase 1 (Plscr1), mRNA.	22038	2807	3660	3530	2883
PMCH	Pmch	Mus musculus pro-melanin-concentrating hormone (Pmch), mRNA.	110312	135	123	129	125
PMM2	Pmm2	Mus musculus phosphomannomutase 2 (Pmm2), mRNA.	54128	1615	2274	2107	2037
PMPCA	Pmpca	Mus musculus peptidase (mitochondrial processing) alpha (Pmpca),	66865	155	164	152	149
PNG1-	Png1-pending			140	129	144	135
PNPT1	Pnpt1	Mus musculus polyribonucleotide nucleotidyltransferase 1 (Pnpt1),	71701	130	134	146	134
POLB	Polb	Mus musculus polymerase (DNA directed), beta (Polb), mRNA.	18970	229	246	279	277
POLI	Poli	Mus musculus polymerase (DNA directed), iota (Poli), transcript variant	26447	304	213	240	218

POPDC2	Popdc2	Mus musculus popeye domain containing 2 (Popdc2), transcript variant	64082	706	399	515	448
POPDC2	Popdc2	Mus musculus popeye domain containing 2 (Popdc2), transcript variant	64082	368	246	350	250
PPA1	Ppa1	Mus musculus pyrophosphatase (inorganic) 1 (Ppa1), mRNA.	67895	16145	14441	10498	11434
PPAP2A	Ppap2a	Mus musculus phosphatidic acid phosphatase 2a (Ppap2a), transcript	19012	1924	1811	2682	2260
PPM1B	Ppm1b	Mus musculus protein phosphatase 1B, magnesium dependent, beta	19043	5029	3072	2692	2974
PPP1R14A	Ppp1r14a	Mus musculus protein phosphatase 1, regulatory (inhibitor) subunit	68458	709	438	486	596
PPP1R16A	Ppp1r16a	Mus musculus protein phosphatase 1, regulatory (inhibitor) subunit	73062	307	317	273	273
PPP1R1C	Ppp1r1c			131	125	141	131
PPP1R3B	Ppp1r3b	Mus musculus protein phosphatase 1, regulatory (inhibitor) subunit	244416	766	581	358	508
PPP2CA	Ppp2ca	Mus musculus protein phosphatase 2 (formerly 2A), catalytic	19052	10718	7854	7954	6673
PPP2R2C	Ppp2r2c	Mus musculus protein phosphatase 2 (formerly 2A), regulatory	269643	251	218	172	200
PPP2R5D	Ppp2r5d	Mus musculus protein phosphatase 2, regulatory subunit B (B56),	21770	192	174	160	172
PPP2R5E	Ppp2r5e			315	210	221	207
PPYR1	Ppyr1	Mus musculus pancreatic polypeptide receptor 1 (Ppyr1), mRNA.	19065	449	170	226	203
PRAMEL4	Pramel4	Mus musculus preferentially expressed antigen in melanoma like 4	347709	11546	12883	16728	16771
PRAP1	Prap1	Mus musculus proline-rich acidic protein 1 (Prap1), mRNA.	22264	157	202	193	180
PRCC	Prcc	Mus musculus papillary renal cell carcinoma (translocation-	94315	166	151	157	169
PRDX6	Prdx6	Mus musculusperoxiredoxin 6 (Prdx6), mRNA.	11758	407	278	231	221
PRDX6	Prdx6	Mus musculusperoxiredoxin 6 (Prdx6), mRNA.	11758	394	292	245	259
PRIM2	Prim2	Mus musculus DNA primase, p58 subunit (Prim2), mRNA.	19076	233	309	307	290
PRKAG1	Prkag1	Mus musculus protein kinase, AMP-activated, gamma 1 non-catalytic	19082	878	935	718	751
PRKD1	Prkd1	Mus musculus protein kinase D1 (Prkd1), mRNA.	18760	141	140	155	156
PRKDC	Prkdc			163	170	153	182
PRKRIP1	Prkrip1	Mus musculus Prkr interacting protein 1 (IL11 inducible) (Prkrip1),	66801	474	632	597	517
PROC	Proc	Mus musculus protein C (Proc), transcript variant 3, mRNA.	19123	147	222	197	159
PRODH	Prodh	Mus musculus proline dehydrogenase (Prodh), nuclear gene	19125	168	225	236	187
PRPF38A	Prpf38a	Mus musculus PRP38 pre-mRNA processing factor 38 (yeast) domain	230596	1560	1687	1858	1998
PRPF4B	Prpf4b			174	159	151	152
PRR16	Prr16	Mus musculus proline rich 16 (Prr16), mRNA.	71373	139	158	158	168
PRSS16	Prss16			134	145	128	143

PSEN2	Psen2	Mus musculus presenilin 2 (Psen2), mRNA.	19165	285	418	408	338
PSMD1	Psmd1	Mus musculus proteasome (prosome, macropain) 26S subunit, non-	70247	4606	6707	6022	6927
PTCHD2	Ptchd2	Mus musculus patched domain containing 2 (Ptchd2), mRNA.	242748	135	127	141	143
PTDSS2	Ptdss2	Mus musculus phosphatidylserine synthase 2 (Ptdss2), mRNA.	27388	752	635	560	547
PTGDS2	Ptgds2	Mus musculus prostaglandin D2 synthase 2, hematopoietic (Ptgds2),	54486	227	169	151	209
PTGDS2	Ptgds2	Mus musculus prostaglandin D2 synthase 2, hematopoietic (Ptgds2),	54486	304	223	178	229
PTGES	Ptges	Mus musculus prostaglandin E synthase (Ptges), mRNA.	64292	191	453	448	351
PTGES	Ptges	Mus musculus prostaglandin E synthase (Ptges), mRNA.	64292	124	179	235	169
PTGS1	Ptgs1	Mus musculus prostaglandin-endoperoxide synthase 1 (Ptgs1),	19224	199	239	333	266
PTHR1	Pthr1	Mus musculus parathyroid hormone receptor 1 (Pthr1), transcript	19228	141	156	196	168
PTMS	Ptms	Mus musculus parathymosin (Ptms), mRNA.	69202	340	250	264	290
PTPN18	Ptpn18	Mus musculus protein tyrosine phosphatase, non-receptor type 18	19253	849	1091	1240	1149
PTPRZ1	Ptprz1	Mus musculus protein tyrosine phosphatase, receptor type Z,	19283	184	139	144	160
PTX3	Ptx3			132	562	382	258
PTX3	Ptx3	Mus musculus pentraxin related gene (Ptx3), mRNA.	19288	119	443	351	244
PVRL3	Pvrl3	Mus musculus poliovirus receptor-related 3 (Pvrl3), transcript	58998	795	653	509	618
PVRL3	Pvrl3	Mus musculus poliovirus receptor-related 3 (Pvrl3), transcript	58998	3093	1963	1391	1803
QDPR	Qdpr	Mus musculus quinoid dihydropteridine reductase (Qdpr), mRNA.	110391	1578	1043	978	950
R3HDM1	R3hdm1	Mus musculus R3H domain 1 (binds single-stranded nucleic acids)	226412	932	774	820	987
RAB11A	Rab11a	Mus musculus RAB11a, member RAS oncogene family (Rab11a),	53869	541	446	362	456
RAB18	Rab18	Mus musculus RAB18, member RAS oncogene family (Rab18), mRNA.	19330	111	123	126	116
RAB27B	Rab27b	Mus musculus RAB27b, member RAS oncogene family (Rab27b),	80718	278	232	174	192
RAB32	Rab32	Mus musculus RAB32, member RAS oncogene family (Rab32), mRNA.	67844	1820	2748	2709	2982
RAB33A	Rab33a	Mus musculus RAB33A, member of RAS oncogene family (Rab33a),	19337	239	165	169	190
RAB35	Rab35	Mus musculus RAB35, member RAS oncogene family (Rab35), mRNA.	77407	1607	1968	2277	2164
RAB3B	Rab3b			175	133	136	135
RAB3C	Rab3c	Mus musculus RAB3C, member RAS oncogene family (Rab3c), mRNA.	67295	126	132	131	118
RAB43	Rab43	Mus musculus RAB43, member RAS oncogene family (Rab43),	69834	307	365	395	346
RAB6B	Rab6b			470	288	364	245
RABL2A	Rabl2a	Mus musculus RAB, member of RAS oncogene family-like 2A	68708	419	326	465	447

RAD50	Rad50	Mus musculus RAD50 homolog (S. cerevisiae) (Rad50), mRNA.	19360	687	557	517	599
RAD9	Rad9	Mus musculus RAD9 homolog (S. pombe) (Rad9), mRNA.	19367	132	133	144	137
RALA	Rala	Mus musculus v-ral simian leukemia viral oncogene homolog A (ras	56044	495	426	346	393
RANBP17	Ranbp17	Mus musculus RAN binding protein 17 (Ranbp17), mRNA.	66011	123	123	139	137
RANBP6	Ranbp6	Mus musculus RAN binding protein 6 (Ranbp6), mRNA.	240614	173	155	143	164
RARS	Rars	Mus musculus arginyl-tRNA synthetase (Rars), mRNA.	104458	1029	1630	1251	1544
RARS2	Rars2	Mus musculus arginyl-tRNA synthetase 2, mitochondrial (Rars2),	109093	888	670	603	620
RASAL2	Rasal2	Mus musculus RAS protein activator like 2 (Rasal2), mRNA.	226525	158	184	186	198
RASEF	Rasef	Mus musculus RAS and EF hand domain containing (Rasef), mRNA.	242505	462	259	191	243
RASEF	Rasef	Mus musculus RAS and EF hand domain containing (Rasef), mRNA.	242505	570	332	251	290
RASGRF1	Rasgrf1	Mus musculus RAS protein-specific guanine nucleotide-releasing	19417	145	129	138	131
RASIP1	Rasip1	Mus musculus Ras interacting protein 1 (Rasip1), mRNA.	69903	212	257	337	266
RBBP4	Rbbp4	Mus musculus retinoblastoma binding protein 4 (Rbbp4), mRNA.	19646	363	451	414	339
RBBP7	Rbbp7	Mus musculus retinoblastoma binding protein 7 (Rbbp7), mRNA.	245688	156	212	208	193
RBM16	Rbm16			126	140	139	129
RBM41	Rbm41	Mus musculus RNA binding motif protein 41 (Rbm41), mRNA.	237073	136	140	127	121
RBP2	Rbp2	Mus musculus retinol binding protein 2, cellular (Rbp2), mRNA.	19660	398	204	174	191
RBP2	Rbp2			421	182	176	190
RDH12	Rdh12	Mus musculus retinol dehydrogenase 12 (Rdh12), mRNA.	77974	137	268	225	205
RDH12	Rdh12			130	148	144	138
RDH14	Rdh14	Mus musculus retinol dehydrogenase 14 (all-trans and 9-cis) (Rdh14),	105014	1305	996	722	891
RECQL	Recql	Mus musculus RecQ protein-like (Recql), mRNA.	19691	156	135	155	143
REG3G	Reg3g	Mus musculus regenerating islet-derived 3 gamma (Reg3g), mRNA.	19695	134	839	3829	3238
RFTN2	Rftn2	Mus musculus raftlin family member 2 (Rftn2), mRNA. XM_920263	74013	341	216	266	223
RFX1	Rfx1			135	127	130	141
RG9MTD3	Rg9mtd3	Mus musculus RNA (guanine-9-) methyltransferase domain containing 3	69934	146	143	128	126
RGMB	Rgmb	Mus musculus RGM domain family, member B (Rgmb), mRNA.	68799	241	168	185	204
RGR	Rgr	Mus musculus retinal G protein coupled receptor (Rgr), mRNA.	57811	117	135	123	119
RGS19	Rgs19	Mus musculus regulator of G-protein signaling 19 (Rgs19), mRNA.	56470	150	153	180	181
RGS9BP	Rgs9bp	Mus musculus regulator of G-protein signalling 9 binding protein	243923	135	150	145	147

RHOJ	Rhoj	Mus musculus ras homolog gene family, member J (Rhoj), mRNA.	80837	1056	2491	2846	1797
RHOT2	Rhot2	Mus musculus ras homolog gene family, member T2 (Rhot2), nuclear	214952	397	357	298	336
RHPN2	Rhpn2	Mus musculus rhophilin, Rho GTPase binding protein 2 (Rhpn2), mRNA.	52428	1739	1210	1337	1457
RILPL2	Rilpl2	Mus musculus Rab interacting lysosomal protein-like 2 (Rilpl2), mRNA.	80291	300	553	565	499
RIMS2	Rims2	Mus musculus regulating synaptic membrane exocytosis 2 (Rims2),	116838	150	134	126	163
RIN2	Rin2	Mus musculus Ras and Rab interactor 2 (Rin2), mRNA.	74030	1946	1268	1687	1266
RIPK2	Ripk2	Mus musculus receptor (TNFRSF)-interacting serine-threonine kinase 2	192656	209	232	266	272
RMND5B	Rmnd5b	Mus musculus required for meiotic nuclear division 5 homolog B (S.	66089	186	219	220	201
RNF144A	Rnf144a	Mus musculus ring finger protein 144A (Rnf144a), transcript variant 2,	108089	202	363	417	361
RNF167	Rnf167	Mus musculus ring finger protein 167 (Rnf167), mRNA.	70510	489	361	366	326
RNF170	Rnf170	Mus musculus ring finger protein 170 (Rnf170), mRNA.	77733	285	260	227	281
RNF38	Rnf38	Mus musculus ring finger protein 38 (Rnf38), transcript variant 2,	73469	150	175	201	165
RNPC3	Rnpc3	Mus musculus RNA-binding region (RNP1, RRM) containing 3 (Rnpc3),	67225	141	142	154	155
ROBO1	Robo1	Mus musculus roundabout homolog 1 (Drosophila) (Robo1), mRNA.	19876	126	127	148	133
ROBO4	Robo4	Mus musculus roundabout homolog 4 (Drosophila) (Robo4), mRNA.	74144	471	596	813	659
ROCK2	Rock2	Mus musculus Rho-associated coiled-coil containing protein kinase 2	19878	198	226	189	232
RP23-RPAP1	Rp23-Rpap1	Mus musculus similar to oxidative stress responsive 1 (Rp23-297j14.5), Mus musculus RNA polymerase II associated protein 1 (Rpap1), mRNA.	10004140 68925	389 145	308 125	277 134	255 123
RPGRIP1L	Rpgrip1l	Mus musculus Rpgrip1-like (Rpgrip1l), mRNA.	244585	183	148	142	152
RPL12	Rpl12	Mus musculus ribosomal protein L12 (Rpl12), mRNA.	269261	16334	18318	17590	16888
RPL18A	Rpl18a	Mus musculus Ribosomal protein L18A (Rpl18a), mRNA.	76808	11302	11700	15442	14267
RPL22	Rpl22	Mus musculus ribosomal protein L22 (Rpl22), mRNA.	19934	2504	1522	1415	1064
RPL32	Rpl32			20280	17335	23023	22103
RPL39	Rpl39	Mus musculus ribosomal protein L39 (Rpl39), mRNA.	67248	21894	20515	25461	25461
RPL9	Rpl9	Mus musculus ribosomal protein L9 (Rpl9), mRNA.	20005	30092	29223	24884	23809
RPS12	Rps12			30407	29074	31710	32651
RPS14	Rps14	Mus musculus ribosomal protein S14 (Rps14), mRNA.	20044	24626	22720	28655	26402
RPS19	Rps19	Mus musculus ribosomal protein S19 (Rps19), mRNA.	20085	22518	24713	22915	22265
RPS2	Rps2	Mus musculus ribosomal protein S2 (Rps2), mRNA.	16898	18930	24421	18367	17760
RPS21	Rps21	Mus musculus ribosomal protein S21 (Rps21), mRNA.	66481	23723	21986	26856	25128

RPS24	Rps24			276	249	291	319
RPS6	Rps6	Mus musculus ribosomal protein S6 (Rps6), mRNA.	20104	14693	15028	13220	12943
RPS6KA4	Rps6ka4	Mus musculus ribosomal protein S6 kinase, polypeptide 4 (Rps6ka4),	56613	367	482	511	550
RPS9	Rps9	Mus musculus ribosomal protein S9 (Rps9), mRNA.	76846	22969	27753	21549	20839
RPS9	Rps9	Mus musculus ribosomal protein S9 (Rps9), mRNA.	76846	15678	15584	14243	13602
RRP1B	Rrp1b	Mus musculus ribosomal RNA processing 1 homolog B (S. cerevisiae)	72462	130	139	154	139
RSHL2A	Rshl2a	Mus musculus radial spokehead-like 2A (Rshl2a), mRNA.	66832	991	834	981	849
RSL1D1	Rsl1d1	Mus musculus ribosomal L1 domain containing 1 (Rsl1d1), mRNA.	66409	768	865	823	940
RSRC2	Rsrc2	Mus musculus arginine/serine-rich coiled-coil 2 (Rsrc2), transcript	208606	1076	818	560	933
RSRC2	Rsrc2	Mus musculus arginine/serine-rich coiled-coil 2 (Rsrc2), transcript	208606	1053	727	487	718
RSU1	Rsu1	Mus musculus Ras suppressor protein 1 (Rsu1), mRNA.	20163	281	287	329	310
RTN4	Rtn4			127	121	122	132
RTP2	Rtp2	Mus musculus receptor transporter protein 2 (Rtp2), mRNA.	224055	132	133	126	123
RTTN	Rttn			140	133	157	132
RUNDC3B	Rundc3b	Mus musculus RUN domain containing 3B (Rundc3b), mRNA.	242819	409	234	256	231
S100A11	S100a11	Mus musculus S100 calcium binding protein A11 (calgizzarin)	20195	9799	23723	18693	19518
SAMD8	Samd8	Mus musculus sterile alpha motif domain containing 8 (Samd8), mRNA.	67630	134	127	143	151
SAR1B	Sar1b	Mus musculus SAR1 gene homolog B (S. cerevisiae) (Sar1b), mRNA.	66397	2640	2771	2578	2486
SAST-	Sast-pending			145	148	169	162
SBNO2	Sbno2	Mus musculus strawberry notch homolog 2 (Drosophila) (Sbno2),	216161	207	296	374	319
SC5D	Sc5d			198	157	168	197
SCAPER	Scaper	Mus musculus S phase cyclin A-associated protein in the ER (Scaper), mR	244891	132	135	139	124
SCD1	Scd1	Mus musculus stearoyl-Coenzyme A desaturase 1 (Scd1), mRNA.	20249	1643	693	889	804
SCEL	Scel	Mus musculus sciellin (Scel), mRNA.	64929	216	150	151	157
SCL0001132	scl0001132.1_		120	127	145	151	
SCL0001233	scl0001233.1_		132	140	147	160	
SCL0001487	scl0001487.1_		511	451	374	350	
SCL0001533	scl0001533.1_		127	146	144	150	
SCL0001849	scl0001849.1_		310	654	944	878	
SCL0002137	scl0002137.1_		126	133	137	130	

SCL0002180	scl0002180.1_		155	136	143	151	
SCL0002617	scl0002617.1_		5064	2871	2994	3857	
SCL0003547	scl0003547.1_			2968	1171	1592	976
SCL000710.	scl000710.1_2		158	143	154	144	
SCL000859.	scl000859.1_3		119	134	130	122	
SCL000911.	scl000911.1_9		850	705	641	964	
SCML2	Scml2	Mus musculus sex comb on midleg-like 2 (Drosophila) (Scml2), mRNA.	107815	137	141	122	129
SCML2	Scml2	Mus musculus sex comb on midleg-like 2 (Drosophila) (Scml2), mRNA.	107815	146	135	137	126
SCN11A	Scn11a	Mus musculus sodium channel, voltage-gated, type XI, alpha (Scn11a),	24046	236	194	210	216
SCN3A	Scn3a			131	127	136	144
SCYA28-	Scya28-			152	145	129	126
SEC14L1	Sec14l1	Mus musculus SEC14-like 1 (S. cerevisiae) (Sec14l1), mRNA.	74136	175	211	227	249
SEC22C	Sec22c	Mus musculus SEC22 vesicle trafficking protein homolog C (S. cerevisiae)	215474	133	133	136	129
SEC31B	Sec31b	Mus musculus Sec31 homolog B (S. cerevisiae) (Sec31b), mRNA.	240667	128	139	148	131
SECTM1A	Sectm1a	Mus musculus secreted and transmembrane 1A (Sectm1a), mRNA.	209588	221	184	164	160
SEL1L	Sel1l	Mus musculus sel-1 suppressor of lin-12-like (C. elegans) (Sel1l),	20338	735	1088	1134	1110
SEL1L	Sel1l	Mus musculus sel-1 suppressor of lin-12-like (C. elegans) (Sel1l),	20338	456	436	703	839
SEMA3B	Sema3b	Mus musculus sema domain, immunoglobulin domain (Ig), short basic	20347	329	284	225	247
SEMA5A	Sema5a			1228	469	595	707
SEMA5A	Sema5a	Mus musculus sema domain, seven thrombospondin repeats (type 1	20356	1594	590	699	853
SEMA6D	Sema6d	Mus musculus sema domain, transmembrane domain (TM), and	214968	124	142	137	145
SENP5	Senp5	Mus musculus SUMO/sentrin specific peptidase 5 (Senp5), mRNA.	320213	135	142	128	135
SENP6	Senp6	Mus musculus SUMO/sentrin specific peptidase 6 (Senp6), mRNA.	215351	142	135	128	137
SENP7	Senp7	Mus musculus SUMO1/sentrin specific peptidase 7 (Senp7), transcript va	66315	498	393	293	409
SEPN1	Sepn1	Mus musculus selenoprotein N, 1 (Sepn1),mRNA.	74777	381	586	736	778
SERHL	Serhl	Mus musculus serine hydrolase-like (Serhl), mRNA.	68607	1402	1401	1098	1190
SERPINA12	Serpina12	Mus musculus serine (or cysteine) peptidase inhibitor, clade A (alpha-	68054	124	127	135	131
SERPINA3F	Serpina3f	Mus musculus serine (or cysteine) peptidase inhibitor, clade A,	238393	137	2009	1403	697
SERPINA3G	Serpina3g	Mus musculus serine (or cysteine) peptidase inhibitor, clade A,	20715	406	4569	3424	2498
SERPINA9	Serpina9			172	144	132	127

SERTAD2	Sertad2	Mus musculus SERTA domain containing 2 (Sertad2), transcript	58172	665	636	535	545
SETD8	Setd8	Mus musculus SET domain containing (lysine methyltransferase) 8	67956	727	601	535	616
SFRP1	Sfrp1	Mus musculus secreted frizzled-related protein 1 (Sfrp1), mRNA.	20377	624	2407	2707	3193
SFRP1	Sfrp1			313	1097	1469	1584
SFRP4	Sfrp4	Mus musculus secreted frizzled-related protein 4 (Sfrp4), mRNA.	20379	124	150	162	164
SFRS7	Sfrs7	Mus musculus splicing factor, arginine/serine-rich 7 (Sfrs7), mRNA.	225027	1145	746	458	753
SGK3	Sgk3	Mus musculus serum/glucocorticoid regulated kinase 3 (Sgk3),	170755	131	141	132	143
SH2D5	Sh2d5	Mus musculus SH2 domain containing 5 (Sh2d5), mRNA.	230863	124	127	132	141
SH3BGR	Sh3bgr			177	136	144	141
SH3RF2	Sh3rf2	Mus musculus SH3 domain containing ring finger 2 (Sh3rf2), mRNA.	269016	387	268	203	226
SH3YL1	Sh3yl1	Mus musculus Sh3 domain YSC-like 1 (Sh3yl1), mRNA.	24057	2302	2095	1769	1950
SHC1	Shc1	Mus musculus src homology 2 domain-containing transforming	20416	3633	4130	4014	4022
SHE	She	Mus musculus src homology 2 domain-containing transforming	214547	148	152	171	162
SHF	Shf	Mus musculus Src homology 2 domain containing F (Shf), mRNA.	435684	153	151	190	167
SHROOM4	Shroom4	Mus musculus shroom family member 4 (Shroom4), mRNA.	208431	138	146	153	136
SIF1	Sif1			17391	15584	18783	22518
SIRPA	Sirpa	Mus musculus signal-regulatory protein alpha (Sirpa), mRNA.	19261	130	152	161	171
SIX5	Six5			209	157	175	206
SKAP2	Skap2	Mus musculus src family associated phosphoprotein 2 (Skap2),	54353	2537	3612	3240	3634
SKIL	Skil	Mus musculus SKI-like (Skil), transcript variant 1, mRNA.	20482	460	350	360	422
SKP2	Skp2			150	158	147	164
SLA	Sla	Mus musculus src-like adaptor (Sla), transcript variant 2, mRNA.	20491	301	1173	1076	829
SLA	Sla	Mus musculus src-like adaptor (Sla), transcript variant 2, mRNA.	20491	128	172	184	158
SLC10A6	Slc10a6	Mus musculus solute carrier family 10 (sodium/bile acid	75750	169	666	714	274
SLC11A1	Slc11a1	Mus musculus solute carrier family 11 (proton-coupled divalent	18173	272	659	1020	809
SLC11A2	Slc11a2			131	137	134	155
SLC13A1	Slc13a1	Mus musculus solute carrier family 13 (sodium/sulphate symporters),	55961	129	123	118	119
SLC13A3	Slc13a3	Mus musculus solute carrier family 13 (sodium-dependent	114644	141	166	222	155
SLC19A1	Slc19a1			124	128	140	138
SLC1A1	Slc1a1	Mus musculus solute carrier family 1 (neuronal/epithelial high	20510	403	317	270	257

SLC20A1	Slc20a1	Mus musculus solute carrier family 20, member 1 (Slc20a1), mRNA.	20515	848	212	302	271
SLC20A1	Slc20a1			207	147	150	154
SLC24A3	Slc24a3	Mus musculus solute carrier family 24 (sodium/potassium/calcium	94249	1808	818	1047	827
SLC25A11	Slc25a11	Mus musculus solute carrier family 25 (mitochondrial carrier	67863	1402	1317	982	1169
SLC25A20	Slc25a20	Mus musculus solute carrier family 25 (mitochondrial	57279	925	784	602	555
SLC25A20	Slc25a20	Mus musculus solute carrier family 25 (mitochondrial	57279	6309	4617	3903	3654
SLC25A34	Slc25a34	Mus musculus solute carrier family 25, member 34 (Slc25a34),	384071	425	315	243	241
SLC27A3	Slc27a3			189	228	238	250
SLC2A13	Slc2a13	Mus musculus solute carrier family 2 (facilitated glucose transporter),	239606	790	467	459	490
SLC2A13	Slc2a13	Mus musculus solute carrier family 2 (facilitated glucose transporter),	239606	1181	589	605	711
SLC2A2	Slc2a2	Mus musculus solute carrier family 2 (facilitated glucose transporter),	20526	158	138	127	129
SLC2A8	Slc2a8	Mus musculus solute carrier family 2, (facilitated glucose	56017	273	221	239	186
SLC30A9	Slc30a9			166	148	149	161
SLC31A2	Slc31a2			184	205	267	213
SLC35A3	Slc35a3	Mus musculus solute carrier family 35 (UDP-N-acetylglucosamine	229782	882	582	416	512
SLC35B4	Slc35b4	Mus musculus solute carrier family 35, member B4 (Slc35b4), mRNA.	58246	781	771	834	889
SLC37A2	Slc37a2	Mus musculus solute carrier family 37 (glycerol-3-phosphate	56857	168	127	131	141
SLC38A11	Slc38a11	Mus musculus solute carrier family 38, member 11 (Slc38a11),	320106	161	145	141	152
SLC46A1	Slc46a1	Mus musculus solute carrier family 46, member 1 (Slc46a1), mRNA.	52466	657	296	218	309
SLC5A4A	Slc5a4a	Mus musculus solute carrier family 5, member 4a (Slc5a4a), mRNA.	64452	132	131	144	123
SLC6A4	Slc6a4			231	170	158	150
SLC7A11	Slc7a11			141	197	195	170
SLC9A10	Slc9a10	Mus musculus solute carrier family 9, isoform 10 (Slc9a10), mRNA.	208169	128	115	129	121
SLIT3	Slit3			136	197	237	242
SLMAP	Slmap	Mus musculus sarcolemma associated protein (Slmap), mRNA.	83997	229	180	158	193
SLMO2	Slmo2	Mus musculus slowmo homolog 2 (Drosophila) (Slmo2), mRNA.	66390	10369	9118	7987	7963
SMAP2	Smap2	Mus musculus stromal membrane-associated GTPase-activating	69780	149	159	177	179
SMARCAD1	Smarcad1	Mus musculus SWI/SNF-related, matrix-associated actin-dependent	13990	432	368	259	303
SMARCD3	Smarcd3	Mus musculus SWI/SNF related, matrix associated, actin dependent	66993	265	184	240	191
SMC3	Smc3	Mus musculus structural maintenace of chromosomes 3 (Smc3),	13006	132	122	115	124

SMCHD1	Smchd1	Mus musculus SMC hinge domain containing 1 (Smchd1), mRNA.	74355	397	299	281	311
SMCR8	Smcr8	Mus musculus Smith-Magenis syndrome chromosome region,	237782	137	150	150	135
SMPD4	Smpd4	Mus musculus sphingomyelin phosphodiesterase 4 (Smpd4), mRNA.	77626	215	237	246	273
SNAI1	Snai1	Mus musculus snail homolog 1 (Drosophila) (Snai1), mRNA.	20613	201	336	354	502
SNAPC2	Snapc2	Mus musculus small nuclear RNA activating complex, polypeptide 2	102209	140	159	163	139
SNORA70	Snora70	Mus musculus small nucleolar RNA, H/ACA box 70 (Snora70), non-	104368	175	203	207	227
SNPH	Snph	Mus musculus syntaphilin (Snph), mRNA.	241727	242	182	199	211
SNTG2	Sntg2	Mus musculus syntrophin, gamma 2 (Sntg2), mRNA.	268534	346	224	282	230
SNX16	Snx16	Mus musculussorting nexin 16 (Snx16), mRNA.	74718	365	287	209	271
SNX21	Snx21	Mus musculus sorting nexin family member 21 (Snx21), mRNA.	101113	545	405	459	327
SNX33	Snx33	Mus musculussorting nexin 33 (Snx33), mRNA.	235406	254	195	201	235
SOCS3	Socs3	Mus musculus suppressor of cytokine signaling 3 (Socs3), mRNA.	12702	288	3819	3867	2547
SORBS2	Sorbs2	Mus musculus sorbin and SH3 domain containing 2 (Sorbs2), mRNA.	234214	311	235	162	191
SOX2	Sox2			140	145	145	135
SOX7	Sox7			143	173	151	165
SPARC	Sparc	Mus musculus secreted acidic cysteine rich glycoprotein (Sparc),	20692	683	1248	2312	2544
SPATA3	Spata3	Mus musculus spermatogenesis associated 3 (Spata3), transcript	70060	124	130	120	128
SPEER4A	Speer4a	Mus musculus spermatogenesis associated glutamate (E)-rich protein	75657	167	135	142	128
SPEER7-PS1	Speer7-ps1	Mus musculus spermatogenesis associated glutamate (E)-rich protein	75858	161	144	128	127
SPG20	Spg20			360	240	281	256
SPG21	Spg21	Mus musculus spastic paraplegia 21 homolog (human) (Spg21),	27965	892	1189	1066	964
SPIN	Spin			311	332	387	485
SPN	Spn	Mus musculus sialophorin (Spn), transcript variant 2, mRNA.	20737	174	159	170	156
SPNR	Spnr			271	230	200	206
SPNS1	Spns1	Mus musculus spinster homolog 1 (Drosophila) (Spns1), mRNA.	73658	349	292	429	320
SPO11	Spo11	Mus musculus sporulation protein, meiosis-specific, SPO11 homolog	26972	125	131	139	144
SPON1	Spon1	Mus musculus spondin 1, (f-spondin) extracellular matrix protein	233744	130	189	271	255
SPRED3	Spred3	Mus musculus sprouty-related, EVH1 domain containing 3 (Spred3),	101809	177	159	135	139
SPRR2A	Sprr2a	Mus musculus small proline-rich protein 2A (Sprr2a), mRNA.	20755	419	299	248	271
SPRR2G	Sprr2g	Mus musculus small proline-rich protein 2G (Sprr2g), non-coding RNA.	20761	127	153	229	137

SRGAP2	Srgap2	PREDICTED: Mus musculus SLIT-ROBO Rho GTPase activating protein	14270	207	213	232	221
SRPK2	Srpk2			235	209	224	247
SRPR	Srpr	Mus musculus signal recognition particle receptor ('docking protein')	67398	878	972	1102	1101
SRPX	Srpx	Mus musculus sushi-repeat-containing protein (Srpx), mRNA.	51795	251	334	459	334
SRXN1	Srxn1	Mus musculus sulfiredoxin 1 homolog (S. cerevisiae) (Srxn1), mRNA.	76650	1173	2028	1583	1661
SSR1	Ssr1	Mus musculus signal sequence receptor, alpha (Ssr1), mRNA.	107513	117	132	124	115
SSX2IP	Ssx2ip	Mus musculus synovial sarcoma, X breakpoint 2 interacting protein	99167	1241	1170	1004	1092
STAG1	Stag1	Mus musculus stromal antigen 1 (Stag1), mRNA. XM_919981	20842	125	120	115	131
STARD3	Stard3	Mus musculus START domain containing 3 (Stard3), mRNA.	59045	445	416	574	477
STBD1	Stbd1	Mus musculus starch binding domain 1 (Stbd1), mRNA.	52331	298	290	347	332
STK24	Stk24			779	919	1006	882
STK32A	Stk32a	Mus musculus serine/threonine kinase 32A (Stk32a), mRNA.	269019	139	139	146	146
STK33	Stk33	PREDICTED: Mus musculus serine/threonine kinase 33 (Stk33),	117229	136	128	124	129
STRBP	Strbp			138	133	138	134
STX18	Stx18	Mus musculus syntaxin 18 (Stx18), mRNA.	71116	400	459	336	419
STX1A	Stx1a	Mus musculus syntaxin 1A (brain) (Stx1a), mRNA.	20907	213	240	274	264
STX3	Stx3	Mus musculus syntaxin 3 (Stx3), transcript variant B, mRNA.	20908	259	178	194	204
STX6	Stx6	Mus musculus syntaxin 6 (Stx6), mRNA.	58244	264	320	385	328
STYXL1	Styxl1	Mus musculus serine/threonine/tyrosine interacting-like 1 (Styxl1),	76571	165	177	145	142
SUCLG1	Suclg1	Mus musculus succinate-CoA ligase, GDP-forming, alpha subunit	56451	173	149	147	154
SULF2	Sulf2	Mus musculus sulfatase 2 (Sulf2), mRNA.	72043	552	1466	1490	1860
SULF2	Sulf2	Mus musculus sulfatase 2 (Sulf2), mRNA.	72043	176	167	186	203
SULT1C1	Sult1c1	Mus musculus sulfotransferase family, cytosolic, 1C, member 1	20888	119	129	137	129
SULT5A1	Sult5a1	Mus musculus sulfotransferase family 5A, member 1 (Sult5a1),	57429	133	141	156	152
SUMO1	Sumo1	Mus musculus SMT3 suppressor of mif two 3 homolog 1 (yeast)	22218	1767	1244	839	932
SUMO1	Sumo1			1581	1212	755	903
SUMO2	Sumo2	Mus musculus SMT3 suppressor of mif two 3 homolog 2 (yeast)	170930	5289	4732	4539	5876
SURF6	Surf6			181	228	235	235
SUZ12	Suz12	Mus musculus suppressor of zeste 12 homolog (Drosophila) (Suz12),	52615	2481	2379	1591	1653
SUZ12	Suz12	Mus musculus suppressor of zeste 12 homolog (Drosophila) (Suz12),	52615	166	161	145	151

SWAP70	Swap70	Mus musculus SWA-70 protein (Swap70), mRNA.	20947	673	470	622	577
SYCN	Sycn	Mus musculus syncollin (Sycn), mRNA.	68416	18598	6121	3662	1874
SYCP2	Sycp2	Mus musculus synaptonemal complex protein 2 (Sycp2), mRNA.	320558	122	124	134	134
SYNC	Sync			194	179	177	163
SYNE2	Syne2	Mus musculus synaptic nuclear envelope 2 (Syne2), mRNA.	319565	165	149	148	151
SYNGR1	Syngr1	Mus musculus synaptogyrin 1 (Syngr1), transcript variant 1b, mRNA.	20972	133	146	159	144
SYNJ2BP	Synj2bp	Mus musculus synaptojanin 2 binding protein (Synj2bp), mRNA.	24071	1016	899	676	846
SYNM	Synm	Mus musculus synemin, intermediate filament protein (Synm),	233335	1818	425	574	406
SYNM	Synm	Mus musculus synemin, intermediate filament protein (Synm),	233335	4177	1367	1765	1109
SYNPO2L	Synpo2l	Mus musculus synaptopodin 2-like (Synpo2l), mRNA.	68760	170	132	144	136
SYT12	Syt12	Mus musculus synaptotagmin XII (Syt12), mRNA.	171180	131	136	128	137
SYTL3	Sytl3	Mus musculus synaptotagmin-like 3 (Sytl3), transcript variant 5,	83672	139	166	162	150
TACC2	Tacc2			128	137	141	134
TACR3	Tacr3	Mus musculus tachykinin receptor 3 (Tacr3), mRNA.	21338	146	125	132	137
TAF7	Taf7			128	119	123	125
TAF8	Taf8	Mus musculus TAF8 RNA polymerase II, TATA box binding protein	63856	128	133	134	147
TAGLN	Tagln	Mus musculus transgelin (Tagln), mRNA.	21345	2015	825	909	685
TATDN2	Tatdn2	Mus musculus TatD DNase domain containing 2 (Tatdn2), mRNA.	381801	227	505	409	361
TBC1D1	Tbc1d1	Mus musculus TBC1 domain family, member 1 (Tbc1d1), mRNA.	57915	181	202	227	213
TBC1D1	Tbc1d1	Mus musculus TBC1 domain family, member 1 (Tbc1d1), mRNA.	57915	355	361	477	419
TBX15	Tbx15			132	133	144	127
TCEAL8	Tceal8	Mus musculus transcription elongation factor A (SII)-like 8 (Tceal8),	66684	1034	835	704	816
TCFAP2B	Tcfap2b	Mus musculus transcription factor AP-2 beta (Tcfap2b), transcript	21419	124	138	128	132
TCIRG1	Tcirg1	Mus musculus T-cell, immune regulator 1, ATPase, H+ transporting,	27060	357	529	579	619
TCIRG1	Tcirg1	Mus musculus T-cell, immune regulator 1, ATPase, H+ transporting,	27060	425	694	752	792
TCP11L1	Tcp11l1	Mus musculus t-complex 11 like 1 (Tcp11l1), mRNA.	320554	123	123	131	117
TDGF1	Tdgf1	Mus musculus teratocarcinoma-derived growth factor (Tdgf1),	21667	125	131	133	123
TDPOZ1	Tdpoz1	Mus musculus TD and POZ domain containing 1 (Tdpoz1), mRNA.	207213	136	150	148	156
TDRD7	Tdrd7	Mus musculus tudor domain containing 7 (Tdrd7), mRNA.	100121	1988	1616	1494	1515
TEAD4	Tead4	Mus musculus TEA domain family member 4 (Tead4), transcript	21679	145	183	185	176

TEP1	Tep1			131	127	122	128
TERF2	Terf2	Mus musculus telomeric repeat binding factor 2 (Terf2), mRNA.	21750	504	547	590	660
TES	Tes	Mus musculus testis derived transcript (Tes), transcript variant 1,	21753	9052	7211	6766	6394
TEX19.1	Tex19.1	Mus musculus testis expressed gene 19.1 (Tex19.1), mRNA.	73679	126	134	142	150
TFPT	Tfpt	Mus musculus TCF3 (E2A) fusion partner (Tfpt), mRNA.	69714	286	321	388	361
TFRC	Tfrc	Mus musculus transferrin receptor (Tfrc), mRNA.	22042	2562	3772	1940	4300
TGFBR2	Tgfbr2	Mus musculus transforming growth factor, beta receptor II (Tgfbr2),	21813	3458	4274	5996	5539
TGFBR2	Tgfbr2			161	158	146	143
TGS1	Tgs1	Mus musculus trimethylguanosine synthase homolog (S. cerevisiae)	116940	274	336	269	329
THBS1	Thbs1	Mus musculus thrombospondin 1 (Thbs1), mRNA.	21825	138	249	386	283
THEM4	Them4	Mus musculus thioesterase superfamily member 4 (Them4), mRNA.	75778	274	195	178	176
THNSL2	Thnsl2	Mus musculus threonine synthase-like 2 (bacterial) (Thnsl2),	232078	603	463	383	369
THNSL2	Thnsl2	Mus musculus threonine synthase-like 2 (bacterial) (Thnsl2),	232078	557	388	315	342
THSD7B	Thsd7b	Mus musculus thrombospondin, type I, domain containing 7B	210417	143	139	154	148
THUMPD1	Thumpd1	Mus musculus THUMP domain containing 1 (Thumpd1), mRNA.	233802	767	678	583	572
TIMM44	Timm44	Mus musculus translocase of inner mitochondrial membrane 44	21856	590	519	546	488
TIMM44	Timm44	Mus musculus translocase of inner mitochondrial membrane 44	21856	627	630	586	540
TIMP1	Timp1			242	2784	4749	3848
TINAG	Tinag	Mus musculus tubulointerstitial nephritisantigen (Tinag), mRNA.	26944	356	181	156	175
TLCD1	Tlcd1	Mus musculus TLC domain containing 1 (Tlcd1), mRNA.	68385	313	208	255	233
TLE4	Tle4	Mus musculus transducin-like enhancer of split 4, homolog of	21888	3109	2416	1959	2246
TLR13	Tlr13	Mus musculus toll-like receptor 13 (Tlr13), mRNA.	279572	144	235	242	227
TLR6	Tlr6			129	133	141	154
TLR6	Tlr6	Mus musculus toll-like receptor 6 (Tlr6), mRNA.	21899	164	268	270	244
TM2D3	Tm2d3	Mus musculus TM2 domain containing 3 (Tm2d3), transcript variant	68634	339	262	221	234
TMC7	Tmc7	Mus musculus transmembrane channel-like gene family 7 (Tmc7),	209760	735	410	441	379
TMED10	Tmed10	Mus musculus transmembrane emp24-like trafficking protein 10	68581	2082	2517	2273	2368
TMED2	Tmed2	Mus musculus transmembrane emp24 domain trafficking protein 2	56334	576	727	839	946
TMED7	Tmed7	PREDICTED: Mus musculus transmembrane emp24 protein transport	66676	1818	1649	1213	1499
TMEM107	Tmem107	Mus musculus transmembrane protein 107 (Tmem107), transcript	66910	174	146	135	143

TMEM120B	Tmem120b	Mus musculus transmembrane protein 120B (Tmem120b), mRNA.	330189	161	181	186	191
TMEM132A	Tmem132a	Mus musculus transmembrane protein 132A (Tmem132a), mRNA.	98170	212	259	271	299
TMEM150	Tmem150	Mus musculus transmembrane protein 150 (Tmem150), mRNA.	232086	271	319	374	355
TMEM168	Tmem168	Mus musculus transmembrane protein 168 (Tmem168), mRNA.	101118	243	173	149	177
TMEM176A	Tmem176a	Mus musculus transmembrane protein 176A (Tmem176a), mRNA.	66058	156	225	302	301
TMEM176B	Tmem176b	Mus musculus transmembrane protein 176B (Tmem176b), mRNA.	65963	2617	4283	5304	6290
TMEM35	Tmem35	Mus musculus transmembrane protein 35 (Tmem35), mRNA.	67564	168	135	134	141
TMEM65	Tmem65	Mus musculus transmembrane protein 65 (Tmem65), mRNA.	74868	331	408	463	417
TMEM81	Tmem81	Mus musculus transmembrane protein 81 (Tmem81), mRNA.	74626	181	174	166	184
TMEM9B	Tmem9b	Mus musculus TMEM9 domain family, member B (Tmem9b), mRNA.	56786	1450	1664	1578	1385
TMEM9B	Tmem9b	Mus musculus TMEM9 domain family, member B (Tmem9b), mRNA.	56786	1535	2032	1867	1736
TMOD2	Tmod2			132	126	142	133
TMOD4	Tmod4	Mus musculus tropomodulin 4 (Tmod4), mRNA.	50874	174	158	144	148
TMSB4X	Tmsb4x	Mus musculus thymosin, beta 4, X chromosome (Tmsb4x), mRNA.	19241	13795	17661	19076	21744
TNA	Tna			222	178	165	189
TNC	Tnc			632	1781	2762	2843
TNFAIP8	Tnfaip8	Mus musculus tumor necrosis factor, alpha-induced protein 8	106869	1303	1699	1750	1941
TNFRSF18	Tnfrsf18	Mus musculus tumor necrosis factor receptor superfamily, member	21936	147	203	225	201
TNFRSF18	Tnfrsf18			136	177	184	171
TNFRSF4	Tnfrsf4	Mus musculus tumor necrosis factor receptor superfamily, member 4	22163	164	371	320	276
TNFSF13B	Tnfsf13b	Mus musculus tumor necrosis factor (ligand) superfamily, member	24099	630	1158	970	1266
TNIK	Tnik	PREDICTED: Mus musculus TRAF2 and NCK interacting kinase,	665113	747	640	582	714
TOM1L2	Tom1l2	Mus musculus target of myb1-like 2 (chicken) (Tom1l2), transcript	216810	142	158	211	176
TPD52	Tpd52	Mus musculus tumor protein D52 (Tpd52), transcript variant 5,	21985	17293	16145	13960	14411
TPM1	Tpm1	Mus musculus tropomyosin 1, alpha (Tpm1), mRNA.	22003	6766	3323	3930	3863
TPM2	Tpm2	Mus musculus tropomyosin 2, beta (Tpm2), mRNA.	22004	10341	3711	5896	5450
TPPP	Tppp	Mus musculus tubulin polymerization promoting protein (Tppp),	72948	255	142	148	157
TRAF6	Traf6	Mus musculus Tnf receptor-associated factor 6 (Traf6), mRNA.	22034	148	193	181	162
TRAFD1	Trafd1	Mus musculus TRAF type zinc finger domain containing 1 (Trafd1),	231712	942	1729	1809	1574
TRAM2	Tram2	Mus musculus translocating chain-associating membrane protein 2	170829	131	132	136	120

TRAPPC3	Trappc3	Mus musculus trafficking protein particle complex 3 (Trappc3),	27096	1288	2243	2146	2072
TRBV6_AE0	TRBV6_AE000		120	131	126	138	
TREM1	Trem1	Mus musculus triggering receptor expressed on myeloid cells 1	58217	131	148	185	168
TRIM2	Trim2	Mus musculus tripartite motif protein 2 (Trim2), mRNA. XM_984114	80890	189	165	155	182
TRIM2	Trim2			138	133	126	131
TRIM23	Trim23	Mus musculus tripartite motif-containing 23 (Trim23), mRNA.	81003	168	161	130	141
TRIM27	Trim27			140	161	151	140
TRIM34	Trim34	Mus musculus tripartite motif protein 34 (Trim34), mRNA.	94094	251	222	233	242
TRIM35	Trim35	Mus musculus tripartite motif-containing 35 (Trim35), mRNA.	66854	127	134	148	160
TRIM38	Trim38	Mus musculus tripartite motif-containing 38 (Trim38), mRNA.	214158	147	132	135	132
TRIM39	Trim39	Mus musculus tripartite motif-containing 39 (Trim39), mRNA.	79263	652	630	710	775
TRIM40	Trim40	Mus musculus tripartite motif-containing 40 (Trim40), mRNA.	195359	180	478	395	395
TRIM7	Trim7			121	118	123	125
TRIM71	Trim71	Mus musculus tripartite motif-containing 71 (Trim71), mRNA.	636931	136	129	143	132
TRIM8	Trim8	Mus musculus tripartite motif protein 8 (Trim8), mRNA.	93679	2590	2776	3351	3406
TRIP6	Trip6	Mus musculus thyroid hormone receptor interactor 6 (Trip6), mRNA.	22051	284	350	462	427
TRMT12	Trmt12	Mus musculus tRNA methyltranferase 12 homolog (S. cerevisiae)	68260	182	163	151	162
TRP53BP1	Trp53bp1	Mus musculus transformation related protein 53 binding protein 1	27223	624	454	481	416
TRPC4AP	Trpc4ap	Mus musculus transient receptor potential cation channel, subfamily	56407	803	887	1014	954
TRPC5	Trpc5			133	135	128	139
TRPD52L3	Trpd52l3	Mus musculus tumor protein D52-like 3 (Trpd52l3), mRNA.	66745	141	128	134	134
TRPM6	Trpm6	Mus musculus transient receptor potential cation channel, subfamily	225997	1218	448	219	287
TRPM6	Trpm6	Mus musculus transient receptor potential cation channel, subfamily	225997	948	372	233	246
TRPM6	Trpm6	Mus musculus transient receptor potential cation channel, subfamily	225997	309	164	138	157
TRPT1	Trpt1	Mus musculus tRNA phosphotransferase1 (Trpt1), mRNA.	107328	199	191	170	162
TSC22D3	Tsc22d3	Mus musculus TSC22 domain family, member 3 (Tsc22d3), transcript	14605	2065	3186	3860	1890
TSC22D3	Tsc22d3	Mus musculus TSC22 domain family, member 3 (Tsc22d3), transcript	14605	204	320	277	209
TSN	Tsn			137	130	135	142
TSPYL3	Tspyl3	Mus musculus TSPY-like 3 (Tspyl3), mRNA.	241732	230	279	303	269
TTC14	Ttc14			477	402	308	381

TTC18	Ttc18	PREDICTED: Mus musculus tetratricopeptide repeat domain 18	76670	126	138	125	128
TTC30B	Ttc30b	Mus musculus tetratricopeptide repeat domain 30B (Ttc30b), mRNA.	72421	485	322	276	375
TTL	Ttl	Mus musculus tubulin tyrosine ligase (Ttl), mRNA.	69737	131	125	138	131
TTLL6	Ttll6	Mus musculus tubulin tyrosine ligase-like family, member 6 (Ttll6),	237930	247	198	177	176
TTLL8	Ttll8	Mus musculus tubulin tyrosine ligase-like family, member 8 (Ttll8),	239591	145	131	119	125
TUBA1A	Tuba1a	Mus musculus tubulin, alpha 1A (Tuba1a), mRNA.	22142	818	784	1431	1395
TUBGCP6	Tubgcp6			137	131	124	130
TUG1	Tug1	Mus musculus taurine upregulated gene 1 (Tug1), non-coding RNA.	544752	245	212	182	200
TULP4	Tulp4	Mus musculus tubby like protein 4 (Tulp4), mRNA.	68842	1607	1242	1207	1407
TXNDC11	Txndc11	Mus musculus thioredoxin domain containing 11 (Txndc11),	106200	158	199	184	175
TYW1	Tyw1	Mus musculus tRNA-yW synthesizing protein 1 homolog (S.	100929	184	170	159	163
UBCE7IP3-	Ubce7ip3-		127	129	126	133	
UBE2I	Ube2i	Mus musculus ubiquitin-conjugating enzyme E2I (Ube2i), mRNA.	22196	208	207	271	278
UBE2N	Ube2n	Mus musculus ubiquitin-conjugating enzyme E2N (Ube2n), mRNA.	93765	592	477	389	499
UBE3A	Ube3a			130	125	134	127
UBR2	Ubr2	Mus musculus ubiquitin protein ligase E3 component n-recognin 2	224826	209	253	279	266
UBR5	Ubr5	Mus musculus ubiquitin protein ligase E3 component n-recognin 5	70790	264	222	214	280
UBTD1	Ubtd1	Mus musculus ubiquitin domain containing 1 (Ubtd1), mRNA.	226122	210	231	282	226
UFC1	Ufc1	Mus musculus ubiquitin-fold modifier conjugating enzyme 1 (Ufc1),	66155	3382	4606	4038	4209
UGT2B34	Ugt2b34	Mus musculus UDP glucuronosyltransferase 2 family, polypeptide	100727	959	547	404	594
UHRF2	Uhrf2	Mus musculus ubiquitin-like, containing PHD and RING finger	109113	533	511	382	505
UNC13A	Unc13a	Mus musculus unc-13 homolog A (C. elegans) (Unc13a), mRNA.	382018	121	125	139	134
UNC13H1	Unc13h1			130	126	134	138
UNC84A	Unc84a	Mus musculus unc-84 homolog A (C. elegans) (Unc84a), mRNA.	77053	269	238	221	199
UPB1	Upb1	Mus musculus ureidopropionase, beta (Upb1), mRNA.	103149	248	160	138	146
UROS	Uros	Mus musculus uroporphyrinogen III synthase (Uros), mRNA.	22276	248	210	193	221
USMG3	Usmg3			161	147	159	143
USP12	Usp12	Mus musculus ubiquitin specific peptidase 12 (Usp12), mRNA.	22217	145	123	139	133
USP2	Usp2	Mus musculus ubiquitin specific peptidase 2 (Usp2), transcript	53376	122	123	129	131
USP28	Usp28	Mus musculus ubiquitin specific peptidase 28 (Usp28), mRNA.	235323	372	275	284	253

USP29	Usp29			124	120	136	131
UTP11L	Utp11l	Mus musculus UTP11-like, U3 small nucleolar ribonucleoprotein,	67205	3214	2976	2292	2767
UTP14B	Utp14b	Mus musculus UTP14, U3 small nucleolar ribonucleoprotein,	195434	140	137	129	131
V1RH5	V1rh5	Mus musculus vomeronasal 1 receptor, H5 (V1rh5), mRNA.	171248	145	144	136	131
VAPB	Vapb	Mus musculus vesicle-associated membrane protein, associated	56491	713	764	975	1005
VAV3	Vav3	Mus musculus vav 3 oncogene (Vav3), transcript variant 1, mRNA.	57257	127	133	117	126
VCAM1	Vcam1			121	130	135	149
VCAN	Vcan	Mus musculusversican (Vcan), transcript variant 1, mRNA.	13003	137	169	173	203
VCAN	Vcan	Mus musculusversican (Vcan), transcript variant 1, mRNA.	13003	137	146	154	159
VCAN	Vcan	Mus musculusversican (Vcan), transcript variant 1, mRNA.	13003	135	184	216	254
VDAC1	Vdac1	Mus musculus voltage-dependent anion channel 1 (Vdac1), mRNA.	22333	13632	11933	11338	10221
VDAC3	Vdac3	Mus musculus voltage-dependent anion channel 3 (Vdac3), mRNA.	22335	5064	3470	2713	3533
VIM	Vim			124	119	134	137
VKORC1L1	Vkorc1l1	Mus musculus vitamin K epoxide reductase complex, subunit 1-like 1	69568	389	389	288	347
VNN3	Vnn3	Mus musculus vanin 3 (Vnn3), mRNA.	26464	133	148	164	150
VSIG2	Vsig2	Mus musculus V-set and immunoglobulin domain containing 2	57276	525	229	285	194
WBP1	Wbp1	Mus musculus WW domain binding protein 1 (Wbp1), transcript	22377	608	549	439	445
WBSCR14	Wbscr14			182	138	136	155
WDFY2	Wdfy2	Mus musculus WD repeat and FYVE domain containing 2 (Wdfy2),	268752	130	151	139	153
WDR19	Wdr19	Mus musculus WD repeat domain 19 (Wdr19), mRNA.	213081	120	114	122	126
WDR20A	Wdr20a	Mus musculus WD repeat domain 20a (Wdr20a), mRNA.	69641	607	658	522	624
WDR33	Wdr33	Mus musculus WD repeat domain 33 (Wdr33), mRNA.	74320	235	203	214	194
WDR41	Wdr41	Mus musculus WD repeat domain 41 (Wdr41), mRNA.	218460	139	131	141	152
WDR55	Wdr55	Mus musculus WD repeat domain 55 (Wdr55), mRNA.	67936	237	315	272	281
WHSC1	Whsc1	PREDICTED: Mus musculus Wolf-Hirschhorn syndrome candidate 1	107823	194	219	204	248
WHSC1	Whsc1	Mus musculus Wolf-Hirschhorn syndrome candidate 1 (human)	107823	132	142	158	154
WWTR1	Wwtr1	Mus musculus WW domain containing transcription regulator 1	97064	984	1160	1518	1411
XKR9	Xkr9	Mus musculus X Kell blood group precursor related family member 9	381246	254	218	157	189
XPR1	Xpr1	Mus musculus xenotropic and polytropic retrovirus receptor 1	19775	2154	1137	971	1165
XPR1	Xpr1	Mus musculus xenotropic and polytropic retrovirus receptor 1	19775	1393	756	661	818

YBX2	Ybx2	Mus musculus Y box protein 2 (Ybx2), mRNA.	53422	297	183	167	189
YBX2	Ybx2			193	136	149	156
YIPF6	Yipf6	Mus musculus Yip1 domain family, member 6 (Yipf6), mRNA.	77929	364	267	223	271
YLPM1	Ylpm1	Mus musculus YLP motif containing 1 (Ylpm1), mRNA.	56531	284	244	262	269
YME1L1	Yme1l1	Mus musculus YME1-like 1 (S. cerevisiae) (Yme1l1), nuclear gene	27377	436	280	236	342
ZAN	Zan	Mus musculus zonadhesin (Zan), mRNA.	22635	935	306	384	553
ZBTB26	Zbtb26	Mus musculus zinc finger and BTB domain containing 26 (Zbtb26),	320633	203	167	146	186
ZBTB37	Zbtb37	Mus musculus zinc finger and BTB domain containing 37 (Zbtb37),	240869	126	118	124	119
ZC3HC1	Zc3hc1	Mus musculus zinc finger, C3HC type 1 (Zc3hc1), mRNA.	232679	354	458	503	421
ZCCHC16	Zcchc16	Mus musculus zinc finger, CCHC domain containing 16 (Zcchc16),	619287	121	119	125	116
ZDHHC12	Zdhhc12	Mus musculus zinc finger, DHHC domain containing 12 (Zdhhc12),	66220	219	264	329	294
ZDHHC21	Zdhhc21	Mus musculus zinc finger, DHHC domain containing 21 (Zdhhc21),	68268	936	1632	832	1527
ZFA	Zfa	Mus musculus zinc finger protein, autosomal (Zfa), mRNA.	22639	129	138	133	124
ZFML	Zfml			152	139	131	157
ZFP101	Zfp101	Mus musculus zinc finger protein 101 (Zfp101), mRNA.	22643	310	243	175	238
ZFP212	Zfp212	Mus musculus Zinc finger protein 212 (Zfp212), mRNA.	232784	1538	1315	1267	1099
ZFP295	Zfp295	Mus musculus zinc finger protein 295 (Zfp295), transcript variant 3,	114565	276	247	207	251
ZFP35	Zfp35	Mus musculus zinc finger protein 35 (Zfp35), mRNA.	22694	270	249	220	257
ZFP36	Zfp36	Mus musculus zinc finger protein 36 (Zfp36), mRNA.	22695	1299	1513	2135	1626
ZFP36L1	Zfp36l1	Mus musculus zinc finger protein 36, C3H type-like 1 (Zfp36l1),	12192	3216	3596	4001	4646
ZFP386	Zfp386	Mus musculus zinc finger protein 386 (Kruppel-like) (Zfp386),	56220	279	250	201	196
ZFP410	Zfp410	Mus musculus zinc finger protein 410 (Zfp410), mRNA.	52708	294	238	281	198
ZFP423	Zfp423	Mus musculus zinc finger protein 423 (Zfp423), mRNA.	94187	123	126	135	128
ZFP426	Zfp426	Mus musculus zinc finger protein 426 (Zfp426), mRNA.	235028	133	122	117	117
ZFP473	Zfp473	Mus musculus zinc finger protein 473 (Zfp473), mRNA.	243963	133	139	131	137
ZFP60	Zfp60	Mus musculus zinc finger protein 60 (Zfp60), transcript variant 2,	22718	262	195	178	211
ZFP622	Zfp622	Mus musculus zinc finger protein 622 (Zfp622), mRNA.	52521	141	139	147	145
ZFP707	Zfp707	Mus musculus zinc finger protein 707 (Zfp707), mRNA.	69020	548	386	308	353
ZFP746	Zfp746	PREDICTED: Mus musculus zinc finger protein 746 (Zfp746), mRNA.	69228	351	360	415	411
ZFP760	Zfp760	Mus musculus zinc finger protein 760 (Zfp760), mRNA.	240034	288	224	188	233

ZFP770	Zfp770	Mus musculus zinc finger protein 770 (Zfp770), mRNA.	228491	242	185	163	207
ZFP817	Zfp817	Mus musculus zinc finger protein 817 (Zfp817), mRNA.	238693	189	172	169	197
ZFP85-RS1	Zfp85-rs1	Mus musculus zinc finger protein 85, related sequence 1 (Zfp85-rs1),	22746	182	172	145	146
ZFY2	Zfy2	Mus musculus zinc finger protein 2, Y linked (Zfy2), mRNA.	22768	138	124	127	130
ZIC2	Zic2			132	130	144	148
ZKSCAN17	Zkscan17	Mus musculus zinc finger with KRAB and SCAN domains 17 (Zkscan17),	268417	234	252	319	261
ZKSCAN3	Zkscan3	Mus musculus zinc finger with KRAB and SCAN domains 3 (Zkscan3),	72739	304	293	345	389
ZMAT5	Zmat5	Mus musculus zinc finger, matrin type 5 (Zmat5), mRNA.	67178	603	523	434	467
ZNRF1	Znrf1	Mus musculus zinc and ring finger 1 (Znrf1), mRNA.	170737	204	252	311	277
ZRANB2	Zranb2	Mus musculus zinc finger, RAN-binding domain containing 2 (Zranb2),	53861	3020	1876	1365	2312
02-Sep	02-Sep	Mus musculus septin 2 (Sept2), mRNA.	18000	7954	5885	5550	6136
03-Sep	03-Sep			136	132	132	144
04-Sep	04-Sep	Mus musculus septin 4 (Sept4), mRNA.	18952	120	128	123	124
382044	382044	Mus musculus predicted gene, 382044 (382044), mRNA.	382044	143	126	134	126
0610007P08RI	0610007P08R	Mus musculus RIKEN cDNA 0610007P08 gene (0610007P08Rik),	76251	165	178	188	194
0610007P22RI	0610007P22R	Mus musculus RIKEN cDNA 0610007P22 gene (0610007P22Rik), mRNA.	68327	286	198	179	181
0610009L18RI	0610009L18Ri			199	162	195	177
0710001C05RI	0710001C05R			144	142	161	154
0910001A06RI	0910001A06R	Mus musculus RIKEN cDNA 0910001A06 gene (0910001A06Rik), mRNA.	223601	201	251	235	285
1110001N06RI	1110001N06R			1029	687	531	795
1110001N06RI	1110001N06R			780	614	401	660
1110001P04RI	1110001P04R			1649	1378	1080	1142
1110003P22RI	1110003P22R			438	635	639	735
1110007L15RI	1110007L15Ri	Mus musculus RIKEN cDNA 1110007L15 gene (1110007L15Rik), mRNA.	67604	968	724	743	610
1110020P15RI	1110020P15R	Mus musculus RIKEN cDNA 1110020P15 gene (1110020P15Rik), mRNA.	66152	21549	23193	18080	17877
1110020P15RI	1110020P15R	Mus musculus RIKEN cDNA 1110020P15 gene (1110020P15Rik), mRNA.	66152	19923	18112	15442	16695
1110021L09RI	1110021L09Ri	PREDICTED: Mus musculus RIKEN cDNA 1110021L09 gene	76306	419	352	472	565
1190005F20RI	1190005F20Ri	Mus musculus RIKEN cDNA 1190005F20 gene (1190005F20Rik), mRNA.	98685	884	640	468	704
1200011I18RIK	1200011I18Ri	Mus musculus RIKEN cDNA 1200011I18 gene (1200011I18Rik), mRNA.	67467	138	137	168	151
1300010F03RI	1300010F03Ri	PREDICTED: Mus musculus RIKEN cDNA 1300010F03 gene	219189	642	393	423	461

1300010M03R	1300010M03	Mus musculus RIKEN cDNA 1300010M03 gene (1300010M03Rik),	67998	133	126	129	118
1500002K03RI	1500002K03R			138	125	142	133
1500041J02RI	1500041J02Ri			181	180	155	159
1520402A15RI	1520402A15R	PREDICTED: Mus musculus RIKEN cDNA 1520402A15 gene	68075	135	133	140	146
1600012H06RI	1600012H06Ri	Mus musculus RIKEN cDNA 1600012H06 gene (1600012H06Rik), transcri	67912	130	120	138	127
1600014C10RI	1600014C10R	Mus musculus RIKEN cDNA 1600014C10 gene (1600014C10Rik),	72244	166	159	186	181
1600014C23RI	1600014C23R			135	146	142	130
1700001E18RI	1700001E18Ri			115	119	115	130
1700006H03RI	1700006H03Ri	PREDICTED: Mus musculus RIKEN cDNA 1700006H03 gene, transcript	74174	151	131	137	122
1700007B14RI	1700007B14R	PREDICTED: Mus musculus RIKEN cDNA 1700007B14 gene, transcript	71831	123	128	133	123
1700009P13RI	1700009P13R			155	151	162	161
1700010H15RI	1700010H15Ri			125	126	136	142
1700011A15RI	1700011A15R	Mus musculus RIKEN cDNA 1700011A15 gene (1700011A15Rik), mRNA.	66322	143	132	118	124
1700012A03RI	1700012A03R	Mus musculus RIKEN cDNA 1700012A03 gene (1700012A03Rik), mRNA.	76382	165	140	124	128
1700019N12RI	1700019N12R	Mus musculus RIKEN cDNA 1700019N12 gene (1700019N12Rik), mRNA.	67077	174	158	133	132
1700024D23RI	1700024D23Ri			119	133	131	128
1700024J04RI	1700024J04Ri			122	115	122	113
1700025K23RI	1700025K23R	Mus musculus RIKEN cDNA 1700025K23 gene (1700025K23Rik), mRNA.	66337	308	233	199	216
1700026N04RI	1700026N04R			122	115	124	132
1700029H14RI	1700029H14Ri	Mus musculus RIKEN cDNA 1700029H14 gene (1700029H14Rik), transcri	66501	135	143	127	141
1700029I15RIK	1700029I15Ri	Mus musculus RIKEN cDNA 1700029I15 gene (1700029I15Rik), mRNA.	75641	193	149	165	158
1700034P14RI	1700034P14R			172	146	142	167
1700052O22RI	1700052O22R			874	961	1438	1221
1700055D16RI	1700055D16Ri			139	127	120	130
1700080O16RI	1700080O16R	PREDICTED: Mus musculus RIKEN cDNA 1700080O16 gene (1700080O16	74279	126	125	128	134
1700095D23RI	1700095D23Ri			133	130	140	145
1700108F19RI	1700108F19Ri			120	123	123	135
1700123J19RI	1700123J19Ri	PREDICTED: Mus musculus RIKEN cDNA 1700123J19 gene (1700123J19Ri	73614	134	142	135	128
1810009O10RI	1810009O10R	Mus musculus RIKEN cDNA 1810009O10 gene (1810009O10Rik), mRNA.	69109	222	203	192	203
1810015C11RI	1810015C11R			1059	533	575	710

1810022C23RI	1810022C23R	Mus musculus RIKEN cDNA 1810022C23 gene (1810022C23Rik), mRNA.	69123	585	320	333	289
1810030J14RI	1810030J14Ri	Mus musculus RIKEN cDNA 1810030J14 gene (1810030J14Rik), mRNA.	66289	23341	1633	471	249
1810030J14RI	1810030J14Ri	Mus musculus RIKEN cDNA 1810030J14 gene (1810030J14Rik), mRNA.	66289	14623	1005	321	198
1810062O14RI	1810062O14R			134	144	157	155
1810062O18RI	1810062O18R			274	196	206	184
2010309E21RI	2010309E21Ri	Mus musculus RIKEN cDNA 2010309E21 gene (2010309E21Rik), mRNA.	66488	121	122	125	128
2210012G02RI	2210012G02Ri	Mus musculus RIKEN cDNA 2210012G02 gene (2210012G02Rik), mRNA.	66526	143	168	187	161
2210037E17RI	2210037E17Ri			168	147	146	155
2210408F11RI	2210408F11Ri			1202	761	611	782
2210414H16RI	2210414H16Ri			202	150	147	152
2310001A20RI	2310001A20R	Mus musculus RIKEN cDNA 2310001A20 gene (2310001A20Rik), mRNA.	71881	1476	1360	1259	1050
2310002F18RI	2310002F18Ri			366	348	480	466
2310006J04RI	2310006J04Ri			129	138	136	119
2310007F21RI	2310007F21R	Mus musculus RIKEN cDNA 2310007F21 gene (2310007F21Rik), mRNA.	66939	1058	768	778	897
2310014D11RI	2310014D11R			248	268	313	319
2310015A05RI	2310015A05R	PREDICTED: Mus musculus RIKEN cDNA 2310015A05 gene	72315	130	134	131	138
2310016C08RI	2310016C08R	Mus musculus RIKEN cDNA 2310016C08 gene (2310016C08Rik), mRNA.	69573	251	395	364	309
2310016C08RI	2310016C08R	Mus musculus RIKEN cDNA 2310016C08 gene (2310016C08Rik), mRNA.	69573	741	1383	1209	1016
2310031L18RI	2310031L18R			141	146	132	150
2310035K24RI	2310035K24R	Mus musculus RIKEN cDNA 2310035K24 gene (2310035K24Rik), mRNA.	69596	934	797	777	710
2310045I24RIK	2310045I24R			133	130	140	147
2310045K21RI	2310045K21R			148	136	151	170
2310075M15R	2310075M15Ri			253	219	315	327
2310079G19RI	2310079G19R	PREDICTED: Mus musculus RIKEN cDNA 2310079G19 gene	69699	2670	377	232	301
2310081J21RI	2310081J21R	PREDICTED: Mus musculus RIKEN cDNA 2310081J21 gene (2310081J21Ri	69211	128	127	118	120
2400010G15RI	2400010G15R			130	140	143	128
2410002O22RI	2410002O22R	Mus musculus RIKEN cDNA 2410002O22 gene (2410002O22Rik), transcri	66975	434	407	322	456
2410018M08R	2410018M08	Mus musculus RIKEN cDNA 2410018M08 gene (2410018M08Rik),	71970	139	133	160	153
2410081M15R	2410081M15	Mus musculus RIKEN cDNA 2410081M15 gene (2410081M15Rik),	73680	335	361	279	281
2410129H14RI	2410129H14R	Mus musculus RIKEN cDNA 2410129H14 gene (2410129H14Rik), mRNA.	76789	922	598	553	479

2410146L05RI	2410146L05R	Mus musculus RIKEN cDNA 2410146L05 gene (2410146L05Rik), mRNA.	67968	318	217	190	189
2500002A22RI	2500002A22R			214	196	161	172
2500003M10R	2500003M10Ri			410	432	354	325
2510049J12RI	2510049J12R	PREDICTED: Mus musculus RIKEN cDNA 2510049J12 gene, transcript vari	70291	1278	1813	1498	1639
2600011E07RI	2600011E07R	Mus musculus RIKEN cDNA 2600011E07 gene (2600011E07Rik), mRNA.	72125	141	169	172	180
2610002B11RI	2610002B11R			135	132	124	150
2610020J05RI	2610020J05R			160	138	135	149
2610021J01RI	2610021J01R			139	127	134	126
2610037P13RI	2610037P13R			254	192	187	220
2610204L23RI	2610204L23R			1236	1016	732	925
2610209A20RI	2610209A20R	Mus musculus RIKEN cDNA 2610209A20 gene (2610209A20Rik), mRNA.	67164	285	219	201	196
2610301F02RI	2610301F02R	Mus musculus RIKEN cDNA 2610301F02 gene (2610301F02Rik), mRNA.	545428	140	144	162	147
2610510H03RI	2610510H03R			123	121	128	139
2610524H06RI	2610524H06R	Mus musculus RIKEN cDNA 2610524H06 gene (2610524H06Rik), mRNA.	330173	182	223	252	194
2700008B19RI	2700008B19R			125	136	134	141
2700060E02RI	2700060E02R	Mus musculus RIKEN cDNA 2700060E02 gene (2700060E02Rik), mRNA.	68045	246	362	551	545
2810005O12RI	2810005O12R			127	131	128	141
2810021B0	2810021B07R	Mus musculus RIKEN cDNA 2810021B07 gene (2810021B07Rik), mRNA.	66308	533	346	280	334
2810046L0	2810046L04Ri			262	280	358	369
2810405K0	2810405K07R			159	144	164	176
2810406K1	2810406K13R	PREDICTED: Mus musculus RIKEN cDNA 2810406K13 gene, transcript	72184	116	120	123	131
2810407C0	2810407C02R	Mus musculus RIKEN cDNA 2810407C02 gene (2810407C02Rik), mRNA.	69227	280	389	358	446
2810408P1	2810408P10R	Mus musculus RIKEN cDNA 2810408P10 gene (2810408P10Rik), mRNA.	242747	301	241	196	261
2810430P2	2810430P21R			179	157	147	155
2810436B1	2810436B12R			436	273	259	342
2810439F0	2810439F02Ri	Mus musculus RIKEN cDNA 2810439F02 gene (2810439F02Rik), mRNA.	72747	136	165	214	169
2810440N0	2810440N09R			151	159	133	144
2810452K2	2810452K22R	Mus musculus RIKEN cDNA 2810452K22 gene (2810452K22Rik), mRNA.	67236	134	132	143	142
2810453H1	2810453H10Ri			148	167	161	171
3010027A0	3010027A04R			263	246	257	285

3110001O0	3110001O07R			515	452	405	432
3110018K0	3110018K01R			156	189	194	188
3110033D1	3110033D18Ri			204	186	156	177
3110043A1	3110043A19R	PREDICTED: Mus musculus RIKEN cDNA 3110043A19 gene	73216	128	133	160	151
3110043J09	3110043J09Ri	Mus musculus RIKEN cDNA 3110043J09 gene (3110043J09Rik), mRNA.	73167	272	266	251	225
3110043O2	3110043O21R	Mus musculus RIKEN cDNA 3110043O21 gene (3110043O21Rik), mRNA.	73205	263	323	353	365
3110062M0	3110062M04	Mus musculus RIKEN cDNA 3110062M04 gene (3110062M04Rik),	78412	139	147	128	122
3300002N1	3300002N10R			153	148	152	162
3732412D2	3732412D22Ri			134	146	131	122
3830612M2	3830612M24			541	330	305	366
4631416I11	4631416I11Ri			149	169	176	159
4631426J05	4631426J05Ri			249	290	336	290
4632401N0	4632401N01R			403	1111	1651	1726
4632404H1	4632404H12Ri	Mus musculus RIKEN cDNA 4632404H12 gene (4632404H12Rik), mRNA.	74034	128	141	135	149
4632408I12	4632408I12Ri			125	128	125	132
4632412I06	4632412I06Ri			151	141	131	136
4632419K2	4632419K20R			136	127	127	140
4632433K1	4632433K11R	Mus musculus RIKEN cDNA 4632433K11 gene (4632433K11Rik), mRNA.	77043	285	234	236	227
4732418C0	4732418C07R	Mus musculus RIKEN cDNA 4732418C07 gene (4732418C07Rik), mRNA.	230648	778	539	580	645
4732418C0	4732418C07R	Mus musculus RIKEN cDNA 4732418C07 gene (4732418C07Rik), mRNA.	230648	1953	1351	1391	1550
4732450N0	4732450N03R			127	137	143	150
4831437C03RI	4831437C03R			174	201	289	307
4833413D08RI	4833413D08R	Mus musculus RIKEN cDNA 4833413D08 gene (4833413D08Rik), mRNA.	71425	125	124	136	137
4833418A01RI	4833418A01R			142	140	131	151
4833419K08RI	4833419K08R			124	126	133	124
4833426J09RI	4833426J09R	Mus musculus RIKEN cDNA 4833426J09 gene (4833426J09Rik), mRNA.	382051	312	200	175	187
4833426J09RI	4833426J09R	Mus musculus RIKEN cDNA 4833426J09 gene (4833426J09Rik), mRNA.	382051	133	122	126	128
4921507O14RI	4921507O14R			117	124	127	120
4921511H13RI	4921511H13R	PREDICTED: Mus musculus RIKEN cDNA 4921511H13 gene	207932	156	140	152	146
4921513D23RI	4921513D23R			1526	1126	898	1273

4921524L21RI	4921524L21R	PREDICTED: Mus musculus RIKEN cDNA 4921524L21 gene, transcript	70901	138	130	145	130
4921525L17RI	4921525L17R			137	133	149	154
4921530L21RI	4921530L21R	Mus musculus RIKEN cDNA 4921530L21 gene (4921530L21Rik), mRNA.	66732	125	129	146	124
4930403C10RI	4930403C10R			719	654	916	896
4930403J07RI	4930403J07R	PREDICTED: Mus musculus RIKEN cDNA 4930403J07 gene (4930403J07Ri	75773	137	133	121	141
4930407I10RIK	4930407I10R	PREDICTED: Mus musculus RIKEN cDNA 4930407I10 gene	328573	135	126	152	137
4930415O10RI	4930415O10R			120	128	126	126
4930417M19R	4930417M19Ri			121	135	137	151
4930418I18RIK	4930418I18R			207	169	172	188
4930421P05RI	4930421P05R	PREDICTED: Mus musculus RIKEN cDNA 4930421P05 gene	73771	127	121	137	143
4930447K03RI	4930447K03R			128	120	122	126
4930521I23RIK	4930521I23R			119	133	121	127
4930533K18RI	4930533K18R			375	664	871	893
4930534B04RI	4930534B04R	Mus musculus RIKEN cDNA 4930534B04 gene (4930534B04Rik), mRNA.	75216	148	157	151	180
4930538K18RI	4930538K18R	Mus musculus RIKEN cDNA 4930538K18 gene (4930538K18Rik), mRNA.	75180	119	120	130	126
4930560E09RI	4930560E09R	PREDICTED: Mus musculus RIKEN cDNA 4930560E09 gene	67737	127	136	140	120
4930562C15RI	4930562C15R	PREDICTED: Mus musculus RIKEN cDNA 4930562C15 gene	78809	142	130	147	137
4930563A19RI	4930563A19R			140	137	145	155
4930572J05RI	4930572J05R	Mus musculus RIKEN cDNA 4930572J05 gene (4930572J05Rik), mRNA.	223626	448	724	814	855
4930579E17RI	4930579E17R			213	182	193	182
4930597O21RI	4930597O21R	PREDICTED: Mus musculus RIKEN cDNA 4930597O21 gene (4930597O21	75373	118	129	125	122
4930599N23RI	4930599N23R			160	146	135	146
4931408C20RI	4931408C20R	Mus musculus RIKEN cDNA 4931408C20 gene (4931408C20Rik), mRNA.	210940	133	135	124	122
4931428F04RI	4931428F04R	Mus musculus RIKEN cDNA 4931428F04 gene (4931428F04Rik), mRNA.	74356	135	141	150	154
4931432M23R	4931432M23	Mus musculus RIKEN cDNA 4931432M23 gene (4931432M23Rik),	70993	126	122	146	133
4932411K1	4932411K12			128	143	130	147
4932412H1	4932412H11R	Mus musculus RIKEN cDNA 4932412H11 gene (4932412H11Rik), mRNA.	242838	139	154	157	144
4932439E0	4932439E07R			259	230	208	198
4933402P0	4933402P03R	Mus musculus RIKEN cDNA 4933402P03 gene (4933402P03Rik), mRNA.	108803	128	128	133	123
4933403G1	4933403G14R	Mus musculus RIKEN cDNA 4933403G14 gene (4933403G14Rik), mRNA.	74393	242	174	165	195

4933406B1	4933406B17R	PREDICTED: Mus musculus RIKEN cDNA 4933406B17 gene	71040	138	132	129	129
4933428A1	4933428A15R			650	370	236	309
4933429E1	4933429E10R	Mus musculus RIKEN cDNA 4933429E10 gene (4933429E10Rik), mRNA.	380701	130	121	131	123
5031409G2	5031409G22R			126	134	129	135
5031414D1	5031414D18R	Mus musculus RIKEN cDNA 5031414D18 gene (5031414D18Rik), mRNA.	271221	127	141	139	145
5031439A0	5031439A09R			234	193	177	203
5033424B0	5033424B07R			141	153	137	136
5330417K0	5330417K06R			132	121	140	124
5330426P1	5330426P16R	PREDICTED: Mus musculus RIKEN cDNA 5330426P16 gene	68190	136	152	178	182
5330432B2	5330432B20R	PREDICTED: Mus musculus RIKEN cDNA 5330432B20 gene	99937	164	129	136	142
5430400L1	5430400L16Ri			138	158	162	158
5430420E1	5430420E18R			129	125	126	134
5530400K2	5530400K22R			1815	915	766	968
5630401D2	5630401D24R	Mus musculus RIKEN cDNA 5630401D24 gene (5630401D24Rik), mRNA.	71449	131	154	131	141
5730478M0	5730478M09			161	175	165	176
5730494M1	5730494M16			129	129	139	143
5730494N0	5730494N06R	Mus musculus RIKEN cDNA 5730494N06 gene (5730494N06Rik), mRNA.	70612	1070	790	831	832
5730507C0	5730507C01R	Mus musculus RIKEN cDNA 5730507C01 gene (5730507C01Rik), mRNA.	236366	163	164	134	147
5730525O2	5730525O22R			367	451	483	380
5730598B0	5730598B06			138	147	137	151
5830416P1	5830416P10R	PREDICTED: Mus musculus RIKEN cDNA 5830416P10 gene	381232	138	126	136	124
5830417I10	5830417I10Ri	PREDICTED: Mus musculus RIKEN cDNA 5830417I10 gene	76022	147	135	136	149
5830427D0	5830427D03R	Mus musculus RIKEN cDNA 5830427D03 gene (5830427D03Rik), mRNA.	76061	253	264	343	287
5830431I07	5830431I07Ri			276	153	210	287
5830432E0	5830432E09R			134	129	134	133
5830433M1	5830433M19			136	132	127	137
5930403H1	5930403H17R			126	126	123	130
6030405A1	6030405A18			128	137	140	139
6030434H1	6030434H13R			150	164	172	188
6030453H1	6030453H13R			115	123	122	129

6130401L2	6130401L20Ri	PREDICTED: Mus musculus RIKEN cDNA 6130401L20 gene, transcript	75740	182	136	141	129
6330403A0	6330403A02R	Mus musculus RIKEN cDNA 6330403A02 gene (6330403A02Rik), mRNA.	381310	180	137	125	141
6330403M2	6330403M23R			1837	977	703	1568
6330407A0	6330407A03R			136	210	190	256
6330411D2	6330411D24R	PREDICTED: Mus musculus RIKEN cDNA 6330411D24 gene, transcript	70725	131	124	120	131
6330416G1	6330416G13Ri	Mus musculus RIKEN cDNA 6330416G13 gene (6330416G13Rik), mRNA.	230279	409	538	553	457
6330417G0	6330417G02Ri	PREDICTED: Mus musculus RIKEN cDNA 6330417G02 gene	74004	128	133	120	126
6330439K1	6330439K17R	Mus musculus RIKEN cDNA 6330439K17 gene (6330439K17Rik), mRNA.	241688	127	131	140	147
6330500D0	6330500D04R	Mus musculus RIKEN cDNA 6330500D04 gene (6330500D04Rik), transcri	193385	172	195	233	196
6330532G1	6330532G10Ri			130	144	140	124
6330566F1	6330566F14Ri			160	145	126	131
6430537F0	6430537F04			194	157	170	176
6430544C0	6430544C07R			136	149	131	143
6430561B1	6430561B16R			127	135	126	134
6430574F2	6430574F24Ri			139	128	142	147
6530404N2	6530404N21Ri	PREDICTED: Mus musculus RIKEN cDNA 6530404N21 gene (6530404N21	67795	143	131	128	137
6530415H1	6530415H11R			569	337	377	552
6620401M0	6620401M08R			236	170	205	211
6720431C0	6720431C02R			124	125	132	135
6720435I21	6720435I21Ri			111	125	124	121
6720470G1	6720470G16Ri			159	187	229	250
7420700D1	7420700D11R			356	292	268	281
8030401N1	8030401N12Ri			124	120	121	117
8030447N1	8030447N19Ri			154	150	167	170
8430408G2	8430408G22Ri	Mus musculus RIKEN cDNA 8430408G22 gene (8430408G22Rik), mRNA.	213393	209	428	363	187
8430419L0	8430419L09Ri	Mus musculus RIKEN cDNA 8430419L09 gene (8430419L09Rik), mRNA.	74525	127	140	144	137
9030024J15	9030024J15Ri			569	751	633	889
9030409G1	9030409G11Ri	Mus musculus RIKEN cDNA 9030409G11 gene (9030409G11Rik), mRNA.	71529	133	138	144	132
9030421J09	9030421J09Ri	Mus musculus RIKEN cDNA 9030421J09 gene (9030421J09Rik), mRNA.	245282	114	142	147	123

9030605I04	9030605I04Ri			250	160	156	195
9030625A1	9030625A11R			362	181	188	168
9130019O2	9130019O22R	Mus musculus RIKEN cDNA 9130019O22 gene (9130019O22Rik), mRNA.	78921	541	376	393	421
9130024O2	9130024O20R			903	366	323	548
9130201A12RI	9130201A12R			117	129	125	121
9130208D14RI	9130208D14R			178	140	134	155
9130230H23RI	9130230H23R			123	120	130	136
9130230L23RI	9130230L23R	PREDICTED: Mus musculus RIKEN cDNA 9130230L23 gene	231253	174	157	150	162
9230110F15RI	9230110F15R	PREDICTED: Mus musculus RIKEN cDNA 9230110F15 gene	77080	128	126	137	137
9330132O05RI	9330132O05R			162	171	190	204
9330155G14RI	9330155G14R			179	168	179	169
9330160L15RI	9330160L15R			123	133	142	144
9330171D12RI	9330171D12R			259	240	234	206
9330175B10RI	9330175B10R			124	125	128	126
9330185J12RI	9330185J12R			250	280	407	370
9430022P05RI	9430022P05R			128	134	150	140
9430023L20RI	9430023L20R	Mus musculus RIKEN cDNA 9430023L20 gene (9430023L20Rik), mRNA.	68118	2195	1771	1676	1351
9430028L06RI	9430028L06R	Mus musculus RIKEN cDNA 9430028L06 gene (9430028L06Rik), mRNA.	225617	230	178	183	187
9430079M16R	9430079M16Ri			127	132	135	149
9430080K19RI	9430080K19R			815	1188	1513	1235
9430093I07RIK	9430093I07R			315	222	239	246
9530001D23RI	9530001D23R			145	150	152	149
9530048O09RI	9530048O09R	PREDICTED: Mus musculus RIKEN cDNA 9530048O09 gene (9530048O09	78611	158	193	172	171
9530051E16RI	9530051E16R			182	162	145	162
9530081N05RI	9530081N05R			212	191	198	215
9630009A06RI	9630009A06R	PREDICTED: Mus musculus RIKEN cDNA 9630009A06 gene	78568	194	140	125	132
9630011N22RI	9630011N22R			150	166	156	179
9630031F12RI	9630031F12R	Mus musculus RIKEN cDNA 9630031F12 gene (9630031F12Rik), mRNA.	58227	222	163	148	168
9830118G07RI	9830118G07R			149	164	168	145
9830134C10RI	9830134C10R	Mus musculus RIKEN cDNA 9830134C10 gene (9830134C10Rik), mRNA.	442827	139	161	152	152

9830144J08RI	9830144J08R			136	139	181	187
A130001G05R	A130001G05R			145	171	176	205
A130019A16RI	A130019A16R			163	210	223	217
A130026C10R	A130026C10R			347	413	482	486
A130028H19RI	A130028H19Ri			141	138	158	163
A130033H05RI	A130033H05Ri			149	161	169	181
A130035O14RI	A130035O14Ri			131	127	138	148
A130038M19R	A130038M19			212	164	165	191
A130053N1	A130053N17			147	130	133	137
A130092J06	A130092J06Ri	Mus musculus RIKEN cDNA A130092J06 gene (A130092J06Rik), mRNA.	241303	208	369	464	296
A230028O0	A230028O05			142	132	127	122
A230050P2	A230050P20R	Mus musculus RIKEN cDNA A230050P20 gene (A230050P20Rik), mRNA.	319278	131	134	147	163
A230054D0	A230054D04R	Mus musculus RIKEN cDNA A230054D04 gene (A230054D04Rik), mRNA.	665775	216	215	182	266
A230080K1	A230080K19R			130	127	124	137
A230087F1	A230087F16R			123	122	135	129
A330008J08	A330008J08Ri			118	115	123	117
A330043L1	A330043L12			147	133	137	145
A330057G1	A330057G13			682	497	298	597
A330086O2	A330086O21			191	154	159	148
A430005L1	A430005L14R	Mus musculus RIKEN cDNA A430005L14 gene (A430005L14Rik), mRNA.	97159	320	362	263	286
A430068O1	A430068O14			130	136	137	123
A430075I06	A430075I06Ri			141	146	127	138
A430091O2	A430091O22			146	133	127	137
A430093F1	A430093F15R	PREDICTED: Mus musculus RIKEN cDNA A430093F15 gene	403202	129	167	172	142
A430106H1	A430106H13R			188	192	219	264
A430108E0	A430108E01R			126	121	125	124
A430110N2	A430110N23	Mus musculus RIKEN cDNA A430110N23 gene (A430110N23Rik), mRNA.	269855	134	140	159	156
A530018G0	A530018G09			128	126	133	144
A530065E1	A530065E19R			128	141	135	133
A530098C1	A530098C11R	Mus musculus RIKEN cDNA A530098C11 gene (A530098C11Rik), mRNA.	433294	141	141	129	128

A630008E1	A630008E13R			143	146	136	152
A630014I05	A630014I05Ri			129	123	134	136
A630043I21	A630043I21Ri			168	165	158	148
A630051D1	A630051D19R			139	126	128	139
A630053E1	A630053E16R			130	120	127	128
A630091F0	A630091F01R			446	377	299	337
A730036E1	A730036E13R	PREDICTED: Mus musculus RIKEN cDNA A730036E13 gene	320291	213	178	163	182
A730043L2	A730043L23R			210	182	163	182
A730054J21	A730054J21Ri			171	182	215	263
A730061M	A730061M06			115	131	127	129
A730081F2	A730081F20R			150	138	145	140
A730091E0	A730091E08R			125	125	138	135
A830010M	A830010M20	PREDICTED: Mus musculus RIKEN cDNA A830010M20 gene, transcript va	231570	136	142	129	135
A830015G1	A830015G10R			204	159	150	148
A830021M	A830021M18			127	137	144	136
A830060N1	A830060N17			271	192	178	184
A830073O2	A830073O21R			139	136	132	126
A930006D2	A930006D20R			134	130	139	152
A930010I20	A930010I20Ri			182	151	152	167
A930015K1	A930015K17R			151	125	144	151
A930021K2	A930021K20R			183	157	144	159
A930039F1	A930039F13R			147	140	126	139
AA536717	AA536717	Mus musculus expressed sequence AA536717 (AA536717), transcript	105428	288	229	216	239
AA987161	AA987161	PREDICTED: Mus musculus expressed sequence AA987161, transcript	380856	128	125	150	133

Supplementary Table 3. Therapeutic effects of DAPP on DSS treated intestine

Ingenuity Canonical Pathways	-log(p-value)	Molecules
Hepatic Fibrosis / Hepatic Stellate Cell Activation	6.8	IL1RL1, COL12A1, FN1, MMP9, COL3A1, COL4A2, IL1R2, ACTA2, LBP
LXR/RXR Activation	5.91	LYZ, IL1RL1, MMP9, KNG1, IL1R2, LBP
Acute Phase Response Signaling	5.08	KRAS, CFB, PIK3R3, FN1, LBP, IL6ST
Actin Cytoskeleton Signaling	4.53	KRAS, PIK3R3, FN1, KNG1, ACTA2, LBP
Inhibition of Angiogenesis by TSP1	3.98	MMP9, HSPG2, THBS1
Atherosclerosis Signaling	3.4	LYZ, MMP9, COL3A1, PLA2G1B
Glioma Invasiveness Signaling	3.23	KRAS, PIK3R3, MMP9
Gap Junction Signaling	3.04	KRAS, TUBA1A, PIK3R3, ACTA2
Agrin Interactions at Neuromuscular Junction	3.03	KRAS, LAMC1, ACTA2
IL-10 Signaling	3.01	IL1RL1, IL1R2, LBP
Germ Cell-Sertoli Cell Junction Signaling	2.98	KRAS, TUBA1A, PIK3R3, ACTA2
Hepatic Cholestasis	2.96	IL1RL1, IL1R2, LBP, HNF4A
ILK Signaling	2.75	PIK3R3, FN1, MMP9, ACTA2
Bladder Cancer Signaling	2.72	KRAS, MMP9, THBS1
FAK Signaling	2.72	KRAS, PIK3R3, ACTA2
Intrinsic Prothrombin Activation Pathway	2.54	KNG1, COL3A1
HIF1α Signaling	2.53	KRAS, PIK3R3, MMP9
Role of NANOG in Mammalian Embryonic Stem Cell Plur	2.42	KRAS, PIK3R3, IL6ST
p38 MAPK Signaling	2.34	IL1RL1, PLA2G1B, IL1R2
FcγRIIB Signaling in B Lymphocytes	2.21	KRAS, PIK3R3
Melanoma Signaling	2.19	KRAS, PIK3R3
eNOS Signaling	2.16	PIK3R3, KNG1, AQP8
Glucocorticoid Receptor Signaling	2.12	KRT36, KRAS, PIK3R3, IL1R2
MSP-RON Signaling Pathway	2.11	PIK3R3, ACTA2
Epithelial Adherens Junction Signaling	2.1	KRAS, TUBA1A, ACTA2
Endometrial Cancer Signaling	2.01	KRAS, PIK3R3
IL-2 Signaling	1.99	KRAS, PIK3R3
Thrombopoietin Signaling	1.96	KRAS, PIK3R3
Arginine Degradation I (Arginase Pathway)	1.94	ARG1
ErbB4 Signaling	1.92	KRAS, PIK3R3
Myc Mediated Apoptosis Signaling	1.92	KRAS, PIK3R3
Endothelin-1 Signaling	1.91	KRAS, PIK3R3, PLA2G1B
NF-κB Signaling	1.9	KRAS, PIK3R3, IL1R2
Role of JAK1 and JAK3 in Î³c Cytokine Signaling	1.89	KRAS, PIK3R3
Sertoli Cell-Sertoli Cell Junction Signaling	1.87	KRAS, TUBA1A, ACTA2
Estrogen-Dependent Breast Cancer Signaling	1.86	KRAS, PIK3R3
Role of NFAT in Cardiac Hypertrophy	1.85	KRAS, PIK3R3, IL6ST
ERK5 Signaling	1.85	KRAS, IL6ST
Airway Pathology in Chronic Obstructive Pulmonary Dise	1.82	CXCL3
IL-8 Signaling	1.81	KRAS, PIK3R3, MMP9

Erythropoietin Signaling	1.8	KRAS, PIK3R3
Neurotrophin/TRK Signaling	1.8	KRAS, PIK3R3
Renal Cell Carcinoma Signaling	1.78	KRAS, PIK3R3
Role of Macrophages, Fibroblasts and Endothelial Cells i	1.77	FN1, IL1R2, IL6
Arginine Degradation VI (Arginase 2 Pathway)	1.77	ARG1
Breast Cancer Regulation by Stathmin1	1.76	KRAS, TUBA1A, PIK3R3
IL-3 Signaling	1.75	KRAS, PIK3R3
Leukocyte Extravasation Signaling	1.75	PIK3R3, MMP9, ACTA2
IL-4 Signaling	1.73	KRAS, PIK3R3
NF-κB Activation by Viruses	1.73	KRAS, PIK3R3
Prolactin Signaling	1.73	KRAS, PIK3R3
Sperm Motility	1.71	PLA2G1B, ZAN
Acute Myeloid Leukemia Signaling	1.7	KRAS, PIK3R3
HER-2 Signaling in Breast Cancer	1.7	KRAS, PIK3R3
IL-6 Signaling	1.69	IL1R2, IL6
Acyl-CoA Hydrolysis	1.69	HNF4A
Systemic Lupus Erythematosus Signaling	1.67	KRAS, PIK3R3, KNG1
Role of Pattern Recognition Receptors in Recognition of	1.67	IL6, PTX3
LPS/IL-1 Mediated Inhibition of RXR Function	1.66	IL1RL1, IL1R2, LBP
Ceramide Signaling	1.66	KRAS, PIK3R3
FXR/RXR Activation	1.63	KNG1, HNF4A
Role of Osteoblasts, Osteoclasts and Chondrocytes in Rh	1.63	IL1RL1, PIK3R3, IL1R2
Melanocyte Development and Pigmentation Signaling	1.62	KRAS, PIK3R3
Role of IL-17A in Psoriasis	1.61	CXCL3
ErbB Signaling	1.61	KRAS, PIK3R3
UVA-Induced MAPK Signaling	1.59	KRAS, PIK3R3
Chronic Myeloid Leukemia Signaling	1.54	KRAS, PIK3R3
T Cell Receptor Signaling	1.51	KRAS, PIK3R3
Telomerase Signaling	1.51	KRAS, PIK3R3
CDK5 Signaling	1.49	KRAS, LAMC1
p53 Signaling	1.49	PIK3R3, THBS1
Maturity Onset Diabetes of Young (MODY) Signaling	1.43	HNF4A
NGF Signaling	1.43	KRAS, PIK3R3
Natural Killer Cell Signaling	1.42	KRAS, PIK3R3
fMLP Signaling in Neutrophils	1.42	KRAS, PIK3R3
PPARα/RXRα Activation	1.41	IL1R2, IL6
Granulocyte Adhesion and Diapedesis	1.41	IL1R2, CXCL3
Superpathway of Citrulline Metabolism	1.4	ARG1
PKCÎ¸ Signaling in T Lymphocytes	1.38	KRAS, PIK3R3
Agranulocyte Adhesion and Diapedesis	1.36	FN1, CXCL3
Glycolysis I	1.35	ENO3
Gα12/13 Signaling	1.35	KRAS, PIK3R3
P2Y Purigenic Receptor Signaling Pathway	1.35	KRAS, PIK3R3

Role of JAK family kinases in IL-6-type Cytokine Signaling	1.33	IL6
Gluconeogenesis I	1.33	ENO3
PI3K/AKT Signaling	1.33	KRAS, PIK3R3
Clathrin-mediated Endocytosis Signaling	1.32	LYZ, HSPA8
ERK/MAPK Signaling	1.32	DUSP1, PLA2G1B
IL-15 Production	1.3	IL6

DSS/DAPP-400 vs DSS alone

Supplementary Table 4. Prophylactic effects of DAPP on DSS treated intestine

Ingenuity Canonical Pathways	-log(p-value)	Molecules
Hepatic Fibrosis / Hepatic Stellate Cell Activation	6.15	FN1, COL3A1, COL4A2, COL1A2, IL1R2, CXCL3, IL6
IL-6 Signaling	6.01	IL1RL1, KRAS, PIK3R3, IL1R2, LBP, IL6ST
Atherosclerosis Signaling	5.51	LYZ, COL3A1, PLA2G1B, COL1A2, IL6
Glucocorticoid Receptor Signaling	4.96	DUSP1, TSC22D3, HSPA8, IL1R2, CXCL3, IL6
Intrinsic Prothrombin Activation Pathway	4.7	KNG1, COL3A1, COL1A2
LXR/RXR Activation	4.11	LYZ, KNG1, IL1R2, IL6
Virus Entry via Endocytic Pathways	3.91	KRAS, PIK3R3, ACTA2, TFRC
Role of Macrophages, Fibroblasts and Endothelial Cells i	3.78	IL1RL1, KRAS, PIK3R3, FN1, IL1R2, IL6ST
CNTF Signaling	3.43	KRAS, PIK3R3, IL6ST
LPS-stimulated MAPK Signaling	2.92	KRAS, PIK3R3, LBP
PPARα/RXRα Activation	2.89	IL1RL1, KRAS, IL1R2, ADIPOQ
VEGF Family Ligand-Receptor Interactions	2.87	KRAS, PIK3R3, PLA2G1B
p38 MAPK Signaling	2.85	DUSP1, PLA2G1B, IL1R2
Clathrin-mediated Endocytosis Signaling	2.72	LYZ, PIK3R3, ACTA2, TFRC
eNOS Signaling	2.68	HSPA8, KNG1, AQP8
VEGF Signaling	2.67	KRAS, PIK3R3, ACTA2
PPAR Signaling	2.66	IL1RL1, KRAS, IL1R2
Mouse Embryonic Stem Cell Pluripotency	2.6	KRAS, PIK3R3, IL6ST
Paxillin Signaling	2.55	KRAS, PIK3R3, ACTA2
Hepatic Cholestasis	2.48	IL1R2, HNF4A, IL6
Pancreatic Adenocarcinoma Signaling	2.46	KRAS, PIK3R3, MMP9
Fc Epsilon RI Signaling	2.42	KRAS, PIK3R3, PLA2G1B
Acute Phase Response Signaling	2.41	FN1, C1S, IL6
Dendritic Cell Maturation	2.4	COL3A1, COL1A2, IL6
CCR3 Signaling in Eosinophils	2.38	KRAS, PIK3R3, PLA2G1B
Colorectal Cancer Metastasis Signaling	2.37	KRAS, PIK3R3, MMP9, IL6ST
Oncostatin M Signaling	2.37	KRAS, IL6ST
14-3-3-mediated Signaling	2.35	KRAS, TUBA1A, PIK3R3
Unfolded protein response	2.34	HSPA8, SEL1L
Complement System	2.32	CFB, CFD
Inhibition of Matrix Metalloproteases	2.27	MMP9, HSPG2

Neuroprotective Role of THOP1 in Alzheimer's Disease	2.23	MMP9, KNG1
Ovarian Cancer Signaling	2.21	KRAS, PIK3R3, MMP9
PXR/RXR Activation	2.2	HNF4A, IL6
IL-17A Signaling in Airway Cells	2.19	CXCL3, IL6
IL-10 Signaling	2.13	IL1R2, IL6
Axonal Guidance Signaling	2.13	KRAS, TUBA1A, PIK3R3, MMP9, ADAMTS2
TREM1 Signaling	2.12	CXCL3, IL6
ErbB2-ErbB3 Signaling	1.95	KRAS, PIK3R3
Granulocyte Adhesion and Diapedesis	1.93	IL1RL1, MMP9, IL1R2
Antiproliferative Role of Somatostatin Receptor 2	1.89	KRAS, PIK3R3
Agranulocyte Adhesion and Diapedesis	1.86	FN1, MMP9, ACTA2
GM-CSF Signaling	1.86	KRAS, PIK3R3
NRF2-mediated Oxidative Stress Response	1.85	KRAS, PIK3R3, ACTA2
Angiopoietin Signaling	1.83	KRAS, PIK3R3
Non-Small Cell Lung Cancer Signaling	1.83	KRAS, PIK3R3
IL-15 Signaling	1.81	KRAS, PIK3R3
Remodeling of Epithelial Adherens Junctions	1.81	TUBA1A, ACTA2
Regulation of the Epithelial-Mesenchymal Transition Pa	1.81	KRAS, PIK3R3, MMP9
Role of MAPK Signaling in the Pathogenesis of Influenza	1.8	KRAS, PLA2G1B
ERK/MAPK Signaling	1.79	KRAS, PIK3R3, PLA2G1B
GDNF Family Ligand-Receptor Interactions	1.79	KRAS, PIK3R3
Macropinocytosis Signaling	1.79	KRAS, PIK3R3
Urea Cycle	1.77	ARG1
FLT3 Signaling in Hematopoietic Progenitor Cells	1.75	KRAS, PIK3R3
PEDF Signaling	1.75	KRAS, PIK3R3
IL-17 Signaling	1.74	KRAS, PIK3R3
JAK/Stat Signaling	1.74	KRAS, PIK3R3
Integrin Signaling	1.74	KRAS, PIK3R3, ACTA2
PDGF Signaling	1.69	KRAS, PIK3R3
VDR/RXR Activation	1.69	IL1RL1, HR
Prostate Cancer Signaling	1.66	KRAS, PIK3R3
Airway Pathology in Chronic Obstructive Pulmonary Dis	1.64	MMP9
Citrulline Biosynthesis	1.64	ARG1
Neuregulin Signaling	1.6	KRAS, PIK3R3
TGF-β Signaling	1.59	KRAS, HNF4A
PAK Signaling	1.58	KRAS, PIK3R3
Fcγ Receptor-mediated Phagocytosis in Macrophages an	1.53	PIK3R3, ACTA2
Glioma Signaling	1.53	KRAS, PIK3R3
SAPK/JNK Signaling	1.53	KRAS, PIK3R3
Nitric Oxide Signaling in the Cardiovascular System	1.52	PIK3R3, KNG1
Acyl-CoA Hydrolysis	1.51	HNF4A
IGF-1 Signaling	1.5	KRAS, PIK3R3
Aldosterone Signaling in Epithelial Cells	1.48	DUSP1, HSPA8

Differential Regulation of Cytokine Production in Macro	1.47	IL6
phagosome formation	1.46	PIK3R3, FN1
HGF Signaling	1.45	KRAS, PIK3R3
Rac Signaling	1.45	KRAS, PIK3R3
Renin-Angiotensin Signaling	1.42	KRAS, PIK3R3
Role of Tissue Factor in Cancer	1.42	KRAS, PIK3R3
Type II Diabetes Mellitus Signaling	1.37	PIK3R3, ADIPOQ
HMGB1 Signaling	1.35	KRAS, PIK3R3
p70S6K Signaling	1.35	KRAS, PIK3R3
PTEN Signaling	1.35	KRAS, PIK3R3
FXR/RXR Activation	1.3	KNG1, HNF4A

DAPP-200 /DSS vs DSS alone

7. DISCUSSION

La lumière de l'intestin est constamment exposée aux oxydants provenant de l'ingestion de nutriments, de l'alcool, du cholestérol oxydé et de la consommation simultanée de fer et d'acide ascorbique. De plus, les microbes et les infections, l'ischemie/reperfusion, la production d'acide gastrique et l'administration d'anti-inflammtoires peuvent promouvoir la formation de RLO (449-451), causant bien des dégâts au niveau des biomolécules de l'organisme. Lors de l'inflammation intestinale l'influx de neutrophiles et de monocytes peuvent également produire des RLO via la stimulation des enzymes du métabolisme oxydatif et la production des prostaglandines et des leucotriènes. Même si l'étiologie des MII doit être encore élucidée, la relation entre le stress oxydant et l'inflammation est bien incriminée depuis plusieurs années (160, 455, 456, 458, 656). En raison de leur puissante capacité antioxydante, nous avons émis l'hypothèse que les polyphénols aideraient à maintenir l'homéostasie intestinale en situation de stress oxydant et d'inflammation lors de MII.

Le début de ce projet de doctorat consistait à trouver un aliment fonctionnel facilement accessible en abondance et capable de prévenir et/ou réduire les maladies chroniques. Nous avons donc arrêté notre choix sur la pomme pour diverses raisons. Le Québec est le plus grand producteur de pommes qui sont peu dispendieuses et largement disponibles durant toute l'année. En outre, la pomme est fortement recommandée à travers les générations et se retrouve déjà dans nos habitudes alimentaires. De plus, la revue de Boyer *et al*. a bien illustré que les polyphénols de la pomme avaient déjà fait l'objet de plusieurs études scientifiques montrant leur capacité à diminuer le stress oxydant qui règne dans certaines maladies chroniques telles que le cancer, le diabète de type II, les maladies cardiovasculaires et pulmonaires, et l'asthme (657). L'étude de la littérature existante sur la composition des polyphénols de la pomme, nous a démontré que les polyphénols se retrouvent en concentration plus élevée dans la pelure de pomme que dans la chaire sans omettre que certains d'entre eux (phlorétine glycosylée, la phloridzine et l'acide chlorogénique) se retrouvent uniquement dans la pelure (658). Puisque les conditions d'extraction des polyphénols peuvent moduler l'activité

antioxydante et les concentrations de ces molécules, une attention spéciale a été portée sur les DAPP, obtenus grâce à des procédés de purification non délètères.

Les polyphénols de la pelure pommes ont été extraits par une méthode semblable à celle de Liu *et al*., mais grandement améliorée (465, 659, 660). La méthode d'extraction des polyphénols de la pomme s'est effectuée pour la première fois dans des conditions à froid afin de favoriser le rendement (moins de dégradation due à la température) et l'extraction de toutes les classes de polyphénols (661, 662). Comme la teneur en polyphénols dans les pommes est très élevée dans la pelure comparativement à la chair (658), la méthode d'extraction a été largement adaptée. Ainsi, l'étude du volet 1 expérimental s'est portée sur l'extrait de pelure de pomme (nommé AB powder) ainsi que sur une fraction purifiée (nommée JC-047) par chromatographie préparative. Nous avons également voulu une fraction purifiée contenant principalement des flavan-3-ols étant donné que cette classe de polyphénols a fait l'objet de plusieurs études *in vitro* et *in vivo* quant à son potentiel remarquable d'agent antioxydant.

Différentes concentrations de polyphénols purifiés ou d'extraits ont été utilisées par la communauté scientifique afin de prouver leur activité antioxydante. Dans le souci d'employer une dose physiologique dans nos travaux, nous avons basé nos calculs sur la consommation estimée de 1g de polyphénols par jour que l'on retrouve dans la diète occidentale (275). Étant donné que le volume intestinal est d'environ 6.25 litres, nous avons estimé que les entérocytes étaient exposés à une concentration de 235 µg/mL. Si le côlon à lui seul à un volume approximatif de 4.25 litres, même une concentration plus élevée est possible. Nous pensons donc que notre choix d'utiliser une concentration de 250 µg/mL pour les études *in vitro* des volets 1 et 2 expérimentaux de ce programme scientifique est justifiée et physiologiquement représentative de ce qui est possiblement retrouvé au niveau du côlon intraluminal (542).

L'étude de la composition des polyphénols de la pomme par spectrométrie de masse à haute résolution (HPLC-ESI-MS TOF) a démontré que l'extrait brut de la pelure de pomme est principalement composé de flavonols et que la fraction purifiée contient bien des flavan-3-ols et leurs oligomères. La quercétine représente le flavonols prépondérant dans l'extrait de la pomme. Des études antérieures ont affirmé que la quercétine possède des activités

antioxydantes et anti-inflammaoires, prévient l'agrégation plaquettaire et stimule la relaxation des muscles cardiovasculaires lisses (488).

Les effets antioxydants et anti-inflammatoires potentiels des polyphénols de la pelure de pomme ont été investigués en employant la lignée cellulaire Caco-2/15 d'origine intestinale. Ces cellules épithéliales sont dérivées d'un adénocarcinome colorectal et ont la capacité de se différencier et d'acquérir l'ensemble des caractéristiques physiologiques de l'intestin grêle humain (663). Elles sont cultivées sur filtre durant 10 jours, ce qui permet leur polarisation apicale et différenciation spontanée, simultanément à la formation de jonctions serrées permettant de constituer une barrière hermétique entre le compartiment apical (lumière intestinale) et le compartiment basolatéral (circulation sanguine) à l'instar de l'humain. Ces cellules sont hautement reconnues pour représenter le meilleur modèle servant à étudier l'absorption et le transport intestinal de plusieurs nutriments, particulièrement les lipides, leur assemblage avec les apolipoprotéines, et leur sécrétion sous forme de lipoprotéines (664, 665). Plus important encore est le fait que ces cellules constituent un outil de choix pour l'investigation du stress oxydant, la défense antioxydante et l'inflammation (666) en relation directe avec nos propres objectifs. Par conséquent, le modèle cellulaire Caco-2/15 est pleinement approprié à l'exploration de la biodisponibilité de l'impact des polyphénols de pommes. Il est à souligner que des études antérieures avaient démontré que les cellules Caco-2 produisent bien les métabolites sulfatés et glucuronidés suite à l'exposition du resvératrol (540, 541).

L'induction d'un stress oxydant dans les cellules Caco-2/15 a été réalisée par le complexe fer/ascorbate, un système efficace pour la production de radicaux d'oxygène et de lipides peroxydés comme rapporté à de nombreuses reprises par notre équipe de laboratoire (139, 476, 478, 481, 482). L'ajout de l'acide ascorbique permet d'amplifier le potentiel oxidatif du fer (476). Les données de notre étude indiquent clairement que le complexe Fer/ascorbate appliqué aux cellules Caco-2/15 a bien déclenché une peroxidation lipidique considérable étant donné la production de MDA, la dégradation des PUFA et la production des eicosanoïdes pro-inflammatoires témoignant donc de la présence de stress oxydant. De plus, ce complexe a déséquilibré la balance antioxydante/prooxydant en vue de la détérioration des antioxydants endogènes (SOD, GPx). Ainsi, il est possible d'imaginer qu'une co-supplémentation en fer et en vitamine C peut empirer l'étendue du stress oxydant dans

plusieurs situations pathophysiologiques et même mener à une exacerbation des maladies inflammatoires de l'intestin allant jusqu'au développement de cancers (490).

La supplémentation de l'extrait DAPP ou encore de la fraction purifiée a significativement contré la peroxidation lipidique en empêchant l'attaque sur les PUFA n-3 et en renforçant la défense antioxydante endogène (article 1). Selon nos données, l'un des mécanismes sous-jacents au raffermissement de la défense antioxydante a impliqué le facteur de transcription Nrf2 qui généralement coordonne la réponse antioxydante par sa liaison aux sites ARE sur le promoteur des gènes antioxydants afin d'activer leur transcription (492, 493). L'ajout de DAPP à notre modèle cellulaire a certainement permis au facteur Nrf2 d'échapper à la dégradation protéasomale médiée par Keap-1 et de se transloquer dans le noyau pour induire l'expression génique d'une série de protéines antioxydantes et cytoprotectives comme la SOD et la GPx. Étant donné que le PGC1α co-active plusieurs récepteurs nucléaires impliqués dans le métabolisme oxydatif, incluant la biogenèse mitochondriale et la respiration (494, 495), il nous a semblé raisonnable d'évaluer sa modulation par le DAPP. Nos observations, démontrant l'augmentation de l'expression protéique de PGC1α suite à l'administration de DAPP, suggèrent que le PGC1α confère un avantage aux cellules intestinales Caco-2/15 de diminuer le stress oxydant en interaction avec le Nrf2 qui régule à la hausse la transcription des gènes codant pour les enzymes antioxydantes endogènes SOD et GPx. La possibilité qu'il y ait un « cross-talk » entre le PGC1α et le Nrf2 suite à l'ajout de DAPP aux cellules épithéliales intestinales demeure hypothétique, ce qui exige d'autres expériences scientifiques pour établir la relation et les mécanismes d'action.

L'inflammation dans les cellules Caco-2/15 a été induite dans nos travaux par l'ajout de la LPS. Cette lipopolysaccharide issue de bactéries à Gram négatif peut passer la barrière intestinale avec l'augmentation de la perméabilité, causer l'endotoxémie et induire la réponse immunitaire de l'hôte de par sa capacité à stimuler la cascade des cytokines pro-inflammatoires (447, 491). Dans notre étude, la LPS a mené à l'amplification de la réponse inflammatoire des cellules Caco-2/15 par une production élevée de PGE_2 (due à l'élévation de COX-2) et de l'expression protéique de TNFα et IL-6 en réponse au facteur de transcription NF-κB. DAPP s'est révélé être un puissant agent dans la prévention de l'inflammation en maitenant le NF-κB inactivé dans le cytoplasme et sans lui permettre de franchir la membrane

nucléaire pour induire la transcription de COX-2, TNFα et IL-6. L'implication de COX-2 et NF-κB a été mise en évidence non seulement par la détermination de l'expression protéique, mais aussi par l'incubation des cellules avec leur inhibiteur spécifique indométhacine heptyl ester et CAPE, respectivement. Si l'addition de CAPE aux cellules traitées préalablement avec le DAPP n'a pas amplifié les effets anti-inflammatoires excercés par le DAPP, la combinaison de l'indométhacine heptyl ester et le DAPP a diminué davantage l'inflammation. Un mécanisme synergétique semble donc être présent lorsque l'indométhacine et le DAPP sont combinés. Puisque l'indométhacine est un anti-inflammatoire souvent administré aux patients atteints de MII, le traitement de surcroit avec le DAPP favoriserait la réduction de la dose d'indométhacine et donc les effets secondaires. Des essais cliniques sont requis pour tester cette proposition.

En résumé, le volet 1 expérimental de mon projet de recherche a permis de mettre en lumière la capacité des DAPP à augmenter la défense antioxydante et anti-inflammatoire par i) la prévention de l'inflammation induite par la LPS via la diminution de l'expression protéique et l'activité de COX-2; ii) la diminution de cytokines pro-inflammatoires via la régulation à la baisse du facteur de transcription NF-κB; et iii) la régulation à la hausse de l'expression des facteurs de transcription Nrf2 et PGC1α. L'étude de ces différents mécanismes d'action a démontré que le DAPP pourrait représenter une nouvelle stratégie dans la prévention du stress oxydant et l'inflammation impliqués dans les MII.

Dans le 2^{e} volet expérimental, nous avons voulu comparer les résultats de la pomme (volet 1) avec ceux de la canneberge qui est considérée comme référence dans la littérature en vue de sa richesse en plusieurs classes de polyphénols. Par conséquent, nous avons décidé dans un premier temps de caractériser les polyphénols de la canneberge et, par la suite, de définir leur métabolisme intracellulaire, d'examiner leur caractère antioxydant et anti-inflammatoire, et d'élucider les mécanismes d'action. Nous étions plus particulièrement intéressés dans ce volet à déterminer les classes de polyphénols responsables de l'activité antioxydante et anti-inflammatoire.

Suite à l'extraction des polyphénols de la canneberge, nous avons procédé à la séparation de trois fractions par chromatographie d'exclusion afin de faciliter leur identification. Ces différentes fractions de canneberge ont donc été séparées selon leur poids moléculaire par chromatographie et leurs structures chimiques ont été identifiées par différentes techniques dont la colorimétrie, le HPLC à fluorescence et la chromatographie liquide ultra-haute performance couplée à un spectromètre de masse à triple quadripôle (UPLC-TDQ). La caractérisation globale des polyphénols extraits de la canneberge a démontré que les acides phénoliques sont majoritairement présents dans la fraction de canneberge de petit poids moléculaire (LC), les flavonoïdes et les procyanidines dimériques/trimériques dans la fraction de poids moléculaire moyen (MC), et les procyanidines oligomériques/polymériques dans la fraction contenant les molécules de haut poids moléculaire (HC).

Les observations et les mécanismes d'action des polyphénols de la canneberge au niveau des cellules Caco-2/15 sont présentés de façon très sommaire dans cette section puisqu'ils sont comparables à ceux retrouvés dans l'étude du volet 1. En fait, les polyphénols de la canneberge ont exhibé leur potentiel à rétablir la plupart des perturbations pro-oxydantes induites par le Fe/Asc, soit le rétablissement de la peroxydation lipidique tel que démontré par les niveaux de MDA, le rétablissement des concentrations des acides gras polyinsaturés n-3 et n-6, l'augmentation de l'activité de la SOD et la diminution de la GPx et de la catalase. Par ailleurs, les polyphénols de la canneberge ont permis de rétablir la plupart des perturbations pro-inflammatoires induites par la LPS, soit l'inhibition de l'expression protéique des marqueurs inflammatoires (COX-2, PGE_2, TNFα et IL-6) et la diminution de l'expression protéique du facteur de transcription pro-inflammatoire NF-κB.

Nous avons arboré dans la recension des écrits que la mitochondrie est la principale source de stress oxydant étant donné sa production abondante de RLO. L'autre raison incitative de mettre l'emphase sur la mitochondrie était basée sur les observations que (i) les polyphénols de pépins de raisin (procyanidines oligomériques) ont l'habileté à moduler le métabolisme énergétique de la mitochondrie dans le muscle squelettique (667); et (ii) la quercétine s'accumule préférentiellement dans la mitochondrie tout en empêchant les RLO d'agir (332). Dans ce deuxième volet, nous avons concentré nos efforts sur les polyphénols de la fraction HC des canneberges étant donné l'ampleur du travail.

Les expressions pro-apoptotique du cytochrome c (cyt C) et anti-apoptotique de Bcl2 démontrent bien que le stress oxydant induit par le Fer/ascorbate active la voie de signalisation de l'apoptose. En présence de stress oxydant, l'expression protéique du cyt C s'est vue à la hausse tandis que celle de Bcl2 est à la baisse dans les cellules Caco-2/15. Une accumulation de sous-produits provenant du stress oxydant dans la mitochondrie constituerait probablement l'amorcement de la cascade qui mène à l'apoptose (668). Dans ce contexte, notre étude a démontré les effets anti-apoptotiques des flavonols et des procyanidines de la fraction HC en induisant l'expression de Bcl2 et en réduisant l'expression du cyt C et d'AIF. Étant donné que le Bcl2 est un régulateur anti-apoptotique clé de la perméabilisation membranaire de la mitochondrie tout en représentant un prérequis pour la sortie du cyt C de la mitochondrie vers le cytosol, la modulation positive de cette voie de signalisation par les flavonols et les procyanidines de la canneberge suggèrent définitivement un effet inhibiteur de l'apoptose. Il est à noter que des études précédentes ont démontré que la quercétine empêche le dysfonctionnent mitochondriale par la régulation de l'homéostasie du Ca^{2+} intracellulaire et par la prévention de l'apoptose (330).

La biogenèse mitochondriale est dépendante de l'échange entre les génomes nucléaires et mitochondriaux orchestré par le facteur de transcription PGC1α (131). Le PGC1α contribue également à la transcription et à la réplication de l'ADN mitochondrial par les facteurs de transcription mitochondriaux A (TFAM) et B (TFB1M et TFB2M) codés par des gènes nucléaires (669). Notre étude supporte la notion que les flavonols et les procyanidines de la canneberge ont la capacité de restaurer le fonctionnement de la mitochondrie en rétablissant la synthèse de l'ATP en réponse à l'augmentation de l'expression protéique de PGC1α. Des études supplémentaires sont à envisager afin de délimiter si la stimulation de la production de l'ATP par les polyphénols de canneberge est accomplie par la biogénese mitochondrial et/ou par l'efficacité bioénergétique de la mitochondrie. Finalement, le stress oxydant peut endommager l'ADN et initier la formation de RLO, mais l'action positive des flavonols et des procyanidines sur l'expression d'OGG1, l'enzyme de réparation de l'ADN, démontre bel et bien que ces polyphénols sont capables de freiner le stress oxydant à son initiation dans la mitochondrie.

L'étude du métabolisme des polyphénols de la canneberge dans les cellules Caco-2/15 est terminée et le manuscrit est maintenant finalisé (article 4).

Des résultats fort intéressants ont été observés quant à l'absorption et au métabolisme des polyphénols de la canneberge au niveau des cellules Caco-2/15 en présence de stress oxydant. La caractérisation des polyphénols par spectrométrie de masse a démontré que les acides cinnamiques et benzoïques (fraction LC), la quercétine glycosylée et conjuguée ainsi que les procyanidines dimériques de type A (fraction MC) et l'épicatéchine et les procyanidines dimérique (fraction HC) sont absorbés au niveau de l'entérocyte. Les processus de métabolisation ont permis le transport des polyphénols surtout sous leur forme conjuguée (méthylé, glucuronidé et sulfaté). À noter que les procyanidines oligomériques ayant un degré de polymérisation supérieur à 2 (fraction HC) semblent adhérer aux cellules Caco-2/15. L'épicatéchine, suivi par les procyanidines dimériques de type A, ont été trouvés prépondérants au niveau des mitochondries. L'analyse des procyanidines oligomériques et polymériques par UPLC-MS QTOF a révélé qu'il est possible d'observer des procyanidines ayant des DP jusqu'à 8 dans le lysat de cellules Caco-2/15 et jusqu'à 11 dans la fraction mitochondriale. Actuellement, la technique d'isolation des mitochondries utilisée ne nous permet pas de déterminer si ces procyanidines, ayant un DP élevé, sont adsorbées ou s'incorporent directement à la mitochondrie. Des études subséquentes devront être réalisées afin de déterminer si ces molécules polyphénoliques sont adsorbées (liaisons chimiques spécifiques) ou intégrées (mécanismes spécifiques) aux mitochondries.

Les études du volet 1 et 2 démontrent bien la régulation du stress oxydant et de l'inflammation par les polyphénols de la pelure de pomme et de la canneberge dans les cellules Caco-2/15. Les mécanismes d'action régissant les propriétés protectrices des polyphénols de ces deux fruits sont comparables dans l'intestin. Même si les polyphénols de la canneberge ont été les seuls à être explorés dans la mitochondrie, on peut d'attendre à ce que la richesse des pommes en quercétine offre également une bonne protection à la mitochondrie lors de perturbations reliées au stress oxydant.

Le troisième volet expérimental de mon programme scientifique consistait à évaluer les aspects préventifs et thérapeutiques des polyphénols dans un modèle murin de MII en spécifiant leurs bénéfices cliniques et voies mécanistiques.

Le choix d'utiliser la pomme ou la canneberge pour effectuer cette étude s'est arrêté principalement sur ces deux faits: les mécanismes antioxydants et anti-inflammatoires des polyphénols de la pelure de pomme sont comparables à ceux de la canneberge (article 1 et 2); et que les Canadiens et Américains consomment majoritairement (environ 20%) les polyphénols provenant de la pomme selon le dernier rapport de la MAPAQ. Ainsi, l'extrait de pelure de pomme DAPP a été administré au modèle murin en concentration proche de celle de l'humain consommant quotidiennement 100g de pomme donc environ 357 mg polyphénols (670, 671). Une autre considération nous a renforçé dans le choix de la concentration et se rapporte à la définition de la dose équivalente chez l'humain tenant compte de la surface corporelle de la souris selon l'équation de US Food and Drug Administration's guidelines (672). Ainsi, la dose de 16 mg/kg chez l'humain serait équivalente à 200 mg/kg chez la souris. Nous avons également décidé de doubler la dose à 400 mg/kg afin d'examiner si des effets indésirables à une forte concentration de polyphenols provenant de cet extrait étaient possibles.

L'induction de l'inflammation intestinale chez les souris C57BL6 a été réalisée par l'administration *per os* de l'agent inflammatoire DSS. Ce modèle d'inflammation est bien établi et largement utilisé par la communauté scientifique oeuvrant sur la pathogenèse des MII (673, 674). Il exhibe de nombreuses caractéristiques similaires à la colite chez l'humain, incluant la progression de la réponse inflammatoire, les signes cliniques (diarrhée, sang dans les selles, saignement rectal, raccourcissement du côlon), les changements histologiques de l'intestin et les modifications du microbiote intestinal (194, 675). La littérature démontre bien que les résultats obtenus dans ce modèle de MII sont pertinents à l'humain (676). Les conditions d'administration du DSS (2.5% pour 10 jours) ont été choisies afin d'induire une colite modérée qui pourrait répondre à un essai nutritionnel préventif ou thérapeutique (194, 673, 677, 678).

Nous avons effectué une caractérisation du contenu polyphénolique de cet extrait par spéctrométrie de masse à haute résolution avant de l'administrer aux souris. La présence des sous-classes des flavonoïdes : flavonols, flavan-3-ols, dihydrochalcones et acides hydroxycinnamiques étaient majoritaires dans le DAPP. Nous avions donc un extrait ayant un potentiel comparable à celui de l'étude *in vitro* (volet 1) pouvant développer des effets antioxydants et anti-inflammatoires au niveau intestinal (311).

L'évaluation des effets préventifs et thérapeutiques de DAPP dans notre modèle murin de MII a démontré une amélioration des signes cliniques induit par le DSS, tels qu'un allégement de la perte de poids corporel, de la diarrhée et du saignement dans les selles. De plus, la supplémentation de DAPP a amoindri le raccourcissement du côlon et les dommages histologiques du côlon induits par le DSS. Les observations histologiques de la muqueuse du côlon et la diminution de l'activité de la MPO permettent d'affirmer que le DAPP restreint le recrutement de neutrophiles au niveau du côlon. De plus, les groupes de souris ayant reçu du DAPP ont un score DAI plus bas que celui du groupe DSS. Pris dans leur ensemble, ces données démontrent l'efficacité préventive et thérapeutique de DAPP afin de contrer le développement de la colite par le DSS. L'effet préventif maximal de DAPP a surtout été noté à la dose de 200 mg/kg.

Un grand nombre de données expérimentales et cliniques suggère que l'inflammation intestinale chronique est la résultante d'une surproduction soutenue de cytokines pro-inflammatoires (376, 679). Puisque les cytokines TNFα et IL-6 semblent jouer un rôle important dans la pathogénèse de la colite chez les souris, nous avons analysé leur expression par RT-qPCR et Western Blot. En accord avec des études antérieures (680), les niveaux de ces cytokines pro-inflammatoires ont été trouvés positivement corrélés à la sévérité de la colite chez nos souris.

Afin de déterminer le mécanisme d'action anti-inflammatoire de DAPP, nous avons évalué l'expression de NF-κB qui a comme fonction de transcrire de nombreux gènes pro-inflammatoires (681). Plusieurs travaux rapportent que le NF-κB est un marqueur très élevé dans les tissus coloniques des animaux avec une colite (682, 683). L'évaluation de NF-κB et de son inhibiteur IκB (capable de prévenir la translocation de NF-κB dans le noyau et l'activation de la transcription des gènes pro-inflammatoires) a démontré la capacité de DAPP à contenir l'augmentation de NF-κB et la dégradation de IκB cytoplasmique dans les souris ayant une colite. Ces résultats sont en accord avec les effets anti-inflammatoires des polyphénols de la pelure de pomme dans les cellules Caco-2/15 (311) et avec les observations démontrant l'efficacité des polyphénols de la pomme à empêcher l'activation de NF-κB dans les lignées cellulaires humaines où l'inflammation a été induite par LPS/IFNy (684).

La régulation à la hausse de certaines protéines, dont le COX-2, est également impliquée dans le dysfonctionnement du système immunitaire des individus atteints de MII. L'augmentation de l'expression protéique de COX-2 résulte en une réponse inflammatoire excessive, une atteinte de l'intégrité de la muqueuse du côlon et contribue au développement des dommages intestinaux (685). L'activité anti-inflammatoire de DAPP a été nouvellement confirmée par la mesure des niveaux de COX-2 et de ses produits PGE2 qui se sont avérés réduits. Dans un premier temps, nous pouvons conclure que les bénéfices préventifs et thérapeutiques de la supplémentation de DAPP proviennent de leurs effets anti-inflammatoires probablement par le contrôle de la voie de signalisation du NF-κB (686).

La communauté scientifique a rapporté largement qu'une combinaison de réponses immunitaires déréglées et d'un débalancement entre la production de RLO et d'antioxydants peut amorcer le développement d'une MII (687, 688). Étant donné la corrélation existante entre l'activité des RLO et la sévérité du DAI (689), nous avons évalué l'impact de DAPP sur la peroxidation lipidique qui est responsable de la diminution de l'intégrité et de l'étanchéité de la membrane cellulaire. Nos résultats supportent clairement le rôle protecteur de DAPP dans la régulation de stress oxydant puisque les niveaux de MDA sont à la baisse. Nos données soulignent également que les DAPP ont un effet antioxydant indirect par l'induction des antioxydants endogènes SOD et GPx suite à l'activation de Nrf2 qui orchestre la transcription des gènes pour des protéines cytoprotectrices antioxydantes (690).

La désorganisation structurale de la mitochondrie a été observée dans les tissus des individus avec un côlon inflammé (691) et dans les monocouches de cellules épithéliales traitées avec des prooxydants (139). Bien qu'il y ait des données limitées sur le rôle de la mitochondrie dans la colite, il y a un intérêt croissant à cibler le stress oxydant majeur généré par la mitochondrie ainsi que les fonctions inhérentes afin de réduire la perméabilité intestinale et le dysfonctionnement cellulaire (692). Nos résultats démontrent l'efficacité des DAPP à améliorer la génération de l'ATP mitochondriale et à réduire l'apoptose comme en témoigne la chute de l'expression protéique de l'AIF et du cyt C dans les souris atteintes de colite ulcéreuse. De plus, l'extrait DAPP a réussi à éviter la baisse de l'expression d'OGG1, une enzyme hydrolysant les bases nucléiques anormales de l'ADN. Ces données sont concordantes avec l'étude de Carrasco-Pozo *et al*. qui ont démontré la capacité des

polyphénols à protéger la mitochondrie contre la perte de potentiel membranaire, l'augmentation de la peroxidation lipidique et la chute de l'ATP induits par l'indométhacine dans les cellules Caco-2/15 (335).

Mécanistiquement, la régulation mitochondriale par les DAPP peut être modulée via l'augmentation de PGC1α, ce qui serait concordant avec le volet 2 expérimental. Nos observations ont validé cette hypothèse. Il est donc tentant de spéculer que les polyphénols de notre extrait de pelure de pomme (DAPP) peuvent avoir des effets salutaires via l'induction de PGC1α sur le dysfonctionnement mitochondrial puisque nous avons vu précédemment le rôle de PGC1α dans la biogenèse mitochondriale et l'évidence que la quercétine en abondance dans notre extrait peut exercer sur le PGC1α (693).

Dans cette étude, nous avons exploité la technologie des puces à ADN (microarray), pour évaluer l'état transcriptionnel des gènes coloniques suite à l'exposition de DAPP en situation de stress oxydant et d'inflammation induits par DSS. Les voies de signalisation « IL-6 signalling », « Atherosclerosis signalling », « LXR/RXR activation », « Acute phase response sinalling » et « IL-10 signalling » ont été identifiées dans notre modèle murin de MII. Ainsi, le DAPP pourrait moduler différentes voies de signalisation inflammatoire. Nos résultats ont démontré que certaines fonctions biologiques sont régulées de façon exclusive par l'utilisation du DAPP en prévention ou en thérapeutique. Les effets préventifs de DAPP modulent les voies de « PPAR signalling », « Fc epsilon RI signalling » and « Dendritic maturation » alors que les voies « Gap junction signalling », « FcyRIIB signalling in B lymphocytes » et « Epithelial adherents junctions signalling » ont été modulées dans les groupes recevant le DAPP en thérapeutique, suggérant des effets bénéfiques dépendamment de la période où le DAPP est administré. Les résultats de cette étude transcriptomique sont concordants avec l'étude histologique effectuée sur le côlon distal où la dose thérapeutique de 400 mg/kg/jour de DAPP joue son plus grand rôle sur l'épithélium de surface du côlon alors que la dose préventive de 200 mg/kg/j protège particulièrement la muqueuse et la sous-muqueuse du côlon.

Comme nous avons vu dans la recension des écrits, le microbiote intestinal joue un rôle extrêmement important dans les MII en plus de moduler la biodisponibilité et les effets

antioxydants des polyphénols. Par conséquent, nous avons évalué l'effet des DAPP sur la dysbiose intestinale induite par le DSS. Nous avons effectué l'analyse métagénomique sur les différents groupes de souris. Le microbiote intestinal du groupe contrôle a été corrélé de façon positive avec les trois phylotypes bactériens : *Anaerostipes, Parabacteroides* et *Barnesiella*.
Il a été démontré que, chez des individus atteints de CU ou de syndrome de l'intestin irritable, les *Parabactéroides* se retrouvaient en faible quantité (694). La *Barnesielle* est un des genres les plus abondants dans le côlon murin (695, 696). Des niveaux de *Barnesiella* ont été corrélés avec des niveaux d'activité inférieures de la colite chez des souris déficientes en interleukine-10 (697). Une augmentation de l'abondance relative d'*Enterobascteriaceae* et de *Peptostreptococceae* ont été observée avec l'utilisation du DSS afin d'induire la colite dans notre modèle murin. Les effets du DSS sur l'épithélium intestinal sont associés à une augmentation du mucus, de la perméabilité intestinale et des dommages aiguës sur la barrière intestinale. Par conséquent, l'altération de la barrière intestinale facilitera la translocation des produits microbiens inflammatoires dans la paroi intestinale et dans la circulation du sang (698, 699). Les effets préventifs de 200 mg/kg/jour de DAPP ont démontrés qu'il y avait une légère diminution de l'activité de la MPO dans le côlon distal. Osman *et al*. ont aussi observé en 2008 que la myrtille réduisait l'infiltration des leucocytes dans la muqueuse par la diminution de la MPO (700). Le nombre d'*Enterobacteriaceae* a diminué significativement avec l'administration de myrtille comparativement au groupe contrôle. Dans notre étude, une diminution de l'abondance relative d'*Enterobacteriaceae* a également été constatée, suggérant ainsi que l'administration de polyphénols en prévention exercent bien un effet antioxydant sur la muqueuse inflammée de l'intestin. De plus, la proportion de séquences attribuées à l'*Akkermansia* était plus élevée dans le métagénome des souris ayant reçu une dose préventive de 200 mg/kg/j de DAPP. Il est possible d'expliquer ce fait, en se basant sur des études faites sur le syndrome métabolique, documentant l'augmentation de la libération du mucus comme moyen de protection contre l'inflammation. En fait, le mucus est le substrat préféré de *l'Akkermansia.* Donc, les propos retirés d'une conférence de Patrice Cani : « *C'est comme si la bactérie disait à l'organisme qu'en échange de ses bons services, elle commandait plus de nourriture »* nous démontrent bien l'échange qui existe entre l'hôte et cette bactérie pour le rétablissement du bon fonctionnement de l'intestin.

Cette dernière étude de mon programme de recherche a fourni la preuve que l'administration de DAPP dans un modèle *in vivo* diminue le stress oxydant par la modulation de la voie de signalisation Nrf2/ARE. De plus, nous avons confirmé que le DAPP diminue l'inflammation intestinale par la réduction de l'infiltration de PNN et du facteur de transciption NF-κB. L'activation de ces mécanismes régulerait au moins partiellement les fonctions mitochondriales, le phénotype de l'ARN messager et le microbiote intestinale.

Les trois volets de ce projet de recherche ne sont pas exempts de limites. Une mesure de la régulation de l'activation de NF-κB aurait été plus adéquate que la mesure du ratio NF-κB/IκB. La présentation du ratio NF-κB/IκB ne permet pas de déterminer l'intensité et la durée de l'activation de NF-κB. Une mesure de la phosphorylation et/ou l'acétylation de NF-κB (701, 702) aurait été plus adéquate pour comprendre davantage les divers processus cellulaires impliqués dans le stress oxydant et l'inflammation. Dans le deuxième volet, l'analyse des complexes protéiques de la chaîne respiratoire (particulièrement I et III) aurait permis d'étoffer nos hypothèses quant à l'origine et à la compréhension de la diminution du stress oxydant par les polyphénols de la canneberge. Dans l'étude *in vivo*, l'ajout d'un groupe de souris recevant uniquement l'extrait de pelure de pomme aurait éliminé l'hypothèse que l'extrait puisse générer à lui seul un léger stress oxydant et/ou une inflammation. De plus, le design de l'étude *in vivo* ne permet pas de mimer les périodes de rechute et de rémission des patients atteints de MII. L'ajout de groupes de souris mimant une rechute de MII ou une rémission auraient permis d'examiner les effets des polyphénols de la pelure de pomme durant ces périodes.

8. CONCLUSIONS

Dans ce programme de doctorat, les mécanismes d'action impliqués dans la régulation du stress oxydant et de l'inflammation par les polyphénols de la pelure de pomme et de la canneberge ont été élucidés dans les cellules Caco-2/15 et ont fait l'objet de deux publications scientifiques. De plus, un manuscrit a été dédié à une caractérisation exhaustive des structures chimiques des polyphénols de la canneberge et aux résultats de leur métabolisme dans les

cellules Caco-2/15. Nous avons par la suite démontré les effets préventifs et thérapeutiques des polyphénols de la pelure de pomme dans un modèle murin de MII tout en illustrant la modulation du microbiote et les voies de signalisation par microarray, ce qui a amené à la soumission d'une quatrième publication.

Une étude clinique débutera prochainement afin d'évaluer si tous les bienfaits de la consommation de polyphénols provenant de la pelure de pomme sont transposables à l'humain atteint de MII. Il sera donc possible pour la première fois d'identifier le rôle des polyphénols de la pelure de pomme dans les pathologies inflammatoires intestinales chez l'humain. Plus globalement, de nouvelles stratégies préventives et thérapeutiques mettant en évidence l'association entre la consommation des polyphénols, provenant de la pomme, et la protection de l'organisme pourront être suggérées.

9. RÉFÉRENCES

1. Von Rosenvinge EC, O'May GA, Macfarlane S, Macfarlane GT, Shirtliff ME. Microbial biofilms and gastrointestinal diseases. Pathog Dis 2013;67:25-38.

2. Gelberg HB. Comparative anatomy, physiology, and mechanisms of disease production of the esophagus, stomach, and small intestine. Toxicol Pathol 2014;42:54-66.

3. Tortora GJ, Grabowski SR. Principles of Anatomy and Physiology, Seventh ed. 1993.

4. Rescigno M, Urbano M, Valzasina B, Francolini M, Rotta G, Bonasio R et al. Dendritic cells express tight junction proteins and penetrate gut epithelial monolayers to sample bacteria. Nat Immunol 2001;2:361-7.

5. Furuse M, Hirase T, Itoh M, Nagafuchi A, Yonemura S, Tsukita S, Tsukita S. Occludin: a novel integral membrane protein localizing at tight junctions. J Cell Biol 1993;123:1777-88.

6. Tsukita S, Furuse M, Itoh M. Multifunctional strands in tight junctions. Nat Rev Mol Cell Biol 2001;2:285-93.

7. Ando-Akatsuka Y, Saitou M, Hirase T, Kishi M, Sakakibara A, Itoh M et al. Interspecies diversity of the occludin sequence: cDNA cloning of human, mouse, dog, and rat-kangaroo homologues. J Cell Biol 1996;133:43-7.

8. Saitou M, Ando-Akatsuka Y, Itoh M, Furuse M, Inazawa J, Fujimoto K, Tsukita S. Mammalian occludin in epithelial cells: its expression and subcellular distribution. Eur J Cell Biol 1997;73:222-31.

9. Van Itallie CM, Anderson JM. Claudins and epithelial paracellular transport. Annu Rev Physiol 2006;68:403-29.

10. Amasheh S, Meiri N, Gitter AH, Schoneberg T, Mankertz J, Schulzke JD, Fromm M. Claudin-2 expression induces cation-selective channels in tight junctions of epithelial cells. J Cell Sci 2002;115:4969-76.

11. Gunzel D, Stuiver M, Kausalya PJ, Haisch L, Krug SM, Rosenthal R et al. Claudin-10 exists in six alternatively spliced isoforms that exhibit distinct localization and function. J Cell Sci 2009;122:1507-17.

12. Tamura A, Hayashi H, Imasato M, Yamazaki Y, Hagiwara A, Wada M et al. Loss of claudin-15, but not claudin-2, causes Na+ deficiency and glucose malabsorption in mouse small intestine. Gastroenterology 2011;140:913-23.

13. Vetrano S, Rescigno M, Cera MR, Correale C, Rumio C, Doni A et al. Unique role of junctional adhesion molecule-a in maintaining mucosal homeostasis in inflammatory bowel disease. Gastroenterology 2008;135:173-84.

14. Barrett JC, Lee JC, Lees CW, Prescott NJ, Anderson CA, Phillips A et al. Genome-wide association study of ulcerative colitis identifies three new susceptibility loci, including the HNF4A region. Nat Genet 2009;41:1330-4.

15. Wapenaar MC, Monsuur AJ, van Bodegraven AA, Weersma RK, Bevova MR, Linskens RK et al. Associations with tight junction genes PARD3 and MAGI2 in Dutch patients point to a common barrier defect for coeliac disease and ulcerative colitis. Gut 2008;57:463-7.

16. Darsigny M, Babeu JP, Dupuis AA, Furth EE, Seidman EG, Levy E et al. Loss of hepatocyte-nuclear-factor-4alpha affects colonic ion transport and causes chronic inflammation resembling inflammatory bowel disease in mice. PLoS One 2009;4:e7609.

17. McGuckin MA, Eri R, Simms LA, Florin TH, Radford-Smith G. Intestinal barrier dysfunction in inflammatory bowel diseases. Inflamm Bowel Dis 2009;15:100-13.

18. Sheng YH, Hasnain SZ, Florin TH, McGuckin MA. Mucins in inflammatory bowel diseases and colorectal cancer. J Gastroenterol Hepatol 2012;27:28-38.

19. McGuckin MA, Eri R, Simms LA, Florin TH, Radford-Smith G. Intestinal barrier dysfunction in inflammatory bowel diseases. Inflamm Bowel Dis 2009;15:100-13.

20. Franke A, McGovern DP, Barrett JC, Wang K, Radford-Smith GL, Ahmad T et al. Genome-wide meta-analysis increases to 71 the number of confirmed Crohn's disease susceptibility loci. Nat Genet 2010;42:1118-25.

21. Moehle C, Ackermann N, Langmann T, Aslanidis C, Kel A, Kel-Margoulis O et al. Aberrant intestinal expression and allelic variants of mucin genes associated with inflammatory bowel disease. J Mol Med (Berl) 2006;84:1055-66.

22. Kyo K, Muto T, Nagawa H, Lathrop GM, Nakamura Y. Associations of distinct variants of the intestinal mucin gene MUC3A with ulcerative colitis and Crohn's disease. J Hum Genet 2001;46:5-20.

23. Lievin-Le M, V, Servin AL. The front line of enteric host defense against unwelcome intrusion of harmful microorganisms: mucins, antimicrobial peptides, and microbiota. Clin Microbiol Rev 2006;19:315-37.

24. Naslund E, Hellstrom PM. Appetite signaling: from gut peptides and enteric nerves to brain. Physiol Behav 2007;92:256-62.

25. Date Y, Kojima M, Hosoda H, Sawaguchi A, Mondal MS, Suganuma T et al. Ghrelin, a novel growth hormone-releasing acylated peptide, is synthesized in a distinct endocrine cell type in the gastrointestinal tracts of rats and humans. Endocrinology 2000;141:4255-61.

26. Cummings DE, Purnell JQ, Frayo RS, Schmidova K, Wisse BE, Weigle DS. A preprandial rise in plasma ghrelin levels suggests a role in meal initiation in humans. Diabetes 2001;50:1714-9.

27. Nagaya N, Kojima M, Uematsu M, Yamagishi M, Hosoda H, Oya H et al. Hemodynamic and hormonal effects of human ghrelin in healthy volunteers. Am J Physiol Regul Integr Comp Physiol 2001;280:R1483-R1487.

28. Chu JY, Cheng CY, Sekar R, Chow BK. Vagal afferent mediates the anorectic effect of peripheral secretin. PLoS One 2013;8:e64859.

29. Gutniak M, Orskov C, Holst JJ, Ahren B, Efendic S. Antidiabetogenic effect of glucagon-like peptide-1 (7-36)amide in normal subjects and patients with diabetes mellitus. N Engl J Med 1992;326:1316-22.

30. Farilla L, Bulotta A, Hirshberg B, Li CS, Khoury N, Noushmehr H et al. Glucagon-like peptide 1 inhibits cell apoptosis and improves glucose responsiveness of freshly isolated human islets. Endocrinology 2003;144:5149-58.

31. Batterham RL, Bloom SR. The gut hormone peptide YY regulates appetite. Ann N Y Acad Sci 2003;994:162-8.

32. Grenier E, Garofalo C, Delvin E, Levy E. Modulatory role of PYY in transport and metabolism of cholesterol in intestinal epithelial cells. PLoS One 2012;7:e40992.

33. Walker JA, Barlow JL, McKenzie AN. Innate lymphoid cells--how did we miss them? Nat Rev Immunol 2013;13:75-87.

34. Sonnenberg GF, Monticelli LA, Alenghat T, Fung TC, Hutnick NA, Kunisawa J et al. Innate lymphoid cells promote anatomical containment of lymphoid-resident commensal bacteria. Science 2012;336:1321-5.

35. Kaser A, Zeissig S, Blumberg RS. Inflammatory bowel disease. Annu Rev Immunol 2010;28:573-621.

36. Crohn BB. Inflammatory diseases of the small intestine. J Omaha Midwest Clin Soc 1946;7:77-83.

37. Silverberg MS, Satsangi J, Ahmad T, Arnott ID, Bernstein CN, Brant SR et al. Toward an integrated clinical, molecular and serological classification of inflammatory bowel disease: report of a Working Party of the 2005 Montreal World Congress of Gastroenterology. Can J Gastroenterol 2005;19 Suppl A:5A-36A.

38. Strober W, Fuss I, Mannon P. The fundamental basis of inflammatory bowel disease. J Clin Invest 2007;117:514-21.

39. Saibeni S, Cortinovis I, Beretta L, Tatarella M, Ferraris L, Rondonotti E et al. Gender and disease activity influence health-related quality of life in inflammatory bowel diseases. Hepatogastroenterology 2005;52:509-15.

40. Bernklev T, Jahnsen J, Aadland E, Sauar J, Schulz T, Lygren I et al. Health-related quality of life in patients with inflammatory bowel disease five years after the initial diagnosis. Scand J Gastroenterol 2004;39:365-73.

41. Robertson DA, Ray J, Diamond I, Edwards JG. Personality profile and affective state of patients with inflammatory bowel disease. Gut 1989;30:623-6.

42. Sajadinejad MS, Asgari K, Molavi H, Kalantari M, Adibi P. Psychological issues in inflammatory bowel disease: an overview. Gastroenterol Res Pract 2012;2012:106502.

43. Vidal A, Gomez-Gil E, Sans M, Portella MJ, Salamero M, Pique JM, Panes J. Health-related quality of life in inflammatory bowel disease patients: the role of psychopathology and personality. Inflamm Bowel Dis 2008;14:977-83.

44. Longobardi T, Bernstein CN. Health care resource utilization in inflammatory bowel disease. Clin Gastroenterol Hepatol 2006;4:731-43.

45. Dagli U. Turkish Inflammatory Bowel Disease Society recommendations on selected topics of Crohn's disease. Turk J Gastroenterol 2010;21:78-9.

46. Bernstein CN, Longobardi T, Finlayson G, Blanchard JF. Direct medical cost of managing IBD patients: a Canadian population-based study. Inflamm Bowel Dis 2012;18:1498-508.

47. Longobardi T, Bernstein CN. Utilization of health-care resources by patients with IBD in Manitoba: a profile of time since diagnosis. Am J Gastroenterol 2007;102:1683-91.

48. Bernstein CN, Loftus EV, Jr., Ng SC, Lakatos PL, Moum B. Hospitalisations and surgery in Crohn's disease. Gut 2012;61:622-9.

49. Soon IS, Molodecky NA, Rabi DM, Ghali WA, Barkema HW, Kaplan GG. The relationship between urban environment and the inflammatory bowel diseases: a systematic review and meta-analysis. BMC Gastroenterol 2012;12:51.

50. Loftus EV, Jr. Clinical epidemiology of inflammatory bowel disease: Incidence, prevalence, and environmental influences. Gastroenterology 2004;126:1504-17.

51. Pinsk V, Lemberg DA, Grewal K, Barker CC, Schreiber RA, Jacobson K. Inflammatory bowel disease in the South Asian pediatric population of British Columbia. Am J Gastroenterol 2007;102:1077-83.

52. Bernstein CN, Wajda A, Svenson LW, MacKenzie A, Koehoorn M, Jackson M et al. The epidemiology of inflammatory bowel disease in Canada: a population-based study. Am J Gastroenterol 2006;101:1559-68.

53. Bernstein CN, Blanchard JF, Rawsthorne P, Wajda A. Epidemiology of Crohn's disease and ulcerative colitis in a central Canadian province: a population-based study. Am J Epidemiol 1999;149:916-24.

54. Lowe AM, Roy PO, Poulin M, Michel P, Bitton A, St-Onge L, Brassard P. Epidemiology of Crohn's disease in Quebec, Canada. Inflamm Bowel Dis 2009;15:429-35.

55. Bernstein CN, Wajda A, Svenson LW, MacKenzie A, Koehoorn M, Jackson M et al. The epidemiology of inflammatory bowel disease in Canada: a population-based study. Am J Gastroenterol 2006;101:1559-68.

56. Williams R, Bosnic N, Duncan AW, Brogan M, Cook SF. Prevalence of opioid dispensings and concurrent gastrointestinal medications in an elderly population from Ontario, Canada. J Opioid Manag 2008;4:193-200.

57. Binder V, Orholm M. Familial occurrence and inheritance studies in inflammatory bowel disease. Neth J Med 1996;48:53-6.

58. Monsen U, Bernell O, Johansson C, Hellers G. Prevalence of inflammatory bowel disease among relatives of patients with Crohn's disease. Scand J Gastroenterol 1991;26:302-6.

59. Romier B, Schneider YJ, Larondelle Y, During A. Dietary polyphenols can modulate the intestinal inflammatory response. Nutr Rev 2009;67:363-78.

60. Winter SE, Keestra AM, Tsolis RM, Baumler AJ. The blessings and curses of intestinal inflammation. Cell Host Microbe 2010;8:36-43.

61. Khor B, Gardet A, Xavier RJ. Genetics and pathogenesis of inflammatory bowel disease. Nature 2011;474:307-17.

62. Hugot JP, Chamaillard M, Zouali H, Lesage S, Cezard JP, Belaiche J et al. Association of NOD2 leucine-rich repeat variants with susceptibility to Crohn's disease. Nature 2001;411:599-603.

63. Ogura Y, Bonen DK, Inohara N, Nicolae DL, Chen FF, Ramos R et al. A frameshift mutation in NOD2 associated with susceptibility to Crohn's disease. Nature 2001;411:603-6.

64. Russell RK, Drummond HE, Nimmo EE, Anderson N, Smith L, Wilson DC et al. Genotype-phenotype analysis in childhood-onset Crohn's disease: NOD2/CARD15 variants consistently predict phenotypic characteristics of severe disease. Inflamm Bowel Dis 2005;11:955-64.

65. Heresbach D, Gicquel-Douabin V, Birebent B, D'halluin PN, Heresbach-Le BN, Dreano S et al. NOD2/CARD15 gene polymorphisms in Crohn's disease: a genotype-phenotype analysis. Eur J Gastroenterol Hepatol 2004;16:55-62.

66. Koloski NA, Bret L, Radford-Smith G. Hygiene hypothesis in inflammatory bowel disease: a critical review of the literature. World J Gastroenterol 2008;14:165-73.

67. Calkins BM. A meta-analysis of the role of smoking in inflammatory bowel disease. Dig Dis Sci 1989;34:1841-54.

68. Kaplan GG, Hubbard J, Korzenik J, Sands BE, Panaccione R, Ghosh S et al. The inflammatory bowel diseases and ambient air pollution: a novel association. Am J Gastroenterol 2010;105:2412-9.

69. Danese S, Fiocchi C. Ulcerative colitis. N Engl J Med 2011;365:1713-25.

70. Carter MJ, Lobo AJ, Travis SP. Guidelines for the management of inflammatory bowel disease in adults. Gut 2004;53 Suppl 5:V1-16.

71. Hanauer SB. Inflammatory bowel disease: epidemiology, pathogenesis, and therapeutic opportunities. Inflamm Bowel Dis 2006;12 Suppl 1:S3-S9.

72. Itzkowitz SH, Harpaz N. Diagnosis and management of dysplasia in patients with inflammatory bowel diseases. Gastroenterology 2004;126:1634-48.

73. CCFC. The impact of inflammatory bowel disease in Canada. 2012. Ref Type: Edited Book
74. Tromm A, Griga T, May B. Oral mesalazine for the treatment of Crohn's disease: clinical efficacy with respect to pharmacokinetic properties. Hepatogastroenterology 1999;46:3124-35.

75. Otley A, Steinhart AH. Budesonide for induction of remission in Crohn's disease. Cochrane Database Syst Rev 2005;CD000296.

76. Dear KL, Compston JE, Hunter JO. Treatments for Crohn's disease that minimise steroid doses are associated with a reduced risk of osteoporosis. Clin Nutr 2001;20:541-6.

77. Stasi C, Orlandelli E. Role of the brain-gut axis in the pathophysiology of Crohn's disease. Dig Dis 2008;26:156-66.

78. Curkovic I, Egbring M, Kullak-Ublick GA. Risks of inflammatory bowel disease treatment with glucocorticosteroids and aminosalicylates. Dig Dis 2013;31:368-73.

79. Colombel JF, Sandborn WJ, Reinisch W, Mantzaris GJ, Kornbluth A, Rachmilewitz D et al. Infliximab, azathioprine, or combination therapy for Crohn's disease. N Engl J Med 2010;362:1383-95.

80. Peyrin-Biroulet L. Anti-TNF therapy in inflammatory bowel diseases: a huge review. Minerva Gastroenterol Dietol 2010;56:233-43.

81. Brandse JF, Peters CP, Gecse KB, Eshuis EJ, Jansen JM, Tuynman HA et al. Effects of Infliximab Retreatment After Consecutive Discontinuation of Infliximab and Adalimumab in Refractory Crohn's Disease. Inflamm Bowel Dis 2013.

82. Guidi L, Pugliese D, Armuzzi A. Update on the management of inflammatory bowel disease: specific role of adalimumab. Clin Exp Gastroenterol 2011;4:163-72.

83. Steenholdt C, Svenson M, Bendtzen K, Thomsen OO, Brynskov J, Ainsworth MA. Acute and delayed hypersensitivity reactions to infliximab and adalimumab in a patient with Crohn's disease. J Crohns Colitis 2012;6:108-11.

84. Singh JA, Wells GA, Christensen R, Tanjong GE, Maxwell L, Macdonald JK et al. Adverse effects of biologics: a network meta-analysis and Cochrane overview. Cochrane Database Syst Rev 2011;CD008794.

85. Silburn S, McIvor E, McEntegart A, Wilson H. Guillain-Barre syndrome in a patient receiving anti-tumour necrosis factor alpha for rheumatoid arthritis: a case report and discussion of literature. Ann Rheum Dis 2008;67:575-6.

86. Sarzi-Puttini P, Ardizzone S, Manzionna G, Atzeni F, Colombo E, Antivalle M et al. Infliximab-induced lupus in Crohn's disease: a case report. Dig Liver Dis 2003;35:814-7.

87. Esser AC, Abril A, Fayne S, Doyle JA. Acute development of multiple keratoacanthomas and squamous cell carcinomas after treatment with infliximab. J Am Acad Dermatol 2004;50:S75-S77.

88. Kansal S, Wagner J, Kirkwood CD, Catto-Smith AG. Enteral Nutrition in Crohn's Disease: An Underused Therapy. Gastroenterol Res Pract 2013;2013:482108.

89. Wiese DM, Lashner BA, Lerner E, DeMichele SJ, Seidner DL. The effects of an oral supplement enriched with fish oil, prebiotics, and antioxidants on nutrition status in Crohn's disease patients. Nutr Clin Pract 2011;26:463-73.

90. Sanders ME, Akkermans LM, Haller D, Hammerman C, Heimbach J, Hormannsperger G et al. Safety assessment of probiotics for human use. Gut Microbes 2010;1:164-85.

91. Cabre E, Manosa M, Gassull MA. Omega-3 fatty acids and inflammatory bowel diseases - a systematic review. Br J Nutr 2012;107 Suppl 2:S240-S252.

92. Uchiyama K, Nakamura M, Odahara S, Koido S, Katahira K, Shiraishi H et al. N-3 polyunsaturated fatty acid diet therapy for patients with inflammatory bowel disease. Inflamm Bowel Dis 2010;16:1696-707.

93. Suibhne TN, Cox G, Healy M, O'Morain C, O'Sullivan M. Vitamin D deficiency in Crohn's disease: prevalence, risk factors and supplement use in an outpatient setting. J Crohns Colitis 2012;6:182-8.

94. Kelly P, Suibhne TN, O'Morain C, O'Sullivan M. Vitamin D status and cytokine levels in patients with Crohn's disease. Int J Vitam Nutr Res 2011;81:205-10.

95. Hou JK, Abraham B, El-Serag H. Dietary intake and risk of developing inflammatory bowel disease: a systematic review of the literature. Am J Gastroenterol 2011;106:563-73.

96. Pavlick KP, Laroux FS, Fuseler J, Wolf RE, Gray L, Hoffman J, Grisham MB. Role of reactive metabolites of oxygen and nitrogen in inflammatory bowel disease. Free Radic Biol Med 2002;33:311-22.

97. Pravda J. Radical induction theory of ulcerative colitis. World J Gastroenterol 2005;11:2371-84.

98. Karp SM, Koch TR. Oxidative stress and antioxidants in inflammatory bowel disease. Dis Mon 2006;52:199-207.

99. Grisham MB. Oxidants and free radicals in inflammatory bowel disease. Lancet 1994;344:859-61.

100. Jourd'heuil D, Morise Z, Conner EM, Grisham MB. Oxidants, transcription factors, and intestinal inflammation. J Clin Gastroenterol 1997;25 Suppl 1:S61-S72.

101. Buffinton GD, Doe WF. Depleted mucosal antioxidant defences in inflammatory bowel disease. Free Radic Biol Med 1995;19:911-8.

102. Lih-Brody L, Powell SR, Collier KP, Reddy GM, Cerchia R, Kahn E et al. Increased oxidative stress and decreased antioxidant defenses in mucosa of inflammatory bowel disease. Dig Dis Sci 1996;41:2078-86.

103. Halliwell B. Free radicals and antioxidants: a personal view. Nutr Rev 1994;52:253-65.

104. Andreyev AY, Kushnareva YE, Starkov AA. Mitochondrial metabolism of reactive oxygen species. Biochemistry (Mosc) 2005;70:200-14.

105. Cadenas E, Boveris A, Ragan CI, Stoppani AO. Production of superoxide radicals and hydrogen peroxide by NADH-ubiquinone reductase and ubiquinol-cytochrome c reductase from beef-heart mitochondria. Arch Biochem Biophys 1977;180:248-57.

106. Turrens JF, Boveris A. Generation of superoxide anion by the NADH dehydrogenase of bovine heart mitochondria. Biochem J 1980;191:421-7.

107. Turrens JF, Alexandre A, Lehninger AL. Ubisemiquinone is the electron donor for superoxide formation by complex III of heart mitochondria. Arch Biochem Biophys 1985;237:408-14.

108. Hansford RG, Hogue BA, Mildaziene V. Dependence of H2O2 formation by rat heart mitochondria on substrate availability and donor age. J Bioenerg Biomembr 1997;29:89-95.

109. Herrero A, Barja G. Sites and mechanisms responsible for the low rate of free radical production of heart mitochondria in the long-lived pigeon. Mech Ageing Dev 1997;98:95-111.

110. Cadenas E, Boveris A, Ragan CI, Stoppani AO. Production of superoxide radicals and hydrogen peroxide by NADH-ubiquinone reductase and ubiquinol-cytochrome c reductase from beef-heart mitochondria. Arch Biochem Biophys 1977;180:248-57.

111. Liu Y, Fiskum G, Schubert D. Generation of reactive oxygen species by the mitochondrial electron transport chain. J Neurochem 2002;80:780-7.

112. Genova ML, Ventura B, Giuliano G, Bovina C, Formiggini G, Parenti CG, Lenaz G. The site of production of superoxide radical in mitochondrial Complex I is not a bound ubisemiquinone but presumably iron-sulfur cluster N2. FEBS Lett 2001;505:364-8.

113. Kushnareva Y, Murphy AN, Andreyev A. Complex I-mediated reactive oxygen species generation: modulation by cytochrome c and NAD(P)+ oxidation-reduction state. Biochem J 2002;368:545-53.

114. Turrens JF, Alexandre A, Lehninger AL. Ubisemiquinone is the electron donor for superoxide formation by complex III of heart mitochondria. Arch Biochem Biophys 1985;237:408-14.

115. Voet, D. and Voet, J. G. Biochimie. 2e. 1998. Ref Type: Edited Book

116. Scarpulla RC. Nuclear control of respiratory gene expression in mammalian cells. J Cell Biochem 2006;97:673-83.

117. Tiranti V, Savoia A, Forti F, D'Apolito MF, Centra M, Rocchi M, Zeviani M. Identification of the gene encoding the human mitochondrial RNA polymerase (h-mtRPOL) by cyberscreening of the Expressed Sequence Tags database. Hum Mol Genet 1997;6:615-25.

118. Bogenhagen DF. Interaction of mtTFB and mtRNA polymerase at core promoters for transcription of Xenopus laevis mtDNA. J Biol Chem 1996;271:12036-41.

119. Larsson NG, Wang J, Wilhelmsson H, Oldfors A, Rustin P, Lewandoski M et al. Mitochondrial transcription factor A is necessary for mtDNA maintenance and embryogenesis in mice. Nat Genet 1998;18:231-6.

120. Ekstrand MI, Falkenberg M, Rantanen A, Park CB, Gaspari M, Hultenby K et al. Mitochondrial transcription factor A regulates mtDNA copy number in mammals. Hum Mol Genet 2004;13:935-44.

121. Falkenberg M, Gaspari M, Rantanen A, Trifunovic A, Larsson NG, Gustafsson CM. Mitochondrial transcription factors B1 and B2 activate transcription of human mtDNA. Nat Genet 2002;31:289-94.

122. McCulloch V, Seidel-Rogol BL, Shadel GS. A human mitochondrial transcription factor is related to RNA adenine methyltransferases and binds S-adenosylmethionine. Mol Cell Biol 2002;22:1116-25.

123. Matsushima Y, Adan C, Garesse R, Kaguni LS. Drosophila mitochondrial transcription factor B1 modulates mitochondrial translation but not transcription or DNA copy number in Schneider cells. J Biol Chem 2005;280:16815-20.

124. Rantanen A, Gaspari M, Falkenberg M, Gustafsson CM, Larsson NG. Characterization of the mouse genes for mitochondrial transcription factors B1 and B2. Mamm Genome 2003;14:1-6.

125. Asin-Cayuela J, Gustafsson CM. Mitochondrial transcription and its regulation in mammalian cells. Trends Biochem Sci 2007;32:111-7.

126. Scarpulla RC. Transcriptional activators and coactivators in the nuclear control of mitochondrial function in mammalian cells. Gene 2002;286:81-9.

127. Virbasius JV, Scarpulla RC. Activation of the human mitochondrial transcription factor A gene by nuclear respiratory factors: a potential regulatory link between nuclear and mitochondrial gene expression in organelle biogenesis. Proc Natl Acad Sci U S A 1994;91:1309-13.

128. Zaid A, Li R, Luciakova K, Barath P, Nery S, Nelson BD. On the role of the general transcription factor Sp1 in the activation and repression of diverse mammalian oxidative phosphorylation genes. J Bioenerg Biomembr 1999;31:129-35.

129. Wu Z, Puigserver P, Andersson U, Zhang C, Adelmant G, Mootha V et al. Mechanisms controlling mitochondrial biogenesis and respiration through the thermogenic coactivator PGC-1. Cell 1999;98:115-24.

130. Vega RB, Huss JM, Kelly DP. The coactivator PGC-1 cooperates with peroxisome proliferator-activated receptor alpha in transcriptional control of nuclear genes encoding mitochondrial fatty acid oxidation enzymes. Mol Cell Biol 2000;20:1868-76.

131. Ruchko M, Gorodnya O, LeDoux SP, Alexeyev MF, Al-Mehdi AB, Gillespie MN. Mitochondrial DNA damage triggers mitochondrial dysfunction and apoptosis in oxidant-challenged lung endothelial cells. Am J Physiol Lung Cell Mol Physiol 2005;288:L530-L535.

132. Kondo S, Toyokuni S, Tanaka T, Hiai H, Onodera H, Kasai H, Imamura M. Overexpression of the hOGG1 gene and high 8-hydroxy-2'-deoxyguanosine (8-OHdG) lyase activity in human colorectal carcinoma: regulation mechanism of the 8-OHdG level in DNA. Clin Cancer Res 2000;6:1394-400.

133. Liao J, Seril DN, Lu GG, Zhang M, Toyokuni S, Yang AL, Yang GY. Increased susceptibility of chronic ulcerative colitis-induced carcinoma development in DNA repair enzyme Ogg1 deficient mice. Mol Carcinog 2008;47:638-46.

134. Green DR, Reed JC. Mitochondria and apoptosis. Science 1998;281:1309-12.

135. Reed JC. Mechanisms of apoptosis. Am J Pathol 2000;157:1415-30.

136. Cai J, Yang J, Jones DP. Mitochondrial control of apoptosis: the role of cytochrome c. Biochim Biophys Acta 1998;1366:139-49.

137. Cai J, Yang J, Jones DP. Mitochondrial control of apoptosis: the role of cytochrome c. Biochim Biophys Acta 1998;1366:139-49.

138. Finucane DM, Bossy-Wetzel E, Waterhouse NJ, Cotter TG, Green DR. Bax-induced caspase activation and apoptosis via cytochrome c release from mitochondria is inhibitable by Bcl-xL. J Biol Chem 1999;274:2225-33.

139. Taha R, Seidman E, Mailhot G, Boudreau F, Gendron FP, Beaulieu JF et al. Oxidative stress and mitochondrial functions in the intestinal Caco-2/15 cell line. PLoS One 2010;5:e11817.

140. Reed JC, Jurgensmeier JM, Matsuyama S. Bcl-2 family proteins and mitochondria. Biochim Biophys Acta 1998;1366:127-37.

141. Cheng EH, Wei MC, Weiler S, Flavell RA, Mak TW, Lindsten T, Korsmeyer SJ. BCL-2, BCL-X(L) sequester BH3 domain-only molecules preventing BAX- and BAK-mediated mitochondrial apoptosis. Mol Cell 2001;8:705-11.

142. Boots AW, Haenen GR, Bast A. Health effects of quercetin: from antioxidant to nutraceutical. Eur J Pharmacol 2008;585:325-37.

143. Marnett LJ. Lipid peroxidation-DNA damage by malondialdehyde. Mutat Res 1999;424:83-95.

144. Valko M, Rhodes CJ, Moncol J, Izakovic M, Mazur M. Free radicals, metals and antioxidants in oxidative stress-induced cancer. Chem Biol Interact 2006;160:1-40.

145. Haleng J, Pincemail J, Defraigne JO, Charlier C, Chapelle JP. [Oxidative stress]. Rev Med Liege 2007;62:628-38.

146. Halliwell B. Antioxidant defence mechanisms: from the beginning to the end (of the beginning). Free Radic Res 1999;31:261-72.

147. Kruidenier L, Kuiper I, van DW, Marklund SL, van Hogezand RA, Lamers CB, Verspaget HW. Differential mucosal expression of three superoxide dismutase isoforms in inflammatory bowel disease. J Pathol 2003;201:7-16.

148. Jones P, Suggett A. The catalse-hydrogen peroxide system. Kinetics of catalatic action at high substrate concentrations. Biochem J 1968;110:617-20.

149. Kruidenier L, Kuiper I, Van DW, Mieremet-Ooms MA, van Hogezand RA, Lamers CB, Verspaget HW. Imbalanced secondary mucosal antioxidant response in inflammatory bowel disease. J Pathol 2003;201:17-27.

150. Brigelius-Flohe R, Kipp A. Glutathione peroxidases in different stages of carcinogenesis. Biochim Biophys Acta 2009;1790:1555-68.

151. Avissar N, Whitin JC, Allen PZ, Wagner DD, Liegey P, Cohen HJ. Plasma selenium-dependent glutathione peroxidase. Cell of origin and secretion. J Biol Chem 1989;264:15850-5.

152. Valko M, Leibfritz D, Moncol J, Cronin MT, Mazur M, Telser J. Free radicals and antioxidants in normal physiological functions and human disease. Int J Biochem Cell Biol 2007;39:44-84.

153. Brigelius-Flohe R, Traber MG. Vitamin E: function and metabolism. FASEB J 1999;13:1145-55.

154. Liebler DC, Kling DS, Reed DJ. Antioxidant protection of phospholipid bilayers by alpha-tocopherol. Control of alpha-tocopherol status and lipid peroxidation by ascorbic acid and glutathione. J Biol Chem 1986;261:12114-9.

155. Burton GW, Ingold KU. beta-Carotene: an unusual type of lipid antioxidant. Science 1984;224:569-73.

156. Halliwell B. The wanderings of a free radical. Free Radic Biol Med 2009;46:531-42.

157. Babior BM, Lambeth JD, Nauseef W. The neutrophil NADPH oxidase. Arch Biochem Biophys 2002;397:342-4.

158. Goto Y, Kiyono H. Epithelial barrier: an interface for the cross-communication between gut flora and immune system. Immunol Rev 2012;245:147-63.

159. Kruidenier L, Kuiper I, Van DW, Mieremet-Ooms MA, van Hogezand RA, Lamers CB, Verspaget HW. Imbalanced secondary mucosal antioxidant response in inflammatory bowel disease. J Pathol 2003;201:17-27.

160. Kruidenier L, Verspaget HW. Review article: oxidative stress as a pathogenic factor in inflammatory bowel disease--radicals or ridiculous? Aliment Pharmacol Ther 2002;16:1997-2015.

161. Garrett WS, Gordon JI, Glimcher LH. Homeostasis and inflammation in the intestine. Cell 2010;140:859-70.

162. Camilleri M, Madsen K, Spiller R, Greenwood-Van MB, Verne GN. Intestinal barrier function in health and gastrointestinal disease. Neurogastroenterol Motil 2012;24:503-12.

163. Neuman MG. Immune dysfunction in inflammatory bowel disease. Transl Res 2007;149:173-86.

164. Bach JF. The effect of infections on susceptibility to autoimmune and allergic diseases. N Engl J Med 2002;347:911-20.

165. Baumgart DC, Carding SR. Inflammatory bowel disease: cause and immunobiology. Lancet 2007;369:1627-40.

166. Ponder A, Long MD. A clinical review of recent findings in the epidemiology of inflammatory bowel disease. Clin Epidemiol 2013;5:237-47.

167. Wilkens KA, Naver A, Bisgaard K, Nordgaard-Lassen I, Becker U, Krag A, Slinde F. Nutrition impact symptoms, handgrip strength and nutritional risk in hospitalized

patients with gastroenterological and liver diseases. Scand J Gastroenterol 2015;50:1191-8.

168. Calsbeek H, Rijken M, Dekker J, van Berge Henegouwen GP. Disease characteristics as determinants of the labour market position of adolescents and young adults with chronic digestive disorders. Eur J Gastroenterol Hepatol 2006;18:203-9.

169. Targownik LE, Sexton KA, Bernstein MT, Beatie B, Sargent M, Walker JR, Graff LA. The Relationship Among Perceived Stress, Symptoms, and Inflammation in Persons With Inflammatory Bowel Disease. Am J Gastroenterol 2015;110:1001-12.

170. Danese S, Fiocchi C. Etiopathogenesis of inflammatory bowel diseases. World J Gastroenterol 2006;12:4807-12.

171. Baumgart DC, Carding SR. Inflammatory bowel disease: cause and immunobiology. Lancet 2007;369:1627-40.

172. Cortot A, Pineton de CG, Vernier-Massouille G, Vigneron B, Gower RC. [Inflammatory bowel disease: genetic or environmental diseases?]. Gastroenterol Clin Biol 2009;33:681-91.

173. Macdonald TT, Monteleone G. Immunity, inflammation, and allergy in the gut. Science 2005;307:1920-5.

174. Clemente JC, Ursell LK, Parfrey LW, Knight R. The impact of the gut microbiota on human health: an integrative view. Cell 2012;148:1258-70.

175. Eckburg PB, Bik EM, Bernstein CN, Purdom E, Dethlefsen L, Sargent M et al. Diversity of the human intestinal microbial flora. Science 2005;308:1635-8.

176. Neuman MG. Immune dysfunction in inflammatory bowel disease. Transl Res 2007;149:173-86.

177. Papadakis KA, Targan SR. Role of cytokines in the pathogenesis of inflammatory bowel disease. Annu Rev Med 2000;51:289-98.

178. Sanchez-Munoz F, Dominguez-Lopez A, Yamamoto-Furusho JK. Role of cytokines in inflammatory bowel disease. World J Gastroenterol 2008;14:4280-8.

179. Erridge C, Bennett-Guerrero E, Poxton IR. Structure and function of lipopolysaccharides. Microbes Infect 2002;4:837-51.

180. Ishioka T, Kuwabara N, Oohashi Y, Wakabayashi K. Induction of colorectal tumors in rats by sulfated polysaccharides. Crit Rev Toxicol 1987;17:215-44.

181. Okayasu I, Hatakeyama S, Yamada M, Ohkusa T, Inagaki Y, Nakaya R. A novel method in the induction of reliable experimental acute and chronic ulcerative colitis in mice. Gastroenterology 1990;98:694-702.

182. Okayasu I, Hatakeyama S, Yamada M, Ohkusa T, Inagaki Y, Nakaya R. A novel method in the induction of reliable experimental acute and chronic ulcerative colitis in mice. Gastroenterology 1990;98:694-702.

183. Cooper HS, Murthy SN, Shah RS, Sedergran DJ. Clinicopathologic study of dextran sulfate sodium experimental murine colitis. Lab Invest 1993;69:238-49.

184. Elson CO, Sartor RB, Tennyson GS, Riddell RH. Experimental models of inflammatory bowel disease. Gastroenterology 1995;109:1344-67.

185. Wirtz S, Neurath MF. Mouse models of inflammatory bowel disease. Adv Drug Deliv Rev 2007;59:1073-83.

186. Araki Y, Sugihara H, Hattori T. In vitro effects of dextran sulfate sodium on a Caco-2 cell line and plausible mechanisms for dextran sulfate sodium-induced colitis. Oncol Rep 2006;16:1357-62.

187. Yamada M, Ohkusa T, Okayasu I. Occurrence of dysplasia and adenocarcinoma after experimental chronic ulcerative colitis in hamsters induced by dextran sulphate sodium. Gut 1992;33:1521-7.

188. Axelsson LG, Landstroëm E, Bylund-Fellenius AC. The degree of sulfate content and the molecular weight of dextran sulfate and carrageenan are important for the induction of colitis in mice. Gastroenterology 1996;110:858-69.

189. Cooper HS, Murthy SN, Shah RS, Sedergran DJ. Clinicopathologic study of dextran sulfate sodium experimental murine colitis. Lab Invest 1993;69:238-49.

190. Murthy SN, Cooper HS, Shim H, Shah RS, Ibrahim SA, Sedergran DJ. Treatment of dextran sulfate sodium-induced murine colitis by intracolonic cyclosporin. Dig Dis Sci 1993;38:1722-34.

191. Kitajima S, Takuma S, Morimoto M. Histological analysis of murine colitis induced by dextran sulfate sodium of different molecular weights. Exp Anim 2000;49:9-15.

192. Vowinkel T, Kalogeris TJ, Mori M, Krieglstein CF, Granger DN. Impact of dextran sulfate sodium load on the severity of inflammation in experimental colitis. Dig Dis Sci 2004;49:556-64.

193. Kullmann F, Messmann H, Alt M, Gross V, Bocker T, Scholmerich J, Ruschoff J. Clinical and histopathological features of dextran sulfate sodium induced acute and chronic colitis associated with dysplasia in rats. Int J Colorectal Dis 2001;16:238-46.

194. Okayasu I, Hatakeyama S, Yamada M, Ohkusa T, Inagaki Y, Nakaya R. A novel method in the induction of reliable experimental acute and chronic ulcerative colitis in mice. Gastroenterology 1990;98:694-702.

195. Maxwell JR, Brown WA, Smith CL, Byrne FR, Viney JL. Methods of inducing inflammatory bowel disease in mice. Curr Protoc Pharmacol 2009;47:5.58.1-5.58.37.

196. TOBLER A, KOEFFLER HP. Myeloperoxidase: localization, structure, and function., Blood cell biochemistry 3 ed. New york: Plenum Press, 1991:255-288pp.

197. Borregaard N, Cowland JB. Granules of the human neutrophilic polymorphonuclear leukocyte. Blood 1997;89:3503-21.

198. Klebanoff SJ. Myeloperoxidase. Proc Assoc Am Physicians 1999;111:383-9.

199. Matheson NR, Wong PS, Travis J. Isolation and properties of human neutrophil myeloperoxidase. Biochemistry 1981;20:325-30.

200. Nauseef WM, McCormick S, Goedken M. Impact of missense mutations on biosynthesis of myeloperoxidase. Redox Rep 2000;5:197-206.

201. Klebanoff SJ. Myeloperoxidase. Proc Assoc Am Physicians 1999;111:383-9.

202. Krawisz JE, Sharon P, Stenson WF. Quantitative assay for acute intestinal inflammation based on myeloperoxidase activity. Assessment of inflammation in rat and hamster models. Gastroenterology 1984;87:1344-50.

203. Sanchez-Munoz F, Dominguez-Lopez A, Yamamoto-Furusho JK. Role of cytokines in inflammatory bowel disease. World J Gastroenterol 2008;14:4280-8.

204. Van KC, Belaiche J, Louis E. Frequently relapsing Crohn's disease is characterized by persistent elevation in interleukin-6 and soluble interleukin-2 receptor serum levels during remission. Int J Colorectal Dis 2000;15:206-10.

205. DeWitt DL. Prostaglandin endoperoxide synthase: regulation of enzyme expression. Biochim Biophys Acta 1991;1083:121-34.

206. Huang WC, Chen JJ, Inoue H, Chen CC. Tyrosine phosphorylation of I-kappa B kinase alpha/beta by protein kinase C-dependent c-Src activation is involved in TNF-alpha-induced cyclooxygenase-2 expression. J Immunol 2003;170:4767-75.

207. Singer II, Kawka DW, Schloemann S, Tessner T, Riehl T, Stenson WF. Cyclooxygenase 2 is induced in colonic epithelial cells in inflammatory bowel disease. Gastroenterology 1998;115:297-306.

208. Okayama M, Hayashi S, Aoi Y, Nishio H, Kato S, Takeuchi K. Aggravation by selective COX-1 and COX-2 inhibitors of dextran sulfate sodium (DSS)-induced colon lesions in rats. Dig Dis Sci 2007;52:2095-103.

209. Sheibanie AF, Yen JH, Khayrullina T, Emig F, Zhang M, Tuma R, Ganea D. The proinflammatory effect of prostaglandin E2 in experimental inflammatory bowel disease is mediated through the IL-23-->IL-17 axis. J Immunol 2007;178:8138-47.

210. Wang D, DuBois RN. Pro-inflammatory prostaglandins and progression of colorectal cancer. Cancer Lett 2008;267:197-203.

211. Hendel J, Nielsen OH. Expression of cyclooxygenase-2 mRNA in active inflammatory bowel disease. Am J Gastroenterol 1997;92:1170-3.

212. Singer II, Kawka DW, Schloemann S, Tessner T, Riehl T, Stenson WF. Cyclooxygenase 2 is induced in colonic epithelial cells in inflammatory bowel disease. Gastroenterology 1998;115:297-306.

213. Campbell KJ, Perkins ND. Regulation of NF-kappaB function. Biochem Soc Symp 2006;165-80.

214. Rogler G, Brand K, Vogl D, Page S, Hofmeister R, Andus T et al. Nuclear factor kappaB is activated in macrophages and epithelial cells of inflamed intestinal mucosa. Gastroenterology 1998;115:357-69.

215. Atreya I, Atreya R, Neurath MF. NF-kappaB in inflammatory bowel disease. J Intern Med 2008;263:591-6.

216. Scalbert A, Williamson G. Dietary intake and bioavailability of polyphenols. J Nutr 2000;130:2073S-85S.

217. Perez-Jimenez J, Neveu V, Vos F, Scalbert A. Identification of the 100 richest dietary sources of polyphenols: an application of the Phenol-Explorer database. Eur J Clin Nutr 2010;64 Suppl 3:S112-S120.

218. Neveu V, Perez-Jimenez J, Vos F, Crespy V, du CL, Mennen L et al. Phenol-Explorer: an online comprehensive database on polyphenol contents in foods. Database (Oxford) 2010;2010:bap024.

219. Perez-Jimenez J, Neveu V, Vos F, Scalbert A. Systematic analysis of the content of 502 polyphenols in 452 foods and beverages: an application of the phenol-explorer database. J Agric Food Chem 2010;58:4959-69.

220. Kuhnau J. The flavonoids. A class of semi-essential food components: their role in human nutrition. World Rev Nutr Diet 1976;24:117-91.

221. D'Archivio M, Filesi C, Di BR, Gargiulo R, Giovannini C, Masella R. Polyphenols, dietary sources and bioavailability. Ann Ist Super Sanita 2007;43:348-61.

222. Macheix JJ, Sapis JC, Fleuriet A. Phenolic compounds and polyphenoloxidase in relation to browning in grapes and wines. Crit Rev Food Sci Nutr 1991;30:441-86.

223. Crozier A, Jaganath IB, Clifford MN. Dietary phenolics: chemistry, bioavailability and effects on health. Nat Prod Rep 2009;26:1001-43.

224. Ververidis F, Trantas E, Douglas C, Vollmer G, Kretzschmar G, Panopoulos N. Biotechnology of flavonoids and other phenylpropanoid-derived natural products. Part I: Chemical diversity, impacts on plant biology and human health. Biotechnol J 2007;2:1214-34.

225. Hollman PC, Katan MB. Dietary flavonoids: intake, health effects and bioavailability. Food Chem Toxicol 1999;37:937-42.

226. Herrmann KM, Weaver LM. THE SHIKIMATE PATHWAY. Annu Rev Plant Physiol Plant Mol Biol 1999;50:473-503.

227. Casanal A, Zander U, Munoz C, Dupeux F, Luque I, Botella MA et al. The Strawberry Pathogenesis-related 10 (PR-10) Fra a Proteins Control Flavonoid Biosynthesis by Binding to Metabolic Intermediates. J Biol Chem 2013;288:35322-32.

228. Casanal A, Zander U, Munoz C, Dupeux F, Luque I, Botella MA et al. The Strawberry Pathogenesis-related 10 (PR-10) Fra a Proteins Control Flavonoid Biosynthesis by Binding to Metabolic Intermediates. J Biol Chem 2013;288:35322-32.

229. Del RD, Rodriguez-Mateos A, Spencer JP, Tognolini M, Borges G, Crozier A. Dietary (poly)phenolics in human health: structures, bioavailability, and evidence of protective effects against chronic diseases. Antioxid Redox Signal 2013;18:1818-92.

230. Del RD, Rodriguez-Mateos A, Spencer JP, Tognolini M, Borges G, Crozier A. Dietary (poly)phenolics in human health: structures, bioavailability, and evidence of protective effects against chronic diseases. Antioxid Redox Signal 2013;18:1818-92.

231. Stalmach A, Mullen W, Pecorari M, Serafini M, Crozier A. Bioavailability of C-linked dihydrochalcone and flavanone glucosides in humans following ingestion of unfermented and fermented rooibos teas. J Agric Food Chem 2009;57:7104-11.

232. Coward L, Smith M, Kirk M, Barnes S. Chemical modification of isoflavones in soyfoods during cooking and processing. Am J Clin Nutr 1998;68:1486S-91S.

233. Crozier A, Jaganath IB, Clifford MN. Dietary phenolics: chemistry, bioavailability and effects on health. Nat Prod Rep 2009;26:1001-43.

234. Hakkinen S, Auriola S. High-performance liquid chromatography with electrospray ionization mass spectrometry and diode array ultraviolet detection in the identification of flavonol aglycones and glycosides in berries. J Chromatogr A 1998;829:91-100.

235. Zheng W, Wang SY. Oxygen radical absorbing capacity of phenolics in blueberries, cranberries, chokeberries, and lingonberries. J Agric Food Chem 2003;51:502-9.

236. Prior RL, Lazarus SA, Cao G, Muccitelli H, Hammerstone JF. Identification of procyanidins and anthocyanins in blueberries and cranberries (Vaccinium spp.) using high-performance liquid chromatography/mass spectrometry. J Agric Food Chem 2001;49:1270-6.

237. Gu L, Kelm MA, Hammerstone JF, Beecher G, Holden J, Haytowitz D et al. Concentrations of proanthocyanidins in common foods and estimations of normal consumption. J Nutr 2004;134:613-7.

238. Gu L, Kelm M, Hammerstone JF, Beecher G, Cunningham D, Vannozzi S, Prior RL. Fractionation of polymeric procyanidins from lowbush blueberry and quantification of procyanidins in selected foods with an optimized normal-phase HPLC-MS fluorescent detection method. J Agric Food Chem 2002;50:4852-60.

239. Wu X, Gu L, Prior RL, McKay S. Characterization of anthocyanins and proanthocyanidins in some cultivars of Ribes, Aronia, and Sambucus and their antioxidant capacity. J Agric Food Chem 2004;52:7846-56.

240. Gu L, Kelm MA, Hammerstone JF, Beecher G, Holden J, Haytowitz D et al. Concentrations of proanthocyanidins in common foods and estimations of normal consumption. J Nutr 2004;134:613-7.

241. Manach C, Scalbert A, Morand C, Remesy C, Jimenez L. Polyphenols: food sources and bioavailability. Am J Clin Nutr 2004;79:727-47.

242. Wu X, Prior RL. Systematic identification and characterization of anthocyanins by HPLC-ESI-MS/MS in common foods in the United States: fruits and berries. J Agric Food Chem 2005;53:2589-99.

243. Borges G, Degeneve A, Mullen W, Crozier A. Identification of flavonoid and phenolic antioxidants in black currants, blueberries, raspberries, red currants, and cranberries. J Agric Food Chem 2010;58:3901-9.

244. Maatta KR, Kamal-Eldin A, Torronen AR. High-performance liquid chromatography (HPLC) analysis of phenolic compounds in berries with diode array and electrospray ionization mass spectrometric (MS) detection: ribes species. J Agric Food Chem 2003;51:6736-44.

245. Hosseinian FS, Beta T. Saskatoon and wild blueberries have higher anthocyanin contents than other Manitoba berries. J Agric Food Chem 2007;55:10832-8.

246. Taruscio TG, Barney DL, Exon J. Content and profile of flavanoid and phenolic acid compounds in conjunction with the antioxidant capacity for a variety of northwest Vaccinium berries. J Agric Food Chem 2004;52:3169-76.

247. Zadernowski R, Naczk M, Nesterowicz J. Phenolic acid profiles in some small berries. J Agric Food Chem 2005;53:2118-24.

248. Mullen W, Edwards CA, Serafini M, Crozier A. Bioavailability of pelargonidin-3-O-glucoside and its metabolites in humans following the ingestion of strawberries with and without cream. J Agric Food Chem 2008;56:713-9.

249. Hager TJ, Howard LR, Liyanage R, Lay JO, Prior RL. Ellagitannin composition of blackberry as determined by HPLC-ESI-MS and MALDI-TOF-MS. J Agric Food Chem 2008;56:661-9.

250. Mullen W, Stewart AJ, Lean ME, Gardner P, Duthie GG, Crozier A. Effect of freezing and storage on the phenolics, ellagitannins, flavonoids, and antioxidant capacity of red raspberries. J Agric Food Chem 2002;50:5197-201.

251. Mullen W, McGinn J, Lean ME, MacLean MR, Gardner P, Duthie GG et al. Ellagitannins, flavonoids, and other phenolics in red raspberries and their contribution to antioxidant capacity and vasorelaxation properties. J Agric Food Chem 2002;50:5191-6.

252. Mullen W, Yokota T, Lean ME, Crozier A. Analysis of ellagitannins and conjugates of ellagic acid and quercetin in raspberry fruits by LC-MSn. Phytochemistry 2003;64:617-24.

253. Mullen W, Stewart AJ, Lean ME, Gardner P, Duthie GG, Crozier A. Effect of freezing and storage on the phenolics, ellagitannins, flavonoids, and antioxidant capacity of red raspberries. J Agric Food Chem 2002;50:5197-201.

254. Mullen W, Edwards CA, Serafini M, Crozier A. Bioavailability of pelargonidin-3-O-glucoside and its metabolites in humans following the ingestion of strawberries with and without cream. J Agric Food Chem 2008;56:713-9.

255. Lu Y, Foo LY. Identification and quantification of major polyphenols in apple pomace. Food Chem 1997;59:187-94.

256. Guyot S, Marnet N, Laraba D, Sanoner P, Drilleau JF. Reversed-phase HPLC following thiolysis for quantitative estimation and characterization of the four main classes of phenolic compounds in different tissue zones of a french cider apple variety (malus domestica Var. Kermerrien).". J Agric Food Chem 1998;46:1698-705.

257. Tomas-Barberan F, Clifford MN. Dietary hydroxybenzoic acid derivatives - nature, occurrence and dietary burden. Journal of the Science of Food and Agriculture 2000;80:1024-32.

258. Amakura Y, Okada M, Tsuji S, Tonogai Y. High-performance liquid chromatographic determination with photodiode array detection of ellagic acid in fresh and processed fruits. J Chromatogr A 2000;896:87-93.

259. Hakkinen SH, Karenlampi SO, Mykkanen HM, Torronen AR. Ellagic acid content in berries: influence of domestic processing and storage. Journal of Agriculture Food Chem 2000;48:2965.

260. Del RD, Stewart AJ, Mullen W, Burns J, Lean ME, Brighenti F, Crozier A. HPLC-MSn analysis of phenolic compounds and purine alkaloids in green and black tea. J Agric Food Chem 2004;52:2807-15.

261. Seeram NP. Berry fruits: compositional elements, biochemical activities, and the impact of their intake on human health, performance, and disease. J Agric Food Chem 2008;56:627-9.

262. Lyons MM, Yu C, Toma RB, Cho SY, Reiboldt W, Lee J, van Breemen RB. Resveratrol in raw and baked blueberries and bilberries. J Agric Food Chem 2003;51:5867-70.

263. Vastano BC, Chen Y, Zhu N, Ho CT, Zhou Z, Rosen RT. Isolation and identification of stilbenes in two varieties of Polygonum cuspidatum. J Agric Food Chem 2000;48:253-6.

264. Mazur WM, Uehara M, Wahala K, Adlercreutz H. Phyto-oestrogen content of berries, and plasma concentrations and urinary excretion of enterolactone after a single strawberry-meal in human subjects. Br J Nutr 2000;83:381-7.

265. Thompson LU, Robb P, Serraino M, Cheung F. Mammalian lignan production from various foods. Nutr Cancer 1991;16:43-52.

266. Adlercreutz H, Mazur W. Phyto-oestrogens and Western diseases. Ann Med 1997;29:95-120.

267. Finger A, Engelhardt UH, Wray V. Flavonol triglycosides containing galactose in tea. Phytochemistry 1991;30:2057-60.

268. Hammerstone JF, Lazarus SA, Mitchell AE, Rucker R, Schmitz HH. Identification of procyanidins in cocoa (Theobroma cacao) and chocolate using high-performance liquid chromatography/mass spectrometry. J Agric Food Chem 1999;47:490-6.

269. Gu L, Kelm MA, Hammerstone JF, Beecher G, Holden J, Haytowitz D, Prior RL. Screening of foods containing proanthocyanidins and their structural characterization using LC-MS/MS and thiolytic degradation. J Agric Food Chem 2003;51:7513-21.

270. Gil MI, Tomas-Barberan FA, Hess-Pierce B, Holcroft DM, Kader AA. Antioxidant activity of pomegranate juice and its relationship with phenolic composition and processing. J Agric Food Chem 2000;48:4581-9.

271. Mullen W, Boitier A, Stewart AJ, Crozier A. Flavonoid metabolites in human plasma and urine after the consumption of red onions: analysis by liquid chromatography with photodiode array and full scan tandem mass spectrometric detection. J Chromatogr A 2004;1058:163-8.

272. Gee JM, DuPont MS, Rhodes MJ, Johnson IT. Quercetin glucosides interact with the intestinal glucose transport pathway. Free Radic Biol Med 1998;25:19-25.

273. Hollman PC, Katan MB. Dietary flavonoids: intake, health effects and bioavailability. Food Chem Toxicol 1999;37:937-42.

274. Del RD, Borges G, Crozier A. Berry flavonoids and phenolics: bioavailability and evidence of protective effects. Br J Nutr 2010;104 Suppl 3:S67-S90.

275. Scalbert A, Williamson G. Dietary intake and bioavailability of polyphenols. J Nutr 2000;130:2073S-85S.

276. Day AJ, Canada FJ, Diaz JC, Kroon PA, Mclauchlan R, Faulds CB et al. Dietary flavonoid and isoflavone glycosides are hydrolysed by the lactase site of lactase phlorizin hydrolase. FEBS Lett 2000;468:166-70.

277. Hollman PC, de Vries JH, van Leeuwen SD, Mengelers MJ, Katan MB. Absorption of dietary quercetin glycosides and quercetin in healthy ileostomy volunteers. Am J Clin Nutr 1995;62:1276-82.

278. Day AJ, Gee JM, DuPont MS, Johnson IT, Williamson G. Absorption of quercetin-3-glucoside and quercetin-4'-glucoside in the rat small intestine: the role of lactase phlorizin hydrolase and the sodium-dependent glucose transporter. Biochem Pharmacol 2003;65:1199-206.

279. Bonetti A, Marotti I, Dinelli G. Urinary excretion of kaempferol from common beans (Phaseolus vulgaris L.) in humans. Int J Food Sci Nutr 2007;58:261-9.

280. DuPont MS, Day AJ, Bennett RN, Mellon FA, Kroon PA. Absorption of kaempferol from endive, a source of kaempferol-3-glucuronide, in humans. Eur J Clin Nutr 2004;58:947-54.

281. Carkeet C, Clevidence BA, Novotny JA. Anthocyanin excretion by humans increases linearly with increasing strawberry dose. J Nutr 2008;138:897-902.

282. Donovan JL, Crespy V, Manach C, Morand C, Besson C, Scalbert A, Remesy C. Catechin is metabolized by both the small intestine and liver of rats. J Nutr 2001;131:1753-7.

283. Ou K, Percival SS, Zou T, Khoo C, Gu L. Transport of cranberry A-type procyanidin dimers, trimers, and tetramers across monolayers of human intestinal epithelial Caco-2 cells. J Agric Food Chem 2012;60:1390-6.

284. Zumdick S, Deters A, Hensel A. In vitro intestinal transport of oligomeric procyanidins (DP 2 to 4) across monolayers of Caco-2 cells. Fitoterapia 2012;83:1210-7.

285. Manach C, Williamson G, Morand C, Scalbert A, Remesy C. Bioavailability and bioefficacy of polyphenols in humans. I. Review of 97 bioavailability studies. Am J Clin Nutr 2005;81:230S-42S.

286. Rechner AR, Smith MA, Kuhnle G, Gibson GR, Debnam ES, Srai SK et al. Colonic metabolism of dietary polyphenols: influence of structure on microbial fermentation products. Free Radic Biol Med 2004;36:212-25.

287. Williamson G, Clifford MN. Colonic metabolites of berry polyphenols: the missing link to biological activity? Br J Nutr 2010;104 Suppl 3:S48-S66.

288. Haughton E, Clifford MN, Sharp P. Monocarboxylate transporter expression is associated with the absorption of benzoic acid in human intestinal epithelial cells. J Sci Food Agric 2007;87:239-44.

289. Mori S, Takanaga H, Ohtsuki S, Deguchi T, Kang YS, Hosoya K, Terasaki T. Rat organic anion transporter 3 (rOAT3) is responsible for brain-to-blood efflux of homovanillic acid at the abluminal membrane of brain capillary endothelial cells. J Cereb Blood Flow Metab 2003;23:432-40.

290. Cao YG, Zhang L, Ma C, Chang BB, Chen YC, Tang YQ et al. Metabolism of protocatechuic acid influences fatty acid oxidation in rat heart: new anti-angina mechanism implication. Biochem Pharmacol 2009;77:1096-104.

291. Karlsson PC, Huss U, Jenner A, Halliwell B, Bohlin L, Rafter JJ. Human fecal water inhibits COX-2 in colonic HT-29 cells: role of phenolic compounds. J Nutr 2005;135:2343-9.

292. Poquet L, Clifford MN, Williamson G. Transport and metabolism of ferulic acid through the colonic epithelium. Drug Metab Dispos 2008;36:190-7.

293. Konishi Y, Kobayashi S. Microbial metabolites of ingested caffeic acid are absorbed by the monocarboxylic acid transporter (MCT) in intestinal Caco-2 cell monolayers. J Agric Food Chem 2004;52:6418-24.

294. Konishi Y, Kobayashi S. Transepithelial transport of chlorogenic acid, caffeic acid, and their colonic metabolites in intestinal caco-2 cell monolayers. J Agric Food Chem 2004;52:2518-26.

295. Lee MJ, Maliakal P, Chen L, Meng X, Bondoc FY, Prabhu S et al. Pharmacokinetics of tea catechins after ingestion of green tea and (-)-epigallocatechin-3-gallate by humans: formation of different metabolites and individual variability. Cancer Epidemiol Biomarkers Prev 2002;11:1025-32.

296. Walle UK, Galijatovic A, Walle T. Transport of the flavonoid chrysin and its conjugated metabolites by the human intestinal cell line Caco-2. Biochem Pharmacol 1999;58:431-8.

297. Ayrton A, Morgan P. Role of transport proteins in drug absorption, distribution and excretion. Xenobiotica 2001;31:469-97.

298. Walgren RA, Karnaky KJ, Jr., Lindenmayer GE, Walle T. Efflux of dietary flavonoid quercetin 4'-beta-glucoside across human intestinal Caco-2 cell monolayers by apical multidrug resistance-associated protein-2. J Pharmacol Exp Ther 2000;294:830-6.

299. Vaidyanathan JB, Walle T. Transport and metabolism of the tea flavonoid (-)-epicatechin by the human intestinal cell line Caco-2. Pharm Res 2001;18:1420-5.

300. Petri N, Tannergren C, Holst B, Mellon FA, Bao Y, Plumb GW et al. Absorption/metabolism of sulforaphane and quercetin, and regulation of phase II enzymes, in human jejunum in vivo. Drug Metab Dispos 2003;31:805-13.

301. Crespy V, Morand C, Besson C, Cotelle N, Vezin H, Demigne C, Remesy C. The splanchnic metabolism of flavonoids highly differed according to the nature of the compound. Am J Physiol Gastrointest Liver Physiol 2003;284:G980-G988.

302. Crespy V, Morand C, Manach C, Besson C, Demigne C, Remesy C. Part of quercetin absorbed in the small intestine is conjugated and further secreted in the intestinal lumen. Am J Physiol 1999;277:G120-G126.

303. Manach C, Williamson G, Morand C, Scalbert A, Remesy C. Bioavailability and bioefficacy of polyphenols in humans. I. Review of 97 bioavailability studies. Am J Clin Nutr 2005;81:230S-42S.

304. Haldar S, Rowland IR, Barnett YA, Bradbury I, Robson PJ, Powell J, Fletcher J. Influence of habitual diet on antioxidant status: a study in a population of vegetarians and omnivores. Eur J Clin Nutr 2007;61:1011-22.

305. Marc F, Davin A, Deglene-Benbrahim L, Ferrand C, Baccaunaud M, Fritsch P. [Studies of several analytical methods for antioxidant potential evaluation in food]. Med Sci (Paris) 2004;20:458-63.

306. Pietta PG. Flavonoids as antioxidants. J Nat Prod 2000;63:1035-42.

307. Higdon JV, Frei B. Tea catechins and polyphenols: health effects, metabolism, and antioxidant functions. Crit Rev Food Sci Nutr 2003;43:89-143.

308. Cos P, Ying L, Calomme M, Hu JP, Cimanga K, Van PB et al. Structure-activity relationship and classification of flavonoids as inhibitors of xanthine oxidase and superoxide scavengers. J Nat Prod 1998;61:71-6.

309. van Acker SA, van den Berg DJ, Tromp MN, Griffioen DH, van Bennekom WP, van der Vijgh WJ, Bast A. Structural aspects of antioxidant activity of flavonoids. Free Radic Biol Med 1996;20:331-42.

310. Halliwell B. Free radicals and antioxidants: a personal view. Nutr Rev 1994;52:253-65.

311. Denis MC, Furtos A, Dudonne S, Montoudis A, Garofalo C, Desjardins Y et al. Apple peel polyphenols and their beneficial actions on oxidative stress and inflammation. PLoS One 2013;8:e53725.

312. Haleng J, Pincemail J, Defraigne JO, Charlier C, Chapelle JP. [Oxidative stress]. Rev Med Liege 2007;62:628-38.

313. Hollman PC, Cassidy A, Comte B, Heinonen M, Richelle M, Richling E et al. The biological relevance of direct antioxidant effects of polyphenols for cardiovascular health in humans is not established. J Nutr 2011;141:989S-1009S.

314. Holst B, Williamson G. Nutrients and phytochemicals: from bioavailability to bioefficacy beyond antioxidants. Curr Opin Biotechnol 2008;19:73-82.

315. Jones P, Suggett A. The catalse-hydrogen peroxide system. Kinetics of catalatic action at high substrate concentrations. Biochem J 1968;110:617-20.

316. Kruidenier L, Kuiper I, Van DW, Marklund SL, van Hogezand RA, Lamers CB, Verspaget HW. Differential mucosal expression of three superoxide dismutase isoforms in inflammatory bowel disease. J Pathol 2003;201:7-16.

317. Petermann A, Miene C, Schulz-Raffelt G, Palige K, Holzer J, Glei M, Bohmer FD. GSTT2, a phase II gene induced by apple polyphenols, protects colon epithelial cells against genotoxic damage. Mol Nutr Food Res 2009;53:1245-53.

318. Soyalan B, Minn J, Schmitz HJ, Schrenk D, Will F, Dietrich H et al. Apple juice intervention modulates expression of ARE-dependent genes in rat colon and liver. Eur J Nutr 2011;50:135-43.

319. Carrasco-Pozo C, Gotteland M, Speisky H. Apple peel polyphenol extract protects against indomethacin-induced damage in Caco-2 cells by preventing mitochondrial complex I inhibition. J Agric Food Chem 2011;59:11501-8.

320. Chattopadhyay I, Bandyopadhyay U, Biswas K, Maity P, Banerjee RK. Indomethacin inactivates gastric peroxidase to induce reactive-oxygen-mediated gastric mucosal injury and curcumin protects it by preventing peroxidase inactivation and scavenging reactive oxygen. Free Radic Biol Med 2006;40:1397-408.

321. Jakesevic M, Aaby K, Borge GI, Jeppsson B, Ahrne S, Molin G. Antioxidative protection of dietary bilberry, chokeberry and Lactobacillus plantarum HEAL19 in mice subjected to intestinal oxidative stress by ischemia-reperfusion. BMC Complement Altern Med 2011;11:8.

322. Kaser A, Lee AH, Franke A, Glickman JN, Zeissig S, Tilg H et al. XBP1 links ER stress to intestinal inflammation and confers genetic risk for human inflammatory bowel disease. Cell 2008;134:743-56.

323. Maestre R, Douglass JD, Kodukula S, Medina I, Storch J. Alterations in the intestinal assimilation of oxidized PUFAs are ameliorated by a polyphenol-rich grape seed extract in an in vitro model and Caco-2 cells. J Nutr 2013;143:295-301.

324. Maity P, Bindu S, Dey S, Goyal M, Alam A, Pal C et al. Indomethacin, a non-steroidal anti-inflammatory drug, develops gastropathy by inducing reactive oxygen species-mediated mitochondrial pathology and associated apoptosis in gastric mucosa: a novel role of mitochondrial aconitase oxidation. J Biol Chem 2009;284:3058-68.

325. Moreno-Sanchez R, Bravo C, Vasquez C, Ayala G, Silveira LH, Martinez-Lavin M. Inhibition and uncoupling of oxidative phosphorylation by nonsteroidal anti-inflammatory drugs: study in mitochondria, submitochondrial particles, cells, and whole heart. Biochem Pharmacol 1999;57:743-52.

326. Rath E, Berger E, Messlik A, Nunes T, Liu B, Kim SC et al. Induction of dsRNA-activated protein kinase links mitochondrial unfolded protein response to the pathogenesis of intestinal inflammation. Gut 2012;61:1269-78.

327. Rath E, Haller D. Mitochondria at the interface between danger signaling and metabolism: role of unfolded protein responses in chronic inflammation. Inflamm Bowel Dis 2012;18:1364-77.

328. Walter P, Ron D. The unfolded protein response: from stress pathway to homeostatic regulation. Science 2011;334:1081-6.

329. Carrasco-Pozo C, Speisky H, Brunser O, Pastene E, Gotteland M. Apple peel polyphenols protect against gastrointestinal mucosa alterations induced by indomethacin in rats. J Agric Food Chem 2011;59:6459-66.

330. Carrasco-Pozo C, Pastene E, Vergara C, Zapata M, Sandoval C, Gotteland M. Stimulation of cytosolic and mitochondrial calcium mobilization by indomethacin in Caco-2 cells: modulation by the polyphenols quercetin, resveratrol and rutin. Biochim Biophys Acta 2012;1820:2052-61.

331. Carrasco-Pozo C, Morales P, Gotteland M. Polyphenols Protect the Epithelial Barrier Function of Caco-2 Cells Exposed to Indomethacin through the Modulation of Occludin and Zonula Occludens-1 Expression. J Agric Food Chem 2013.

332. Fiorani M, Guidarelli A, Blasa M, Azzolini C, Candiracci M, Piatti E, Cantoni O. Mitochondria accumulate large amounts of quercetin: prevention of mitochondrial damage and release upon oxidation of the extramitochondrial fraction of the flavonoid. J Nutr Biochem 2010;21:397-404.

333. Vreeburg RA, van Wezel EE, Ocana-Calahorro F, Mes JJ. Apple extract induces increased epithelial resistance and claudin 4 expression in Caco-2 cells. J Sci Food Agric 2012;92:439-44.

334. Wagner MC, Rhodes G, Wang E, Pruthi V, Arif E, Saleem MA et al. Ischemic injury to kidney induces glomerular podocyte effacement and dissociation of slit diaphragm proteins Neph1 and ZO-1. J Biol Chem 2008;283:35579-89.

335. Carrasco-Pozo C, Gotteland M, Speisky H. Protection by apple peel polyphenols against indometacin-induced oxidative stress, mitochondrial damage and cytotoxicity in Caco-2 cells. J Pharm Pharmacol 2010;62:943-50.

336. Cos P, Ying L, Calomme M, Hu JP, Cimanga K, Van PB et al. Structure-activity relationship and classification of flavonoids as inhibitors of xanthine oxidase and superoxide scavengers. J Nat Prod 1998;61:71-6.

337. van Acker SA, van den Berg DJ, Tromp MN, Griffioen DH, van Bennekom WP, van der Vijgh WJ, Bast A. Structural aspects of antioxidant activity of flavonoids. Free Radic Biol Med 1996;20:331-42.

338. Petermann A, Miene C, Schulz-Raffelt G, Palige K, Holzer J, Glei M, Bohmer FD. GSTT2, a phase II gene induced by apple polyphenols, protects colon epithelial cells against genotoxic damage. Mol Nutr Food Res 2009;53:1245-53.

339. Maestre R, Douglass JD, Kodukula S, Medina I, Storch J. Alterations in the intestinal assimilation of oxidized PUFAs are ameliorated by a polyphenol-rich grape seed extract in an in vitro model and Caco-2 cells. J Nutr 2013;143:295-301.

340. Jakesevic M, Aaby K, Borge GI, Jeppsson B, Ahrne S, Molin G. Antioxidative protection of dietary bilberry, chokeberry and Lactobacillus plantarum HEAL19 in mice subjected to intestinal oxidative stress by ischemia-reperfusion. BMC Complement Altern Med 2011;11:8.

341. Levine RL. Carbonyl modified proteins in cellular regulation, aging, and disease. Free Radic Biol Med 2002;32:790-6.

342. Richter C, Park JW, Ames BN. Normal oxidative damage to mitochondrial and nuclear DNA is extensive. Proc Natl Acad Sci U S A 1988;85:6465-7.

343. Ames BN, Shigenaga MK, Hagen TM. Oxidants, antioxidants, and the degenerative diseases of aging. Proc Natl Acad Sci U S A 1993;90:7915-22.

344. Cann RL, Wilson AC. Length mutations in human mitochondrial DNA. Genetics 1983;104:699-711.

345. Cortopassi GA, Shibata D, Soong NW, Arnheim N. A pattern of accumulation of a somatic deletion of mitochondrial DNA in aging human tissues. Proc Natl Acad Sci U S A 1992;89:7370-4.

346. Carrasco-Pozo C, Gotteland M, Speisky H. Apple peel polyphenol extract protects against indomethacin-induced damage in Caco-2 cells by preventing mitochondrial complex I inhibition. J Agric Food Chem 2011;59:11501-8.

347. Maity P, Bindu S, Dey S, Goyal M, Alam A, Pal C et al. Indomethacin, a non-steroidal anti-inflammatory drug, develops gastropathy by inducing reactive oxygen species-mediated mitochondrial pathology and associated apoptosis in gastric mucosa: a novel role of mitochondrial aconitase oxidation. J Biol Chem 2009;284:3058-68.

348. Chattopadhyay I, Bandyopadhyay U, Biswas K, Maity P, Banerjee RK. Indomethacin inactivates gastric peroxidase to induce reactive-oxygen-mediated gastric mucosal injury and curcumin protects it by preventing peroxidase inactivation and scavenging reactive oxygen. Free Radic Biol Med 2006;40:1397-408.

349. Moreno-Sanchez R, Bravo C, Vasquez C, Ayala G, Silveira LH, Martinez-Lavin M. Inhibition and uncoupling of oxidative phosphorylation by nonsteroidal anti-inflammatory drugs: study in mitochondria, submitochondrial particles, cells, and whole heart. Biochem Pharmacol 1999;57:743-52.

350. Vreeburg RA, van Wezel EE, Ocana-Calahorro F, Mes JJ. Apple extract induces increased epithelial resistance and claudin 4 expression in Caco-2 cells. J Sci Food Agric 2012;92:439-44.

351. Wagner MC, Rhodes G, Wang E, Pruthi V, Arif E, Saleem MA et al. Ischemic injury to kidney induces glomerular podocyte effacement and dissociation of slit diaphragm proteins Neph1 and ZO-1. J Biol Chem 2008;283:35579-89.

352. Johansson ME, Ambort D, Pelaseyed T, Schutte A, Gustafsson JK, Ermund A et al. Composition and functional role of the mucus layers in the intestine. Cell Mol Life Sci 2011;68:3635-41.

353. Maloy KJ, Powrie F. Intestinal homeostasis and its breakdown in inflammatory bowel disease. Nature 2011;474:298-306.

354. Pierre JF, Heneghan AF, Feliciano RP, Shanmuganayagam D, Roenneburg DA, Krueger CG et al. Cranberry proanthocyanidins improve the gut mucous layer morphology and function in mice receiving elemental enteral nutrition. JPEN J Parenter Enteral Nutr 2013;37:401-9.

355. Sandoval-Acuna C, Ferreira J, Speisky H. Polyphenols and mitochondria: an update on their increasingly emerging ROS-scavenging independent actions. Arch Biochem Biophys 2014;559:75-90.

356. Sandoval-Acuna C, Ferreira J, Speisky H. Polyphenols and mitochondria: an update on their increasingly emerging ROS-scavenging independent actions. Arch Biochem Biophys 2014;559:75-90.

357. Boivin D, Blanchette M, Barrette S, Moghrabi A, Beliveau R. Inhibition of cancer cell proliferation and suppression of TNF-induced activation of NFkappaB by edible berry juice. Anticancer Res 2007;27:937-48.

358. D'Argenio G, Mazzone G, Tuccillo C, Ribecco MT, Graziani G, Gravina AG et al. Apple polyphenols extract (APE) improves colon damage in a rat model of colitis. Dig Liver Dis 2012;44:555-62.

359. Deng S, Palu 'K, West BJ, Su CX, Zhou BN, Jensen JC. Lipoxygenase inhibitory constituents of the fruits of noni (Morinda citrifolia) collected in Tahiti. J Nat Prod 2007;70:859-62.

360. Fawzy AA, Vishwanath BS, Franson RC. Inhibition of human non-pancreatic phospholipases A2 by retinoids and flavonoids. Mechanism of action. Agents Actions 1988;25:394-400.

361. Larrosa M, Gonzalez-Sarrias A, Yanez-Gascon MJ, Selma MV, Azorin-Ortuno M, Toti S et al. Anti-inflammatory properties of a pomegranate extract and its metabolite urolithin-A in a colitis rat model and the effect of colon inflammation on phenolic metabolism. J Nutr Biochem 2010;21:717-25.

362. Lattig J, Bohl M, Fischer P, Tischer S, Tietbohl C, Menschikowski M et al. Mechanism of inhibition of human secretory phospholipase A2 by flavonoids: rationale for lead design. J Comput Aided Mol Des 2007;21:473-83.

363. Rosillo MA, Sanchez-Hidalgo M, Cardeno A, de la Lastra CA. Protective effect of ellagic acid, a natural polyphenolic compound, in a murine model of Crohn's disease. Biochem Pharmacol 2011;82:737-45.

364. Sergent T, Piront N, Meurice J, Toussaint O, Schneider YJ. Anti-inflammatory effects of dietary phenolic compounds in an in vitro model of inflamed human intestinal epithelium. Chem Biol Interact 2010;188:659-67.

365. Vasquez-Martinez Y, Ohri RV, Kenyon V, Holman TR, Sepulveda-Boza S. Structure-activity relationship studies of flavonoids as potent inhibitors of human platelet 12-hLO, reticulocyte 15-hLO-1, and prostate epithelial 15-hLO-2. Bioorg Med Chem 2007;15:7408-25.

366. Yoon JH, Baek SJ. Molecular targets of dietary polyphenols with anti-inflammatory properties. Yonsei Med J 2005;46:585-96.

367. Barnett MP, Cooney JM, Dommels YE, Nones K, Brewster DT, Park Z et al. Modulation of colonic inflammation in Mdr1a(-/-) mice by green tea polyphenols and their effects on the colon transcriptome and proteome. J Nutr Biochem 2013;24:1678-90.

368. Campbell KJ, Perkins ND. Regulation of NF-kappaB function. Biochem Soc Symp 2006;165-80.

369. Comalada M, Ballester I, Bailon E, Sierra S, Xaus J, Galvez J et al. Inhibition of pro-inflammatory markers in primary bone marrow-derived mouse macrophages by naturally occurring flavonoids: analysis of the structure-activity relationship. Biochem Pharmacol 2006;72:1010-21.

370. Crouvezier S, Powell B, Keir D, Yaqoob P. The effects of phenolic components of tea on the production of pro- and anti-inflammatory cytokines by human leukocytes in vitro. Cytokine 2001;13:280-6.

371. Essafi-Benkhadir K, Refai A, Riahi I, Fattouch S, Karoui H, Essafi M. Quince (Cydonia oblonga Miller) peel polyphenols modulate LPS-induced inflammation in human THP-1-derived macrophages through NF-kappaB, p38MAPK and Akt inhibition. Biochem Biophys Res Commun 2012;418:180-5.

372. Femia AP, Luceri C, Bianchini F, Salvadori M, Salvianti F, Pinzani P et al. Marie Menard apples with high polyphenol content and a low-fat diet reduce 1,2-dimethylhydrazine-induced colon carcinogenesis in rats: effects on inflammation and apoptosis. Mol Nutr Food Res 2012;56:1353-7.

373. Hommes DW, Peppelenbosch MP, van Deventer SJ. Mitogen activated protein (MAP) kinase signal transduction pathways and novel anti-inflammatory targets. Gut 2003;52:144-51.

374. Kleemann R, Verschuren L, Morrison M, Zadelaar S, van Erk MJ, Wielinga PY, Kooistra T. Anti-inflammatory, anti-proliferative and anti-atherosclerotic effects of quercetin in human in vitro and in vivo models. Atherosclerosis 2011;218:44-52.

375. Lee SH, Sohn DH, Jin XY, Kim SW, Choi SC, Seo GS. 2',4',6'-tris(methoxymethoxy) chalcone protects against trinitrobenzene sulfonic acid-induced colitis and blocks tumor necrosis factor-alpha-induced intestinal epithelial inflammation via heme oxygenase 1-dependent and independent pathways. Biochem Pharmacol 2007;74:870-80.

376. Papadakis KA, Targan SR. Current theories on the causes of inflammatory bowel disease. Gastroenterol Clin North Am 1999;28:283-96.

377. Paradkar PN, Blum PS, Berhow MA, Baumann H, Kuo SM. Dietary isoflavones suppress endotoxin-induced inflammatory reaction in liver and intestine. Cancer Lett 2004;215:21-8.

378. Romier B, Van De Walle J, During A, Larondelle Y, Schneider YJ. Modulation of signalling nuclear factor-kappaB activation pathway by polyphenols in human intestinal Caco-2 cells. Br J Nutr 2008;100:542-51.

379. Ruiz PA, Haller D. Functional diversity of flavonoids in the inhibition of the proinflammatory NF-kappaB, IRF, and Akt signaling pathways in murine intestinal epithelial cells. J Nutr 2006;136:664-71.

380. Ruiz PA, Braune A, Holzlwimmer G, Quintanilla-Fend L, Haller D. Quercetin inhibits TNF-induced NF-kappaB transcription factor recruitment to proinflammatory gene promoters in murine intestinal epithelial cells. J Nutr 2007;137:1208-15.

381. Waetzig GH, Schreiber S. Review article: mitogen-activated protein kinases in chronic intestinal inflammation - targeting ancient pathways to treat modern diseases. Aliment Pharmacol Ther 2003;18:17-32.

382. Xie C, Kang J, Ferguson ME, Nagarajan S, Badger TM, Wu X. Blueberries reduce pro-inflammatory cytokine TNF-alpha and IL-6 production in mouse macrophages by inhibiting NF-kappaB activation and the MAPK pathway. Mol Nutr Food Res 2011;55:1587-91.

383. Yang F, Oz HS, Barve S, de Villiers WJ, McClain CJ, Varilek GW. The green tea polyphenol (-)-epigallocatechin-3-gallate blocks nuclear factor-kappa B activation by inhibiting I kappa B kinase activity in the intestinal epithelial cell line IEC-6. Mol Pharmacol 2001;60:528-33.

384. Scarpa M, Stylianou E. Epigenetics: Concepts and relevance to IBD pathogenesis. Inflamm Bowel Dis 2012;18:1982-96.

385. Arasaradnam RP, Commane DM, Bradburn D, Mathers JC. A review of dietary factors and its influence on DNA methylation in colorectal carcinogenesis. Epigenetics 2008;3:193-8.

386. Biesalski HK. Polyphenols and inflammation: basic interactions. Curr Opin Clin Nutr Metab Care 2007;10:724-8.

387. Donnelly LE, Newton R, Kennedy GE, Fenwick PS, Leung RH, Ito K et al. Anti-inflammatory effects of resveratrol in lung epithelial cells: molecular mechanisms. Am J Physiol Lung Cell Mol Physiol 2004;287:L774-L783.

388. Fang MZ, Wang Y, Ai N, Hou Z, Sun Y, Lu H et al. Tea polyphenol (-)-epigallocatechin-3-gallate inhibits DNA methyltransferase and reactivates methylation-silenced genes in cancer cell lines. Cancer Res 2003;63:7563-70.

389. Finkel T, Deng CX, Mostoslavsky R. Recent progress in the biology and physiology of sirtuins. Nature 2009;460:587-91.

390. Gilbert ER, Liu D. Flavonoids influence epigenetic-modifying enzyme activity: structure - function relationships and the therapeutic potential for cancer. Curr Med Chem 2010;17:1756-68.

391. Hauser AT, Jung M. Targeting epigenetic mechanisms: potential of natural products in cancer chemoprevention. Planta Med 2008;74:1593-601.

392. Huang YW, Kuo CT, Stoner K, Huang TH, Wang LS. An overview of epigenetics and chemoprevention. FEBS Lett 2011;585:2129-36.

393. Johnson IT, Belshaw NJ. Environment, diet and CpG island methylation: epigenetic signals in gastrointestinal neoplasia. Food Chem Toxicol 2008;46:1346-59.

394. Lavu S, Boss O, Elliott PJ, Lambert PD. Sirtuins--novel therapeutic targets to treat age-associated diseases. Nat Rev Drug Discov 2008;7:841-53.

395. Lee WJ, Shim JY, Zhu BT. Mechanisms for the inhibition of DNA methyltransferases by tea catechins and bioflavonoids. Mol Pharmacol 2005;68:1018-30.

396. Lee WJ, Zhu BT. Inhibition of DNA methylation by caffeic acid and chlorogenic acid, two common catechol-containing coffee polyphenols. Carcinogenesis 2006;27:269-77.

397. Leiro J, Arranz JA, Fraiz N, Sanmartin ML, Quezada E, Orallo F. Effect of cis-resveratrol on genes involved in nuclear factor kappa B signaling. Int Immunopharmacol 2005;5:393-406.

398. Li Y, Tollefsbol TO. Impact on DNA methylation in cancer prevention and therapy by bioactive dietary components. Curr Med Chem 2010;17:2141-51.

399. Manna SK, Mukhopadhyay A, Aggarwal BB. Resveratrol suppresses TNF-induced activation of nuclear transcription factors NF-kappa B, activator protein-1, and apoptosis: potential role of reactive oxygen intermediates and lipid peroxidation. J Immunol 2000;164:6509-19.

400. Michan S, Sinclair D. Sirtuins in mammals: insights into their biological function. Biochem J 2007;404:1-13.

401. Singh JA, Wells GA, Christensen R, Tanjong GE, Maxwell L, Macdonald JK et al. Adverse effects of biologics: a network meta-analysis and Cochrane overview. Cochrane Database Syst Rev 2011;CD008794.

402. Singh UP, Singh NP, Singh B, Hofseth LJ, Price RL, Nagarkatti M, Nagarkatti PS. Resveratrol (trans-3,5,4'-trihydroxystilbene) induces silent mating type information regulation-1 and down-regulates nuclear transcription factor-kappaB activation to

abrogate dextran sulfate sodium-induced colitis. J Pharmacol Exp Ther 2010;332:829-39.

403. Verma M, Maruvada P, Srivastava S. Epigenetics and cancer. Crit Rev Clin Lab Sci 2004;41:585-607.

404. Deng S, Palu 'K, West BJ, Su CX, Zhou BN, Jensen JC. Lipoxygenase inhibitory constituents of the fruits of noni (Morinda citrifolia) collected in Tahiti. J Nat Prod 2007;70:859-62.

405. Vasquez-Martinez Y, Ohri RV, Kenyon V, Holman TR, Sepulveda-Boza S. Structure-activity relationship studies of flavonoids as potent inhibitors of human platelet 12-hLO, reticulocyte 15-hLO-1, and prostate epithelial 15-hLO-2. Bioorg Med Chem 2007;15:7408-25.

406. Lattig J, Bohl M, Fischer P, Tischer S, Tietbohl C, Menschikowski M et al. Mechanism of inhibition of human secretory phospholipase A2 by flavonoids: rationale for lead design. J Comput Aided Mol Des 2007;21:473-83.

407. Fawzy AA, Vishwanath BS, Franson RC. Inhibition of human non-pancreatic phospholipases A2 by retinoids and flavonoids. Mechanism of action. Agents Actions 1988;25:394-400.

408. D'Argenio G, Mazzone G, Tuccillo C, Ribecco MT, Graziani G, Gravina AG et al. Apple polyphenols extract (APE) improves colon damage in a rat model of colitis. Dig Liver Dis 2012;44:555-62.

409. Femia AP, Luceri C, Bianchini F, Salvadori M, Salvianti F, Pinzani P et al. Marie Menard apples with high polyphenol content and a low-fat diet reduce 1,2-dimethylhydrazine-induced colon carcinogenesis in rats: effects on inflammation and apoptosis. Mol Nutr Food Res 2012;56:1353-7.

410. Kleemann R, Verschuren L, Morrison M, Zadelaar S, van Erk MJ, Wielinga PY, Kooistra T. Anti-inflammatory, anti-proliferative and anti-atherosclerotic effects of quercetin in human in vitro and in vivo models. Atherosclerosis 2011;218:44-52.

411. Xie C, Kang J, Chen JR, Nagarajan S, Badger TM, Wu X. Phenolic acids are in vivo atheroprotective compounds appearing in the serum of rats after blueberry consumption. J Agric Food Chem 2011;59:10381-7.

412. Femia AP, Luceri C, Bianchini F, Salvadori M, Salvianti F, Pinzani P et al. Marie Menard apples with high polyphenol content and a low-fat diet reduce 1,2-dimethylhydrazine-induced colon carcinogenesis in rats: effects on inflammation and apoptosis. Mol Nutr Food Res 2012;56:1353-7.

413. Comalada M, Ballester I, Bailon E, Sierra S, Xaus J, Galvez J et al. Inhibition of pro-inflammatory markers in primary bone marrow-derived mouse macrophages by

naturally occurring flavonoids: analysis of the structure-activity relationship. Biochem Pharmacol 2006;72:1010-21.

414. Crouvezier S, Powell B, Keir D, Yaqoob P. The effects of phenolic components of tea on the production of pro- and anti-inflammatory cytokines by human leukocytes in vitro. Cytokine 2001;13:280-6.

415. Banerjee N, Kim H, Talcott S, Mertens-Talcott S. Pomegranate polyphenolics suppressed azoxymethane-induced colorectal aberrant crypt foci and inflammation: possible role of miR-126/VCAM-1 and miR-126/PI3K/AKT/mTOR. Carcinogenesis 2013;34:2814-22.

416. Ruiz PA, Haller D. Functional diversity of flavonoids in the inhibition of the proinflammatory NF-kappaB, IRF, and Akt signaling pathways in murine intestinal epithelial cells. J Nutr 2006;136:664-71.

417. Ruiz PA, Braune A, Holzlwimmer G, Quintanilla-Fend L, Haller D. Quercetin inhibits TNF-induced NF-kappaB transcription factor recruitment to proinflammatory gene promoters in murine intestinal epithelial cells. J Nutr 2007;137:1208-15.

418. Paradkar PN, Blum PS, Berhow MA, Baumann H, Kuo SM. Dietary isoflavones suppress endotoxin-induced inflammatory reaction in liver and intestine. Cancer Lett 2004;215:21-8.

419. Lee SH, Sohn DH, Jin XY, Kim SW, Choi SC, Seo GS. 2',4',6'-tris(methoxymethoxy) chalcone protects against trinitrobenzene sulfonic acid-induced colitis and blocks tumor necrosis factor-alpha-induced intestinal epithelial inflammation via heme oxygenase 1-dependent and independent pathways. Biochem Pharmacol 2007;74:870-80.

420. Romier B, Van De Walle J, During A, Larondelle Y, Schneider YJ. Modulation of signalling nuclear factor-kappaB activation pathway by polyphenols in human intestinal Caco-2 cells. Br J Nutr 2008;100:542-51.

421. Hommes DW, Peppelenbosch MP, van Deventer SJ. Mitogen activated protein (MAP) kinase signal transduction pathways and novel anti-inflammatory targets. Gut 2003;52:144-51.

422. Egerton M, Fitzpatrick DR, Catling AD, Kelso A. Differential activation of T cell cytokine production by the extracellular signal-regulated kinase (ERK) signaling pathway. Eur J Immunol 1996;26:2279-85.

423. Waetzig GH, Schreiber S. Review article: mitogen-activated protein kinases in chronic intestinal inflammation - targeting ancient pathways to treat modern diseases. Aliment Pharmacol Ther 2003;18:17-32.

424. Bergmann M, Hart L, Lindsay M, Barnes PJ, Newton R. IkappaBalpha degradation and nuclear factor-kappaB DNA binding are insufficient for interleukin-1beta and tumor necrosis factor-alpha-induced kappaB-dependent transcription. Requirement for an additional activation pathway. J Biol Chem 1998;273:6607-10.

425. Essafi-Benkhadir K, Refai A, Riahi I, Fattouch S, Karoui H, Essafi M. Quince (Cydonia oblonga Miller) peel polyphenols modulate LPS-induced inflammation in human THP-1-derived macrophages through NF-kappaB, p38MAPK and Akt inhibition. Biochem Biophys Res Commun 2012;418:180-5.

426. Xie C, Kang J, Ferguson ME, Nagarajan S, Badger TM, Wu X. Blueberries reduce pro-inflammatory cytokine TNF-alpha and IL-6 production in mouse macrophages by inhibiting NF-kappaB activation and the MAPK pathway. Mol Nutr Food Res 2011;55:1587-91.

427. Barnett MP, Cooney JM, Dommels YE, Nones K, Brewster DT, Park Z et al. Modulation of colonic inflammation in Mdr1a(-/-) mice by green tea polyphenols and their effects on the colon transcriptome and proteome. J Nutr Biochem 2013;24:1678-90.

428. Senggunprai L, Kukongviriyapan V, Prawan A, Kukongviriyapan U. Quercetin and EGCG Exhibit Chemopreventive Effects in Cholangiocarcinoma Cells via Suppression of JAK/STAT Signaling Pathway. Phytother Res 2013.

429. Huang YW, Kuo CT, Stoner K, Huang TH, Wang LS. An overview of epigenetics and chemoprevention. FEBS Lett 2011;585:2129-36.

430. Verma M, Maruvada P, Srivastava S. Epigenetics and cancer. Crit Rev Clin Lab Sci 2004;41:585-607.

431. Hauser AT, Jung M. Targeting epigenetic mechanisms: potential of natural products in cancer chemoprevention. Planta Med 2008;74:1593-601.

432. Johnson IT, Belshaw NJ. Environment, diet and CpG island methylation: epigenetic signals in gastrointestinal neoplasia. Food Chem Toxicol 2008;46:1346-59.

433. Arasaradnam RP, Commane DM, Bradburn D, Mathers JC. A review of dietary factors and its influence on DNA methylation in colorectal carcinogenesis. Epigenetics 2008;3:193-8.

434. Gilbert ER, Liu D. Flavonoids influence epigenetic-modifying enzyme activity: structure - function relationships and the therapeutic potential for cancer. Curr Med Chem 2010;17:1756-68.

435. Li Y, Tollefsbol TO. Impact on DNA methylation in cancer prevention and therapy by bioactive dietary components. Curr Med Chem 2010;17:2141-51.

436. Michan S, Sinclair D. Sirtuins in mammals: insights into their biological function. Biochem J 2007;404:1-13.

437. Lavu S, Boss O, Elliott PJ, Lambert PD. Sirtuins--novel therapeutic targets to treat age-associated diseases. Nat Rev Drug Discov 2008;7:841-53.

438. Finkel T, Deng CX, Mostoslavsky R. Recent progress in the biology and physiology of sirtuins. Nature 2009;460:587-91.

439. Singh UP, Singh NP, Singh B, Hofseth LJ, Price RL, Nagarkatti M, Nagarkatti PS. Resveratrol (trans-3,5,4'-trihydroxystilbene) induces silent mating type information regulation-1 and down-regulates nuclear transcription factor-kappaB activation to abrogate dextran sulfate sodium-induced colitis. J Pharmacol Exp Ther 2010;332:829-39.

440. Donnelly LE, Newton R, Kennedy GE, Fenwick PS, Leung RH, Ito K et al. Anti-inflammatory effects of resveratrol in lung epithelial cells: molecular mechanisms. Am J Physiol Lung Cell Mol Physiol 2004;287:L774-L783.

441. Manna SK, Mukhopadhyay A, Aggarwal BB. Resveratrol suppresses TNF-induced activation of nuclear transcription factors NF-kappa B, activator protein-1, and apoptosis: potential role of reactive oxygen intermediates and lipid peroxidation. J Immunol 2000;164:6509-19.

442. Leiro J, Arranz JA, Fraiz N, Sanmartin ML, Quezada E, Orallo F. Effect of cis-resveratrol on genes involved in nuclear factor kappa B signaling. Int Immunopharmacol 2005;5:393-406.

443. Biesalski HK. Polyphenols and inflammation: basic interactions. Curr Opin Clin Nutr Metab Care 2007;10:724-8.

444. Fang MZ, Wang Y, Ai N, Hou Z, Sun Y, Lu H et al. Tea polyphenol (-)-epigallocatechin-3-gallate inhibits DNA methyltransferase and reactivates methylation-silenced genes in cancer cell lines. Cancer Res 2003;63:7563-70.

445. Lee WJ, Shim JY, Zhu BT. Mechanisms for the inhibition of DNA methyltransferases by tea catechins and bioflavonoids. Mol Pharmacol 2005;68:1018-30.

446. Lee WJ, Zhu BT. Inhibition of DNA methylation by caffeic acid and chlorogenic acid, two common catechol-containing coffee polyphenols. Carcinogenesis 2006;27:269-77.

447. Parks DA. Oxygen radicals: mediators of gastrointestinal pathophysiology. Gut 1989;30:293-8.

448. Young IS, Woodside JV. Antioxidants in health and disease. J Clin Pathol 2001;54:176-86.

449. Biswas K, Bandyopadhyay U, Chattopadhyay I, Varadaraj A, Ali E, Banerjee RK. A novel antioxidant and antiapoptotic role of omeprazole to block gastric ulcer through scavenging of hydroxyl radical. J Biol Chem 2003;278:10993-1001.

450. Parks DA, Williams TK, Beckman JS. Conversion of xanthine dehydrogenase to oxidase in ischemic rat intestine: a reevaluation. Am J Physiol 1988;254:G768-G774.

451. Sanchez S, Martin MJ, Ortiz P, Motilva V, Alarcon dlL. Effects of dipyrone on inflammatory infiltration and oxidative metabolism in gastric mucosa: comparison with acetaminophen and diclofenac. Dig Dis Sci 2002;47:1389-98.

452. Brown DI, Griendling KK. Nox proteins in signal transduction. Free Radic Biol Med 2009;47:1239-53.

453. Gillespie MN, Pastukh V, Ruchko MV. Oxidative DNA modifications in hypoxic signaling. Ann N Y Acad Sci 2009;1177:140-50.

454. Babbs CF. Oxygen radicals in ulcerative colitis. Free Radic Biol Med 1992;13:169-81.

455. Fiocchi C. Inflammatory bowel disease: etiology and pathogenesis. Gastroenterology 1998;115:182-205.

456. Nishikawa M, Oshitani N, Matsumoto T, Nishigami T, Arakawa T, Inoue M. Accumulation of mitochondrial DNA mutation with colorectal carcinogenesis in ulcerative colitis. Br J Cancer 2005;93:331-7.

457. Pravda J. Radical induction theory of ulcerative colitis. World J Gastroenterol 2005;11:2371-84.

458. Rezaie A, Parker RD, Abdollahi M. Oxidative stress and pathogenesis of inflammatory bowel disease: an epiphenomenon or the cause? Dig Dis Sci 2007;52:2015-21.

459. Bonizzi G, Piette J, Schoonbroodt S, Greimers R, Havard L, Merville MP, Bours V. Reactive oxygen intermediate-dependent NF-kappaB activation by interleukin-1beta requires 5-lipoxygenase or NADPH oxidase activity. Mol Cell Biol 1999;19:1950-60.

460. Campbell KJ, Perkins ND. Regulation of NF-kappaB function. Biochem Soc Symp 2006;165-80.

461. Natarajan R, Ghosh S, Fisher BJ, Diegelmann RF, Willey A, Walsh S et al. Redox imbalance in Crohn's disease intestinal smooth muscle cells causes NF-kappaB-mediated spontaneous interleukin-8 secretion. J Interferon Cytokine Res 2001;21:349-59.

462. Schreck R, Rieber P, Baeuerle PA. Reactive oxygen intermediates as apparently widely used messengers in the activation of the NF-kappa B transcription factor and HIV-1. EMBO J 1991;10:2247-58.

463. Sen CK, Packer L. Antioxidant and redox regulation of gene transcription. FASEB J 1996;10:709-20.

464. Shapiro H, Singer P, Halpern Z, Bruck R. Polyphenols in the treatment of inflammatory bowel disease and acute pancreatitis. Gut 2007;56:426-35.

465. Eberhardt MV, Lee CY, Liu RH. Antioxidant activity of fresh apples. Nature 2000;405:903-4.

466. Kang NJ, Shin SH, Lee HJ, Lee KW. Polyphenols as small molecular inhibitors of signaling cascades in carcinogenesis. Pharmacol Ther 2011;130:310-24.

467. Korycka-Dahl MB, Richardson T. Activated oxygen species and oxidation of food constituents. CRC Crit Rev Food Sci Nutr 1978;10:209-41.

468. Lavelli V, Hippeli S, Peri C, Elstner EF. Evaluation of radical scavenging activity of fresh and air-dried tomatoes by three model reactions. J Agric Food Chem 1999;47:3826-31.

469. Scalbert A, Deprez S, Mila I, Albrecht AM, Huneau JF, Rabot S. Proanthocyanidins and human health: systemic effects and local effects in the gut. Biofactors 2000;13:115-20.

470. Kim DO, Lee KW, Lee HJ, Lee CY. Vitamin C equivalent antioxidant capacity (VCEAC) of phenolic phytochemicals. J Agric Food Chem 2002;50:3713-7.

471. Wolfe K, Wu X, Liu RH. Antioxidant activity of apple peels. J Agric Food Chem 2003;51:609-14.

472. He X, Liu RH. Phytochemicals of apple peels: isolation, structure elucidation, and their antiproliferative and antioxidant activities. J Agric Food Chem 2008;56:9905-10.

473. Kevers C, Pincemail J, Tabart J, Defraigne JO, Dommes J. Influence of cultivar, harvest time, storage conditions, and peeling on the antioxidant capacity and phenolic and ascorbic acid contents of apples and pears. J Agric Food Chem 2011;59:6165-71.

474. Brownmiller C, Howard LR, Prior RL. Processing and storage effects on procyanidin composition and concentration of processed blueberry products. J Agric Food Chem 2009;57:1896-902.

475. Prior RL, Gu L. Occurrence and biological significance of proanthocyanidins in the American diet. Phytochemistry 2005;66:2264-80.

476. Bernotti S, Seidman E, Sinnett D, Brunet S, Dionne S, Delvin E, Levy E. Inflammatory reaction without endogenous antioxidant response in Caco-2 cells exposed to iron/ascorbate-mediated lipid peroxidation. Am J Physiol Gastrointest Liver Physiol 2003;285:G898-G906.

477. Courtois F, Delvin E, Ledoux M, Seidman E, Lavoie JC, Levy E. The antioxidant BHT normalizes some oxidative effects of iron + ascorbate on lipid metabolism in Caco-2 cells. J Nutr 2002;132:1289-92.

478. Courtois F, Seidman EG, Delvin E, Asselin C, Bernotti S, Ledoux M, Levy E. Membrane peroxidation by lipopolysaccharide and iron-ascorbate adversely affects Caco-2 cell function: beneficial role of butyric acid. Am J Clin Nutr 2003;77:744-50.

479. Levy E, Mehran M, Seidman E. Caco-2 cells as a model for intestinal lipoprotein synthesis and secretion. FASEB J 1995;9:626-35.

480. Levy E, Trudel K, Bendayan M, Seidman E, Delvin E, Elchebly M et al. Biological role, protein expression, subcellular localization, and oxidative stress response of paraoxonase 2 in the intestine of humans and rats. Am J Physiol Gastrointest Liver Physiol 2007;293:G1252-G1261.

481. Marcil V, Seidman E, Sinnett D, Boudreau F, Gendron FP, Beaulieu JF et al. Modification in oxidative stress, inflammation, and lipoprotein assembly in response to hepatocyte nuclear factor 4alpha knockdown in intestinal epithelial cells. J Biol Chem 2010;285:40448-60.

482. Precourt LP, Seidman E, Delvin E, Amre D, Deslandres C, Dominguez M et al. Comparative expression analysis reveals differences in the regulation of intestinal paraoxonase family members. Int J Biochem Cell Biol 2009;41:1628-37.

483. Precourt LP, Marcil V, Ntimbane T, Taha R, Lavoie JC, Delvin E et al. Antioxidative properties of paraoxonase 2 in intestinal epithelial cells. Am J Physiol Gastrointest Liver Physiol 2012.

484. Taha R, Seidman E, Mailhot G, Boudreau F, Gendron FP, Beaulieu JF et al. Oxidative stress and mitochondrial functions in the intestinal Caco-2/15 cell line. PLoS One 2010;5:e11817.

485. Spahis S, Vanasse M, Belanger SA, Ghadirian P, Grenier E, Levy E. Lipid profile, fatty acid composition and pro- and anti-oxidant status in pediatric patients with attention-deficit/hyperactivity disorder. Prostaglandins Leukot Essent Fatty Acids 2008;79:47-53.

486. McCord JM, Fridovich I. Superoxide dismutase. An enzymic function for erythrocuprein (hemocuprein). J Biol Chem 1969;244:6049-55.

487. Kalgutkar AS, Marnett AB, Crews BC, Remmel RP, Marnett LJ. Ester and amide derivatives of the nonsteroidal antiinflammatory drug, indomethacin, as selective cyclooxygenase-2 inhibitors. J Med Chem 2000;43:2860-70.

488. Moon SK, Cho GO, Jung SY, Gal SW, Kwon TK, Lee YC et al. Quercetin exerts multiple inhibitory effects on vascular smooth muscle cells: role of ERK1/2, cell-cycle

regulation, and matrix metalloproteinase-9. Biochem Biophys Res Commun 2003;301:1069-78.

489. Brunet S, Thibault L, Lepage G, Seidman EG, Dube N, Levy E. Modulation of endoplasmic reticulum-bound cholesterol regulatory enzymes by iron/ascorbate-mediated lipid peroxidation. Free Radic Biol Med 2000;28:46-54.

490. Qutub AA, Popel AS. Reactive oxygen species regulate hypoxia-inducible factor 1alpha differentially in cancer and ischemia. Mol Cell Biol 2008;28:5106-19.

491. Wells CL, Jechorek RP, Olmsted SB, Erlandsen SL. Effect of LPS on epithelial integrity and bacterial uptake in the polarized human enterocyte-like cell line Caco-2. Circ Shock 1993;40:276-88.

492. Tkachev VO, Menshchikova EB, Zenkov NK. Mechanism of the Nrf2/Keap1/ARE signaling system. Biochemistry (Mosc) 2011;76:407-22.

493. Li J, Lee JM, Johnson JA. Microarray analysis reveals an antioxidant responsive element-driven gene set involved in conferring protection from an oxidative stress-induced apoptosis in IMR-32 cells. J Biol Chem 2002;277:388-94.

494. Martinez-Jimenez CP, Gomez-Lechon MJ, Castell JV, Jover R. Underexpressed coactivators PGC1alpha and SRC1 impair hepatocyte nuclear factor 4 alpha function and promote dedifferentiation in human hepatoma cells. J Biol Chem 2006;281:29840-9.

495. Ramachandran B, Yu G, Gulick T. Nuclear respiratory factor 1 controls myocyte enhancer factor 2A transcription to provide a mechanism for coordinate expression of respiratory chain subunits. J Biol Chem 2008;283:11935-46.

496. Tang Y, Zheng S, Chen A. Curcumin eliminates leptin's effects on hepatic stellate cell activation via interrupting leptin signaling. Endocrinology 2009;150:3011-20.

497. Scalbert A, Morand C, Manach C, Remesy C. Absorption and metabolism of polyphenols in the gut and impact on health. Biomed Pharmacother 2002;56:276-82.

498. Manach C, Scalbert A, Morand C, Remesy C, Jimenez L. Polyphenols: food sources and bioavailability. Am J Clin Nutr 2004;79:727-47.

499. Crespy V, Aprikian O, Morand C, Besson C, Manach C, Demigne C, Remesy C. Bioavailability of phloretin and phloridzin in rats J Nutr 2001;131:3227-30.

500. Donovan JL, Crespy V, Manach C, Morand C, Besson C, Scalbert A, Remesy C. Catechin is metabolized by both the small intestine and liver of rats. J Nutr 2001;131:1753-7.

501. Selma MV, Espin JC, Tomas-Barberan FA. Interaction between phenolics and gut microbiota: role in human health. J Agric Food Chem 2009;57:6485-501.

502. Blaut M, Clavel T. Metabolic diversity of the intestinal microbiota: implications for health and disease. J Nutr 2007;137:751S-5S.

503. Kosinska A, Andlauer W. Cocoa polyphenols are absorbed in Caco-2 cell model of intestinal epithelium. Food Chem 2012;135:999-1005.

504. Graziani G, D'Argenio G, Tuccillo C, Loguercio C, Ritieni A, Morisco F et al. Apple polyphenol extracts prevent damage to human gastric epithelial cells in vitro and to rat gastric mucosa in vivo. Gut 2005;54:193-200.

505. D'Argenio G, Mazzone G, Tuccillo C, Grandone I, Gravina AG, Graziani G et al. Apple polyphenol extracts prevent aspirin-induced damage to the rat gastric mucosa. Br J Nutr 2008;100:1228-36.

506. D'Argenio G, Mazzone G, Tuccillo C, Ribecco MT, Graziani G, Gravina AG et al. Apple polyphenols extract (APE) improves colon damage in a rat model of colitis. Dig Liver Dis 2012;44:555-62.

507. Galleano M, Calabro V, Prince PD, Litterio MC, Piotrkowski B, Vazquez-Prieto MA et al. Flavonoids and metabolic syndrome. Ann N Y Acad Sci 2012;1259:87-94.

508. Landete JM. Updated knowledge about polyphenols: functions, bioavailability, metabolism, and health. Crit Rev Food Sci Nutr 2012;52:936-48.

509. Salah N, Miller NJ, Paganga G, Tijburg L, Bolwell GP, Rice-Evans C. Polyphenolic flavanols as scavengers of aqueous phase radicals and as chain-breaking antioxidants. Arch Biochem Biophys 1995;322:339-46.

510. Artis D. Epithelial-cell recognition of commensal bacteria and maintenance of immune homeostasis in the gut. Nat Rev Immunol 2008;8:411-20.

511. Hooper LV, Macpherson AJ. Immune adaptations that maintain homeostasis with the intestinal microbiota. Nat Rev Immunol 2010;10:159-69.

512. Srigiridhar K, Nair KM. Iron-deficient intestine is more susceptible to peroxidative damage during iron supplementation in rats. Free Radic Biol Med 1998;25:660-5.

513. Gonzalez PK, Doctrow SR, Malfroy B, Fink MP. Role of oxidant stress and iron delocalization in acidosis-induced intestinal epithelial hyperpermeability. Shock 1997;8:108-14.

514. Reifen R, Matas Z, Zeidel L, Berkovitch Z, Bujanover Y. Iron supplementation may aggravate inflammatory status of colitis in a rat model. Dig Dis Sci 2000;45:394-7.

515. Sartor RB, Muehlbauer M. Microbial host interactions in IBD: implications for pathogenesis and therapy. Curr Gastroenterol Rep 2007;9:497-507.

516. Rubas W, Cromwell ME, Shahrokh Z, Villagran J, Nguyen TN, Wellton M et al. Flux measurements across Caco-2 monolayers may predict transport in human large intestinal tissue. J Pharm Sci 1996;85:165-9.

517. Yang F, Wang J, Li X, Ying T, Qiao S, Li D, Wu G. 2-DE and MS analysis of interactions between Lactobacillus fermentum I5007 and intestinal epithelial cells. Electrophoresis 2007;28:4330-9.

518. Sun H, Chow EC, Liu S, Du Y, Pang KS. The Caco-2 cell monolayer: usefulness and limitations. Expert Opin Drug Metab Toxicol 2008;4:395-411.

519. McKay DL, Blumberg JB. Cranberries (Vaccinium macrocarpon) and cardiovascular disease risk factors. Nutr Rev 2007;65:490-502.

520. Puupponen-Pimia R, Nohynek L, Alakomi HL, Oksman-Caldentey KM. Bioactive berry compounds-novel tools against human pathogens. Appl Microbiol Biotechnol 2005;67:8-18.

521. Jiang ZY, Woollard AC, Wolff SP. Lipid hydroperoxide measurement by oxidation of Fe2+ in the presence of xylenol orange. Comparison with the TBA assay and an iodometric method. Lipids 1991;26:853-6.

522. Bohr VA, Stevnsner T, de Souza-Pinto NC. Mitochondrial DNA repair of oxidative damage in mammalian cells. Gene 2002;286:127-34.

523. Esposito LA, Melov S, Panov A, Cottrell BA, Wallace DC. Mitochondrial disease in mouse results in increased oxidative stress. Proc Natl Acad Sci U S A 1999;96:4820-5.

524. Wang SY, Lin HS. Antioxidant activity in fruits and leaves of blackberry, raspberry, and strawberry varies with cultivar and developmental stage. J Agric Food Chem 2000;48:140-6.

525. Sun J, Chu YF, Wu X, Liu RH. Antioxidant and antiproliferative activities of common fruits. J Agric Food Chem 2002;50:7449-54.

526. Wu X, Beecher GR, Holden JM, Haytowitz DB, Gebhardt SE, Prior RL. Lipophilic and hydrophilic antioxidant capacities of common foods in the United States. J Agric Food Chem 2004;52:4026-37.

527. Burleigh AE, Benck SM, McAchran SE, Reed JD, Krueger CG, Hopkins WJ. Consumption of sweetened, dried cranberries may reduce urinary tract infection incidence in susceptible women -- a modified observational study. Nutr J 2013;12:139.

528. Wilson T, Meyers SL, Singh AP, Limburg PJ, Vorsa N. Favorable glycemic response of type 2 diabetics to low-calorie cranberry juice. J Food Sci 2008;73:H241-H245.

529. McKay DL, Blumberg JB. Cranberries (Vaccinium macrocarpon) and cardiovascular disease risk factors. Nutr Rev 2007;65:490-502.

530. Ruel G, Couillard C. Evidences of the cardioprotective potential of fruits: the case of cranberries. Mol Nutr Food Res 2007;51:692-701.

531. Deprez S, Mila I, Huneau JF, Tome D, Scalbert A. Transport of proanthocyanidin dimer, trimer, and polymer across monolayers of human intestinal epithelial Caco-2 cells. Antioxid Redox Signal 2001;3:957-67.

532. Courtois F, Suc I, Garofalo C, Ledoux M, Seidman E, Levy E. Iron-ascorbate alters the efficiency of Caco-2 cells to assemble and secrete lipoproteins. Am J Physiol Gastrointest Liver Physiol 2000;279:G12-G19.

533. Grenier E, Maupas FS, Beaulieu JF, Seidman E, Delvin E, Sane A et al. Effect of retinoic acid on cell proliferation and differentiation as well as on lipid synthesis, lipoprotein secretion, and apolipoprotein biogenesis. Am J Physiol Gastrointest Liver Physiol 2007;293:G1178-G1189.

534. Levy E, Menard D, Suc I, Delvin E, Marcil V, Brissette L et al. Ontogeny, immunolocalisation, distribution and function of SR-BI in the human intestine. J Cell Sci 2004;117:327-37.

535. Levy E, Harmel E, Laville M, Sanchez R, Emonnot L, Sinnett D et al. Expression of Sar1b enhances chylomicron assembly and key components of the coat protein complex II system driving vesicle budding. Arterioscler Thromb Vasc Biol 2011;31:2692-9.

536. Mailhot G, Ravid Z, Barchi S, Moreau A, Rabasa-Lhoret R, Levy E. CFTR knockdown stimulates lipid synthesis and transport in intestinal Caco-2/15 cells. Am J Physiol Gastrointest Liver Physiol 2009;297:G1239-G1249.

537. Marcil V, Delvin E, Seidman E, Poitras L, Zoltowska M, Garofalo C, Levy E. Modulation of lipid synthesis, apolipoprotein biogenesis, and lipoprotein assembly by butyrate. Am J Physiol Gastrointest Liver Physiol 2002;283:G340-G346.

538. Ravid Z, Bendayan M, Delvin E, Sane AT, Elchebly M, Lafond J et al. Modulation of intestinal cholesterol absorption by high glucose levels: impact on cholesterol transporters, regulatory enzymes, and transcription factors. Am J Physiol Gastrointest Liver Physiol 2008;295:G873-G885.

539. Sane AT, Sinnett D, Delvin E, Bendayan M, Marcil V, Menard D et al. Localization and role of NPC1L1 in cholesterol absorption in human intestine. J Lipid Res 2006;47:2112-20.

540. Cencic A, Langerholc T. Functional cell models of the gut and their applications in food microbiology--a review. Int J Food Microbiol 2010;141 Suppl 1:S4-14.

541. Li Y, Shin YG, Yu C, Kosmeder JW, Hirschelman WH, Pezzuto JM, van Breemen RB. Increasing the throughput and productivity of Caco-2 cell permeability assays using liquid chromatography-mass spectrometry: application to resveratrol absorption and metabolism. Comb Chem High Throughput Screen 2003;6:757-67.

542. Farrell TL, Poquet L, Dew TP, Barber S, Williamson G. Predicting phenolic acid absorption in Caco-2 cells: a theoretical permeability model and mechanistic study. Drug Metab Dispos 2012;40:397-406.

543. Suzuki T, Hara H. Quercetin enhances intestinal barrier function through the assembly of zonula [corrected] occludens-2, occludin, and claudin-1 and the expression of claudin-4 in Caco-2 cells. J Nutr 2009;139:965-74.

544. Pierre JF, Heneghan AF, Feliciano RP, Shanmuganayagam D, Roenneburg DA, Krueger CG et al. Cranberry proanthocyanidins improve the gut mucous layer morphology and function in mice receiving elemental enteral nutrition. JPEN J Parenter Enteral Nutr 2013;37:401-9.

545. Lipson SM. Cranberry and Grape Juices Affect Tight Junction Function and Structural Integrity of Rotavirus-Infected Monkey Kidney Epithelial Cell Monolayers. Food Environ Virol 2011;3:46-54.

546. Stichtenoth DO, Thoren S, Bian H, Peters-Golden M, Jakobsson PJ, Crofford LJ. Microsomal prostaglandin E synthase is regulated by proinflammatory cytokines and glucocorticoids in primary rheumatoid synovial cells. J Immunol 2001;167:469-74.

547. Thoren S, Jakobsson PJ. Coordinate up- and down-regulation of glutathione-dependent prostaglandin E synthase and cyclooxygenase-2 in A549 cells. Inhibition by NS-398 and leukotriene C4. Eur J Biochem 2000;267:6428-34.

548. MacMillan-Crow LA, Crow JP. Does more MnSOD mean more hydrogen peroxide? Anticancer Agents Med Chem 2011;11:178-80.

549. Sies H. Role of reactive oxygen species in biological processes. Klin Wochenschr 1991;69:965-8.

550. Cadenas E, Davies KJ. Mitochondrial free radical generation, oxidative stress, and aging. Free Radic Biol Med 2000;29:222-30.

551. Moi P, Chan K, Asunis I, Cao A, Kan YW. Isolation of NF-E2-related factor 2 (Nrf2), a NF-E2-like basic leucine zipper transcriptional activator that binds to the tandem NF-E2/AP1 repeat of the beta-globin locus control region. Proc Natl Acad Sci U S A 1994;91:9926-30.

552. Kobayashi A, Kang MI, Okawa H, Ohtsuji M, Zenke Y, Chiba T et al. Oxidative stress sensor Keap1 functions as an adaptor for Cul3-based E3 ligase to regulate proteasomal degradation of Nrf2. Mol Cell Biol 2004;24:7130-9.

553. Rushmore TH, Morton MR, Pickett CB. The antioxidant responsive element. Activation by oxidative stress and identification of the DNA consensus sequence required for functional activity. J Biol Chem 1991;266:11632-9.

554. Li Q, Verma IM. NF-kappaB regulation in the immune system. Nat Rev Immunol 2002;2:725-34.

555. Yan MH, Wang X, Zhu X. Mitochondrial defects and oxidative stress in Alzheimer disease and Parkinson disease. Free Radic Biol Med 2013;62:90-101.

556. Schapira AH. Mitochondrial diseases. Lancet 2012;379:1825-34.

557. Newsholme P, Gaudel C, Krause M. Mitochondria and diabetes. An intriguing pathogenetic role. Adv Exp Med Biol 2012;942:235-47.

558. Pajuelo D, Diaz S, Quesada H, Fernandez-Iglesias A, Mulero M, Arola-Arnal A et al. Acute administration of grape seed proanthocyanidin extract modulates energetic metabolism in skeletal muscle and BAT mitochondria. J Agric Food Chem 2011;59:4279-87.

559. Wang GW, Klein JB, Kang YJ. Metallothionein inhibits doxorubicin-induced mitochondrial cytochrome c release and caspase-3 activation in cardiomyocytes. J Pharmacol Exp Ther 2001;298:461-8.

560. Ruchko M, Gorodnya O, LeDoux SP, Alexeyev MF, Al-Mehdi AB, Gillespie MN. Mitochondrial DNA damage triggers mitochondrial dysfunction and apoptosis in oxidant-challenged lung endothelial cells. Am J Physiol Lung Cell Mol Physiol 2005;288:L530-L535.

561. Poulsen HE, Prieme H, Loft S. Role of oxidative DNA damage in cancer initiation and promotion. Eur J Cancer Prev 1998;7:9-16.

562. Davis CS, Mock KE, Bentz BJ, Bromilow SM, Bartell NV, Murray BW et al. Isolation and characterization of 16 microsatellite loci in the mountain pine beetle, Dendroctonus ponderosae Hopkins (Coleoptera: Curculionidae: Scolytinae). Mol Ecol Resour 2009;9:1071-3.

563. Fraga CG, Galleano M, Verstraeten SV, Oteiza PI. Basic biochemical mechanisms behind the health benefits of polyphenols. Mol Aspects Med 2010;31:435-45.

564. Johnston K, Sharp P, Clifford M, Morgan L. Dietary polyphenols decrease glucose uptake by human intestinal Caco-2 cells. FEBS Lett 2005;579:1653-7.

565. Alzaid F, Cheung HM, Preedy VR, Sharp PA. Regulation of glucose transporter expression in human intestinal Caco-2 cells following exposure to an anthocyanin-rich berry extract. PLoS One 2013;8:e78932.

566. Solomon TP, Blannin AK. Changes in glucose tolerance and insulin sensitivity following 2 weeks of daily cinnamon ingestion in healthy humans. Eur J Appl Physiol 2009;105:969-76.

567. Qin B, Dawson HD, Schoene NW, Polansky MM, Anderson RA. Cinnamon polyphenols regulate multiple metabolic pathways involved in insulin signaling and intestinal lipoprotein metabolism of small intestinal enterocytes. Nutrition 2012;28:1172-9.

568. Merken HM, Beecher GR. Measurement of food flavonoids by high-performance liquid chromatography: A review. J Agric Food Chem 2000;48:577-99.

569. Merken HM, Beecher GR. Liquid chromatographic method for the separation and quantification of prominent flavonoid aglycones. J Chromatogr A 2000;897:177-84.

570. Nijveldt RJ, van NE, van Hoorn DE, Boelens PG, van NK, van Leeuwen PA. Flavonoids: a review of probable mechanisms of action and potential applications. Am J Clin Nutr 2001;74:418-25.

571. Pappas E, Schaich KM. Phytochemicals of cranberries and cranberry products: characterization, potential health effects, and processing stability. Crit Rev Food Sci Nutr 2009;49:741-81.

572. Ruel G, Couillard C. Evidences of the cardioprotective potential of fruits: the case of cranberries. Mol Nutr Food Res 2007;51:692-701.

573. Neto CC. Cranberry and its phytochemicals: a review of in vitro anticancer studies. J Nutr 2007;137:186S-93S.

574. Burleigh AE, Benck SM, McAchran SE, Reed JD, Krueger CG, Hopkins WJ. Consumption of sweetened, dried cranberries may reduce urinary tract infection incidence in susceptible women -- a modified observational study. Nutr J 2013;12:139.

575. Burger O, Weiss E, Sharon N, Tabak M, Neeman I, Ofek I. Inhibition of Helicobacter pylori adhesion to human gastric mucus by a high-molecular-weight constituent of cranberry juice. Crit Rev Food Sci Nutr 2002;42:279-84.

576. Burger O, Ofek I, Tabak M, Weiss EI, Sharon N, Neeman I. A high molecular mass constituent of cranberry juice inhibits helicobacter pylori adhesion to human gastric mucus. FEMS Immunol Med Microbiol 2000;29:295-301.

577. Gonthier MP, Donovan JL, Texier O, Felgines C, Remesy C, Scalbert A. Metabolism of dietary procyanidins in rats. Free Radic Biol Med 2003;35:837-44.

578. Reed JD. Nutritional toxicology of tannins and related polyphenols in forage legumes. J Anim Sci 1995;73:1516-28.

579. Del RD, Rodriguez-Mateos A, Spencer JP, Tognolini M, Borges G, Crozier A. Dietary (poly)phenolics in human health: structures, bioavailability, and evidence of protective effects against chronic diseases. Antioxid Redox Signal 2013;18:1818-92.

580. Rodriguez-Mateos A, Vauzour D, Krueger CG, Shanmuganayagam D, Reed J, Calani L et al. Bioavailability, bioactivity and impact on health of dietary flavonoids and related compounds: an update. Arch Toxicol 2014;88:1803-53.

581. Pierre JF, Heneghan AF, Feliciano RP, Shanmuganayagam D, Roenneburg DA, Krueger CG et al. Cranberry Proanthocyanidins improve the gut mucous layer morphology and function in mice receiving elemental enteral nutrition. Journal of Parenteral and Enteral Nutrition 2013;37:401-9.

582. Moi P, Chan K, Asunis I, Cao A, Kan YW. Isolation of NF-E2-related factor 2 (Nrf2), a NF-E2-like basic leucine zipper transcriptional activator that binds to the tandem NF-E2/AP1 repeat of the beta-globin locus control region. Proc Natl Acad Sci U S A 1994;91:9926-30.

583. Cote J, Caillet S, Doyon G, Sylvain JF, Lacroix M. Analyzing cranberry bioactive compounds. Crit Rev Food Sci Nutr 2010;50:872-88.

584. Prior RL, Fan E, Ji H, Howell A, Nio C, Payne MJ, Reed J. Multi-laboratory validation of a standard method for quantifying proanthocyanidins in cranberry powders. J Sci Food Agric 2010;90:1473-8.

585. Feliciano RP, Shea MP, Shanmuganayagam D, Krueger CG, Howell AB, Reed JD. Comparaison of isolated Cranberry (Vaccinium macrocarpon Ait.) proanthocyanidins to catechin and procyanidins A2 and B2 for use as standards in the 4-(dimethylamino)cinnamaldehyde assay. Journal of Agricultural and Food Chemistry 2012;60:4578-85.

586. Kelm MA, Johnson JC, Robbins RJ, Hammerstone JF, Schmitz HH. High-performance liquid chromatography separation and purification of cacao (Theobroma cacao L.) procyanidins according to degree of polymerization using a diol stationary phase. J Agric Food Chem 2006;54:1571-6.

587. Robbins RJ, Leonczak J, Johnson JC, Li J, Kwik-Uribe C, Prior RL, Gu L. Method performance and multi-laboratory assessment of a normal phase high pressure liquid chromatography-fluorescence detection method for the quantitation of flavanols and procyanidins in cocoa and chocolate containing samples. J Chromatogr A 2009;1216:4831-40.

588. Wallace DC, Giusti M. Extraction and normal-phase HPLC-fluorescence-electrospray MS characterization and quantification of procyanidins in cranberry extracts. Journal of Food Science 2010;75:C690-C696.

589. Howell AB, Reed JD, Krueger CG, Winterbottom R, Cunningham DG, Leahy M. A-type cranberry proanthocyanidins and uropathogenic bacterial anti-adhesion activity. Phytochemistry 2005;66:2281-91.

590. Foo LY, Lu Y, Howell AB, Vorsa N. A-Type proanthocyanidin trimers from cranberry that inhibit adherence of uropathogenic P-fimbriated Escherichia coli. J Nat Prod 2000;63:1225-8.

591. Neto CC, Krueger CG, Lamoureux TL, Kondo M, Vaisberg AJ, Hurta RAR. MALDI-TOF MS characterization of proanthocyanidins from cranberry fruit Vaccinium macrocarpon that inhibit tumor cell growth and matrix metalloproteinase expression in vitro. Journal of the Science of Food and Agriculture 2006;81:18-25.

592. Porter ML, Krueger CG, Wiebe DA, Cunningham DG, Reed JD. Cranberry proanthocyanidins associate with low-density lipoprotein and inhibit in vitro Cu2+-induced oxidation. Journal of the Science of Food and Agriculture 2001;81:1306-13.

593. Reed JD, Krueger CG, Vestling MM. MALDI-TOF mass spectrometry of oligomeric food polyphenols. Phytochemistry 2005;66:2248-63.

594. Carpenter JL, Caruso FL, Tata A, Vorsa N, Neto CC. Variation in proanthocyanidin content and composition among commonly grown North American cranberry cultivars (Vaccinium macrocarpon). J Sci Food Agric 2014;94:2738-45.

595. Foo LY, Lu Y, Howell AB, Vorsa N. The structure of cranberry proanthocyanidins which inhibit adherence of uropathogenic P-fimbriated Escherichia coli in vitro. Phytochemistry 2000;54:173-81.

596. Feliciano RP, Meudt JJ, Shanmuganayagam D, Krueger CG, Reed JD. Ratio of "A-type" to "B-type" proanthocyanidin interflavan bonds affects extra-intestinal pathogenic Escherichia coli invasion of gut epithelial cells. J Agric Food Chem 2014;62:3919-25.

597. Kevers C, Pincemail J, Tabart J, Defraigne JO, Dommes J. Influence of cultivar, harvest time, storage conditions, and peeling on the antioxidant capacity and phenolic and ascorbic acid contents of apples and pears. J Agric Food Chem 2011;59:6165-71.

598. Marti MP, Pantaleon A, Rozek A, Soler A, Valls J, Macia A et al. Rapid analysis of procyanidins and anthocyanins in plasma by microelution SPE and ultra-HPLC. J Sep Sci 2010;33:2841-53.

599. USDA. USDA database for the flavonoid content of selected foods release. 21 st edn. 2007. USDA, Belstville. Ref Type: Report

600. Rodriguez-Mateos A, Vauzour D, Krueger CG, Shanmuganayagam D, Reed J, Calani L et al. Bioavailability, bioactivity and impact on health of dietary flavonoids and related compounds: an update. Arch Toxicol 2014;88:1803-53.

601. Harborne JB. The Flavonoids: Advances in Research since 1986. In: Chapman and Hall, ed. London, U.K.: 1994.

602. Häkkinen S, Heinonen M, Karenlampi S, Mykkanen H, Ruuskanen J, Torronen R. Screening of selected flavonoids and phenolic acids in 19 berries. Food Res Int 1999;32:345-53.

603. Singleton VL, Orthofer R, and Lamuela-Raventos RM. Analysis of total phenols and other oxidation substrates and antioxidants by means of Folin-Ciocalteu Reagent. Methods in Enzymology 1999;299:152-78.

604. Denis MC, Desjardins Y, Furtos A, Marcil V, Dudonne S, Montoudis A et al. Prevention of oxidative stress, inflammation and mitochondrial dysfunction in the intestine by different cranberry phenolic fractions. Clin Sci (Lond) 2015;128:197-212.

605. Hanton SD. Mass spectrometry of polymers and polymer surfaces. Chem Rev 2001;101:527-69.

606. Alicata R, Montaudo G, Puglisi C, Samperi F. Influence of chain end groups on the matrix-assisted laser desorption/ionization spectra of polymer blends. Rapid Commun Mass Spectrom 2002;16:248-60.

607. Feliciano RP, Krueger CG, Shanmuganayagam D, Vestling MM, Reed JD. Deconvolution of matrix-assisted laser desorption/ionization time-of-flight mass spectrometry isotope patterns to determine ratios of A-type to B-type interflavan bonds in cranberry proanthocyanidins. Food Chem 2012;135:1485-93.

608. Ohnishi-Kameyama M, Yanagida A, Kanda T, Nagata T. Identification of catechin oligomers from apple (Malus pumila cv. Fuji) in matrix-assisted laser desorption/ionization time-of-flight mass spectrometry and fast-atom bombardment mass spectrometry. Rapid Commun Mass Spectrom 1997;11:31-6.

609. Day AJ, Canada FJ, Diaz JC, Kroon PA, Mclauchlan R, Faulds CB et al. Dietary flavonoid and isoflavone glycosides are hydrolysed by the lactase site of lactase phlorizin hydrolase. FEBS Lett 2000;468:166-70.

610. Day AJ, DuPont MS, Ridley S, Rhodes M, Rhodes MJ, Morgan MR, Williamson G. Deglycosylation of flavonoid and isoflavonoid glycosides by human small intestine and liver beta-glucosidase activity. FEBS Lett 1998;436:71-5.

611. Day AJ, Gee JM, DuPont MS, Johnson IT, Williamson G. Absorption of quercetin-3-glucoside and quercetin-4'-glucoside in the rat small intestine: the role of lactase

phlorizin hydrolase and the sodium-dependent glucose transporter. Biochem Pharmacol 2003;65:1199-206.

612. Crespy V, Morand C, Manach C, Besson C, Demigne C, Remesy C. Part of quercetin absorbed in the small intestine is conjugated and further secreted in the intestinal lumen. Am J Physiol 1999;277:G120-G126.

613. Walgren RA, Karnaky KJ, Jr., Lindenmayer GE, Walle T. Efflux of dietary flavonoid quercetin 4'-beta-glucoside across human intestinal Caco-2 cell monolayers by apical multidrug resistance-associated protein-2. J Pharmacol Exp Ther 2000;294:830-6.

614. Vaidyanathan JB, Walle T. Transport and metabolism of the tea flavonoid (-)-epicatechin by the human intestinal cell line Caco-2. Pharm Res 2001;18:1420-5.

615. Petri N, Tannergren C, Holst B, Mellon FA, Bao Y, Plumb GW et al. Absorption/metabolism of sulforaphane and quercetin, and regulation of phase II enzymes, in human jejunum in vivo. Drug Metab Dispos 2003;31:805-13.

616. Crespy V, Morand C, Besson C, Cotelle N, Vezin H, Demigne C, Remesy C. The splanchnic metabolism of flavonoids highly differed according to the nature of the compound. Am J Physiol Gastrointest Liver Physiol 2003;284:G980-G988.

617. Lambert N, Kroon PA, Faulds CB, Plumb GW, McLauchlan WR, Day AJ, Williamson G. Purification of cytosolic beta-glucosidase from pig liver and its reactivity towards flavonoid glycosides. Biochim Biophys Acta 1999;1435:110-6.

618. Wu X, Cao G, Prior RL. Absorption and metabolism of anthocyanins in elderly women after consumption of elderberry or blueberry. J Nutr 2002;132:1865-71.

619. Mojarrabi B, Mackenzie PI. Characterization of two UDP glucuronosyltransferases that are predominantly expressed in human colon. Biochem Biophys Res Commun 1998;247:704-9.

620. Walle UK, Galijatovic A, Walle T. Transport of the flavonoid chrysin and its conjugated metabolites by the human intestinal cell line Caco-2. Biochem Pharmacol 1999;58:431-8.

621. Ayrton A, Morgan P. Role of transport proteins in drug absorption, distribution and excretion. Xenobiotica 2001;31:469-97.

622. Coughtrie MW, Sharp S, Maxwell K, Innes NP. Biology and function of the reversible sulfation pathway catalysed by human sulfotransferases and sulfatases. Chem Biol Interact 1998;109:3-27.

623. Falany CN. Enzymology of human cytosolic sulfotransferases. FASEB J 1997;11:206-16.

624. Silva FA, Borges F, Guimaraes C, Lima JL, Matos C, Reis S. Phenolic acids and derivatives: studies on the relationship among structure, radical scavenging activity, and physicochemical parameters. J Agric Food Chem 2000;48:2122-6.

625. Zuo Y, Wang C, Zhan J. Separation, characterization, and quantitation of benzoic and phenolic antioxidants in American cranberry fruit by GC-MS. J Agric Food Chem 2002;50:3789-94.

626. Yeh CT, Ching LC, Yen GC. Inducing gene expression of cardiac antioxidant enzymes by dietary phenolic acids in rats. J Nutr Biochem 2009;20:163-71.

627. Graf E. Antioxidant potential of ferulic acid. Free Radic Biol Med 1992;13:435-48.

628. Yang F, Oz HS, Barve S, de Villiers WJ, McClain CJ, Varilek GW. The green tea polyphenol (-)-epigallocatechin-3-gallate blocks nuclear factor-kappa B activation by inhibiting I kappa B kinase activity in the intestinal epithelial cell line IEC-6. Mol Pharmacol 2001;60:528-33.

629. Feng R, Lu Y, Bowman LL, Qian Y, Castranova V, Ding M. Inhibition of activator protein-1, NF-kappaB, and MAPKs and induction of phase 2 detoxifying enzyme activity by chlorogenic acid. J Biol Chem 2005;280:27888-95.

630. Karlsson PC, Huss U, Jenner A, Halliwell B, Bohlin L, Rafter JJ. Human fecal water inhibits COX-2 in colonic HT-29 cells: role of phenolic compounds. J Nutr 2005;135:2343-9.

631. Rice-Evans C, Miller N. Measurement of the antioxidant status of dietary constituents, low density lipoproteins and plasma. Prostaglandins Leukot Essent Fatty Acids 1997;57:499-505.

632. Vvedenskaya IO, Rosen RT, Guido JE, Russell DJ, Mills KA, Vorsa N. Characterization of flavonols in cranberry (Vaccinium macrocarpon) powder. J Agric Food Chem 2004;52:188-95.

633. Aherne SA, O'Brien NM. Dietary flavonols: chemistry, food content, and metabolism. Nutrition 2002;18:75-81.

634. Mullen W, Marks SC, Crozier A. Evaluation of phenolic compounds in commercial fruit juices and fruit drinks. J Agric Food Chem 2007;55:3148-57.

635. Yan X, Murphy BT, Hammond GB, Vinson JA, Neto CC. Antioxidant activities and antitumor screening of extracts from cranberry fruit (Vaccinium macrocarpon). J Agric Food Chem 2002;50:5844-9.

636. Vvedenskaya IO, Rosen RT, Guido JE, Russell DJ, Mills KA, Vorsa N. Characterization of flavonols in cranberry (Vaccinium macrocarpon) powder. J Agric Food Chem 2004;52:188-95.

637. Ohnishi R, Ito H, Kasajima N, Kaneda M, Kariyama R, Kumon H et al. Urinary excretion of anthocyanins in humans after cranberry juice ingestion. Biosci Biotechnol Biochem 2006;70:1681-7.

638. Prior RL, Lazarus SA, Cao G, Muccitelli H, Hammerstone JF. Identification of procyanidins and anthocyanins in blueberries and cranberries (Vaccinium spp.) using high-performance liquid chromatography/mass spectrometry. J Agric Food Chem 2001;49:1270-6.

639. Bilyk A, Sapers GM. Varietal differences in the quercetin, kaempferol, and myricetin contents of highbush blueberry, cranberry, and thornless blackberry fruits. J Agric Food Chem 1986;34:585-8.

640. Shih PH, Yeh CT, Yen GC. Effects of anthocyanidin on the inhibition of proliferation and induction of apoptosis in human gastric adenocarcinoma cells. Food Chem Toxicol 2005;43:1557-66.

641. White BL, Howard LR, Prior RL. Proximate and polyphenolic characterization of cranberry pomace. J Agric Food Chem 2010;58:4030-6.

642. Shih PH, Yeh CT, Yen GC. Anthocyanins induce the activation of phase II enzymes through the antioxidant response element pathway against oxidative stress-induced apoptosis. J Agric Food Chem 2007;55:9427-35.

643. Singletary KW, Jung KJ, Giusti M. Anthocyanin-rich grape extract blocks breast cell DNA damage. J Med Food 2007;10:244-51.

644. Turner A, Chen SN, Nikolic D, van BR, Farnsworth NR, Pauli GF. Coumaroyl iridoids and a depside from cranberry (Vaccinium macrocarpon). J Nat Prod 2007;70:253-8.

645. Nakamura Y, Watanabe S, Miyake N, Kohno H, Osawa T. Dihydrochalcones: evaluation as novel radical scavenging antioxidants. J Agric Food Chem 2003;51:3309-12.

646. Harnly JM, Doherty RF, Beecher GR, Holden JM, Haytowitz DB, Bhagwat S, Gebhardt S. Flavonoid content of U.S. fruits, vegetables, and nuts. J Agric Food Chem 2006;54:9966-77.

647. Gu L, Kelm MA, Hammerstone JF, Beecher G, Holden J, Haytowitz D, Prior RL. Screening of foods containing proanthocyanidins and their structural characterization using LC-MS/MS and thiolytic degradation. J Agric Food Chem 2003;51:7513-21.

648. Appeldoorn MM, Vincken JP, Gruppen H, Hollman PC. Procyanidin dimers A1, A2, and B2 are absorbed without conjugation or methylation from the small intestine of rats. J Nutr 2009;139:1469-73.

649. Ou K, Percival SS, Zou T, Khoo C, Gu L. Transport of cranberry A-type procyanidin dimers, trimers, and tetramers across monolayers of human intestinal epithelial Caco-2 cells. J Agric Food Chem 2012;60:1390-6.

650. Gu L, Kelm M, Hammerstone JF, Beecher G, Cunningham D, Vannozzi S, Prior RL. Fractionation of polymeric procyanidins from lowbush blueberry and quantification of procyanidins in selected foods with an optimized normal-phase HPLC-MS fluorescent detection method. J Agric Food Chem 2002;50:4852-60.

651. Rodriguez-Ramiro I, Ramos S, Bravo L, Goya L, Martin MA. Procyanidin B2 induces Nrf2 translocation and glutathione S-transferase P1 expression via ERKs and p38-MAPK pathways and protect human colonic cells against oxidative stress. Eur J Nutr 2012;51:881-92.

652. Fiorani M, Guidarelli A, Blasa M, Azzolini C, Candiracci M, Piatti E, Cantoni O. Mitochondria accumulate large amounts of quercetin: prevention of mitochondrial damage and release upon oxidation of the extramitochondrial fraction of the flavonoid. J Nutr Biochem 2010;21:397-404.

653. Verstraeten SV, Keen CL, Schmitz HH, Fraga CG, Oteiza PI. Flavan-3-ols and procyanidins protect liposomes against lipid oxidation and disruption of the bilayer structure. Free Radic Biol Med 2003;34:84-92.

654. Verstraeten SV, Hammerstone JF, Keen CL, Fraga CG, Oteiza PI. Antioxidant and membrane effects of procyanidin dimers and trimers isolated from peanut and cocoa. J Agric Food Chem 2005;53:5041-8.

655. Verstraeten SV, Lanoue L, Keen CL, Oteiza PI. Relevance of lipid polar headgroups on boron-mediated changes in membrane physical properties. Arch Biochem Biophys 2005;438:103-10.

656. Pravda J. Radical induction theory of ulcerative colitis. World J Gastroenterol 2005;11:2371-84.

657. Boyer J, Liu RH. Apple phytochemicals and their health benefits. Nutr J 2004;3:5.

658. Wolfe K, Wu X, Liu RH. Antioxidant activity of apple peels. J Agric Food Chem 2003;51:609-14.

659. Wolfe K, Wu X, Liu RH. Antioxidant activity of apple peels. J Agric Food Chem 2003;51:609-14.

660. He X, Liu RH. Phytochemicals of apple peels: isolation, structure elucidation, and their antiproliferative and antioxidant activities. J Agric Food Chem 2008;56:9905-10.

661. Tierney MS, Smyth TJ, Rai DK, Soler-Vila A, Croft AK, Brunton N. Enrichment of polyphenol contents and antioxidant activities of Irish brown macroalgae using food-

friendly techniques based on polarity and molecular size. Food Chem 2013;139:753-61.

662. Monrad JK, Srinivas K, Howard LR, King JW. Design and optimization of a semicontinuous hot-cold extraction of polyphenols from grape pomace. J Agric Food Chem 2012;60:5571-82.

663. Hidalgo IJ, Raub TJ, Borchardt RT. Characterization of the human colon carcinoma cell line (Caco-2) as a model system for intestinal epithelial permeability. Gastroenterology 1989;96:736-49.

664. Mehran M, Levy E, Bendayan M, Seidman E. Lipid, apolipoprotein, and lipoprotein synthesis and secretion during cellular differentiation in Caco-2 cells. In Vitro Cell Dev Biol Anim 1997;33:118-28.

665. Mehran M, Seidman E, Marchand R, Gurbindo C, Levy E. Tumor necrosis factor-alpha inhibits lipid and lipoprotein transport by Caco-2 cells. Am J Physiol 1995;269:G953-G960.

666. Courtois F, Seidman EG, Delvin E, Asselin C, Bernotti S, Ledoux M, Levy E. Membrane peroxidation by lipopolysaccharide and iron-ascorbate adversely affects Caco-2 cell function: beneficial role of butyric acid. Am J Clin Nutr 2003;77:744-50.

667. Pajuelo D, Diaz S, Quesada H, Fernandez-Iglesias A, Mulero M, Arola-Arnal A et al. Acute administration of grape seed proanthocyanidin extract modulates energetic metabolism in skeletal muscle and BAT mitochondria. J Agric Food Chem 2011;59:4279-87.

668. Wang GW, Klein JB, Kang YJ. Metallothionein inhibits doxorubicin-induced mitochondrial cytochrome c release and caspase-3 activation in cardiomyocytes. J Pharmacol Exp Ther 2001;298:461-8.

669. Poulsen HE, Prieme H, Loft S. Role of oxidative DNA damage in cancer initiation and promotion. Eur J Cancer Prev 1998;7:9-16.

670. Podsedek A, Wilska-Jeszka J, Anders B, Markowski J. Compositional characterisation of some apple varieties. European Food Research and Technology 2000;210:268-72.

671. Liu RH, Eberhardt MV, Lee CY. Antioxidant and antiproliferative activites of selected New York apple cultivars. N Y Fruit Q 2001;9:15-7.

672. Reagan-Shaw S, Nihal M, Ahmad N. Dose translation from animal to human studies revisited. FASEB J 2008;22:659-61.

673. Murthy SN, Cooper HS, Shim H, Shah RS, Ibrahim SA, Sedergran DJ. Treatment of dextran sulfate sodium-induced murine colitis by intracolonic cyclosporin. Dig Dis Sci 1993;38:1722-34.

674. Wirtz S, Neurath MF. Mouse models of inflammatory bowel disease. Adv Drug Deliv Rev 2007;59:1073-83.

675. Chassaing B, Aitken JD, Malleshappa M, Vijay-Kumar M. Dextran sulfate sodium (DSS)-induced colitis in mice. Curr Protoc Immunol 2014;104:Unit.

676. Perse M, Cerar A. Dextran sodium sulphate colitis mouse model: traps and tricks. J Biomed Biotechnol 2012;2012:718617.

677. Elson CO, Sartor RB, Tennyson GS, Riddell RH. Experimental models of inflammatory bowel disease. Gastroenterology 1995;109:1344-67.

678. Dieleman LA, Ridwan BU, Tennyson GS, Beagley KW, Bucy RP, Elson CO. Dextran sulfate sodium-induced colitis occurs in severe combined immunodeficient mice. Gastroenterology 1994;107:1643-52.

679. Pahl HL. Activators and target genes of Rel/NF-kappaB transcription factors. Oncogene 1999;18:6853-66.

680. Strober W, Fuss IJ. Proinflammatory cytokines in the pathogenesis of inflammatory bowel diseases. Gastroenterology 2011;140:1756-67.

681. Visekruna A, Joeris T, Seidel D, Kroesen A, Loddenkemper C, Zeitz M et al. Proteasome-mediated degradation of IkappaBalpha and processing of p105 in Crohn disease and ulcerative colitis. J Clin Invest 2006;116:3195-203.

682. Dong WG, Liu SP, Yu BP, Wu DF, Luo HS, Yu JP. Ameliorative effects of sodium ferulate on experimental colitis and their mechanisms in rats. World J Gastroenterol 2003;9:2533-8.

683. Andresen L, Jorgensen VL, Perner A, Hansen A, Eugen-Olsen J, Rask-Madsen J. Activation of nuclear factor kappaB in colonic mucosa from patients with collagenous and ulcerative colitis. Gut 2005;54:503-9.

684. Jung M, Triebel S, Anke T, Richling E, Erkel G. Influence of apple polyphenols on inflammatory gene expression. Mol Nutr Food Res 2009;53:1263-80.

685. Sanchez-Fidalgo S, Cardeno A, Villegas I, Talero E, de la Lastra CA. Dietary supplementation of resveratrol attenuates chronic colonic inflammation in mice. Eur J Pharmacol 2010;633:78-84.

686. Li Q, Verma IM. NF-kappaB regulation in the immune system. Nat Rev Immunol 2002;2:725-34.

687. Lih-Brody L, Powell SR, Collier KP, Reddy GM, Cerchia R, Kahn E et al. Increased oxidative stress and decreased antioxidant defenses in mucosa of inflammatory bowel disease. Dig Dis Sci 1996;41:2078-86.

688. Levy E, Rizwan Y, Thibault L, Lepage G, Brunet S, Bouthillier L, Seidman E. Altered lipid profile, lipoprotein composition, and oxidant and antioxidant status in pediatric Crohn disease. Am J Clin Nutr 2000;71:807-15.

689. Alzoghaibi MA. Concepts of oxidative stress and antioxidant defense in Crohn's disease. World J Gastroenterol 2013;19:6540-7.

690. Huang HC, Nguyen T, Pickett CB. Phosphorylation of Nrf2 at Ser-40 by protein kinase C regulates antioxidant response element-mediated transcription. J Biol Chem 2002;277:42769-74.

691. Nazli A, Yang PC, Jury J, Howe K, Watson JL, Soderholm JD et al. Epithelia under metabolic stress perceive commensal bacteria as a threat. Am J Pathol 2004;164:947-57.

692. Wang A, Keita AV, Phan V, McKay CM, Schoultz I, Lee J et al. Targeting mitochondria-derived reactive oxygen species to reduce epithelial barrier dysfunction and colitis. Am J Pathol 2014;184:2516-27.

693. Rayamajhi N, Kim SK, Go H, Joe Y, Callaway Z, Kang JG et al. Quercetin induces mitochondrial biogenesis through activation of HO-1 in HepG2 cells. Oxid Med Cell Longev 2013;2013:154279.

694. Noor SO, Ridgway K, Scovell L, Kemsley EK, Lund EK, Jamieson C et al. Ulcerative colitis and irritable bowel patients exhibit distinct abnormalities of the gut microbiota. BMC Gastroenterol 2010;10:134.

695. Bailey MT, Dowd SE, Parry NM, Galley JD, Schauer DB, Lyte M. Stressor exposure disrupts commensal microbial populations in the intestines and leads to increased colonization by Citrobacter rodentium. Infect Immun 2010;78:1509-19.

696. Weiss GA, Chassard C, Hennet T. Selective proliferation of intestinal Barnesiella under fucosyllactose supplementation in mice. Br J Nutr 2014;111:1602-10.

697. Ye J, Lee JW, Presley LL, Bent E, Wei B, Braun J et al. Bacteria and bacterial rRNA genes associated with the development of colitis in IL-10(-/-) mice. Inflamm Bowel Dis 2008;14:1041-50.

698. Kitajima S, Takuma S, Morimoto M. Changes in colonic mucosal permeability in mouse colitis induced with dextran sulfate sodium. Exp Anim 1999;48:137-43.

699. Mueller C, Macpherson AJ. Layers of mutualism with commensal bacteria protect us from intestinal inflammation. Gut 2006;55:276-84.

700. Osman N, Adawi D, Ahrne S, Jeppsson B, Molin G. Probiotics and blueberry attenuate the severity of dextran sulfate sodium (DSS)-induced colitis. Dig Dis Sci 2008;53:2464-73.

701. Schmitz ML, Bacher S, Kracht M. I kappa B-independent control of NF-kappa B activity by modulatory phosphorylations. Trends Biochem Sci 2001;26:186-90.

702. Vermeulen L, De WG, Notebaert S, Vanden Berghe W, Haegeman G. Regulation of the transcriptional activity of the nuclear factor-kappaB p65 subunit. Biochem Pharmacol 2002;64:963-70.